# Vorwort

Der alljährliche „Paracelsus Science Get Together" konnte auch 2021 durchgeführt werden – adaptiert an die neuen Gegebenheiten in Zeiten der Pandemie wechselten wir heuer zum zweiten Mal auf die virtuelle Plattform #vSGT.

Forschende aus der Universität, den Universitätskliniken in Salzburg und Nürnberg sowie Kooperationspartnern aus Salzburg und Nürnberg folgten der Einladung und reichten insgesamt mehr als 130 internationale Poster (davon 17 Poster von Studierenden der Humanmedizin) ein. Sie stellten ihre aktuellen Forschungsarbeiten vor – virtuell und den ganzen Sommer über auch online verfügbar. Die gezeigten Arbeiten umfassen eine enorme thematische Bandbreite aus den verschiedensten Wissenschaftsbereichen, darunter Medizin, Natur- und Sozialwissenschaften, von Grundlagen- bis zu klinischer Forschung.

Rund 670 Besucherinnen und Besuchern konnte die medizinisch-wissenschaftliche Leistungsschau im bereits elften Jahr ihres Bestehens in neuem Format begeistern, wie auch die zahlreiche Teilnahme am neu eingeführten Publikumsvoting beweist. Mehr als 1240 Seitenaufrufe (!) wurden über den Sommer gezählt.

Herzliche Gratulation an alle Gewinnerinnen und Gewinner der Poster Awards. Das Publikum kürte das Poster von **Christiane Licht** mit dem Titel „Maladjustment of pressure settings of a Codman-Hakim programmable shunt valve by electromagnetic door locks – A case report" von der Klinik für Psychiatrie und Psychotherapie in Nürnberg zum besten Poster.

Die Fachjury entschied sich für **Lara Bieler** (Best Poster female) mit „Retro- and anterograde axonal tracing via injection of AAV particles to study neuroregeneration after spinal cord injury", **Bruno Benedetti** (Best Poster male), „Mechanisms of neuronal maturation in the adult and aging brain", **Katharina Strempfl** (Best PhD Poster), „The anti-asthmatic drug Montelukast improves motor coordination and balance in the Line 61 mouse model of Parkinson's disease" (alle Salzburg) und **Anna-Lena Petersmann** (Best Student Poster), „Externe Validation zweier aktueller MRT-basierter Risikokalkulatoren zur Diagnostik des Prostatakarzinoms" (Nürnberg).

Ein herzlicher Dank gilt unseren Organisatoren rund um Bruno Wöran, dem Leiter des Forschungsservice FMTT und Ralf Bertram, der am Standort Nürnberg für die Abwicklung verantwortlich war, sowie den zahlreichen Unterstützer*innen, die auch in diesem besonderen Jahr die Durchführung des vSGT mitermöglicht haben. 16 internationale Sponsoren, allen voran Hauptsponsor Pfizer Oncology, vertrauten auf das neue Format und ermöglichten das umfangreiche, internationale Netzwerken.

Wir freuen uns, Ihnen zum Abschluss des „Paracelsus virtual Science Get Together – Science Summer" wie in jedem Jahr diesen Abstractband zum besseren Überblick und als Nachschlagewerk übermitteln zu dürfen, wiederum mit einer ISBN-Nummer versehen und damit zitierfähig. Für alle, die noch einen Blick auf die tatsächlichen Poster werfen möchten, die Ausstellung kann nach wie vor unter https://vsgt.pmu.ac.at/ besucht werden.

Der besondere Dank der Universität gilt neben den Mitarbeiterinnen und Mitarbeitern des Forschungsservices im FMTT der gesamten IT, insbesondere der Abteilung Application Management sowie Media Technology, die das neue Format zum Laufen brachten und jetzt bereits im zweiten Jahr etablierten. So wurde der Netzwerkgedanke des vSGT nicht nur von den Teilnehmenden, sondern auch von der Organisation gelebt – ganz im Sinne des Leitbildes der Universität.

Es ist uns ein großes Anliegen, den Vernetzungsgedanken weiter zu verankern und auch gemeinsame Forschungsprojekte zwischen den beiden Universitäts-Standorten Salzburg und Nürnberg im Sinne eines Brückenschlages innerhalb der PMU weiter voranzutreiben und zu fördern.

Für 2022 laufen jetzt schon die Planungen: Es wird den ganzen Sommer über standortübergreifende virtuelle und hybride Veranstaltungen geben. Bleiben Sie gesund und neugierig und freuen Sie sich mit uns auf den „Science Get Together 2022", in dem wir wieder großartige Leistungen präsentieren werden.

Es grüßen Sie herzlich

Univ.-Prof. Dr. Wolfgang Sperl
Rektor

Univ.-Prof. Dr. Ludwig Aigner
Vizerektor für Forschungsangelegenheiten

# Inhaltsverzeichnis

Vorwort I

Sponsor*innen XI

Abstractsammlung

Nr. 1: The Cdk5 inhibitor Dinaciclib as a novel therapeutic approach for biliary tract cancer S. 2

Nr. 2: Mutations in HID1 cause syndromic infantile encephalopathy and hypopituitarism S. 4

Nr. 3: A Rodent Lumbosacral Spinal Cord Injury Model Reflecting Neurological and Urological Deficits of Humans S. 6

Nr. 4: Development of a physiologically relevant, biomechanical test setup considering internal muscle forces for the investigation of complex pelvic ring fractures S. 8

Nr. 5: Protein Metabolism in Preterm and Term Infants using a 15N-Tracer and the Nitrogen Balance Method: A Pilot-Study S. 10

Nr. 6: Evaluation of Tazemetostat as a therapeutically relevant substance in biliary tract cancer S. 12

Nr. 7: Inducing ferroptosis, a new approach to target biliary tract cancer? S. 14

Nr. 8: Mechanisms of neuronal maturation in the adult and aging brain S. 16

Nr. 9: Expression of the amino acid transporter SLC6A20 is regulated by the transcription factor POU3F4 S. 18

Nr. 10: Handinfections – the longer untreated the worse the outcome? S. 20

Nr. 11: Understanding the role of platelets in Alzheimer's Disease S. 22

Nr. 12: Retro- and anterograde axonal tracing via injection of AAV particles to study neuroregeneration after spinal cord injury S. 24

Nr. 13: AML-derived extracellular vesicles convey immunomodulatory potential S. 26

Nr. 14: Die robotisch assistierte, bilaterale Fixation am Cooper Ligament (Pektopexie) zur Behandlung des apikalen Prolapses: Erstbeschreibung und Analyse der perioperativen Ergebnisse S. 28

Nr. 15: Status epilepticus outcome in patients with and without MRI abnormalities S. 30

Nr. 16: Identification of microRNA as regulating somatic factors of adaptive coping in patients with fibromyalgia syndrome S. 32

Nr. 17: The effect of Matrix, Admedus patches and Inspiris aortic valve materials on primary human endothelial cells from the great saphenous vein S. 34

Nr. 18: Das Dilemma der nekrotisierenden Fasziitis ..... S. 36

Nr. 19: Treatment of psoriasiform-like skin inflammation with diacerein influences skin and spleen immune cell subpopulations ..... S. 38

Nr. 20: Ergebnisse der Operation nach Karydakis zur Behandlung eines Sinus pilonidalis ..... S. 40

Nr. 21: PHARMACEUTICAL MEDICATION MANAGEMENT AT HOSPITAL ADMISSION IDENTIFIES RELEVANT DRUG-RELATED PROBLEMS ..... S. 42

Nr. 22: Evidence- Based Patient Selection in Headache Surgery: The Impact of Preoperative RFA Treatment on Surgical Outcomes ..... S. 44

Nr. 23: TAILOR-MADE CARDIOPULMONARY BYPASS ..... S. 46

Nr. 24: Management algorithms and artificial intelligence systems for cardiopulmonary bypass ..... S. 48

Nr. 25: Extracellular vesicles derived from induced pluripotent stem cells in hypoxic conditions enhance angiogenesis ..... S. 50

Nr. 26: Cholinerge Neurone in der humanen Aderhaut eine quantitative Untersuchung ..... S. 52

Nr. 27: Effect of yoga on the psychological well-being of breast cancer patients (depression, anxiety and social support) - Evaluation of the HADS and ESSI questionnaire ..... S. 54

Nr. 28: Regeneration of critical sized defects (csd) by implantation of directed silk scaffolds (SC) in combination with bone morphogenetic protein 2 (BMP-2) and/or hydroxyapatite (HA) in a rat animal model ..... S. 56

Nr. 29: Assessment of the Regenerative Activity of Human Umbilical Cord Mesenchymal Stem Cells - derived Extracellular Vesicles (hUCMSC-EVs) in Osteoporotic Bone – A Femoral Metaphyseal Fracture Defect Model in Rats ..... S. 58

Nr. 30: Comparative Evaluation of Microplate-based Assays for Viable Cell Quantity ..... S. 60

Nr. 31: Establishing the cardiotonic steroid ouabain as a potent anti-cancer drug against biliary tract cancer – Step one ..... S. 62

Nr. 32: Identification of baseline characteristics of HR+/HER2- primary metastatic breast cancer patients at Breast Center Klinikum Nuremberg that drive decision between chemotherapy and CDK4/6 inhibition ..... S. 64

Nr. 33: Potential role of Cullin-RING E3 ubiquitin ligase CRL3Zbtb16 in the premature degradation of pathogenic pendrin variants ..... S. 66

Nr. 34: Self-assembly of human iPSC-derived single cells creates skin organoids and regenerates vascularized human skin ..... S. 68

Nr. 35: Multimodal diagnostic efforts for infratentorial lesions - The suboccipital transcerebellar approach in stereotactic brain biopsy - A single institution experience ..... S. 70

Nr. 36: Auswirkungen der Endokrinen Therapie mit einem CDK4/6 Inhibitor im Vergleich zur Chemotherapie beim metastasierten HR+/HER-2-neg Mammakarzinom in der Erstlinientherapie ..... S. 74

Nr. 37: A spoonful of L-fucose - An efficient therapy for GFUS-CDG, a new glycosylation disorder ..... S. 76

Nr. 38: Customized 3D printed milling templates can significantly improve the fitting of the subchondral bone plate in autologous osteochondral transplants ..... S. 78

Nr. 39: The effects of extracellular potassium on the respiratory burst in neutrophil granulocytes ..... S. 82

Nr. 40: Helping women cope with a traumatic life event: The MALT! program for women. A controlled randomized trial ..... S. 84

Nr. 41: The EJP-RD EBStatMax project: How clinicians and statisticians work together ..... S. 86

Nr. 42: Automated non-contact respiratory rate monitoring of neonates ..... S. 88

Nr. 43: HAIP – Optimiertes Hygienemanagement in der außerklinischen Intensivpflege ..... S. 90

Nr. 44: Integration von biologisch abbaubarem Poly(L-Lactid) (PLLA) auf neu entwickelten bioaktiven Glas Scaffolds (CAR12N) für das Knorpel Tissue Engineering ..... S. 92

Nr. 45: Aufrechterhaltung der Ligamenthomöostase und -differenzierung durch zyklische Dehnung von funktionalisierten PLA/+P[LA-CL]-Kollagenkonstrukten für das Kreuzband-Tissue Engineering ..... S. 94

Nr. 46: Stem cell-based regeneration of muscles ..... S. 96

Nr. 47: ECG-Predictors of postoperative arrhythmia after aortic valve replacement and coronary artery bypass graft ..... S. 98

Nr. 48: Human Platelet Lysate for Skin Regeneration & Immune Modulation ..... S. 100

Nr. 49: Mid-term survival of geriatric patients with septic arthritis of the knee and the influence of risk factors on survival ..... S. 102

Nr. 50: Quantitative echocardiographic analysis of the right atrial size reflects the severity of histopathological confirmed fibrosis in patients undergoing cardiac surgery ..... S. 104

Nr. 51: Hypotonicity Sensitizes Biliary Tract Cancer Cells to Cisplatin Cytotoxicity ..... S. 106

Nr. 52: THE ENHANCER LANDSCAPE PREDETERMINES SKELETAL REGENERATION CAPACITY OF BONE MARROW STROMAL CELLS ..... S. 108

Nr. 53: In-Hospital thrombocytopenia following TAVI – Predictors and Outcomes ..... S. 110

Nr. 54: Do you know if your patient can cross the traffic light during the green period? – a prospective observational study ..... S. 112

Nr. 55: C - reactive protein is a promising indicator of ventricular arrhythmias in pacemaker patients ..... S. 114

Nr. 56: Higher incidence of stroke in severe COVID 19 is not associated with a higher burden of arrhythmias: Comparison to other types of severe pneumonia ..... S. 116

Nr. 57: The Geriatric Patient in the Emergency Department – The Role of Imaging in Patient Care Management ..... S. 118

Nr. 58: Nursing Development Center - Perspectives on safety culture in acute care from health care professionals ..... S. 120

Nr. 59: Nitrerge Neuronen der menschlichen Aderhaut: Eine quantitative Studie ..... S. 122

Nr. 60: Low pH attenuates apoptosis by suppressing the volume-sensitive outwardly rectifying (VSOR) chloride current in chondrocytes ..... S. 124

Nr. 61: Functional characterization of Staphylococcus aureus strains isolated from patients with recessive dystrophic epidermolysis bullosa ..... S. 126

Nr. 62: Ophthalmological Surgeries with a novel Ultrashort Pulse Laser Source ..... S. 128

Nr. 63: The influence of various great saphenous vein graft storage solutions on the ..... S. 130

Nr. 64: Individualized growth trajectories: Evaluation of growth outcomes in the California Perinatal Quality Care Collaborative (CPQCC) ..... S. 132

Nr. 65: Mesoderm induction improves human induced pluripotent stem cell-derived megakaryocyte differentiation and platelet production ..... S. 134

Nr. 66: Sarcopenia is an independent predictor for mortality and morbidity in coronary bypass surgery ..... S. 136

Nr. 67: The relationship of intraspinal to extraspinal disorders in nonidiopathic scoliosis ..... S. 138

Nr. 68: The incidence of lumbo sacral transitional vertebra in scoliosis ..... S. 140

Nr. 69: Upregulation of mitotic bookmarking transcription factors may induce enhanced proliferation of human stromal cells by human platelet lysate ..... S. 142

Nr. 70: Individualized target fortification of breast milk with protein, carbohydrates, and fat for preterm infants - Neurodevelopmental outcomes ..... S. 144

Nr. 71: Intraoperative hemoadsorption reduces sepsis-related death in all-comers undergoing surgery for infective left-sided endocarditis ..... S. 146

Nr. 72: Serum levels of GFAP and NfL are related to the neurological impairment and spinal edema after traumatic spinal cord injury ..... S. 148

Nr. 73: Benefits of pulmonary rehabilitation in COVID-19 a prospective observational cohort study ..... S. 150

Nr. 74: Maladjustment of pressure settings of a Codman-Hakim programmable shunt valve by electromagnetic door locks – A case report ..... S. 152

Nr. 75: Repetitive Transcranial Magnetic Stimulation for Catatonia – a case report ..... S. 154

Nr. 76: Central Nervous System Manifestation of a mantle cell lymphoma at the resection site of a meningioma: a case report ..... S. 156

Nr. 77: Effect of long COVID-19 on respiratory burst of neutrophils. ..... S. 158

Nr. 78: Cytosolic Mineralocorticoid Receptor interacts differentially with other Proteins depending on Ligand ..... S. 160

Nr. 79: Integration of body composition assessments for preterm infants into clinical routine ..... S. 162

Nr. 80: A new exploratory score for determining the prognostic value of MRI in patients with status epilepticus ..... S. 164

Nr. 81: First description of non-obstructing cerebral aqueduct cysts seen in Normal pressure hydrocephalus patients ..... S. 166

Nr. 82: Results from the 10 years follow-up following sutureless aortic valve replacement: survival and hemodynamic outcomes ..... S. 168

Nr. 83: Determinants of hyperglucagonemia in pediatric non-alcoholic fatty liver disease ..... S. 170

Nr. 84: Glucagon, NAFLD and Amino acids- an Evidence map ..... S. 172

Nr. 85: Pathogenicity assessment of pendrin (SLC26A4) variant p.L117F ..... S. 174

Nr. 86: HDAC Screening identifies the HDAC Class I Inhibitor Romidepsin as a promising Epigenetic Drug for Biliary Tract Cancer ..... S. 176

Nr. 87: Standardized single incision laparoscopy for resection in liver segments 7 and 8: retrospective analysis from a center ..... S. 178

Nr. 88: Bestehende therapeutische Antikoagulation und OP-Indikation bei symptomatischer Varikose – Chance oder Widerspruch? ..... S. 180

Nr. 89: A protocol to evaluate and validate implant internal forces and moments ..... S. 182

Nr. 90: Burnout and resilience among hospital staff during the COVID-19 pandemic: cross-sectional results from the international Cope-Corona study ..... S. 184

Nr. 91: Coagulation potential of SARS CoV-2 target cells and their extracellular vesicles ..... S. 186

Nr. 92: Benchmark test of flow sensors for the Sophie ventilator regarding dead space ..... S. 188

Nr. 93: Benchmark test of flow sensors for the Sophie ventilator regarding condensation susceptibility ..... S. 190

Nr. 94: Effects of Angocin® on Microbacteria ..... S. 192

Nr. 95: Targeting Neuroblastoma with Food Additives ..... S. 196

Nr. 96: Analysis of the fibrotic substrate and post-operative ventricular arrhythmias in patients undergoing surgery due to valvular aortic stenosis and left ventricular outflow tract obstruction ..... S. 198

Nr. 97: Externe Validation zweier aktueller MRT-basierter Risikokalkulatoren zur Diagnostik des Prostatakarzinoms ..... S. 200

Nr. 98: Efficient CRISPR/Cas9n-mediated repair of a COL17A1 mutation ..... S. 202

Nr. 99: Retrospective analysis of excipients in drug therapy of premature infants and its potential impact on patient safety ..... S. 204

Nr. 100: Adherence to minimal experimental requirements for defining extracellular vesicles and their functions: a systematic review. S. 206

Nr. 101: Galanin is a modulator of phagocytosis in the human monocytic cell line THP-1 S. 208

Nr. 102: Role of Kir2.1 channels in an oxidative stress-related model of aging neuroglia S. 210

Nr. 103: Health-related quality of life in patients with traumatic spinal cord injury – A longitudinal study S. 212

Nr. 104: Effects of online sleep counselling for shift workers S. 214

Nr. 105: Functional recovery through intralesional application of extracellular vesicles in a rat model of traumatic spinal cord injury. S. 216

Nr. 106: Immediate full weight-bearing with supplemental cerclage? A biomechanical study on the distal tibia S. 218

Nr. 107: Pro- and antiangiogenic effects of human tendon cells depend on oxygen availability S. 220

Nr. 108: Effects of an automatic oxygen system during walking in hypoxemic patients with severe COPD – a randomized controlled double-blind cross over trial S. 222

Nr. 109: MiA - Mentalisierung im Alter – Erste Ergebnisse einer laufenden Studie S. 224

Nr. 110: Augmenting tendon repair with SPARC S. 226

Nr. 111: IN VITRO EVALUATION OF A NANOPARTICLE-BASED mRNA DELIVERY SYSTEM FOR TENDON TISSUE S. 228

Nr. 112: Führt ein unbehandelter Diabetes mellitus Typ II zur Knorpeldegeneration?. Untersuchungen in situ und im in vitro Arthrosemodell S. 230

Nr. 113: Possible Interrelation between Complement and Prolactin Hormone Systems in Chondrocytes in Perspective of Osteoarthritis Pathogenesis S. 232

Nr. 114: Die Bedeutung des interatrialen Blocks für das Auftreten von postoperativem Vorhofflimmern nach isoliertem Aortenklappenersatz und aortocoronarer Bypassoperation S. 234

Nr. 115: Case Report: Tertiäre Nebennierenrindeninsuffizienz bei zerebraler Metastasierung S. 236

Nr. 116: PREDICTION OF CARDIAC SURGERY-ASSOCIATED ACUTE KIDNEY INJURY THROUGH ARTIFICIAL INTELLIGENCE-BASED METHODS S. 238

Nr. 117: The anti-asthmatic drug Montelukast improves motor coordination and balance in the Line 61 mouse model of Parkinson's disease S. 240

Nr. 118: Low-Dose Therapy in Atopic Dermatitis S. 242

Nr. 119: Establishment of a fetal MRI method to measure the body composition for the development of fetal fat mass and fat-free mass trajectories S. 244

Nr. 120: Virtual simulation versus hands-on training in Extracorporeal Life Support (ECLS) and ECMO S. 246

Nr. 121: Transcriptomic characterization of brain CD8+ T-cells identifies gene signature of tissue-resident memory T-cells in Alzheimer's disease transgenic mice. S. 248

Nr. 122: in vitro Enthesisformation mittels Ko-Kultur auf einem triphasisch gestickten Träger für das Kreuzband Tissue Engineering S. 250

Nr. 123: Spondylodiscitis – a retrospective analysis of hospitalized older patients S. 252

Nr. 124: Controlled and randomized study of the psychological effects of yoga during breast cancer therapy S. 254

Nr. 125: Ketogenic diets reduce melanoma growth in vivo regardless of mutation status and metabolic signature S. 256

Nr. 126: Analysing the Neonatal Microbiome by qPCR and Nanopore Sequencing S. 258

Nr. 127: Perfusionsmuster eines hepatozellulären Karzinoms vom fibrolamellären Subtyp in der Kontrastmittelsonographie (CEUS) S. 262

Nr. 128: A DEEP-LEARNING-BASED TECHNIQUE FOR THE QUANTITATIVE ANALYSIS OF FEMOROTIBIAL OSTEOPHYTE AND BONE VOLUMES – DATA FROM THE OSTEOARTHRITIS INITIATIVE S. 264

Nr. 129: FULLY AUTOMATED CARTILAGE SEGMENTATION OF LATE STAGE OSTEOARTHRITIS (KLG4) KNEES USING DEEP LEARNING WITH U-NET ARCHITECTURES – MODEL SPECIFICITY IS IMPORTANT S. 266

Nr. 130: Enhanced angiogenesis and wound healing in vivo induced by extracellular vesicles from therapeutic grade allogeneic human placental stromal cells S. 268

Nr. 131: Does the "Gremlin/BMP-axis" modulate tendon inflammation? S. 270

Nr. 132: Klinische Bedeutung der Targeted axillary dissection (TAD) nach neoadjuvanter Chemotherapie bei Mammakarzinompatientinnen mit prätherapeutisch befallenen Lymphknoten und Konversion zu ycN0 S. 272

Nr. 133: Clinically relevant prognostic biomarkers for immune-checkpoint inhibitor therapy in NSCLC S. 274

Nr. 134: Investigating the effect of β-cyclodextrin on dopamine D2 receptor ligand binding S. 276

Nr. 135: Establishment of a seminal platform for AI Development in a radiological-clinical context S. 278

Liste aller beteiligten Einrichtungen XV

Verzeichnis aller Autor*innen XVI

Der Paracelsus virtual Science Get Together 2021 wurde mit freundlicher Unterstützung folgender Unternehmen ermöglicht:

Pfizer Oncology

bartelt LABOR-KOMPLETTAUSSTATTER Chemikalien · Geräte · Service · Software

BAYER

NEW ENGLAND BioLabs GmbH be INSPIRED | drive DISCOVERY | stay GENUINE

BIOMÉRIEUX

Biozym SCIENCE IS OUR BUSINESS

BRACCO LIFE FROM INSIDE

Cochlear Hear now. And always

COOK MEDICAL

idox

IPSEN Innovation for patient care

LACTAN Chemikalien und Laborgeräte ROTH

MLP Finanzen verstehen. Richtig entscheiden.

NOVARTIS ONCOLOGY

S&T international UG

TERUMO Aortic

# Poster- & Abstractsammlung

# The Cdk5 inhibitor Dinaciclib as a novel therapeutical approach for biliary tract cancer

Celina Ablinger[1], Johanna Pachmayr[2], Daniel Neureiter[3], Markus Ritter[1,2], Tobias Klieser[1,2], Irina Pancic[1], Maximilian Ardelt[4], Christian Mayr[1,5,6], Petra Huber-Cantonati[1,6]

[1] Center for Physiology, [2] Histochemistry and Biochemistry – Studying and Maintaining Cells as Tissue Physiology and Pathophysiology – ICCC Salzburg, Austria; [3] Institute of Pathology, Paracelsus Medical University / Salzburger Landeskliniken (SALK), 5020 Salzburg, Austria; [4] Department of Internal Medicine I, Paracelsus Medical University / Salzburger Landeskliniken (SALK), 5020 Salzburg, Austria; [5] Institute of Pharmacy, Department of Pharmaceutical Technology and Clinical Pharmacy, [6] Paracelsus Medical University, 5020 Salzburg, Austria

Acknowledgements: This work is supported by the PMU Translational Research Fund (PMU-TFF; I-19-03218P, A-TRF)

**Objective:** Biliary tract cancer has a poor survival prognosis due to the lack of sufficient therapies and high rates of recurrence regarding the development of chemoresistance. Cyclin-dependent kinases (Cdks) have gained increased interest as potential cancer therapeutic targets in the last decade. The current study investigates the potential of the new composite Cdk inhibitor Dinaciclib as a novel treatment option for BTC.

**Methods:** For this study, a comprehensive human BTC in vitro model (n = 11 cell lines), including one non-tumourgenous cell line, is used. First, the cytotoxic effect of Dinaciclib in nM range was investigated using Resazurin assays. $IC_{50}$ values were calculated for each biological replicate using linear interpolation based on n = 3 biological replicates (mean ± SEM). Also Cdk expression (1,2,5 and 9) in each cell line was analysed using Western Blot analysis.

**Result 1:** Dose-dependent cytotoxic effect of Dinaciclib on BTC cell lines after 72h treatment. Data are presented as mean ± SEM of n = 3 biological replicates.

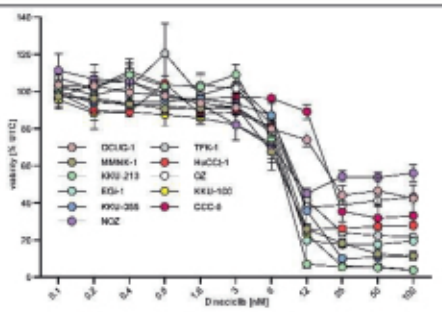


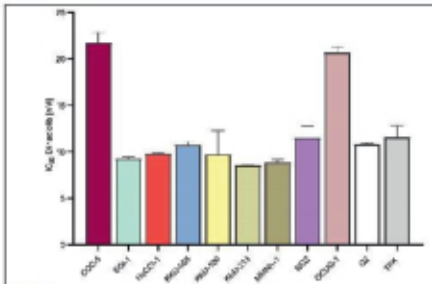


**Result 1:** Calculated Dinaciclib $IC_{50}$ values for BTC cell lines. Data are shown as mean ± SEM of n = 3 biological replicates.

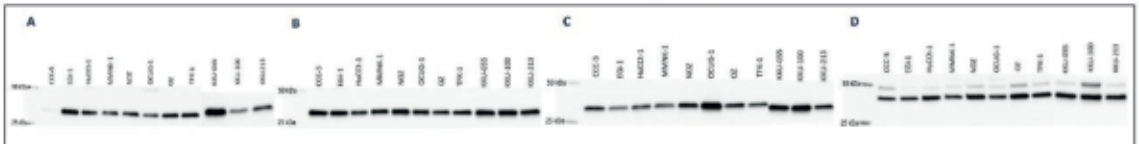


**Results 3:** Representative Western Blot images of preliminary results of Cdk1 (A), Cdk2 (B), Cdk5 (C) and Cdk9 (D) protein expression analysis.

**Outlook:** Next steps include investigation of the effect of Dinaciclib on cell viability (time-resolved) and cell proliferation, either as single drug treatment or in combination with the standard chemotherapeutic Cisplatin. The effect of Dinaciclib/Cisplatin combination on cellular proliferation will be tested via impedance measurement using the xCELLigence device. Furthermore, cell cycle will be analysed following Dinaciclib treatment. Next, we will investigate whether Dinaciclib causes DNA damage via measurement of protein levels of DNA damage-related factors as well as using the COMET assay for detection of double strand breaks in DNA. The expression pattern of Cdk5 is evaluated in resected FFPE BTC samples (N=80) of a well characterized patient cohort with immunohistochemistry.

## The Cdk5 inhibitor Dinaciclib as a novel therapeutic approach for biliary tract cancer

Celina Ablinger[1], Johanna Pachmayr[3], Daniel Neureiter[4], Markus Ritter[1,2], Tobias Kiesslich[1,5], Irina Pancis[1], Maximilian Ardelt[3], Christian Mayr[1,5#], Petra Huber-Cantonati[3#]

[1]Center for Physiology, Pathophysiology and Biophysics - Salzburg and Nuremberg, Institute for Physiology and Pathophysiology - Salzburg, 5020 Salzburg, Austria; [2]Kathmandu University School of Medical Sciences, Dhulikhel, Nepal; [3]Institute of Pharmacy, Department of Pharmaceutical Biology and Clinical Pharmacy, Paracelsus Medical University, 5020 Salzburg, Austria; [4]Institute of Pathology, Paracelsus Medical University / Salzburger Landeskliniken (SALK), 5020 Salzburg, Austria; [5]Department of Internal Medicine I, Paracelsus Medical University / Salzburger Landeskliniken (SALK), 5020 Salzburg, Austria; Contact: celina.ablinger@pmu.ac.at

### Objective
Biliary tract cancer is a rare malignancy and has a poor survival prognosis due to the lack of sufficient therapies and development of chemoresistance. Cyclin-dependent kinases (Cdks) have gained increasing interest as potential cancer therapeutic targets in the last few years. The current study examines the potential of the new composite Cdk inhibitor Dinaciclib as a novel treatment option for BTC.

### Methods
For this study, a comprehensive human BTC in vitro model (n = 11 cell lines, including one non-tumorigenic cell line) is used. The cytotoxic effect of Dinaciclib (nM range) was investigated using Resazurin assays. IC50 values were calculated using linear interpolation based on n = 3 biological replicates (mean ± SEM). Also Cdk expression (1,2,5 and 9) in each cell line was analysed using Western Blot analysis.

### Results
Based on preliminary data, the cytotoxic effect of Dinaciclib was investigated in the complete in vitro model. We found a cell line-specific reduction of viable cells after 72 h of treatment. Since Dinaciclib is described as a Cdk1, 2, 5, and 9 inhibitor, we next measured protein levels of these Cdks in the BTC cells and found a heterogeneous expression distribution.

### Conclusions
Next steps include the investigation of the effect of Dinaciclib on cell viability (time-resolved) and cell proliferation on suitable BTC cells, either as single drug treatment or in combination with the standard chemotherapeutic cisplatin. The effect of the Dinaciclib/Cisplatin combination on cellular proliferation (independent of cellular metabolism) will be tested via impedance measurement using the xCELLigence device. Furthermore, cell cycle will be analysed following Dinaciclib treatment. Next, we will investigate whether Dinaciclib causes DNA damage via measurement of protein levels of DNA damage-related factors as well as using the COMET assay for detection of double strand breaks in DNA.

### Acknowledgements
This work is supported by the PMU Forschungsförderungsfond (PMU-FFF E-19/30/157-ARD)

# Mutations in *HID1* cause syndromic infantile encephalopathy and hypopituitarism

Melanie T. Achleitner[1,*], Anne Schlinzer[2,*], HIDI Study Group, Blake Hummer[3], René G. Feichtinger[1], Johannes A. Mayr[1], Saskia B. Wortmann[1,4,5,6] and Axel Weber[7]

1 University Children's Hospital, Paracelsus Medical University (PMU), Salzburg, Austria, 2 Institute of Neuropathology, Justus-Liebig-University, Giessen, Germany, 3 Molecular and Cellular Biophysics Program, Dept. of Biological Sciences, University of Denver, 4 Radboud Center for Mitochondrial Medicine, Department of Pediatrics, Amalia Children's Hospital, Radboudumc, Nijmegen, The Netherlands, 5 Institute of Human Genetics, Helmholtz Center Munich, Neuherberg, Germany, 6 Institute of Human Genetics, Technical University Munich, Munich, Germany, 7 Institute of Human Genetics, Justus-Liebig-University, Giessen, Germany, * These authors contributed equally to this work

## INTRODUCTION

Precursors of peptide hormones undergo posttranslational modifications within the trans-Golgi network (TGN). Dysfunction of proteins involved at different steps of this process cause several complex syndromes affecting the central nervous system (CNS). We aimed to clarify the genetic cause in a group of patients characterized by hypopituitarism in combination with brain atrophy, thin corpus callosum, severe developmental delay, visual impairment, and epilepsy.



**Figure 1. Clinical phenotype and MRI images of patients with bi-allelic HID1 variants**
(A) Patient I:II-2 at age 3 months (A1, A2). T2-weighted sagittal (A3) and coronal (A4) brain MR images of patient I:II-2 at age 4 months indicating hypoplasia of the corpus callosum and a small sella turcica (white arrows). (B) I:III-3 at age 2 months (B1, B2), at age 2 years (B3), and at age 3 years (B4), respectively. T2-weighted sagittal and coronal brain MR images of patient I:III-3 at age 4 months (B5, B6) and at age 3 years and 3 months (B7, B8), respectively. Note the small pituitary gland and the thin and dysplastic corpus callosum (B6 white arrows). Note also distinct cortical atrophy and enlargement of the inner ventricles evolving during the course of disease in patient I:III-3 (B7, B8). An unspecific signal alteration of the ventral part of the pons (B7, white arrow) is also marked. (C) Patient 2:IV-3 at age 3 years (C1) and at age 21 years (C2, C3). T1-weighted brain MR image displays a relatively small pituitary gland and a small corpus callosum. No generalized brain atrophy is visible. (D) Patient 3:IV-1 at age 3 years (D1, D2). T2-weighted brain MR image displays a thin corpus callosum (D3, white arrows). (E) Facial gestalt of patient 4:II-2 at age 8 months (E1, E2). T2 (E3) and T1-weighed (E4) sagittal brain MR images show a thin corpus callosum. T1-weighted coronal image depicts enlarged lateral ventricles and suggests gyral atrophy. (F) Patient 5:II-1 at age 2 weeks (F1), 20 months with cushingoid face (F2) and 3 years, respectively (F3). Sagittal T1-weighted MR image at age 18 months indicates a dysplastic corpus callosum and a small pituitary gland (F4), while a coronal FLAIR image indicates mild gyral atrophy (F5).

## RESULTS

We identified bi-allelic variants in the gene *HID1* domain-containing protein 1 (HID1) in seven patients [PMID:33999436][1]. Post mortem examination confirmed cerebral atrophy with enlarged lateral ventricles. Markedly reduced expression of pituitary hormones was found in pituitary gland tissue. Co-localization of HID1 protein with the TGN was not altered in fibroblasts of patients compared to controls, while the extracellular acidification rate (ECAR) upon stimulation with potassium chloride was significantly reduced in patient fibroblasts compared to controls.

Our findings indicate that mutations in HID1 cause an early infantile encephalopathy with hypopituitarism as the leading presentation, and expand the list of syndromic CNS diseases caused by interference of TGN function.

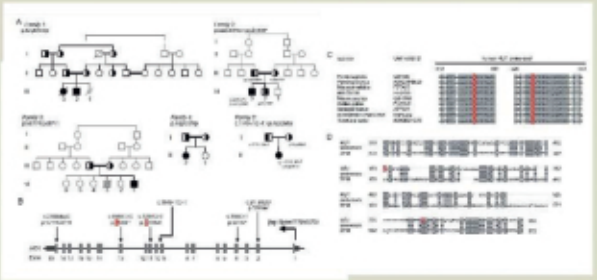

**Figure 2. *HID1* variants**
(A) Pedigrees of families reported (1 to 5). Family members who underwent genetic testing for the respective HID1 variants are indicated with black and white symbols. Grey-and-white symbols correspond to family members not tested for the familial *HID1* variant.
(B) The human *HID1* gene (NM_030630) consists of 19 exons on the minus strand of chromosome 17 (hg19 coordinates: chr17:72946837-72968854). *HID1* variants found in the families reported are highlighted. Missense variants are indicated white with red background. (C) Alignment of the protein sequences in vicinity to amino acids D28, R433 and L533, between human and homologous HID1 proteins. R433, L533 and adjacent amino acids are widely conserved between species. D28 is also highly conserved except for nematods. (D) Partial alignment of human HID1 (NP_065133.1) and DYM (NP_060123.3) amino acid sequences. Regions depicted in result of the BLASTP search, displayed as pairs of matches between query (HID1) and subject (DYM) sequence. Identities present the letter, conservative substitutions present a "+" and nothing otherwise within the consensus line. Amino acids R433 and L533 in HID1 are highlighted

**FUNDING**
Supported by the ERA PerMed project PerMitn (Austrian Science Fund FWF, I4704-B) to S.B.W. and ERA E-RARE-3 project GENOMIT (Austrian Science Fund FWF, I2741-B26 and I4995-B) to J.A.M., and by the German Science Foundation Collaborative Research Centre (CRC) 870.

Achleitner A, Achleitner M, Trübenbach D, Abdel I, Alhenaky R, Abdulwahab MW, Brett PA, Mosberg S, Mansour S, Feichtinger RG, Mayr JA, Wortmann SB, Jochum H, Rudolf-Schlotthauer S, Rad A, Bultas F, Sánchez JP, Flora S, Hamilton T, Kido IG, Wieczorek IM, Neubauer BA, Anton T, Rohrbacher RK, Jamsheer C, Bertoncelj C, Akinyemi RS, Alfayad MD, Hehr A, Weber A. Mutations in HID1 cause syndromic infantile encephalopathy and hypopituitarism. Am Neurol. 2021 May 17. doi: 10.1002/ana.26127. [Epub ahead of print] PMID: 33999436.

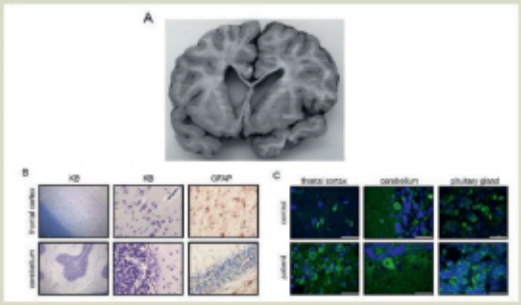

**Figure 3. Neuropathological findings of patient 1:III-3**
(A) Gross examination of a coronal brain section of patient 1:III-3 at age 3 years showing cerebral atrophy (brain weight 702 grams), enlargement of the lateral ventricles and a thin corpus callosum. The cortical gray matter is well distinguished from the white matter. (B) Klüver Barrera (KB) staining displays normal cortical architecture in the frontal cortex and cerebellum, no signs of de- or hypomyelination (magnification x40 1st column; x400 2nd column). Activated glial cells are numerous in frontal cortex as confirmed with antibodies against GFAP (magnification x400).
(C) Analysis of the pituitary gland shows normal adenoid morphology. Staining with antibodies against pituitary hormones depicts moderate ACTH reduction, while FSH, HGH, LH, Prolactin (Prol) and TSH are strongly reduced compared to the control (inlay) (magnification 200x). (B) Immunofluorescence analysis with antibodies against HID1 shows a cytoplasmic expression in neuronal cells of the frontal cortex and cerebellum and in adenoid cells of the pituitary gland in patient 1:III-3 and control (magnification x630, white bars correspond 50 µm).

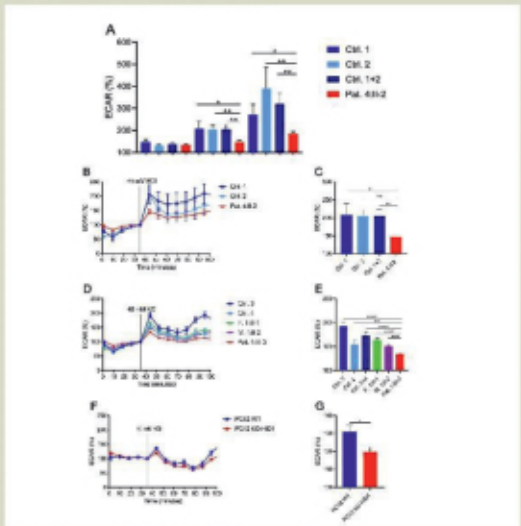

**Figure 3. Extracellular acidification rate (ECAR) dependent on HID1 function**
(A) Analysis of the mean relative ECAR change demonstrates that addition of 22.5 mM KCl was not sufficient to induce a significant increase of ECAR in any individual, while addition of 45 and 90 mM KCl induced a significantly higher increase in controls than in the affected individual 4:II-2. A parametric t-test was used to analyze the differences between the affected individuals and controls. Mean ± SEM are shown. *p<0.05, **p<0.01. (B-G) Baseline ECAR and relative change in (ECAR) in fibroblasts and PC12 cells after addition of potassium chloride (KCl). (B) Analysis of the relative change in ECAR over time shows lower values at all time points after addition of 45 mM KCl for the affected bi-allelic individual (4:II-2; n=16 wells) compared to two controls (each n=8 wells). (C) Analysis of the mean relative change of ECAR directly after 45 mM KCl addition reveals a significantly lower value in patient 4:II-2 compared to controls (time point 6 compared to time point 5). (D) Relative change in ECAR in the affected bi-allelic individual (1:III-3; n=32 wells), heterozygous parents (father 1:II-1; n=16 wells and mother 1:II-2; n= 16 wells) and two controls (each n=14 wells) over time. (E) Mean relative change directly after 45 mM KCl addition is significantly lower in 1:III-3 compared to controls and heterozygous parents (time point 6 compared to time point 5). (F) Relative change in ECAR in PC12 wild-type and HID1 knockout cells over time. (G) Mean relative change directly after 90 mM KCl addition is significantly lower in HID1-knockout compared to wild-type cells (time point 6 compared to time point 5). A parametric t-test was used to analyze the differences between the affected individuals and controls. Mean ± SEM are shown. *p<0.05, **p<0.01, ***p<0.001, ****p<0.0001.

## DISCUSSION AND CONCLUSIONS

- Confirmed cerebral atrophy with enlarged lateral ventricles
- Markedly reduced expression of pituitary hormones
- No altered co-localization of HID1 protein with the TGN
- Reduced ECAR upon stimulation with KCl in patient fibroblasts
- HID1 deficiency is a novel, recognizable syndrome

**Our findings indicate that mutations in HID1 cause an early infantile encephalopathy with hypopituitarism as the leading presentation, and expand the list of syndromic CNS diseases caused by interference of TGN function.**

contact: s.wortmann@salk.at

## Mutations in HID1 cause syndromic infantile encephalopathy and hypopituitarism

Melanie T. Achleitner[1], Anne Schänzer[2], Blake Hummer[3], René G. Feichtinger[1], Johannes A. Mayr[1], Saskia B. Wortmann[1,4,5,6], Axel Weber[7]

[1]University Children´s Hospital, Paracelsus Medical University (PMU), Salzburg, Austria; [2]Institute of Neuropathology, Justus-Liebig-University, Giessen, Germany; [3]Molecular and Cellular Biophysics Program, Dept. of Biological Sciences, University of Denver; [4]Radboud Center for Mitochondrial Medicine, Department of Pediatrics, Amalia Children's Hospital, Radboudumc, Nijmegen, The Netherlands; [5]Institute of Human Genetics, Helmholtz Center Munich, Neuherberg, Germany; [6]Institute of Human Genetics, Technical University Munich, Munich, Germany; [7]Institute of Human Genetics, Justus-Liebig-University, Giessen, Germany; Contact: me.achleitner@salk.at

### Objective

Precursors of peptide hormones undergo posttranslational modifications within the trans-Golgi network (TGN). Dysfunction of proteins involved at different steps of this process cause several complex syndromes affecting the central nervous system (CNS). We aimed to clarify the genetic cause in a group of patients characterized by hypopituitarism in combination with brain atrophy, thin corpus callosum, severe developmental delay, visual impairment, and epilepsy.

### Results

We identified bi-allelic variants in the gene HID1 domain-containing protein 1 (HID1) in seven patients [PMID: 33999436]. Post mortem examination confirmed cerebral atrophy with enlarged lateral ventricles. Markedly reduced expression of pituitary hormones was found in pituitary gland tissue. Co-localization of HID1 protein with the TGN was not altered in fibroblasts of patients compared to controls, while the extracellular acidification rate (ECAR) upon stimulation with potassium chloride was significantly reduced in patient fibroblasts compared to controls.

Our findings indicate that mutations in HID1 cause an early infantile encephalopathy with hypopituitarism as the leading presentation, and expand the list of syndromic CNS diseases caused by interference of TGN function.

### Conclusions

- Ø Confirmed cerebral atrophy with enlarged lateral ventricles
- Ø Markedly reduced expression of pituitary hormones
- Ø No altered co-localization of HID1 protein with the TGN
- Ø Reduced ECAR upon stimulation with KCl in patient fibroblasts
- Ø HID1 deficiency is a novel, recognizable syndrome

### Funding

Supported by the ERA PerMed project PerMim (Austrian Science Fund FWF, I4704-B) to S.B.W, and ERA E-RARE-3 project GENOMIT (Austrian Science Fund FWF, I2741-B26 and I4695-B) to JAM, and by the German Science Foundation Collaborative Research Centre (CRC) 870.

### References

1. Schänzer A, Achleitner M, Trümbach D, Hubert L, Munnich A, Ahlemeyer B, AlAbdulrahim MM, Greif PA, Vosberg S, Hummer B, Feichtinger RG, Mayr JA, Wortmann SB, Aichner H, Rudnik-Schöneborn S, Ruiz A, Gabau E, Sánchez JP, Ellard S, Homfray T, Stals KL, Wurst W, Neubauer BA, Acker T, Bohlander SK, Asensio C, Besmond C, Alkuraya FS, AlSayed MD, Hahn A, Weber A. Mutations in HID1 cause syndromic infantile encephalopathy and hypopituitarism. Ann Neurol. 2021 May 17. doi: 10.1002/ana.26127. Epub ahead of print. PMID: 33999436.

# "A Rodent Lumbosacral Spinal Cord Injury Model Reflecting Neurological and Urological Deficits of Humans"

**Behnaz Afrashteh[1,2,3], Karin Roider[1,2,3], Lukas Lusuardi[3], Ludwig Aigner[1,2,3], Esra Keller[1,2,3]**

[1] Institute of Molecular Regenerative Medicine, Paracelsus Medical University Salzburg
[2] Spinal Cord Injury and Tissue Regeneration Center Salzburg, Paracelsus Medical University Salzburg
[3] Department of Urology, University Clinic, Paracelsus Medical University, Salzburg, Austria

## Introduction

The lumbosacral spinal cord contains critical motor centers, including the parasympathetic preganglionic neurons (innervating bladder detrusor smooth muscle) and Onuf's nucleus (innervating external urethral sphincter (EUS)[1,2].

Damage to these centers following lumbosacral spinal cord injury (SCI) disrupts crucial bladder function, resulting in an underactive bladder pathology[3].

There is no trustworthy lumbosacral SCI rat model available to date that describes locomotor and bladder dysfunction during chronic follow up.

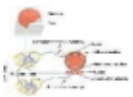

## Aims

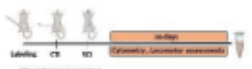


CTI: catheter implantation
SCI: spinal cord injury at Lumbosacral level

1. Retrograde labeling the Onuf's nucleus at the lumbosacral spinal cord
2. Qualification of the lesion size and degree of sparing projections from the lesions by using contrast-enhanced µCT-based 3D reconstruction
3. Characterization of bladder function (Cystometry), locomotor function (BBB locomotion score, Catwalk gait analysis) and structure of the bladder (histology) following severe contusion at the lumbosacral spinal cord, in the region of Onuf's nucleus

## Conclusion

- A severe contusion at L6-S1 level of spinal cord leads to an underactive bladder (flaccid bladder) with high compliance.
- The lumbosacral SCI rats with different severities in the lesion sites show similar deficit in the bladder function.
- Lumbosacral SCI at L6-S1 spinal cord results in a minor disruption in the locomotor function.
- Bladder tissue analysis shows a hypertrophy with fibrosis development in lumbosacral SCI bladders.
- This model closely mimics human lumbosacral injuries: allows testing of therapies.

## Results

### Neurons innervating the EUS are located in ventrolateral portion of L 6 and S 1 spinal cord

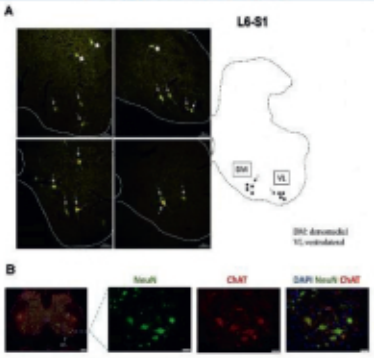


Retrograde labeling showed two distinct of motoneuron pools. The neurons located in VL are Onuf's nucleus motoneurons innervating the EUS and the neurons in dorsomedial (DM) portion are levator ani motoneurons, innervating the skeletal pelvic floor muscle. (B) Onuf's nucleus motoneurons as gamma cholinergic neurons (NeuN+, ChAT+). ON: Onuf's nucleus , scale bar 200 µm

### µCT scanning revealed 3 distinct injury groups

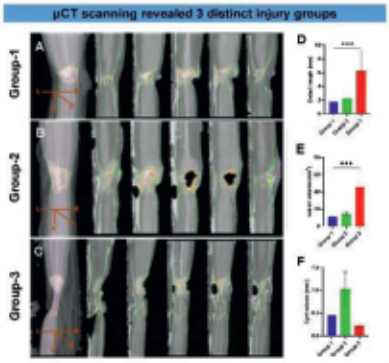


(A-C) The µCT imaging showing that the variation in the lesion level along the rostro-caudal axis. (A) Lesion area, rostral to caudal, from mid of L6 to beginning of S1. (A) Lesion area from beginning of L6 to mid of S1. (C) Lesion area from beginning to end of S1. Magnification 20x, scale bar 200 µm.

V; Ventral, D; Dorsal, L; Left, R; Right (D-F) Quantification of the defect length, lesion and cyst volumes. Data points present the mean ± standard deviation of the mean. Statistics: (two-way ANOVA, *ns, P< 0.5, *** P< 0.0005).

### Lumbosacral SCI caused detrusor underactivity with high compliance

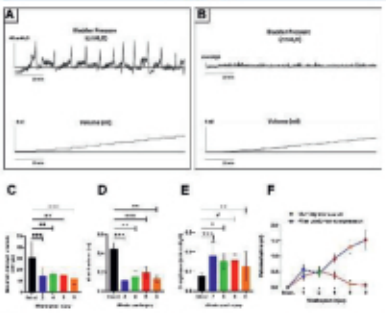


(A) Urodynamic data from an intact rat showing a regular voiding patterns, stable basal pressure and voiding volumes (B) Urodynamic data from a SCI rat showing underactive bladder with bladder leak-point pressure and leak volumes. C) Quantification of the maximum bladder pressure showing a significant decrease in the bladder pressure and (D) voiding volume, with (E) higher compliance. (F) Quantification of the bladder expression in morning showing a decrease of the retained urine that indicates no obstruction in the bladder and expressing bladder after each urodynamic study also showing the higher bladder capacity in the injured rats.

("Compliance"= (Δ *Volume*) / (Δ *Pressure*)).

Data points present the mean + standard deviation of the mean. Statistics: (two-way ANOVA, * P< 0.05, ** P< 0,005, *** P< 0,0005). PRI, Pre SCI; WPI, weeks post SCI.

### SCI rats showed minor disruption in locomotor function and high recovery

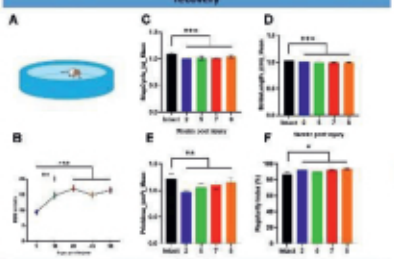


(A) schematic diagram of the open-field locomotor scores (BBB score). (B) Post-SCI, BBB score showing plateaued at 14 score until the end 56 days follow up period. (C-F) Gait analyses at different time points pre and post-SCI including (C) print area, (D) stride length, (E) step cycle and (F) regularity index showing no disruption in limb function in SCI rats. Data points present the mean ± standard deviation of the mean. Statistics: (one-way ANOVA, * P< 0.05, ** P< 0.005, *** P< 0.0005).

### Underactive bladder showed severe atrophy after lumbosacral SCI

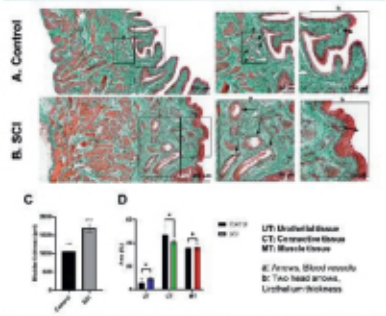


(A, B) Masson-Goldner staining of the bladder section showing bladder wall in the SCI group was significantly ticker compared to the control group. (a) Higher magnification of the connective tissue showing changes in the blood vessels with thickened endothelia in SCI bladders. (b) Higher magnification of the urothelial tissue showing a hypertrophy with urothelial cell proliferation in SCI bladders. (C) Quantification of the bladder thickness showing a 1.5-fold increase in the thickness of SCI bladders vs. Control bladders.

(D) Quantification of the bladder layers showing a significant increase in the urothelial layer and a slight thickening of the detrusor smooth muscle tissue and a decreased intramuscular connective tissue were observed in the SCI bladders..(two-way ANOVA, * P< 0.05, ** P< 0.005, *** P< 0.0005).

### Bladder underwent development of fibrosis after lumbosacral SCI

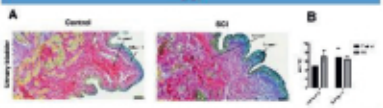


(A) Herovici staining of the bladder section showing the collagen Type-II as a major collagen type in the control bladders.
In SCI bladders, the percentage of collagen Type-III increases in the connective tissue beneath the urothelial layer.
(B) Quantification of the percentage of the collagen Type-III and Type-I showing the 40% increase in the ratio of collagen Type III to Type I in the SCI bladders (as a fibrosis indicator).
(two-way ANOVA, ns, P< 0,5), scale bar 200 µm

## References

1. Beckel JM, de Groat WC, Beckel JM, de Groat WC. Neural Control of Lower Urinary Tract Function. Oxford Research Encyclopedia of Neuroscience. 2019; 1–36 p.
2. Fowler CJ, Griffiths D, Groat WC De. Neural control of micturition (review). 2010;9(6):453–66.
3. Aizawa N, Igawa Y. Pathophysiology of the underactive bladder. Investig Clin Urol. 2017;58:883–8.

## Acknowledgements

This study is conducted with Prof. Ludwig Aigner's Lab and supported by the Paracelsus Medical University Forschungsförderungsfond (FFF) (R-19 / 03 / 119-AFR)

## A Rodent Lumbosacral Spinal Cord Injury Model Reflecting Neurological and Urological Deficits of Humans

Behnaz Afrashteh[1,2,3], Karin Roider[1,2,3], Lukas Lusuardi[3], Ludwig Aigner[1, 2, 3], Esra Keller[1,2,3]

[1]Institute of Molecular Regenerative Medicine, Paracelsus Medical University Salzburg; [2]Spinal Cord Injury and Tissue Regeneration Center Salzburg, Paracelsus Medical University Salzburg; [3]Department of Urology, University Clinic, Paracelsus Medical University, Salzburg, Austria; Contact: behnaz.afrashteh@pmu.ac.at

### Objective

The lumbosacral spinal cord injury (SCI) contains critical motor centers, including the parasympathetic neurons innervating the bladder detrusor smooth muscle and Onuf's nucleus innervating the external urethral sphincter (EUS) (1). In SCI patients with a lesion at the lumbosacral level, damage to these centers disrupts crucial bladder function, resulting in an underactive or flaccid bladder(2).Most animal SCI models have focused on the cervical or thoracic spinal cord(3) but no standardized lumbosacral model is available to test therapeutic strategies for restoring bladder function after lumbosacral SCI. Accordingly, we described a rat lumbosacral spinal cord contusion model with reproducible anatomical, histological, and functional outcomes similar to human lumbosacral injuries.

### Methods

Motoneurons innervating EUS was detected by using Fluorgold retrograde labelling. A severe incomplete severe contusion SCI was conducted at the level of detected labelled neurons. Two months after SCI, the lesion size and volume and also the sparing of white and gray matters were quantified by using an advanced $\mu$CT imaging. The urodynamic study was done to evaluate the bladder function and BBB score and catwalk analysis were also done to identify the locomotor function. The structure of bladder in control and SCI group was also evaluated by histology studies.

### Results

Neurons innervating the EUS are specially located in L 6-S 1 spinal cord. The urodynamic study showed that severe contusion injuries at lumbosacral level results in an underactive bladder and provide relevant clinical content. The $\mu$CT analysis also showed that the disruption of bladder function is not due to differences in lesion size or to differential sparing of the white and gray matters. After SCI, a significant increase in urothelial tissue was seen. Elastic fibers were reduced in numbers and diameter length. The results of locomotor function showed a high recovery in SCI rats.

### Conclusions

In this study, we developed a consistent, reproducible contusion lumbosacral SCI model that mimics human urinary tract complications following lumbosacral SCI. Our experiments show that severe contusion at the L6-S1 spinal cord produces an underactive bladder with development of fibrosis. The animal model in this study can be used in subsequent translationally oriented studies aimed at preventing and restoring bladder function in lumbosacral spinal cord contusions.

### References

1. Beckel JM, de Groat WC, Beckel JM, de Groat WC. Neural Control of Lower Urinary Tract Function. Oxford Research Encyclopedia of Neuroscience. 2019. 1–38 p.
2. Blok BFM, De Weerd H, Holstege G. The pontine micturition center projects to sacral cord GABA immunoreactive neurons in the cat. Neurosci Lett. 1997;233(2–3).
3. Noto H, Roppolo JR, Steers WD, de Groat WC. Electrophysiological analysis of the ascending and descending components of the micturition reflex pathway in the rat. Brain Res. 1991

# Development of a physiologically relevant, biomechanical test setup considering internal muscle forces for the investigation of complex pelvic ring fractures

Dirk Baumeister[1], Martin Winkler[2], Peter Augat[1, 2]
[1] Institute for Biomechanics, BG Unfallklinik Murnau, Germany
[2] Institute for Biomechanics, Paracelsus Medical University Salzburg, Austria

BGU Murnau
Berufsgenossenschaftliche Unfallklinik Murnau

## Introduction

The human pelvis is a ring-shaped bone structure, designed to transfer the load of the upper body to the lower extremities. Fractures of the pelvis can lead to disruptions of the ring-shaped structure which results in mechanical destabilization. Forces and moments can then no longer be transmitted by the pelvis. In order to address the existing instability, fractures of the pelvic ring require a mechanically stable osteosynthetic treatment, for which a variety of different methods are available. Previous biomechanical studies do not fully consider the complex loading situation at the pelvis, so that there is still a lack of knowledge about the mechanical stability of the different osteosynthetic treatments.

**The aim of this project is to build a test setup able to determine the stability of different fixation methods for complex pelvic ring fractures under a loading situation simulating human gait: The weight of the upper body is alternately transferred to the legs via both hip joints. In addition, muscles at the pelvis counteract a tilting of the pelvis.**

## Material and Methods

Three different types of forces are considered that act on the pelvis during human gait:

- **Force of the trunk:** Khoo et al. [1] developed a dynamic biomechanical model to determine loads at the lumbosacral joint-center during the stance phase of normal level walking. Their findings showed that the resultant loads at the lumbosacral joint-center were between 1.5 and 2 times body-weight. A force of this magnitude will be applied to the sacrum in vertical direction in the test setup.
- **Muscle forces:** Rajagopal et al. [2] built up a musculoskeletal model including bony geometry for the full body with 37 degrees of freedom to define joint kinematics, Hill-type muscle models of 80 muscle-tendon units and 17 ideal torque actuators driving the upper body. They also provide the simulation data of a 31 year old individual walking with a speed of 1.5 m/s. These data were used to determine the muscle forces that act on the pelvis during walking. For the purpose of experimentally realizing the muscle actions the individual muscles were combined into two muscle groups (anterior and posterior muscle group, **Table 1**).

  The sum of the considered muscle forces acting on the pelvis reach two maxima during gait, similar to the pattern in the ground reaction force. The second, higher maximum is reached at approximately 48 % of the gait cycle. The resulting muscle forces (magnitude and direction) for the two muscle groups were calculated at this time point. These data are used (adapted to the simulated body weight) for the muscle simulation in the test setup.

| Combined muscle group | Muscle (part) | Resulting force | Representation of muscles in OpenSim Model [4] |
|---|---|---|---|
| Posterior muscle group | Gluteus maximus (superior, middle) | 1290 N |  |
| | Gluteus medius (anterior, middle, posterior) | | |
| | Gluteus minimus (anterior, middle, posterior) | | |
| | Tensor fascia latae | | |
| Anterior muscle group | Iliacus | 1216 N |  |
| | Sartorius | | |
| | Rectus femoris | | |

Table 1: Muscles and muscle parts from the simulation of Rajagopal et al. [2] were combined to muscle groups. The resulting forces for these muscle groups were calculated (48 % gait cycle for the simulation data of the single subject). Some muscles from the simulation (not shown) were neglected because of too low values.

- **Force of the free-hanging contralateral leg:** During gait the weight of the free-hanging leg pulls at the corresponding side at the pelvis. This force can be considered by a constant weight of 16 % of the simulated body weight. [3]

## Test Setup

The mechanical test setup was constructed in a CAD-model (Figure 1). The vertical force of the trunk is applied on the sacrum via a hydraulic testing machine. In order to avoid uncontrollable shear forces between sacrum and testing machine, a linear bearing allows translational movement in the horizontal plane and a ball bearing mounted directly to the sacrum allows rotational movement around all three spatial axes.

A hip joint endoprosthesis with three rotational degrees of freedom is mounted to each acetabulum. The shafts of the endoprostheses are embedded to vertically moveable embedding pots. During the simulated stance phase of the corresponding leg, the (green) aluminum rod is fixated to the upper position to lock the vertical movement of the acetabulum (anatomical left side in figure 1). At the same time, the other acetabulum is free to move vertically, corresponding to the swing leg phase.

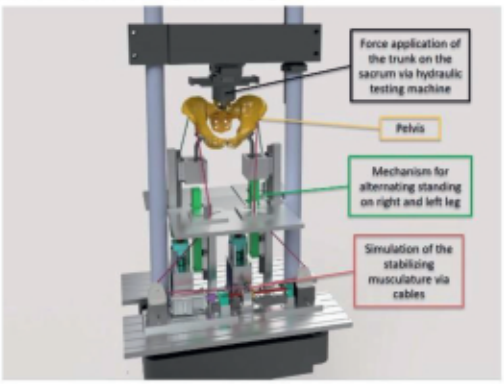


Figure 1: Rendering of the CAD-model of the test setup from the frontal perspective. The red cables represent the anterior muscle group, the green cables the posterior muscle groups. Not shown is the drive unit for the posterior muscle mechanism and the force application of the free-hanging contralateral leg.

Muscle forces are applied to the standing leg side by attaching ropes to the pelvis, which are tensioned by means of electric motors. Force sensors measure the current muscle force.

By alternately loading the right and left acetabulum, several thousand gait cycles can be simulated.

The stability of the pelvis after fracture fixation will be assessed by measuring the fracture gap movements during testing by an optical measurement system.

## Discussion

To date, biomechanical experiments on pelvises have been performed primarily on single-leg stance or double-leg stance models. In single-leg stand models, only one half of the pelvis (fracture side) is loaded. Thus, loads arising on the other "healthy" side are neglected, although these loads can also have an influence on the stability on the fracture side. In double-leg stand models, only bipodal standing is simulated by simultaneously loading on both sides. With the newly constructed test setup, the aforementioned limitations can be overcome: By alternately loading the hip joints of a pelvis, a kind of walking can be simulated.

However, some simplifications are made for the test setup: The determination and application of the muscle forces and forces acting between femoral head and acetabulum occurs only at a single time point of the gait cycle. Thus, the test scenario corresponds primarily to a cyclic change in the maximum loads on the right and left pelvic side. Furthermore, different muscles have been combined into muscle groups and other muscles and soft tissue contacts are neglected.

**In summary, the newly designed test setup can be used to evaluate the fatigue strength of osteosynthetic constructs used for complex pelvic ring fractures under loads that are similar to the loads that occur thousands of times between surgery and healing of the bone.**

Literature:
[1] Khoo, K., et al. (1994). Medical Engineering & Physics, 17(1), 27-35.
[2] Rajagopal, A., et al. (2016). IEEE Transactions on Biomedical Engineering, 63(10), 2068-2079.
[3] Schildhauer, T. A., et al. (2006). Journal of Orthopaedic Trauma, 20(1), 22-30.
[4] Delp, S. L., et al. (2007). IEEE Transactions on Biomedical Engineering, vol. 54, pp. 1940-1950.

Kontakt:
Dirk Baumeister, M.Sc.
E-Mail: dirk.baumeister@bgu-murnau.de
Telefon: +49 8841 48-2508
Fax: +49 8841 48-4373

BG Kliniken Murnau,
Institut für Medizinische Forschung und Biomechanik
Prof.-Küntscher-Str. 8
82418 Murnau am Staffelsee
www.bgu-murnau.de

Paracelsus Science Day Salzburg 2021 - Virtual Conference

## Development of a physiologically relevant, biomechanical test setup considering internal muscle forces for the investigation of complex pelvic ring fractures

Dirk Baumeister[1], Martin Winkler[1], Peter Augat[1,2]

[1]Institute for Biomechanics, BG Unfallklinik Murnau, Germany; [2]Institute for Biomechanics, Paracelsus Medical University Salzburg, Austria; Contact: dirk.baumeister@bgu-murnau.de

### Objective

Fractures of the human pelvis can lead to disruptions of the ring-shaped structure which results in mechanical destabilization of the pelvic ring. A variety of different methods for an osteosynthetic treatment are available, but there is still a lack of knowledge about the mechanical stability of these methods. The aim of this project is to build a test setup able to determine the stability of different fixation methods for complex pelvic ring fractures under a loading situation simulating human gait.

### Methods

During gait, the human pelvis is loaded mainly by the weight of the trunk, muscle forces and the weight of the free-hanging leg in swing leg phase. Rajagopal et al. (1) built up a musculoskeletal model and provide simulation data of a 31-year old individual walking with a speed of 1.5 m/s. The muscle forces from this simulation were summarized into an anterior and a posterior muscle group.

### Results

The vertical force of the trunk is applied on the sacrum via a hydraulic testing machine. Hip joint endoprostheses are mounted to the acetabuli of the specimen. The vertical movement of the hip joint endoprostheses can either be released (swing leg phase) or locked (stance leg phase). Muscle forces are applied with the help of ropes and their magnitude is determined with force sensors. By alternately loading the right and left acetabulum, several thousand gait cycles can be simulated.

### Conclusions

To date, biomechanical experiments on pelvises have been performed primarily on single-leg stance or double-leg stance models. Because these do not fully take into account the complex loading situation during gait, the new test setup was developed. Simplifications were made to account for the applied loads, especially the muscle forces. The new test setup can be used to evaluate the fatigue strength of osteosynthetic constructs used for complex pelvic ring fractures.

### References

1. A. Rajagopal, C. L. Dembia, M. S. DeMers, D. D. Delp, J. L. Hicks and S. L. Delp, "Full-Body Musculoskeletal Model for Muscle-Driven Simulation of Human Gait," in IEEE Transactions on Biomedical Engineering, vol. 63, no. 10, pp. 2068-2079, Oct. 2016, doi: 10.1109/TBME.2016.2586891.

PARACELSUS MEDIZINISCHE PRIVATUNIVERSITÄT

Klinikum Nürnberg
Wir sind für Sie da!

# Protein Metabolism in Preterm and Term Infants using a $^{15}$N-Tracer and the Nitrogen Balance Method: A Pilot-Study

Sabrina Beck[1], Christoph Fusch[1,2], Jan Däbritz[3], Gerhard Fusch[2], Birgit Salewski[3], Klaus Wutzke[3], Niels Rochow[1,2,3]

[1]Pediatrics, Paracelsus Medical University, Nuremberg; [2]Pediatrics, McMaster University, Hamilton, Canada; [3]Pediatrics, University Medicine Rostock, Rostock

## INTRODUCTION

- It is desired to provide preterm infants with nutrition that supports accrual of protein and fat-free mass.
- To maximize the utilization of protein building blocks, to optimize growth, excess protein oxidation and related urea production should be avoided.
- The composition of feedings determined by
  1) availability of macronutrients
  2) protein (gram) to energy ratio and
  3) carbs to fat ratio affects protein oxidation.

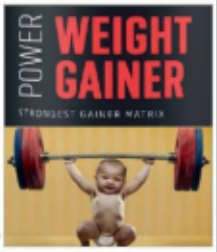


- Kinetic of urinary N excretion using $^{15}$N-labeled amino acids (Tracer) can measure protein turnover, protein gain and urea production.
- This pilot study aims to establish a tracer method in preparation for a double-blind, randomized clinical trial (RCT) to identify a composition of fortified breast milk which maximizes protein accretion.

## OBJECTIVES

- To analyze nitrogen balance, protein turnover and net protein gain using $^{15}$N-labeled amino acid tracer in preterm infants.

## METHODS

- Stable growing newborns with no gastrointestinal diseases which affect nutritional absorption were enrolled at McMaster Children's Hospital.
- Nitrogen kinetic was measured using a single shot (1mL/kg) $^{15}$N-labeled amino acid mixture (ALGAL Amino Acid Mixture; 3.3 mg AA/mL).
- Urine was collected over a 36 hours period in 3 hours intervals.
- Urinary $^{15}$N was measured using an elemental analyzer Solid Liquid (SL™, SerCon, CREWE, U.K.) and urea and creatinine were measured using standard clinical chemistry.
- Based on the three-compartment model (TCM), nitrogen balance, protein turnover and net protein gain were calculated (g/kg/d).

**Three-Compartment Model (TCM)**

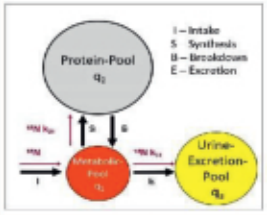


**Nitrogen flux**

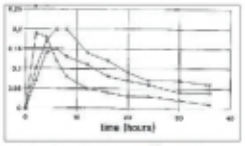


Example of urinary $^{15}$N amino acid kinetic (Wutzke et al. 1992)

## RESULTS

- 18 preterm male infants were enrolled (gestational age: 25 to 39 weeks, birth weight: 720 to 2770 g) and tracer were given between day of life 3 to 97.
- No adverse events were reported during the study.

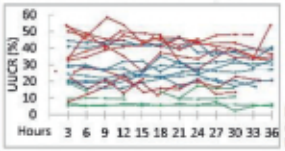


- Participants demonstrate individual starting levels of UUCR.
- Time course per participant seems to be stable with a constant intake.

**Fig. 1: Urinary urea creatinine ratio (UUCR)**
Colors represent the standard deviation (red: SD > 3.5%; blue: SD ≥ 1.6% to ≤ 3.5%; green: SD ≤ 1.5%).

## RESULTS

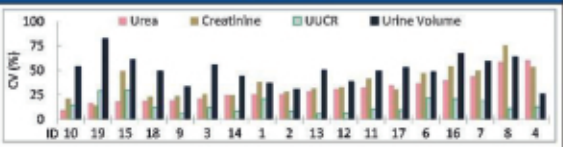


**Fig. 2: Individual coefficient of variation (CV), 3 hours intervals**

- The individual CV for urea ranges from 9.9 % to 60.3 %, for creatinine from 14.5 % to 75.6 %, for UUCR from 5.6 % to 29.6 % and for urine volume from 25.9 % to 82.3 %.
- Based on the CV of urea up to 60.3 %, spot urine does not seem sufficient in determining protein accretion.

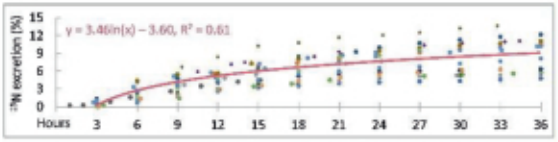


**Fig. 3: Cumulative urinary $^{15}$N-Tracer excretion (36 hour period)**

- The cumulative urinary excretion dose from tracer varies between 4 % and 14 %.
- 86 % to 96 % of the tracer dose were stored in the body.
- Urinary $^{15}$N kinetic curves plateaued at 36 hours.

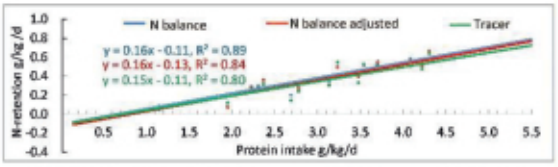


**Fig. 4: Method comparison - Nitrogen retention per protein intake.**
(N balance adjusted: N multiplied by factor 1.25 for other N containing components in urine)

- N balance, N balance adjusted and the tracer method yield similar slopes of regression lines.
- A linear relation is observed between nitrogen retention and protein intake from 1.25 to 5.5 g/kg/d.
- X-axis intercept at ~1.0 g protein /kg/d compares favorably with results of previous studies (Koletzko et al., 2014).

## CONCLUSION

- A $^{15}$N-Tracer has been established which is an useful and safe tool to analyze the protein metabolism. Additionally to common nitrogen balance studies, protein synthesis, protein breakdown, protein turnover and net protein gain can be calculated from urinary $^{15}$N kinetics.
- The $^{15}$N urinary measurements demonstrate a similar kinetic with a plateau at 36 hours which is comparable to data from the literature.
- The similarity of the results between tracer kinetic and balance method indicates the reliability of the $^{15}$N-Tracer method.
- To optimize non-protein composition of fortified breast milk, protein synthesis will be studied in a double-blind RCT using $^{15}$N-Tracer comparing low and high carbs nutrition with similar protein intake (table).

| Group 1* Low Carbs/High Fat | | Group 2* High Carbs/Low Fat | |
|---|---|---|---|
| Carbs | 5.5 | Carbs | 11 |
| Protein | 3 | Protein | 3 |
| Fat | 5.5 | Fat | 3 |
| Sum kcal | 86 | Sum kcal | 85.3 |

*Values for 100 mL breast milk

Niels Rochow, MD, PhD, Pediatrics, Paracelsus Medical University, niels.rochow@klinikum-nuernberg.de

## Protein Metabolism in Preterm and Term Infants using a 15N-Tracer and the Nitrogen Balance Method: A Pilot-Study

Sabrina Beck[1], Christoph Fusch[1,2], Jan Däbritz[3], Gerhard Fusch[2], Birgit Salewski[3], Klaus Wutzke[3], Niels Rochow[1,2,3]

[1]Pediatrics, Paracelsus Medical University, Nuremberg; [2]Pediatrics, McMaster University, Hamilton, Canada; [3]Pediatrics, University Medicine Rostock, Rostock; Contact: sabrina.beck@stud.pmu.ac.at

### Objective
It is desired to provide preterm infants with nutrition that supports accrual of protein and fat-free mass. To maximize the utilization of protein building blocks, to optimize growth, excess protein oxidation and related urea production should be avoided. This pilot study analyzes nitrogen balance, protein turnover and net protein gain using a $^{15}N$-labeled amino acid tracer in preterm infants. It aims to establish a tracer method in preparation for a double-blind, randomized clinical trial (RCT) to identify a composition of fortified breast milk which maximizes protein accretion.

### Methods
Stable growing newborns with no gastrointestinal diseases which affect nutritional absorption were enrolled at McMaster Children's Hospital. Nitrogen kinetic was measured using a single shot (1mL/kg) $^{15}N$-labeled amino acid mixture (ALGAL Amino Acid Mixture; 3.3 mg AA/mL). Urine was collected over a 36 hours period in 3 hours intervals. Urinary $^{15}N$ was measured using an elemental analyzer Solid Liquid (SLTM, SerCon, CREWE, U.K.) and urea and creatinine were measured using standard clinical chemistry. Based on the three-compartment model (TCM), nitrogen balance, protein turnover and net protein gain were calculated (g/kg/d).

### Results
Eighteen infants with birth weight 1215 ± 592 g and gestational age 29 ± 4 weeks were recruited. Based on the CV of urea up to 60.3 %, spot urine does not seem sufficient in determining protein accretion. 86 % to 96 % of the tracer dose were stored in the body. Urinary $^{15}N$ kinetic curves plateaued at 36 hours. A linear relation is observed between nitrogen retention and protein intake from 1.25 to 5.5 g/kg/d. X-axis intercept at −1.0 g protein/kg/d compares favorably with results of previous studies (Koletzko et al., 2014).

### Conclusions
A $^{15}N$-Tracer has been established as a tool to analyze the protein metabolism. Additionally to common nitrogen balance studies, protein synthesis, protein breakdown, protein turnover and net protein gain can be calculated from urinary $^{15}N$ kinetics. The $^{15}N$ urinary measurements demonstrate a similar kinetic with a plateau at 36 hours which is comparable to data from the literature. The similarity of the results between tracer kinetic and balance method indicates the reliability of the $^{15}N$-Tracer method.

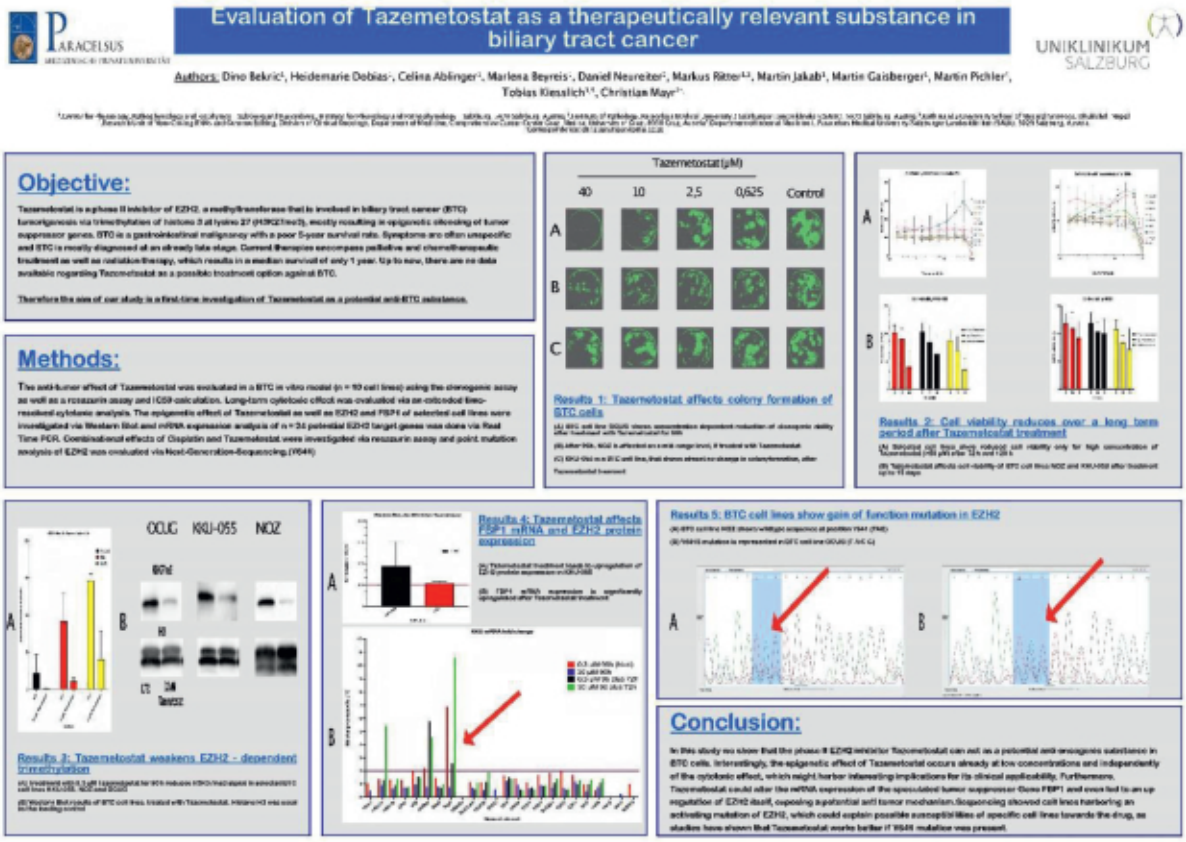
Evaluation of Tazemetostat as a therapeutically relevant substance in biliary tract cancer
PARACELSUS
UNIKLINIKUM SALZBURG
Authors: Dino Bekric[1], Heidemarie Dobias[1], Celina Ablinger[1], Marlena Beyreis[1], Daniel Neureiter[2], Markus Ritter[1,3], Martin Jakab[1], Martin Gaisberger[1], Martin Pichler[1], Tobias Klesslich[1,3], Christian Mayr[2]
Objective:
Methods:
Tazemetostat (µM)
40
10
2,5
0,625
Control
A
B
C
Results 1: Tazemetostat affects colony formation of BTC cells
Results 2: Cell viability reduces over a long term period after Tazemetostat treatment
OCUG
KKU-055
NOZ
Results 3: Tazemetostat weakens EZH2 - dependent trimethylation
Results 4: Tazemetostat affects FBP1 mRNA and EZH2 protein expression
Results 5: BTC cell lines show gain of function mutation in EZH2
Conclusion:

## Evaluation of Tazemetostat as a therapeutically relevant substance in biliary tract cancer

Dino Bekric[1], Heidemarie Dobias[1], Celina Ablinger[1], Marlena Beyreis[1], Daniel Neureiter[2], Markus Ritter[1,3], Martin Jakab[1], Martin Gaisberger[1], Martin Pichler[4], Tobias Kiesslich[1,5], Christian Mayr[1,5]

[1]Center for Physiology, Pathophysiology and Biophysics - Salzburg and Nuremberg, Institute for Physiology and Pathophysiology - Salzburg, 5020 Salzburg, Austria; [2]Institute of Pathology, Paracelsus Medical University / Salzburger Landeskliniken (SALK), 5020 Salzburg, Austria; [3]Kathmandu University School of Medical Sciences, Dhulikhel, Nepal; [4]Research Unit of Non-Coding RNAs and Genome Editing, Division of Clinical Oncology, Department of Medicine, Comprehensive Cancer Center Graz, Medical University of Graz, 8036 Graz, Austria; [5]Department of Internal Medicine I, Paracelsus Medical University/Salzburger Landeskliniken (SALK), 5020 Salzburg, Austria; Contact: dino.bekric@pmu.ac.at

### Objective
Tazemetostat is an FDA approved inhibitor of EZH2, a methyltransferase that is involved in cancer progression. Biliary tract cancer (BTC) is a malignancy with a poor overall survival and limited treatment option. Currently, there is no data displaying a potential use of Tazemetostat as an anti-BTC agent.

### Methods
The clonogenic assay as well as a resazurin assay and IC50 calculation were used to evaluate the anti-tumor effect of Tazemetostat in a BTC in vitro model. To investigate long term cytotoxic effects, an extended time-resolved cytotoxic analysis was used. The epigenetic effect of Tazemetostat was evaluated using Western Blot (H3K27me3 levels) and mRNA expression analysis of potential EZH2 target genes. Point-mutation analysis of EZH2 (Y641) in BTC cells will be investigated via sequencing.

### Results
Tazemetostat reduced clonogenic growth of BTC cells in a cell line-dependent manner. We observed a latency of the cytotoxic effect of Tazemetostat, as treatment of BTC cells with Tazemetostat for 72h did not result in a decline of cell viability, whereas treatment for up to 15 days did - a phenomenon that was already described in other tumor entities. Interestingly, the epigenetic effect following Tazemetostat treatment (= lower H3K27me3 levels) was already observed 72h after treatment with low concentrations. Real time-PCR unveiled a significant upregulation of the potential tumor suppressor gene, Fructose 1,6 bisphosphatase 1 (FBP1), whereas its protein levels did not change, after drug treatment.

### Conclusions
In this study, we can show that the FDA approved EZH2 inhibitor Tazemetostat has potential anti-tumor effects in BTC cells. Notably, despite the late cytotoxic effect of Tazemetostat, its epigenetic effects occur at low concentrations and independent of the cytotoxic effects. Currently, we are analyzing the mutation status of EZH2 in our BTC cell line model as Tazemetostat was shown to effectively target tumor cells harboring a EZH2 mutation.

# Inducing ferroptosis, a new approach to target biliary tract cancer?

Authors: Dino Bekric[1,2], Heidemarie Dobias[1-4], Marlena Beyreis[1], Martina Winklmayr[4], Daniel Neureiter[2], Markus Ritter[1,3],Tobias Kiesslich[1,3], Christian Mayr[1,3]

## Objective:

In 2012, Dixon et al. described a new form of regulated cell death, called ferroptosis. Ferroptosis is defined as an iron- and ROS-dependent non-apoptotic form of regulated cell death that leads to excessive peroxidation of polyunsaturated fatty acids (PUFAs), which ultimately results in cell death.
Biliary tract cancer (BTC) is a deadly malignancy, with a poor overall survival rate, which lacks efficient therapeutic options.
Therefore, the aim of this study is a first-time investigation of ferroptosis as an anti-BTC strategy.

## Methods:

Resazurin assay and $IC_{50}$ calculation were used to evaluate the anti-tumor effect of ferroptosis in a BTC in vitro model, using six different potential ferroptosis inducing substances. Mitochondrial changes will be imaged via transmission electron microscopy and cell morphology will be photo-led via microscopy.
Iron assay kit and Glutathione assay kit will be used to investigate cellular ferrous iron levels and GPX4 protein activity as well as GSH/GSSG levels. To determine lipid ROS and levels of NADP(H) in cells, BODIPY 581/591 and Colorimetric NADP/NADPH Ratio Assay Kit will be used.
Biomarkers of ferroptosis will be evaluated via real time PCR and Western Blot. Combinational effects of ferroptosis with a cisplatin are going to be investigated via resazurin assay.

## Conclusion & Outlook:

In this study, we can show in a first step, that cell lines react differently on cell viability and morphological levels, after treatment with ferroptosis-inducing substances.
To evaluate, if the observed reduction of cell viability is due to ferroptosis, different ferroptosis and apoptosis as well as necrosis inhibitors will be applied simultaneously, and levels of lipid ROS will be measured.
In a next step, we will evaluate several potential biomarkers, with the aim to connect the heterogenic cytotoxicity profile of the different BTC cell lines with these factors. Therefore, we will measure cellular iron levels, GPX4 protein levels and activity, NADP(H) levels/ratio, GSH/GSSG levels/ratio as well as the expression of genes and proteins that are connected with ferroptosis.
Lastly, cisplatin will be combined with ferroptosis inducers for evaluation of possible combinatory effects.

## Mechanism of ferroptosis

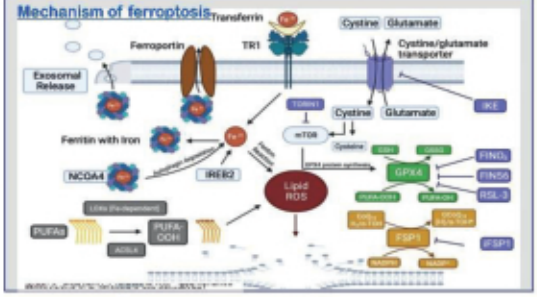


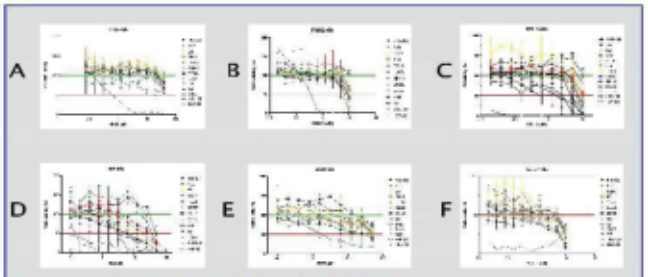


Results 1: BTC cell lines show heterogeneity towards different ferroptosis inducer

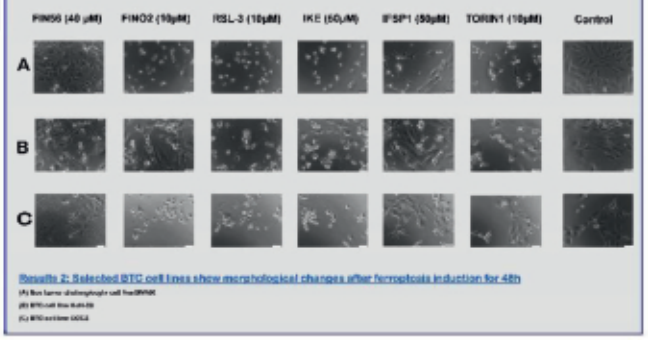


Results 2: Selected BTC cell lines show morphological changes after ferroptosis induction for 48h

## Inducing ferroptosis, a new approach to target biliary tract cancer?

Dino Bekric[1,4], Heidemarie Dobias[1,4], Daniel Neureiter[2], Markus Ritter[1,3], Marlena Beyreis[1], Martina Winklmayr[6], Tobias Kiesslich[1,5], Christian Mayr[1,5]

[1]Center for Physiology, Pathophysiology and Biophysics - Salzburg and Nuremberg, Institute for Physiology and Pathophysiology - Salzburg, 5020 Salzburg, Austria; [2]Institute of Pathology, Paracelsus Medical University / Salzburger Landeskliniken (SALK), 5020 Salzburg, Austria 3. Kathmandu University School of Medical Sciences, Dhulikhel, Nepal; [3]Kathmandu University School of Medical Sciences, Dhulikhel, Nepal; [4]Gastein Research Institute, Paracelsus Medical University, 5020 Salzburg, Austria; [5]Department of Internal Medicine I, Paracelsus Medical University/Salzburger Landeskliniken (SALK), 5020 Salzburg, Austria; [6]Ludwig Boltzmann Institute for Arthritis and Rehabilitation, Paracelsus Medical University, 50202 Salzburg, Austria; Contact: dino.bekric@pmu.ac.at

### Objective

In 2012, Dixon et al. described a new form of regulated cell death, called ferroptosis. Ferroptosis is defined as an iron- and ROS-dependent non-apoptotic form of regulated cell death that leads to excessive peroxidation of polyunsaturated fatty acids (PUFAs), which ultimately results in cell death. Biliary tract cancer (BTC) is a deadly malignancy, with a poor overall survival rate, which lacks efficient therapeutic options. Therefore, the aim of this study is a first-time investigation of ferroptosis as an anti-BTC strategy.

### Methods

Resazurin assay and IC50 calculation were used to evaluate the anti-tumor effect of ferroptosis in a BTC in vitro model, using six different potential ferroptosis inducing substances. Mitochondrial changes will be imaged via transmission electron microscopy and cell morphology will be pictured via microscopy. Iron assay kit and Glutathione assay kit will be used to investigate cellular ferrous iron levels and GPX4 protein activity as well as GSH/GSSG levels. To determine lipid ROS and levels of NADP(H) in cells, BODIPY
581/591
and Colorimetric NADP/NADPH Ratio Assay Kit will be used. Biomarkers of ferroptosis will be evaluated via real time PCR and Western Blot. Combinational effects of ferroptosis with a cisplatin are going to be investigated via resazurin assay.

### Results

The first results indicate a relatively heterogenous susceptibility of BTC cells towards ferroptosis inducing substances and morphological changes can be seen after a short period of time for selected cell lines. Cell death can be induced relatively early and with a low concentration in HEP-G2 and HuH-28 cells, whereas signs of resistance towards ferroptosis induced cell death can be seen in OCUG and OZ.

### Conclusions

In this study, we can show in a first step, that cell lines react differently on cell viability and morphological levels, after treatment with ferroptosis-inducing substances. To evaluate, if the observed reduction of cell viability is due to ferroptosis, different ferroptosis and apoptosis as well as necrosis inhibitors will be applied simultaneously, and levels of lipid ROS will be measured. In a next step, we will evaluate several potential biomarkers, with the aim to connect the heterogenic cytotoxicity profile of the different BTC cell lines with these factors. Therefore, we will measure cellular iron levels, GPX4 protein levels and activity, NADP(H) levels/ratio, GSH/GSGG levels/ratio as well as the expression of genes and proteins that are connected with ferroptosis. Lastly, cisplatin will be combined with ferroptosis inducers for evaluation of possible combinatory effects.

### Acknowledgements

This Project is part of the PhD Programm Medical Sciences (Doctoral Student: Dino Bekric) and is funded by the PMU-FFF research fund.

# Mechanisms of neuronal maturation in the adult and aging brain

Bruno Benedetti[1,2,3], Gabriele Gabriele[1,2,3], Maximilian Reisinger[1,2,3], Christina Kreutzer[1,2,3], Rodolphe Poupardin[2,4], Sébastien Couillard-Després[1,2,3]

[1]Institute of Experimental Neuroregeneration, Paracelsus Medical University; [2]Salzburg, Austria; Spinal Cord Injury and Tissue Regeneration Center Salzburg (SCI-TReCS), [3]Austrian Cluster for Tissue Regeneration, 1200 Vienna, Austria; [4] Institute of Experimental and Clinical Cell Therapy, Paracelsus Medical University, Salzburg, Austria

BEST POSTER (male)

**Objective**
Maturation of neuronal precursors in the adult brain occurs spontaneously in the neurogenic niches and, as we recently documented, in some cortical areas. Such maturation requires necessarily mechanisms that are different from those regulating the embryonic and neonatal development, as precursors must interface with and wire into fully developed brain networks. In this project, we questioned whether brain aging affects neuronal precursor maturation. Furthermore, we searched for molecular mechanisms that may trigger the maturation of latent precursors in the adult brain.

**Methods**
A transgenic mouse model (DCX-CreRT2::fl-eGFP) allowed tracing the maturation of precursors in the adult (9 months) or aged (15 months) murine brain. In these genetically engineered animals, tamoxifen administration induces permanent green labelling of precursors, which were thereafter analysed six months after induction. Morphological and immunohistochemical traits of aged precursors were analysed ex vivo. Additionally, transcriptome analysis allowed to identify candidate proteins selectively enriched in the neuronal precursors that may control their maturation in the adult brain. Finally, functional correlates of putative triggers of maturation were analysed with single-cell patch clamp experiments.

**Results**
We found that aging affects precursor maturation; i.e. neurons derived from latent immature precursors in the aged brain are morphologically different from neurons derived from precursors which maturation occurs during early-adulthood. Precursors that matured in the aged brain had a bigger soma, more dendrites and shorter axon initial segment, implying different functional properties in comparison to early-matured precursors. Focusing on precursor maturation in cortical areas, we could identify the likely triggers of maturations in the adult brain, impinging on two specific neurotransmitter receptors. Single-cell patch clamp experiment revealed that chronic modulation of these receptors by an endogenous agonist causes mild increase in ionic conductance in the precursors of the piriform cortex, recapitulating a more mature functional profile.

## 1. Tracing early- and late-maturing precursors

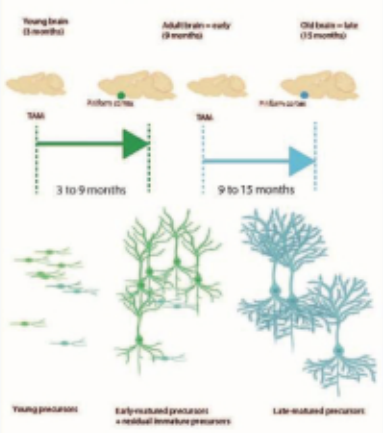


Transgenic mice allowed to trace the maturation of neuronal precursors in the adult brain. In the DCX-CreRT2/fl-eGFP mouse, tamoxifen (TAM) activates a recombinase leading to permanent green labelling (eGFP) of neuronal precursors that express doublecortin (DCX) at the moment of TAM administration. Early- and late-maturing precursors (expressing DCX) were labelled by TAM administration at 3 months (early) or 9 months (late) respectively. Early- and late-matured precursors were thereafter analysed, six months after TAM administration.

## 2a. The piriform cortex generates neuronal precursors during development, which mature during adulthood

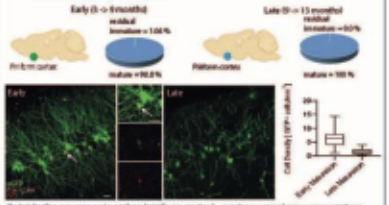


Outside the neurogenic niches (piriform cortex), most neuronal precursor mature during early adulthood (3 -> 9 months). However, some precursors retain latent immaturity and still express DCX and PSA-NCAM, immature neuronal markers, at 9 months of age. The residual precursors eventually undergo maturation (9 -> 15 months) and TAM induction at 9 months allows to detect some eGFP positive late-matured precursors, at 15 months. At 15 months there are no residual immature precursors as the reservoir has extinguished. Scale bars = 20 µm

## 2b. The neurogenic niches generate new neuronal precursors continuously during development and during adulthood

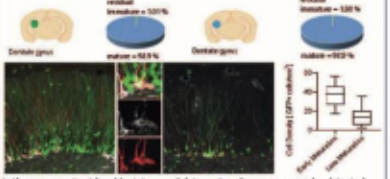


In the neurogenic niches (dentate gyrus), late-matured precursors can be detected readily. At 15 months, residual immature precursors can still be found as the reservoir is replenished by proliferative precursors. Scale bars = 20 µm

## 3. Early- and late matured precursors have different morphologies

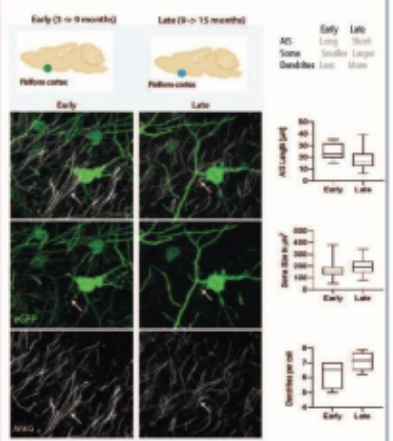


Even though late-maturing precursors retain capacity of becoming neurons, brain aging may affect their morphological and functional traits. In the piriform cortex, late-matured precursors are endowed with shorter axon initial segment (AIS), slightly larger soma, and slightly more dendrites that early-matured precursors. Morphological differences herald different functional traits and lead questioning whether the mechanisms of maturation change with age or whether maturation itself is overridden by the general process of brain aging. Scale bars = 20 µm

## 4. Analysis of precursor synaptic integration after maturation in the aged brain

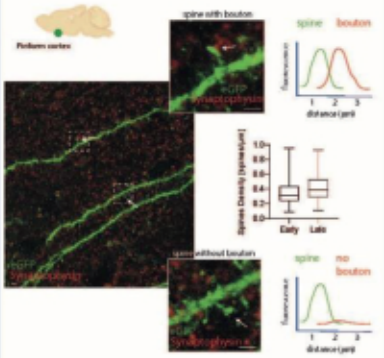


The formation of functional synaptic contact between matured precursors and other neurons is crucial for network integration. Early- and late-matured precursors have a comparable density of synaptic spines on their dendrites. Proximity of bouton localization by synaptophysin-labelling allows to estimate how many of the precursor spines are actually contacted by presynaptic terminals (ongoing work). Scale bars = 2µm

## 5. Single-cell transcriptome analysis on molecular mechanisms of precursor maturation

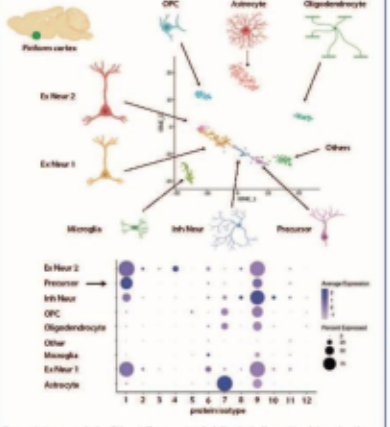


Transcriptome analysis of the piriform cortex (adult mice) allowed to determine the cell-specific patterns of gene transcription. According to Gene Ontology enrichment profile, precursors express a combination of specific protein isotypes, known to control neurogenesis. These receptors are the likely triggers of maturation of the piriform cortex precursors, prompting to question whether prolonged latent immaturity of some precursors correlates with lower expression levels (outlook).

## 6. Functional precursor responses can be triggered by endogenous agonist-mediated neuromodulation

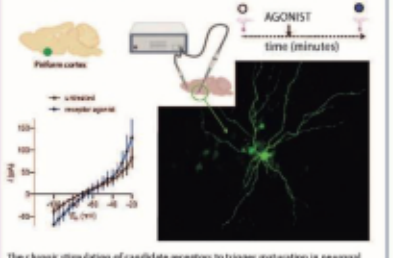


The chronic stimulation of candidate receptors to trigger maturation in neuronal precursors of the piriform cortex causes increase in ionic currents. Stimulation is carried out ex vivo, by endogenous neuromodulator application. The results prompt questioning whether chronic neuromodulation in vivo may influence the course of precursor maturation and to further question the relevant behavioural correlates (outlook).

## Conclusions

Our results indicate that although neuronal precursor maturation can occur outside the neurogenic niches, the outcomes vary according to the time of maturation onset. Thus, immature precursors look different upon maturation in the young-adult or in the old brain. Better understanding of molecular mechanisms controlling precursor maturation will allow to modulate the process pharmacologically and evaluate the effects of early vs. late precursor integration in the brain in vivo.

SIGNIFICANCE:

Maturation and functional integration of endogenous (or transplanted) neuronal precursors in the adult brain pivots on intrinsic precursor properties as well as on the molecular cues of the hosting niche. The latter is not only context-dependent, but also likely subject to age-dependent changes. Elements of neuromodulation outside the adult neurogenic niches, may help precursor maturation in a young-adult brain, but might be missing or waning in the old brain.
Our results show that even if neuronal maturation in the old brain is possible, the outcomes of the process differ from those occurring in the young brain. Discovering pathways of neuromodulation that promote or hinder the maturation will help to identify and overcome bottlenecks for a more efficient and less age-dependent precursor integration in the adult and old brain.

## ACKNOWLEDGMENTS

We thank Ariane Benedetti, Paracelsus Medical University Salzburg, Austria, for the excellent support in the management of the mouse colonies and the tamoxifen induction procedures. We acknowledge the support of Dr. A. Fleischmann, Brown University, Providence RI, USA for the raw data used for transcriptomic analysis. We thank Dr. Simona Covello and Prof. Juan Nacher, Universitat de Valencia, Spain, for the insightful discussions and suggestions on matters of precursor analysis.

## FUNDING

We are grateful for the support provided by the PMU-FFF through grants: PMU-FFF: R-20/02/130-BEN and PMU-FFF: R-16/04/084-BEN

## Mechanisms of neuronal maturation in the adult and aging brain

Bruno Benedetti[1,2,3], Gabriele Gabriele[1,2,3], Maximilian Reisinger[1,2,3], Christina Kreutzer[1,2,3], Rodolphe Poupardin[2,4], Sébastien Couillard-Després[1,2,3]

[1]Institute of Experimental Neuroregeneration, Paracelsus Medical University; [2]Salzburg, Austria; Spinal Cord Injury and Tissue Regeneration Center Salzburg (SCI-TReCS); [3]Austrian Cluster for Tissue Regeneration, 1200 Vienna, Austria; [4]Institute of Experimental and Clinical Cell Therapy, Parecelsus Medical University, Salzburg, Austria; Contact: bruno.benedetti@pmu.ac.at

### Objective
Maturation of neuronal precursors in the adult brain occurs spontaneously in the neurogenic niches and, as we recently documented, in some cortical areas. Such maturation requires necessarily mechanisms that are different from those regulating the embryonic and neonatal development, as precursors must interface with and wire into fully developed brain networks. In this project, we questioned whether brain aging affects neuronal precursor maturation. Furthermore, we searched for molecular mechanisms that may trigger the maturation of latent precursors in the adult brain.

### Methods
A transgenic mouse model (DCX-CreRT2::fl-eGFP) allowed tracing the maturation of precursors in the adult (9 months) or aged (15 months) murine brain. In these genetically engineered animals, tamoxifen administration induces permanent green labelling of precursors, which were thereafter analysed six months after induction. Morphological and immunohistochemical traits of aged precursors were analysed ex vivo. Additionally, transcriptome analysis allowed to identify candidate proteins selectively enriched in the neuronal precursors that may control their maturation in the adult brain. Finally, functional correlates of putative triggers of maturation were analysed with single-cell patch clamp experiments.

### Results
We found that aging affects precursor maturation; i.e. neurons derived from latent immature precursors in the aged brain are morphologically different from neurons derived from precursors which maturation occurs during early-adulthood. Precursors that matured in the aged brain had a bigger soma, more dendrites and shorter axon initial segment, implying different functional properties in comparison to early-matured precursors. Focusing on precursor maturation in cortical areas, we could identify the likely triggers of maturation in the adult brain, impinging on two specific neurotransmitter receptors. Single-cell patch clamp experiment revealed that chronic modulation of these receptors by an endogenous agonist causes mild increase in ionic conductance in the precursors of the piriform cortex, recapitulating a more mature functional profile.

### Conclusions
Our results indicate that although neuronal precursor maturation can occur outside the neurogenic niches, the outcomes vary according to the time of maturation onset. Thus, immature precursors look different upon maturation in the young-adult or in the old brain. Better understanding of molecular mechanisms controlling precursor maturation will allow to modulate the process pharmacologically and evaluate the effects of early vs. late precursor integration in the brain in vivo.

### Acknowledgements
We are grateful for the support provided by the PMU-FFF through grants:
PMU FFF: R-20/02/130-BEN and PMU-FFF: R-16/04/084-BEN
We thank Ariane Benedetti, Paracelsus Medical University Salzburg, Austria, for the tamoxifen induction procedure. We acknowledge the support of Dr. A. Fleischmann, Brown University, Providence RI, USA for the raw data used for transcriptomic analysis.

# Expression of the amino acid transporter SLC6A20 is regulated by the transcription factor POU3F4

Emanuele Bernardinelli[1], Sebastian Roesch[2], Gerd Rasp[2], Laura Astolfi[3], Silvia Dossena[1], Antonio Sarikas[1]

[1]Institute of Pharmacology and Toxicology, Paracelsus Medical University, Salzburg
[2]Department of Otorhinolaryngology, Head and Neck Surgery, Paracelsus Medical University, Salzburg
[3]Bioacustic Research Laboratory, Department of Neuroscience, University of Padua

## Background and objective

Hearing loss is the most common sensory defect, affecting 450 million people worldwide in a disabling form (1). Defects in the *POU3F4* gene on the X chromosome, encoding for the transcription factor of the same name (3), are causative of X-linked deafness type 3 (DFN3), the most common type of X-linked deafness (2). The pathomechanism underlying POU3F4-related deafness is largely unknown, as are its transcriptional targets. In the present project we identified a potential transcriptional targets of POU3F4 and investigated its expression in mouse cochlea as well as its regulation following POU3F4 overexpression or silencing.

## Methods

- RNAseq analysis was performed on mRNA extracted from Hek293Phoenix cells overexpressing POU3F4 or a negative control.
- RT-qPCR was performed on mRNA extracted from cells in which POU3F4 was either overexpressed or silenced by transient transfection and on mRNA extracted from wild type mouse cochlea.
- IHC: cochleae were fixed in Shandon Glyo-Fixx™ (Thermo), decalcified in Surgipath Decalcifier II® (Leica Biosystems) and paraffinated. Fixed samples were sectioned with a thickness of 5µm. Sections were blocked in goat serum before incubation with primary antibodies. Primary antibodies were detected with appropriate secondary antibodies.
- Statistics: One Way ANOVA with Bonferroni's Post Test or unpaired Student's t-test were applied.

## POU3F4 regulates *SLC6A20* transcript

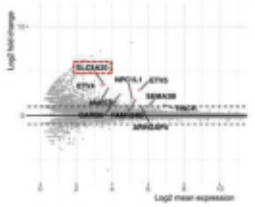

**Figure 1: SLC6A20 is upregulated in POU3F4 overexpressing HEK293Phoenix cells.** The RNAseq analysis was performed on RNA extracted from three independent subcultures of HEK293Phoenix cells transiently transfected with WT POU3F4 or an empty control vector. Above the 0 line are transcripts upregulated in POU3F4 WT cells versus the negative control

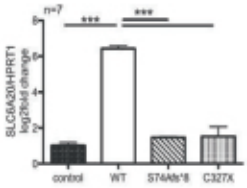


**Figure 2: The SLC6A20 transcript is upregulated in HEK293Phoenix cells overexpressing POU3F4 WT, but not in cells overexpressing pathogenic variants of POU3F4.** HEK293Phoenix cells were transiently transfected with plasmid vectors coding for WT POU3F4 or two potentially pathogenic variants identified in patients of the Austrian cohort. Cells transfected with an empty vector served as negative control. Total RNA was reverse-transcribed and subjected to RT-qPCR. The levels of the SLC6A20 transcript were normalized to the housekeeping HPRT1. ***: p<0.001, OneWay ANOVA with Bonferroni's post-test.

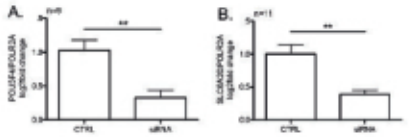


**Figure 3: Silencing of Pou3f4 in MEFs leads to reduced Slc6a20 expression.** RT-qPCR on mRNA extracted from MEFs transfected with a combination of siRNAs designed to silence Pou3f4 or with a scrambled control siRNA. A: relative expression of Pou3f4 in siRNA transfected cells vs. control (silencing -70% ± 7.2); B: relative expression of Slc6a20 in siRNA transfected cells vs. control (-60.9% ± 3.5) (**:p<0.01, unpaired Student's t-test.). POLR2A was used as housekeeping.

## *Slc6a20* and *Pou3f4* in the mouse cochlea

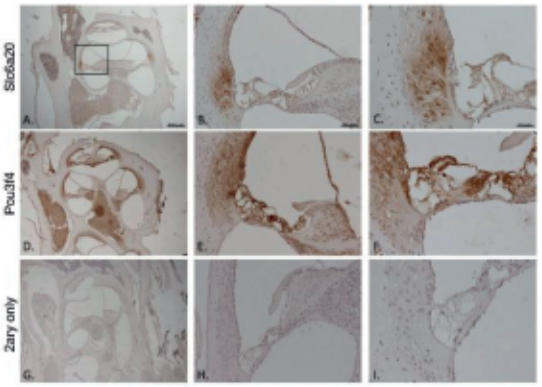


**Figure 4: Slc6a20 and Pou3f4 are expressed in WT mouse cochlea.** Immunostaining of tissue slices from mouse cochlea. A-C: primary Antibody anti-Slc6a20; D-E: primary Antibody anti-Pou3f4; G-I: negative control, secondary Antibody only. Slc6a20 show a clear signal localized in the spiral ligament, Pou3f4 show a more diffuse signal in different structures of the cochlea, including the spiral ligament.

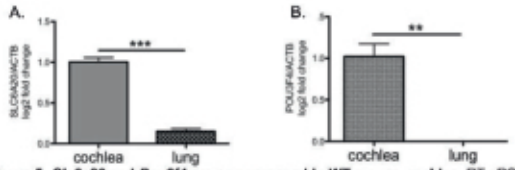


**Figure 5: *Slc6a20* and *Pou3f4* are co-expressed in WT mouse cochlea.** RT-qPCR on mRNA extracted from mouse cochlea or lung. A: relative expression of *Slc6a20* transcript in mouse tissues (n=5, ***:p<0.001, unpaired Student's t-test.). B: relative expression of *Pou3f4* transcript in mouse tissues (**:p<0.01, unpaired Student's t-test.). Lung was taken as negative control. ACTB was used as housekeeping.

## Conclusions and outlook

The present study we identified and validated a putative transcriptional target of POU3F4, the aminoacid transporter SLC6A20. We could show an upregulation of SLC6A20 in overexpression of POU3F4 WT but not when overexpressing pathogenic variants of the transcription factor. Accordingly, a downregulation of SLC6A20 transcript was observed when POU3F4 was silenced by siRNA. Furthermore, we could assess the expression of both *Pou3f4* and *Slc6a20* in mouse cochlea, both on the transcript and protein level. The underlying pathomechanism of POU3F4-SLC6A20-related deafness remains to be elucidated. It is tempting to speculate that a diminished POU3F4 activity results in reduced expression of SLC6A20 and in a defective transport of betaine in the fibrocytes of the spiral ligament of the cochlea. Reduced betaine concentration in turn would lead to the toxic accumulation of Homocysteine and the structural defects observed in POU3F4-deafness (4).

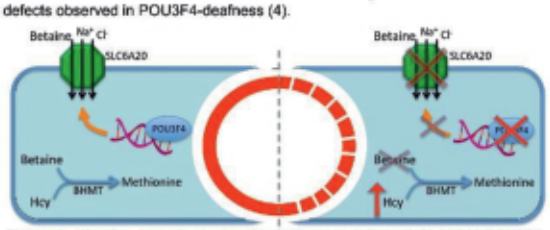


**Figure 6: Working hypothesis for the pathomechanism of SLC6A20-POU3F4-related deafness**

***References:*** ***(1)*** Sheffield, A.M., and Smith, R.J.H. (2019). The Epidemiology of Deafness. Cold Spring Harb Perspect Med 9.; ***(2)*** de Kok, Y.J. et al. (1995). Association between X-linked mixed deafness and mutations in the POU domain gene POU3F4. Science 267, 685-688.; ***(3)*** Phippard, D., et a. (1999). Targeted mutagenesis of the POU-domain gene Brn4/Pou3f4 causes developmental defects in the inner ear. J Neurosci 19, 5980-5989.; ***(4)*** Song, M.H.et al. (2011). Pou3f4 deficiency causes defects in otic fibrocytes and stria vascularis by different mechanisms. Biochem Biophys Res Commun 404, 528-533.

## Expression of the amino acid transporter SLC6A20 is regulated by the transcription factor POU3F4

Emanuele Bernardinelli[1], Sebastian Roesch[2], Gerd Rasp[2], Laura Astolfi[3], Silvia Dossena[1], Antonio Sarikas[1]

[1]Institute of Pharmacology and Toxicology, Paracelsus Medical University, Salzburg, Austria; [2]Department of Otorhinolaryngology, Head and Neck Surgery, Paracelsus Medical University, Salzburg, Austria; [3]Bioacustic Research Laboratory, Department of Neuroscience, University of Padua; Contact: e.bernardinelli@pmu.ac.at

### Objective
Hearing loss is the most common sensory defect, affecting 450 million people worldwide in a disabling form. Defects in the POU3F4 gene on the X chromosome, encoding the transcription factor POU3F4, are causative of X-linked deafness type 3 (DFN3), the most common type of X-linked deafness. The pathomechanism underlying POU3F4-related deafness is largely unknown, as are its transcriptional targets. In the present project we identified a potential transcriptional target of POU3F4 and investigated its expression in mouse cochlea as well as its regulation following POU3F4 overexpression or silencing.

### Methods
RNAseq analysis was performed on mRNA extracted from Hek293Phoenix cells overexpressing POU3F4 or a negative control. RT-qPCR was performed on mRNA extracted from cells in which POU3F4 was either overexpressed or silenced by transient transfection and on mRNA extracted from wild type mouse cochlea. We determined the expression of Pou3f4 and Slc6a20 in isolated cochleae of C57BL/6J mice both by RT-qPCR and immunostaining.

### Results
The amino acid transporter SLC6A20 was identified among the upregulated transcripts from RNAseq analysis (FDR-adj. p-value=0,001281, log2fold change=3.488). The upregulation was confirmed by RT-qPCR on RNA from cells overexpressing POU3F4 WT, compared to a negative control (log2fold change=6.43±0.15, $p<0.001$), but not in cells overexpressing POU3F4 pathogenic variants. Correspondingly, silencing of POU3F4 by siRNA resulted in a decrease of the transcript level of SLC6A20 (POU3F4 silencing: -70%±7.2, $p<0.01$, unpaired Student's t-test; SLC6A20 decrease: -60.9%±3.5, $p<0.01$, unpaired Student's t-test). Pou3f4 transcript was highly expressed in the cochlea while not detectable in the lung. Slc6a20 transcript also was significantly expressed in the cochlea when compared to lung tissue ($p<0.001$, $n=5$ cochleae). Immunostaining of cochlea slices with antibodies against Pou3f4 and Slc6a20 also showed an expression of both proteins in different structures, including the spiral ligament of the cochlea.

### Conclusions
The present study identified aminoacid transporter SLC6A20 as a potential transcriptional target of POU3F4. We show an upregulation of SLC6A20 in overexpression of POU3F4 WT but not when overexpressing pathogenic variants of the transcription factor. Accordingly, POU3F4 silencing by siRNA resulted in downregulation of SLC6A20. Pou3f4 and Slc6a20 were detected in mouse cochlea, both on the transcript and protein level. The underlying pathomechanism of POU3F4-SLC6A20-related deafness remains to be elucidated. It is tempting to speculate that a diminished POU3F4 activity results in reduced expression of SLC6A20 and in a defective transport of betaine in the fibrocytes of the spiral ligament of the cochlea. Reduced betaine concentration in turn would lead to the toxic accumulation of Homocysteine and the structural defects observed in POU3F4-deafness.

PARACELSUS
MEDIZINISCHE PRIVATUNIVERSITÄT

Klinikum Nürnberg
Wir sind für Sie da!

# Handinfections – the longer untreated the worse the outcome?

## Course of hand infections as a function of the latency period until presentation at the specialist clinic

Maresa Berns, Moritz Billner, Bert Reichert

[1]Department of Plastic surgery, Paracelsus Medical University; Nuremberg, Germany; Contact: maresa.berns@klinikum-nuernberg.de

**Abstract**

**Background:** Being one of the most useful human tools the hand plays a vital role for every human being. As hands are used for nearly every activity they are especially exposed to the environment. Even commonplace injuries may lead to a significant morbidity, including serious loss of function and even amputation. The aim of this retrospective study was to analyse if there is a correlation between delay of event and consultation of specialist.

**Hypothesis:** Delay between triggering event and consultation of a hand surgery department affect the clinical course of hand infection along with other factors.

**Material and methods:** Over a 4.33 year period data from 976 patients with the diagnostic key ICD-10 L03.0 and L03.1 were obtained of which 493 could be analysed. The case files were evaluated by using statistical programme.

**Results:** There was a significant difference in the required period of treatment between patients, who consulted a medical specialist in the first 2 days after a triggering event and those who wait for more then 2 days. U = 39.495,500;
Z =5,847, p < .001 Kolmogorov-Smirnov p < .05

There was a significant difference in the number of operations between patients, who consulted a medical specialist in the first 2 days after a triggering event and those who wait for more then 2 days. U = 35.110,500; Z 3,723; p < .001 Kolmogorov-Smirnov p < .05.

**Conclusions:** An early consultation of medical specialist in many cases leads to an improved course of infection and therefore to a better outcome at all.

### Introduction and Objective

Hand infections are a common and versatile disease. Due to the ubiquitous use of the hands, they are particularly exposed to the environment. The exposed position of the hand as a human tool leads more often to injuries. Nevertheless, minor injuries are often trivialised, which leads to delays between the triggering event and the presentation in the hospital. In order to find out how the course of a hand infection can be influenced, latency period, length of stay in the clinic and number of operations were analysed.

### Methods

The present study is a retrospective, monocentric, epidemiological study. Shapiro-Wilk test was started to check for normal distribution. Since no normal distribution was present, Mann-Whitney-U tests and Spearman correlations were performed. (Significance level alpha 5%, P-value of <0.05). A total of 976 cases with the ICD 10 code phlegmon on fingers (ICD L03.0 and L03.1) were examined, of which 493 cases were included in the study. (see fig.1)



figure 1

### Results:

- Latency and treatment duration correlated positively, r = .222, p < .001.
- Latency and number of necessary operations correlated slightly positive, r = .140, p= < .002.
- Age of patients at baseline and latency correlated slightly positive, r = .123, p < .001.
- Age at the beginning of treatment and number of necessary surgical interventions correlated slightly positive, r = .102, p < .001
- Treatment duration and number of necessary surgical interventions correlated strongly positive, r = .653, p < .001.
- There was significant difference in treatment duration between patients who presented within the first 2 days after triggering event and those presented to specialist only after more than 2 days. U = 39,495.500; Z =5,847, p < .001
- There was significant difference in number of operations between patients presented within the first 2 days after the triggering event and those who presented to the specialist clinic only after more than 2 days. U = 35,110.500; Z = 3,723; p < .001.

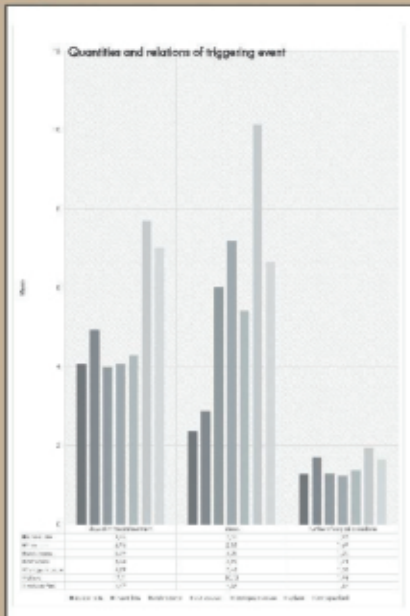


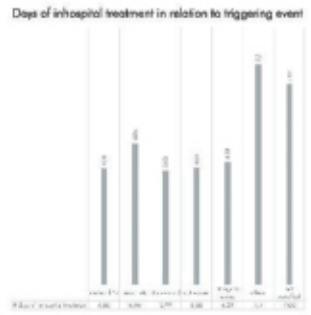


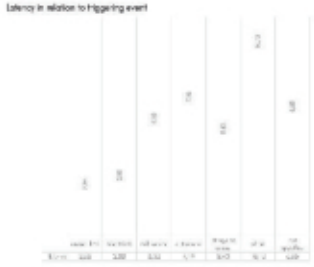


### Conclusions & Perspectives

- the longer the delay in visiting specialists, the longer the length of stay in hospital afterwards
- the longer the delay in visiting specialists, the more necessary surgical interventions

→ Importance of early specialist treatment at least after potentially critical events.

- However results do not show exact causality between latency and outcome

→ Further studies needed (additional aspects on outcome); especially to develop recommendations

### References and Acknowledgements

- Infektionen der Hand. Schirmer S, Vogt PM. In: Praxis der Plastischen Chirurgie. Springer; 2011:531-545
- Handinfektion als Folge einer Bagatellverletzung v. Minimalverletzungen. Reichert,O-FP, Maßnahmen. Vo 39(2). Handchir Mikrochir Plast Chir.2007:124 127.
- Infektionen an der Hand. Ziegler B, Bickert B. Orthopädie und Unfallchirurgie up2date. 2018;13(01):55-64.

## Handinfections – the longer untreated the worse the outcome?

Maresa Berns[1], Moritz Billner[1], Bert Reichert[1]

[1]Department of Plastic and Hand surgery, Burn surgery Paracelsus Medical University, Nuremberg, Germany; Contact: maresa.berns@klinikum-nuernberg.de

### Objective

Hand infections are a common and versatile disease. Due to the ubiquitous use of the hands, they are particularly exposed to the environment. The exposed position of the hand as a human tool leads more often to injuries. Nevertheless, minor injuries are often trivialised, which leads to delays between the triggering event and the presentation in the hospital. In order to find out how the course of a hand infection can be influenced, latency period, length of stay in the clinic and number of operations were analysed.

### Methods

The present study is a retrospective, monocentric, epidemiological study. Shapiro-Wilk test was started to check for normal distribution. Since no normal distribution was present, Mann-Whitney-U tests and Spearman correlations were performed. (Significance level alpha 5%, P-value of $<0.05$). A total of 976 cases with the ICD 10 code phlegmon on fingers (ICD L03.0 and L03.1) were examined, of which 493 cases were included in the study. (see fig.1)

### Results

Latency and treatment duration correlated positively, $r = .222$, $p < .001$.
Latency and number of necessary operations correlated slightly positive, $r = .140$, $p = < .002$.
Age of patients at baseline and latency correlated slightly positive, $r = .123$, $p<.001$.
Age at the beginning of treatment and number of necessary surgical interventions correlated slightly positive, $r=.102$, $p<.001$
Treatment duration and number of necessary surgical interventions correlated strongly positive, $r=.653$, $p<.001$.
There was significant difference in treatment duration between patients who presented within the first 2 days after triggering event and those presented to specialist only after more than 2 days. $U=39,495.500$; $Z=5,847$, $p<.001$
There was significant difference in number of operations between patients presented within the first 2 days after the triggering event and those who presented to the specialist clinic only after more than 2 days. $U=35,110.500$; $Z=3,723$; $p<.001$.

### Conclusions

As expected the longer the delay in visiting a specialist clinic, the longer the length of stay in hospital afterwards and the more necessary surgical interventions. These findings underline the importance of early specialist treatment at least after potentially critical events. However our results do not show the exact causality between latency and outcome. Further studies are needed to rule out additional aspects on outcome like individual immun status, spectrum of pathogenic agents or gender aspects. Especially to develop effective recommendations the difference in triggering causes must be analyzed more in detail.

# Understanding the role of platelets in Alzheimer's Disease

Diana M Bessa de Sousa[1,2], Michael S Unger[1,2], Heike Mrowetz[1,2], Barbara Altendorfer[1,3], Arianne Benedetti[1,3], Rodolphe Poupardin[1,4], Thomas Fröhlich[5], Ludwig Aigner[1,2,6], Kathrin Kniewallner[1,2]

1: Institute of Molecular Regenerative Medicine, Paracelsus Medical University, Salzburg, Austria. 2: Spinal Cord Injury and Tissue Regeneration Center Salzburg (SCI-TReCS), Paracelsus Medical University, Salzburg, Austria. 3: Institute of Experimental Regeneration, Paracelsus Medical University, Salzburg, Austria. 4: GolTherapy Institute, Paracelsus Medical University, Salzburg, Austria. 5: Laboratory of Functional Genome Analysis (LAFUGA), Gene Center, Ludwig Maximilian University of Munich, Germany. 6: Austrian Cluster for Tissue Regeneration, Vienna, Austria.

## Introduction

In Alzheimer's disease (AD) platelets become dysfunctional contributing to vascular injury and neuroinflammation.

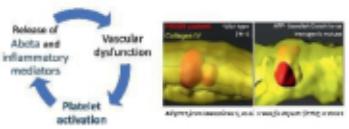


However, the molecular changes of platelets in AD and their impact on the pathology remain largely unexplored. Under the hypothesis, that platelets in AD are activated, have an aggressive phenotype and actively contribute to disease pathogenesis, we aim to better understand the role of platelets in AD using a transgenic AD mouse model (i.e., APP Swedish PS1 dE9, APP-PS1).

## Experimental setup

**A. Molecular and cellular characterization of APP-PS1 platelets**

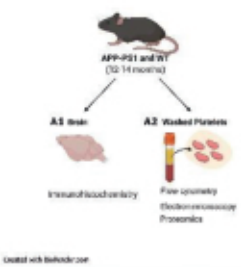


**B. Immune-mediated platelet depletion in APP-PS1 mice**

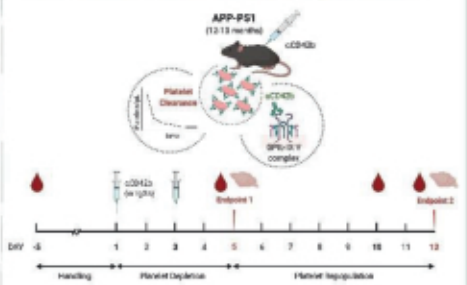


## A1 Platelets in APP-PS1 mice are activated and invade the brain[1]

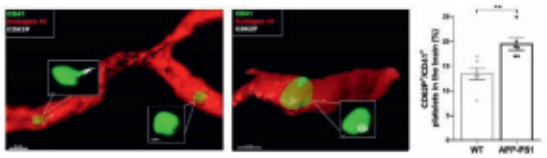


**Figure 1. Immunohistochemical analysis of platelets activation status in APP-PS1 mice.** An increased percentage of CD41+ platelets (green) expressing the activation marker CD62P (white) circulate within cerebral blood vessels (red), in APP-PS1 compared to age-matched WT. Statistical analysis was performed by unpaired Student's t test (**p < 0.01; n=6/genotype). Scale: 5 µm and 1 µm (zoom in).

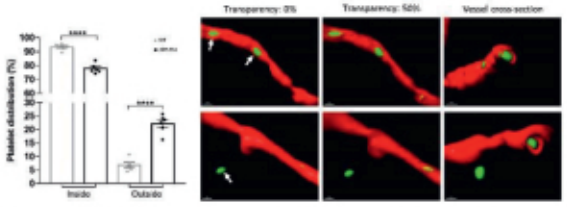


**Figure 2. Immunohistochemical analysis of platelet distribution in the brain of APP-PS1 mice.** In APP-PS1 and age matched WT mice, CD41+ platelets were mainly located within the cerebral blood vessels (counted as inside). However, in APP-PS1 mice, platelets were frequently seen in the brain parenchyma or at the blood vessel wall, suggesting extravasation (counted as outside, arrows). Statistical analysis was performed by two-way ANOVA with Tukey's multiple comparison test (****p < 0.0001; n=6/genotype). Scale: 3 µm.

## A2 Characterization of peripheral blood platelets

**Figure 3. Activation status and ultrastructure analysis of peripheral blood platelets in APP-PS1 mice.**[1] Surface expression of CD62P by blood-isolated CD41+ platelets was assessed by flow cytometry. CD62P+/CD41+ platelets were detected in APP-PS1 and WT mouse blood, but the percentage of activated platelets in the bloodstream of APP-PS1 and WT was not significantly different. APP-PS1 platelets showed morphological features of activation: membrane protrusions (arrows), microparticle (MP,*) formation, and a 30% smaller area. Statistical analysis was performed by unpaired Student's t test (n=7/genotype).

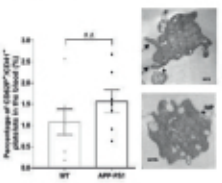





**77** misregulated proteins
**in APP-PS1 platelets**

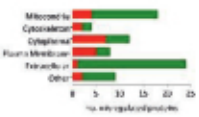

**Figure 4. Proteomic analysis of peripheral blood platelets in APP-PS1 mice.** Volcano plot of significantly differentially expressed proteins and their respective fold changes in APP-PS1 and WT mice (n=3/genotype). GO term analysis of dysregulated proteins related to their cellular components in APP-PS1 mouse platelets (**red**: downregulation; **green**: upregulation)

## B Immune-mediated platelet depletion induced transient thrombocytopenia in APP-PS1 mice

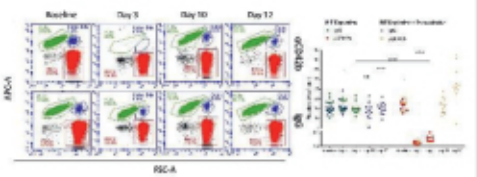


**Figure 5. Immune-mediated platelet depletion in APP-PS1 mice induces a transient thrombocytopenia.** APP-PS1 mice intraperitoneal injected with an anti-CD42b antibody (2µg/g of body weight) presented platelet depletion with up to 99% efficacy. Platelet counts were monitored by flow cytometry using blood collected from the saphenous vein (baseline, day 3 and 10) or by cardiac puncture (day 5 and 12). Diluted whole blood samples were stained with allophycocyanin (APC)-labelled anti mouse CD41 antibody to identify platelets (PLTs). Withdrawal of the antibody treatment had a rebound effect on platelet production, resulting in thrombocytosis by day 12. Non-immune rat immunoglobulins (IgG) were used as depletion control (n=8-12/group).

## Outlook

**Investigate the impact of platelet depletion onto:**

- **Amyloid pathology**

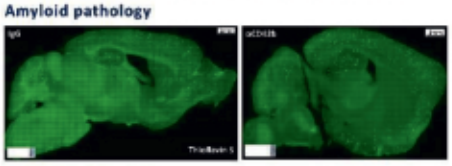


**Figure 6.** Thioflavin S stained amyloid plaques in the brain of APP-PS1 mice treated with IgG or αCD42b for 5 days.

- **Neuroinflammation**

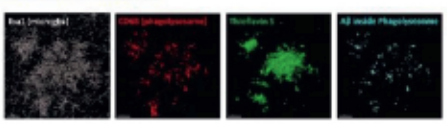


**Figure 7.** Amyloid beta (Aβ) phagocytosis by microglia, upon platelet depletion and repopulation, will be investigated using immunohistochemistry and 3D surface rendering.

- **Differential Gene Expression (Hippocampus)**

**Acknowledgments:** The authors thank the microscopy core facility of SCI-TReCS (Spinal Cord Injury and Tissue Regeneration Center Salzburg). This study was supported by the Austrian Science Fund: (P24734-B24), the PMU Rise Project (PMU-FFF) (R17/04/007-KNI) and the PMU postgraduate students support program DISCITE! (D-19/01/008-BES).

[1] Kniewallner KM, et al. Front Neurosci. 2020;14:129. doi:10.3389/fnins.2020.00129

## Understanding the role of platelets in Alzheimer's Disease

Diana Marisa Bessa de Sousa[1,2], Michael Stefan Unger[1,2], Heike Mrowetz[1,2], Barbara Altendorfer[1,2], Ariane Benedetti[2,3], Rodolphe Poupardin[2,4], Thomas Fröhlich[5], Ludwig Aigner[1,2,6], Kathrin Maria Kniewallner[1,2]

[1]Institute of Molecular Regenerative Medicine, Paracelsus Medical University, Salzburg, Austria; [2]Spinal Cord Injury and Tissue Regeneration Center Salzburg (SCI-TReCS), Paracelsus Medical University, Salzburg, Austria; [3]Institute of Experimental Regeneration, Paracelsus Medical University, Salzburg, Austria; [4]Cell Therapy Institute, Paracelsus Medical University, Salzburg, Austria; [5]Laboratory of Functional Genome Analysis (LAFUGA), Gene Center, Ludwig Maximilian University of Munich, Germany; [6]Austrian Cluster for Tissue Regeneration, Vienna, Austria; Contact: diana.bessa@pmu.ac.at

### Objective
In Alzheimer's disease (AD) platelets become dysfunctional. However, it remains unclear whether the platelet alterations occurring in AD are a consequence of the ongoing pathological events or a driver of the disease. Aiming to characterise platelets at the molecular and cellular level, we analysed platelets in a transgenic mouse model of AD (APP Swedish PS1 dE9, APP-PS1).

### Methods
We assessed the platelet activation status (CD62P expression) and the proteome of blood isolated platelets in 14 months old APP-PS1 mice and wild type (WT) age-matched controls. Further, we induced short term immune-mediated platelet depletion in 12-13 months old APP-PS1 mice by intraperitoneal injections of an anti-CD42b antibody.

### Results
APP-PS1 mice showed significantly higher percentages of activated platelets in the brain, but only a slight, non-significant, higher platelet activation in the bloodstream. Nevertheless, preliminary proteomics data revealed the existence of 77 differentially expressed proteins in APP-PS1 blood isolated platelets compared to WT mice. Interestingly, in the APP-PS1 mouse brain, about 20% of the platelets located extravascularly. Antibody treatment with anti-CD42b induced transient thrombocytopenia (>99%) in APP-PS1 mice, which could be reversed by the withdrawal of the antibody treatment. A rebound effect on platelet production was observed 9 days after the last antibody injection, suggesting the occurrence of thrombocytosis. Effects on AD pathology are currently under investigation.

### Conclusions
Platelets might present an altered cellular and molecular profile in AD. Short-term platelet depletion will help to enlighten the involvement of platelets in AD pathogenesis, particularly in amyloid plaque formation and microglial function, and potentially to identify novel targets of platelet biology, which might be developed as new drugs or drug targets.

### Acknowledgements
The authors thank the microscopy core facility of SCI-TReCS (Spinal Cord Injury and Tissue Regeneration Center Salzburg). This study was supported by the Austrian Science Funds (P24734-B24), the PMU Rise Project (PMU-FFF) (R17/04/097-KNI) and the PMU postgraduate students support program DISCITE! (D-19/01/008-BES).

# Retro- and anterograde axonal tracing via injection of AAV particles to study neuroregeneration after spinal cord injury

Bieler L[1,2], Jakubecova D[1,2], Swann V[1,2], Kreutzer C[1,2], Couillard-Després S[1,2,3]
[1]Institute of Experimental Neuroregeneration, Paracelsus Medical University, Salzburg, Austria
[2]Spinal Cord Injury and Tissue Regeneration Center Salzburg (SCI-TReCS), Austria
[3]Austrian Cluster for Tissue Regeneration
✉ Lara.Bieler@pmu.ac.at

BEST POSTER (female)

PARACELSUS MEDIZINISCHE PRIVATUNIVERSITÄT

## 1 Background

Axonal tracing is a useful technique to determine the degree of regeneration or reinnervation following neuroregenerative therapies. Various chemicals are available on the market for retrograde as well as anterograde tracing. However, these substances present limitations in regard to uptake, stability, speed of transport and distribution within the cellular compartments (i.e. retrograde tracing labels the somata only, while anterograde tracing mainly labels the axons). The low uptake of most substances by uninjured axons is particularly problematic. To circumvent this obstacle, we established a retro- as well as anterograde axonal fiber tracing based on adeno-associated dependoparvovirus (AAV) encoding fluorescent proteins under the control of a neuron-specific promotor.

In this poster, we show examples of anterograde bilateral labeling of cortical motor neurons and follow the axonal projections from the motor cortex to the corticospinal tract (CST) in the spinal cord. Additionally, we injected AAV in the lamina 5 of the cervical spinal cord (unilateral) and labeled the upper motor neurons projecting in this area.

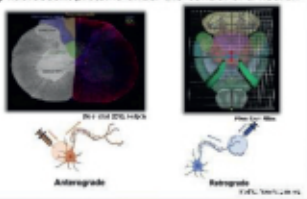


## 2 Material and Methods




For anterograde tracing, rats were slowly injected with AAV9-hSyn-eGFP in the motor cortex of one hemisphere and AAV1-hSyn-mCherry in the other hemisphere, respectively, using a stereotactic frame and a blunt 25 G Hamilton syringe. For retrograde tracing, AAVeg-hSyn-eGFP was injected unilaterally in the lamina 5 of the spinal cord at cervical level 4 using a blunt 33 G Hamilton syringe. After 21 days, for anterograde tracing, or 7 days, for retrograde tracing, rats were transcardially perfused with heparinized saline followed by phosphate-buffered 4 % PFA and tissue was processed for immunohistochemical analyses.

## 3 Anterograde labeling of axons from cortical motor neurons

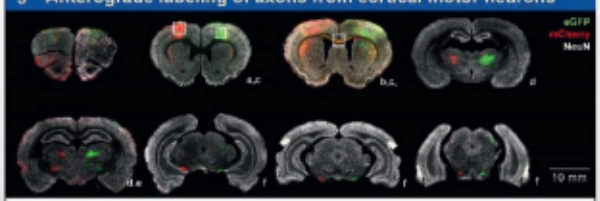


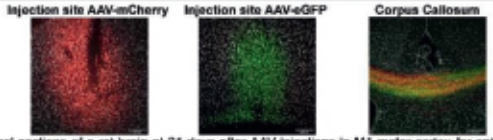


Coronal sections of a rat brain at 21 days after AAV injections in M1 motor cortex for anterograde labeling of axonal projections. Axons can be traced from (a) the injection sites to (b) the corpus callosum, (c) caudate putamen, (d) ventro-posteromedial nucleus in the thalamus, (e) zona incerta dorsal and ventral part as well as (f) the cerebral peduncle. (NeuN: neuronal marker)

## 4 Retrograde labeling of neurons in the motor cortex

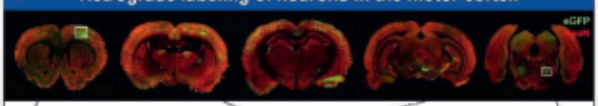


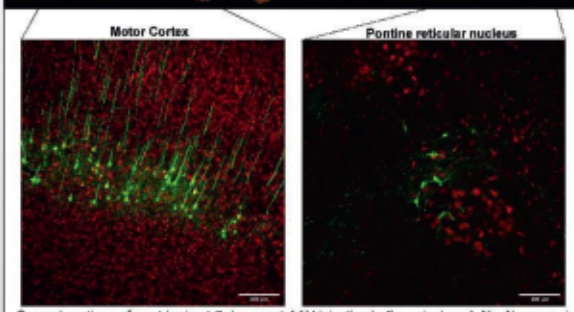


Coronal sections of a rat brain at 7 days post-AAV injection in the spinal cord. NeuN expressing neurons are detected in red. Somata and dendrites of neurons retrogradely labeled are visualized in green in the motor cortex and in the reticular formation. (NeuN: neuronal marker)

## 5 Anterograde labeling of CST in the cervical spinal cord

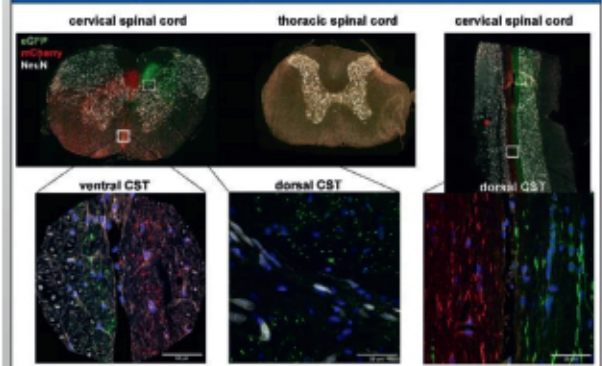


Coronal and horizontal sections of the spinal cord at 21 days post-AAV injection in the M1 motor cortex. In the cervical segment, the fibers of the dorsal as well as ventral CST were labelled. Crossing and non-crossing CST axons were revealed using different reporter colors for each hemisphere. Additional labeling was observed in the intermediomedial tract and in the laminae 5 and 6 of the gray matter. Injections were performed in the motor cortex innervating the front limbs and labeling thus was absent in and below the thoracic segments of the spinal cord. Scale bar = 50 µm

## 6 Retrograde labeling in the Spinal Cord

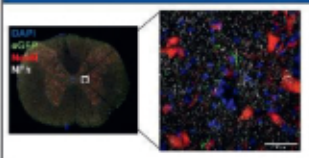


Coronal section of the cervical spinal cord rostral to the injection site 7 days after injection. The very low number of structures expressing eGFP in the grey matter indicates a very low labeling rate of interneurons in the spinal cord. Retrograde AAV injections to label upper motor neurons will lead at later time point (e.g. 21 days) to the labeling of their projections in the CST as well.

## 7 Conclusion

The labeling with the different AAV-serotypes to anterogradely or retrogradely label axonal tracts was efficient. The fluorescence intensity of reporters was strong enough to be detected without enhancement. However, enhancement using specific antibodies increased the signal intensity substantially and allowed for the resolution of very fine cellular structures. Due to the large volume of the motor cortex, coordinates of AAV injection must be carefully selected to label the motor neuron population projecting at the spinal segment(s) of interest.

## 8 Outlook

Axonal labeling with AAVs offers a wide range of future usage and will be implemented in ongoing projects:

**Mapping neuronal connectivity**

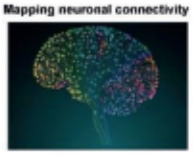

**Assessment of axonal regeneration and sprouting**

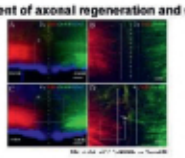

**Optimized morphological analysis**

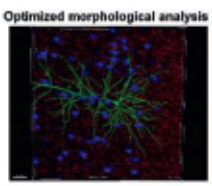

**Targeted electrophysiological measurements**

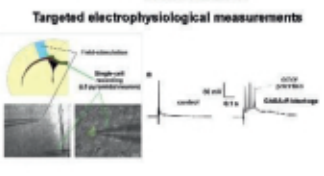

**Further ideas or questions?** → **Contact me!**

## Retro- and anterograde axonal tracing via injection of AAV particles to study neuroregeneration after spinal cord injury

Lara Bieler[1,2], Dominika Jakubecova[1,2], Victoria Swann[1,2], Christina Kreutzer[1,2], Sebastien Couillard-Despres[1,2,3]

[1]Institute of Experimental Neuroregeneration, Paracelsus Medical University Salzburg, Austria; [2]Spinal Cord Injury and Tissue Regeneration Center Salzburg, Austria; [3]Austrian Cluster for Tissue Regeneration; Contact: lara.bieler@pmu.ac.at

### Objective
Axonal tracing is a useful technique to determine the degree of regeneration or reinnervation following neuroregenerative therapies. Various chemicals are available on the market for retrograde as well as anterograde tracing. However, these substances present limitations in regard to uptake, stability, speed of transport and distribution within the cellular compartments. The low uptake of most substances by uninjured axons is particularly problematic. To circumvent this obstacle, we established a retro- as well as anterograde axonal fiber tracing based on adeno-associated dependoparvovirus (AAV) encoding fluorescent proteins under the control of a neuron-specific promotor. The AAV particles used are replication deficient and have no pathogenic potential in mammals. In this poster, we show examples of anterograde bilateral labeling of cortical motor neurons and follow the axonal projections from the motor cortex to the corticospinal tract (CST) in the spinal cord. Additionally, we injected AAV in the lamina 5 of the cervical spinal cord and labeled the upper motor neurons projecting in this area.

### Methods
For anterograde tracing, rats were stereotactically injected with AAV9-hSyn-eGFP in the motor cortex of the right hemisphere and AAV1-hSyn-mCherry in the left hemisphere. For retrograde tracing, AAVrg-hSyn-eGFP was injected unilaterally in the lamina 5 of the spinal cord at cervical level 4. After 21 days, for anterograde tracing, or 7 days, for retrograde tracing, tissue was processed for immunohistochemical analyses.

### Results
Twenty-one days after bilateral AAV injections in motor cortex (front limb area) using different reporter colors for each hemisphere, neuronal projections were labeled in an anterograde fashion and axons could be traced within the brain from the injection sites to the spinal cord. In the spinal cord, crossing and non-crossing CST axons were revealed based on the different reporter colors for each hemisphere. Additional labeling was observed in the of the gray matter. As injections were performed in the motor cortex innervating the front limbs, labeling was absent in and below the thoracic segments of the spinal cord.
Seven days following spinal injection of AAV for retrograde labeling, the very low number of structures expressing the reporter in the grey matter rostral to the injection site indicated a low rate of labeling for spinal interneurons. However, strong reporter expression was detected in the somata and dendrites of upper motor neurons in the motor cortex and in the reticular formation.

### Conclusions
The anterograde and retrograde of axonal tracts was efficient. The fluorescence intensity of reporters was strong enough to be detected without enhancement. However, enhancement using specific antibodies increased the signal intensity substantially and allowed for the resolution of very fine cellular structures. Due to the large volume of the motor cortex, coordinates of AAV injection must be carefully selected to anterogradely label the motor neuron population projecting at the spinal segment(s) of interest. With this labeling technique we established a method, which can be used in a variety of research questions in the field of neuroscience such as connectome analyses, assessment of axonal regeneration, enhanced morphological analyses and targeted electrophysiological measurements.

# AML-derived extracellular vesicles convey immunomodulatory potential

H.-M. Binder[1], N. Maeding[1] B. Vári[1], A. Raninger[1], M. Wolf[1], T. Heuser[2], A. Obermayr[3], G. Brachtl[1], K. Schallmoser[4], D. Strunk[1]

[1] Experimental and Clinical Cell Therapy Institute (ExCT), Spinal Cord Injury and Tissue Regeneration Center Salzburg (SCI-TreCS), Paracelsus Medical University, Salzburg, Austria
[2] Vienna Biocenter Core Facilities, Medical University, Vienna, Austria
[3] Department of Cell Biology, Biomedical Ultrastructure Research Group, University of Salzburg, Salzburg, Austria
[4] Department of Transfusion Medicine, Paracelsus Medical Private University, Salzburg, Austria

nicole.maeding@pmu.ac.at

## INTRODUCTION

Acute myeloid leukemia (AML) is the most common type of acute leukemia in adults and in 2018 it claimed more than 10000 lives in the US only. Although 80-85% of patients show complete remission after initial treatment with anthracycline and cytarabine, the overall outcome remains poor (Moschoi et al., 2016). According to the National Cancer Institute of the US, 27.4% of people diagnosed with AML survive five or more years. AML is a cancer of the myeloid blood cell lineage exhibiting defective control of its proliferation, differentiation and maturation. It is widely accepted that it arises from the transformation of a single cell which is maintained by a small population of leukemia initiating cells (LICs). These LICs are hypothesized to instruct their **niche** directly or by secreting soluble factors and/or extracellular vesicles (EVs) to become **permissive** resulting in enhanced leukemia progression and relapse.

## HYPOTHESIS

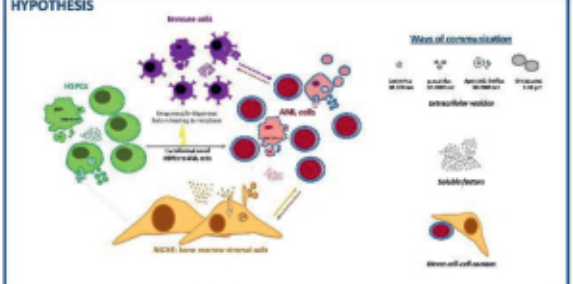


**Figure 1: AML cells communicate bi-directionally with their niche and the immune system in various ways**, including exchange of cell-derived matrix (adapted from Binder et al., 2017).

## METHODS

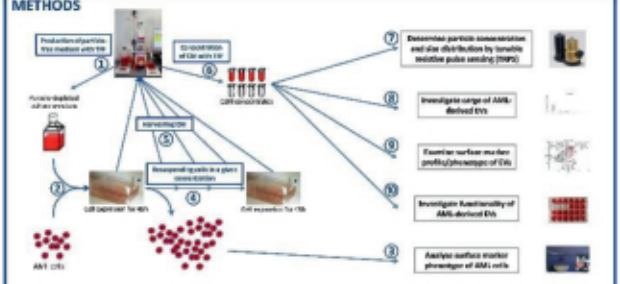

**Figure 2:** AML cells were grown in particle-depleted medium to exclude serum-derived particles and enable the characterization of cell-derived particles. Since the cell lines used reached confluency within 48 hours, cells were reseeded every 2 days at optimal density and conditioned media (CM) were pooled from several harvests. After collecting, concentrating and washing the CM with buffered saline solution, we performed in-depth characterization of the AML-derived EVs concerning their cargo, surface marker profile and functionality.

## QUANTITY & SIZE OF AML-DERIVED EVs

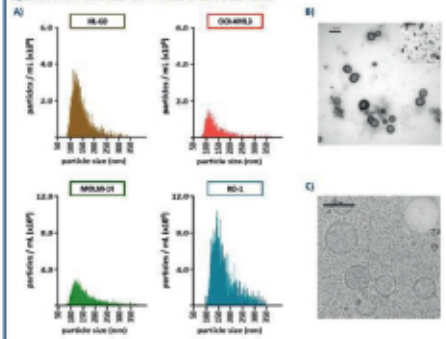


**Figure 3:** *A)* Size distribution and concentration of AML-derived particles measured by TRPS *B)* Transmission electron microscopy of MOLM-14 EVs *C)* Cryogenic electron microscopy of MOLM-14 EVs

## FUNCTION (IMMUNE RESPONSE & OSTEOGENESIS MODULATION)

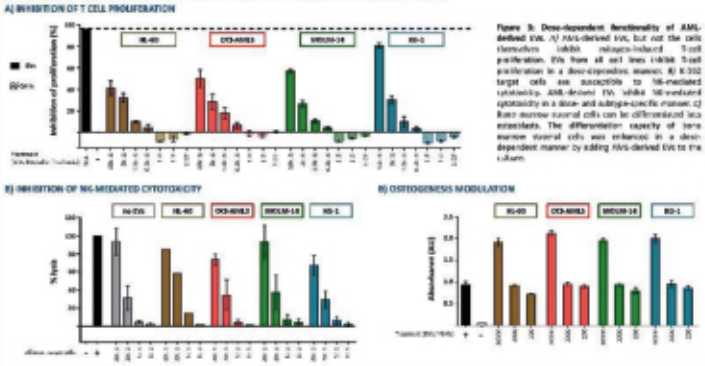


**Figure 4: Dose-dependent functionality of AML-derived EVs.** *A)* AML-derived EVs, but not the cells themselves, inhibit mitogen-induced T-cell proliferation. EVs from all cell lines inhibit T-cell proliferation in a dose-dependent manner. *B)* K-562 target cells are susceptible to NK-mediated cytotoxicity. AML-derived EVs inhibit NK-mediated cytotoxicity in a dose- and subtype-specific manner. *C)* Bone marrow stromal cells can be differentiated into osteoblasts. The differentiation capacity of bone marrow stromal cells was enhanced in a dose-dependent manner by adding AML-derived EVs to the culture.

## IMMUNE PHENOTYPE OF AML CELL LINES

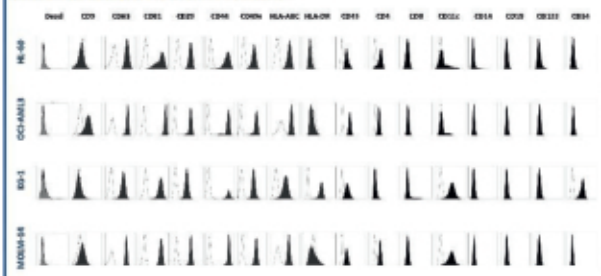


**Figure 5: The surface-marker phenotype of four AML cell lines** was analyzed by flow cytometry. We investigated various markers related to haematopoiesis (CD49, CD4, CD8, CD33c, CD14, CD15) and antigen presentation (HLA-ABC, HLA-DR), the leukemia-related marker CD133 and the hematopoietic stem/progenitor cell marker CD34. Black histograms show isotype, the respective antibody stain, while histograms are the corresponding isotype controls.

## IMMUNE PHENOTYPE OF AML derived EVs

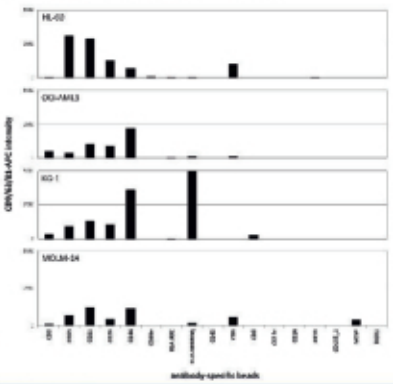


**Figure 6: Immune phenotype of AML-derived EVs.** Investigating the surface marker phenotype of EVs with MACS Plex® multiplex bead-based flow cytometer showed high expression levels of classical tetraspanins (CD81, CD63, CD9) as well as intercellular matrix interaction and adhesion proteins such as integrin β1 (CD29) and the hyaluronic receptor CD44. Differential expression among the AML cell line derived EVs was observed for the MHC class I and II markers (HLA-ABC and HLA-DRDQDP), neuro-/activin, melanoma-associated chondroitin sulphate proteoglycan (MCSP) and receptor tyrosine kinase like Orphan Receptor 1 (ROR1). The hematopoietic markers observed on cells were represented in most cases on EV surfaces (CD34, CD38, CD133). Interestingly, CD45, a marker of lymphocytes and CD11c, a marker of dendritic cells were exclusively expressed on cells, not on EVs.

## RNA CARGO OF AML-DERIVED EVs

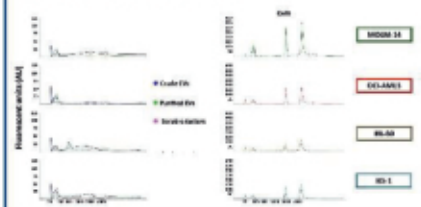


**Figure 7: AML-derived EV preparations contain small RNA species as well as longer RNA molecules,** including ribosomal RNA. Further investigations are needed to determine which molecules are inside the EVs and which ones are outside (associated with the EV corona), but protected.

## SUMMARY

- Acute myeloid leukemia (AML) cells secrete extracellular vesicles (EVs) and soluble factors into their environment. EV-containing conditioned medium can be purified by tangential flow filtration (TFF) to enrich particles in a given size and separate EVs from soluble factors.
- Different AML cell lines show limited variability in their immune phenotype.
- AML EVs display EV-specific surface markers including canonical tetraspanins, extracellular matrix interaction molecules and fibronectin receptors. The composition and expression levels of the detected surface markers reflected their AML cell line origin.
- AML-derived EVs contain high levels of small RNA species. Longer RNA molecules, including ribosomal RNAs show lower abundance compared to total the RNA profile of the cells, however they are still present in the EV preparations.
- AML-derived EVs, but not the cells exhibit immune modulation capacity in a dose-dependent manner. AML-derived EVs induce supra-optimum osteogenic differentiation in a dose-dependent manner.

## ACKNOWLEDGEMENTS

This work is part of a project that has received funding from the Cancer Cluster Salzburg (CCS) foundation.

## AML-derived extracellular vesicles convey immunomodulatory potential

Heide-Marie Binder[1], Nicole Maeding[1], Balazs Vari[1], Anna Raninger[1], Martin Wolf[1], Thomas Heuser[2], Astrid Obermayr[3], Gabriele Brachtl[1], Katharina Schallmoser[4], Dirk Strunk[1]

[1]Experimental and Clinical Cell Therapy Institute (ExCT), Spinal Cord Injury and Tissue Regeneration Center Salzburg (SCI-TreCS), Paracelsus Medical University, Salzburg, Austria; [2]Vienna Biocenter Core Facilities, Medical University, Vienna, Austria; [3]Department of Cell Biology, Biomedical Ultrastructure Research Group, University of Salzburg, Salzburg, Austria; [4]Department of Transfusion Medicine, Paracelsus Medical Private University, Salzburg, Austria; Contact: nicole.maeding@pmu.ac.at

### Objective
Acute myeloid leukemia (AML) cells can secrete trophic factors including extracellular vesicles (EVs) instructing the stromal leukemic niche. The mechanisms by which AML-derived EVs contribute to the immunosuppressive microenvironment and instruction of the leukemic niche remain poorly understood. We have previously observed immunomodulatory functions of different hematopoietic and non-hematopoietic cell-derived EVs. We therefore asked if AML-EVs can directly target immune cell functions.

### Methods
AML-derived EVs were obtained by large-scale culture of AML cell lines HL-60, MOLM-14, OCI-AML3 and KG-1, to collect conditioned medium. EVs were enriched >100x and separated from AML-derived soluble factors by two sequential rounds of tangential flow filtration (TFF). EVs were characterized by electron microscopy, immunoblotting and bead-based flow cytometry, confirming the double-membrane morphology, purity and identity. To highlight functional capacities, purified AML-derived EVs were used as active agent in assays interrogating immune modulation during T cell proliferation and NK cell-dependent cytotoxicity.

### Results
Purified EVs showed a significant dose-dependent inhibition of PHA-stimulated T cell proliferation that was not observed with AML cells or the isolated soluble factors. Furthermore, AML-derived EVs were able to reduce NK cell-mediated lysis of K-562 target cells in a calcein release assay, with the exception of MOLM14-derived EVs. In addition, osteogenic differentiation capacity of bone marrow stromal cells was increased by AML-EVs. Analysis of surface marker expression by MACSPlex for EVs and flow cytometry for AML cells showed a comparable pattern of immune-related surface markers, thus reflecting the AML cell origin of the investigated EVs. In contrast to AML cells, AML-derived EVs showed only miniscule levels of HLA-ABC (MHC I) which would be necessary for presentation of altered self. RNA cargo analysis of EVs using an Agilent Bioanalyzer revealed that AML-EVs contain small RNA species (e.g. miRNAs) as well as longer RNA molecules, albeit to a lesser extent.

### Conclusions
We show that AML-EVs, but not AML cells or their secreted soluble factors, inhibit T cell proliferation and NK cell functionality while enhancing osteogenic differentiation capacity of bone marrow stroma. These effects could contribute to the creation of a leukemia-permissive niche and immune escape of AML mediated by their EVs. The underlying molecular mechanisms need further investigation.2

# Die robotisch assistierte, bilaterale Fixation am Cooper Ligament (Pektopexie) zur Behandlung des apikalen Prolapses: Erstbeschreibung und Analyse der perioperativen Ergebnisse




D.I. Bolovis[1], W. Hitzl[2], C. Brucker[1]

[1]Klinik für Frauenheilkunde und Geburtshilfe, Universitätsklinik der Paracelsus Medizinischen Privatuniversität, Nürnberg; [2]Abteilung für Ophthalmologie und Optometrie, [2]Abteilung für Forschung und Innovation, Paracelsus Medizinische Privatuniversität, Salzburg


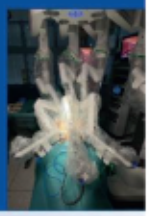

Senkungsbeschwerden des weiblichen Genitale betreffen 33-50% der Frauen. Für die definitive Therapie ist eine chirurgische Behandlung erforderlich. Die Sakrokolpopexie ist der Goldstandard zur anatomischen Prolapskorrektur seit den 1990er Jahren. Vor kurzem wurde die Pektopexie als neue Operationsmethode zur Behandlung des apikalen Deszensus etabliert (1). Die vorliegende Arbeit beschreibt erstmals das Verfahren als robotische Operation und stellt die Ergebnisse der ersten 30 Fälle vor.

## Fragestellung

Ziel dieser Arbeit ist die Etablierung der robotisch assistierten netzgestützten bilateralen Pektopexie sowie die klinische Analyse der perioperativen Ergebnisse bei einem nicht selektierten Patientinnen-Kollektiv. Es wird postuliert, dass die robotisch assistierte Pektopexie ein sicheres und effektives Operationsverfahren zur Korrektur des apikalen Prolapses darstellt.

## Methoden

Die Operation wurde unter Zuhilfenahme des da Vinci® OP-Roboters etabliert und anhand der ersten 30 Patientinnen, die im Zeitraum Januar 2018 bis Januar 2020 mit dieser neuen Methode behandelt wurden, im Rahmen einer retrospektiven klinischen Beobachtungsstudie evaluiert. Die Patientinnendaten wurden bezüglich des geschätzten Blutverlustes, der Operationsdauer sowie Komplikationen und Konversionen anhand der Krankenakte ausgewertet. Der Behandlungserfolg wurde nach 3-6 Monaten mit Hilfe eines Komposit-Endpunkts, bestehend aus anatomischen und subjektiven Parametern beurteilt (Tab. 1).

*Tab. 1: Komposit-Endpunkt zur Bewertung des Behandlungserfolgs (modifiziert nach 2)*

| Kriterium | Ergebnis bei Kontrolluntersuchung |
|---|---|
| Objektiver Befund | Ein POP-Q Stadium von ≤ 1 für den tiefsten Punkt der vorderen oder apikalen Scheidenwand |
| Subjektive Wahrnehmung | Abwesenheit von vaginalem Senkungsgefühl |
| Notwendigkeit Re-Operation | Keine Notwendigkeit für eine erneute Operation bei vorderem oder apikalem Deszensus |

*Abb. 1: Operationsschritte der robotischen Pektopexie*



*Abb. 1a: Eröffnen des Spatium vesikozervikale, Abschieben der Harnblase von der Zervix/Vagina.*
*Abb. 1b: Inzision des Peritoneums entlang des Lig. rotundum und Präparation in Richtung Lig. pektineum.*
*Abb. 1c: Legen eines Ethibond-Fadens am rechten Lig. Pektineum.*
*Abb. 1d: Die laterale Meshfixierung wird beidseits auf Höhe des M. psoas über dem Lig. pektineum durchgeführt.*

*Tab. 2: Zusätzliche chirurgische Maßnahmen im Hinblick auf die Art der robotischen Pektopexie (Hystero-, Zerviko- oder Vaginopektopexie)*

| | Hysteropektopexie (n=18) | Zervixpektopexie (n=6) | Vaginopektopexie (n=6) |
|---|---|---|---|
| Supracervicale HE | 0 (0%) | 6 (100%) | 0 (0%) |
| Vordere Plastik | 1 (5.6%) | 3 (50%) | 0 (0%) |
| Hintere Plastik | 1 (5.6%) | 3 (50%) | 1 (17%) |
| Perineoplastik | 1 (5.6%) | 2 (33%) | 1 (17%) |
| Burch Kolposuspension | 0 (0%) | 2 (33%) | 0 (0%) |
| Sakrospinale Fixation | 2 (0%) | 1 (17%) | 0 (0%) |
| Adnexektomie | 0 (0%) | 2 (33%) | 0 (0%) |
| Sakralgiektomie | 1 (5.6%) | 0 (0%) | 0 (0%) |
| Tubenligatur | 1 (5.6%) | 0 (0%) | 0 (0%) |
| Zystektomie | 1 (5.6%) | 0 (0%) | 0 (0%) |
| Abrasio | 1 (5.6%) | 0 (0%) | 0 (0%) |
| Vaginalpolyp | 0 (0%) | 0 (0%) | 1 (17%) |

*Abb. 2a: Whisker plot der Anzahl zusätzlicher Eingriffe bei der Zervikо-, Hystero- und Vaginopexie mit Mittelwert und 95% Konfidenzintervallen für den Mittelwert*
*Abb. 2b: Whisker plot der Operationsdauer bei der Zervikо-, Hystero- und Vaginopexie mit Mittelwert und 95% Konfidenzintervallen für den Mittelwert*

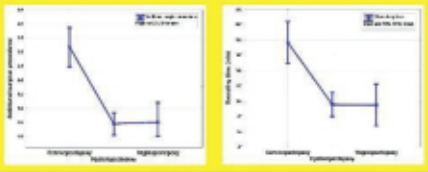

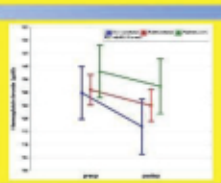

*Abb. 3: Veränderung der Hämoglobinwerte prä- und postoperativ im Hinblick auf die Art der Pektopexie*

*Whisker plot der Hämoglobinwerte prä- und postoperativ bei der Zervikо-, Hystero- und Vaginopexie mit Mittelwert und 95% Konfidenzintervallen für den Mittelwert*

*Tab. 3: Perioperative Befunde bei der robotischen Pektopexie mit Interventionsbedarf*

| Befund | Intervention | Status |
|---|---|---|
| postoperative Anämie | Bluttransfusion | ambulant |
| Beeinträchtigung des Plexus brachialis | MRT kein morphologisches Korrelat | Keine Residuen |
| Erhöhter Blutdruck | Passagere medikamentöse Behandlung | Keine Residuen |
| Persistierende Kopfschmerzen | CT, kein morphologisches Korrelat | Keine Residuen |


**References**

[1] Banerjee C, Noé KG: Laparoscopic pectopexy (2011) A new technique of prolapse surgery for obese patients. Arch Gynecol Obstet 284:631-635

2]Barber MD, Maher C. Epidemiology and outcome assessment of pelvic organ prolapse (2013) Int Urogynecol J 24(11):1783-1790


## Ergebnisse

Die Pektopexie wurde auf Basis der von Banerjee und Noe (1) beschriebenen Methode unter Verwendung eines vorgefertigten Netzes (DynaMesh®PRP) modifiziert für die Anwendung im robotischen Setting (Abb. 1). Bei uteriner Pathologie wurde zusätzlich eine suprazervikale Hysterektomie (LASH) durchgeführt. Bei der Operation wurden die präoperativ vorliegenden anatomischen Verhältnisse berücksichtigt.

Somit erhielten 18 Patientinnen mit unauffälligem Uterus eine Hysteropektopexie, 6 Patientinnen erhielten bei fehlendem Uterus eine Vaginopektopexie und weitere 6 Patientinnen eine Zervikopektopexie mit LASH. Bei insgesamt 14 Patientinnen wurden Zusatzeingriffe durchgeführt (Tab. 2), und dies hatte einen Einfluss auf die Operationsdauer (Abb. 2a,b) und den intraoperativen Blutverlust (Abb. 3). Perioperativ zeigten vier Patientinnen Befunde mit Interventionsbedarf (Tab. 3), die jedoch nicht in direktem Zusammenhang mit der Operationsmethode standen. Intraoperative Komplikationen oder Konversionen zum offenen Vorgehen traten nicht auf. Ein Behandlungserfolg im Sinne einer erfolgreichen Rekonstruktion des Beckenbodens wurde bei allen 30 Patientinnen (100%) entsprechend des Komposit-Endpunkts nachgewiesen.

## Schlussfolgerung

Zusammenfassend handelt es sich bei der Pektopexie um ein operatives Verfahren zur Korrektur des apikalen Deszensus. Die robotische Technik erlaubt dabei im Vergleich zur konventionellen Laparoskopie eine ideale anatomische Präparation und beseitigt den chirurgischen Kompromiss. Die Platzierung von Netz- und Nahtmaterial gelingt schnell und exakt, wodurch die Operationsdauer reduziert und das chirurgische Trauma minimiert wird. Die Technik ist sicher und die anatomischen Ergebnisse sind exzellent.

## Die robotisch assistierte, bilaterale Fixation am Cooper Ligament (Pektopexie) zur Behandlung des apikalen Prolapses: Erstbeschreibung und Analyse der perioperativen Ergebnisse

Dimitrios Ilias Bolovis[1], Cosima Brucker[1], W. Hitzl[2]

[1]Department of Gynaecologie, Paracelsus Medical University, Nuremberg, Germany; [2]Abteilung für Ophthalmologie, Universität Salzburg; Contact: dimitrios.bolovis@klinikum-nuernberg.de

### Objective

Pelvic organ prolapse affects 30-50% of the female population. For definitive treatment surgery is unavoidable. Sacrocolpopexy has been the gold standard for anatomical correction of pelvic organ prolapse since the 1990s. Recently, pectopexy has been introduced as a new surgical procedure to correct apical prolapse. We have translated the laparoscopic pectopexy into a robotic procedure.

### Methods

The method was established and the charts of the first 30 consecutive patients who underwent robotic pectopexy at the department for robotic and pelvic floor surgery were reviewed. All patients were analyzed for estimated blood loss, operation time, as well as complications. Treatment success was evaluated after 3-6 months using a composite endpoint including anatomical and subjective components.

### Results

Of the 30 patients analyzed, 18 underwent hysteropectopexy (n= 18), 6 patients underwent vaginopectopexy and 6 patients underwent cervicopectopexy. Additional procedures were performed in 14 patients, and this influenced operation time and intraoperative blood loss. No intraoperative complications were noted and no conversions were necessary. Treatment success according to the primary composite endpoint was achieved in 30 (100%) patients. Furthermore, neither de novo urgency nor obstructive bowel symptoms were noted in any if the patients treated with robotic pectopexy.

### Conclusions

Similar to Sacrocolpopexy, pectopexy is designed for prolapse repair. The robotic technique for pectopexy capitalizes on the advantages of robotic surgery as compared to conventional laparoscopy, since it allows for anatomical preparation and simplification of applying sutures and mesh material, reducing operating time and minimizing surgical trauma. The technique is safe, and anatomical outcomes are excellent.

### References

1. Hendrix SL, Clark A, Nygaard I, Aragaki A, Barnabei V, McTiernan A (2002) Pelvic organ prolapse in the Women's Health Initiative: gravity and gravidity. Am J Obstet Gynecol 186:1160-1166

# Status epilepticus outcome in patients with and without MRI abnormalities

**Bosque Varela P[1,2], Machegger L[3], Zimmermann G[4], Oellerer A[3], Steinbacher J[3], McCoy M[3], Pfaff J[3], Trinka E[1,2], Kuchukhidze G[1,2]**

[1] Department of Neurology, Christian Doppler Klinik, Affiliated Member of the European Reference Network EpiCARE, and Centre for Cognitive Neuroscience, Paracelsus Medical University of Salzburg, Austria

[2] Neuroscience Institute, Christian Doppler Klinik, Salzburg, Austria

[3] University Institute of Neuroradiology, Christian Doppler Klinik, Paracelsus Medical University of Salzburg, Austria

[4] Team Biostatistics and Big Medical Data, Intelligent Data Analytics Lab, Paracelsus Medical University of Salzburg, Austria

**Background**: Status epilepticus (SE) is a neurological emergency frequently associated with peri-ictal MRI abnormalities (PMA). PMA commonly include diffusion restriction, hyperperfusion and high signal in T2-weighted images (including FLAIR – fluid attenuated inversion recovery). PMA affect particular brain areas such as neocortex, pulvinar of thalamus, hippocampus, corpus callosum and cerebellum. PMA can be completely reversible or persist and be followed by permanent alterations such as cortical laminar necrosis, mesial temporal sclerosis and focal brain atrophy. The aim of this study was to compare the outcome of SE in patients with and without PMA.

**Methods:** We prospectively recruited 247 patients with SE at our institution between February 2019 and November 2020. In an acute phase (within 48 h after the onset of SE), 142/247 (57%) patients underwent MRI with a standard protocol due to their clinical needs. The MRI protocol included following sequences: diffusion weighted, T1-weighted with and without contrast application, FLAIR, arterial spin labelling (ASL), MR-perfusion and time of flight (ToF). All patients underwent thorough neurological examination and electroencephalography (EEG).

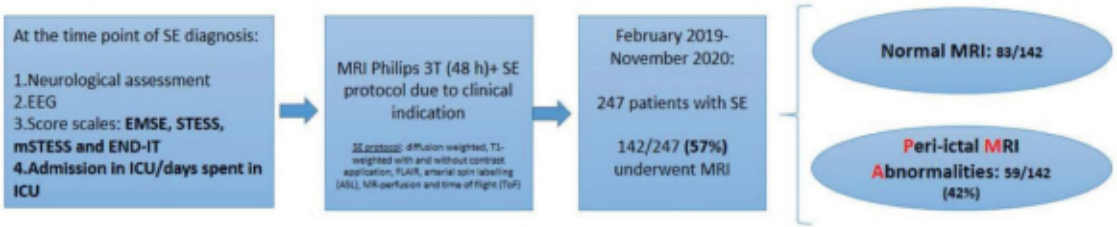


**Results:** PMA were observed in 59/142 (42%) of patients (51% female; mean age: 62yo; range: 19-93). In 83 (58%) of patients no PMA were seen. (36% female; mean age: 64,6 yo; range: 19-89). Mean values (with range) of STESS, mSTESS and EMSE did not differ in patients with PMA vs. patients without PMA: STESS (2.8, 0-6) vs. (2.8, 0-6) p=0.577; mSTESS (3.3, 0-7) vs. (3.2, 0-7) p=0.629; EMSE (49.1, 4-153) vs. (43.6, 4-113) p=0.631.

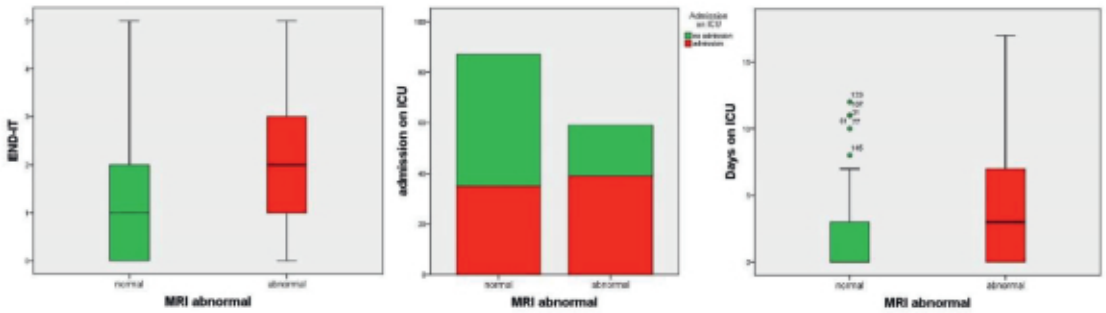


Fig. END-IT score was significantly higher (p<0.001) in patients with PMA (mean 2.4, range 0-5) compared to patients without (mean 1.3, range 0-5). More patients with PMA (38/59; 64%) were admitted on ICU as compared to those without PMA (33/83; 40%) (p=0.004). Patients with PMA spent significantly more days on ICU (mean 4.9, SD 8.3) as compared to those without (mean 3.1, SD 7.2) (p=0.006).

**Conclusions:** MRI abnormalities in patients with SE are associated with worse outcome, need of admission on ICU and longer duration of treatment there. Acute changes in MRI may serve as prognostic biomarker in patients with SE.

**Acknowledgments:** Dr. Bosque-Varela P. has received a 2-year grant by Alfonso Martin Escudero fundation (Madrid, Spain)

## Status epilepticus outcome in patients with and without MRI abnormalities

Pilar Bosque Varela[1,2], Lukas Machegger[3], Georg Zimmermann[4], Andreas Oellerer[3], Jürgen Steinbacher[3], Mark McCoy[2], Johannes Pfaff[3], Eugen Trinka[1,2], Giorgi Kuchukhidze[1,2]

[1]Department of Neurology, Christian Doppler Klinik, Affiliated Member of the European Reference Network EpiCARE, and Centre for Cognitive Neuroscience, Paracelsus Medical University of Salzburg, Austria; [2]Neuroscience Institute, Christian Doppler Klinik, Salzburg, Austria; [3]University Institut of Neuroradiology, Christian Doppler Klinik, Paracelsus Medical University of Salzburg, Austria; [4]Team Biostatistics and Big Medical Data, Intelligent Data Analytics Lab, Paracelsus Medical University of Salzburg, Austria; Contact: pilar.bosquev@gmail.com

### Objective
Status epilepticus (SE) is a neurological emergency frequently associated with peri-ictal MRI abnormalities (PMA) including diffusion restriction, hyperperfusion and high signal in T2-weighted images (including FLAIR). PMA can be completely reversible or persistent. It can be followed by permanent alterations such as cortical laminar necrosis, mesial temporal sclerosis and focal brain atrophy. We aimed comparing the outcome of SE in patients with and without PMA

### Methods
We prospectively recruited 247 patients with SE between February 2019 and November 2020. 142/247 (57%) patients underwent MRI within 48 h after the onset of SE.
SE-outcome scores as well as admission to intensive care unit (ICU) and days spent at the ICU were compared in two groups of patients: those with and without PMA

### Results
PMA was observed in 59/142 (42%) of patients (51% female; mean age 62.0 years, range 19-93 years). In 83 (58%) of patients no PMA were seen (36% female; mean age 64.6 years, range 19-89 years).
Mean values (with range) of STESS, mSTESS and EMSE did not differ in patients with PMA vs. patients without PMA: STESS (2.8, 0-6) vs. (2.8, 0-6) $p=0.577$; mSTESS (3.3, 0-7) vs. (3.2, 0-7) $p=0.629$; EMSE (49.1, 4-153) vs. (43.6, 4-113) $p=0.631$. END-IT score was significantly higher ($p<0.001$) in patients with PMA (mean 2.4, range 0-5) compared to patients without (mean 1.3, range 0-5). More patients with PMA (38/59; 64%) were admitted to ICU as compared to those without PMA (33/83; 40%) ($p=0.004$). Patients with PMA spent significantly more days in ICU (mean 4.9, SD 8.3) as compared to those without (mean 3.1, SD 7.2) ($p=0.006$).

### Conclusions
MRI abnormalities in patients with SE are associated with worse outcome, need of admission to ICU and longer duration of treatment there. Acute changes in MRI may serve as prognostic biomarker in patients with SE

# Identification of microRNA as regulating somatic factors of adaptive coping in patients with fibromyalgia syndrome

Braun A [1], Evdokimov D [2], Frank J [2], Sommer C [2], Üçeyler N [2]

[1] Clinic of Psychosomatic Medicine and Psychotherapy, Paracelsus Medical Private University, Nürnberg, Germany | [2] Neurological Clinic and Policlinic, Department of Neurology, University Clinic, Würzburg, Germany

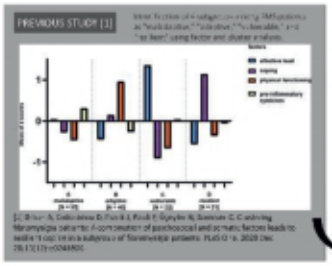


BACKGROUND

SUBJECTS AND METHODS

32 FMS patients

16 healthy controls

MicroRNA (miRNA) mainly inhibit post-transcriptional gene expression of specific targets and may modulate disease severity.

miR103a-3p
miR107
miR130a-3p
miR125a-5p

in white blood cell (WBC) RNA

***Identification of cluster specific miRNA signatures related to resilience and disability potentially usable as diagnostic tool***

RESULTS

**Figure 1: Gene expression between patients and controls.**

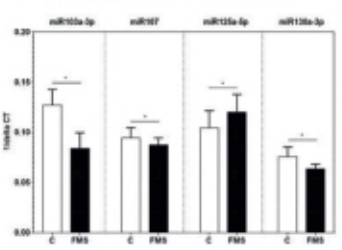


Lower relative gene expression levels of miR103a-3p, miR107, and miR130a-3p in patients (FMS) compared to healthy controls (C), except for miR125a-5p.

STRUCTURE

**Table 1:** Relative gene expression of miRNA was correlated with clinical scores of pain, stress, and resilience - related questionnaires.

| miR | Clinical score | r |
|---|---|---|
| miR103a-3p | HQ | 0.4* |
| miR107 | CTQ physical abuse | -0.5* |
| miR125a-5p | PCS | 0.4* |

*Spearman coefficient r
**Significance level p < 0.05
Gene expression of miR-1 Pro-3p was associated with the sum score of the PCS questionnaire (r = 0.4, p < 0.05).
HQ: Hannover Questionnaire / CTQ: Childhood Trauma Questionnaire, subscale physical abuse / PCS: Pain Catastrophizing Questionnaire

**Figure 2: Gene expression among patient clusters.**

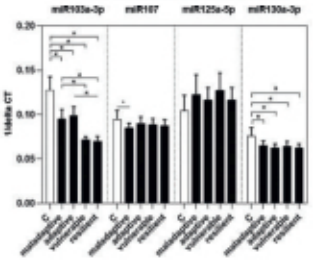


MiR103a-3p is differential expressed among individual clusters. Mean miR107 gene expression did not differ among clusters but tended to be higher in the adaptive cluster. Since miR107 forms a family with miR103 and has valid data for influence on inflammation and adaptation we included it to the synopsis.

CONCLUSION

SYNOPSIS

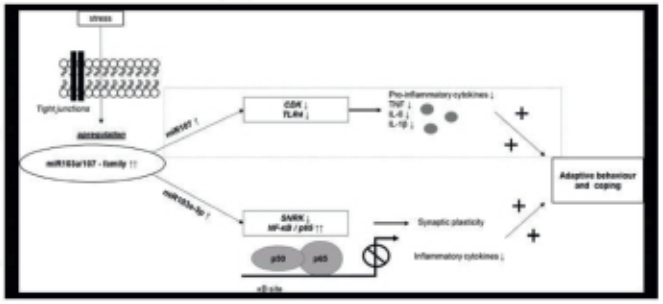


Upregulation of miR103a-3p and miR107 in the adaptive cluster of FMS patients might promote adaptive behavior by targeting genes which are involved in signaling cascades. We speculate that higher miR107 gene expression may lead to lower expression of CDK (cyclin dependent kinases) and TLR4 (Toll like receptor 4) resulting in low pro-inflammatory cytokine levels. A pro-inflammatory profile may lead to depressive behavior whereas low levels of pro-inflammatory cytokines favor permissive behavior. MiR103a-3p is linked to stress and inflammation by regulating the SNRK / NF-κB / p65 signaling pathway. Higher gene expression of miR103a-3p may lead to suppression of sucrose non-fermentable serine/threonine protein kinase (SNRK) and ultimately lead to an over-activation of the transactivating subunit protein 65 (p65) of nuclear factor kappa B (NF-κB). NF- κB was reported to be linked to epigenetic resilience promoting mechanisms and synaptic plasticity resulting in adaptive processes.

## Identification of microRNA as regulating somatic factors of adaptive coping in patients with fibromyalgia syndrome

Alexandra Braun[1], Dimitar Evdokimov[2], Johanna Frank[2], Claudia Sommer[2], Nurcan Üçeyler[2]

[1]Clinic of Psychosomatic Medicine and Psychotherapy, Paracelsus Medical Private University, Nürnberg, Germany; [2]Neurological Clinic and Policlinic, Department of Neurology, University Clinic, Würzburg, Germany; Contact: Alexandra.Braun@klinikum-nuernberg.de

### Objective
Identification of cluster specific miRNA signatures related to resilience and disability.

### Methods
A previous study identified 4 subgroups among FMS patients and characterized them as "maladaptive," "adaptive," "vulnerable," and "resilient" using factor and cluster analysis [1]. Thirty-two FMS patients and sixteen healthy controls were selected to analyze the relative gene expression of miR103a-3p, miR107, miR130a-3p and miR125a-5p in white blood cell (WBC) RNA. The relative gene expression of miRNA was correlated with clinical scores of pain, stress, and resilience-related questionnaires. Potential target genes of the selected miRNA were determined with the online tool "Target Scan Human" and a cluster-specific miRNA-mediated regulation scheme was created.

### Results
MiR103a-3p, miR107 and miR130a-3p were lower expressed in FMS patients compared to healthy controls ($p < 0.05$). The highest relative gene expression was shown by miR103a in the adaptive cluster ($p < 0.05$), the patient group with the lowest disability in all symptom categories, and correlated with disease-related disability ($p < 0.05$). MiR107 tended to slightly increased expression in the adaptive cluster and correlated with the total score of the trauma questionnaire "physical abuse" ($p < 0.05$). Target Scan Human" identified serine / threonine protein kinase (SNRK), nuclear factor kappa-b, cyclin-dependent kinase (CDK) and toll-like receptor 4 (TLR4) as target genes of the miR103a/107 miRNA family.

### Conclusions
We show an association between upregulated gene expression of miR103a, tending to include miR107, and adaptive coping in FMS patients. Validation of this miRNA family might lead to the identification of a somatic resilience factor in FMS.

### References
1. Braun A, Evdokimov D, Frank J, Pauli P, Üçeyler N, Sommer C. Clustering fibromyalgia patients: A combination of psychosocial and somatic factors leads to resilient coping in a subgroup of fibromyalgia patients. PLoS One. 2020 Dec 28;15(12):e0243806.

PARACELSUS MEDIZINISCHE PRIVATUNIVERSITÄT

Klinikum Nürnberg
wir sind für Sie da.

Contact: tobias.braun@klinikum-nuernberg.de
maria.kokozidou@pmu.ac.at

Science Get Together, 2021
Nuremberg, Germany

# The effect of Matrix, Admedus patches and Inspiris aortic valve materials on primary human endothelial cells from the great saphenous vein

**Tobias Braun[1]*, Maria Kokozidou[2]*, Julia Mladek[2], Gundula Schulze-Tanzil[2], Theodor Fischlein[1]**

[1] Department of Cardiac Surgery (Cardiovascular Center), Klinikum Nürnberg, Paracelsus Medical University, Nuremberg, Germany
[2] Institute for Anatomy, Paracelsus Medical University, Nuremberg, Germany
* The authors have equally contributed

## Objective

Heart disease remains a leading problem for the public health. Ischaemic injuries and myocardial infarction can cause irreversible damage of the heart tissue. Several cell types have been used to study cellular retention and vascularisation of cardiac paches in order to benefit heart ischaemic injury. We used the Matrix and Admedus patches and the Inspiris aortic valve graft to explore the adhesion of primary human endothelial cells (ECs) isolated from the great saphenous vein (GSV).

## Methods

1. Primary human endothelial cells (hECs) were isolated from GSV (Ethic Commission No. 15073) and cultivated in culture medium (CM) to 80-90% confluence.
2. 18.000 cells were seeded onto round patch sections (Ø 6 mm) from Matrix, Admedus patches and Inspiris aortic valve and grown in culture medium (CM) in a 96-well plate. After 24 h, 7 d, 10 d and 14 d, the colonized patch surface area was documented using live-dead staining under a Confocal Laser-Scanning-Microscope. Pictures were analysed using Image J. Fixed patches (cross sections) were stained with DAPI to evaluate the depth of penetration of hECs into the different patch materials.
3. Extracts (48 h) of possible toxins of the three patch materials were prepared in CM. Following hECs (n=3) and L929 mouse fibroblast cell line (n=1) were seeded into a 96-well plate, 10.000/well (triplicates) and were allowed to adhere for 24 h. Consequently, the cells were incubated with the extracts for a further 24 h. Cell viability was determined using CellTiter 96® AQueous One Solution Cell Proliferation Assay (MTS, Promega).

## Results

All Patch materials were colonized to a certain degree (Figure 2A a-i). There where no significant differences between the materials used, nevertheless Matrix was the one that increased its colonised surface steadily till 14 d compared to Inspiris and Admedus (Figure 3 A).
DAPI staining of cross sections showed no ingrowth into the Patch materials for all materials (Figure 2 B a-f), but a gradually increased cell-layer thickness from 1 d to 14 d for the Matrix Patch material (Figure 2 B a-b).
The MTS assay revealed high metabolic activity for hECs and the L929 on both materials, Matrix and Admedus.

## Conclusion

Matrix patch material is a material that allows a steady colonization with hECs and it shows to have no cytotoxic effects on them. More research is necessary for all materials to explore their promising ability to be colonized by hECs along with their vascularization potential.

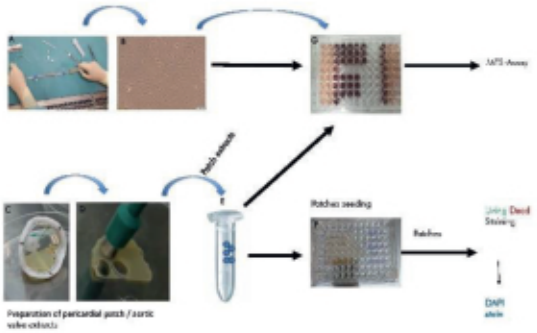


**Figure 1 Work flow chart of the experiments:** primary ECs were isolated from GSV and were cultured in CM (A-B). The patch materials from Matrix, Admedus and Inspiris aortic valve were dissected onto round patch sections (Ø 6mm) (C-D) and were allowed to extract (48 h) their possible toxins (E). ECs were seeded on the patch sections (F) and cultured for 24 h, 7 d, 10 d and 14 d and then processed to Living/Dead and DAPI staining. ECs and L929 cells were cultured in a 96-well plate and incubated with the patch extracts (G). MTS assay followed. ECs: endothelial cells, L929: mouse fibroblast cell line.

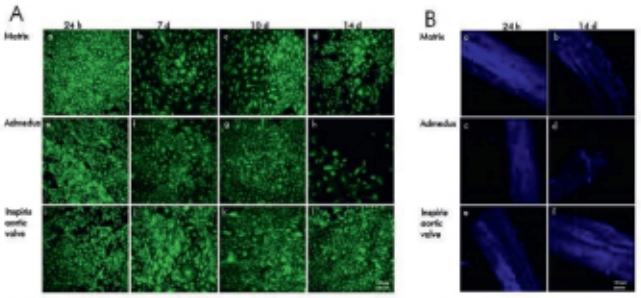


**Fig 2 A: Living/dead staining of the hECs** on patch materials, Matrix (a-d), Admedus (e-h), Inspiris aortic valve (i-l). Patches were photographed after 24h, 7 d, 10 d and 14 d (A: a-l). **B: DAPI staining of the paches' sections from** A, for Matrix (a-b), Admedus (c-d) and Inspiris aortic valve (e, f), at time points 24 h & 14 d. hECs: primary human endothelial cells. Scale bars:100 µm

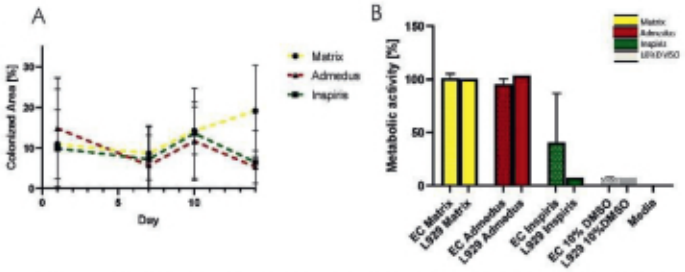


**Figure 3:** Charts show hECs confluence rates (%) depending on the patch material and time point (A) and MTS-Assay to evaluate cytotoxicity of patch extracts compared on hECs and L929 (B). hECs: primary human endothelial cells, L929: mouse fibroblast cell line.

This study was financed by Manfred Roth foundation.

## The effect of Matrix, Admedus patches and Inspiris aortic valve materials on primary human endothelial cells from the great saphenous vein

Tobias Braun[1], Maria Kokozidou[2], Julia Mladek[1], Gundula Schulze-Tanzil[2], Theodor Fischlein[1]

[1]Department of Cardiac Surgery (Cardiovascular Center), Klinikum Nürnberg, Paracelsus Medical University, Nuremberg, Germany; [2]Institute of Anatomy and Cell Biology, Paracelsus Medical University, Nuremberg, Germany; Contact: maria.kokozidou@pmu.ac.at

### Objective
Heart disease remains a leading problem for the public health. Ischaemic injuries and myocardial infarction can cause irreversible damage of the heart tissue. Several cell types have been used to study cellular retention and vascularisation of cardiac paches in order to benefit heart ischaemic injury. We used the Matrix and Admedus patches and the Inspiris aortic valve graft to explore the adhesion of primary human endothelial cells (ECs) isolated from the great saphenous vein (GSV).

### Methods
a) Primary human endothelial cells (hECs) were isolated from GSV (Ethic Commission No. 15073) and cultivated in culture medium (CM) to 80-90% confluence.

b) 18.000 cells were seeded onto round patch sections (Ø 6 mm) from Matrix, Admedus patches and Inspiris aortic valve and grown in culture medium (CM) in a 96-well plate. After 24 h, 7 d, 10 d and 14 d, the colonized patch surface area was documented using live-dead staining under a Confocal Laser-Scanning-Microscope. Pictures were analysed using Image J. Fixed patches (cross sections) were stained with DAPI to evaluate the depth of penetration of hECs into the different patch materials.
c) Extracts (48 h) of possible toxins of the three patch materials were prepared in CM. Following hECs (n=3) and L929 mouse fibroblast cell line (n=1) were seeded into a 96-well plate, 10.000/well (triplicates) and were allowed to adhere for 24 h. Consequently, the cells were incubated with the extracts for a further 24 h. Cell viability was determined using CellTiter 96® AQueous One Solution Cell Proliferation Assay (MTS, Promega)

### Results
All patch materials were colonized to a certain degree. There were no significant differences between the materials used, nevertheless, Matrix was the one that increased its colonised surface steadily till 14 d compared to Inspiris and Admedus.
DAPI staining of cross sections showed no ingrowth into the patches for all materials tested, but a gradually increased cell-layer thickness from 1 d to 14 d for the Matrix patch material.
The MTS assay revealed high metabolic activity for hECs and the L929 on both patch materials, Matrix and Admedus.

### Conclusions
Matrix patch material is a material that allows a steady colonization with hECs and it shows to have no cytotoxic effects on them. More research is necessary for all materials to explore their promising ability to be colonized by hECs along with their vascularization potential.

### References
1. no references

PARACELSUS MEDIZINISCHE PRIVATUNIVERSITÄT

Klinikum Nürnberg

# Das Dilemma der nekrotisierenden Fasziitis

**D. Breidung, A. Barth, M. Billner, A. Marti, B. Reichert**

Universitätsklinik für Plastische, Wiederherstellende und Handchirurgie, Zentrum für Schwerbrandverletzte,
Paracelsus Medizinische Privatuniversität - Klinikum Nürnberg

## Einleitung

Bei der nekrotisierenden Faszitis (NF) handelt es sich um eine lebensbedrohliche Weichteilinfektion. Eine frühe Diagnosestellung ist hierbei von entscheidender Bedeutung und beeinflusst maßgeblich das klinische Outcome. Die klinischen Zeichen und Symptome einer NF (Tabelle 2) sind häufig nicht eindeutig und erlauben keine Diagnosestellung basierend auf diesen allein. Der LRINEC Score wurde von Wong et al. 2004 vorgestellt und soll als Hilfestellung für die Operationsindikation dienen. Die Parameter des LRINEC Scores, sowie deren Gewichtung sind in Tabelle 1 dargestellt. Anhand der Score-Punkte erfolgt eine Einteilung in Risikogruppen. Ein LRINEC Score < 6 bedeutet ein niedriges Risiko (<50%) für das Vorliegen einer nekrotisierenden Fasziitis, ein Score von 6-7 ein moderates Risiko (50-75%) sowie ein Score ≥8 ein hohes Risiko (>75%), was eine operative Diagnosesicherung unabdingbar macht.

## Material

Es erfolgte eine retrospektive Analyse von Patienten mit einer histologisch bestätigten nekrotisierenden Fasziitis, welche auf unserer Abteilung für Plastische Chirurgie behandelt wurden. Dabei wurden demographische Daten, Komorbiditäten, Laborwerte sowie klinische Parameter ausgewertet. Es konnten 123 Fälle nekrotisierender Faszitis sowie 262 Fälle chirurgisch behandelter Weichteilinfektionen als Kontrollgruppe, in die Studie inkludiert werden. Als Einschlusskriterium in der Kontrollgruppe galt eine Weichteilinfektion mit einer Operationsdauer von mindestens 60 Minuten sowie eine intravenöse Antibiotikatherapie. Beide Gruppen wurden miteinander verglichen und der LRINEC Score hinsichtlich seiner Aussagekraft über das Vorliegen einer NF untersucht.

| Variable | Wert | Score |
|---|---|---|
| **C-reaktives Protein, mg/dl** | <15 | 0 |
| | ≥15 | 4 |
| **Leukozyten, pro mm²** | <15 | 0 |
| | 15-25 | 1 |
| | >25 | 2 |
| **Hämoglobin, g/dl** | >13,5 | 0 |
| | 11-13,5 | 1 |
| | <11 | 2 |
| **Natrium, mmol/l** | ≥135 | 0 |
| | <135 | 2 |
| **Kreatinin, mg/dl** | ≤1,6 | 0 |
| | >1,6 | 2 |
| **Glukose, mg/dl** | ≤180 | 0 |
| | >180 | 1 |

Tabelle 1. Der LRINEC Score (vorgestellt von Wong et al.)

**Klinische Manifestationen**

- Schmerzen und Druckempfindlichkeit
- Bullae (Blasenbildung)
- Rötung – livide Verfärbung
- Überwärmung
- Hautnekrose
- Schwellung
- Fieber
- Tachykardie
- Hypotension
- Dyspnoe

Tabelle 2. Klinische Manifestationen einer nekrotisierenden Fasziitis




Abbildung 1. (A) Präoperativer Befund einer nekrotisierenden Fasziitis (B) Intraoperativer Befund



Abbildung 2. Lytische Faszie als Zeichen des Infektes

## Ergebnisse

Die Mortalitätsrate beträgt in unserer Studie 14%. In den meisten Fällen nekrotisierender Fasziitis konnte eine Mischinfektion (32%) mit mehreren Erregern nachgewiesen werden. Die häufigsten Erreger waren Bakterien der Staphylokokkus oder Streptokokkus Gattung (24%).

Die Lokalisationen der Fälle von nekrotisierender Fasziitis waren in absteigender Häufigkeit: untere Extremität (42%), obere Extremität (22%), Perineum/Genital (20%), Oberkörper (4%) sowie Hals (1%). In 11% der Fälle waren mehrere Körperregionen betroffen.

Die Auswertung der diagnostischen Gütekriterien des LRINEC Scores, eine Evaluation des Scores zur Prognose des Krankheitsverlaufes sowie eine biostatistische Analyse der Komorbiditäten sind noch ausstehend und sind für die nächsten Monate geplant.

## Diskussion

In anderen Studien aus den USA und Europa zeigten sich ebenfalls Gram-positive Bakterien als häufigste Erreger während sich im asiatischen Raum Mikroorganismen aus dem Gram-negativen Bereich (insbesondere Bakterien der Gattung Vibrio und Aeromas) aus NF-Kulturen isolieren ließen. Infektionen durch Gruppe-A-Streptokokken (GAS) gelten als besonders bedrohlich und gehen mit einer hohen Mortalität einher.

Die frühzeitige Diagnosesicherung und rasche Entfernung des nekrotisierenden Weichteilgewebes stellen den wichtigsten Faktor für das Outcome des Patienten dar. Vor allem bei klinisch nicht eindeutigen Weichteilinfektionen dient der Score als eine gute Hilfestellung für den Chirurgen. Anhand der Erregerstatistik kann eine kalkulierte Antibiotikatherapie bei Diagnosestellung begonnen werden. Mit den zukünftigen Ergebnissen der Studie erhoffen wir eine Überprüfung des Scores für den klinischen Einsatz sowie bei unbefriedigenden Ergebnissen, Anhaltspunkte für Verbesserungen des Scoring-Systems zu erhalten.

Literatur

1. Gelbard RB, Ferrada P, Yeh DD, et al. Optimal timing of initial debridement for necrotizing soft tissue infection: A Practice Management Guideline from the Eastern Association for the Surgery of Trauma. J Trauma Acute Care Surg. 2018;85(1):208-214. doi:10.1097/TA.0000000000001857
2. Wong C-H, Khin L-W, Heng K-S, Tan K-C, Low C-O. The LRINEC (Laboratory Risk Indicator for Necrotizing Fasciitis) score: a tool for distinguishing necrotizing fasciitis from other soft tissue infections. Crit Care Med. 2004;32(7):1535-1541. doi:10.1097/01.ccm.0000129486.35458.7d
3. Goh T, Goh LG, Ang CH, Wong CH. Early diagnosis of necrotizing fasciitis. Br J Surg. 2014;101(1):e119-125. doi:10.1002/bjs.9371
4. Wang J-M, Lim H-K. Necrotizing fasciitis: eight-year experience and literature review. Braz J Infect Dis Off Publ Braz Soc Infect Dis. 2014;18(2):137-143. doi:10.1016/j.bjid.2013.06.003
5. Leitch HA, Palopu A, Fernandes CM. Necrotizing fasciitis secondary to group A streptococcus. Morbidity and mortality still high. Can Fam Physician. 2000;46:1460-1466.

## Das Dilemma der nekrotisierenden Fasziitis

David Breidung[1], André Barth[1], Moritz Billner[1], Alejandro Marti[1], Bert Reichert[1]

[1]Department of Plastic, Reconstructive and Hand Surgery, Center of Severe Burn Injuries Nuremberg General Hospital, Paracelsus Medical University Nuremberg, Germany; Contact: david.breidung@icloud.com

### Objective
Überprüfung des Laboratory risk indicator for necrotizing fasciitis (LRINEC) Scores zur Differenzierung von Fällen nekrotisierender Fasziitis und anderen Weichteilinfektionen.

### Methods
Es erfolgte eine retrospektive Analyse von Patienten mit einer histologisch bestätigten nekrotisierenden Fasziitis, welche auf unserer Abteilung für Plastische Chirurgie behandelt wurden. Dabei wurden demographische Daten, Komorbiditäten, Laborwerte sowie klinische Parameter ausgewertet. Es konnten 123 Fälle nekrotisierender Fasziitis sowie 262 Fälle chirurgisch behandelter Weichteilinfektionen in die Studie inkludiert werden. Als Einschlusskriterium in der Kontrollgruppe galt eine Weichteilinfektion mit einer Operationsdauer von min. 60 Minuten sowie eine intravenöse Antibiotikatherapie. Beide Gruppen wurden miteinander verglichen und der LRINEC Score hinsichtlich seiner Aussagekraft über das Vorliegen einer NF untersucht.

### Results
Die Mortalitätsrate beträgt in unserer Studie 14%. In den meisten Fällen nekrotisierender Fasziitis konnte eine Mischinfektion (32%) mit mehreren Erregern nachgewiesen werden. Die häufigsten Erreger waren Bakterien der Staphylokokkus oder Streptokokkus Gattung (24%). Die häufigste Lokalisation war die untere Extremität. In 11% der Fälle waren mehrere Körperregionen betroffen. Die Auswertung der diagnostischen Gütekriterien des LRINEC Scores, eine Evaluation des Scores zur Prognose des Krankheitsverlaufes sowie eine biostatistische Analyse der Komorbiditäten sind noch ausstehend und sind für die nächsten Monate geplant.

### Conclusions
Die frühzeitige Diagnosesicherung und rasche Entfernung des nekrotisierenden Weichteilgewebes stellen den wichtigsten Faktor für das Outcome des Patienten dar. Vor allem bei klinisch nicht eindeutigen Weichteilinfektionen dient der Score als eine gute Hilfestellung für den Chirurgen. Anhand der Erregerstatistik kann eine kalkulierte Antibiotikatherapie bei Diagnosestellung begonnen werden. Mit den zukünftigen Ergebnissen der Studie erhoffen wir eine Überprüfung des Scores für den klinischen Einsatz in der Notaufnahme sowie bei unbefriedigenden Ergebnissen, Anhaltspunkte für Verbesserungen des Scoring-Systems zu erhalten.

### References
1. Gelbard RB, Ferrada P, Yeh DD, et al. Optimal timing of initial debridement for necrotizing soft tissue infection: A Practice Management Guideline from the Eastern Association for the Surgery of Trauma. J Trauma Acute Care Surg. 2018;85(1):208-214. doi:10.1097/TA.0000000000001857
2. Wong C-H, Khin L-W, Heng K-S, Tan K-C, Low C-O. The LRINEC (Laboratory Risk Indicator for Necrotizing Fasciitis) score: a tool for distinguishing necrotizing fasciitis from other soft tissue infections. Crit Care Med. 2004;32(7):1535-1541. doi:10.1097/01.ccm.0000129486.35458.7d
3. Goh T, Goh LG, Ang CH, Wong CH. Early diagnosis of necrotizing fasciitis. Br J Surg. 2014;101(1):e119-125. doi:10.1002/bjs.9371
4. Wang J-M, Lim H-K. Necrotizing fasciitis: eight-year experience and literature review. Braz J Infect Dis Off Publ Braz Soc Infect Dis. 2014;18(2):137-143. doi:10.1016/j.bjid.2013.08.003
5. Leitch HA, Palepu A, Fernandes CM. Necrotizing fasciitis secondary to group A streptococcus. Morbidity and mortality still high. Can Fam Physician. 2000;46:1460-1466.

# Treatment of psoriasiform-like skin inflammation with diacerein influences skin and spleen immune cell subpopulations

Susanne M. Brunner[1,2], Andrea Ramspacher[1], Caroline Rieser[1], Julia Leitner[1], Hannah Heil[1], Barbara Kofler[1], Roland Lang[3], Verena Wally[4]

[1]RESEARCH PROGRAM FOR RECEPTOR BIOCHEMISTRY AND TUMOR METABOLISM, DEPARTMENT OF PEDIATRICS, PARACELSUS MEDICAL UNIVERSITY, SALZBURG, AUSTRIA; [2]RESEARCH PROGRAM FOR EXPERIMENTAL OPHTHALMOLOGY, DEPARTMENT OF OPHTHALMOLOGY AND OPTOMETRY, PARACELSUS MEDICAL UNIVERSITY, SALZBURG, AUSTRIA; [3]DEPARTMENT OF DERMATOLOGY, PARACELSUS MEDICAL UNIVERSITY, SALZBURG, AUSTRIA; [4]EB HOUSE AUSTRIA, RESEARCH PROGRAM FOR MOLECULAR THERAPY OF GENODERMATOSES, DEPARTMENT OF DERMATOLOGY AND ALLERGOLOGY, UNIVERSITY HOSPITAL OF THE PARACELSUS MEDICAL UNIVERSITY SALZBURG, AUSTRIA.

## OBJECTIVE

Psoriasis is an inflammatory skin disease characterized by increased neo-vascularization, keratinocyte hyperproliferation, a proinflammatory cytokine milieu and immune cell infiltration.[1] Diacerein is an anti-inflammatory drug, currently approved for the treatment of osteoarthritis. Diacerein has an impact on several proinflammatory cytokines, like IL-1ß, IL-6 and TNFα, in different diseases like epidermolysis bullosa simplex and diabetes.[2,3] Therefore, we hypothesized that topical application of diacerein has beneficial effects on the course of psoriasis. The aim of the present study was to elucidate the ability of topical diacerein to delay or reduce the severity of psoriasis in a mouse model of psoriasiform-induced inflammation.

## METHODS

To induce psoriasiform inflammation, the shaved and depilated dorsal skin of mice (C57BL/6N males, 9 weeks old) was treated daily with 62.5 or 80 mg Aldara cream (5% imiquimod, IMQ) or vehicle for 3 or 6 consecutive days. At least 6 hours after IMQ administration, 100 mg of a diacerein cream (2.5%, 5% or 10%) or placebo cream was applied topically, or the skin was left untreated. Macroscopic images of the skin were recorded daily and erythema, scaling, and thickening were scored independently on a scale from 0 to 4 in a double-blinded fashion. The cumulative score (scale 0–12) served as an indicator for clinical severity. At sample collection, mice were euthanized and the spleen was excised and weighed. Single cell suspensions were obtained from treated skin areas and spleens for further flow cytometry analyses.[4]

## RESULTS

- Daily treatment with IMQ increased the severity score compared to vehicle treatment. However, topical application of diacerein did not influence the severity of the inflammation compared to placebo treatment (Fig. 1).
- At day 4, flow cytometry analysis of the skin revealed that IMQ reduced the fraction of live CD4⁺ and CD8⁺ T cells but increased the fraction of neutrophils, NK cells, eosinophils and CD11b⁺ myeloid cells compared to vehicle-treated skin (Fig. 2A-F). Remarkably, 10% diacerein significantly diminished the fraction of CD11b⁺ CD11c⁺ myeloid dendritic cells in the IMQ-treated skin compared to placebo control (Fig. 2G).
- At day 7, treatment with a 10% diacerein cream resulted in significant reduction of the IMQ-induced splenomegaly compared to placebo (Figure 3). At day 4, similar results were obtained for the splenic mass (data now shown).
- At day 4, flow cytometry analysis revealed that IMQ significantly increased the fraction of live CD19⁺ B cells, neutrophils, MHCII⁺ monocytes and macrophages, myeloid and lymphoid dendritic cells in the spleen (Fig. 4A-E) and significantly decreased the fraction of live CD4⁺ or CD8⁺ T cells, eosinophils, CD11c⁺ dendritic cells and red-pulp macrophages (Fig. 4F-J) compared to daily treatment with a vehicle cream. Importantly, compared to treatment with a placebo cream, the topical application of 10% diacerein significantly reduced the fraction of live lymphoid dendritic cells (Fig. 4E) and red-pulp macrophages (Fig. 4J).

## CONCLUSIONS

Consequently, we conclude that diacerein does not influence clinical severity of psoriasiform-like skin inflammation in an IMQ-induced mouse model, but it has an anti-inflammatory impact on immune cells in the skin and spleen. The spleen is probably affected via a systemic effect.

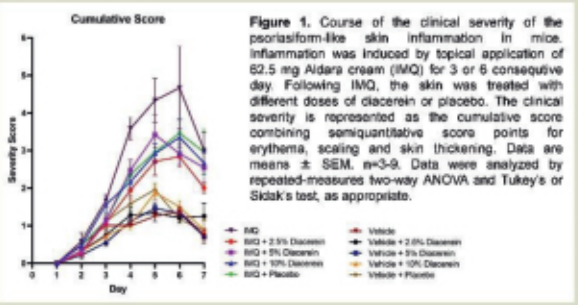


**Figure 1.** Course of the clinical severity of the psoriasiform-like skin inflammation in mice. Inflammation was induced by topical application of 62.5 mg Aldara cream (IMQ) for 3 or 6 consequtive day. Following IMQ, the skin was treated with different doses of diacerein or placebo. The clinical severity is represented as the cumulative score combining semiquantitative score points for erythema, scaling and skin thickening. Data are means ± SEM. n=3-9. Data were analyzed by repeated-measures two-way ANOVA and Tukey's or Sidak's test, as appropriate.

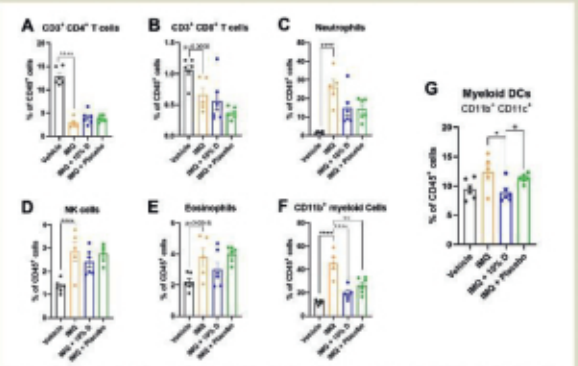


**Figure 2.** Flow cytometry analysis of skin single cell suspensions of IMQ-treated mice. The immune cell subpopulations studied were CD4⁺ (A) and CD8⁺ T cells (B), neutrophils (C), NK cells (D), eosinophils (E), CD11b⁺ myeloid cells (F) and CD11b⁺/CD11c⁺ myeloid dendritic cells (G). Data are means ± SEM. n=5-6. Data were analyzed by one-way ANOVA and Tukey's test (****p<0.0001, **p<0.01, *p<0.05) or unpaired t-test (*p<0.05).

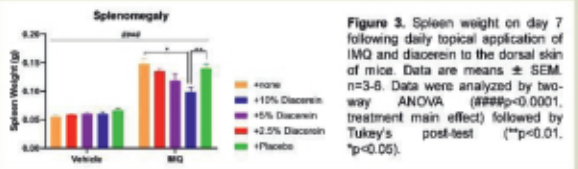


**Figure 3.** Spleen weight on day 7 following daily topical application of IMQ and diacerein to the dorsal skin of mice. Data are means ± SEM. n=3-8. Data were analyzed by two-way ANOVA (####p<0.0001, treatment main effect) followed by Tukey's post-test (**p<0.01, *p<0.05).

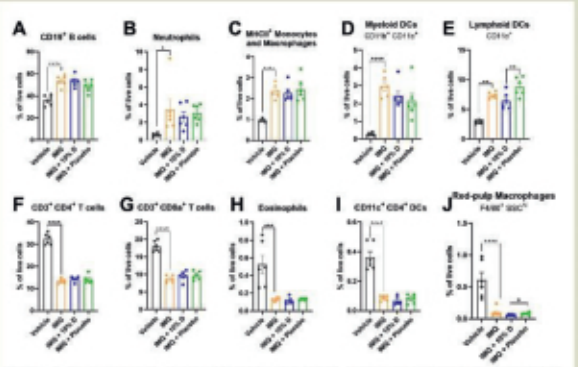


**Figure 4.** Flow cytometry analysis of splenic single cell suspensions of IMQ-treated animals. The immune cell subpopulations studied were CD19+ B cells (A), neutrophils (B), monocytes/macrophages (C), myeloid (D) and lymphoid dendritic cells (E), CD4⁺ (F) and CD8⁺ T cells (G), eosinophils (H), CD11c⁺/CD4⁺ dendritic cells (I) and red-pulp macrophages (J). Data are means ± SEM. n=5-6. Data were analyzed by one-way ANOVA and Tukey's test (****p<0.0001, ***p<0.001, **p<0.01, *p<0.05) or unpaired t-test (*p<0.05).

**References**

[1]Clin Exp Dermatol. 28(4):314-320. [2]Ther Adv Musculoskelet Dis. 3(2):95-104. [3]Free Radic Biol Med. 72:104-112. [4]J Immunol. 173(5):3051-61.

Contact: su.brunner@salk.at

This study is supported by the Paracelsus Medical University Salzburg (PMU-FFF, E-18/27/145-WAL).

## Treatment of psoriasiform-like skin inflammation with diacerein influences skin and spleen immune cell subpopulations

Susanne M Brunner[1, 2], Andrea Ramspacher[1], Caroline Rieser[1], Julia Leitner[1], Hannah Heil[1], Barbara Kofler[1], Roland Lang[3], Verena Wally[4]

[1]Research Program for Receptor Biochemistry and Tumor Metabolism, Department of Pediatrics, Paracelsus Medical University, Salzburg, Austria; [2]Research Program for Experimental Ophthalmology, Department of Ophthalmology and Optometry, Paracelsus Medical University, Salzburg, Austria; [3]Department of Dermatology, Paracelsus Medical University, Salzburg; [4]EB House Austria, Research Program for Molecular Therapy of Genodermatoses, Department of Dermatology and Allergology, Paracelsus Medical University Salzburg, Austria; Contact: su.brunner@salk.at

### Objective
Psoriasis is an inflammatory skin disease characterized by increased neovascularization, keratinocyte hyperproliferation, a proinflammatory cytokine milieu and immune cell infiltration. Diacerein is an antiinflammatory drug, currently approved for osteoarthritis treatment. Diacerein influences several proinflammatory cytokines, like IL-1ß, IL-6 and TNFα, in different diseases like epidermolysis bullosa simplex and diabetes. Therefore, we hypothesized that topical diacerein has beneficial effects on the course of psoriasis. The aim of the present study was to elucidate the ability of diacerein to delay or reduce the severity of psoriasis in a mouse model of psoriasiform-induced inflammation.

### Methods
To induce psoriasiform inflammation, the dorsal skin of mice (C57BL/6N males, 9 wks old) was treated daily with 62.5 or 80 mg 5% imiquimod (IMQ) or vehicle for 3 or 6 consecutive days. At least 6 hours after IMQ, 100 mg of a diacerein cream (2.5, 5 or 10%) or placebo cream was applied topically, or the skin was left untreated. Macroscopic images of the skin were recorded daily and erythema, scaling and thickening were scored independently on a scale from 0 to 4 in a double-blinded fashion. The cumulative score (scale 0–12) served as an indicator for clinical severity. At sample collection, mice were euthanized and the spleen was excised and weighed. Single cell suspensions were obtained from treated skin areas and spleens for flow cytometry analyses.

### Results
Daily IMQ increased the severity score compared to vehicle treatment. However, topical diacerein did not influence the severity of the inflammation compared to placebo. At day 4, flow cytometry analysis of the skin revealed that IMQ reduced the fraction of live $CD4^+$ and $CD8^+$ T cells but increased the fraction of neutrophils, NK cells, eosinophils and $CD11b^+$ myeloid cells compared to vehicle-treated skin. Remarkably, 10% diacerein significantly diminished the fraction of $CD11b^+$ $CD11c^+$ myeloid dendritic cells in the IMQ-treated skin compared to placebo. Treatment with 10% diacerein resulted in a significant reduction of the IMQ-induced splenomegaly compared to placebo. At day 4, flow cytometry analysis revealed that IMQ significantly increased the fraction of live $CD19^+$ B cells, neutrophils, $MHCII^+$ monocytes/macrophages, myeloid and lymphoid dendritic cells in the spleen and significantly decreased the fraction of live $CD4^+$ or $CD8^+$ T cells, eosinophils, $CD11c^+$ dendritic cells and red-pulp macrophages compared to the vehicle cream. Importantly, compared to treatment with placebo, the topical application of 10% diacerein significantly reduced the fraction of live red-pulp macrophages and lymphoid dendritic cells in the spleen.

### Conclusions
We conclude that diacerein does not influence clinical severity of psoriasiform-like skin inflammation in an IMQ-induced mouse model, but it has antiinflammatory effects on immune cells in the skin and spleen. The spleen is probably affected via a systemic effect.

### Acknowledgements
Funding: PMU-FFF stand-alone project to V. Wally (E-18/27/145-WAL).

PARACELSUS
MEDIZINISCHE PRIVATUNIVERSITÄT

Klinikum Nürnberg

# Ergebnisse der Operation nach Karydakis zur Behandlung eines Sinus pilonidalis

**Philipp Buben, André A. Barth, Moritz Billner, Alejandro Marti, Bert Reichert, Reiner Sievers**

Universitätsklinik für Plastische, Wiederherstellende und Handchirurgie, Zentrum für Schwerbrandverletzte,
Paracelsus Medizinische Privatuniversität - Klinikum Nürnberg

## Einleitung

Beim Sinus pilonidalis handelt es sich um eine akut sowie chronisch auftretende Weichteilinfektion im perinealen Bereich (v.a. Gesäßfalte). Die hohe Rezidivrate und Wundkomplikationen stellen den Plastischen Chirurgen vor eine Herausforderung. Zahlreiche Behandlungsmethoden werden in der Literatur beschrieben, jedoch konnte bisher kein Goldstandard festgelegt werden. Zur Reevaluation unserer klinischen Ergebnisse nach der Operation nach Karydakis, wurde eine retrospektive Outcomeanalyse durchgeführt und die Ergebnisse mit der Literatur und anderen Verfahren verglichen.

## Material und Methoden

Es erfolgte eine retrospektive Analyse der Patienten welche wegen eines Sinus pilonidalis in unserer Klinik für Plastischen Chirurgie behandelt wurden. Dabei wurden demographische Daten, Komorbiditäten, Laborwerte sowie klinische Parameter aus unserer Klinikdatenbank in Microsoft Excel zusammengetragen und ausgewertet. Anschließend wurde entweder mittels eines standardisierten Telefongespräches oder persönlich in unserer Sprechstunde die Patienten zu postoperativen Parametern nachuntersucht. Die Daten wurden mit der Literatur (lokale Exzision, Limberg Lappenplastik) verglichen.



**Abb 1:** Präoperative Präsentation des Sinus pilonidalis mit den typischen Pori in der Mittellinie.



**Abb 2:** Die Exzision nach Karydakis. Exzision bis auf die präsakrale Faszie.

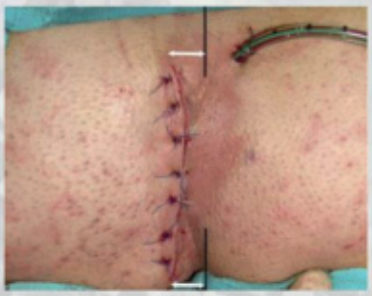

**Abb 3:** Wunde mit einer paramedian liegenden Narbe.

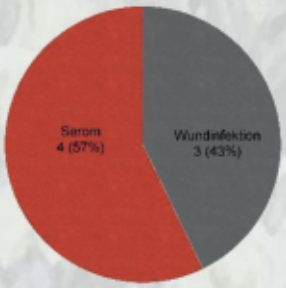


**Abb 4:** Minor- Komplikationen

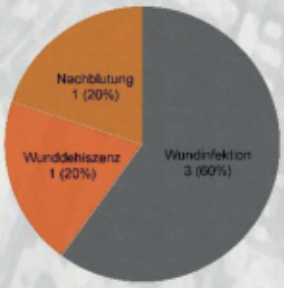


**Abb 5:** Major- Komplikationen



**Abb 6:** Offene Wundheilung nach der Exzision eines Sinus pilonidalis

## Ergebnisse

Insgesamt konnten 103 Patienten in die Studie eingeschlossen werden. Die Rezidivrate nach der Operation nach Karydakis betrug 6,8 %. Die durchschnittliche Follow-up Zeit betrug 4.9 Jahre. Die postoperative Wundheilungsdauer der Patienten betrug durchschnittlich 21 Tage (range 8-35 Tage). Insgesamt erlitten drei Patienten eine Wundinfektion und vier Patienten entwickelten ein Serom (Minor Komplikationen). Eine Revision musste in fünf Fällen aufgrund postoperativer Komplikationen durchgeführt werden (Major Komplikation).

## Schlussfolgerung

Der Sinus pilonidalis führt bei Betroffenen zu einer deutlichen Einschränkung der Lebensqualität. Bei Erstauftreten mit akuten Symptomen ist die rasche Entlastung mit Stichinzision die Therapie der Wahl. Bei unseren Patienten hat sich in den meisten Fällen eine insuffiziente Vorbehandlung gezeigt, weshalb eine Operation mit lokaler Lappenplastik indiziert war. Eine radikale Exzision führt zu einer deutlichen Reduktion der Rezidivrate. Die offene Wundbehandlung ist in vielen Zentren eine häufige Behandlungsalternative, führt jedoch zu einer teils mehreren Monaten andauernden Wundbehandlung.

Die von uns durchgeführte Operation nach Karydakis zeigt eine geringere Wundheilungsdauer, geringe Komplikations- und Rezidivrate und eine hohe Patientenzufriedenheit, weshalb wir den Eingriff in unserer Klinik weiterhin als die Therapie der Wahl bei chronischen Sinusleiden empfehlen.

Literatur
Harris CL, Holloway S. Development of an evidence-based protocol for care of pilonidal sinus wounds healing by secondary intent using a modified reactive Delphi procedure. Part one: the literature review". Int Wound J. 2012;9(2):156-172. doi:10.1111/j.1742-481X.2011.00874.x
Karydakis GE. New approach to the problem of pilonidal sinus. Lancet. 1973;2(7843):1414-1415. doi:10.1016/s0140-6736(73)92803-1
Can MF, Sevinç MM, Hanoğulları O, Yilmaz M, Yagci G. Multicenter prospective randomized trial comparing modified Limberg flap transposition and Karydakis flap reconstruction in patients with sacrococcygeal pilonidal disease. Am J Surg. 2010;299(3):319-327. doi:10.1016/j.amjsurg.2009.08.042

## Ergebnisse der Operation nach Karydakis zur Behandlung eines Sinus pilonidalis

Philipp Buben[1], André A. Barth, Moritz Billner, Alejandro Marti[1], Bert Reichert[1], Reiner Sievers[1]

[1]Universitätsklinik für Plastische, Wiederherstellende und Handchirurgie, Zentrum für Schwerbrandverletzte, Paracelsus Medizinische Privatuniversität, Nürnberg, Deutschland; Contact: philipp.buben@stud.pmu.ac.at

### Objective
Beim Sinus pilonidalis handelt es sich um eine akut sowie chronisch auftretende Weichteilinfektion im perinealen Bereich (v.a. Gesäßfalte). Die hohe Rezidivrate und Wundkomplikationen stellen den Plastischen Chirurgen vor eine Herausforderung. Zahlreiche Behandlungsmethoden werden in der Literatur beschrieben, jedoch konnte bisher kein Goldstandard festgelegt werden. Zur Reevaluation unserer klinischen Ergebnisse nach der Operation nach Karydakis, wurde eine retrospektive Outcomeanalyse durchgeführt und die Ergebnisse mit der Literatur und anderen Verfahren verglichen.

### Methods
Es erfolgte eine retrospektive Analyse der Patienten welche wegen eines Sinus pilonidalis in unserer Klinik für Plastischen Chirurgie behandelt wurden. Dabei wurden demographische Daten, Komorbiditäten, Laborwerte sowie klinische Parameter aus unserer Klinikdatenbank in Microsoft Excel zusammengetragen und ausgewertet. Anschließend wurde entweder mittels eines standardisierten Telefongespräches oder persönlich in unserer Sprechstunde die Patienten zu postoperativen Parametern nachuntersucht. Die Daten wurden mit der Literatur (lokale Exzision, Limberg Lappenplastik) verglichen.

### Results
Insgesamt konnten 103 Patienten in die Studie eingeschlossen werden. Die Rezidivrate nach der Operation nach Karydakis betrug 6,8 %. Die durchschnittliche Follow-up Zeit betrug 4.9 Jahre. Die postoperative Wundheilungsdauer der Patienten betrug durchschnittlich 21 Tage (range 8- 35 Tage). Insgesamt erlitten drei Patienten eine Wundinfektion und vier Patienten entwickelten ein Serom (Minor Komplikationen). Eine Revision musste in fünf Fällen aufgrund postoperativer Komplikationen durchgeführt werden (Major Komplikation).

### Conclusions
Der Sinus pilonidalis führt bei Betroffenen zu einer deutlichen Einschränkung der Lebensqualität. Bei Erstauftreten mit akuten Symptomen ist die rasche Entlastung mit Stichinzision die Therapie der Wahl. Bei unseren Patienten hat sich in den meisten Fällen eine insuffiziente Vorbehandlung gezeigt, weshalb eine Operation mit lokaler Lappenplastik indiziert war. Eine radikale Exzision führt zu einer deutlichen Reduktion der Rezidivrate. Die offene Wundbehandlung ist in vielen Zentren eine häufige Behandlungsalternative, führt jedoch zu einer teils mehreren Monaten andauernden Wundbehandlung. Die von uns durchgeführte Operation nach Karydakis zeigt eine geringere Wundheilungsdauer, geringe Komplikations- und Rezidivrate und eine hohe Patientenzufriedenheit, weshalb wir den Eingriff in unserer Klinik weiterhin als die Therapie der Wahl bei chronischen Sinusleiden empfehlen.

## PHARMACEUTICAL MEDICATION MANAGEMENT AT HOSPITAL ADMISSION IDENTIFIES RELEVANT DRUG-RELATED PROBLEMS

Stephanie Buchegger[1], Peter Gerner[2], Christina Hofer-Dückelmann[1, 3], Maria Flamm[4, 5], Johanna Pachmayr[1, 5]

[1]Pharmacy, Pharmaceutical Biology&Clinical Pharmacy, Paracelsus Medical University, Salzburg, Austria.; [2]Department of Anesthesiology, Perioperative Medicine and Intensive Care Medicine, University Hospital, Salzburg, Austria.; [3]Landesapotheke am St. Johanns-Spital, Salzburg, Austria.; [4]Institute of General Practice, Family Medicine and Preventive Medicine, Paracelsus Medical University, Salzburg, Austria.; [5]Center of Public Health and Health Services Research, Paracelsus Medical University, Salzburg, Austria.; Contact: stephanie.buchegger@pmu.ac.at

### Objective
The aim of our study is to evaluate the impact of clinical-pharmaceutical service at the pre-anaesthetic outpatient clinic (PAOC) on medication safety of patients undergoing elective surgery on three different wards: orthopaedics/traumatology, vascular surgery and general surgery.

### Methods
The study was designed as a single arm, retrospective study. Documented DRPs were analyzed and classified by the Pharmaceutical Care Network Europe (PCNE)-system Version 9.00 (1) to identify their cause and furthermore evaluated according to their clinical significance (2). Physician's acceptance rate of the PIs was evaluated by the time of hospital discharge. The study was approved by the local ethics committee [1112/2020].

### Results
During six months of observation (January-June 2018), 188 DRPs were identified in 137 admitted patients. The average age of the patients was 70.03 years (ranges 40-92) and 56.2% were male. 18% of DRPs were very significant at the initial phase of hospital admission. A total of 197 DRP causes were identified (one DRP can be induced by more causes). Under-prescribing (lack of indicated drug) was the major cause of DRPs (23.4%), followed by drug-drug-interactions (16.8%), inappropriate drug monitoring (13%) and over-prescribing (no indication for drug) (11.4%). Additionally, more than half of the PIs were medically accepted by the physicians and/or a change was made in the prescription or in non-pharmacological interventions such as drug monitoring or monitoring clinical laboratory parameters.

### Conclusions
Our results show that clinical pharmacists can play a crucial role in identifying and solving DRPs. Under-prescribing as well as over-prescribing represent a major problem in the drug therapy of patients. In patient-centered pharmacy, the screening of long-term medication is clinically relevant. The establishment of a pharmaceutical discharge management could further increase the quality assurance in routine clinical pharmacy practice.

### References
1. PCNE, P.C.N.E.A. PCNE Classification for Drug-Related Problems V9.00 (2019).
2. Hind T. Hatoum, R.A.H., Kenneth W. Witte, and George P. Newby. Evaluation of the contribution of clinical pharmacists: inpatient care and cost reduction. Drug Intel/ Clin Pharm 1988;22:252-9. (1988).

# Evidence- Based Patient Selection in Headache Surgery: The Impact of Preoperative RFA Treatment on Surgical Outcomes

Maria Emilia Casari

Division of Plastic and Reconstructive Surgery, Massachusetts General Hospital, Harvard Medical School, Boston, MA 02114, USA

Harvard Medical School

## INTRODUCTION

Radiofrequency ablation (RFA) of the greater occipital nerve is a minimally-invasive treatment option, commonly used in patients with occipital neuralgia.[1] Patients who undergo occipital surgery for headaches after failed RFA treatment present a unique opportunity to evaluate RFA- treated nerves and determine the impact of RFA on headache surgery outcomes.

## OBJECTIVES

To explore:

- Intraoperative anatomy of patients with previous RFA treatment and without
- Wether previous RFA treatment has an impact on the surgical outcome or treatment

## METHODS

- A study population of 115 patients with occipital trigger site deactivation surgery and a diagnosis of chronic occipital neuralgia/ migraine/ headache were prospectively enrolled.
- Comparison of patients with a history of RFA treatment versus patients with no history of RFA treatment was conducted.
- Outcome scores were collected preoperatively –
  1) Migraine Headache Index (MHI).
  2) Pain Self Efficacy Questionnaires (PSEQ).
  3) Patient Health Questionnaire-2 (PHQ-2).
- Unpaired t-tests were performed to compare preoperative and postoperative MHI, PSEQ and PHQ-2 scores between patients with previous RFA versus without RFA treatment, as well as between RFA patients with and RFA patients without damaged nerves.
- Chi-square test was performed For analysis of the anatomical characteristics and surgical sites.
- For subgroup analysis of nerve transection all sites of trigger site deactivation surgery were included increasing the study population of that specific data analysis to 154 patients.

**ACKNOWLEDGEMENTS**

Lisa Gfrerer, M.D, PhD;
William G. Austen Jr., MD;
Priv.-Doz. Dr. rer. nat. Martin Jokeb

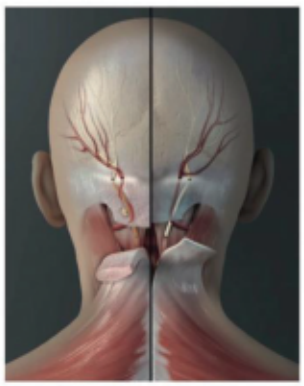

***Figure 1:*** *Pictorial representation of a migraine patient with thickened trapezius fascia (right side) versus a healthy subject (left side).*[2]

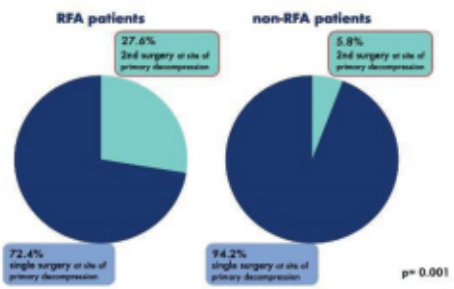


***Figure 2:*** *More patients with history of RFA treatment required a same-site second surgery (27.6%) compared to patients who had not undergone RFA (5.8%) (p=0.001).*

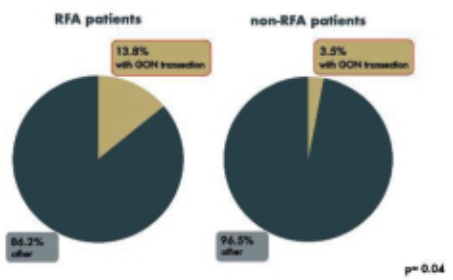


***Figure 3:*** *RFA patients were also more likely to require a greater occipital nerve (GON) transection (p=0.04, 13.8% in RFA patients, 3.5% in non-RFA patients)*

## RESULTS

- RFA-treated patients had a higher rate of macroscopic nerve damage (45%) than non RFA-treated patients (24%) (p=0.03).
- Subgroup analysis of RFA patients with and without a damaged nerve revealed no significant difference in preoperative MHI scores (134.4±92.7 and 116.4±80.8, respectively; p=0.29)
- RFA patients were significantly more likely to require a second surgery at the site of primary decompression (27.6% versus 5.8%; p=0.001), as well as greater occipital nerve (GON) transection (13.8% versus 3.5%; p=0.04).
- Patients who underwent nerve transection achieved similar outcome scores (MHI, PSEQ, and PHQ-2) to patients without nerve transection (p=0.09, p=0.45, and p=0.48 respectively)
- Outcome scores at the last follow up visit were comparable between RFA- treated and non RFA- treated patients (p=0.15).

## CONCLUSIONS

- RFA patients have a good outcome after occipital trigger site deactivation surgery and did comparable to patients with no history of RFA treatment.
- Macroscopically, RFA patients showed to have significantly more damaged nerves. Our findings were consistent with reported nerve damage after RFA treatment of several other studies.[3,4]
- RFA patients required significantly more reoperations at site of primary decompression and also showed to have more nerve transections of the GON. However, preoperative migraine severity scores were comparable between groups.
- We recommend physicians conducting to inform about the higher likelihood of requirement of reoperations and possible nerve transections to achieve an acceptable outcome, as well as the subsequent effects, such as loss of sensation.

### REFERENCES

I. Abd-Elsayed A, Kreuger L, Wheeler S, Robillard J, Seeger S, Dulli D. Radiofrequency Ablation of Peripheral Nerves for Treating Headache Conditions: A Promising Option for Patients. Ochsner J. 2018;18(1):59-62.

II. Gfrerer L, Hanasoge MA, Ortiz R, Chartier C, Nealon KP, Austen WG, Jr. Muscle Fascia Changes in Patients with Occipital Neuralgia, Headache, or Migraine. Plast Reconstr Surg. 2021;147(1):176-180.

III. Kapural L, Malkhasyan N. Radiofrequency ablation for chronic pain control. Curr Pain Headache Rep. 2001;5(6):517-525.

IV. Bunch TJ, Bruce GK, Mahapatra S, et al. Mechanisms of phrenic nerve injury during radiofrequency ablation of the pulmonary vein ostium. J Cardiovasc Electrophysiol. 2005;16(12):1318-1325.

## Evidence- Based Patient Selection in Headache Surgery: The Impact of Preoperative RFA Treatment on Surgical Outcomes

Maria Emilia Casari[1], Christian Chartier[1], Lisa Gfrerer[1], William G. Austen[1]

[1]Massachusetts General Hospital, Harvard Medical School; Contact: maria.casari@stud.pmu.ac.at

### Objective
Radiofrequenz Ablation (RFA) ist eine minimal-invasive Therapieoption für Patienten, die an occitpitalen Kopfschmerzen leiden. In dieser Studie werden makroskopische Nervenschädigungen in RFA-Patienten evaluiert und Unterschiede in den Therapiefolgen einer Migräne Operation des Nervus occipitalis major, durch vorhergegangen RFA-Therapie, untersucht.

### Methods
In dieser Studie wurden 115 Patienten mit occipitaler Migräne Operation inkludiert, 29 dieser Gruppe haben eine Patientengeschichte mit RFA-Therapie. Migraine Headache Index, Pain Self-Efficacy Questionnaire, und Pain Health Questionnaire-2 Ergebnis-Scores wurden präoperativ aufgenommen und schließlich bei den folgenden Nachsorgeuntersuchungen. Intraoperative makroskopische Nervenschädigungen und Operative Ergebnisse wurden zwischen RFA und nicht-RFA Patienten mittels Chi-square Test und T-Test verglichen.

### Results
RFA-behandelte Patienten haben eine höhere Rate an makroskopischen Nervenschädigungen (45%) im Vergleich zu Patienten ohne RFA-Therapie (24%) ($p=0.03$), und hatten eine signifikant höhere Wahrscheinlichkeit eine sekundäre Operation am primären Lokus zu benötigen (27.6% versus 5.8%, $p=0.001$), sowie eine Nervendurchtrennung des Nervus occipitalis major statt Dekompression (13.8% versus 3.5%, $p=0.04$). Die Ergebnis-Scores der letzten Nachsorgeuntersuchung waren zwischen den RFA-Patienten und jenen ohne RFA-Therapie vergleichbar.

### Conclusions
Obwohl RFA-Patienten und Patienten ohne RFA-Therapie ein äquivalentes Ergebnis der occipitalen Migräne Operation erlangen, waren eine höhere Anzahl an sekundären Operationen am primären Lokus und häufigere Nervendurchtrennungen des Nervus occipitalis major in RFA-Patienten notwendig. Jene Patienten sollten über die zusätzlichen Risiken von multiplen Operationen und Durchtrennung von Nerven, welche zu einem akzeptablen und erfolgreichen operativen Ergebnis führen, aufgeklärt werden.

# TAILOR-MADE CARDIOPULMONARY BYPASS

I. Condello, V. Cosco, L.M. Macrì, A.F. Coletta, P. Mastroroberto, G. Speziale, T. Fischlein, G. Santarpino.

## I. *INTRODUCTION*

Despite advances in surgical techniques, CPB technology, anesthesia management and patient care, cardiac surgery is still chatacterized by significant morbidity and subsequent mortality. In particular, one of the adverse effects related to the use of CPB is SIRS, a phenomenon that can be controlled and reduced by managing the perfusion temperature, hemodilution, circuit miniaturization and biocompatibility. In this regard, a prospective study was carried out between 2015 and 2020 to compare the techniques that can be adopted in the field of extracorporeal circulation, with particular reference to conventional CPB and MiECC.

## II. *OBJECTIVE*

Demonstrate the need to carry out a correct and careful intraoperative management by the cardiac surgeon, anesthetist and perfusionist, with particular regard to extracorporeal circulation. It is therefore essential in terms of outcome to use an approach that is designed and tailored to each patient.

## III. *METHOD*

Between 2015 and 2020, a comparative study was conducted on 100 patients candidates for aortocoronary bypass procedure. The study is based on two different historical periods in which a retrospective analysis of 50 patients treated with conventional CPB and a prospective analysis of 50 patients treated with MiECC were compared. The data collected and compared between the two groups are: consumption of blood products, the incidence of acute renal failure, markers of myocardial ischemia, hospitalization time in ICU, incidence of post-operative cognitive disorders, adverse events during the procedures. [Table 1]

TAB. 1. Basic characteristics of the study samples Total sample (n=100)

| | STUDY GROUP (n=50) | CONTROL GROUP (n=50) |
|---|---|---|
| Age (a) (mean) | 68.4 | 69.7 |
| Body surface area (m2) | 1.86 | 1.85 |
| Left ventricular ejection fraction % (mean) | 48 | 49 |
| NYHA class (median) | 2 | 2 |
| Euroscore II | 4.9 | 4.4 |
| Pre-CPB Hematocrit (%, mean +- SEM) | 32.6 ± 1.9 | 32.4 ± 1.2 |
| Pre-CPB Hb (g/dl) | 10.8 ± 1.2 | 10.4 ± 1.1 |
| Creatinine (mg/dl) (mean) | 1.06 ± 0.9 | 1.17 ± 0.6 |
| CPB time (min) | 90 ± 8.37 | 112 ± 15.2 |
| Aortic cross-clamp time (min) | 69 ± 7 | 59 ± 9 |
| Elective | 146 | 148 |
| Urgent | 4 | 2 |

- **FIRST HISTORICAL PERIOD** (2015-2017) The first historical period foresees only one conventional CPB system [Figure 1], without metabolic monitoring systems.
- **SECOND HISTORICAL PERIOD** (2018-2020) The second historical period foresees a change of approach to the CPB structured on:
  1. Type of procedure
  2. Type of patient
  3. Surgical technique with four different methodologies with metabolic monitoring system



Figure 1: Conventional CPB

This type of approach has been favored by the evolution from type 1 design to type 4 design of MiECC systems that took place in the last decade:

- **Type 1**: It is a standard closed-circuit system that includes an afferent tube, which drains the blood from the right atrium to the pump and then to the oxygenator, and returns it to the arterial circulation with the efferent tube. [Figure 2]
- **Type 2**: It is equipped with an air removal device added to the standard MiECC circuit to facilitate air treatment and avoid air capture in the venous line. [Figure 3]
- **Type 3**: It has a soft shell reservoir added to the circuit to collect volume from the patient and return it during perfusion if needed. [Figure 4]
- **Type 4**: It features a hard shell reservoir, added as an extra component, integrated into the venous line to convert the system into an open circuit, which could facilitate blood management or any other intraoperative problem. [Figure 5]

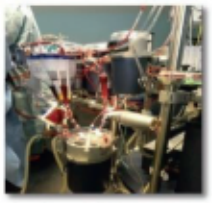

Figure 2: MiECC Type 1



Figure 3: MiECC Type 2



Figure 4: MiECC Type 3



Figure 5: MiECC Type 4

## IV. *RESULTS*

The study revealed a substantial difference between the two study groups in terms of:

- **Consumption of blood products in operating room and intensive care units:** 35% less use was evaluated in patients treated with MiECC
- **Reduction in the incidence of acute kidney injury:** 15% reduction was evaluated in patients treated with MiECC [Figure 6]
- **Reduction time of stay in intensive care unit**: 39% reduction was evaluated in patients treated with MiECC, which was also associated with a reduction in POCD (post-operative cognitive impairment) [Figure 7]
- **Reduction of markers for myocardial ischemia:** an important reduction in TnT ng / L (24H) myocardial ischaemia markers was evaluated in patients treated with MiECC.
- **The adjustments during CPB for**: ultrafiltration (3 study vs 36 control), use of a diuretic Lasix 5 mg (3 patient study vs 28 patient control) and liquids administration mean value for each procedure during of liquids balance during cardiac surgery procedure (700 ml study vs 2100 ml control).

Figure 6: Acute kidney incidence

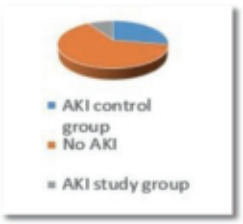


Figure 7: Mean value of stay in intensive care ICU.

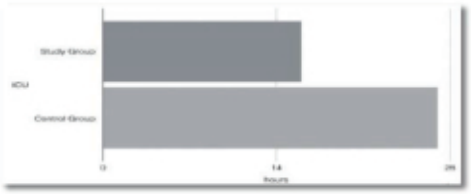


## V. *DISCUSSION*

The tailor-made approach involves a knowledge of the pathophysiology and a shared working method; The main limitations of this study are: 1 only selected patients were chosen mainly with a low risk of mortality.

## VI. *CONCLUSION*

The tailor-made CPB approach showed in this retrospective analysis a better outcome in the patient candidate for cardiac surgery with statistically significant values for incidence of time of stay in intensive care units, consumption of blood products, myocardial suffering marker, incidence POCD, and AKI. However, this technique needs larger samples and the treatments of more fragile patients to have more evidence.

## TAILOR-MADE CARDIOPULMONARY BYPASS

Ignazio Condello, Valeria Cosco, Lucrezia Macrí, Anna Franca Coletta, Pasquale Mastroroberto, Giuseppe Speziale, Theodor Fischlein, Giuseppe Santarpino

[1]Anthea Hospital GVM Care & Research, BARI ITALY; [2]Magna Graecia University, CATANZARO ITALY; [3]Paracelsus Medical University, NUREMBERG GERMANY; Contact: ignicondello@hotmail.it

### Objective

Despite advances in surgical techniques, CPB technology, anesthesia management and patient care, cardiac surgery is still chatacterized by significant morbidity and subsequent mortality. In particular, one of the adverse effects related to the use of CPB is SIRS, a phenomenon that can be controlled and reduced by managing the perfusion temperature, hemodilution, circuit miniaturization and biocompatibility. In this regard, a prospective study was carried out between 2015 and 2020 to compare the techniques that can be adopted in the field of extracorporeal circulation, with particular reference to conventional CPB and MiECC.

### Methods

Between 2015 and 2020, a comparative study was conducted on 100 patients candidates for aortocoronary bypass procedure. The study is based on two different historical periods in which a retrospective analysis of 50 patients treated with conventional CPB and a prospective analysis of 50 patients treated with MiECC were compared. The data collected and compared between the two groups are: consumption of blood products, the incidence of acute renal failure, markers of myocardial ischemia, hospitalization time in ICU, incidence of post-operative cognitive disorders, adverse events during the procedures.

### Results

The study revealed a substantial difference between the two study groups in terms of: •Consumption of blood products in operating room and intensive care units: 35% less use was evaluated in patients treated with MiECC
•Reduction in the incidence of acute kidney injury: 15% reduction was evaluated in patients treated with MiECC
•Reduction time of stay in intensive care unit: 39% reduction was evaluated in patients treated with MiECC, which was also associated with a reduction in POCD (post-operative cognitive impairment)
•Reduction of markers for myocardial ischemia: an important reduction in TnT ng / L (24H) myocardial ischaemia markers was evaluated in patients treated with MiECC.
•The adjustments during CPB for: ultrafiltration (3 study vs 36 control), use of a diuretic Lasix 5 mg (3 patient study vs 28 patient control) and liquids administration mean value for eachprocedure during of liquids balance during cardiac surgery procedure (700 ml study vs 2100 ml control).

### Conclusions

The tailor-made CPB approach showed in this retrospective analysis a better outcome in the patient candidate for cardiac surgery with statistically significant values for incidence of time of stay in intensive care units, consumption of blood products, myocardial suffering marker, incidence POCD, and AKI. However, this technique needs larger samples and the treatments of more fragile patients to have more evidence.

PARACELSUS
MEDIZINISCHE PRIVATUNIVERSITÄT

**Corresponding Author**
Ignazio Condello, PhD
GVM Care & Research, Perfusion service, Anthea Hospital, Via Camillo Rosalba 35/37, 70124 Bari, Italy.
Tel. +39 080 5644560
Fax +39 080 5644560
E-mail: ignicondello@hotmail.it

# Management algorithms and artificial intelligence systems for cardiopulmonary bypass

I. Condello[1], A. Critelli, A.F. Coletta[1], P. Mastroroberto[3], G. Speziale[1], T. Fischlein[2], G. Santarpino[2]

[1]Department of Cardiac Surgery, Anthea Hospital - GVM Care & Research, Bari, Italy
[2]Department of Cardiac Surgery, Paracelsus Medical University, Nuremberg, Germany
[3]Cardiac Surgery Unit, Department of Experimental and Clinical Medicine-University "Magna Graecia" of Catanzaro, Italy

## Abstract

This article introduces management algorithms to support operators in choosing the best strategy for metabolic management during cardiopulmonary bypass using artificial intelligence systems. We developed algorithms for the identification of the optimal way for assessing metabolic parameters. Different management algorithms for extracorporeal procedures interfaced with metabolic monitoring systems already exist on the market and are applied in clinical practice.

## Introduction

Extracorporeal circulation devices have become technologically advanced, intuitive and simple. There has been a reduction in size and a qualitative selection of materials and electronic systems, leading to the development of systems for the safe management and monitoring of vital parameters.

The devices, most commonly known as simulators, consist mainly of a traditional heart-lung machine, interfaced with a simulator controlled by programs that simulate the characteristics of a patient during the procedure. These biomedical devices are developed with the aim of translating and quantifying blood parameters through sensors that use spectrophotometry and ultrasound.

The Model for the quantification of fluid dynamics parameters with the support of artificial intelligence is described by EACTS/EACTA/EBCP guidelines on CPB in adult cardiac surgery.

The anticoagulation process is managed by an algorithm which, using the reference value of ACT in clinical practice, simplifying this complex task.

The end-tidal $CO_2$ management together with the management of CVP represents the indirect parameter of cardiac output, thus an increase in end-tidal $CO_2$ correlates with increased cardiac output and, as a result, increased blood in- and outflow from the pulmonary circulation correlates with CVP in non-pathological hemodynamic situations between 7-11 mmHg. Further, a reduction in end-tidal $CO_2$ concentration correlates with reduced cardiac output entering and leaving the pulmonary circulation with a reduction also in CVP.

At the beginning of CPB, the correction of venous return during the first minutes does not allow an immediate assessment of the pathophysiological mechanisms that can influence it and the cardiac index is interdependent on parameters such as venous return, vascular resistance.

To correct $SaO_2$ values <100% is adviced to follow eight steps, so the perfusionist should click on the monitor every time a suggested step has been performed.

The ideal value of mean arterial pressure during extracorporeal circulation is reported to be between 50 and 70 mmHg.

Using a weak AI some Algorithms could be implemented to cover typical metabolic problems and to provide possible corrective solutions for experienced and non-experienced perfusionists.

As in any new system, this management algorithm has a limitation, in that the system should be validated in further and larger-scale studies that will be undertaken shortly.

## Conclusions

The advantage of AI applied to metabolic management during extracorporeal circulation resides in the possibility of integrating the calculated and highly variable metabolic parameters into the monitoring systems. Goal directed perfusion has improved metabolic management resulting in a lower incidence of acute renal failure. However, there have not been systems with algorithms for the identification of the optimal way to resolve metabolic problems. Different management algorithms for extracorporeal procedures interfaced with metabolic monitoring systems already exist on the market and are applied in clinical practice. These algorithms could provide guidance for selecting the best metabolic strategy with the aim at reducing human error and orienting young operators towards optimized management.



**Figure 1.** Console for traditional extracorporeal circulation.

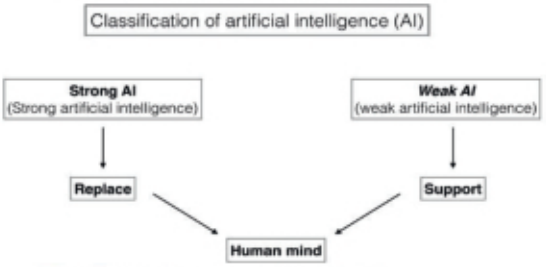


**Figure 2.** Artificial intelligence (AI) classifications.

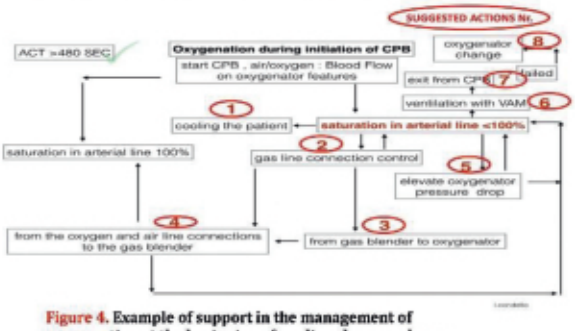


**Figure 4.** Example of support in the management of oxygenation at the beginning of cardiopulmonary bypass.

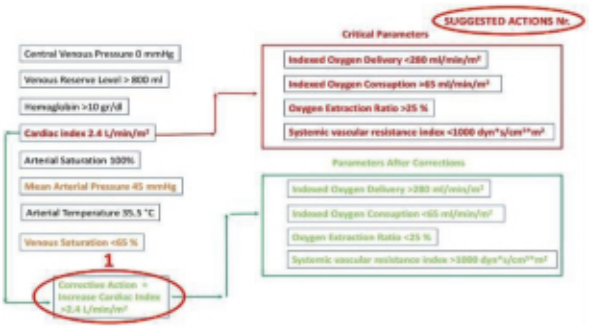


**Figure 7.** Example of goal directed perfusion.

## Management algorithms and artificial intelligence systems for cardiopulmonary bypass

Ignazio Condello, Alessandra Critelli, Anna Franca Coletta, Pasquale Mastroroberto, Giuseppe Speziale, Theodor Fischlein, Giuseppe Santarpino

[1]Anthea Hospital GVM Care & Research, BARI ITALY; [2]Magna Graecia University, CATANZARO ITALY; [3]Paracelsus Medical University, NUREMBERG GERMANY; Contact: ignicondello@hotmail.it

### Objective

Extracorporeal circulation devices have become technologically advanced, intuitive and simple. There has been a reduction in size and a qualitative selection of materials and electronic systems, leading to the development of systems for the safe management and monitoring of vital parameters.

### Methods

The devices, most commonly known as simulators, consist mainly of a traditional heart-lung machine, interfaced with a simulator controlled by programs that simulate the characteristics of a patient during the procedure. These biomedical devices are developed with the aim of translating and quantifying blood parameters through sensors that use spectrophotometry and ultrasound. The Model for the quantification of fluid dynamics parameters with the support of artificial intelligence is described by EACTS/EACTA/EBCP guidelines on CPB in adult cardiac surgery.

### Results

The anticoagulation process is managed by an algorithm which, using the reference value of ACT in clinical practice, simplifying this complex task. The end-tidal CO2 management together with the management of CVP represents the indirect parameter of cardiac output, thus an increase in end-tidal CO2 correlates with increased cardiac output and, as a result, increased blood in- and outflow from the pulmonary circulation correlates with CVP in non-pathological hemodynamic situations between 7-11 mmHg. Further, a reduction in end-tidal CO2 concentration correlates with reduced cardiac output entering and leaving the pulmonary circulation with a reduction also in CVP. At the beginning of CPB, the correction of venous return during the first minutes does not allow an immediate assessment of the pathophysiological mechanisms that can influence it and the cardiac index is interdependent on parameters such as venous return, vascular resistance. To correct SaO2 values <100% is adviced to follow eight steps, so the perfusionist should click on the monitor every time a suggested step has been performed. The ideal value of mean arterial pressure during extracorporeal circulation is reported to be between 50 and 70 mmHg. Using a weak AI some Algorithms could be implemented to cover typical metabolic problems and to provide possible corrective solutions for experienced and non-experienced perfusionists.

### Conclusions

The advantage of AI applied to metabolic management during extracorporeal circulation resides in the possibility of integrating the calculated and highly variable metabolic parameters into the monitoring systems. Goal directed perfusion has improved metabolic management resulting in a lower incidence of acute renal failure. However, there have not been systems with algorithms for the identification of the optimal way to resolve metabolic problems. Different management algorithms for extracorporeal procedures interfaced with metabolic monitoring systems already exist on the market and are applied in clinical practice. These algorithms could provide guidance for selecting the best metabolic strategy with the aim at reducing human error and orienting young operators towards optimized management.

# Extracellular vesicles derived from induced pluripotent stem cells in hypoxic conditions enhance angiogenesis

André Cronemberger Andrade [1], Martin Wolf [1], Heide-Marie Binder [1], Fausto Gueths Gomes [2], Felix Manstein[3], Patricia Ebner Peking [1], Rodolphe Poupardin [1], Robert Zweigerdt[3], Katharina Schallmoser [2] and Dirk Strunk [1]

[1] Experimental and Clinical Cell Therapy Institute (LCCT), Spinal Cord Injury and Tissue Regeneration Center, Paracelsus Medical University, Salzburg, Austria
[2] Department of Transfusion Medicine, Paracelsus Medical University Salzburg, Austria
[3] Department of Cardiac, Thoracic, Transplantation and Vascular Surgery, Leibniz Research Laboratories for Biotechnology and Artificial Organs (LEBAO), Hannover Medical School, Hannover, Germany

andre.cronemberger@pmu.ac.at

## INTRODUCTION

Stem cells secrete paracrine factors including EVs that are important in cellular communication and can support the regeneration of injured tissues. Reduced oxygen conditions (hypoxia) are crucial for proliferation and self-renewal of stem cells. Hypoxia is a key regulator in regeneration, and it may also be an important factor influencing cellular communication via EVs. There is evidence that, depending on the method of vesicle isolation, there is an impact on EV function. Therefore, we investigated whether hypoxic pre-conditioning could impact iPSC-EV quantity, quality and function.

## GRAPHICAL ABSTRACT

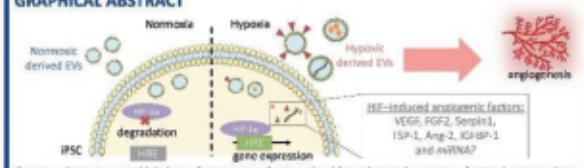


Figure 1. In this study we established a purification strategy for EV produced from a large-scale expansion of iPSC in hypoxic conditions. Upon hypoxia an accumulation of HIF-1α leads to binding of HIF complex to the hypoxia-response element (HRE) in the promoter of target genes. HIFs regulate the expression of several angiogenic genes. Angiogenic molecules can associate with EVs and serve as carriers for target cells boosting the angiogenesis potential.

## METHODOLOGY FOR EV PRODUCTION AND PURIFICATION

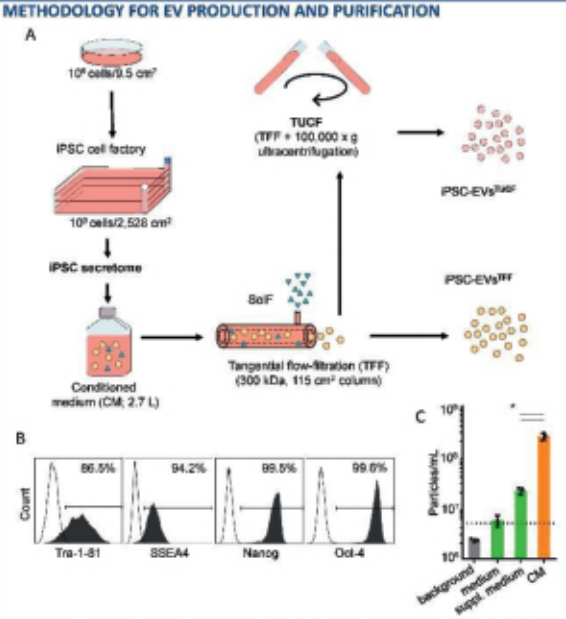


Figure 2. (A) We start iPSC cultures from six well plates. iPSCs were then expanded directly to 1225 flasks and consequently to four layered cell factories for EV production within eight days. EVs were purified from culture conditioned medium (CM) and separated from soluble factors (SolF) by tangential flow filtration (TFF) and further concentrated by ultracentrifugation (TUCF). (B) After large scale expansion iPSC cultures maintained the pluripotency state (Tra-1-81, SSEA-4, Nanog, OCT-4) when analyzed by flow cytometry. (C) The defined medium was suitable for EV production presenting low particle numbers in comparison with CM.

## MONITORING iPSC-EV PURIFICATION

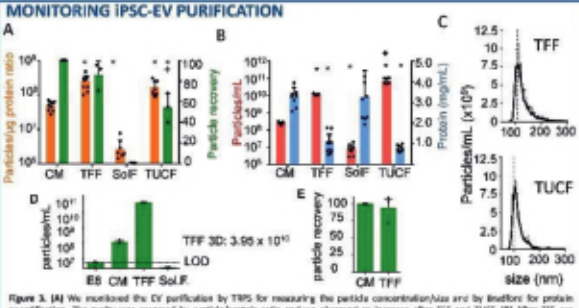


Figure 3. (A) We monitored the EV purification by TRPS for measuring the particle concentration/size and by BioRad for protein quantification. The purity was accessed by particle/protein ratio and we observed an increase after TFF and TUCF. (B) After TFF, we obtained an enrichment in particles and a depletion in protein amount, the subsequent enrichment by ultracentrifugation further increased particles and depleted proteins. Efficiency of TFF is higher compared to TUCF. (C) Particle-size distribution for TFF and TUCF revealed a mode of diameter 109 and 103 nm respectively (dotted lines). (D, E) 3D (bioreactor) purifications after TFF compared to CM.

## CHARACTERIZATION OF HUMAN iPSC-EVs

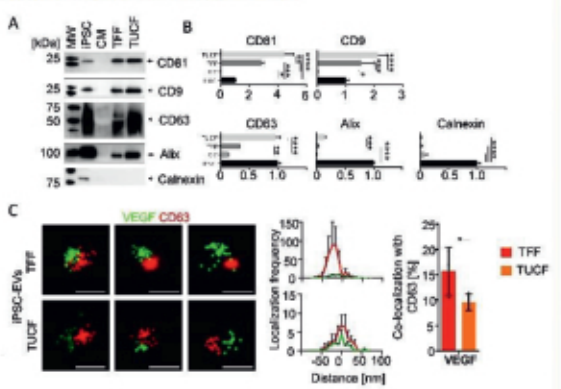


Figure 4. (A) (B) EV identity was determined by immunoblotting and we could observe an enrichment for tetraspanins (CD9, CD63 and CD81) and Alix after TFF and TUCF. As expected the EV samples were negative for Calnexin. (C) Using super-resolution direct stochastic optical microscopy (dSTORM), we detected the presence of CD63 and VEGF on the EVs. Scale bar 100nm. Co-localization signal of VEGF with CD63 was higher in TFF samples compared with TUCF.

## HYPOXIC CONDITIONS OF HUMAN iPSC CULTURES

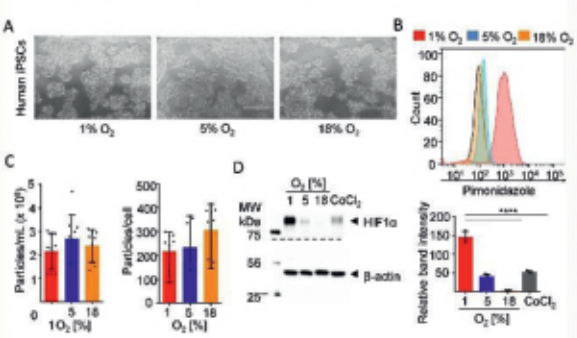


Figure 5. (A) iPSCs cultured under 1%, 5% and 18% oxygen conditions showing typical morphology (B) Using the hypoxiprobe pimonidazole we observed a higher signal after 1% oxygen culture. (C) After culturing iPSCs under different oxygen conditions the particle number and particle/cell displayed no alterations. (D) immunoblotting for HIF-1α expression confirms higher levels of HIF-1α at 1% oxygen conditions.

## ANGIOGENIC POTENTIAL OF HUMAN iPSC-EVs

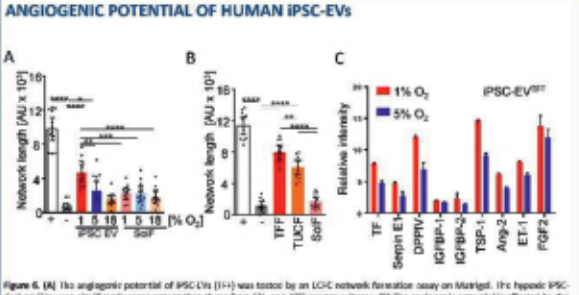


Figure 6. (A) The angiogenic potential of iPSC-EVs (TFF) was tested by an LCHC network formation assay on Matrigel. The hypoxic iPSC-derived EVs were significantly more potent than those from 5% and 18% oxygen cultures. (B) The angiogenic potential is affected by the method of choice when comparing TFF with TUCF EVs from iPSC 1% cultures. (C) We also compared the angiogenic protein profile of iPSC-EVs from 1% and 5%-oxygen cultures where proteins related to angiogenesis showed higher expression levels in the iPSC-EVs (TFF).

## SUMMARY/OUTLOOK

- We produced iPSC-EVs from large-scale iPSC cultures by tangential flow filtration and further concentrated these by ultracentrifugation, giving a good particle enrichment/quality.
- iPSC-EVs (TFF) from hypoxic condition cultures have a greater pro-angiogenic effect compared with iPSC-EVs derived from 5% and 18% conditions and soluble factors.
- An extended purification method to further concentrate the EVs by ultracentrifugation (TUCF) after TFF reduced the pro-angiogenic effect and showed a reduced amount of growth factor (VEGF) on the EVs.

## ACKNOWLEDGEMENTS

This work was funded by the European Union's Horizon 2020, Cancer Cluster Salzburg—Smart Specialization Center (CCS); Transfer Center for Extracellular Vesicles Theralytic Technologies (EVTT); European Union H2020 project TECHNOLOGY PACE.

EVTT

## Extracellular vesicles derived from induced pluripotent stem cells in hypoxic conditions enhance angiogenesis

André Cronemberger Andrade[1], Martin Wolf[1], Heide-Marie Binder[1], Fausto Gueths[2], Felix Manstein[3], Patricia Ebner[1], Rodolphe Poupardin[1], Robert Zweigerdt[3], Katharina Schallmoser[2], Dirk Strunk[1]

[1]Cell Therapy Institute, Spinal Cord Injury and Tissue Regeneration Center Salzburg (SCI-TReCS), Paracelsus Medical University (PMU), Salzburg, Austria; [2]Department of Transfusion Medicine and SCI-TReCS, Paracelsus Medical University (PMU), Salzburg, Austria; [3]3Department of Cardiac, Thoracic, Transplantation and Vascular Surgery, Leibniz Research Laboratories for Biotechnology and Artificial Organs (LEBAO), Hannover Medical School, Hannover, Germany; Contact: andre.cronemberger@pmu.ac.at

### Objective
Stem cells secrete paracrine factors including EVs that are important in cellular communication and can support the regeneration of injured tissues. As hypoxia is a key regulator in development and regeneration it may be an important factor influencing cellular communication via EVs. Therefore, we investigated whether hypoxic pre-conditioning can influence iPSC-EV EV quantity, quality and, EV-based angiogenic potential.

### Methods
We start iPSC cultures from six-well plates then expanded directly to T225 flasks and consequently to four-layered cell factories for EV production within eight days. EVs were purified from a culture-conditioned medium (CM) and separated from soluble factors (SolF) by tangential flow filtration (TFF) and further concentrated by ultracentrifugation (TUCF). We quantified and characterized EVs by tunable resistive pulse sensing (TRPS), immunoblotting for EV markers, and super-resolution microscopy (dSTORM). To evaluate the functionality of the EVs derived from different oxygen conditions we performed an ECFC network formation assay on matrigel.

### Results
We observed superior EV recovery by TFF compared to TUCF. We confirmed hypoxia efficacy by HIF-1α stabilization and pimonidazole hypoxyprobe. EV quantity did not differ significantly at different oxygen conditions. In immunoblots, we found enrichment of the tetraspanins and Alix for the EV purifications and not for Calnexin. We observed an elevated angiogenic potential on iPSC-EVs derived from 1% oxygen culture by TFF compared with iPSC-EVs from 5% and 18% conditions and soluble factors. An extended purification method to further concentrate the EVs by ultracentrifugation (TUCF) after TFF reduced the pro-angiogenic effect and showed a reduced amount of growth factor (VEGF) on the EVs. Data thus demonstrate that cell-culture oxygen conditions and mode of EV preparation affect iPSC-EV function.

### Conclusions
We produced iPSC-EVs from large-scale iPSC cultures by TFF and concentrated by TUCF, giving good particle enrichment. The iPSC-EVs derived from hypoxic conditions had a greater pro-angiogenic effect compared with iPSC-EVs derived from 5% and 18% conditions and soluble factors. We conclude that selecting appropriate protocols will further improve the production of particularly potent iPSC-EV-based therapeutics.

# Cholinerge Neurone in der humanen Aderhaut - eine quantitative Untersuchung

Lisa Danklmaier[1,2], Christian Platzl[2], Heidi Wolfmeier[2], Alexandra Kaser-Eichberger[2], Falk Schrödl[2]

[1] Abschlussarbeit BSc Studium Pharmazie JG2018

[2]Zentrum für Anatomie und Zellbiologie, Institut für Anatomie und Zellbiologie Salzburg, Paracelsus Medizinische Privatuniversität Salzburg

## Einleitung

Die Aderhaut ist die mittlere Augenschicht, die zwischen Augenbecher und Netzhaut liegt. Sie erfüllt eine Vielzahl von Funktionen im Auge. Die Steuerung dieser Funktionen, z.B. Augendruck oder Blutfluss, wird hierbei vom autonomen Nervensystem und zusätzlich von Nervenzellen innerhalb der Aderhaut, sog. intrinsischen choroidalen Neuronen (ICN), übernommen. Die Bedeutung dieser Nervenzellen ist jedoch noch nicht genau verstanden.

**Das Ziel dieser Arbeit war das Vorliegen und den Anteil cholinerger Neurone an der Gesamtpopulation der ICN zu bestimmen und damit Beiträge für ein mögliches Konzept zur pharmakologischen Therapie für Fehlsichtigkeiten, wie z.B. Myopie, zu entwickeln.**

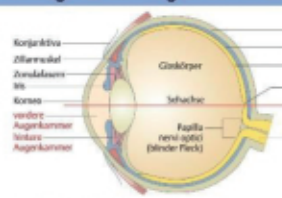


Das Auge ist eines unserer wichtigsten Sinnesorgane. Es ist aus drei Schichten aufgebaut als äußerste Schicht findet sich im vorderen Abschnitt die durchsichtige Hornhaut, die sich im hinteren Augenabschnitt in den Augenbecher (die Sklera) fortsetzt.[1] Im Inneren befindet sich die Netzhaut mit dem angrenzenden retinalen Pigmentepithel, die mittlere Schicht wird von der sogenannten Aderhaut (Choroidea) gebildet.[2]

Abb. 1 – Aufbau des Auges im Längsschnitt.[3]

## Material und Methoden

Es wurde menschliches Gewebe aus dem Spenderwesen des Institutes für Anatomie und Zellbiologie, Paracelsus Medizinische Privatuniversität, für immunhistochemische Färbung aufbereitet. Die Gesamtpopulation aller Neuronen wurde mittels Neurofilament (NF) 160/200 und cholinerge Neurone mittels Cholinacetyltransferase (ChAT) dargestellt. Die quantitative Auswertung erfolgte am Fluoreszenzmikroskop.

### Anfertigung der Aderhaut-Flachschnitte

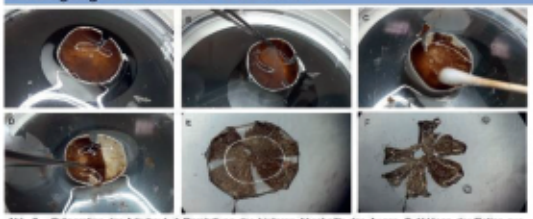

Abb. 2 – Präparation der Aderhaut. A Darstellung des hinteren Abschnitts des Auges. B Ablösen der Retina aus dem Augenbecher. C Abstreifen des RPE mittels feuchten Wattetupfer. D Ablösen der Aderhaut und Abtrennung von anhaftenden Nerven. E Flache Auslegung der Aderhaut in Saccharoselösung auf einem Stück Paraffin. F Isolierte Aderhaut auf einem Stück Paraffin abgetupft.



Abb. 3 – Auftragen der Aderhaut. A Gefrorene Aderhaut im Cryotom eingespannt. B Auf Objektträger aufgetragene Caroideschnitte nach dem Schneiden. Hier werden Beispielschnitte dargestellt.

## Ergebnisse

Die immunmarkierten Nervenzellen wurden anschließend unter Verwendung von Fluoreszenzmikroskopie ausgezählt.

### Mikroskop Ergebnisse

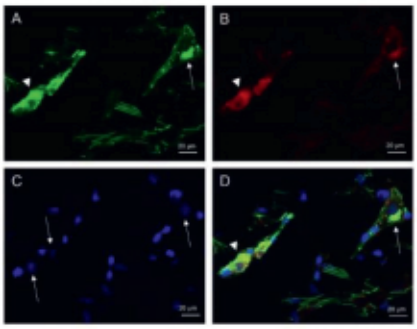

Abb. 4 – Bilder A-D zeigen links eine immunmarkierte ChAT-positive (Pfeilspitze) und rechts eine immunmarkierte ChAT-negative Nervenzelle (Pfeil) in der menschlichen Aderhaut. Auf dem Bild A ist das NF in grün dargestellt und auf dem Bild B ist links die ChAT-positive und rechts die ChAT-negative Nervenzelle in rot dargestellt. Die Verbleibende Färbung ist durch autofluoreszente Lipofuszingranula hervorgerufen, die eigentliche Zelle bleibt unmarkiert. Auf dem Bild C werden die blau gefärbten Zellkerne mit DAPI dargestellt (Pfeile) und Bild D zeigt alle drei Kanäle elektronisch kombiniert. Die Bilder A-D werden bei einer 40-fachen Vergrößerung dargestellt.

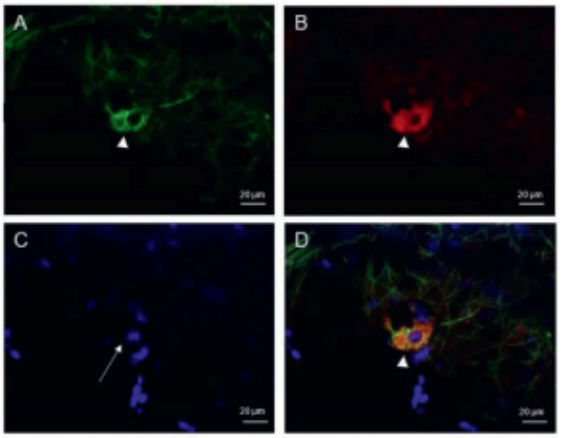

Abb. 5 – Bilder A-D zeigen eine exemplarisch dargestellte immunmarkierte ChAT-positive Nervenzelle (Pfeilspitze) in der menschlichen Aderhaut. Bild A zeigt NF in grün, Bild B zeigt ChAT in rot, Bild C zeigt die blau gefärbten Zellkerne mit DAPI (Pfeil) und Bild D zeigt eine Überlagerung aller drei Kanäle elektronisch. Die Bilder A-D werden bei einer 40-fachen Vergrößerung dargestellt.

### Quantitative Auswertung

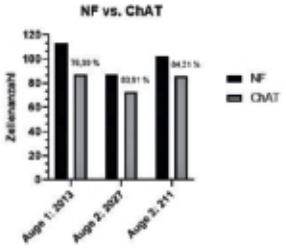


Abb. 6 – Quantitative Evaluation der drei Spenderaugen. Dargestellt ist die Gesamtzahl der ICN (NF, schwarzer Balken) und die Anzahl der ChAT-positiven Nervenzellen (ChAT, grauer Balken). Die Prozentzahl der ChAT-positiven Nervenzellen an der Gesamtzellzahl findet sich angegeben.

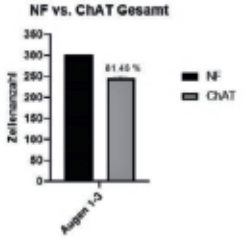


Abb. 7 – Quantitative Evaluation der drei Spenderaugen gesamt. Dargestellt ist die Gesamtzahl der ICN (NF, schwarzer Balken) und die Anzahl der ChAT-positiven Nervenzellen (ChAT, grauer Balken). Die Prozentzahl der ChAT-positiven Nervenzellen an der Gesamtzellzahl findet sich angegeben. Aus dem Mittelwert des prozentuellen Anteils der ChAT-positiven Nervenzellen an der Gesamtzellzahl ergibt sich eine Standardabweichung von 4,12.

## Zusammenfassung

In dieser Arbeit wurde die menschliche Aderhaut mit dem besonderen Fokus auf ICN und cholinerge Neurone untersucht. Die verwendete immunhistochemische Methode hat gut funktioniert. In den entsprechenden Kanälen waren die ICN und die cholinergen Neurone im Fluoreszenzmikroskop gut sichtbar und konnten gut ausgezählt werden. Die Morphologie der cholinergen Neurone kann in zukünftigen Studien weiter charakterisiert werden. Ebenso könnten in weiteren Studien die Funktionen der Aderhaut und der cholinergen Neurone untersucht werden. Weiters könnten unsere Befunde als Grundlage dazu dienen, eine pharmakologische Therapie gegen Myopie zu entwickeln, welche bereits im Kindesalter eingesetzt werden könnte.

Diese Arbeit ist Teil der Abschlussarbeit BSc Studium Pharmazie JG2018

## Danksagung

Ich danke dem Spenderwesen des Institutes für Anatomie und Zellbiologie für die Bereitstellung der menschlichen Gewebe. Ebenso richtet sich ein großer Dank an meine Betreuer Frau Priv.-Doz. Dr. Alexandra Kaser-Eichberger und Herrn Prof. Dr. med. Falk Schrödl für die fachliche Unterstützung und Ermöglichung dieses Projektes.

## Referenzen

[1] SPECKMANN, E.-J. and WITTKOWSKI, W. (2020) Handbuch Anatomie : Bau und Funktion des menschlichen Körpers. In) 21. Auflage ed. München, Deutschland : Elsevier, pp. 107-111.

[2]GRAY, H. and LEWIS, W. H. (1918) Anatomy of the human body. Philadelphia: Lea & Febiger.

[3]BOMMAS-EBERT, U. (2011) Seh-, Hör- und Gleichgewichtsorgan. In: BOMMASEBERT, U., et al. (Eds.) Kurzlehrbuch Anatomie und Embryologie. 3. Auflage ed. Georg Thieme Verlag, p. 437.

## Cholinerge Neurone in der humanen Aderhaut eine quantitative Untersuchung

Lisa Danklmaier[1,2], Christian Platzl[2], Heidi Wolfmeier[2], Alexandra Kaser-Eichberger[2], Falk Schrödl[2]

[1]Abschlussarbeit BSc Studium Pharmazie JG2018; [2]Zentrum für Anatomie und Zellbiologie, Institut für Anatomie und Zellbiologie Salzburg; Contact: falk.schroedl@pmu.ac.at

### Objective
Die Aderhaut ist die mittlere Augenschicht, die zwischen Augenbecher und Netzhaut liegt. Sie ist für eine Vielzahl von Augenfunktionen verantwortlich. Die Steuerung dieser Funktionen, z.B. Augendruck oder Blutfluss, wird hierbei vom autonomen Nervensystem und zusätzlich von Nervenzellen innerhalb der Aderhaut, sog. intrinsischen choroidalen Neuronen (ICN), übernommen. Die Bedeutung dieser Nervenzellen ist jedoch noch nicht genau verstanden.

### Methods
Es wurde menschliches Gewebe (n= 3) aus dem Spenderwesen des Institutes für Anatomie und Zellbiologie, Paracelsus Medizinische Privatuniversität, für immunhistochemische Färbung aufbereitet, um das Vorliegen und den Anteil cholinerger Neurone an der Gesamtpopulation der ICN zu bestimmen. Die Gesamtpopulation aller Neuronen wurde mittels Neurofilament (NF) 160/200 und cholinerge Neurone mittels Cholinacetyltransferase (ChAT) dargestellt. Die Auswertung erfolgte am Fluorenzenzmikroskop.

### Results
Die quantitative Auswertung der Zellen ergab beim Spender 1 einen Anteil von 76,99 % ChAT-positiver Neurone gemessen an der Gesamtzellanzahl, beim Spender 2 waren es 83,91 % und beim Spender 3 84,31 %. Im Durchschnitt fanden sich damit 81,46 % ± 4,12 ChAT-positive Neurone gegenüber der Gesamtzellanzahl (NF +).

### Conclusions
Die Methode hat bei allen Schnitten und bei allen Spendern gut funktioniert, da NF und ChAT in den Nervenzellen der Choroidea nachgewiesen werden konnte. Da die cholinergen Neurone für vielfältige Funktionen verantwortlich sein könnten, wäre es möglich ein Konzept zur pharmakologischen Therapie für Fehlsichtigkeiten, wie z.B. Myopie, zu entwickeln.

PARACELSUS
MEDIZINISCHE PRIVATUNIVERSITÄT

Klinikum Nürnberg
wir sind für Sie da!

# Effect of yoga on the psychological well-being of breast cancer patients
## (depression, anxiety and social support) - Evaluation of the HADS and ESSI questionnaire


Noam Leander Degner[1,2,*]

[1] Paracelsus Medical University, Nuremberg; [2] Department of Obstetrics and Gynecology, University Hospital Nuremberg, Paracelsus Medical University; all Germany;
*Contact: noam.degner@stud.pmu.ac.at


### *Introduction & Objective*

The prevalence of breast cancer in women proceeds to rise, but mortality rates decrease continuously. This leads to a growing number of breast cancer survivors. To support women during the challenging period of neoadjuvant chemotherapy or radiation therapy and prevent comorbidities like anxiety and depression we evaluated an accompanying course of viniyoga for usefulness. Also, an effect on perceived social support was examined. Systematic reviews could already prove numerous positive effects of yoga on various psychological pathologies.[3,4] Neoadjuvant chemotherapy is a particularly challenging period where adding yoga to the therapy regimen may have beneficial influence.[5]

### *Materials and Methods*

- 77 women with breast cancer
- Weekly viniyoga practice vs control group of 2x counseling on complementary medicine
- ENRICHD Social Support Inventory (ESSI) evaluates social support
- Hospital Anxiety and Depression Scale (HADS) evaluates depression/ anxiety




### ESSI sum score - radiation group

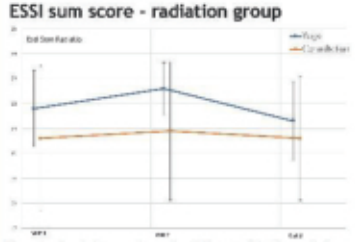

Perceived social support may be influenced in the radiation group. The analysis on the right shows how:

### ESSI Radiation Group - % of patients with good social support

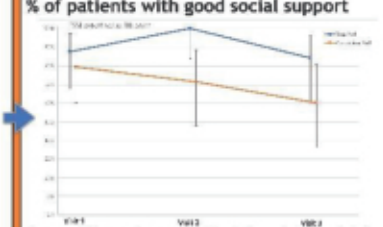

A group difference becomes evident when stratifying data by the originally proposed cut-off value.

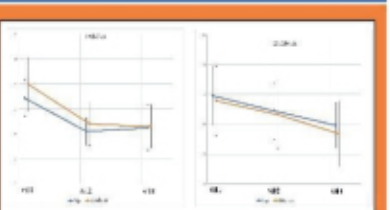

The screening scores for depression and anxiety were lowered in almost all study groups over the study period. Only the radiation group was roughly consistent. Yet, in neither case a significant difference between the groups became evident.

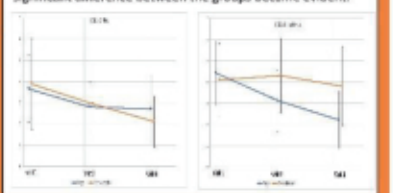

### ESSI sum score - neoadjuvant group

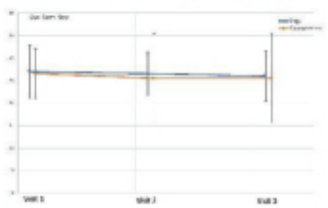

Perceived social support seems not to be influenced in the neoadjuvant group.

➡ Perceived social support seems to be influenced positively in the radiation group - although not statistically significantly, when only looking at the total sum score.

The difference becomes more evident when stratifying data by the proposed cut-off value of 18 points and using a dichotomous scale. This indicates a better social support in the Yoga vs. the control group ($p=0.02$)

The group difference vanished after yoga therapy was stopped.

### *Conclusions*

Perceived social support seems to be influenced positively by a weekly session of viniyoga during radiation therapy. A weekly session of viniyoga did not seem to influence screenings for anxiety and depression differently than two counselings on complementary medicine in the control group. If favored by the patient yoga could be recommended to patients receiving radiation or neoadjuvant therapy especially because of the safety of the program.

Further studies could focus on identifying the type/style of yoga with the greatest efficacy to explain the discrepancy in current literature.

### References and Acknowledgements


- [3] Buffart LM, et al. Physical and psychosocial benefits of yoga in cancer patients and survivors, a systematic review and meta-analysis of randomized controlled trials. BMC Cancer. Nov 2012; 2:559
- [4] Cramer H, et al. Non-pharmacological therapies for depressive symptoms in breast cancer patients: Systematic review and meta-analysis of randomized clinical trials. Breast. Apr 2019;44:135-143.
- [5] Jong MC, et al. A Randomized Study of Yoga for Fatigue and Quality of Life in Women with Breast Cancer Undergoing (Neo) Adjuvant Chemotherapy. J Altern Complement Med. 20(8 Sep/Oct 2018;24(9-10):942953



This study was funded with the help of the „Förderverein des Tumorzentrums Erlangen-Nürnberg e.V." (10.000 Euro in total).

## Effect of yoga on the psychological well-being of breast cancer patients (depression, anxiety and social support) - Evaluation of the HADS and ESSI questionnaire

Noam Leander Degner[1,2]

[1]Paracelsus Medical University, Nuremberg; [2]Department of Obstetrics and Gynecology, University Hospital Nuremberg, Paracelsus Medical University; Contact: noam.degner@stud.pmu.ac.at

### Objective
Background: The prevalence of breast cancer in women proceeds to rise, but mortality rates decrease continuously. This leads to a growing number of breast cancer survivors. To support women during the challenging period of neoadjuvant chemotherapy or radiation therapy and prevent comorbidities like anxiety and depression we evaluated an accompanying course of viniyoga for usefulness. Also, an effect on perceived social support was examined.

### Methods
Materials and Methods: 77 women newly diagnosed with breast cancer were randomized into a group of weekly viniyoga practice for the duration of their neoadjuvant chemo- or radiation therapy, or a control group who received two times complementary medical counseling. Three visits each were scheduled, one at baseline, after 6 months of therapy, and after a 6 months follow-up. The social support was evaluated using the ESSI (ENRICHD Social Support Inventory) Questionnaire and depression and anxiety were evaluated by the HADS (Hospital Anxiety and Depression Scale) Questionnaire.

### Results
Results: Social support measured by ESSI was significantly influenced by yoga exercises. At the second visit a significantly higher number of subjects who participated in the yoga class during radiation therapy rate themselves in a score range above the cut-off value of 18 points, signifying better social support ($p=0.02$). A significant decrease in scores for depression and anxiety was measured over time. A difference between two groups of cases and controls however was not measured.

### Conclusions
Conclusions: Perceived social support seems to be influenced by a weekly session of viniyoga during radiation therapy. A weekly session of viniyoga did not seem to influence screenings for anxiety and depression differently than two counselings on complementary medicine in the control group. If favored by the patient viniyoga could be recommended to patients receiving radiation or neoadjuvant therapy.

# Regeneration of critical sized defects (csd) by implantation of directed silk scaffolds (SC) in combination with bone morphogenetic protein 2 (BMP-2) and/or hydroxyapatite (HA) in a rat animal model

Christian Deininger[1], Herbert Tempfer[1], Nadja Weißenbacher[1], Andrea Wagner[1], Bettina Schwemberger[1], Amelie Deluca[1], Andreas Teuschl[2], Andreas Traweger[1]

[1]Institute of Tendon and Bone Regeneration, Paracelsus Medical University, Salzburg, Austria

[2]Technikum Wien Tissue Engineering and Regenerative Medicine, Vienna, Austria

*The silk road to bone regeneration?*

*Objective:*

Regeneration of critical sized defects (csd) by implantation of directed silk scaffolds (SC) in combination with bone morphogenetic protein 2 (BMP2) and/or hydroxyapatite (HA) in a rat animal model

*Methods:*

In this study a combination of osteoinductive SC and BMP2 and/or HA were evaluated to support the functional repair of a 5mm critical-sized, segmental defect in the right femur of 30 rats. Four groups were defined: SC only, SC + HA, SC + BMP2 and SC + HA + BMP2. The defect was stabilized with an angle-stable plate system. Subsequently, the preparations are examined for regenerated bone volume using µ-Computed tomography (µCT) and histological features.

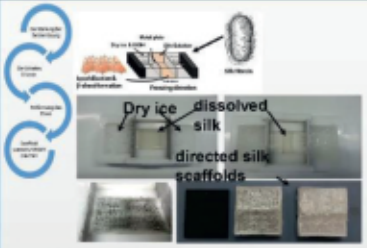


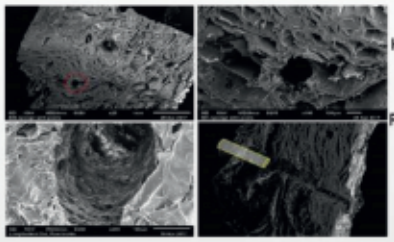

Process of "directed-freezing" to simulate a structure similar to physiological cancellous bone with pores (yellow and red).

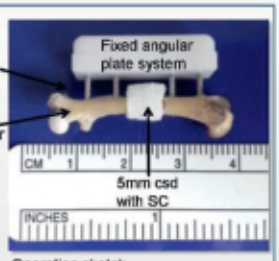


Operation sketch

*Results:*

All groups showed increased bone formation in the defect zone. Direct comparison of the groups showed a significantly higher bone volume in the SC + HA + BMP2 group compared to the SC + HA group. In comparison of all other groups, no significant differences were found, but there was a tendency for more bone substance in the BMP2 groups. The mean regenerated bone substance was 23.31% (±8.2%) for SC only, 22.66% (±9.5%) for SC + HA, 29.83% (±14.3%) for SC + BMP2 and 42.41% (±15.2%) for SC + HA + BMP2. A complete bony healing of the defect with this measurement method corresponds to 80%. 6 of the 28 femora (21.43%) were bony fused, 1 from the SC + BMP2 group and 5 from the SC + HA + BMP2 group.

X-Rays postoperative, 2, 6 and 10 weeks after treatment with a SC + HA + BMP2 (A) and an empty defect (B).

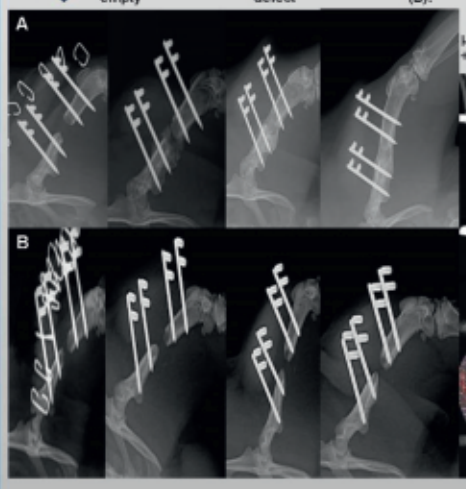


µCT of the corresponding SC + HA + BMP2 X-Ray sample

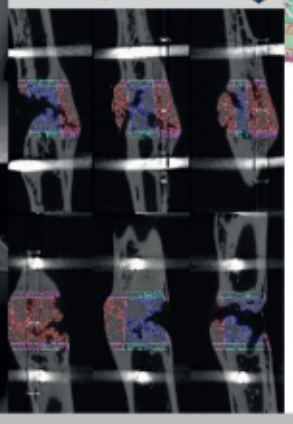

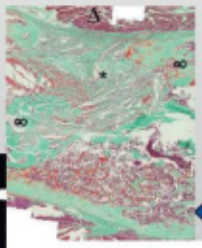


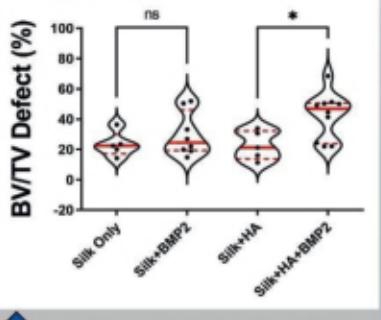


Violin plot with significantly increased bone mass between group Silk + HA + BMP2 and Silk + HA

*Conclusions:*

All groups showed an increased bone regeneration in the defect zone compared to the "empty defect". Six of the 28 femoral bones (21.43%) healed and bridged the defect of the femora and resulted in a clinically stable situation. The amount of BMP2 was significantly reduced in combination with HA and silk. A low dose of BMP-2 results in increased bone volume if combined with a HA-treated silk scaffold. More baseline studies are needed to analyze SC full potency.

*Outlook:*

Longterm goal: Development of a simple "out of the shelf" therapy option for pseudarthrosis or larger bone defects.

## Regeneration of critical sized defects (csd) by implantation of directed silk scaffolds (SC) in combination with bone morphogenetic protein 2 (BMP-2) and/or hydroxyapatite (HA) in a rat animal model

Christian Deininger[1], Herbert Tempfer[1], Nadja Weißenbacher[1], Andrea Wagner[1], Bettina Schwemberger[1], Amelie Deluca[1], Andreas Teuschl[2], Andreas Traweger[1]

[1]Institute of Tendon and Bone Regeneration, Paracelsus Medical University, Salzburg, Austria; [2]Technikum Wien Tissue Engineering and Regenerative Medicine, Vienna, Austria; Contact: christian.deininger@hotmail.com

### Objective

Regeneration of critical sized defects (csd) by implantation of directed silk scaffolds (SC) in combination with bone morphogenetic protein 2 (BMP2) and/or hydroxyapatite (HA) in a rat animal model

### Methods

In this study a combination of osteoinductive SC and BMP2 and/or HA were evaluated to support the functional repair of a 5mm critical-sized, segmental defect in the right femur of 30 rats. Four groups were defined: SC only, SC + HA, SC + BMP2 and SC + HA + BMP2. The defect was stabilized with an angle-stable plate system. Subsequently, the preparations are examined for regenerated bone volume using µ-Computed tomography (µCT) and histological features.

### Results

All groups showed increased bone formation in the defect zone. Direct comparison of the groups showed a significantly higher bone volume in the SC + HA + BMP2 group compared to the SC + HA group. In comparison of all other groups, no significant differences were found, but there was a tendency for more bone substance in the BMP2 groups. The mean regenerated bone substance was 23.31% (±8.2%) for SC only, 22.66% (±9.5%) for SC + HA, 29.83% (±14.3%) for SC + BMP2 and 42.41% (±15.2%) for SC + HA + BMP2. A complete bony healing of the defect with this measurement method corresponds to 80%. 6 of the 28 femora (21.43%) were bony fused, 1 from the SC + BMP2 group and 5 from the SC + HA + BMP2 group.

### Conclusions

All groups showed an increased bone regeneration in the defect zone compared to the "empty defect". Six of the 28 femoral bones (21.43%) healed and bridged the defect of the femora and resulted in a clinically stable situation. The amount of BMP2 was significantly reduced in combination with HA and silk. A low dose of BMP-2 results in increased bone volume if combined with a HA-treated silk scaffold. More baseline studies are needed to analyze SC full potency

Outlook:

Longterm goal: Development of a simple "out of the shelf" therapy option for pseudarthrosis or larger bone defects.

### References

1. Nadja Kunkel et al, Comparing the osteogenic potential of bone marrow and tendon-derived stromal cells to repair a critical-sized defect in the rat femur, J Tissue Eng Regen Med (2015)

# Assessment of the Regenerative Activity of Human Umbilical Cord Mesenchymal Stem Cells - derived Extracellular Vesicles (hUCMSC-EVs) in Osteoporotic Bone – A Femoral Metaphyseal Fracture Defect Model in Rats

Amelie Deluca[1,2], Christian Deininger[1,3], Bettina Schwemberger[1], Andrea Wagner[1], Herbert Tempfer[1], Ernst J. Müller[2], Andreas Traweger[1]

[1] Institute of Tendon and Bone Regeneration, Spinal Cord Injury & Tissue Regeneration Center Salzburg, Paracelsus Medical University, Salzburg, Austria
[2] Department of Trauma Surgery, KABEG-Klinikum Klagenfurt a.W., Klagenfurt, Austria
[3] Department of Orthopedics and Traumatology, Salzburg University Hospital, Salzburg, Austria

amelie.kanovsky@pmu.ac.at

**Hypothesis:** The local application of hUCMSC-EVs has the capability of enhancing the osseointegration, bone regeneration and fracture stability in an osteoporotic metaphyseal fracture.

## Materials & Methods:

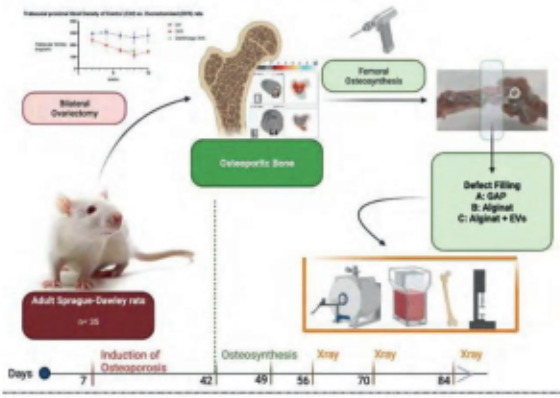


Fig. 1: Estrogen dysregulation combined with a dietary treatment[1] was achieved with a ventral ovariectomy (OVX) performed on 35 female Sprague Dawley rats. Ovariectomized (OVX) rats were analyzed by peripheral quantitative computed tomography (pQCT) at biweekly time points over 14 weeks. After 8 weeks, a 1mm fracture of the right distal metaphysis of the femur was internally stabilized with a Y-shaped mini plate. OVX rats were divided into three subgroups: [A]-OVX without vehicle (n=3), [B]-OVX with alginate scaffold (n=16), [C]-OVX with hUCMSC-EVs on alginate scaffold (2.0 x $10^9$ hUCMSC-EVs) (n=16). The corresponding treatments were administered directly into the fracture gap and monitored with weekly X-rays.

**Results:** pQCT analysis of the proximal tibia metaphysis showed a significant difference in the volumetric cancellous bone mineral density (Trabecular density/TRAB_DEN) between OVX and CTRL rats ($P$<0.0001; Pearson correlation test). TRAB_DEN for OVX rats revealed a mean of 176.0 mg/cm$^3$±57.1 and 284.9 mg/cm$^3$±31.5 for CTRL rats. A significant difference was also observed in the volumetric total bone mineral density (Total density /TOT_DEN) with a mean of 518.2 mg/cm$^3$±31.1 for OVX and 637.0 mg/cm$^3$±11.1 for CTRL rats ($P$<0.0001; Fig. 1).

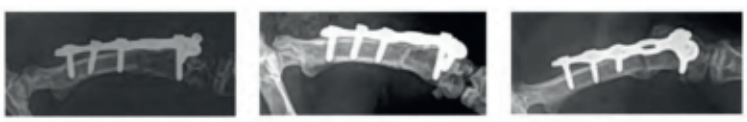

[A]-empty gap,; 6 weeks post surgery | [B]-Alginat,; 6 weeks post surgery | [C]-Alginat+EVs,; 6 weeks post surgery

Fig. 2: Fracture consolidation on X-ray was observed in all three groups after 6 weeks. hUCMSC-EVs-Alginat scaffold [C] depicts macroscopicly the most new bone formation.

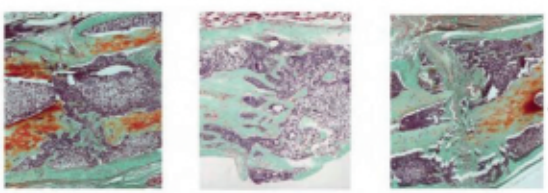

[A]-empty gap | [B]-Alginat | [C]-Alginat+EVs

Fig. 4: All results were confirmed by histology at 6-weeks post-surgery on formalin-fixed paraffin-embedded femoral sections. Masson Goldner stains showed minimal new bone formation in [A], fracture healing in [B] and new bone formation in [C].

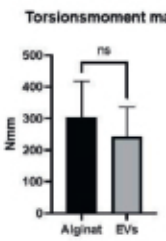


Fig. 3: Biomechanical comparison of [B] versus [C]. After 6 weeks biomechanical testing for bending stiffness in group [B], mean 264.7 Nmm, compared to group [C], mean 255.4 Nmm, did not show a significant difference between them (P=0.4848; t-test).

**Conclusion:** Osteoporotic fracture healing in rats is enhanced by the direct application of hUCMSC-EVs using alginate as a carrier into the fracture to improve callus formation. Although the enhanced bone formation does not result in an improved biomechanical outcome.

[1] C. Heiss *et al.*, Induction of osteoporosis with its influence on osteoporotic determinants and their interrelationships in rats by DEXA. *Med Sci Monit* 18, BR199-207 (2012).

Funding: AO Trauma Nachwuchsförderung –DACH ; Lorenz Böhler Fond #1-21

## Assessment of the Regenerative Activity of Human Umbilical Cord Mesenchymal Stem Cells - derived Extracellular Vesicles (hUCMSC-EVs) in Osteoporotic Bone – A Femoral Metaphyseal Fracture Defect Model in Rats

Amelie Deluca[1, 2], Christian Deininger[1, 3], Andrea Wagner[1], Herbert Tempfer[1], Bettina Schwamberger[1], Andreas Traweger[1], Ernst Müller[2]

[1]Institute of Tendon and Bone Regeneration, Spinal Cord Injury & Tissue Regeneration Center Salzburg, Paracelsus Medical University, Salzburg, Austria; [2]Department of Trauma Surgery, KABEG-Klinikum Klagenfurt a.W., Klagenfurt, Austria; [3]Department of Orthopedics and Traumatology, Salzburg University Hospital, Salzburg, Austria; Contact: amelie.kanovsky@pmu.ac.at

### Objective

Hypothesis: The local application of hUCMSC-EVs has the capability of enhancing the osseointegration, bone regeneration and fracture stability in an osteoporotic metaphyseal fracture.

### Methods

Methods and Materials: Estrogen dysregulation combined with a dietary treatment was achieved with a ventral ovariectomy performed on 35 female Sprague Dawley rats at 12 weeks. The osteoporotic effect was enhanced in all ovariectomized (OVX) rats by a phosphate-, vitamin D3-, soja, and phytoestrogen reduced diet for 6 weeks post-surgery. OVX rats were analyzed by peripheral quantitative computed tomography (pQCT) at biweekly time points to confirm reduced bone mineral density and content compared to controls (CTRL) over 14 weeks. After 8 weeks, a 1mm fracture of the right distal metaphyseal area of the femur was internally stabilized with a Y-shaped mini plate. OVX rats were divided into three subgroups: [A]-OVX without vehicle (n=3), [B]-OVX with alginate scaffold carrier (n=16), and [C]-OVX with hUCMSC-EVs on alginate scaffold (2.0 x 109 hUCMSC-EVs) (n=16). The corresponding treatments were administered directly into the fracture gap and monitored with weekly X-rays.

### Results

Results: pQCT analysis of the proximal tibia metaphysis showed a significant difference in the volumetric cancellous bone mineral density (Trabecular density/TRAB_DEN) between OVX and CTRL rats ($P<0.0001$; Pearson correlation test). TRAB_DEN for OVX rats revealed a mean of 176.0 mg/cm3±57.1 and 284.9 mg/cm3±31.5 for CTRL rats. A significant difference was also observed in the volumetric total bone mineral density (Total density /TOT_DEN) with a mean of 518.2 mg/cm3±31.1 for OVX and 637.0 mg/cm3±11.1 for CTRL rats ($P<0.0001$).
Fracture consolidation on X-ray was observed in all three groups after 6 weeks. hUCMSC-EVs-Alginat scaffold [C] depicts macroscopicly the most new bone formation.
All results were confirmed by histology at 6-weeks post-surgery on formalin-fixed paraffin-embedded femoral sections. Masson Goldner stains showed minimal new bone formation in [A], fracture healing in [B] and new bone formation in [C].
After 6 weeks the biomechanical comparison of [B] versus [C] did not show a significant difference for bending stiffness in group [B], mean 264.7 Nmm, compared to group [C], mean 255.4 Nmm ($P=0.4848$; t-test).

### Conclusions

Conclusion: Osteoporotic fracture healing in rats is enhanced by the direct application of hUCMSC-EVs using alginate as a carrier into the fracture to improve callus formation. Although the enhanced bone formation does not result in an improved biomechanical outcome.

# Comparative Evaluation of Microplate-based Assays for Viable Cell Quantity

Heidemarie Dobias[1,2], Christian Mayr[1,3], Marlena Beyreis[1], Markus Ritter[1,2,4], Tobias Kiesslich[1,3]

[1]Center for Physiology, Pathophysiology and Biophysics - Salzburg and Nuremberg, Institute for Physiology and Pathophysiology - Salzburg, Paracelsus Medical University, Salzburg, Austria; [2]Gastein Research Institute, Paracelsus Medical University, Salzburg, Austria; [3]Department of Internal Medicine I, University Hospital Salzburg, Paracelsus Medical University, Salzburg, Austria; [4]Ludwig Boltzmann Institute for Arthritis and Rehabilitation, Paracelsus Medical University, Salzburg, Austria.
Contact: heidi.dobias@pmu.ac.at | https://www.pmu.ac.at/physiologie.html

## Objective

Methods for determining viable cell numbers (or cell mass) are central to basic cell biology research by providing information on cell viability, cytotoxicity and proliferation. The 96-well microplate format allows for medium to high throughput analyses including control samples on each plate. This project aims at a comprehensive characterisation and direct comparison of ten widely used microplate-based assays using a dilution series of HeLa cervical cancer cells.

## Methods

Dilution series of HeLa cells were seeded into 96-well microplates and assayed for viable cell mass using the assays and protocols described in Figure 1. The results were analyzed for repeatability (coefficient of variation, CV), linear range, sensitivity towards cell number changes (slope of linear range), and reproducibility.

## Results (I)

- **Repeatability** (Figure 2): a CV threshold of 0.5 was set to restrict the subsequent analyses to cell numbers with an acceptable signal variability.
- Representative plots of the **linear range** of two assays are shown in Figure 3 – nuclear count (Hoechst 33342 staining) and the MTS assay. The linear range and the linear regression was limited to the range of data points resulting in a COD (coefficient of determination) >0.99.

**Figure 4. Assay characteristics**

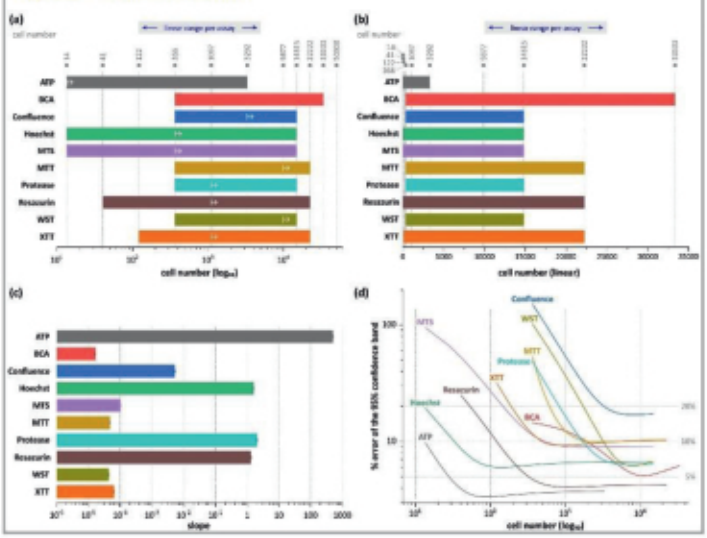


## Results (II)

The **assay characteristics** summarized in Figure 4 allow for the following statements:

- Most assays tested showed a linear range between ~400 and 15,000 cells.
- The linear range of intracellular ATP content, nuclear count (Hoechst), the MTS and the Resazurin assay extends down to 100 cells and below.
- The ATP assay, followed by fluorescence assays (Hoechst-based nuclei count, Resazurin, live-cell protease) show the highest slope of the linear regression, i.e. the highest sensitivity towards changes in analyte concentration (cell number).
- Although confluence measurement showed the highest experiment-to-experiment variability, this is the only label-free assay in the current methods' selection, thus allowing for any downstream application.

This study was supported by funds of the federal government of Salzburg (Wirtschafts- und Forschungsförderung, 20102-P1600889-FPR01-2016).

**Figure 1. Workflow and protocol overview**

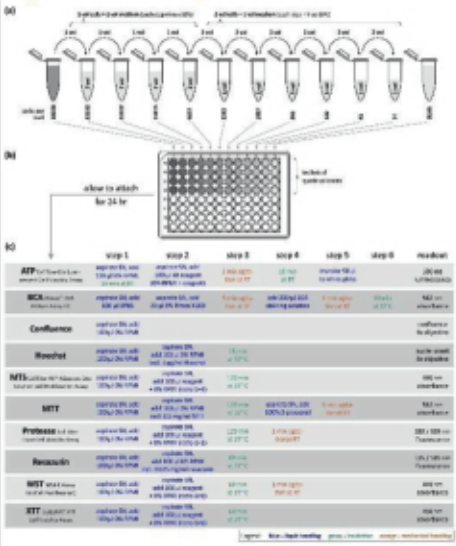


**Figure 2. Assay repeatability**

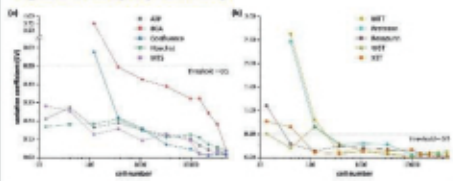


**Figure 3. Linear regression, linear range**

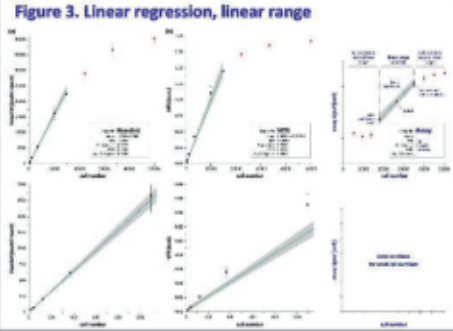

## Conclusions

The results confirm that luminometric measurement of intracellular ATP content is the gold standard surrogate parameter for determination of cell number in terms of lower limit of quantification and assay sensitivity towards changes in cell number. This assay is followed by nuclear count (Hoechst 33342 staining) and the Resazurin assay. For intermediate cell numbers, additional considerations such as costs, hands-on time, instrument availability or subsequent applications are relevant in choosing the most appropriate method.

## Comparative Evaluation of Microplate-based Assays for Viable Cell Quantity

Heidemarie Dobias[1,2], Christian Mayr[1,3], Marlena Beyreis[1], Markus Ritter[1,2,4], Tobias Kiesslich[1,3]

[1]Center for Physiology, Pathophysiology and Biophysics - Salzburg and Nuremberg, Institute for Physiology and Pathophysiology - Salzburg, Paracelsus Medical University, Austria; [2]Gastein Research Institute, Paracelsus Medical University, Salzburg, Austria; [3]Department of Internal Medicine I, University Hospital Salzburg, Paracelsus Medical; [4]Ludwig Boltzmann Institute for Arthritis and Rehabilitation, Paracelsus Medical University, Salzburg, Austria; Contact: heidi.dobias@pmu.ac.at

### Objective
Methods for determining the viable cell quantity (or cell mass) are central to basic cell biology research by providing information on cell viability, cytotoxicity and proliferation. The 96-well microplate format allows for medium to high throughput analyses including control samples on each plate. This project aims at a comprehensive characterisation and direct comparison of ten widely used microplate-based assays using a HeLa cell line dilution series.

### Methods
Serial dilutions of HeLa cervical cancer cells were seeded into 96-well microplates and assayed on the subsequent day after cell attachment. Viable cell mass assays were based on metabolic/enzymatic activity (MTT, MTS, Resazurin, WST and XTT), intracellular ATP content, confluence, nuclear count (Hoechst 33342 staining), live cell protease activity, or total cellular protein (BCA). For each assay, the results were evaluated for repeatability (coefficient of variation, CV), linear range, sensitivity towards cell number changes (slope of linear range), and reproducibility.

### Results
All assays tested showed a linear range between ~400 and 15,000 cells (except for intracellular ATP with a maximum of 3300 cells within the linear range). Lower cell numbers are well quantifiable using assays for intracellular ATP, nuclear count (Hoechst 33342) or metabolic/enzymatic activity-based assays (MTS, Resazurin, XTT). In most assays, a signal plateau was observed when 25,000 or more cell were seeded – most probably due to reduced proliferation (overnight) at these cell densities. The ATP assay, followed by fluorescence assays (Hoechst-based nuclei count, Resazurin, live-cell protease) showed the highest slope of the linear regression, i.e. indicating the highest sensitivity towards changes in analyte concentration (cell number). Reproducibility over biological replicates indicated by the width of the linear fits' confidence band was highest for ATP, followed by Resazurin and Hoechst-based nuclear count.

### Conclusions
The results confirm that luminometric measurement of intracellular ATP content is the gold standard surrogate parameter for determination of cell number in terms of lower limit of quantification and assay sensitivity towards changes in cell number. This assay is followed by nuclear count (Hoechst 33342 staining) and the Resazurin assay. For intermediate cell numbers, additional considerations such as costs, hands-on time, instrument availability or subsequent applications are relevant in choosing the most appropriate method.

### References
1. no references

# Establishing the cardiotonic steroid ouabain as a potent anti-cancer drug against biliary tract cancer – Step one

Heidemarie Dobias[1,2], Tobias Kiesslich[1,3], Markus Ritter[1,2,4], Daniel Neureiter[5], Elen Neureiter[5], Marlena Beyreis[1], Dino Bekric[1,2], Celina Ablinger[1,2], Christian Mayr[1,3]

[1]Center for Physiology, Pathophysiology and Biophysics - Salzburg and Nuremberg, Institute for Physiology and Pathophysiology - Salzburg, Paracelsus Medical University, Austria; [2]Gastein Research Institute, Paracelsus Medical University, Salzburg, Austria; [3]Department of Internal Medicine I, University Hospital Salzburg, Paracelsus Medical University, Salzburg, Austria; [4]Ludwig Boltzmann Institute for Arthritis and Rehabilitation, Paracelsus Medical University, Salzburg, Austria; [5]Department of Pathology, Cancer Cluster, University Hospital Salzburg, Paracelsus Medical University, Salzburg, Austria;

*Correspondence: heidi.dobias@pmu.ac.at; https://www.pmu.ac.at/physiologie.html

This work is supported by the PMU Research Fund PMU-FFF (R-17/04/095-DOB)

## Objective

Cardiotonic steroids (CTS) like ouabain are $Na^+/K^+$-ATPase (NKA) inhibitors which bind to the α-subunit of the enzyme and inhibit its ion pump function at saturating (millimolar) concentrations, which results in breakdown of the electrochemical gradients across the cell membrane ("ionic pathway"). However, in subsaturating (nanomolar) concentrations CTS have been reported to exert anti-tumor effects. These effects uncover a novel receptor function of the NKA. Activation of the NKA receptor results in its interaction with other signaling receptors like the EGF receptor and activation of intracellular pathways which in turn regulate cell functions including proliferation, migration and apoptosis ("signaling pathway"). The aim of the current project is to evaluate whether subsaturating concentrations of ouabain exert cytotoxic effects on several BTC cells.

## Methods

Dose-response analysis of ouabain cytotoxicity on different BTC cell lines (n=8) and one non-tumor cholangiocyte (MMNK-1) cell line was assessed using fluorescent resazurin labeling. NKA subunit expression was analyzed with Real Time PCR. Ouabain-induced mode of cell death was tested by Caspase-Glo®3/7 Assay (apoptosis), LDH-Glo™ Cytotoxicity Assay (necrosis), RealTime-Glo™ Annexin V Apoptosis and Necrosis Assay (apoptosis and/or necrosis).

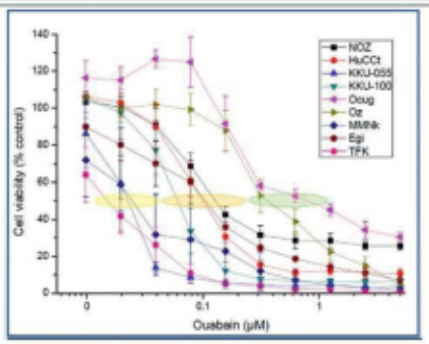


**Results 1. Cytotoxicity of ouabain.** Ouabain shows cell line dependent cytotoxicity at subsaturating nanomolar concentrations.

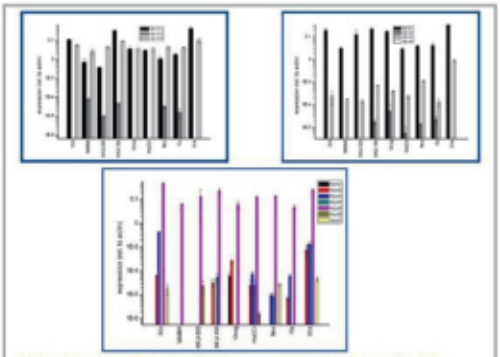

**Results 2. NKA subunit expression analysis.** NKA subunit expression analysis revealed cell type specific expression of different NKA subunits. Some isoforms of the alpha and beta subunits (e.g. atp1a1, atp1a3, atp1b1) and fxyd5 are expressed in all tested cell lines.

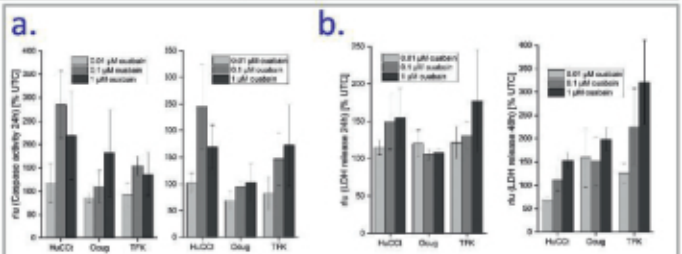


**Results 3a/b.** For investigation of the mode of cytotoxicity, we grouped the cell lines in the categories 'very sensitive' (TFK, MMNK, KKU-055), 'sensitive' (NOZ, HuCCt, Egi) and 'less sensitive' (Ocug, Oz) cells (see Results 1. represented by yellow, orange, green ellipses). Ouabain shows only marginal cell line and concentration dependent effects in caspase activation (after 24 und 48 h of incubation; a) and LDH release (after 48 h of incubation; b).

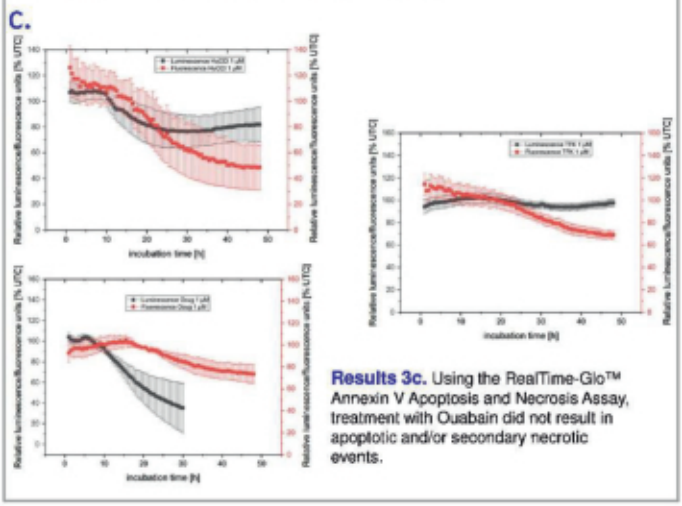


**Results 3c.** Using the RealTime-Glo™ Annexin V Apoptosis and Necrosis Assay, treatment with Ouabain did not result in apoptotic and/or secondary necrotic events.

## Conclusion and Outlook

Ouabain has a cell line-dependent cytotoxic effect at nanomolar concentrations in all tested cell lines. No correlation was found between NKA subunit expression and ouabain sensitivity in the tested *in vitro* models. Regarding the mode of cytotoxicity initiated by ouabain in BTC cells, further experiments are required as the current results (Caspase-Glo®3/7 3D Assay LDH-Glo™ Cytotoxicity Assay, RealTime-Glo™ Annexin V Apoptosis and Necrosis Assay) do not point towards these modes of cell death.

Therefore, we will perform time-resolved cytotoxic analysis as well as combinatory treatments of BTC cells using ouabain and established cell death inhibitors (inhibitors of apoptosis, necrosis, ferroptosis). Furthermore, we will evaluate whether the used ouabain concentrations are indeed in the subsaturating range, i.e. we will assess whether or not these concentrations interfere with the electrochemical gradients across the cell membrane, e.g. by measuring the cell membrane potential in the absence and presence of ouabain at different concentrations.

## Establishing the cardiotonic steroid ouabain as a potent anti-cancer drug against biliary tract cancer – Step one

Heidemarie Dobias[1,2], Tobias Kiesslich[1,3], Markus Ritter[1,2,4], Daniel Neureiter[5], Elen Neureiter[5], Marlena Beyreis[1], Dino Bekric[1,2], Celina Ablinger[1,2], Christian Mayr[1,3]

[1]Center for Physiology, Pathophysiology and Biophysics - Salzburg and Nuremberg, Institute for Physiology and Pathophysiology - Salzburg, Paracelsus Medical University, Austria; [2]Gastein Research Institute, Paracelsus Medical University, Salzburg, Austria; [3]Department of Internal Medicine I, University Hospital Salzburg, Paracelsus Medical; [4]Ludwig Boltzmann Institute for Arthritis and Rehabilitation, Paracelsus Medical University, Salzburg, Austria; [5]Department of Pathology, Cancer Cluster, University Hospital Salzburg, Paracelsus Medical University, Salzburg, Austria;; Contact: heidi.dobias@pmu.ac.at

### Objective
Identification of therapeutically relevant substances for the treatment of biliary tract cancer (BTC) is of utmost importance. Cardiotonic steroids (CTS) like ouabain are Na+/K+-ATPase (NKA) inhibitors which bind to the α-subunit of the enzyme and inhibit its ion pump function at saturating (millimolar) concentrations, which results in breakdown of the electrochemical gradients across the cell membrane ("ionic pathway"). However, in subsaturating (nanomolar) concentrations CTS have been reported to exert anti-tumor effects. These effects uncover a novel receptor function of the NKA. Activation of the NKA receptor results in its interaction with other signaling receptors like the EGF receptor and activation of intracellular pathways which in turn regulate cell functions including proliferation, migration and apoptosis ("signaling pathway"). The aim of the current project is to evaluate whether subsaturating concentrations of ouabain exert cytotoxic effects on several BTC cells.

### Methods
Dose-response analysis of ouabain cytotoxicity on different BTC cell lines (n=8) and one non-tumor cholangiocyte (MMNK-1) cell line was assessed using fluorescent resazurin labeling. NKA subunit expression was analyzed with Real Time PCR. Ouabain-induced mode of cell death was tested by Caspase-Glo®3/7 Assay (apoptosis), LDH-Glo™ Cytotoxicity Assay (necrosis), RealTime-Glo™ Annexin V Apoptosis and Necrosis Assay (apoptosis and/or necrosis).

### Results
Ouabain shows cell line dependent cytotoxicity at subsaturating nanomolar concentrations. NKA subunit expression analysis revealed cell type specific expression of different NKA subunits. Some isoforms of the alpha and beta subunits and the fxyd5 subunit are expressed in all tested cell lines. For investigation of the mode of cytotoxicity, we grouped the cell lines in the categories ´very sensitive´ (TFK, MMNK, KKU-055), ´sensitive´ (NOZ, HuCCt, Egi) and ´less sensitive´ (Ocug, Oz) cells. Surprisingly, treatment of BTC cells with ouabain did not result in significant initiation of apoptosis or necrosis.

### Conclusions
Ouabain has a cell line-dependent cytotoxic effect at nanomolar concentrations in all tested cell lines. No correlation was found between NKA subunit expression and ouabain sensitivity. Regarding the mode of cytotoxicity initiated by ouabain in BTC cells, further experiments are required as the current results do not point towards these modes of cell death.Therefore, we will perform time-resolved cytotoxic analysis as well as combinatory treatments of BTC cells using ouabain and established cell death inhibitors (inhibitors of apoptosis, necrosis, ferroptosis). Furthermore, we will evaluate whether the used ouabain concentrations are indeed in the subsaturating range, i.e. we will assess whether or not these concentrations interfere with the electrochemical gradients across the cell membrane, e.g. by measuring the cell membrane potential in the absence and presence of ouabain at different concentrations.

### References
no references

Klinikum Nürnberg
PARACELSUS MEDIZINISCHE PRIVATUNIVERSITÄT

# Identification of baseline characteristics of HR+/HER2- primary metastatic breast cancer patients at Breast Center Klinikum Nuremberg that drive decision between chemotherapy and CDK4/6 inhibition

Christiane Dormann[1], Prof. Dr. Cosima Brucker[2], Dr. Fabian Winterholler[3]
1) Paracelsus Medical University Nuremberg, Germany 2) Department of Gynecology Paracelsus Medical University - Klinikum Nuremberg, Germany 3) Department of Gynecology Klinikum Fürth, Germany

**Objective.** Breast cancer is the most frequent malignant tumour in women worldwide with HR+/HER2- breast carcinoma as the most common subtype. In 2016, the drug class of cyclin-dependent kinases 4/6 inhibitors was approved by international drug administrations offering an alternative to conventional cytostatic chemotherapy for primary metastatic disease. This study's aim is to evaluate the changes of first-line systemic treatment choices for HR+/HER2- primary metastatic breast cancer at Klinikum Nuremberg comparing CDK4/6 inhibitors to cytostatic chemotherapy and to evaluate if the results match international guideline suggestions.

**Methods.** We retrospectively included all patients with HR+/HER2- primary metastatic breast cancer who received any systemic treatment from 2015 to 2019. Based on protocols of tumour board meetings at Klinikum Nuremberg patient, tumour characteristics and recommended initial systemic therapy were collected. Initial metastatic sites were classified as solely osseous, visceral or multiple metastases (both bone and visceral metastases). Possible initial systemic therapy options were CDK4/6 inhibiting agents combined with endocrine therapy, endocrine monotherapy or chemotherapy. The chosen first-line systemic therapy was analysed for the total cohort and defined subgroups. Data were checked for consistency and normality. Independent t-tests and univariate logistic regression models were applied to evaluate data.

Table 1: Baseline characteristics of first-line systemic treatment (Cohort 1)

| 2015 - 2019 | CT N = 17 (19%) | CDK4/6 + ET N = 47 (52%) | ET N = 27 (30%) | Total N = 91 |
|---|---|---|---|---|
| Age at diagnosis | | | | |
| Mean age | 55 | 65 | 81 | 66 |
| premenopausal | 7 (47%) | 8 (53%) | 0 (0%) | 15 |
| postmenopausal | 10 (13%) | 39 (52%) | 27 (36%) | 76 |
| < 70 y/o | 15 (30%) | 28 (56%) | 7 (14%) | 50 |
| ≥ 70 y/o | 2 (5%) | 19 (46%) | 20 (49%) | 41 |
| Initial metastatic sites | | | | |
| Bone only | 6 (17%) | 21 (60%) | 8 (23%) | 35 |
| Visceral only | 9 (26%) | 15 (43%) | 11 (31%) | 35 |
| Multiples | 2 (10%) | 11 (52%) | 8 (38%) | 21 |

*CT: chemotherapy; ET: endocrine therapy; y/o: years old*

Table 2: First-line systemic treatment choices (Cohort 1)

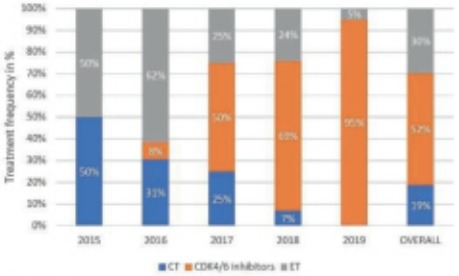


Table 3: Baseline characteristics of first-line systemic treatment (Cohort 2)

| 2015 - 2019 | CT N = 17 (27%) | CDK4/6 + ET N = 47 (73%) | Total N = 64 |
|---|---|---|---|
| Age at diagnosis | | | |
| Mean age | 55 | 65 | 62 |
| premenopausal | 7 (47%) | 8 (53%) | 15 |
| postmenopausal | 10 (20%) | 39 (80%) | 49 |
| < 70 y/o | 15 (35%) | 28 (65%) | 43 |
| ≥ 70 y/o | 2 (10%) | 19 (90%) | 21 |
| Initial metastatic sites | | | |
| Bone only | 6 (22%) | 21 (78%) | 27 |
| Visceral only | 9 (38%) | 15 (62%) | 24 |
| Multiples | 2 (15%) | 11 (85%) | 13 |

*CT: chemotherapy; ET: endocrine therapy; y/o: years old*

Table 4: First-line systemic treatment choices (Cohort 2)

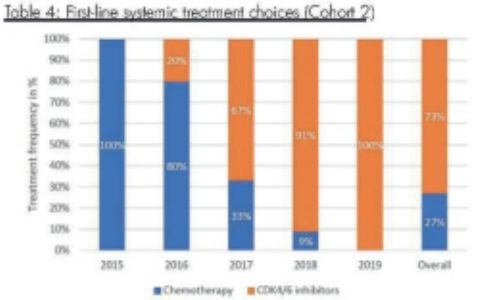


**Results.** Based on the chosen first line systemic therapy patients were subdivided into two cohorts. Cohort 1 with 91 patients received CDK4/6 inhibiting drugs (52%), endocrine monotherapy (30%) and chemotherapy (19%) as initial systemic treatment (Table 1). In Cohort 2 patients who received endocrine monotherapy were excluded. Cohort 2 consists of 64 patients who were treated with CDK4/6 inhibiting drugs (73%) and chemotherapy (27%) (Table 3). Table 2 and 4 show the shift of first-line systemic treatment choices towards CDK4/6 inhibiting therapy in both cohorts.

In 2015 exclusively chemotherapeutic treatment was used in Cohort 2, whereas in 2019 all first line systemic treatments were CDK4/6 inhibiting therapies (Table 4). The mean age of the patients treated with CDK4/6 inhibitors is significantly higher than the one of the patients receiving chemotherapy (p=0.01). In patients who receive either chemotherapy or a CDK4/6 inhibiting therapy, the probability of being treated with CDK4/6 inhibitors significantly increases with age (p=0.01). Initial metastatic sites did not constitute criteria for preferring a chemotherapeutic treatment or a CDK4/6 inhibiting treatment.

**Conclusion.**
CDK4/6 inhibiting drugs were increasingly included at Breast Center Klinikum Nuremberg since their approval. The use of cytostatic chemotherapy was declining respectively. First-line systemic treatment choices at Breast Center Klinikum Nuremberg correspond to international guideline suggestions.

**Contact:** christiane.dormann@stud.pmu.ac.at

© Paracelsus Medizinische Privatuniversität – Universitätsklinik für Gynäkologie und Geburtshilfe

## Identification of baseline characteristics of HR+/HER2- primary metastatic breast cancer patients at Breast Center Klinikum Nuremberg that drive decision between chemotherapy and CDK4/6 inhibition

Christiane Dormann[1], Cosima Brucker[2], Fabian Winterholler[3]

[1]Paracelsus Medical University, Nuremberg, Germany; [2]Department of Gynecology and Obstetrics, Paracelsus Medical University, Nuremberg, Germany; [3]Department of Gynecology and Obstetrics, Klinikum Fürth; Contact: christiane.dormann@stud.pmu.ac.at

### Objective
Breast cancer is the most frequent malignant tumour in women worldwide with HR+/HER2- breast carcinoma as the most common subtype. In 2016, the drug class of cyclin-dependent kinases 4/6 inhibitors was approved by international drug administrations offering an alternative to conventional cytostatic chemotherapy for primary metastatic disease. This study's aim is to evaluate the changes of first-line systemic treatment choices for HR+/HER2- primary metastatic breast cancer at Klinikum Nuremberg comparing CDK4/6 inhibitors to cytostatic chemotherapy and to evaluate if the results match international guideline suggestions.

### Methods
We retrospectively included all patients with HR+/HER2- primary metastatic breast cancer who received any systemic treatment from 2015 to 2019. Based on protocols of tumour board meetings at Klinikum Nuremberg patient, tumour characteristics and recommended initial systemic therapy were collected. Initial metastatic sites were classified as solely osseous, visceral or multiple metastases (both bone and visceral metastases). Possible initial systemic therapy options were CDK4/6 inhibiting agents combined with endocrine therapy, endocrine monotherapy or chemotherapy. The chosen first-line systemic therapy was analysed for the total cohort and defined subgroups. Data were checked for consistency and normality. Independent t-tests and univariate logistic regression models were applied to evaluate data.

### Results
Based on the chosen first line systemic therapy patients were subdivided into two cohorts. Cohort 1 with 91 patients received CDK4/6 inhibiting drugs (52%), endocrine monotherapy (30%) and chemotherapy (19%) as initial systemic treatment (Table 1). In Cohort 2 patients who received endocrine monotherapy were excluded. Cohort 2 consists of 64 patients who were treated with CDK4/6 inhibiting drugs (73%) and chemotherapy (27%) (Table 3). Table 2 and 4 show the shift of first-line systemic treatment choices towards CDK4/6 inhibiting therapy in both cohorts. In 2015 exclusively chemotherapeutic treatment was used in Cohort 2, whereas in 2019 all first line systemic treatments were CDK4/6 inhibiting therapies (Table 4). The mean age of the patients treated with CDK4/6 inhibitors is significantly higher than the one of the patients receiving chemotherapy ($p=0.01$). In patients who receive either chemotherapy or a CDK4/6 inhibiting therapy, the probability of being treated with CDK4/6 inhibitors significantly increases with age ($p=0.01$). Initial metastatic sites did not constitute criteria for preferring a chemotherapeutic treatment or a CDK4/6 inhibiting treatment.

### Conclusions
CDK4/6 inhibiting drugs were increasingly included at Breast Center Klinikum Nuremberg since their approval. The use of cytostatic chemotherapy was declining respectively. First-line systemic treatment choices at Breast Center Klinikum Nuremberg correspond to international guideline suggestions.

# Potential role of Cullin-RING E3 ubiquitin ligase $CRL3^{Zbtb16}$ in the premature degradation of pathogenic pendrin variants

Silvia Dossena[1], Emanuele Bernardinelli[1], Zhen-Qiang Pan[2], Robert Konrat[3], Antonio Sarikas[1]

[1]Institute of Pharmacology and Toxicology, Paracelsus Medical University, Salzburg, Austria
[2]Department of Oncological Sciences, Icahn School of Medicine at Mount Sinai, New York, USA
[3]Department of Structural and Computational Biology, University of Vienna, Austria

## Background and Objectives

- Pendrin (SLC26A4) is a $Cl^-/HCO_3^-$ exchanger expressed in the inner ear and is essential for a normal hearing function.
- Genetically inherited pathogenic variants of pendrin are involved in determining Pendred syndrome (OMIM ID_274600) and non-syndromic autosomal recessive deafness B4 (DFNB4, OMIM ID_600791), which are two of the most common forms of hereditary hearing loss.
- Recently, we have shown that the ubiquitin proteasome system controls the protein levels of pendrin and leads to an accelerated degradation of its pathogenic variants [1,2].
- A yeast two-hybrid screening of a library of mouse kidney proteins with the C-terminus of pendrin identified the zinc-finger and BTB domain-containing protein Zbtb16 as a pendrin binding partner. However, the biological significance of this molecular interaction is currently unknown.
- Zbtb16 forms a Cullin-RING E3 ubiquitin ligase comprising Cullin3 and Rocl ($CRL3^{Zbtb16}$) [3] (**Figure 1**). Therefore, we hypothesized that the $CRL3^{Zbtb16}$ E3 ubiquitin ligase might recruit wild type pendrin and its pathogenic variants to proteasomal degradation.

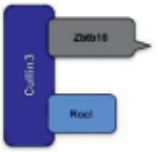


**Figure 1. Specific composition of the $CRL3^{Zbtb16}$ E3 ligase.** Cullin proteins are molecular scaffolds that assemble multi-subunit cullin-RING E3 ubiquitin ligase (CRL) complexes. In the $CRL3^{Zbtb16}$, a cullin protein (Cullin3) tethers both an adaptor/substrate-recognition subunit (Zbtb16) and the RING finger component Rocl. BTB, Bric-a-brac, Tramtrack, Broad-complex domain; RING, really interesting new gene. Redrawn from [3].

## Methods

- Expression of pendrin, Zbtb16, Cullin3 and Rocl transcripts in the inner ear and other mouse tissues was verified by RT-qPCR.
- Co-localization between pendrin and Zbtb16 in the mouse inner ear was verified by immunchistochemistry of cochlear sections.
- The direct molecular interaction between pendrin and Zbtb16 proteins was verified in intact cells by fluorescence resonance energy transfer (FRET).
- The protein structure and protein-protein interaction score were determined by protein meta-analysis [4].

## Results

- Zbtb16, Cullin3 and Rocl transcripts were abundantly expressed in the inner ear and kidney cortex, which are known to express pendrin (**Figure 2**).
- In the inner ear, the Zbtb16 protein resulted prominently expressed in the organ of Corti and co-localized with pendrin in the *stria vascularis* (**Figure 3**).
- Wild type pendrin as well as four pendrin pathogenic variants frequently found in the Caucasian population (p.L236P, p.R409H, p.G149R and p.Q431R) established a direct molecular interaction with Zbtb16 (wild type pendrin FRET efficiency: 0.105±0.013, n=18, p<0.01) (**Figure 4A**).
- Sequential deletions of the C-terminus of pendrin guided by protein-protein interaction score followed by FRET indicated that Zbtb16 binds to amino acids 584-673 of pendrin (**Figure 4B-C**). This region is structurally disordered but contains six putative Ser/Thr phosphorylation and two ubiquitination sites and a local alpha-helix organization, which represents a typical protein-protein interaction motif (**Figure 5**).

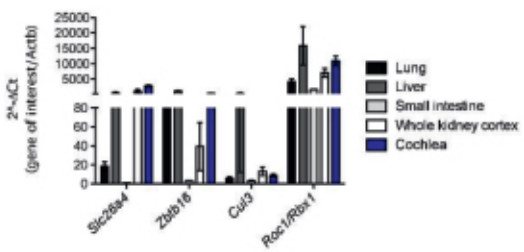


**Figure 2. Zbtb16 is expressed in the mouse cochlea.** Expression levels of the indicated transcripts determined by RT-qPCR on total mRNA extracted from mouse tissues (n=3 independent samples) and normalized for the housekeeping transcript *Actb*.

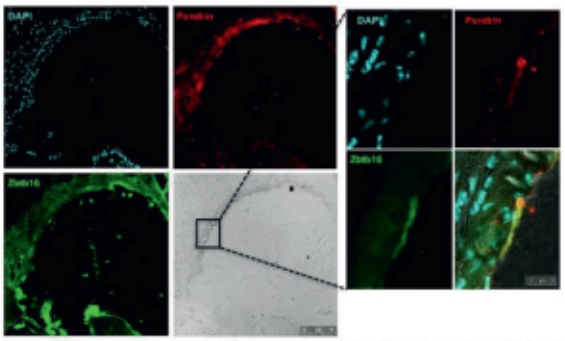


**Figure 3. Zbtb16 co-localizes with pendrin in the *stria vascularis*.** Expression and co-localization of Zbtb16 and pendrin in 8-weeks old mice cochlea sections imaged by confocal microscopy following immunostaining with anti-pendrin (rabbit polyclonal, H-195, Santa Cruz) and anti-Zbtb16 (mouse monoclonal, D-8, Santa Cruz) antibodies. Endogenous mouse IgG were blocked with an unlabeled goat anti-mouse IgG (Abcam, ab6668, 0.1 mg/ml) to reduce background.

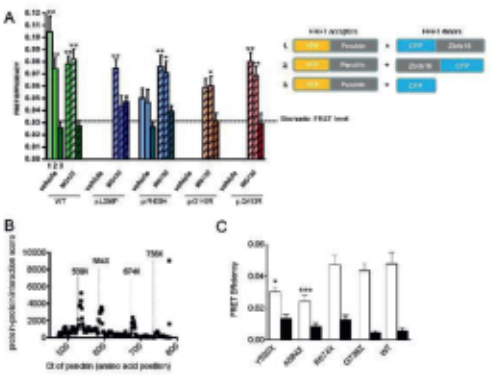


**Figure 4. Zbtb16 binds wild type pendrin and its pathogenic variants. (A).** HeLa cells were transfected for 72 hours with plasmid vectors encoding the indicated FRET donors and acceptors pairs (samples #1, 2 and 3) and treated with the proteasome inhibitor MG132 (10 μM). FRET was determined following photobleaching of the acceptor. **: p<0.01, *: p<0.05 compared to stochastic FRET (sample #3), one-way ANOVA with Dunnet's post-test. **(B).** Protein-protein interaction score of the C-terminus of pendrin. Arrows indicate sequential deletions for which the interaction with Zbtb16 was probed by FRET **(C).** ***: p<0.001, *: p<0.05 compared the wild type, two-tailed, unpaired Student's t test.

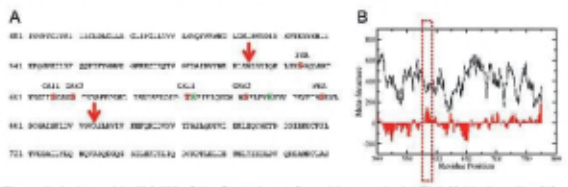


**Figure 5. Amino acids 584-673 of the C-terminus of pendrin contain the Zbtb16 binding site. (A).** Amino acid sequence of human pendrin. Red arrows encompass the Zbtb16 binding site as determined by FRET. Red and green letters indicate putative phosphorylation and poly-ubiquitination sites, respectively, according to http://www.cbs.dtu.dk/services/NetPhos/ and http://www.ubpred.org/cgi-bin/ubpred/ubpred.cgi. **(B).** Meta-structure of the C-terminus of pendrin. The bottom graph (red) indicates the protein secondary structure and the top graph (black) the structural compactness. The dotted rectangle indicates the putative Zbtb16 binding site. Positive values of protein secondary structure associated with high compactness indicate that this region is organized in an alpha helix.

## Conclusions

- Cullin-RING E3 ubiquitin ligase $CRL3^{Zbtb16}$ may contribute to the accelerated degradation of pendrin pathogenic variants following their recruitment to the ubiquitin proteasome system.
- The characterization of the mechanism underlying pendrin degradation may lead to the identification of novel therapeutic targets for hereditary hearing loss.

## References

1. De Moraes, V.C.S.; Bernardinelli, E.; ... Dossena, S. Reduction of cellular expression levels is a common feature of functionally affected pendrin (SLC26A4) protein variants. Mol Med. 2016, 22:41-53
2. Roesch, S.; Bernardinelli, E.; ... Dossena, S. Functional testing of SLC26A4 variants-clinical and molecular analysis of a cohort with enlarged vestibular aqueduct from Austria. Int J Mol Sci. 2018, 19(1):209
3. Sarikas, A.; Hartmann, T.; Pan, Z-Q. The cullin protein family. Genome Biol. 2011, 12(4):220
4. Konrat, R. The protein meta-structure: a novel concept for chemical and molecular biology. Cell Mol Life Sci. 2009, 66(22):3625-3639

## Potential role of Cullin-RING E3 ubiquitin ligase CRL3Zbtb16 in the premature degradation of pathogenic pendrin variants

Silvia Dossena[1], Emanuele Bernardinelli[1], Zhen-Qiang Pan[2], Robert Konrat[3], Antonio Sarikas[1]

[1]Institute of Pharmacology and Toxicology, Paracelsus Medical University, Salzburg, Austria; [2]Department of Oncological Sciences, Icahn School of Medicine at Mount Sinai, New York, USA; [3]Department of Structural and Computational Biology, University of Vienna, Austria; Contact: silvia.dossena@pmu.ac.at

### Objective
Pendrin (SLC26A4) is a $Cl^-/HCO_3^-$ exchanger expressed in the inner ear and is essential for a normal hearing function. Genetically inherited pathogenic variants of pendrin are involved in determining Pendred syndrome (OMIM ID_274600) and non-syndromic autosomal recessive deafness B4 (DFNB4, OMIM ID_600791), which are two of the most common forms of hereditary hearing loss. Recently, we have shown that the ubiquitin proteasome system controls the protein levels of pendrin and leads to an accelerated degradation of its pathogenic variants. A yeast two-hybrid screening of a library of mouse kidney proteins with the C-terminus of pendrin identified the zinc-finger and BTB domain-containing protein Zbtb16 as a pendrin binding partner. However, the biological significance of this molecular interaction is currently unknown. Zbtb16 forms a Cullin-RING E3 ubiquitin ligase comprising Cullin3 and RocI ($CRL3^{Zbtb16}$). Therefore, we hypothesized that the $CRL3^{Zbtb16}$ E3 ubiquitin ligase might recruit wild type pendrin and its pathogenic variants to proteasomal degradation.

### Methods
Expression of pendrin, Zbtb16, Cullin3 and RocI transcripts in the inner ear and other mouse tissues was verified by RT-qPCR. Co-localization between pendrin and Zbtb16 in the mouse inner ear was verified by immunohistochemistry of cochlear sections. The direct molecular interaction between pendrin and Zbtb16 proteins was verified in intact cells by fluorescence resonance energy transfer (FRET). The protein structure and protein-protein interaction score were determined by protein meta-analysis.

### Results
Zbtb16, Cullin3 and RocI transcripts were abundantly expressed in the inner ear and kidney cortex, which are known to express pendrin. In the inner ear, the Zbtb16 protein resulted prominently expressed in the organ of Corti and co-localized with pendrin in the *stria vascularis*. Wild type pendrin as well as four pendrin pathogenic variants frequently found in the Caucasian population (p.L236P, p.R409H, p.G149R and p.Q431R) established a direct molecular interaction with Zbtb16 (wild type pendrin FRET efficiency: $0.105 \pm 0.013$, $n=18$, $p<0.01$). Sequential deletions of the C-terminus of pendrin guided by protein-protein interaction score followed by FRET indicated that Zbtb16 binds to amino acids 584-673 of pendrin. This region is structurally disordered but contains six putative Ser/Thr phosphorylation and two ubiquitination sites and a local alpha-helix organization, which represents a typical protein-protein interaction motif.

### Conclusions
Cullin-RING E3 ubiquitin ligase $CRL3^{Zbtb16}$ may contribute to the accelerated degradation of pendrin pathogenic variants following their recruitment to the ubiquitin proteasome system. Characterization of the mechanism underlying pendrin degradation may lead to the identification of novel therapeutic targets for hereditary hearing loss.

# Self-assembly of iPSC-derived single cells creates organoids and regenerates vascularized human skin

Patricia Ebner[1], Linda Krisch[1,2], Martin Wolf[1], Anna Hoog[1], Sarah Hochmann[1], Balázs Vári[1], Katharina Muigg[1], Rodolphe Poupardin[1], Cornelia Scharler[3], Sabine Schmidhuber[3], Elisabeth Russe[4], Cornelia Hauser-Kronberger[5], Harald Stachelscheid[6], Achim Schneeberger[3], Katharina Schallmoser[2], Dirk Strunk[1]

[1]Cell Therapy Institute, Spinal Cord Injury and Tissue Regeneration Center Salzburg (SCI-TReCS), Paracelsus Medical University, Salzburg, Austria; [2]Department of Transfusion Medicine, Paracelsus Medical University, Salzburg, Austria; [3]Accanis Biotech, Biocenter Vienna, Austria; [4]Department of Plastic, Aesthetic and Reconstructive Surgery, Hospital Barmherzige Brueder, Salzburg, Austria; [5]Department of Pathology, Paracelsus Medical University Salzburg, Austria; [6]Stem Cell Core Facility, Charité, Berlin Institute of Health, Berlin, Germany.

## 1) Introduction

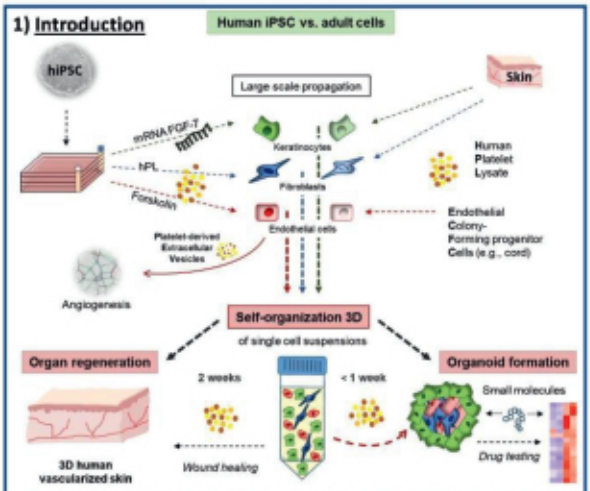


Self-assembly of adult and hiPSC-derived keratinocytes, fibroblasts and endothelial cells was promoted by platelet-derived growth factors, creating novel skin organoids within 6 days. Human skin organoids were properly characterized expressing markers of all skin layers and were used for high-content screening. We also established a humanized skin regeneration mouse model, based on self-assembly of adult as compared to iPSC-derived skin cell lineages under xeno-free conditions resulting in organized neo-vascularized human skin.

## 2) Platelet growth factors (HPL) support 3D organoid assembly

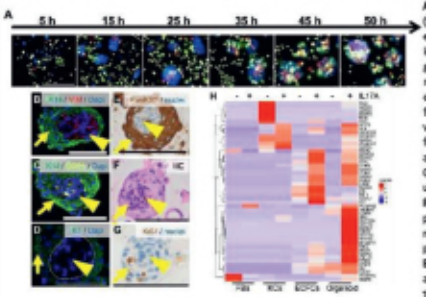


**A:** Nanoparticle labelling (fibroblasts (FBs) blue, endothelial cells (ECs)= red, keratinocytes (KCs) = green) and live cell imaging revealed sequential organoid assembly starting from initial stromal-vascular aggregation and followed by the superficial anchorage of adult KC. **B-G:** Organoid characterization using skin (VIM, K14, PanMKT), vessel (CD31) and proliferation (Ki67) markers. **H:** Proteome profiling of single FBs, ECFCs, KCs and organoids after 12 h stimulation in the absence (HCL control) or presence of IL17A. Z-scores.

## 3) Human iPSC-derived cell characterization

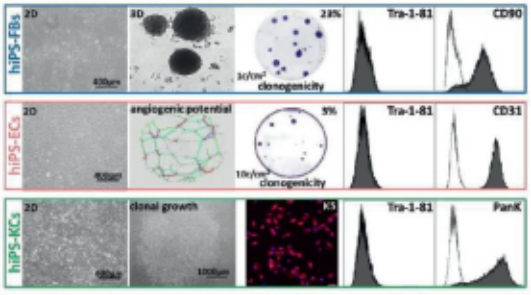


Cell characterization of hiPS-FBs, hiPS-ECs and hiPS-KCs revealed the cell type-specific morphology and marker expression. Tra-1-81 negative cell populations confirmed the lack of pluripotency in all three cell types. The angiogenic potential of iPS-EC was shown in a tube-like structure formation assay and iPS-FB and iPS-KC revealed clonogenic potential. Data from iPSC derived cells of two independent donors, repeated 2-6 times.

## 4) HPL supports rapid layered human skin organization *in vivo*

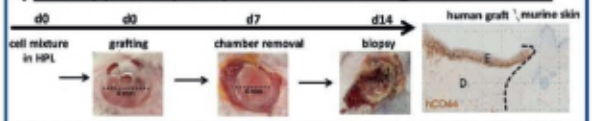


Schema of the skin cell transplantation model, where cells in animal serum-free 10% HPL or 10% FBS (Wang et al. 2000, JID) were transplanted. Anti-human CD44 (hCD44) staining of two weeks old skin grafts showed human cell organization into epidermis (E) and dermis (D) and the border between the human graft and the murine skin (dotted line).

## 5) Improved neo-vascularized skin in the presence of HPL

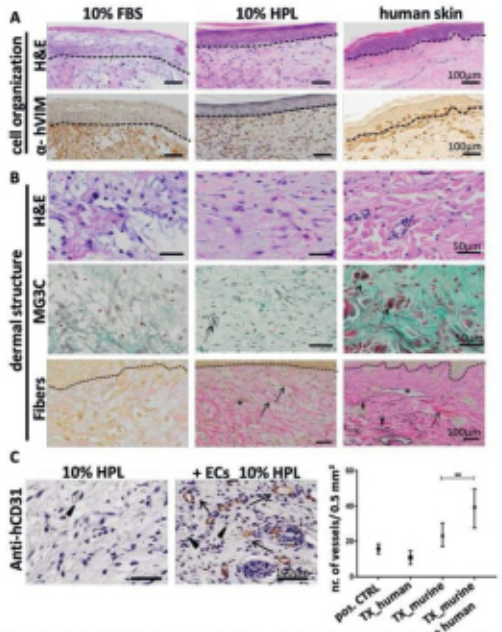


**A:** H&E of cell grafts in 10% HPL shows normal cell organization, whereas cell grafts in 10% FBS result in hyperkeratosis indicated by the thickened epidermis. **B:** Comparison of the dermal structures via H&E, MG3C and collagen fiber staining confirms the increased quality of 10% HPL by a regular fibroblast organization, blood vessels (dotted arrow), ground substance (asterisk) and collagen fiber production (arrow). **C:** Anti-human CD31 staining showed the formation of human blood vessels within the human skin upon co-transplantation of ECs. Quantification showed significantly increased vessel numbers upon co-transplantation of EC. Data from 3 biological and 3 technical replicates. Scale bar = 100 µm.

## 6) Successful iPSC-based self-organized skin regeneration

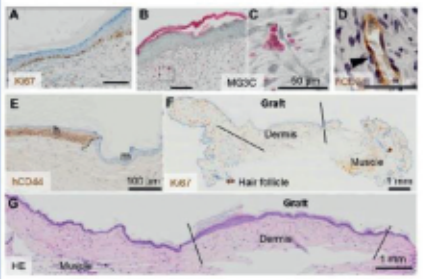


Human iPSC grafts, two weeks (**A-D**) and 3 months (**E-G**) after transplantation. **A:** Ki67 staining showed proliferation at the basal epidermal layer (brown). **B-C:** MG3C staining showed a vascularized dermis, (**C**) higher magnification, day 14. **D:** hCD31$^+$ human vessel. **E:** hCD44 staining showed border between human graft and murine skin, 3 mo. **F-G:** Ki67 and HE staining showed the absence of tumorigenic structures in serial full section scans three months after grafting. 2 animals per condition.

## 7) Conclusion

These data show that self-assembly of adult and human iPSC-derived human KCs+FBs combined with co-transplantation of ECs can create complex organoids *in vitro* and patent neo-vascularized human skin *in vivo* in a platelet-derived growth factor dependent manner. This technology has broad applicability in studies of skin regeneration and skin pharmacology, building the basis for novel therapeutic strategies.

Funding: European Union's Horizon 2020; grant agreement N°668724 – TECHNOBEAT.

Cell Therapy Institute, PMU Salzburg
Dr. Patricia Ebner, patricia.ebner@pmu.ac.at

## Self-assembly of human iPSC-derived single cells creates skin organoids and regenerates vascularized human skin

Patricia Ebner[1], Linda Krisch[1,2], Martin Wolf[1], Anna Hoog[1], Sarah Hochmann[1], Balász Vári[1], Katharina Muigg[1], Rodolphe Poupardin[1], Cornelia Scharler[1], Sabine Schmidhuber[3], Elisabeth Russe[4], Harald Stachelscheid[5], Achim Schneeberger[3], Katharina Schallmoser[2], Dirk Strunk[1]

[1]Cell Therapy Institute, Spinal Cord Injury and Tissue Regeneration Center Salzburg (SCI-TReCS), Paracelsus Medical University, Salzburg, Austria; [2]Department of Transfusion Medicine, Paracelsus Medical University, Salzburg, Austria.; [3]Accanis Biotech, Biocenter Vienna, Austria.; [4]Department of Plastic, Aesthetic and Reconstructive Surgery, Hospital Barmherzige Brueder, Salzburg, Austria.; [5]Stem Cell Core Facility, Charité, Berlin Institute of Health; Berlin, Germany.; Contact: patricia.ebner@pmu.ac.at

### Objective
Stem/progenitor cells can self-organize into organoids in culture, bearing the potential to model tissue function and regeneration. Here we demonstrated the 3D self-assembly of clonally expanded primary skin-derived mixed progenitors into spheroid organoids in vitro and the well-organized layered arrangement of human induced pluripotent stem cell (hiPSC)-derived and healthy adult skin-derived single cell suspension transplants into vascularized human skin in vivo.

### Methods
Umbilical cord blood-derived hiPSCs were differentiated into endothelial cells (hiPS-ECs), fibroblasts (hiPS-FBs) and keratinocytes (hiPS–KCs) according to efficiency-optimized protocols. Primary ECs, FBs and KCs were isolated from human tissues and polyclonally propagated under 2D xeno-free conditions. Cell identity and purity were confirmed by flow cytometry and clonogenicity indicated their stem/progenitor potential.

### Results
Human platelet-derived growth factors promoted the sequential organoid-like assembly of FBs, ECs and KCs in an orchestrated initial stromal-vascular aggregation step followed by superficial anchorage of KCs. Transplanting adult or hiPSC-derived single cell suspensions into full-thickness skin wounds of immune-deficient mice resulted in formation of layered human skin with a stratified epidermis and a vascularized dermis. Co-transplantation of ECs significantly boosted vascularization resulting in well-vascularized perfused transplants after 2wk only, compared to FBs/KCs transplants without ECs. No tumorigenesis was induced upon in vivo grafting, indicating the purity and lineage restriction of mature hiPSC-derived cells. Increased skin quality was revealed upon engraftment in human platelet lysate (HPL) compared to standard bovine serum, identified via following parameters: fiber/ground substance production/distribution, fibroblast density, dermal blood vessel content and epidermal stratification.

### Conclusions
We here developed an hiPSC-based skin regeneration strategy supported by HPL, showing that self-assembly of KCs+FBs combined with co-transplanting ECs forms organoids in culture and neo-vascularized human skin in vivo.

PARACELSUS
MEDIZINISCHE PRIVATUNIVERSITÄT

Klinikum Nürnberg
wir sind für Sie da.

# Multimodal diagnostic efforts for infratentorial lesions
# The suboccipital transcerebellar approach in stereotactic brain biopsy
# A single institution experience

**Thomas Eibl [1], Michael Schrey [1], Markus Holtmannspoetter [2], Cristiane Blechschmidt [3], Hans-Herbert Steiner [1]**

1 Department of Neurosurgery, Paracelsus Medical University, Nuremberg, Germany
2 Department of Radiology, Section Neuroradiology, Paracelsus Medical University, Nuremberg, Germany
3 Department of Pathology, Paracelsus Medical University, Nuremberg, Germany
Correspondence to: Thomas.eibl@klinikum-nuernberg.de

**Background:** Stereotactic brain biopsy is a core procedure in neurosurgical departments around the world. Almost any target site can be reached but yet lesions within the posterior fossa and the brainstem still remain challenging for the surgeon considering the approach and operative technique for technical as well as neuroanatomical reasons.

**Objective:** To describe a possible operative technique for a suboccipital route for stereotactic brain biopsy focusing on operative setting, success rates and complications of the transcerebellar route for stereotactic biopsy.

**Materials and Methods:** We present a retrospective analysis of patients' records who underwent diagnostic stereotactic biopsy via a suboccipital approach in out institution between 2011 and 2020.

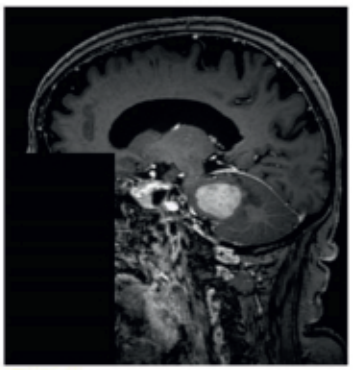

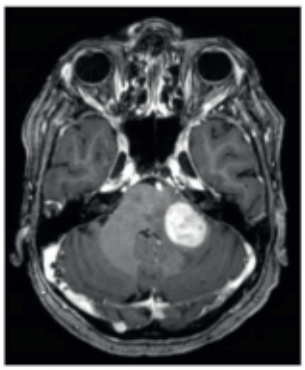

**Figure 1:** Left-sided cerebellar and contrast enhancing tumor (MRI, T1 with contrast-enhancement), histologic diagnosis: lymphoma

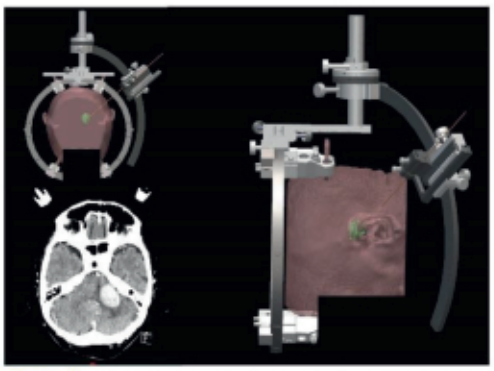

**Figure 2:** Trajectory planning for a left-sided transcerebellar biopsy

**Results:** 13 Patients (69.2% female) with 14 biopsied lesions were included, the mean age was 63.77 years, diagnostic yield was 12/13 (92.31%), a major complication occurred in 1 patient (7.7%). All biopsies were performed in a prone position under general anesthesia. We used the Zamorano-Dujovny stereotactic system without modifications with a straight but inversely (feet-)mounted frame.
Biopsies were obtained from the cerebellar hemispheres in 8 cases, cerebellar peduncles in 4 cases, the pons 1 case and the brainstem in 1 case. Histologic diagnoses were cerebral lymphoma in 5 cases, metastasis in 2 cases, glioblastoma WHO°IV, anaplastic astrocytoma WHO°III, diffuse astrocytoma WHO°II, progressive multifocal leucencephalopathy (PML) and abscess in 1 case each.

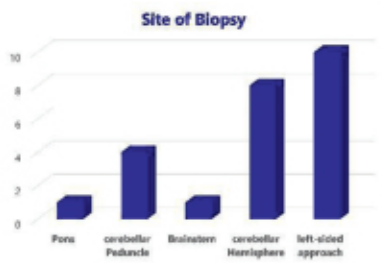


| Patients | |
|---|---|
| All patients | 13 |
| female (%) | 69.23 |
| mean age (yrs) | 63.77 |
| steroids prior to biopsy (%) | 30.77 |
| **Imaging** | |
| singular lesion (%) | 69.23 |
| MR-contrast enhancement (%) | 78.6 |
| biopsy samples per procedure (n) | 7.8 |
| diagnostic samples (%) | 92.3 |
| **Outcome** | |
| new deficit (%) | 0 |
| asymptomatic bleeding (%) | 23.1 |
| death (%) | 7.7 |

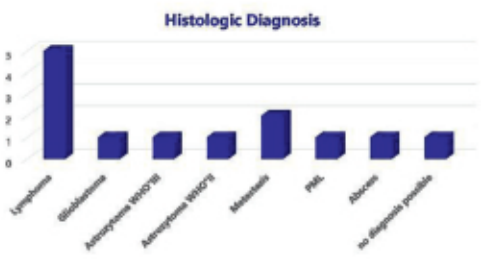


**Conclusion:** The suboccipital transcerebellar route is a safe way to perform biopsies from lesions in the posterior fossa and the brainstem when a diagnosis cannot be made without invasive methods.

## Multimodal diagnostic efforts for infratentorial lesions - The suboccipital transcerebellar approach in stereotactic brain biopsy - A single institution experience

Thomas Eibl[1], Michael Schrey[1], Markus Holtmannspoetter[2], Cristiane Blechschmidt[3], Hans-Herbert Steiner[1]

[1]Department of Neurosurgery, Paracelsus Medical University, Nuremberg, Germany; [2]Department of Radiology, Section Neuroradiology, Paracelsus Medical University, Nuremberg, Germany; [3]Department of Pathology, Paracelsus Medical University, Nuremberg, Germany; Contact: thomas.eibl@stud.pmu.ac.at

### Objective
Stereotactic brain biopsy is a core procedure in neurosurgical departments around the world. Almost any target site can be reached but yet lesions within the posterior fossa and the brainstem still remain challenging for the surgeon considering the approach and operative technique for technical as well as neuroanatomical reasons.
The objective is to describe a possible operative technique for a suboccipital route for stereotactic brain biopsy focusing on operative setting, success rates and complications of the transcerebellar route for stereotactic biopsy.

### Methods
We present a retrospective analysis of patients' records who underwent diagnostic stereotactic biopsy via a suboccipital approach in out institution between 2011 and 2020.

### Results
13 Patients (69.2% female) with 14 biopsied lesions were included, the mean age was 63.77 years, diagnostic yield was 12/13 (92.31%), a major complication occurred in 1 patient (7.7%). All biopsies were performed in a prone position under general anesthesia. We used the Zamorano-Dujovny stereotactic system without modifications with a straight but inversely (feet-)mounted frame. Biopsies were obtained from the cerebellar hemispheres in 8 cases, cerebellar peduncles in 4 cases, the pons 1 case and the brainstem in 1 case. Histologic diagnoses were cerebral lymphoma in 5 cases, metastasis in 2 cases, glioblastoma WHO°IV, anaplastic astrocytoma WHO°III, diffuse astrocytoma WHO°II, progressive multifocal leucencephalopathy (PML) and abscess in 1 case each.

### Conclusions
The suboccipital transcerebellar route is a safe way to perform biopsies from lesions in the posterior fossa and the brainstem when a diagnosis cannot be made without invasive methods.


WENIGER AUFWAND.
BESSERE VERSORGUNG.
BAYER
medrad Centargo
CT Injection System
Richtungsweisend
Für die Radiologie.
medrad Centargo
CT Injection System

BRACCO
LIFE FROM INSIDE

Bracco.
The Contrast Imaging Specialists.

Seit 35 Jahren Ihr zuverlässiger Partner im Bereich der Life Sciences




Laborkunststoffe - Biochemikalien - Laborgeräte

Biozym
SCIENCE IS OUR BUSINESS

Biozym Biotech Trading GmbH
Tel.: 01 / 334 0156 0, Fax: 01 / 334 0156 88
Mail: wien@biozym.com

www.biozym.com

Biozym Scientific
@BiozymS
Biozym Scientific
Newsletter

PARACELSUS
MEDIZINISCHE PRIVATUNIVERSITÄT

Klinikum Nürnberg
Wir sind für Sie da.

# Auswirkungen der Endokrinen Therapie mit einem CDK4/6 Inhibitor im Vergleich zur Chemotherapie beim metastasierten HR+/HER-2-neg Mammakarzinom in der Erstlinientherapie

Rahel Erling[1], Prof. Dr. Cosima Brucker[2], Dr. Fabian Winterholler[2]
1) Paracelsus Medizinische Privatuniversität, Nürnberg; 2) Klinik für Frauenheilkunde und Geburtshilfe, Klinikum Nürnberg

Jährlich erkranken immer mehr Frauen an Brustkrebs.[1] Die Entwicklung von CDK4/6 Inhibitoren verändert die Aussicht auf Erfolge beim metastasierten HR+/Her2neg Mammakarzinom und wird hier inzwischen auch als Erstlinientherapie von den AGO-Guidelines empfohlen.[2] In Studien zeigen sie gute Ergebnisse in Bezug auf Wirksamkeit, Verträglichkeit und Lebensqualität. Trotzdem werden noch sehr viele Patientinnen mit einer Chemotherapie als Erstlinientherapie behandelt. [3]

## Zielsetzung:

Die Datenlage bezüglich eines Vergleiches von CDK4/6-Inhibitoren und einer Chemotherapie ist im Moment noch spärlich. Daher sollen diese beiden Therapiekonzepte in folgenden Punkten miteinander verglichen werden:

- Wirksamkeit
  - Gesamtüberleben
  - Progressionsfreies Überleben
- Verträglichkeit
- Lebensqualität

## Methoden:

Mittels Literaturrecherche wurden Daten zur Chemotherapie und zur endokrinen Therapie mit einem CDK4/6-Inhibitor gesammelt. Diese wurden bezüglich des progressionsfreien Überlebens, des Gesamtüberlebens, der Verträglichkeit und der Lebensqualität miteinander verglichen.

## Ergebnisse:

Es zeichnet sich ein Vorteil zugunsten der CDK4/6-Inhibitoren in den Bereichen progressionsfreies Überleben, Verträglichkeit und Lebensqualität ab.

- Ein deutlicher Unterschied ist insbesondere beim Progressionsfreien Überleben zu erkennen.
- Im Bereich Gesamtüberleben ist ein Vorteil schwer auszumachen.
- Bei der Verträglichkeit differieren die Ergebnisse je nach Nebenwirkungsprofil des verwendeten Chemotherapeutikums.
- Die Lebensqualität setzt sich aus verschiedenen Faktoren wie beispielsweise dem progressionsfreien Überleben, den Nebenwirkungen oder auch Ängsten zusammen. Auch hier scheinen die CDK4/6 Inhibitoren überlegen zu sein

Abbildung 1: Progressionsfreies Überleben in Monaten

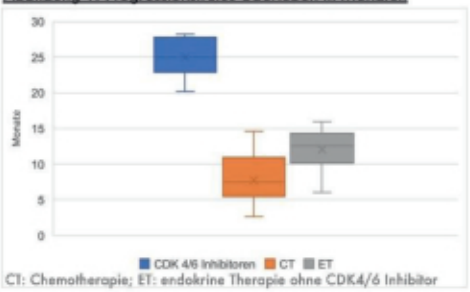


CT: Chemotherapie; ET: endokrine Therapie ohne CDK4/6 Inhibitor

Abbildung 2: Gesamtüberleben in Monaten

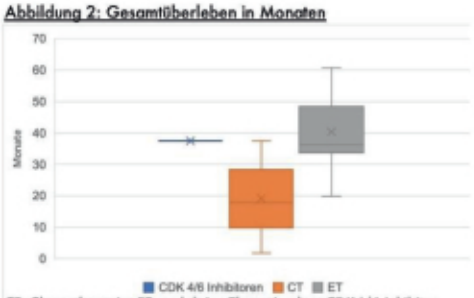


CT: Chemotherapie; ET: endokrine Therapie ohne CDK4/6 Inhibitor

Abbildung 3: Häufigkeit von Nebenwirkungen in Prozent

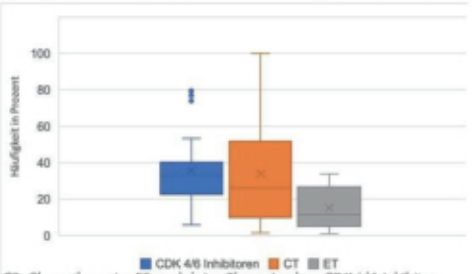


CT: Chemotherapie; ET: endokrine Therapie ohne CDK4/6 Inhibitor

Tabelle 1: Häufigkeit von Nebenwirkungen in Prozent

| Nebenwirkung % | CDK4/6 Inhibitoren | Chemotherapie | Endokrine Therapie |
|---|---|---|---|
| Neutropenie | 70,3 (+/- 14,4) | 90,2 (+/- 8,5) | 5,2 (+/- 1,8) |
| Übelkeit | 39,20 (+/- 11,1) | 30,2 (+/- 18,7) | 23,6 (+/- 6,6) |
| Durchfall | 37 (+/- 22,9) | 13,7 (+/- 10,7) | 20,80 (+/- 6,6) |
| Erschöpfung | 36,4 (+/- 6,8) | 34,4 (+/- 18,4) | 28,3 (+/- 3,8) |
| Leukopenie | 33,3 (+/- 7,6) | 44,3 (+/- 37,4) | 3,5 (+/- 1,1) |
| Gelenkbeschwerden | 29,3 (+/- 4,4) | 24,1 (+/- 13,8) | 27,7 (+/- 7,1) |
| Anämie | 24,7 (+/- 6) | 25,5 (+/- 28,7) | 6,7 (+/- 2,3) |
| Thrombozythämie | 10,6 (+/- 5) | 14,5 (+/- 18,7) | 1,5 (+/- 0,5) |

## Schlussfolgerung:

Die Arbeit konnte zeigen, dass die CDK4/6 Inhibitoren in vielen Bereichen Vorteile gegenüber der Chemotherapie versprechen. Dennoch ist die Studienlage nicht so eindeutig, dass eine generelle Präferenz ausgesprochen werden kann. So ist eine Therapieentscheidung immer individuell und in enger Zusammenarbeit mit der Patientin und deren Umfeld zu treffen. Beim metastasierten HR+/Her2neg Mammakarzinom hat die Lebensqualität aufgrund des langen Überlebens den größten Impact. Ziel ist es, die beste Lebensqualität in der Palliativsituation zu erreichen. Die Therapieentscheidung ist im Verlauf auch gegebenenfalls abzuändern, wenn das die Situation verbessert. Die Literaturrecherche gibt Anlass dazu, die Erkenntnisse der Arbeit in randomisierten Studien zu überprüfen.

**Referenzen:** [1]: Robert Koch-Institut, Gesellschaft der epidemiologischen Krebsregister in Deutschland e.V.. Krebs in Deutschland für 2015/ 2016. Berlin. 2019; 12. Ausgab.
[2]: Onkologie L. Interdisziplinäre S3-Leitlinie für die Früherkennung , Nachsorge des Mammakarzinoms Wesentliche Neuerungen; 2020
[3]: Hartkopf AD, Huober J, Volz B, et al. Treatment landscape of advanced breast cancer patients with hormone receptor positive HER2 negative tumors; 2018

**Danksagung:** Herzlicher Dank geht an die Betreuung von Frau Prof. Dr. Cosima Brucker und Herrn Dr. Fabian Winterholler sowie die Unterstützung durch Freunde und Familie.

## Auswirkungen der Endokrinen Therapie mit einem CDK4/6 Inhibitor im Vergleich zur Chemotherapie beim metastasierten HR+/HER-2-neg Mammakarzinom in der Erstlinientherapie

Rahel Erling[1]

[1]Paracelsus Medical University, Nuremberg, Germany; Contact: rahel.erling@stud.pmu.ac.at

### Objective
Each year the number of women who develop breast cancer increases. But scientific knowledge is also increasing, and a lot of energy is being invested in the development of new drugs changing the way we go about treating diseases. The CDK4 / 6 inhibitors join the ranks, as they have shown good results in terms of efficacy, tolerability and quality of life in the latest studies. Therefore, the AGO guidelines recommend endocrine therapy as first-line therapy for metastatic HR + / Her2neg breast cancer. Nevertheless, many patients are still being treated with first-line chemotherapy. The data situation regarding a comparison of CDK4/6 inhibitors and chemotherapy is still poor currently.

### Methods
Employing literature research data has been collected regarding efficacy, tolerability and quality of life comparing chemotherapy with endocrine therapy plus CDK4/6 inhibitors.

### Results
In terms of progression free survival, tolerability and quality of life CDK4/6 inhibitors tend to have an advantage over chemotherapy. Depending on the chemotherapy regimen this advantage varies particularly regarding side effects. With respect to overall survivability there is no evidence of a significant change.

### Conclusions
Although the CDK4/6 inhibitors are showing promising results in contrast to chemotherapy, decisions regarding therapy should be made in collaboration with the patient and its close relations. There should be also room for changing an ongoing therapy. Since patients with HR+/Her2neg metastatic breast cancer tend to survive long, quality of life should be the main concern. Therefore the goal is to reach the best quality of life in the palliative situation. This term is very complex as there are a lot of variables that have a major impact.

# A spoonful of L-fucose - An efficient therapy for GFUS-CDG, a new glycosylation disorder

René G. Feichtinger[1], Andreas Hüllen[2], Andreas Koller[3], Dieter Kotzot[4], Valerian Grote[5], Erdmann Rapp[5,6], Peter Hofbauer[7], Karin Brugger[1], Christian Thiel[2], Johannes A. Mayr[1], Saskia B. Wortmann[1,8]

[1]University Children's Hospital, Salzburger Landeskliniken (SALK) and Paracelsus Medical University (PMU), Salzburg, Austria; [2]Centre for Child and Adolescent Medicine, Department Pediatrics, University of Heidelberg, Heidelberg, Germany; [3]Research Program for Experimental Ophthalmology, Department of Ophthalmology and Optometry, Salzburger Landeskliniken (SALK) and Paracelsus Medical University (PMU), Salzburg, Austria; [4]Clinical Genetics Unit, Salzburger Landeskliniken (SALK) and Paracelsus Medical University (PMU), Salzburg, Austria; [5]Max Planck Institute for Dynamics of Complex Technical Systems, Bioprocess Engineering, Magdeburg, Germany; [6]glyXera GmbH, Magdeburg, Germany; [7]Landesapotheke Salzburg, Department of Production, Hospital Pharmacy, Salzburg, Austria; [8]Radboud Center for Mitochondrial Medicine, Department of Pediatrics, Amalia Children's Hospital, Radboudumc, Nijmegen, The Netherlands

## INTRODUCTION

Congenital disorders of glycosylation (CDG) are a genetically and phenotypically heterogeneous family of diseases affecting the co- and posttranslational modification of proteins. Using exome sequencing, we detected biallelic variants in GFUS (Fig. 1,2) in a patient presenting with global developmental delays, mild coarse facial features and faltering growth.

GFUS encodes GDP-L-fucose synthase the terminal enzyme in the de novo synthesis of GDP-L-fucose, which is the basis for fucosylation of N- and O-glycans.

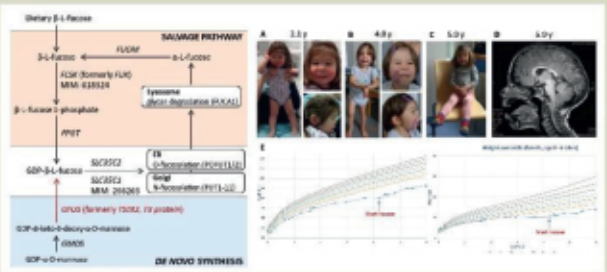


**Figure 1.** Synthesis of GDP-L-fucose by the de novo and salvage pathway.
Shown are the two metabolic pathways for GDP-L-fucose synthesis by the salvage and de novo pathways. In the salvage pathway, fucose obtained from diet or lysosomal degradation is converted to GDP-fucose in two steps by L-fucose kinase (FCSK) followed by fucose-1-phosphate guanylyltransferase (FPGT). In the de novo synthesis, which is responsible for most of the GDP-fucose yielded, GDP-fucose is obtained from GDP-mannose. The enzymes involved are GDP-mannose-4,6-dehydratase (GMDS) and GDP-L-fucose synthase (GFUS). GDP-fucose is then transported to the endoplasmic reticulum (ER) and to the Golgi by transporters SLC35C2 and SLC35C1, respectively. Genes with previously described disease-causing mutations are indicated by their respective MIM numbers.
**Clinical and neuroimaging findings in one individual with biallelic GFUS variants.** A Photo of the individual with 2.1 years. B Photo of the individual with 4 years. C Photo of the individual with 5.9 years. D Magnetic resonance imaging (MRI) of the affected individual at the age of 5.9 years. E Growth charts / anthropometry of the patient before and after treatment with fucose. Written and informed consent was obtained from the parents to show the full face of the affected individual.

## RESULTS

We found reduced GFUS protein and decreased GDP-L-fucose levels leading to a general hypofucosylation determined in patient´s serum, leukocytes, thrombocytes, and fibroblasts (Fig. 3,4,5). Viral complementation of patient-derived fibroblasts with the wildtype GFUS-cDNA restored normal fucosylation of glycoproteins. Making use of the GDP-L-fucose salvage pathway, oral fucose supplementation was initiated and normalised fucosylation of proteins within four weeks as measured in patient serum and leukocytes. During the follow up of 19 months, a moderate improvement of the growth was seen, as well as a clear improvement of cognitive skills as measured by the Kaufmann ABC (Fig 1).

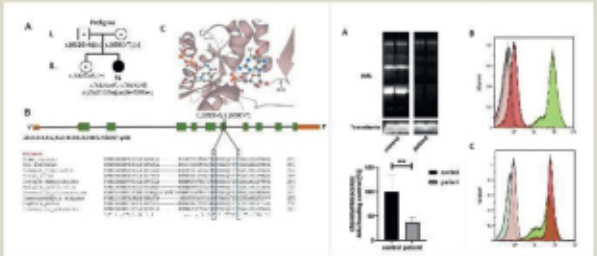


**Figure 2** Mutations identified in GFUS in one family. GFUS gene organization, partial structure of GFUS protein
A Compound-heterozygous mutations were identified in GFUS in one family. B (Top) Gene structure of GFUS and localization of variants. Introns length was reduced 1.5-fold. 5' and 3' UTR is shown in brown and the coding exons in green. (Bottom) Alignment and conservation of GFUS protein sequences from different species by Clustal Omega. Partial protein structure of GFUS. Amino acid Gly284 is localized close to the GDP-mannose substrate binding domain whereas amino acid Ser213 is in neighborhood to the binding domain of the cofactor NADPH (Zhou et al., 2013).




**Figure 3.** Aleuria aurantia lectin blot of the affected individual and controls and FACS analysis
A *Aleuria aurantia* lectin (AAL) was used to address the fucosylation level in sera of controls and the patient (left) which revealed significant loss of fucose residues in case of the patient. B,C FACS analysis of PBMCs. Results of flow cytometry analysis of patient (red) and control (green) PBMCs stained with 1 µg/ml FAA lectin without (dark) or with 200 mM L-fucose (light) before the start of fucose therapy and 6 weeks after therapy start.

**FUNDING**
Supported by the Anniversary Fund of the Oesterreichische Nationalbank grant 18023 to S.B.W. and the Deutsche Forschungsgemeinschaft (DFG, German Research Foundation; Forschungsgruppe FOR 2509, Project-ID TH1461/7–2 to C.T. and RA2992/1-2 to E.R.) and the European Commission (E-Rare-3 Joint Transnational Call 2018/ EUROGLYCANOMICS in association with the DFG, Project-ID TH1461/9–1).
We thank Ann-Katrin Schlosser (C.C.A.M. Heidelberg) for her outstanding contribution to this project and Dr. Marcus Hoffmann (MPI Magdeburg) for his excellent guidance and support during the assessment of the N-glycan analysis data.

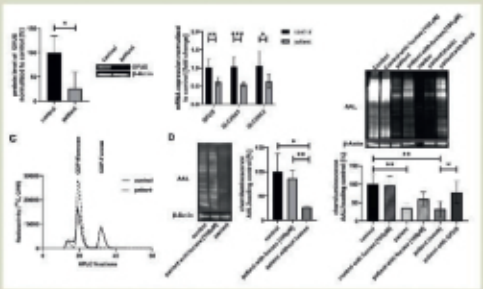


**Figure 4.** Biochemical characterization of GFUS deficiency in patient-derived fibroblasts
A Western blot analysis and quantification of GFUS. Expression of GFUS was analyzed by Western blotting on a 15% SDS PAGE with cytosolic fractions derived from control and patient fibroblasts. Quantification revealed a significant decrease of GFUS protein.
B mRNA expression studies. qRT-PCR studies showed a significant decrease in mRNA level of GFUS by 46.0% (± 9.3%, $^{***}p = 0.0010$) normalized to a control. Also, expression of SLC35C1 and SLC35C2 were significantly decreased in patient-derived fibroblasts. C Conversion of GDP-D-mannose into GDP-L-fucose. The conversion GDP-D-[2-3H]mannose to GDP-L-[2-3H]fucose was analyzed in an in-vitro assay. After 1 h nearly half of GDP-mannose was transformed to GDP-fucose in the control cell line, whereas the patient's fibroblasts were nearly unable to catalyze the reaction. D Lectin binding studies and quantification in fibroblasts. *Aleuria aurantia* lectin (AAL) was used to address the fucosylation level in fibroblasts. AAL staining was performed before and after treatment of the patient cell line with 100 µM L-fucose. Before sugar supplementation a significant loss of AAL signal strength was measured, whereas after treatment a significant re-fucosylation was detected. E Complementation study with patient-derived fibroblasts. Viral infection was used to introduce an empty cloning vector and the wild-type GFUS DNA in patient cells, respectively. For analysis lysates of a control cell-line, a control cell-line supplemented with 100 µM fucose, patient cells, patient cells supplemented with 100 µM fucose, patient cells transfected with an empty vector and patient cells transfected with wild type GFUS were analyzed by AAL staining clearly indicating the disease-causing influence of the defective GFUS in the patient.

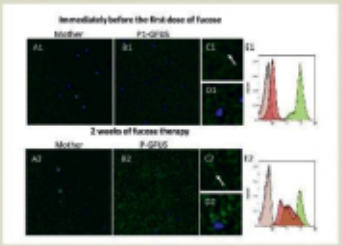


**Figure 5.** *Aleuria aurantia* lectin staining of blood smears and FACS analysis from the affected individual, the mother and an additional control. A1-A4,B1-B4,C1-C4,D1-D4 Merge of lectin (green) and DAPI (blue) staining A1-A4,C1-C4 Staining of blood smears of the mother. B1-B4,D1-D4 Staining of blood smears of the affected individual. E1-E4 FACS analysis of PBMCs of the affected individual and her mother A1-D1 Lectin staining of blood smears immediately before start of fucose treatment. E1 FACS analysis of lectin of PBMCs immediately before start of fucose treatment. A2-D2 Lectin staining of blood smears two weeks after start of fucose treatment. E2 FACS analysis of lectin of PBMCs two weeks after start of fucose treatment. Green: *Aleuria aurantia* lectin; Blue: DAPI. PBMCs are highlighted by a white arrow in panel E. Platelets are highlighted by white arrows. Fluorescence images were taken with a 20x magnification. Results of flow cytometry analysis of patient (red) and control (green) PBMCs stained with 1 µg/ml FAA lectin without (dark) or with 200 mM L-fucose (light) before the start of fucose therapy.



**Figure 6.** Comparison of clinical presentation of known genetic defects in fucose metabolism.

## DISCUSSION AND CONCLUSIONS

- GFUS deficiency is the first disorder of de novo fucose synthesis.
- GFUS deficiency seems to be rare, maybe due to a narrow degree of residual activity, which results in disease (less might be lethal, more might be normal)
- Due to the existence of a salvage pathway, treatment with oral fucose seems to allow a complete correction of the glycosylation defect and result in a clear improvement of the development of the affected individual. In SLC35C1, a carrier of GDP-fucose, treatment with oral fucose has been reported previously (Fig. 6).
- Despite of its rarity, we think that GFUS deficiency is a good candidate for newborn screening.

contact: s.wortmann@salk.at

## A spoonful of L-fucose - An efficient therapy for GFUS-CDG, a new glycosylation disorder

René Günther Feichtinger[1], Andreas Hüllen[2], Andreas Koller[3], Dieter Kotzot[4], Valerian Grothe[5], Erdmann Rapp[5,6], Peter Hofbauer[7], Karin Brugger[1], Christian Thiel[2], Johannes Adalbert Mayr[1], Saskia Wortmann[1,8]

[1]University Children's Hospital, Salzburger Landeskliniken (SALK) and Paracelsus Medical University (PMU), Salzburg, Austria; [2]Centre for Child and Adolescent Medicine, Department Pediatrics, University of Heidelberg, Heidelberg, Germany; [3]Research Program for Experimental Ophthalmology, Department of Ophthalmology and Optometry, Salzburger Landeskliniken (SALK) and Paracelsus Medical University (PMU), Salzburg, Austria; [4]Clinical Genetics Unit, Salzburger Landeskliniken (SALK) and Paracelsus Medical University (PMU), Salzburg, Austria; [5]Max Planck Institute for Dynamics of Complex Technical Systems, Bioprocess Engineering, Magdeburg, Germany; [6]glyXera GmbH, Magdeburg, Germany; [7]Landesapotheke Salzburg, Department of Production, Hospital Pharmacy, Salzburg, Austria; [8]Radboud Center for Mitochondrial Medicine, Department of Pediatrics, Amalia Children's Hospital, Radboudumc, Nijmegen, The Netherlands; Contact: r.feichtinger@salk.at

### Objective
Congenital disorders of glycosylation (CDG) are a genetically and phenotypically heterogeneous family of diseases affecting the co- and posttranslational modification of proteins. Using exome sequencing, we detected biallelic variants in GFUS in a patient presenting with global developmental delays, mild coarse facial features and faltering growth. GFUS encodes GDP-L-fucose synthase the terminal enzyme in the de novo synthesis of GDP-L-fucose, which is the basis for fucosylation of N- and O-glycans.

### Methods
Alterations of fucosylation were analyzed in patient derived skin fibroblasts and PBMCs using immunofluorescence stainings and lectin blotting. Furthermore, the activity of GFUS was determined. Additionally, N-glycans were determined by glycomics.

### Results
We found reduced GFUS protein and decreased GDP-L-fucose levels leading to a general hypofucosylation determined in patient´s serum, leukocytes, thrombocytes, and fibroblasts. Viral complementation of patient-derived fibroblasts with the wildtype GFUS-cDNA restored normal fucosylation of glycoproteins. Making use of the GDP-L-fucose salvage pathway, oral fucose supplementation was initiated and normalised fucosylation of proteins within four weeks as measured in patient serum and leukocytes. During the follow up of 19 months, a moderate improvement of the growth was seen, as well as a clear improvement of cognitive skills as measured by the Kaufmann ABC.

### Conclusions
>GFUS deficiency is the first disorder of de novo fucose synthesis.
>GFUS deficiency seems to be rare, maybe due to a narrow degree of residual activity, which results in disease (less might be lethal, more might be normal)
>Due to the existence of a salvage pathway, treatment with oral fucose seems to allow a complete correction of the glycosylation defect and result in a clear improvement of the development of the affected individual.
>In SLC35C1, a carrier of GDP-fucose, treatment with oral fucose has been reported previously.
>Despite of its rarity, we think that GFUS deficiency is a good candidate for newborn screening.

Supported by the Anniversary Fund of the Oesterreichische Nationalbank grant 18023 to S.B.W. and the Deutsche Forschungsgemeinschaft (DFG, German Research Foundation; Forschungsgruppe FOR 2509, Project-ID TH1461/7–2 to C.T. and RA2992/1-2 to E.R.) and the European Commission (E-Rare-3 Joint Transnational Call 2018/ EUROGLYCANOMICS in association with the DFG, Project-ID TH1461/9–1).

# Customized 3D printed milling templates can significantly improve the fitting of the subchondral bone plate in autologous osteochondral transplants

Authors: L. Fricke*, J. Wittig**, A. Auffarth*, A. Wittig-Draenert*

*University Hospital for Orthopedic and Trauma Surgery, PMU, Salzburg, Austria
**University Hospital for Maxillofacial Surgery, PMU, Salzburg, Austria

***Background*** One of the key aspects for the success of autologous osteochondral transplantations is the fit of the subchondral bone plate of the transplant to the recipient area. (Baumbach et al., Draenert et al.)[1,2]. Therefore, we hypothesise that the use of milling-templates will significantly improve the fit of the subchondral bone plate at the transplant site. The aim of this study was to find a way to create precise milling templates and to check whether an experienced surgeon can improve his results by using templates in an animal cadaver study.

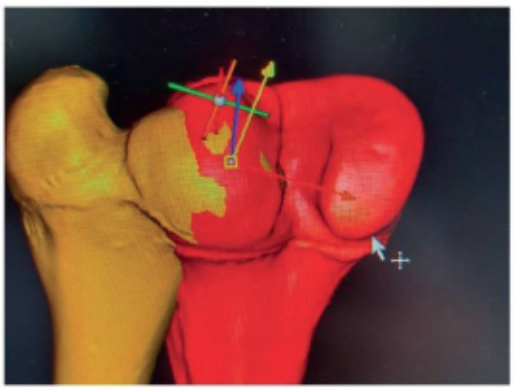

Figure 1: Matching articular surfaces

***Methods*** We performed autologous osteochondral transplants of the posterior lateral condyle to the femoral head of the same bone on 50 femoral pig bones. For 25 bones milling templates were created and used in the transplant process. To generate the milling templates, Cone Beam Computer Tomography scans of the bones were done. For matching the articular surface of the lateral femoral condyle with the femoral head a 3D reconstruction model was used (Materialise mimics inprint 3D Software) (Figure 1). Templates (Figure 2) were printed using a photopolymer jetting system (Formlabs 2). For the transplantation the surgical diamond instruments by BoneArtis were used. To analyse the fit of the subchondrol bone plate, CT scans with the Siemens Emotion 6 were carried out (Figure 3). The scans then were uploaded into the Materialise mimics inprint 3D Software and the fit of the subchondral bone plate of the transplant to the surrounding subchondral bone plate was measured in millimetres at four different sites (0°, 90°, 180°, 270°) of the transplant cylinder.

***Results*** The average gap between the subchondral bone plate of the transplant and that of the implant site was 0.27mm in the group with milling-templates and 0.73mm in the group without. We performed a t-test, showing that the milling template transplants outperformed the transplant without a template at a 1% significance level ($p<0.01$). Furthermore, milling template displayed a 72% lower variance ($\sigma^2 = 0.086$) versus the transplants without a template ($\sigma^2 = 0.312$).

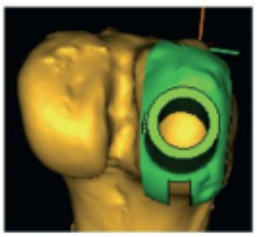

Figure 2: Milling template on lat. condyle

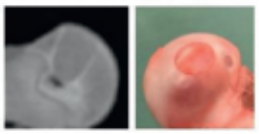

Figure 3: CT scan and final transplant after template

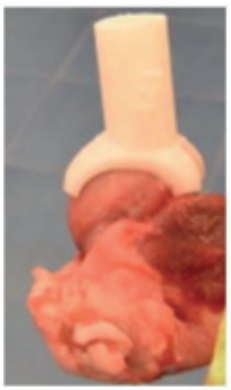

Figure 4: Template on femoral head

***Conclusion*** The results show that the use of 3D printed milling-templates can improve the fit of the subchondral bone plate in autologous osteochondrol transplantation. Furthermore, the study shows that the use of templates creates a more replicable result throughout the series of surgeries, as displayed by the difference in variance.

***Clinical relevance*** This study indicates a benefit of using 3D software to match the donors and recipients articular surface curvatures to make sure that the subchondral bone plate achieves an optimal fit, increasing the chances of successful transplantation. Further studies are necessary in order to use the customised milling templates in a clinical setting.

*Especially we would like to thank Dipl. Ing. Johan Fierlbeck and his team of the Institute of Clinical Innovation, PMU, Salzburg*

[1] K. Baumbach, J-P. Petersen, P. Uebelacker, J. Schröder, C. Gopfert, A. Stork, J. M. Rieger, M. Anning, N. M. Meen (2007) The fate of osteochondral grafts after autologous osteochondral transplantation: a one-year follow-up study in a minipig model. Arthroscopy and Sports Medicine 1251255-1262

[2] K. Draenert, Y. Draenert, T. Pohlemann, G. Regel (2012), Autologous Resurfacing and Fracture Dowelling, ISBN 978-3-642-24610-6

## Customized 3D printed milling templates can significantly improve the fitting of the subchondral bone plate in autologous osteochondral transplants

Leonard Fricke[1], Jörn Wittig[2], Alexander Auffarth[1], Alice Wittig-Draenert[1]

[1]University Hospital for Orthopedic and Trauma Surgery, PMU, Salzburg, Austria; [2]University Hospital for Maxillofacial Surgery, PMU, Salzburg; Austria; Contact: leonard.fricke@pmu.stud.ac.at

### Objective

Background One of the key aspects for the success of autologous osteochondral transplantations is the fit of the subchondral bone plate of the transplant to the donor area. (Baumbach et al., Draenert et al.)1,2. Therefore, we hypothesise that the use of milling-templates will significantly improve the fit of the subchondral bone plate at the transplant site. The aim of this study was to find a way to create precise milling templates and to check whether an experienced surgeon can improve his results by using templates in an animal cadaver study.

### Methods

Methods We performed autologous osteochondral transplants of the posterior lateral condyle to the femoral head of the same bone on 50 femoral pig bones. For 25 bones milling templates were created and used in the transplant process. To generate the milling templates, Cone Beam Computer Tomography scans of the bones were done. For matching the articular surface of the lateral femoral condyle with the femoral head a 3D reconstruction model was used (Materialise mimics inprint 3D Software) (Figure 1). Templates (Figure 2) were printed using a photopolymer jetting system (Formlabs 2). For the transplantation the surgical diamond instruments by BoneArtis were used. To analyse the fit of the subchondrol bone plate, CT scans with the Siemens Emotion 6 were carried out (Figure 3). The scans then were uploaded into the Materialise mimics inprint 3D Software and the fit of the subchondral bone plate of the transplant to the surrounding subchondral bone plate was measured in millimetres at four different sites (0°, 90°, 180°, 270°) of the transplant cylinder.

### Results

Results The average gap between the subchondral bone plate of the transplant and that of the implant site was 0.27mm in the group with milling-templates and 0.73mm in the group without. We performed a t-test, showing that the milling template transplants outperformed the transplant without a template at a 1% significants level ($p<0.01$). Furthermore, milling template displayed a 72% lower variance ($\sigma^2 = 0.086$) versus the transplants without a template ($\sigma^2 = 0.312$).

### Conclusions

Conclusion The results show that the use of 3D printed milling-templates can improve the fit of the subchondral bone plate in autologous osteochondrol transplantation. Furthermore, the study shows that the use of templates creates a more replicable result throughout the series of surgeries, as displayed by the difference in variance.

Clinical relevance This study indicates a benefit of using 3D software to match the donors and recipients articular surface curvatures to make sure that the subchondral bone plate achieves an optimal fit, increasing the chances of successful transplantation. In order to use the customised milling templates in a clinical setting, FDA approval has to be achieved. Nonetheless, the novel evidence presented in this study warrants further research and actions for approval of the templates.

### References

1. K. Baumbach, J-P. Petersen, P. Ueblacker, J. Schröder, C. Göpfert, A. Stork, J. M. Rieger, M. Amning, N. M. Meen (2007) The fate of osteochondral grafts after autologous osteochondral transplantation: a one-year follow-up study in a minipig model. Arthroscopy and Sports Medicine 128:1255-1262
2. K. Draenert and Y. Draenert (2015), Autologous Resurfacing. Micrsoscopy Research and Technique 78:40-51

FÜR FACHKREISE




Cochlear™ Osia® System

# Sowas haben Sie noch nie gehört

Das Cochlear™ Osia® System ist ein einzigartiges Hörimplantatsystem. Es ist das weltweit erste osseointegrierte dauerhafte Implantat (Osseointegrated Steady-State Implant, OSI), das digital piezoelektrische Reize nutzt, um beschädigte Bereiche des natürlichen Gehörsystems zu umgehen und Klänge direkt an die Cochlea zu senden für ein ausgezeichnetes Sprachverständnis und perfekte Klangqualität.

- **Cochlear Osia 2 Soundprozessor:** ein schlanker und komfortabler[1] frei vom Ohr getragener Soundprozessor mit SmartSound® iQ Signalverarbeitung und drahtloser Konnektivität, der sich außerhalb des Ohres befindet.
- **Cochlear Osia OSI200 Implantat:** ein leistungsfähiges Implantat mit einem Anpassbereich von bis zu 55 dB SNHL, das sich mit einem unkomplizierten chirurgischen[2] Eingriff implantieren lässt.
- **Cochlear BI300 Implantat:** die stabile osseointegrierte Basis[3] des Systems für eine effektive Schallübertragung.[4]

**www.cochlear.at**

1. Mylanus EAM, Hua H, Wigren S, et al. Multicenter Clinical Investigation of a New Active Osseointegrated Steady-State Implant System. Otol Neurotol. 2020;41(9):1249-1257.
2. Lau K, Scotta G, Wright K, et al. First United Kingdom experience of the novel Osia active transcutaneous piezoelectric bone conduction implant. Eur Arch Otorhinolaryngol. 2020;10.
3. Vansteit B. Literature review and Evaluation: BI300 implant years and survival rate. Cochlear Bone Anchored Solutions AB, Sweden. 2019; D1322539.
4. Rigato C, Reinfeldt S, Håkansson B, Fredén Jansson K-J, Renvall E, Eeg-Olofsson M. Effect of transducer attachment on vibration transmission and transcranial attenuation for direct drive bone conduction stimulation. Hear Res. 2019;15:381:107763.

Dieses Material ist für Fachkräfte im Gesundheitswesen vorgesehen. Wenn Sie Kunde bzw. Kundin sind, informieren Sie sich bei Ihrem Arzt über die Möglichkeiten der Behandlung von Hörverlust. Ergebnisse können abweichen; Ihr Arzt berät Sie bezüglich der Faktoren, die Ihr Ergebnis beeinflussen könnten. Lesen Sie stets das Benutzerhandbuch. Nicht alle Produkte sind in allen Ländern erhältlich. Für Produktinformationen wenden Sie sich bitte an Ihren Vertreter von Cochlear vor Ort. Cochlear, Hear now. And always, Human Design, Osia, SmartSound und das elliptische Logo sind Marken beziehungsweise eingetragene Marken von Cochlear Limited oder Cochlear Bone Anchored Solutions AB.

© Cochlear Limited 2021. D1697611 V1 2021-06 German Translation of D1884030 V1 2021-06



# Beste Renditeaussichten mit Immobilien.

Nutzen Sie Immobilien als soliden Anlagebaustein und investieren Sie in Wachstum am deutschen Immobilienmarkt. Die Investitionen in Sachwerte bieten Ihnen dabei Schutz vor Inflation. MLP präsentiert Ihnen ein breites Objektangebot vom Neubau bis zur denkmalgeschützten Immobilie aus dem Portfolio erfahrener Anbieter.

**Tel 0173 • 40 21 323**

MLP Finanzberatung SE
Geschäftsstelle Erlangen 1
bert.hellrung@mlp.de, www.bert-hellrung.de

MLP
Finanzen verstehen. Richtig entscheiden.

PARACELSUS
MEDIZINISCHE PRIVATUNIVERSITÄT

Klinikum Nürnberg
wir sind für Sie da!

# The effects of extracellular potassium on the respiratory burst in neutrophil granulocytes

Martin Geltinger[1], Gustavo Chaves-Barboza[2] and Boris Musset[3]
[1] Medical student, Paracelsus Medical University Nuremberg, Germany
[2] Institute of Physiology, Paracelsus Medical University Nuremberg, Germany
[3] Institute of Physiology, Paracelsus Medical University Nuremberg, Germany

## Abstract

Reactiveoxygen species (ROS) are one of the most effective weapons of the innate immune response to pathogenic microbes. The respiratory burst of polymorphonuclear leucocytes (PMNs) is the underlying process of phagolysosomal hydrogen peroxide, which is converted to the extremely bactericidal hypochloric acid by the myeloperoxidase (MPO). Our experiments should shed light whether alterations in extracellular potassium have an impact on the $H_2O_2$-production. These changes may occur, for example, in the event of massive cell death due to necrosis or crush injuries. In the first experiments, the PMNs were activated in different potassium chloride concentrations.The hydrogen peroxide productions was measured using a fluorescence-based assay. At a concentration of 100 mM potassium chloride, a delay in the start of ROS production of about 5 minutes and a delay in the maximum production rate of 10 minutes were found. This phenomenon could also be reproduced in measurements with 100 mM potassummethanesulfonate, sodium chloride, sodium methanesulfonate and 200 mM sucrose. In further experiments showing time dependence the concentration of ions or sugar were increased 3, 6, 10, 20 and 40 minutes after activation of the cells. The production of hydrogen peroxide was similar to control recordings after 3, 6 and 10 minutes. After 20 and 40 minutes, the production stopped abruptly. In summary, it can be stated that the osmotic forces of extracellular substances can delay the production of hydrogen peroxide in PMN and that the electrostatic effect of the different cations has no influence on the production behavior of $H_2O_2$ of the PMN. The phenomenon observed is attributed to the osmotic toxicity caused by the substances added. In addition, the respiratory burst can be divided into an osmotically non-vulnerable early phase (approx. 0-10 min. after activation) and a vulnerable late phase (from 20 min.).

## The measurement of $H_2O_2$-production




Amplex Red → Resorufin

Taken from BioTek.com

The conversion of Amplex Red to resorufin allows accurate quantification of hydrogen peroxide production in polymorphonuclear granulocytes.

## How does the NADPH-Oxidase work?

$$2\ O_2 + NADPH \rightarrow 2\ O_2^{\bullet-} + NADP^+ + H^+$$

## The Respiratory Burst

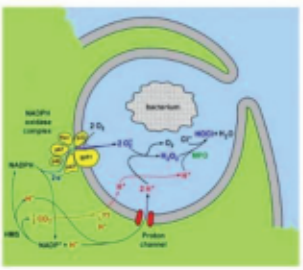

The NADPH oxidase complex has assembled after successful activation at the phagolysosomal membrane. Now, two electrons are translocated from the intracellular space to the phagolysosome by the oxidation of NADPH by the NOX2 subunit [gp91$^{phox}$] to produce hyperoxide anions ($O_2^{\bullet-}$), which react very rapidly to form hydrogen peroxide and O2 due to their instability.

Taken from Murphy & DeCoursey, 2006

## The osmotic effects on the Respiratory Burst

### Concentration dependence

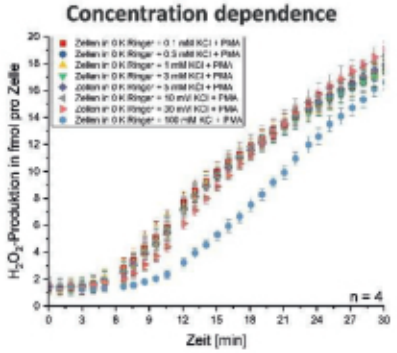


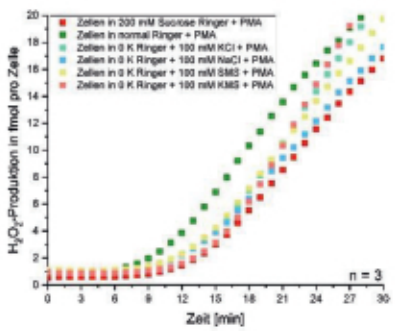


### Time dependence

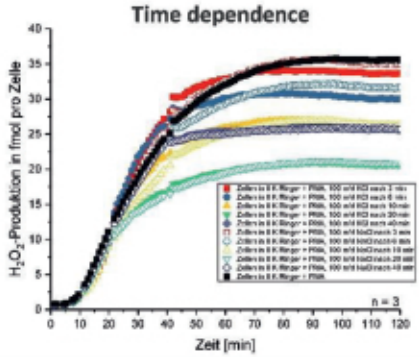


### Results

- $H_2O_2$-production during the respiratory burst in human polymorphonuclear granulocytes can be delayed by increasing extracellular osmotic forces
- The substrates potassium, sodium, chloride and sucrose affect hydrogen peroxide production to the same extent
- The respiratory burst can be divided into an osmotically vulnerable (about 0-10 minutes after activation) and nonvulnerable phase (starting at about 20 minutes)

## The effects of extracellular potassium on the respiratory burst in neutrophil granulocytes

Martin Geltinger[1], Dr. Gustavo Chaves-Barboza[2], Prof. DDr. Boris Musset[2]

[1]medical student, Paracelsus Medical University, Nuremberg, Germany; [2]Institute of Physiology, Paracelsus Medical University, Nuremberg, Germany; Contact: martin.geltinger@stud.pmu.ac.at

### Objective
Reactiveoxygen species (ROS) are one of the most effective weapons of the innate immune response to pathogenic microbes. The respiratory burst of polymorphonuclear leucocytes (PMNs) is the underlying process of phagolysosomal hydrogen peroxide, which is converted to the extremely bactericidal hypochloric acid by the myeloperoxidase (MPO). Our experiments should shed light whether alterations in extracellular potassium have an impact on the $H_2O_2$-production. These changes may occur, for example, in the event of massive cell death due to necrosis or crush injuries.

### Methods
The hydrogen peroxide productions was measured using a fluorescence-based assay.

### Results
In the first experiments, the PMNs were activated in different potassium chloride concentrations. At a concentration of 100 mM potassium chloride, a delay in the start of ROS production of about 5 minutes and a delay in the maximum production rate of 10 minutes were found. This phenomenon could also be reproduced in measurements with 100 mM potassiummethanesulfonate, sodium chloride, sodium methanesulfonate and 200 mM sucrose. In further experiments showing time dependence the concentration of ions or sugar were increased 3, 6, 10, 20 and 40 minutes after activation of the cells. The production of hydrogen peroxide was similar to control recordings after 3, 6 and 10 minutes. After 20 and 40 minutes, the production stopped abruptly.

### Conclusions
In summary, it can be stated that the osmotic forces of extracellular substances can delay the production of hydrogen peroxide in PMN and that the electrostatic effect of the different cations has no influence on the production behavior of $H_2O_2$ of the PMN. The phenomenon observed is attributed to the osmotic tonicity caused by the substances added. In addition, the respiratory burst can be divided into an osmotically non-vulnerable early phase (approx. 0-10 min. after activation) and a vulnerable late phase (from 20 min.).

PARACELSUS MEDIZINISCHE PRIVATUNIVERSITÄT

MALT!

Klinikum Nürnberg
wir sind für Sie da!

# Helping women cope with a traumatic life event: The MALT! program for women. A controlled randomized trial

Gerber, L[1,2], Braun, A[1], Müller, MM[1], Rohleder, N[2], Ruff, M[2], Stein, B[1], Tausch, A[2], Waller, C[1]

[1]Department of Psychosomatic Medicine and Psychotherapy, Paracelsus Medical University, General Hospital Nuremberg. Contact: Lois.Gerber@klinikum-nuernberg.de
[2]Department of Psychology, Chair of Health Psychology, Friedrich Alexander University Erlangen-Nuremberg

## Abstract

Objective: Traumatic life events have a great impact on the individuals' life and their mental and physical health. However, there are hardly any studies on treatments before the onset of PTSD. Equally, there are no studies on the biological influences of art therapy. The aim of this study is to understand what effect a specific art therapy program has on psychological and biological stress induced reactions associated with traumatic symptoms and if an implementation of this program after a traumatic event can reduce the traumatic symptoms.

Methods: Women between the ages of 18 to 50 are recruited at cooperating clinics and counseling centers in Nuremberg. The women either experienced a recent miscarriage or accident. If they match the criteria, they will be examined twice: after the event and three months after the first examination. In the examination, blood, saliva and an array of psychological questionnaires will be taken, before and after partaking in the Socially Evaluated Cold Pressor Test to induce a stress reaction. In between the two examinations participants will be randomized to a weekly Art Therapy program for 8 weeks or a Watchful Waiting group.

Results: We expect that trauma focused Art Therapy will lead to an improvement of the psychological symptomatology but also a reduction of the immunological and cellular stress reactivity of the individual. We also expect a healthy control group, that did not experience acute trauma to have a different biological reaction to induced stress.
Conclusion: The study is designed to help shed more light on biological influences on PTSD and help further the advancement of preventive methods. We hope that we will be able to offer a treatment to help prevent PTSD after traumatic events for women.

## Why this study?

- Need for treatment options after traumatic event
- Hardly any studies on treatments before the onset of post-traumatic stress disorder (PTSD)
- Art Therapy is used successfully as part of a PTSD therapy
- No studies yet on biological influences of art therapy

## Art Therapy

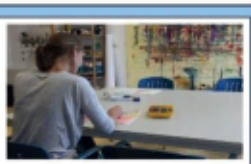

- Focusing on the **emotional, sensory level.**
- Strengthening the **sense of self-efficacy and appreciation** of the experience.
- **Non-verbal processing** and integration.

## MALTI-Process

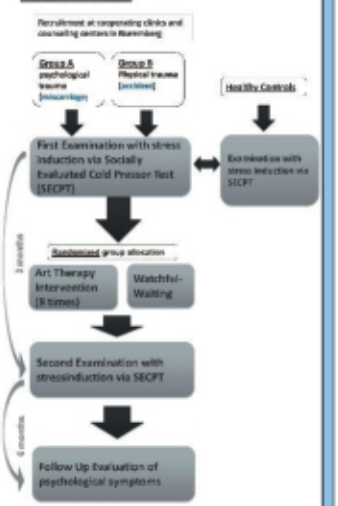


## MALTI- Examination

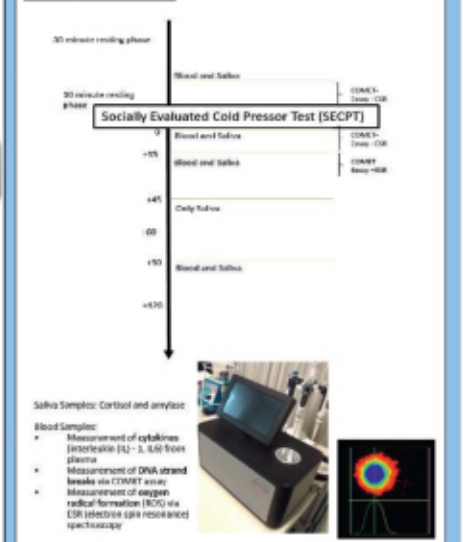


Saliva Samples: Cortisol and amylase

Blood Samples:
- Measurement of cytokines (interleukin (IL) - 1, -6) from plasma
- Measurement of DNA strand breaks via COMET assay
- Measurement of oxygen radical formation (ROS) via ESR (electron spin resonance) spectroscopy





## SECPT (Socially Evaluated Cold Pressor Test)

Activation of autonomic and neuroendocrine stress axes by cold stimulus and social evaluation

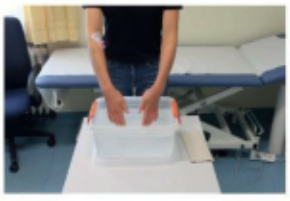

## Expected Results/ Hypthesis

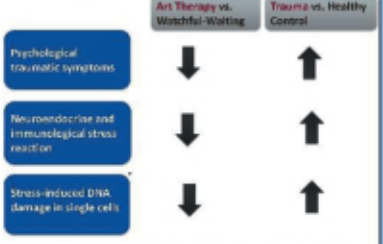


## Team and Cooperations

Klinikum Nürnberg wir sind für Sie da!

PARACELSUS MEDIZINISCHE PRIVATUNIVERSITÄT

FAU FRIEDRICH-ALEXANDER UNIVERSITÄT ERLANGEN-NÜRNBERG

UNIVERSITÄTS KLINIKUM ULM

## Goals and Challenges

- Shed more light on biological influences on PTSD, especially before the actual onset
- Provide insight on the biological effects of Art Therapy
- The COVID 19 pandemic might have an impact on the results
- Longitudinal Stress studies often have a habituation effect considering the method to induce stress

## Acknowledgements

This research project is made possible by the contributions and commitment of all participating parties.

Funding is provided by Staedtler Stiftung

The authors declare that there are no conflicts of interest.

STAEDTLER STIFTUNG

MALT!

## Helping women cope with a traumatic life event: The MALT! program for women. A controlled randomized trial

Luis Gerber[1,2], Alexandra Braun[1], Markus Müller[1], Nicolas Rohleder[2], Marleen Ruff[2], Barbara Stein, Andreas Tausch, Christiane Waller

[1]Department of Psychosomatic Medicine and Psychotherapy, Paracelsus Medical University, General Hospital Nuremberg;; [2]Department of Psychology, Chair of Health Psychology, Friedrich-Alexander University Erlangen-Nuremberg; Contact: Luis.Gerber@klinikum-nuernberg.de

### Objective
Traumatic life events have a great impact on the individuals' life and their mental and physical health. However, there are hardly any studies on treatments before the onset of PTSD. Equally, there are no studies on the biological influences of art therapy. The aim of this study is to understand what effect a specific art therapy program has on psychological and biological stress induced reactions associated with traumatic symptoms and if an implementation of this program after a traumatic event can reduce the traumatic symptoms.

### Methods
Women between the ages of 18 to 50 are recruited at cooperating clinics and counseling centers in Nuremberg. The women either experienced a recent miscarriage or accident. If they match the criteria, they will be examined twice: after the event and three months after the first examination. In the examination, blood, saliva and an array of psychological questionnaires will be taken, before and after partaking in the Socially Evaluated Cold Pressor Test to induce a stress reaction. In between the two examinations participants will be randomized to a weekly Art Therapy program for 8 weeks or a Watchful Waiting group.

### Results
We expect that trauma focused Art Therapy will lead to an improvement of the psychological symptomatology but also a reduction of the immunological and cellular stress reactivity of the individual. We also expect a healthy control group, that did not experience acute trauma to have a different biological reaction to induced stress.

### Conclusions
The study is designed to help shed more light on biological influences on PTSD and help further the advancement of preventive methods. We hope that we will be able to offer a treatment to help prevent PTSD after traumatic events for women

# The EJP-RD EBStatMax project: How clinicians and statisticians work together

Geroldinger M [a, b], Zimmermann G [a, b], Laimer M [c], Bauer JW [c]

[a] Team Biostatistics and Big Medical Data, IDA Lab Salzburg, Paracelsus Medical University, Salzburg, Austria
[b] Department of Research and Innovation, Paracelsus Medical University, Salzburg, Austria
[c] University Clinic of Dermatology and Allergology, Paracelsus Medical University, Salzburg, Austria

## Starting point of the project

In a randomized, placebo-controlled, 2-period crossover phase 2/3 trial, the immunomodulatory impact of 1% diacerein cream vs. placebo in reducing the number of blisters in EBS (=Epidermolysis bullosa simplex) was assessed.[1] 15 patients were randomized to either placebo or diacerein for a 4-week treatment and a 3-month follow-up in period 1. After a washout (mean 5.6 months), patients were crossed over during period 2. Of the patients receiving diacerein, 86% in episode 1 and 37.5% in episode 2 met the primary end point, i.e. a reduction of number of blisters by more than 40% from baseline in selected areas over the treatment episode (vs 14% and 17% with placebo, respectively). No adverse effects were observed.

## Statistical challenges

From a statistical point of view, small sample sizes represent a major challenge in drawing conclusions from that trial. Since this is an inherent statistical property of rare skin diseases, a methodologically sound consideration of alternative analysis options has the potential to exploit the limited information in the data in an optimized way and thus to provide valuable additional insights.

## What is EBStatMax?

EBStatMax is a "demonstration project" funded by the European Joint Programme on Rare Diseases[2], aimed at bridging the gap between challenges arising from clinical practice and their potential statistical solutions. An international consortium of statisticians (Austria, Belgium, Sweden) with different overlapping and complementing areas of expertise, is

- (A) reanalyzing and simulating data using different state-of-the-art methodologies, trying to exploit the longitudinal nature of the data as much as possible,
- (B) investigating the impact that certain characteristics of the trial have on the statistical analysis,
- (C) developing strategies and design recommendations for future trials in this area, but also transferable to other rare diseases,
- (D) devising computational tools that can be used by practitioners in order to implement (A) - (C) in concrete trial planning and analysis, and
- (E) preparing educational material.

(D) and (E) are considered as means to ensure transferability and high dissemination of the results.

## Work packages of the project:

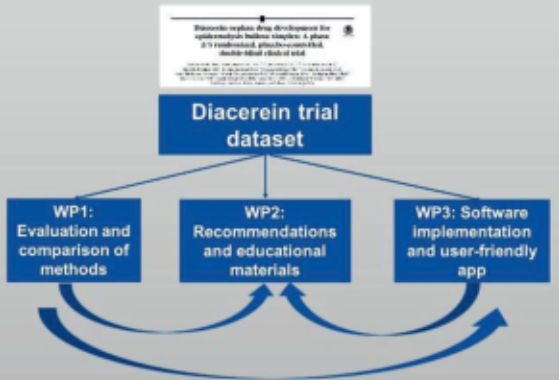


## Project timeline




## Why do we need this project?

- For rare diseases, detailed evaluations of innovative statistical methods (instead of short-time statistical consulting) are much needed to optimize data aquisition and interpretation while limiting the trial burden in a vulnerable cohort.
- The continuous collaboration between statisticians and clinicians ensures that the disease-specific challenges and patients' priorities are adequately taken into account.
- Importantly, new methodological developments should be disseminated and communicated to relevant stakeholders. Accordingly, international networks play a key role as facilitators.

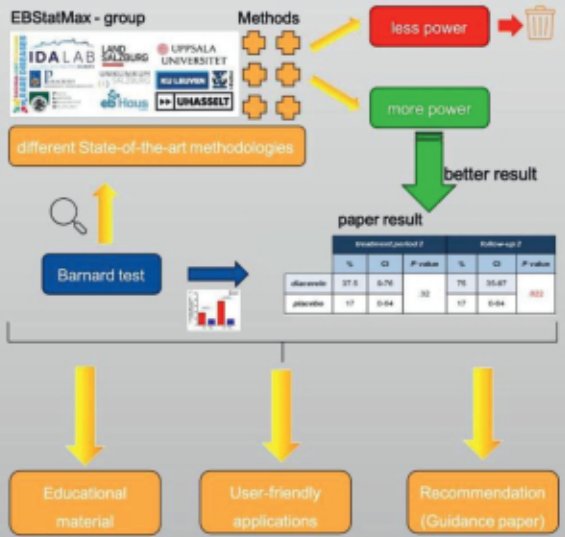


1: Wally et al., *J Am Acad Dermatol* 2018; 78(5):892-901.e7. 2: https://www.ejprarediseases.org/funded-projects-demonstration/

This project has received funding from the European Union's Horizon 2020 research and innovation programme under grant agreement No 825575.

for further questions: martin.geroldinger@pmu.ac.at

## The EJP-RD EBStatMax project: How clinicians and statisticians work together

Martin Geroldinger[1,2], Georg Zimmermann[1,2], Martin Laimer[3], Johann Bauer[3]

[1]Team Biostatistics and Big Medical Data, IDA Lab Salzburg, Paracelsus Medical University, Salzburg, Austria; [2]Department of Research and Innovation, Paracelsus Medical University, Salzburg, Austria; [3]Department of Dermatology and Allergology, Paracelsus Medical University, Salzburg, Austria; Contact: martin.geroldinger@pmu.ac.at

### Objective

Small sample sizes represent a major challenge in drawing conclusions from trials in rare diseases. Since being confronted with small cohorts is an inherent statistical property of rare skin diseases, a methodologically sound consideration of alternative analysis options, which make use of the limited information in the data in an optimized way, might provide valuable additional insights.

### Methods

Currently, we are re-analyzing a randomized, placebo-controlled, 2-period crossover phase 2/3 trial with 15 patients on the immunomodulatory impact of 1% diacerein cream vs. placebo in reducing the number of blisters in Epidermolysis Bullosa Simplex (1).

This re-analysis is performed within EBStatMax, a "demonstration project" funded by the European Joint Programme on Rare Diseases (EJP-RD) (2), aimed at bridging the gap between challenges arising from clinical practice and their potential statistical solutions.

### Results

An international consortium of statisticians with different, overlapping and complementing, areas of expertise, is currently (A) reanalyzing the data using different state-of-the-art methodologies, trying to exploit the longitudinal nature of the data as much as possible. Further key aims of the project will be to (B) investigate the impact that certain characteristics of the trial have on the statistical analysis, (C) develop strategies and design recommendations for future trials in this area, but also transferable to other rare diseases, and (D), as means to ensure transferability and high dissemination of the results, devise computational tools that can be used by practitioners in order to implement (A) - (C) in concrete trial planning and analysis, and (E) provide educational material.

### Conclusions

The aim of this presentation is to provide an overview of the status quo, and to give an outlook to the next steps and the expected outcomes, hoping that thus, the ongoing interdisciplinary exchange might be extended to an even broader audience.

This project has received funding from the European Union's Horizon 2020 research and innovation programme under grant agreement No 825575.

GZ gratefully acknowledges the support of the WISS 2025 project 'IDA-Lab Salzburg' (20204-WISS/225/197-2019 and 20102-F1901166-KZP)

### References

1. https://www.ejprarediseases.org/funded-projects-demonstration/
2. Wally et al., J Am Acad Dermatol 2018; 78(5):892-901.e7

TECHNISCHE HOCHSCHULE NÜRNBERG
GEORG SIMON OHM

## Current respiratory monitoring on the Neonatal Intensive Care Unit (NICU)



Skin irritations from electrode removal [1]



Pulse oxymeter [2]



Ventilated preterm neonate [3]

### Aim

Automated non-contact respiratory rate monitoring to minimize risks, increase comfort and allow an easier handling of the baby

## Related work

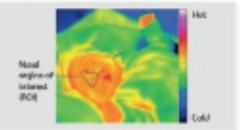


Thermal imaging of a neonate with marked ROI [4]



Radar and ToF for respiratory volume detection [5]

### Gaps

- face needs to be visible (line of sight)
- RGB is light-dependent
- radar is sensitive towards motion artifacts
- some approaches only tested on adults

## Automated non-contact respiratory rate monitoring of neonates

Sensor integration
Signal processing
Synchronization

### Radar sensor



The microwave interferometric radar sensor measures the change in displacement caused by the respiration and is even capable of sensing the small movements due to the heartbeat.
Several signal processing steps are required to deliver the respiratory rate in breaths per minute (BPM).



Radar distance signal at a respiratory rate of 40 BPM.

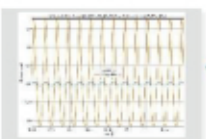

### Baby thorax simulator

with reference measurement

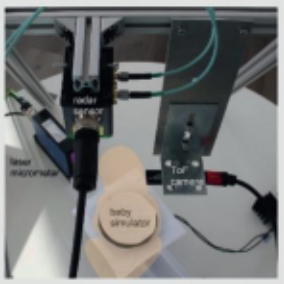


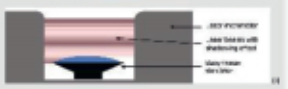

A laser micrometer measures the displacement caused by the thorax simulator movement and acts as gold standard

TIME SYNCHRONIZATION

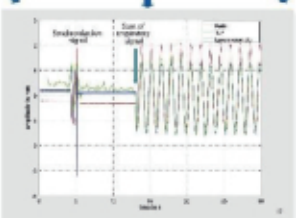

Section of the respiratory signal at 45 BPM measured by the ToF camera, the radar sensor and the laser micrometer.
At the beginning, the synchronization signal can be seen. The signals of the different sensors are in phase.

### ToF camera





The time-of-flight (ToF) camera (top) delivers 3D point clouds of the baby thorax simulator (bottom) which can be used to calculate the change in distance due to the movement of the thorax.
The point cloud is processed using several filters, segmentation and a peak detection to return the respiratory rate in BPM.



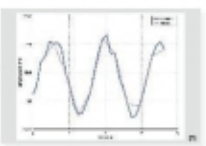

Unfiltered (blue) and filtered (magenta) section of the respiratory signal at 20 BPM.

Measurements were taken for simulated respiratory rates between 5 and 80 BPM. Our approach delivers very precise results within the norm respiratory rate range of 20 to 60 BPM with a maximum difference of 3 BPM. For low respiratory rates at 5 and 10 BPM the drawback of the ToF camera due to noise needed to be compensated by the radar.

## Future steps

- Measurements with real babies within the NICU
- Test how fast our system reacts towards changing respiratory rates
- Fusion with additional sensor data

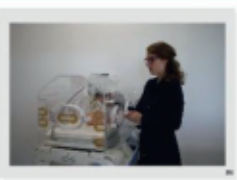

References

NeoWatch: Non-contact monitoring system for neonates on the NICU
Funding reference: 13FH548IX6

Johanna Gleichauf, johanna.gleichauf@th-nuernberg.de
Christine Niebler, christine.niebler@th-nuernberg.de

In cooperation with:
Universitätsklinikum Erlangen
InnoSenT

## Automated non-contact respiratory rate monitoring of neonates

Johanna Gleichauf[1], Sven Herrmann[1], Lukas Hennemann[1], Hannes Krauss[1], Janina Nitschke[1], Philipp Renner[1], Christine Niebler[1], Alexander Koelpin[2]

[1]Technische Hochschule Nürnberg; [2]Technische Universität Hamburg; Contact: johanna.gleichauf@th-nuernberg.de

### Objective

Preterm neonates on the Neonatal Intensive Care Unit (NICU) require continuous monitoring of their vital signs such as the respiratory and heart rate and the body temperature. For monitoring the respiratory rate impedance pneumography using electrodes and the ventilator itself are used. These methods have the drawback that they are cable based and are in direct contact with the baby's skin. As premature neonates are underdeveloped, they react very sensitive to these methods which can lead to pressure marks, eczemas, skin irritations and even the removal of the skin. Within the BMBF project NeoWatch we research and develop non-contact monitoring approaches to minimize these risks, to increase the comfort and to allow an easier handling of the baby.

### Methods

Within our latest research we showed that it is possible to determine the respiratory rate based on the synchronous evaluation of a microwave interferometric radar sensor and a 3D-time-of-flight (ToF) camera [1]. Radar sensors have the advantage that they can measure distance changes caused by the respiration or even the heartbeat [2]. 3D-time-of-flight cameras deliver 3D point clouds which can be used to detect distance changes caused by the movement of the thorax and calculate the respiratory rate from it. Both sensors have the advantage that they are not light-dependent, do not require markers or the baby's face visible as would be necessary for thermal imaging [3] or RGB cameras. Furthermore, many of the existing approaches have only been tested on adults [4]. By evaluating the radar sensor and the ToF camera data synchronously we hope to compensate the drawbacks of each sensor to allow robust monitoring. Our approach was validated with a self-developed baby simulator at respiratory rates between 5 and 80 breaths per minute (BPM). The baby simulator consists of a speaker, an amplifier circuit and a laser micrometer as reference measurement.

### Results

We showed that our approach delivers very precise results within the norm respiratory rate range of 20 to 60 BPM with a maximum difference of 3 BPM [1]. For low respiratory rates at 5 and 10 BPM the drawback of the ToF camera due to noise needed to be compensated by the radar sensor measurements. Within the norm range the ToF camera performed slightly better than the radar sensor.

### Conclusions

In the future we intend to test our approach with real babies within the NICU and to investigate how fast our system reacts towards changing respiratory rates.

### References

1. Gleichauf, J.; Herrmann, S.; Hennemann, L.; Krauss, H.; Nitschke, J.; Renner, P.; Niebler, C.; Koelpin, A. Automated Non-Contact Respiratory Rate Monitoring of Neonates Based on Synchronous Evaluation of a 3D Time-of-Flight Camera and a Microwave Interferometric Radar Sensor. Sensors 2021, 21, 2959
2. Vinci, G.; Lindner, S.; Barbon, F.; Mann, S.; Hofmann, M.; Duda, A.; Weigel, R.; Koelpin, A. Six-port radar sensor for remote respiration rate and heartbeat vital-sign monitoring. IEEE Trans. Microw. Theor. Techniq. 2013, 61, 2093–2100
3. Abbas, A.K.; Heimann, K.; Jergus, K.; Orlikowsky, T.; Leonhardt, S. Neonatal non-contact respiratory monitoring based on real-time infrared thermography. BioMed. Eng. OnLine 2011, 5, 1124–1135
4. Nguyen, P.; Transue, S.; Choi, M.H.; Halbower, A.C.; Vu, T. WiKiSpiro: Non-contact respiration volume monitoring during sleep. In Proceedings of the Annual International Conference on Mobile Computing and Networking, MOBICOM, New York City, NY, USA, 3–7 October 2016; pp. 27–29

# HAIP

## Optimiertes **H**ygienemanagement in der **a**ußerklinischen **I**ntensiv**p**flege

Irmela Gnass[1], Stefanie Berger[1], Anna Brandauer[1], Nicole Freywald[1], Isabel Höppchen[1], Patrick Kutschar[1], Annemarie Strobl[1], Carola Walter[1]

[1] Institut für Pflegewissenschaft und -praxis, Paracelsus Medizinische Privatuniversität, Strubergasse 21, 5020 Salzburg, Österreich

### Hintergrund

In der Versorgung von Menschen mit Beatmungsbedarf nimmt das Hygienemanagement zur Vermeidung und Kontrolle beatmungsassoziierter Infektionen in Wohngemeinschaften (WG) der außerklinischen Intensivpflege einen hohen Stellenwert ein, wird in der Pflegeforschung jedoch bisher wenig behandelt [1-4].

### Ziel

Optimierung des Hygienemanagements für Menschen mit Beatmungsbedarf in WG der außerklinischen Intensivpflege der Deutschen Pflegegruppe [DPG].

### Übergeordnete Forschungsfrage des Gesamtprojektes (März 2019 bis Juli 2021)

Welche strukturellen und personellen Gegebenheiten und Herausforderungen im Hygienemanagement zeigen sich für Menschen mit Beatmungsbedarf in WG der außerklinischen Intensivpflege?

### Methodik Projektstränge

I. Strang: Scoping Review

II. Strang: a) Standardisierte Strukturdatenerhebung der hygiene- und infektionsspezifischen Versorgungssituation in 31 WG
b) Online- und papierbasierte standardisierte Befragung von Pflegefachkräften zum Wissensstand und zu Informationsbedarfen

III. Strang: Bildungsoffensive für Pflegefachkräfte der DPG mit Schwerpunkt Hygiene; Entwicklung und Implementierung von E-Learning Kursen

### Ergebnisse

**I. Hygienemanagement, 8 Studien inkludiert**

Evidenz für die Bereiche:
- … Infektionskritische Tätigkeiten
- … Qualitätsmanagement für Hygiene
- … Schulung und Ausbildung von Pflegefachkräften

Wenig bis keine Evidenz für die Bereiche:
- … Küchenhygiene
- … Hygiene bei Angehörigen/Besucher*innen
- … Abfallmanagement

**IIa. Ergebnisse der Strukturdatenanalyse**

… zeigten Optimierungsbedarfe bei den Themen Infektionsmanagement, Umgang mit Antibiotika und Arbeitsschutz sowie Impfungen

**IIb. Pflegefachkräfte** (n=147/482, 30% Rücklaufquote)

… schätzen ihr Wissen zu hygienespezifischen Themen im Schnitt zwischen Sehr gut und Gut* ein

… benennen häufigste Herausforderungen im Versorgungsalltag:
- > Kommunikation und Abstimmung mit Angehörigen
- > Versorgung von Klient*innen mit multiresistenter Keimbesiedelung
- > Verfügbarkeit von Materialressourcen

*(Sehr gut (1) bis Ungenügend (6))

**III. E-Learning Kurse für Pflegefachkräfte**

Hygiene 1 Kurse:
- … Übertragung von Infektionskrankheiten und Infektionsabwehr
- … Maßnahmen zur Verhütung und Bekämpfung übertragbarer Krankheiten

Hygiene 2 Kurse:
- … Arbeitsschutzmaßnahmen (Hautschutz, -pflege, Immunisierung, Gefahrenstoffe, Abfallentsorgung)
- … Multiresistente Erreger (MRSE, MRGN, VRE)

### Diskussion

Die mit dem Projekt HAIP gewonnenen Erkenntnisse liefern wichtige Aspekte für die Versorgung von Menschen mit Beatmungsbedarf und untermauern die hohe Relevanz weiterführender Forschungsarbeiten. Zudem ist die Notwendigkeit einheitlicher Standards in WG der außerklinischen Intensivpflege zu vermuten [2], die das Antibiotikamanagement sowie Bereiche des Arbeitsschutzes weiter verdeutlichen. Die von den Pflegefachkräften genannten Herausforderungen und Wissenslücken im Versorgungsalltag implizieren die Wichtigkeit weiterführender Fortbildungsangebote, die neue fachliche wie gesetzliche Entwicklungen berücksichtigen [5,6].

### Referenzen

[1] Gnass, I., Volle, P., Strobl, A., Pelgrim, T., Kutschar, P., Lohrmann, C., Mayer, H. (2019). Hygienemanagement in der außerklinischen Intensivpflege. Erfassung von Herausforderungen und Handlungsbedarfen. Pflegewissenschaft, 21(1), 43-53.

[2] Gnass, I., Halbeck, Sabine, C., Schmitt, B. L., Fabri, M., Gastmeier, P. & Hübl, E. (2019). Hygienemanagement und Infektionsprävention in Wohngemeinschaften der außerklinischen Intensivpflege. Bundesgesundheitsblatt - Gesundheitsforschung - Gesundheitsschutz, 62(2), 227-235.

[3] Strobl, A., Gnass, I., Kutschar, P., Rabensteiner, E., Pichler, W. Ausmaß und Risikofaktoren der Kolonisation mit multiresistenten gramnegativen Bakterien bei Menschen mit Tracheostoma in Wohngemeinschaften der außerklinischen Intensivpflege. (2019) Gesundheitswesen (Bundesverband der Ärzte des Öffentlichen Gesundheitsdienstes (Germany)), 81(10), 871-877. doi: 10.1055/a-0662-7547

[4] Robert Koch-Institut (2016). Anforderungen an die Hygiene bei der Aufbereitung von Medizinprodukten. Empfehlung der Kommission für Krankenhaushygiene und Infektionsprävention beim Robert Koch-Institut. Bundesgesundheitsblatt 59, 358–386. https://www.rki.de/DE/Content/Kommissionen/KRINKO/Empfehlungen/Aufbereitung_Medizinprodukte.pdf?__blob=publicationFile

[5] Deutsches Institut für Normung e.V. (2018). Anforderungen an Hygiene bei der Aufbereitung von Medizinprodukten – Besondere Anforderungen an die Aufbereitung invasiver oder kritischer Medizinprodukte; Deutsche Fassung EN 17664:2017. Beuth Verlag GmbH. https://www.beuth.de/de/norm/din-en-17664/281650650

**Korrespondenz:** Ass.-Prof. Dr. Irmela Gnass, Paracelsus Medizinische Privatuniversität, Institut für Pflegewissenschaft und -praxis, irmela.gnass@pmu.ac.at, Tel. +43662 2420-80397

## HAIP – Optimiertes Hygienemanagement in der außerklinischen Intensivpflege

Irmela Gnass[1], Stefanie Berger[1], Anna Brandauer[1], Nicole Freywald[1], Isabel Höppchen[1], Patrick Kutschar[1], Annemarie Strobl[1], Carola Walter[1]

[1]Institute of Nursing Science and Practice, Paracelsus Medical University, Salzburg, Austria; Contact: irmela.gnass@pmu.ac.at

### Objective

In der Versorgung von Menschen mit Beatmungsbedarf nimmt das Hygienemanagement zur Vermeidung und Kontrolle beatmungsassoziierter Infektionen in Wohngemeinschaften (WG) der außerklinischen Intensivpflege einen hohen Stellenwert ein, wird in der Pflegeforschung jedoch bisher wenig behandelt [1].
Ziel des Projektes HAIP ist die Optimierung des Hygienemanagements für Menschen mit Beatmungsbedarf in WG der außerklinischen Intensivpflege eines deutschlandweit agierenden Betreibers.

### Methods

Der Thematik wurde mit drei Projektsträngen begegnet. (I) Um den aktuellen Erkenntnisstand zum Hygienemanagement in der außerklinischen Intensivpflege abbilden zu können, wurde eine umfassende Literaturrecherche in wissenschaftlichen Datenbanken durchgeführt. (IIa) Des Weiteren wurden relevante strukturelle Gegebenheiten in den ambulant betreuten WG standardisiert erhoben. (IIb) Zudem fand eine standardisierte Befragung von in den WG tätigen Pflegefachkräften zum eigenen aktuellen Wissensstand und Informationsbedarfen hinsichtlich Hygiene und Infektionen bei der Versorgung von Menschen mit Beatmungsbedarf statt. (III) Diese Erkenntnisse bildeten in weiterer Folge die Grundlage für die Entwicklung eines E-Learning basierten Weiterbildungsangebots für Pflegefachkräfte der WG.

### Results

Die Ergebnisse der Literaturrecherche zum Hygienemanagement (I) zeigen u.a. Belege für die Bereiche infektionskritische Tätigkeiten, Qualitätsmanagement für Hygiene sowie Schulung und Ausbildung. Wenig bis keine Evidenz ist für die Bereiche Küchenhygiene, Hygiene bei Angehörigen/Besucher*innen und Abfallmanagement vorhanden. Aus den Ergebnissen der Strukturdatenanalyse (IIa) lässt sich Optimierungsbedarf bei den Themen Infektionsmanagement, Umgang mit Antibiotika und Arbeitsschutz sowie Impfungen ableiten. Die Ergebnisse der Befragung der Pflegefachkräfte (IIb) zeigen, dass die Pflegefachkräfte ihr eigenes Wissen zu hygienespezifischen Themen im Schnitt zwischen Sehr gut und Gut einschätzen. Als häufigste Herausforderungen im Versorgungsalltag wurden die Themen Kommunikation und Abstimmung mit Angehörigen, Versorgung von Klient*innen mit multiresistenter Keimbesiedelung und Verfügbarkeit von Materialressourcen genannt. Auf Basis der Erkenntnisse wurden zwei E-Learning Kurse (III) im Zuge einer Bildungsoffensive entwickelt.

### Conclusions

Die aus dem Projekt HAIP gewonnenen Erkenntnisse untermauern die hohe Relevanz weiterführender Forschungsarbeiten zur Thematik. Zudem konnte die Notwendigkeit einheitlicher Standards im Setting der WG der außerklinischen Intensivpflege gezeigt werden [1]. Die von den Pflegefachkräften genannten Herausforderungen und Wissenslücken im Versorgungsalltag implizieren zudem die Wichtigkeit weiterführender Fortbildungsangebote.

### References

1. Gleich, S., Horvath, Böhm, D., Dodenhoff, E., Fulle, W., Gstöttner, H. & Hille, S. (2019). Hygiene in der außerklinischen Intensivpflege - Anforderungen an Struktur und Prozessqualität - Ergebnisse einer Risikoanalyse der AG Hygiene. https://knaib.de/wp-content/uploads/2016/06/Hygiene-2019.pdf

PARACELSUS MEDIZINISCHE PRIVATUNIVERSITÄT

Klinikum Nürnberg
Wir sind für Sie da.

Kontakt: clemens.goegele@pmu.ac.at

Virtueller Paracelsus Science Get Together, 02. Juli 2021

# Integration von biologisch abbaubarem Poly(L-Lactid) (PLLA) auf neu entwickelten bioaktiven Glas Scaffolds (CAR12N) für das Knorpel Tissue Engineering

**Clemens Gögele[1,2], Silvana Müller[3], Andreas Pradel[3], Sven Wiltzsch[3], Armin Lenhart[3], Markus Hornfeck[3], Achim Rübling[3], Hannes Kühl[3], Kerstin Schäfer-Eckart[4], Thomas Martin Weiger[2] und Gundula Schulze-Tanzil[1]**

1 Institut für Anatomie und Zellbiologie, Paracelsus Medizinische Privatuniversität, Nürnberg und Salzburg, Nürnberg, Deutschland
2 Fachbereich für Biowissenschaften, Paris Lodron Universität Salzburg, Salzburg, Österreich
3 Fakultät für Werkstofftechnik, Technische Hochschule Nürnberg Georg Simon Ohm, Nürnberg, Deutschland
4 Klinik für Onkologie/Hämatologie, Klinikum Nürnberg Nord, Nürnberg, Deutschland

## Fragestellung

Knorpelverletzungen sind schwerwiegende Gewebeschäden, da die Regenerationsfähigkeit des Knorpels äußerst gering ist. Ein Knorpelverlust führt zu dauerhaften Schäden, die sich mit der Zeit ausweiten und zum Ausgangspunkt für Arthrose werden können. In der Vergangenheit wurden bioaktive Glas (BG) Scaffolds (z.B. BG1393 und BG45S5) für den Knochenersatz entwickelt und einige dieser Varianten wurden auch mit Knorpelzellen (Chondrozyten) besiedelt. Allerdings ist nicht nur die in diesen BG Scaffolds übliche Bildung von Hydroxylapatit als typischer Bestandteil des Knochens, sondern auch die geringe mechanische Stabilität für die Knorpelbildung wenig geeignet.

Ziel dieses interdisziplinären Projektes war es, unser patentiertes neuartiges, langsam abbaubares BG Scaffold (Car12N) mit einem biologisch abbaubaren Polymer Poly(L-Lactid) (PLLA) zu verstärken und zu prüfen, ob es nach erfolgreicher Besiedlung mit chondrogenen Zellen zur Bildung einer knorpelspezifischen Extrazellulären Matrix (EZM) kommt.

## Material und Methoden

BG Scaffolds wurden mittels Phasentrennung mit einem Lösungsmittel gelösten PLLA infiltriert. Eine detaillierte Charakterisierung der Scaffold Varianten [reine Car12N Scaffolds als Kontrolle und Car12N Scaffolds, die mit einem, zwei oder drei Polymer-Infiltrationsschritten behandelt wurden], wurde durchgeführt. Die biomechanischen Festigkeit, pH-Änderungen während der sauren 0,1 M HCl-Auslaugung und die Porosität wurden berechnet. Assay-basierte Zytotoxizitätstests wurden gemäß den internationalen Standards durchgeführt. Zur Untersuchung des Zellwachstums wurden die Scaffolds mit porcinen Gelenkchondrozyten (pGC) oder humanen mesenchymalen Stromazellen (hMSC) (27778 Zellen/mm³) für bis zu 35 Tage in einer dynamischer Rotationskultur besiedelt **(Abb.1)**. Das Überleben der Zellen wurde mit einem Vitalitäts-Assay überprüft. Anhand des DNA-Gehalts wurde die Zellproliferation bestimmt. Die Synthese von sulfatierten Glykosaminoglykanen (sGAG) in der Kultur wurde mit einem quantitativen Dimethylmethylenblau-Assay nachgewiesen. Die Stoffwechselaktivität der Zellen wurde mit dem Alamar Blue Test gemessen.

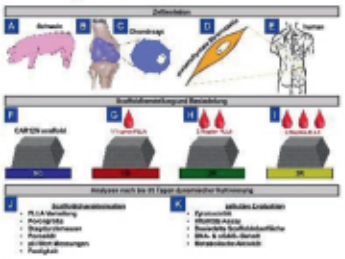

**Abb.1: Versuchsaufbau.** Aus dem Schwein (A) wurden Kniegelenke (B) entnommen um native Chondrozyten daraus zu isolieren (C). Mesenchymale Stromazellen (D) wurden aus dem humanen Beckenkamm (E) gewonnen. Primäre Zellen wurden anschließend auf reine bioaktive Glasscaffolds (BG,F), einmal (1R,G), zweimal (2R,H) oder dreimal (3R,I) mit PLLA infiltrierte Scaffolds angesiedelt. Vor der Besiedelung wurden umfangreiche Analysen zur Charakterisierung der Materialeigenschaften (J) durchgeführt. Nach bis zu 35 Tagen in einer dynamischen Rotationskultur wurden die zellulären Veränderungen näher untersucht (K).

## Ergebnisse und Diskussion

Die PLLA Verteilung war im BG Gerüst nicht homogen. Es gab signifikante Unterschiede in der Glassteglänge und der Porengröße zwischen Scaffolds mit und ohne PLLA Infiltration **(Abb.2)**. Die Porosität nahm mit zunehmendem PLLA ab **(Abb.3)**. Der Auslaugvorgang führte zur Bildung einer Gelschicht (4,2 µm) und nach 8 Tagen Auslaugung blieb der pH-Wert stabil. Die PLLA Infiltration stabilisierte die Scaffolds im Vergleich zum reinen BG Scaffold **(Abb.4)**. Keine der vier Scaffold Varianten war zytotoxisch. Die Vitalität (über 85%) und Adhärenz der beiden Zelltypen auf den Scaffolds konnte noch nach 35 Tagen nachgewiesen werden **(Abb.5)**.

Die DNA- und sGAG-Gehalte der mit beiden Zelltypen besiedelten Scaffolds stiegen bis zu 35 Tagen an, waren aber bei den PLLA infiltrierten Scaffolds im Vergleich zu den BG Kontrollscaffolds höher. Die Stoffwechselaktivität der verschiedenen Zelltypen auf den BG Scaffolds mit und ohne PLLA zeigten keine signifikanten Unterschiede.

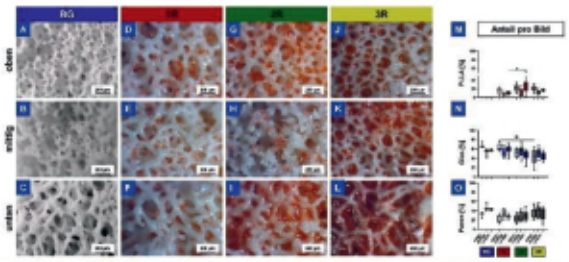

**Abb.2: Native Mikrokopaufnahmen.** Der obere (A, D, G, J), der mittige (B, E, H, K) und untere (C, F, I, L) Abschnitt von vertikal halbierten BG (A, B, C), 1R (D, E, F), 2R (G, H, I) und 3R (J, K, L) Scaffolds wurde aufgenommen. PLLA wurde rot eingefärbt um es vom Glas besser unterscheiden zu können. Maßstab: 200 µm. Der PLLA- (M), Glas- (N) und Poren- (O) Anteil wurde für jeden Abschnitt der unterschiedlichen Scaffolds berechnet. Drei unabhängige Versuche ergaben signifikante Unterschiede nach einer one-way ANOVA Testung mit (*) für p<0,05.

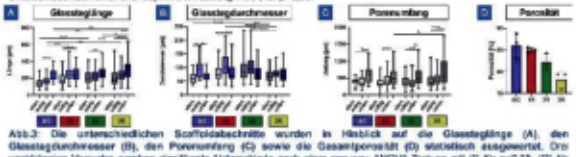

**Abb.3: Die unterschiedlichen Scaffoldabschnitte wurden in Hinblick auf die Glassteglänge (A), den Glassteg durchmesser (B), den Porenumfang (C) sowie die Gesamtporosität (D) statistisch ausgewertet.** Drei unabhängige Versuche ergaben signifikante Unterschiede nach einer one-way ANOVA Testung mit (*) für p<0,05; (**) für p<0,01; (***) für p<0,001 und mit (****) für p< 0,0001.

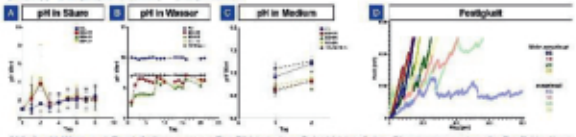

**Abb.4: pH Wert und Festigkeitsmessung.** Zur Bildung einer Gelschicht auf den Glasstegen wurden die Scaffolds über einen Zeitraum von 8 Tagen in 0,1 M Salzsäure ausgelaugt (A). Danach wurden die Scaffolds in Wasser überführt und gelagert (B) bevor sie vor der Kultivierung in Medium überführt wurden (C). Die Festigkeit der Scaffolds vor und nach der Auslaugung gemessen (D).

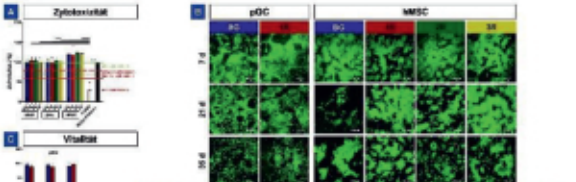

**Abb.5: Zytotoxizitätstestung (A), Vitalitäts-Assay (B), Vitalitäts-Messung (C).** Signifikante Unterschiede zur positiven Dimethylensulfoxid (DMSO) Kontrolle nach einer one-way ANOVA Testung mit (****) für p<0,0001. Im Vitalitäts-Assay werden lebende und tote porcine Gelenkchondrozyten (pGCs) bzw. humanen mesenchymale Stromazellen (hMSCs) unterschieden. Basierend auf dem Vitalitäts-Assay wurde die pGC/hMSC Vitalität berechnet. Die Besiedelungen von 2R und 3R Scaffolds mit pGCs wurden noch nicht durchgeführt.

## Schlussfolgerung und Ausblick

Der Polymerinfiltrationsprozess muss optimiert werden, um eine homogenere Polymerverteilung innerhalb des BG Scaffolds zu erreichen. Nicht nur das reine Car12N, sondern auch die polymerinfiltrierten neu entwickelten BG Scaffolds sind bis zu 35 Tage stabil und erlauben die Adhärenz und Proliferation von pGCs und hMSCs. Die Charakterisierung der knorpelspezifischen EZM Gen- und Proteinexpression, einschließlich Kollagen Typ II, Aggrecan und des chondrogenen Transkriptionsfaktors SOX9, wird in Zukunft durchgeführt.

## Integration von biologisch abbaubarem Poly(L-Lactid) (PLLA) auf neu entwickelten bioaktiven Glas Scaffolds (CAR12N) für das Knorpel Tissue Engineering

Clemens Gögele[1,2], Silvana Müller[3], Andreas Pradel[3], Sven Wiltzsch[3], Armin Lenhart[3], Markus Hornfeck[3], Achim Rübling[3], Hannes Kühl[3], Kerstin Schäfer-Eckart[4], Thomas M. Weiger[2], Gundula Schulze-Tanzil[1]

[1]Institut für Anatomie und Zellbiologie, Paracelsus Medizinische Privatuniversität, Nürnberg und Salzburg, Nürnberg, Deutschland; [2]Fachbereich für Biowissenschaften, Paris Lodron Universität Salzburg, Salzburg, Österreich; [3]Fakultät für Werkstofftechnik, Technische Hochschule Nürnberg Georg Simon Ohm, Nürnberg, Deutschland; [4]Klinik für Onkologie/Hämatologie, Klinikum Nürnberg Nord, Nürnberg, Deutschland; Contact: clemens.goegele@pmu.ac.at

### Objective

Knorpelverletzungen sind schwerwiegende Gewebeschäden, da die Regenerationsfähigkeit des Knorpels äußerst gering ist. Ein Knorpelverlust führt zu dauerhaften Schäden, die sich mit der Zeit ausweiten und zum Ausgangspunkt für Arthrose werden können. In der Vergangenheit wurden bioaktive Glas (BG) Scaffolds für den Knochenersatz entwickelt. Allerdings ist nicht nur die in diesen BG Scaffolds übliche Bildung von Hydroxylapaptit als typischer Bestandteil des Knochens, sondern auch die geringe mechanische Stabilität für die Knorpelbildung wenig geeignet. Ziel dieses interdisziplinären Projektes war es, unser patentiertes neuartiges, langsam abbaubares BG Scaffold (Car12N) mit einem biologisch abbaubaren Polymer Poly(L-Lactid) (PLLA) zu verstärken und zu prüfen, ob es nach erfolgreicher Besiedlung mit chondrogenen Zellen zur Bildung einer knorpelspezifischen Extrazellulären Matrix (EZM) kommt.

### Methods

BG Scaffolds wurden mittels Phasentrennung mit PLLA infiltriert. Eine Charakterisierung der Scaffold Varianten [reine Car12N Scaffolds als Kontrolle und Car12N Scaffolds, die mit einem, zwei oder drei Polymer-Infiltrationsschritten behandelt wurden], wurde durchgeführt. Die Festigkeit, pH-Änderungen während der Auslaugung und die Porosität wurden berechnet. Assay-basierte Zytotoxizitätstests wurden durchgeführt. Zur Untersuchung des Zellwachstums wurden die Scaffolds mit porcinen Gelenkchondrozyten (pGC) oder humanen mesenchymalen Stromazellen (hMSC) (27778 Zellen/mm3) für bis zu 35 Tage in einer dynamischer Rotationskultur besiedelt. Das Überleben der Zellen wurde mit einem Vitalitäts- Assay überprüft. Anhand des DNA-Gehalts wurde die Zellproliferation bestimmt.

### Results

Die PLLA Verteilung war im BG Gerüst nicht homogen. Es gab signifikante Unterschiede in der Glassteglänge und der Porengröße zwischen Scaffolds mit und ohne PLLA Infiltration. Die Porosität nahm mit zunehmendem PLLA ab. Der Auslaugvorgang führte zur Bildung einer Gelschicht (4,2 µm) und nach 8 Tagen Auslaugung blieb der pH Wert stabil. Die PLLA Infiltration stabilisierte die Scaffolds im Vergleich zum reinen BG Scaffold. Keine der vier Scaffold Varianten war zytotoxisch. Die Vitalität (über 85%) und Adhärenz der beiden Zelltypen auf den Scaffolds konnte noch nach 35 Tagen nachgewiesen werden. Die DNA- Gehalte der mit beiden Zelltypen besiedelten Scaffolds stieg bis zu 35 Tagen an, war aber bei den PLLA infiltrierten Scaffolds im Vergleich zu den BG Kontrollscaffolds höher. Die Stoffwechselaktivität der verschiedenen Zelltypen auf den BG Scaffolds mit und ohne PLLA zeigten keine signifikanten Unterschiede.

### Conclusions

Der Polymerinfiltrationsprozess muss optimiert werden, um eine homogenere Polymerverteilung innerhalb des BG Scaffolds zu erreichen. Nicht nur das reine Car12N, sondern auch die polymerinfiltrierten neu entwickelten BG Scaffolds sind bis zu 35 Tage stabil und erlauben die Adhärenz und Proliferation von pGCs und hMSCs. Die Charakterisierung der knorpelspezifischen EZM Gen- und Proteinexpression wird in Zukunft durchgeführt.

PARACELSUS MEDIZINISCHE PRIVATUNIVERSITÄT

Klinikum Nürnberg
Wir sind für Sie da.

Kontakt: clemens.goegele@pmu.ac.at

Virtueller Paracelsus Science Get Together, 02. Juli 2021

# Aufrechterhaltung der Ligamenthomöostase und -differenzierung durch zyklische Dehnung von funktionalisierten PLA/+P[LA-CL]-Kollagenkonstrukten für das Kreuzband-Tissue Engineering

**Clemens Gögele[1,2], Jens Konrad[3], Bernd Hoffmann[3], Judith Hahn[4], Annette Breier[4], Michael Meyer[5], Michaela Schröpfer[5], Gundula Schulze-Tanzil[1]**

[1]Institut für Anatomie und Zellbiologie, Paracelsus Medizinische Privatuniversität, Salzburg und Nürnberg, Nürnberg, Deutschland
[2]Fachbereich für Biowissenschaften, Paris Lodron Universität Salzburg, Österreich
[3]Institut für Biologische Informationsverarbeitung: IBI-2 Forschungszentrum Jülich, Deutschland
[4]Leibniz Institut für Polymerforschung (IPF) Dresden, Deutschland
[5]FILK Freiberg Institute, Freiberg, Deutschland

## Fragestellung

Die Rekonstruktion eines rupturierten vorderen Kreuzbandes (VKB) ist limitiert durch die Verfügbarkeit geeigneter Autografts und die Spendermorbidität. Um diese Einschränkungen zu umgehen könnten zukünftig Tissue engineerte Zellträger (Scaffolds) zum Einsatz kommen. Durch eine angepasste Sticktechnik mit einem Unterfaden aus Polymilchsäure (PLA) und einem Polycaprolacton (PCL)-basierten Oberfaden können solche dreidimensionalen Scaffolds hergestellt werden. Da die Zelladhärenz auf PLA oft sehr unbefriedigend ist, werden die Scaffolds zuerst mittels Gasphasenfluorierung hydrophiliert und anschließend mit Kollagenschaum infiltriert (Funktionalisierung).

**Dabei ist das Ziel dieses Projekts den Einfluss zyklischer Dehnung auf die Adhärenz, das Wachstum, das F-Aktin Zytoskelett und die Expression von Bänder-assoziierter Faktoren lapiner Kreuzbandzellen (LKBs) zu testen.**

## Material und Methoden

Zwei Scaffoldvarianten (mit und ohne Funktionalisierung) wurde mit 8333 lapinen Kreuzbandzellen (LKBs)/mm³ in der Suspensions- und der Sphäroidkultur besiedelt. Auf eine Adhärenzphase folgte die Dehnungsphase (4% Dehnung, 0,3 Hz, 3 Tage) **(Abb.1)**. Das Zellüberleben wurde mittels Vitalitäts Assay unter dem Konfokalen Laser Mikroskop überprüft **(Abb.2)**. Basierend auf diesen Daten konnte die besiedelte Fläche auf den Scaffolds durch das Program ImageJ ermittelt werden **(Abb.3A)**. Mit dem CyQuant Assay wurde die Zellzahl pro Scaffold bestimmt **(Abb.3B)**. Der Dimethylmethylen Blau (DMMB) Assay wurde herangezogen, um sulfatierte Glykosaminoglykane zu messen **(Abb.3C)**. Mittels immuncytochemischer Färbungen wurde der Proliferationsmarker ki67, Paxillin, alpha smooth muscle actin (αSMA), F-Aktin und die Zellkerne dargestellt **(Abb.4)**. Die relative Genexpression von Kollagen Typ I, Decorin, Tenascin C, Tenomodulin, Mohawk und Connexin 43 wurde mittels real-time PCR quantifiziert **(Abb.5)**.

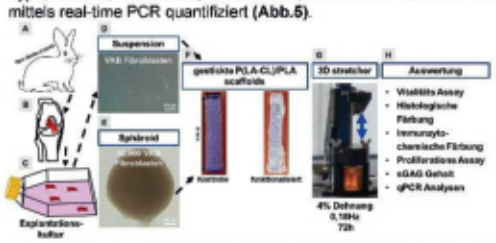


**Abb.1: Versuchsaufbau.** Aus dem Kaninchen (A) wurden native Kreuzbänder (B) entnommen. Vordere Kreuzband (VKB) Fibroblasten wurden in der Zellkultur gezüchtet (C). Mittels Zellsuspension (D) oder Sphäroidkultur (E) wurden gestickte Scaffolds (F) aus PLA und PCL besiedelt bevor sie anschließend in einem 3D Stretcher 72h gestreckt wurden. Eine umfangreiche Auswertung (H) soll helfen das Verhalten von LKBs auf zyklische Dehnung besser zu verstehen. Hz =Hertz, sGAG=sulfatierte Glycosaminoglykane.

## Ergebnisse und Diskussion

Die zyklische Dehnung hatte keinen Einfluss auf die Zellvitalität. Funktionalisierte Scaffolds zeigten eine höhere Zelladhärenz und signifikant größere Oberflächenbesiedelung als unfunktionalisierte. LKBs breiteten sich gleichmäßiger auf den gedehnten Fäden aus als auf der ungedehnten Variante. Die Proliferationsrate war in der Suspensionskultur bei unfunktionalisierten und ungedehnten Scaffolds am höchsten. Die relative Genexpression von Kollagen Typ I, Decorin und Tenascin C wurde in der Sphäroidkultur im Vergleich zur Suspensionskultur hochreguliert, wohingegen Tenomodulin, Mohawk und Connexin 43 in beiden Scaffoldvarianten und in beiden Kultursystemen durch die Dehnung hochreguliert wurde.

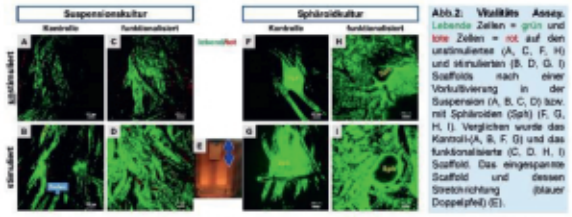


**Abb.2: Vitalitäts Assay.** Lebende Zellen = grün und tote Zellen = rot auf den unstimulierten (A, C, F, H) und stimulierten (B, D, G, I) Scaffolds nach einer Vorfluffvierung in der Suspension (A, B, C, D) bzw. mit Sphäroiden (Sph) (F, G, H, I). Verglichen wurde das Kontroll-(A, B, F, G) und das funktionalisierte (C, D, H, I) Scaffold. Das eingespannte Scaffold und dessen Streichrichtung (blauer Doppelpfeil) (E).

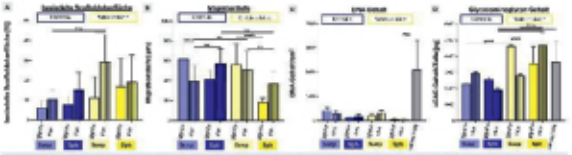

**Abb.3: Statistische Auswertung der besiedelten Scaffoldoberfläche (A), der Migrationstiefe (B), des DNA Gehalts (C) und des sGAG Gehalts (D) aus der Suspensions (Susp)- und Sphäroid (Sph)- Kultur.** Signifikante Unterschiede werden nach einer one-way ANOVA Testung mit (****) für $p< 0,0001$ angegeben. unstim=unstimuliert, stim=stimuliert, VKB = Vorderes Kreuzband.

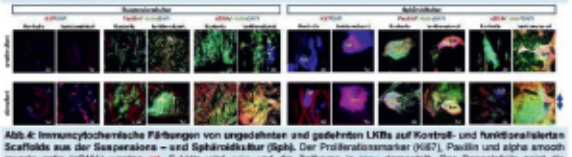

**Abb.4: Immuncytochemische Färbungen von ungedehnten und gedehnten LKBs auf Kontroll- und funktionalisierten Scaffolds aus der Suspensions – und Sphäroidkultur (Sph).** Der Proliferationsmarker (Ki67), Paxillin und alpha smooth muscle actin (αSMA) werden rot, F-Aktin wird grün und die Zellkerne in blau dargestellt. Der Doppelpfeile zeigt die Streichrichtung. Maßstab = 100µm

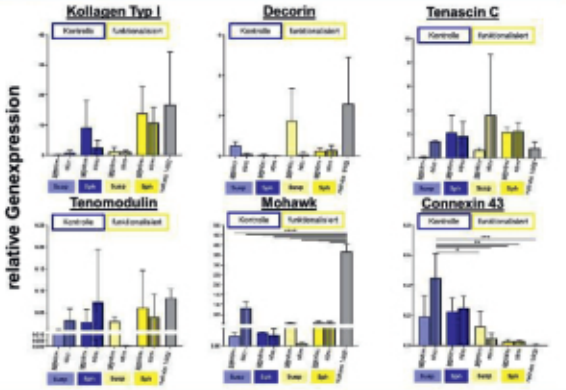


**Abb.5: Relative Genexpression von Ligament-assoziierten Matrixproteinen (Kollagen Typ I, Decorin, Tenascin C), dem Markerprotein (Tenomodulin), dem Transkriptionsfaktor (Mohawk) und dem Protein für Zell-Zell-Kontakte (Connexin 43).** Native Kreuzbänder dienten als Referenz. Drei unabhängige Versuche ergaben signifikante Unterschiede nach einer one-way ANOVA Testung mit (*) für $p<0,05$; (**) für $p<0,01$; (***) für $p<0,001$ und mit (****) für $p< 0,0001$.

## Schlussfolgerung und Ausblick

In dieser Studie konnte gezeigt werden, dass eine zyklische Dehnung funktionalisierter Kreuzbandscaffolds zu einer gleichmäßigen Zelladhärenz und größerer Oberflächenbesiedelung nicht nur in der Suspensions- sondern auch in der Sphäroidkultur führt und dass dadurch die Ligamenthomöostase und -differenzierung aufrechterhalten wird.

Die Arbeiten sind assoziiert mit einem durch die Deutsche Forschungsgemeinschaft (SCHU1079, 14-1) geförderten Projekt zum Tissue engineerten Kreuzbandersatz. Der Einsatzt bedankt sich recht herzlich bei Herrn Prof. Traweger für die Betreuung seiner PhD Arbeit.

## Aufrechterhaltung der Ligamenthomöostase und -differenzierung durch zyklische Dehnung von funktionalisierten PLA/+P[LA-CL]-Kollagenkonstrukten für das Kreuzband-Tissue Engineering

Clemens Gögele[1,2], Jens Konrad[3], Bernd Hoffmann[3], Judith Hahn[4], Annette Breier[4], Michael Meyer[5], Michaela Schröpfer[5], Gundula Schulze-Tanzil[1]

[1]nstitut für Anatomie und Zellbiologie, Paracelsus Medizinische Privatuniversität, Salzburg und Nürnberg, Nürnberg, Deutschland; [2]Fachbereich für Biowissenschaften, Paris Lodron Universität Salzburg, Österreich; [3]nstitut für Biologische Informationsverarbeitung: IBI-2 Forschungszentrum Jülich, Deutschland; [4]Leibniz Institut für Polymerforschung (IPF) Dresden, Deutschland; [5]FILK Freiberg Institute, Freiberg, Deutschland; Contact: clemens.goegele@pmu.ac.at

### Objective

Die Rekonstruktion eines rupturierten vorderen Kreuzbandes (VKB) ist limitiert durch die Verfügbarkeit geeigneter Autografts und die Spendermorbidität. Um diese Einschränkungen zu umgehen könnten zukünftig Tissue engineerte Zellträger (Scaffolds) zum Einsatz kommen. Durch eine angepasste Sticktechnik mit einem Unterfaden aus Polymilchsäure (PLA) und einem Polycaprolacton (PCL)-basierten Oberfaden können solche dreidimensionalen Scaffolds hergestellt werden. Da die Zelladhärenz auf PLA oft sehr unbefriedigend ist, werden die Scaffolds zuerst mittels Gasphasenfluorierung hydrophiliert und anschließend mit Kollagenschaum infiltriert (Funktionalisierung). Dabei ist das Ziel dieses Projekts den Einfluss zyklischer Dehnung auf die Adhärenz, das Wachstum, das F-Aktin Zytoskelett und die Expression von Bänder- assoziierter Faktoren lapiner Kreuzbandzellen (LKBs) zu testen.

### Methods

Zwei Scaffoldvarianten (mit und ohne Funktionalisierung) wurde mit 8333 lapinen Kreuzbandzellen (LKBs)/mm3 in der Suspensions- und der Sphäroidkultur besiedelt. Auf eine Adhärenzphase folgte die Dehnungsphase (4% Dehnung, 0,3 Hz, 3 Tage). Das Zellüberleben wurde mittels Vitalitäts Assay unter dem Konfokalen Laser Mikroskop überprüft. Basierend auf diesen Daten konnte die besiedelte Fläche auf den Scaffolds durch das Program ImageJ ermittelt werden. Mit dem CyQuant Assay wurde die Zellzahl pro Scaffold bestimmt. Der Dimethylmethylen Blau (DMMB) Assay wurde herangezogen, um sulfatierte Glykosaminoglykane zu messen. Mittels immuncytochemischer Färbungen wurde der Proliferationsmarker ki67, Paxillin, alpha smooth muscle actin (αSMA), F-Aktin und die Zellkerne dargestellt. Die relative Genexpression von Kollagen Typ I, Decorin, Tenascin C, Tenomodulin, Mohawk und Connexin 43 wurde mittels real-time PCR quantifiziert.

### Results

Die zyklische Dehnung hatte keinen Einfluss auf die Zellvitalität. Funktionalisierte Scaffolds zeigten eine höhere Zelladhärenz und signifikant größere Oberflächenbesiedelung als unfunktionalisierte. LKBs breiteten sich gleichmäßiger auf den gedehnten Fäden aus als auf der ungedehnten Variante. Die Proliferationsrate war in der Suspensionskultur bei unfunktionalisierten und ungedehnten Scaffolds am höchsten. Die relative Genexpression von Kollagen Typ I, Decorin und Tenascin C wurde in der Sphäroidkultur im Vergleich zur Suspensionskultur hochreguliert, wohingegen Tenomodulin, Mohawk und Connexin 43 in beiden Scaffoldvarianten und in beiden Kultursystemen durch die Dehnung hochreguliert wurde.

### Conclusions

In dieser Studie konnte gezeigt werden, dass eine zyklische Dehnung funktionalisierter Kreuzbandscaffolds zu einer gleichmäßigen Zelladhärenz und größerer Oberflächenbesiedelung nicht nur in der Suspensionssondern auch in der Sphäroidkultur führt und dass dadurch die Ligamenthomöostase und -differenzierung aufrechterhalten wird.

# Stem cell-based regeneration of muscles

Grabner C[1,3], Benedetti A[1,3], Kreutzer C[1,3], Romanelli P[1,2], Thurner M[2], Couillard-Després S[1,3,4]

[1]Institute of Experimental Neuroregeneration, Paracelsus Medical University, Salzburg, Austria
[2]Innovacell AG, Innsbruck, Austria
[3]Spinal Cord Injury and Tissue Regeneration Center Salzburg (SCI-TReCS), Austria
[4]Austrian Cluster for Tissue Regeneration, Austria
✉ Christian.Grabner@pmu.ac.at

PARACELSUS MEDIZINISCHE PRIVATUNIVERSITÄT

## 1 Background

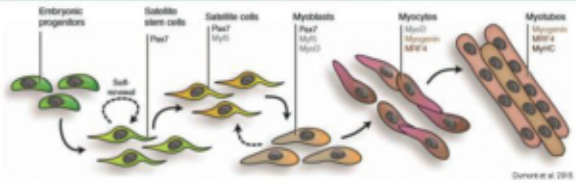


Satellite cells are able to quickly repair mature myofibers of skeletal muscles after massive injuries because of their myogenic regenerative capacities. Residing between the basal lamina and the myofiber membrane in a dormant state, satellite cells are activated after injury by various signals arising from the damaged tissue. Along the myogenic lineage progression, they migrate toward the injury site and proliferate to become mononucleated myoblasts. After differentiating into mature myocytes, they can regenerate skeletal muscle by fusing to multinucleated myotubes. This regenerative process is controlled by a vast network of transcription factors specific to the different steps of myogenesis. A good survival of muscle stem cells after implantation is crucial for an effective regenerative cell therapy. Monitoring and modulating the integration and persistence of transplanted cells is essential to find and optimize conditions of cell administration.

## 2 Aim of the project

Strategies for autologous cells transplantation to cure impaired tissue regeneration are currently heavily investigated. The regenerative capacities of satellite cells can be used for the development of regenerative therapies required following muscle lesion (e.g. fecal and urinary incontinence) and in cases of myopathies (e.g. Duchenne- and Becker Muscular Dystrophy).

Recent studies using autologous skeletal muscle derived cells (SMDC) for the treatment of fecal and urinary incontinence reported promising results in clinical trials. However, the detailed mode of action remains to be elucidated and cell engraftment and persistence following implantation has to be optimized.

The aim of this project is to get a better understanding of the potential of skeletal muscle-derived stem cells for muscle regeneration therapies.

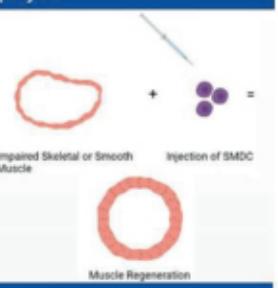


## 3 Material and Methods

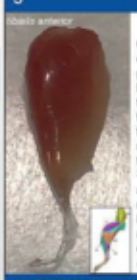


Cell culture techniques allow for the isolation and expansion of skeletal muscle-derived cells (SMDC; a heterogeneous pool of muscle stem cells and myogenic progenitor cells) after muscle biopsy. Transgenic donor SMDC (expressing bioluminescent and fluorescent reporter genes) are used to track cells after transplantation. Cells expressing a bioluminescent reporter (firefly luciferase) allow for a sensitive detection *in vivo* of engrafted cells. Expression in grafted cells of a fluorescent reporter (eGFP, tdTomato) allows for the detection on histological sections at a cellular resolution. To mimic the clinical situation of autologous cell transplantation, cells are injected in a syngeneic fashion (by using a B6(Cg)-Tyr$^{c-2J}$/J mouse for cell isolation and host). For implantation, one million cells are administered into the *tibialis anterior (TA)* using a Luer adaptor holding four 30G needles for simultaneous injection. SMDC were monitored via repeated bioluminescence acquisition for 9 weeks post-transplantation. Finally, cryosections and immunohistology are performed to analyse SMDC engraftment and expression of specific cell markers and transcription factors.

Charles et al. 2016

## 4 TdTomato expression of engrafted cells following transplantation

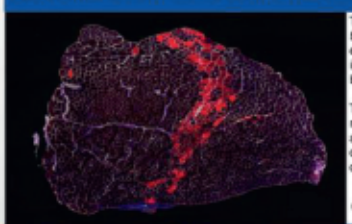

The micrograph shows a cross-section of a *tibialis anterior* with transplanted SMDC expressing tdTomato (red). Laminin is shown in white and the nuclear staining DAPI in blue.

The successful engraftment of SMDC is revealed by the presence of normal appearing myotubes expressing tdTomato. In contrast to the other results, this result was obtained in immunodeficient host mice.

Messner et al. 2021

## 5 Monitoring of skeletal muscle-derived cells after transplantation

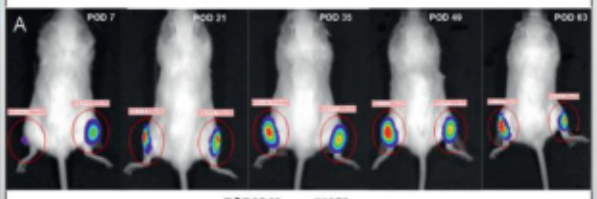


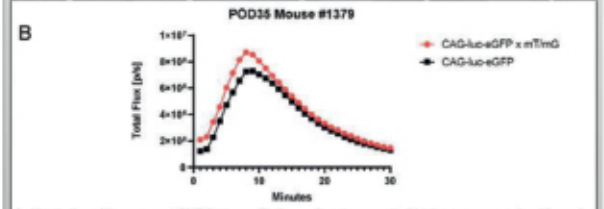


A: Monitoring of transplanted SMDC at specific time points. Increment of bioluminescence signal intensity of engrafted SMDC at post operative day (POD) 7, 21, 35, 49 and 63.
B: Luciferase signals emitted by grafted SMDC (one measurement per minute over a time period of 30 minutes) were quantified to calculate the area under the curve (AUC) on day 35 post-implantation. Background corrected signals expressed in photons/second (p/s)

## 6 Transplanted SMDC persist in muscles for at least 9 weeks

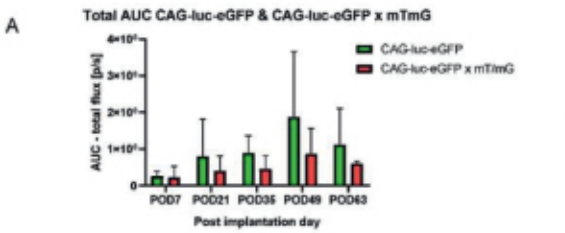


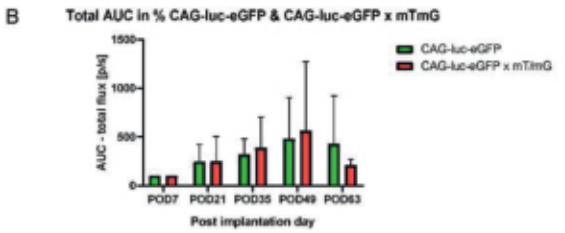


**Luciferase signal over time:** Bioluminescence measurement of transplanted SMDC at specific post-operative days (POD). Luciferase signal integration (area under the curve; AUC) of mice that received 1*10$^6$ SMDC of CAG-luc-eGFP or CAG-luc-eGFP x mT/mG in the *tibialis anterior*. Comparison of the bioluminescence signal intensities of all mice in (A) total AUC and (B) % AUC normalized to day 7 measurements (set as 100%). The graphs indicate an increase in signal intensity up to a fivefold until POD49 and survival and maintenance at POD63.

## 7 Outlook

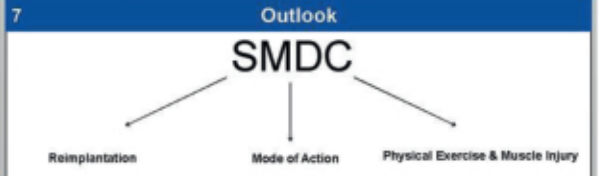


## 8 Acknowledgements

We gratefully thank the support from our collaboration partner the Innovacell AG, Innsbruck!

References:

Messner et al. Stem Cell Research & Therapy (2021) 12:148 https://doi.org/10.1186/s13287-021-02208-w
Dumont et al. Compr Physiol 5:1027-1059, 2015
Charles et al. (2016) Musculoskeletal Geometry, Muscle Architecture and Functional Specialisations of the Mouse Hindlimb. PLoS ONE 11(4): e0147889

## Stem cell-based regeneration of muscles

Christian Grabner[1,3], Ariane Benedetti[1,3], Christina Kreutzer[1,3], Pasquale Romanelli[1,2], Marco Thurner[2], Sébastien Couillard-Després[1,3,4]

[1]Institute of Experimental Neuroregeneration, Paracelsus Medical University, Salzburg, Austria; [2]Innovacell AG, Innsbruck, Austria; [3]Spinal Cord Injury and Tissue Regeneration Center Salzburg (SCI-TReCS), Austria; [4]Austrian Cluster for Tissue Regeneration, Austria; Contact: christian.grabner@pmu.ac.at

### Objective
Strategies for autologous cells transplantation to cure impaired tissue regeneration are currently heavily investigated. The regenerative capacities of satellite cells can be used for the development of regenerative therapies to address yet unmet medical needs (e.g. fecal and urinary incontinence, Duchenne- and Becker Muscular Dystrophy). Residing between the basal lamina and the myofiber membrane in a dormant state, satellite cells are activated after injury by various signals arising from the damaged tissue. After differentiating into mature myocytes, they can regenerate skeletal muscle by fusing to multinucleated myotubes. Recent studies using autologous skeletal muscle-derived cells (SMDC; a heterogeneous pool of muscle stem cells and myogenic progenitor cells) for the treatment of fecal and urinary incontinence reported promising results in clinical trials. However, the detailed mode of action remains to be elucidated and cell engraftment and persistence following implantation must be optimized. The aim of this project is to get a better understanding of the potential of SMDC for muscle regeneration therapies.

### Methods
A good survival of muscle stem cells after implantation is crucial for an effective regenerative cell therapy. Monitoring and modulating the integration and persistence of transplanted cells is essential to find and optimize conditions of cell administration. Cell culture techniques allow for the isolation and expansion of SMDC after muscle biopsy. Transgenic mouse donor SMDC expressing reporter genes were used to track cells in vivo and ex vivo after transplantation. To mimic the clinical situation of autologous cell transplantation, cells were injected in a syngeneic fashion for cell isolation and host. One million SMDC were administered into the tibialis anterior (TA) and were monitored via repeated bioluminescence acquisition for 9 weeks post-transplantation. Immunohistology was performed to analyze SMDC engraftment and expression of specific cell markers and transcription factors.

### Results
The recording of bioluminescence and the detection of normal appearing myotubes expressing tdTomato during histological analysis of the tibialis anterior revealed the successful engraftment of SMDC.

### Conclusions
SMDC can integrate into the host muscle and remain available for regenerative processes for a period of at least 9 weeks. In ongoing studies, we are analyzing the impact of SMDC re-implantations in the same muscle segment at several timepoints, the potential mode of action for functional muscle regeneration, as well as the effects of physical exercise and induced muscle lesion on regenerative processes after SMDC transplantation.

PARACELSUS MEDIZINISCHE PRIVATUNIVERSITÄT

University of Ljubljana

Klinikum Nürnberg
Wir sind für Sie da!

# EKG-Prädiktoren für postoperative Rhythmusstörungen nach chirurgischem Aortenklappenersatz und Aorto-Coronarer-Bypass-Operation

Günzler V [1], Kallsnik JM [2], Stuet P [1], Kocet L [3], Zibert J [3], Sirch J [2], Fittkau M [2], Fischlein T [2]

[1]Paracelsus Medizinische Privatuniversität Nürnberg, Deutschland; [2]Klinik für Herzchirurgie, Klinikum Nürnberg Süd, Deutschland; [3]Fakultät für Gesundheitswissenschaften, Universität Ljubljana, Slowenien.
Kontakt: valentin.guenzler@stud.pmu.ac.at

## Einleitung

Herzrhythmusstörungen zählen zu den häufigsten Komplikationen nach herzchirurgischen Operationen. Ihre Prävalenz liegt bei knapp 50 % aller herzoperierten Patient*Innen[1] Die häufigste Gruppe stellen hier mit ca. 20-30 % die Schmalkomplex-Tachyarrhythmien aufgrund von Vorhofflimmern dar.[2] Postoperative Bradyarrhythmien treten dagegen seltener auf, bergen aber in Form einer kompletten atrioventrikulären Blockierung ein enormes Risiko einer Herzinsuffizienz bis hin zum Herzstillstand.[3]

## Zielsetzung

Diese Arbeit setzt sich das Ziel, Prädiktoren für das postoperative Neuauftreten von Vorhofflimmern (poVHF) und einer kompletten atrioventrikulären Blockierung (poAVB III°) zu eruieren. Der Fokus dieser Studie liegt vor allem auf der Analyse präoperativer EKG-Parameter.

## Methodik

1155 Patient*Innen, die in der Herzchirurgie des Klinikums Nürnberg eine isolierte Aorto-Coronare-Bypass-Operation (= ACB; im Zeitraum: 11.06.2018-31.12.2019) oder einen isolierten chirurgischen Aortenklappenersatz (= AKE; im Zeitraum: 13.04.2015-31.12.2019) erhielten, wurden in dieser Studie retrospektiv untersucht. 286 Patient*innen (24,76 %) mussten ausgeschlossen werden. Die zu analysierenden Parameter wurden mittels der archivierten Patientenakte und der Operationsdokumentation erfasst. Das letzte präoperative EKG wurde jeweils gesondert analysiert. Eine Übersicht des Studienkollektives findet sich in Fenster 1, die analysierten Parameter in Fenster 2.

### Studienkollektiv 1

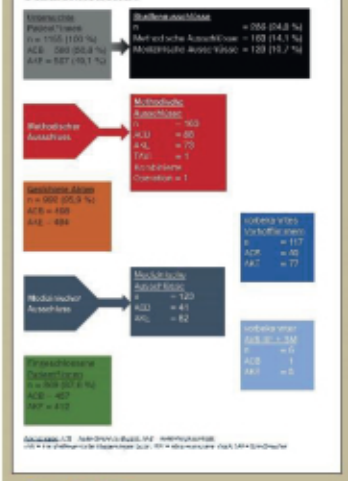


### Analysierte EKG-Parameter 2

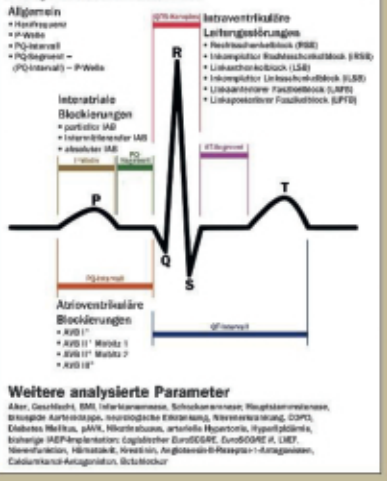


**Weitere analysierte Parameter**

Alter, Geschlecht, BMI, Infarktanamnese, Schockanamnese, Reoptisternotomie, Bisherige Aortenklappe, neurologische Erkrankung, Nierenersatzung, COPD, Diabetes Mellitus, pAVK, Nikotinabusus, arterielle Hypertonie, Hypercholesterinämie, bisherige (AE)Pumpfunktion: Ergebnisse EuroSCORE, EuroSCORE II, LVEF, Niereninsuffizienz, Hämatokrit, Kreatinin, Angiotensin-II-Rezeptor-1-Antagonisten, Calciumkanal-Antagonisten, Betablocker

### Präoperative Rhythmusstörungen 3

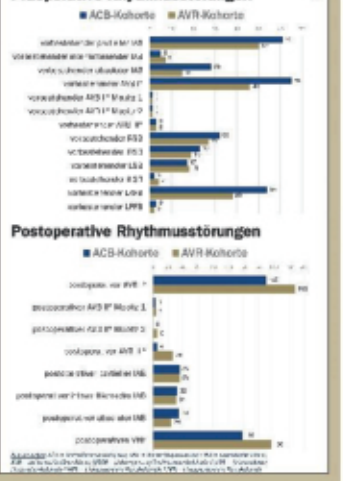


### Postoperative Rhythmusstörungen




## Ergebnisse

### Analysen zu postoperativen Vorhofflimmern 4

**Univariate Analyse**

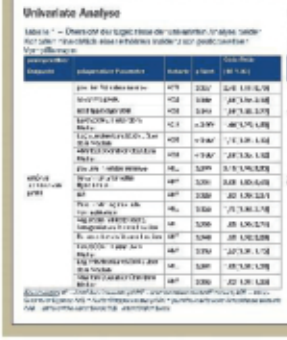

**Multivariate Analyse**

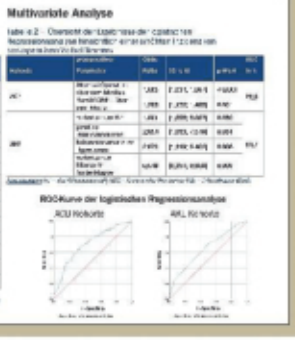

**ROC-Kurve der logistischen Regressionsanalyse**




### Analysen zu postoperativen AV-Blockierungen III° 5

**Univariate Analyse**

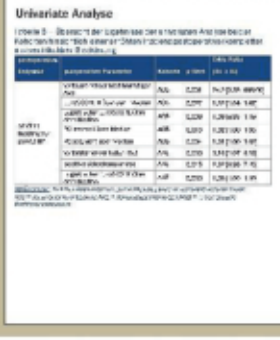

**Multivariate Analyse**

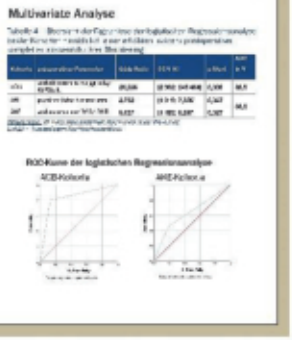

**ROC-Kurve der logistischen Regressionsanalyse**




## Schlussfolgerungen

Die Ergebnisse dieser Studie sollen den Fokus der präoperativen Risikoeinschätzung vermehrt auf das EKG richten. EKG-Parameter konnten in dieser Studie als signifikante Risikofaktoren und Prädiktoren sowohl für poVHF, also auch für poAVB III° beschrieben werden.

- vorbestehender IAB und AKE geplant
- → erhöhtes Risiko für das Entwickeln eines poVHF
- niedriggradiger AV-Block und ACB geplant
- → erhöhtes Risiko für das Entwickeln eines poAVB III°
- vorbestehender RSB/IRSB und AKE geplant
- → erhöhtes Risiko für das Entwickeln eines poAVB III°

## Referenzen


- [1]Boriani G, Fauchier L, Aguinaga L, et al. European Heart Rhythm Association (EHRA) consensus document on management of arrhythmias and cardiac electronic devices in the critically ill and post-surgery patient. Europace. 2019.
- [2]Mathew JP, Fontes ML, Tudor IC, et al. A multicenter risk index for atrial fibrillation after cardiac surgery. JAMA. 2004.
- [3]Peretto G, Durante A, Limite LR, Cianflone D. Postoperative arrhythmias after cardiac surgery: incidence, risk factors, and therapeutic management. Cardiol Res Pract. 2014.

## ECG-Predictors of postoperative arrhythmia after aortic valve replacement and coronary artery bypass graft

Valentin Günzler[1], Jurij Matija Kalisnik[2], Patrick Sluet[1], Laura Kocet[3], Janez Zibert[3], Joachim Sirch[2], Martin Fittkau[2], Theodor Fischlein[2]

[1]Paracelsus Medical University, Nuremberg, Germany; [2]Department of cardiac surgery, Paracelsus Medical University, Nuremberg, Germany; [3]Faculty of health sciences, University of Ljubljana, Slovenia; Contact: valentin.guenzler@stud.pmu.ac.at

### Objective

Actually nearly 50% of all heart surgical patients develop a post-operative arrhythmia (1). Most of them suffer from a supraventricular tachycardia, predominantly based on atrial fibrillation (2). Postoperative bradyarrhythmias caused by complete atrio ventricular blockage appear less often, but are associated with a high risk of heart insufficiency or also possible cardiac arrest (3). Although many studies have investigated the etiology of post-operative atrial fibrillation (poAF) and post-operative complete atrio ventricular blockage (poAVB III°) and tried to classify predictors, only a few focused on parameters of the routine pre-operative ECG.

### Methods

In a single-center retrospective observational case-control study of 1155 patients without prior history of AF and implanted pacemaker, we examined patients, who underwent isolated coronary artery bypass surgery (=CABG; in the period of 11.06.18–31.12.19), or isolated surgical aortic valve replacement (=AVR; in the period of 13.04.15–31.12.19). 286 patients have been excluded for medical or methodical reasons. Parameters for analyses were collected from pre-operative ECGs and patient records. For further analysis data of operation-documentation were added. Univariate analysis and multivariate logistic regression analysis were used to identify risk factors.

### Results

The rate of poAF was 118 (25,82%) after CABG-operation and 156 (37,86%) after surgical AVR. A higher risk of developing poAF was shown by patients in the CABG-cohort with an advanced age (OR=1,07 [1,03;1,10], p=<0,001) and a high EuroSCORE II (OR=1,28 [1,11;1,49], p=0,001) but in the AVR-cohort a pre-existing interatrial block (OR=1,80 [1,06;3,07], p=0,030), a former myocardial infarction (OR = 2,85 [1,08;7,52], p=0,034) or a pre-existing hypertension (OR=2,67 [1,32;5,40], p=0,006) have been identified as risk factors. Patients with a pre-existing bicuspid aortic valve (OR=0,55 [0,35;0,86], p=0,009) had a lower incidence of poAF. In the cohorts 1,1% of the patients following CABG (n=5) and 5,88% of the patients following AVR (n=24) were affected by new-onset poAVB III°. Through investigating only a pre-existing low atrio ventricular blockage (OR = 26,97 [2,96;245,46], p=0,003) was highly significant for CABG-cohort. In the AVR-cohort a former shock (OR=2,73 [1,02;7,36], p=0,047) and a pre-existing (incomplete) right bundle branch block (OR=3,07 [1,14;8,29], p=0,027) were shown as cohort-specific risk factors.

### Conclusions

This study proved that patients with pre-existing interatrial block have a higher risk of developing post-operative poAF if an AVR is planned, as well as a pre-existing low atrio ventricular blockage in case of planned CABG and a pre-existing (incomplete) right bundle branch block in case of getting AVR are risk factors for poAVB III°. This study is limited by the single-center retrospective design and should be validated in further studies.

### References

1. Boriani G, et al. EHRA consensus document on management of arrhythmias and cardiac electronic devices in the critically ill and post-surgery patient, endorsed by HRS, APHRS, CASSA, and LAHRS. Europace. 2019
2. Mathew JP, et al. A multicenter risk index for atrial fibrillation after cardiac surgery. JAMA. 2004
3. Peretto G, et al. Postoperative arrhythmias after cardiac surgery. Cardiol Res Pract. 2014

# Human Platelet Lysate for Skin Regeneration & Immune Modulation

Fausto Gueths Gomes [1], André Cronemberger Andrade [2], Martin Wolf [2], Sarah Hochman [2], Linda Krisch [1], Christof Regl [3], Patricia Ebner-Peking [2], Christian Huber [3], Nicole Meisner-Kober [3], Katharina Schallmoser [1] and Dirk Strunk [2]

[1]Department of Transfusion Medicine, Paracelsus Medical University, Salzburg, Austria
[2]Experimental and Clinical Cell Therapy Institute (CCT), Spinal Cord Injury and Tissue Regeneration Center, Paracelsus Medical University, Salzburg, Austria
[3]Department for Biosciences, Paris Lodron University Salzburg, Austria

fausto.gueths@pmu.ac.at

## Introduction/main goals

Platelet derivatives, particularly platelet-rich plasma, have been extensively evaluated regarding their possible application for regeneration purposes (Etulain, Platelets 2018). Human-platelet lysate (HPL) promotes cell growth more effectively than fetal bovine serum but has not yet been thoroughly evaluated towards a possible regenerative therapeutic role. On a parallel note, platelet extracellular vesicles (PEVs) have been shown to promote re-epithelization of chronic wounds in mice (Guo et al., Theranostics 2017), angiogenesis (Ohtsuka et al., Atherosclerosis 2013), among others. However, the functional characteristics of PEVs can differ depending on how the platelets were prepared for EV production (e.g. resting/activated state; Puhm et al., ATVB 2021) and little is known about HPL-EVs.

Our main goal in the present study is, therefore, to evaluate the effects of HPL in skin regeneration and immunomodulation using a novel type of skin organoid (Ebner-Peking et al., BioRxiv 2021) and our standardized immune modulation assay (Ketterl et al., Stem Cell Res Ther 2015), with particular interest in the role of HPL-derived EVs in combination or not with HPL protein-rich preparations.

## Sample characterization

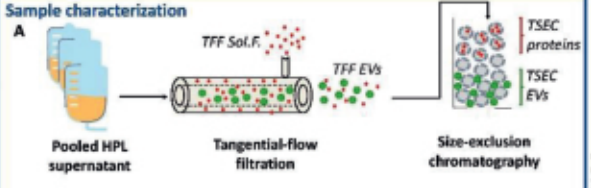


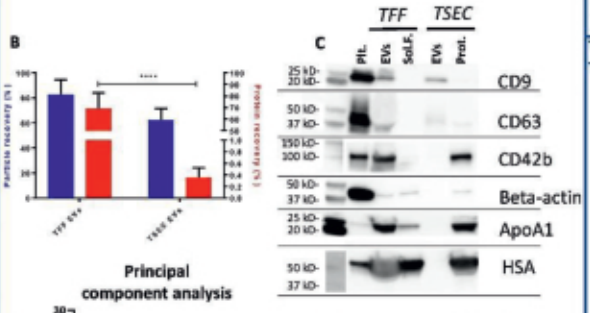


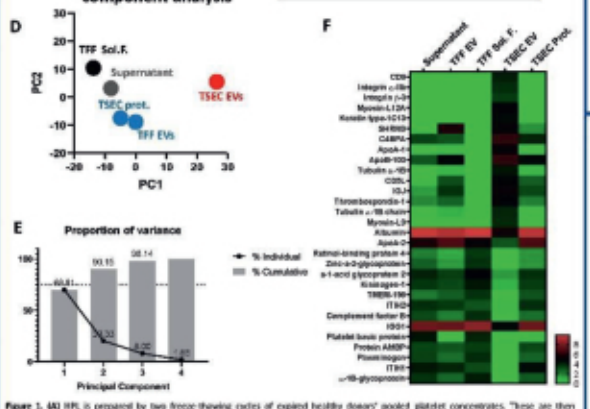


**Figure 1.** **(A)** HPL is prepared by two freeze-thawing cycles of expired healthy donors' pooled platelet concentrates. These are then centrifuged at 3,000 × g, 30 min, filtered at 0.22 µm, 10× diluted in cell culture media and put through one round of TFF (500 kD) where we collect the soluble factors as permeate and EVs as retentate. TFF EVs are then further purified in initial SEC fractions, while remaining proteins are also collected on later fractions. **(B)** Particle (measured by Tunable Resistive Pulse Sensing) and protein (DC protein assay) recovery related to total supernatant levels were calculated for each method. Of note, both methods recover particles efficiently, while proteins are mostly depleted on TSEC. n=3. **(C)** Western blot showing presence of EV marker CD9 on both TFF and TSEC EVs, whereas depletion of serum components such as HSA was only observed in TSEC EVs. **(D)**, **(E)** Principal component analysis - which classifies groups of proteins responsible for the biggest amount of variance between samples - of label free proteomics shows that TSEC EVs differed from the other samples mostly by PC1, which explained ~ 70% of variance between samples. **(F)** By compiling 30 of the most relevant proteins in PC1 across the different HPL samples, we see upregulation of EV marker CD9 and platelet markers integrin alfa/β-3 in TSEC EVs. n=3.

## Skin-organoid/fibrosphere formation was more prominently induced by TFF EVs and TSEC protein fractions

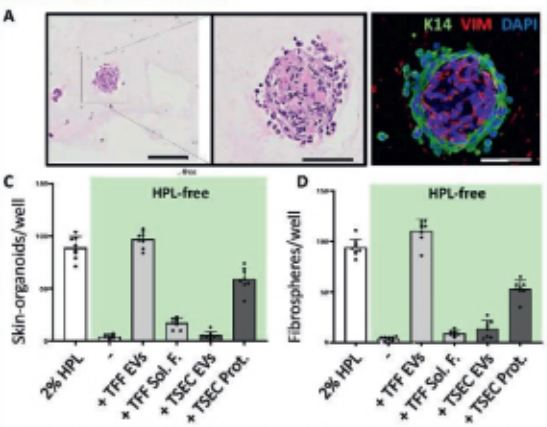


**Figure 2.** We incubated human primary keratinocytes, fibroblasts and endothelial cells on a 2:1:1 ratio in 96-well ultra-low attachment plates for 6 days, 37°C, 5% $CO_2$/$O_2$. The suspensions were then embedded in paraffin followed by **(A)** H&E staining and immunostaining with Keratin 14-AF488, showing the surrounding keratinocyte layer and Vimentin-555, showing the dermal core of the skin organoids. **(C)** We then quantified the number of skin organoids and **(D)** fibrospheres (fibroblasts alone)-per well following treatments with 100k EVs/well from different EV preparations and matching volumes for soluble factors and protein fractions. TFF EVs notably induced structure formation in both experimental setups (* 100/well), followed by TSEC protein fractions (*50/well). Scale bars from left to right: 250, 100 and 50 µm. n=3

## TFF EV-induced immunomodulation is partially reproduced by combining TSEC EV and protein fractions

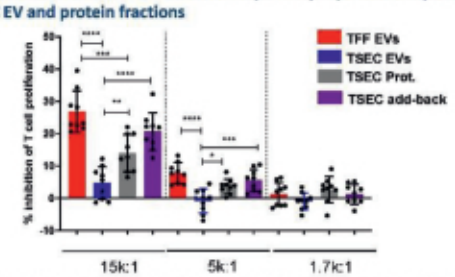


**Figure 3.** We performed an immunomodulation assay in which we incubated CFSE-stained PBMCs (pool of 10 donors) with HPL-derived samples for 4 days, 37°C, 5% $CO_2$, 18% $O_2$. On day 0, PBMCs were also treated with phycoerythrin (PHA) as a mitogenesis inducer, and we observe the samples' potential to inhibit PHA-induced T cell (CD3+) proliferation. We observed that, although TFF EVs were most efficient in inhibiting T cell proliferation at a concentration of 15k EVs per cell, the combination of TSEC EV (at the same EV concentration) and TSEC prot. (at the same protein concentration) got closer to recapitulate "TF EVs' effect. TFF EVs were significantly more potent than TSEC Prot, but not from TSEC add-back, at 15k:1 concentration. n=3.

## HPL EV uptake by Peripheral-blood mononuclear cells (PBMCs)

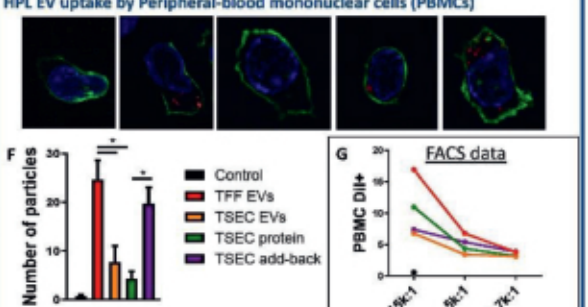


**Figure 4.** We stained EV/protein samples with the lipophilic dye DiI and incubated them with unlabeled PBMCs for 24h, 37°C, 5% $CO_2$, 18% $O_2$. Cells were then stained with phalloidin-488 (actin cytoskeleton) and DAPI and imaged using the ONI super resolution microscope, 100× objective. (A-E) DiI control, TFF EVs, TSEC EVs, TSEC protein, TSEC add-back, respectively, at the highest EV/protein concentration (15k:1). (F) Three fields per condition were quantified using IMARIS software, showing highest uptake on TFF EVs and TSEC add-back conditions. TSEC EVs and TSEC Prot. were not as effectively uptaken by PBMCs. (G) Flow cytometry data on 6x; however, shows highest uptake of TFF EVs, followed by TSEC protein fractions, with less uptake by "TSEC EVs and add-back. Scale bar: 5 µm, n=3

## SUMMARY/OUTLOOK

- TFF+SEC is a scalable approach that allows us to effectively concentrate/purify/separate HPL-EVs and proteins, making it feasible to evaluate the effects of different HPL components, isolated or combined;
- HPL-TFF-EV samples but not soluble factors were highly efficient in promoting skin organoid assembly and inhibiting PHA-induced T-cell proliferation; SEC farther separated EVs from functional corona proteins;
- We plan to further evaluate the mode of action and molecular mechanism of HPL-EV and their associated corona proteins.

## ACKNOWLEDGEMENTS

This work was funded by the European Union's Horizon 2020, Cancer Cluster Salzburg—Smart Specialization Center (CCS), Transfer Center for Extracellular Vesicles Therapies Technologies (EVTT), European Union H2020 project "ECHOBOLAT; PACE.

EVTT

## Human Platelet Lysate for Skin Regeneration & Immune Modulation

Fausto Gueths Gomes[1], André Cronemberger Andrade[2], Martin Wolf[2], Sarah Hochmann[2], Linda Krisch[1], Christof Regl[3], Patricia Ebner-Peking[2], Christian Huber[3], Nicole Meisner-Kober[3], Katharina Schallmoser[1], Dirk Strunk[2]

[1]Department of Transfusion Medicine, Paracelsus Medical University, Salzburg, Austria; [2]Experimental and Clinical Cell Therapy Institute (ExCT), Spinal Cord Injury and Tissue Regeneration Center, Paracelsus Medical University, Salzburg, Austria; [3]Department for Biosciences, Paris Lodron University Salzburg, Austria; Contact: fausto.gueths@pmu.ac.at

### Objective
Platelet derivatives, particularly platelet-rich plasma, have been extensively evaluated regarding their possible application for regeneration purposes. Human-platelet lysate (HPL) promotes cell growth more effectively than fetal bovine serum but has not yet been thoroughly evaluated towards a possible therapeutic role. On a parallel note, platelet extracellular vesicles (PEVs) have been shown to promote re-epithelization of chronic wounds, angiogenesis, among others. However, the functional characteristics of PEVs can differ depending on how the platelets were prepared for EV production (e.g. resting/activated state) and little is known about HPL-EVs. Our main goal in the present study is, therefore, to evaluate the effects of HPL in skin regeneration and immunomodulation using a novel type of skin organoid (Ebner-Peking et al., BioRxiv 2020) and our standardized immune modulation assay (Ketterl et al., Stem Cell Res Ther 2015), with particular interest in the role of HPL-derived EVs in combination or not with HPL protein-rich preparations.

### Methods
HPL supernatant was concentrated by tangential-flow filtration (TFF; 500 kD) and further purified by size-exclusion chromatography (TSEC). Particle concentration was measured by tunable resistive pulse sensing (TRPS) and protein content by detergent compatible (DC) protein assay. Western blot and label-free proteomics were done to further characterize samples. Skin-organoid/fibrosphere formation was quantified using NIS software and stained by hematoxylin & eosin and immunostained for keratin 14 (K14), vimentin (VIM) and DAPI. Immunomodulation assay was also performed in combination with DiI-labelled EV uptake analysis on peripheral mononucleated cells.

### Results
Western blot showed the presence of the EV marker tetraspanin CD9 on both TFF-EVs and TSEC-EVs and depletion of serum components in TSEC-EVs. Also, proteomic analysis demonstrated the presence of platelet markers (α-IIb/β-III integrin) upregulated in TSEC EVs. Functionally, TFF-EVs induced skin-organoid and fibrosphere formation more efficiently than other samples, followed by TSEC protein fractions. Immunostaining showed clear outside layer of K14-positive keratinocytes, with an inner VIM-positive dermal core. TFF-EVs were also most efficient in inhibiting phycoerythrin-induced T cell proliferation, while add-back of TSEC protein (same protein concentration of TFF) to purified TSEC-EV (same particle concentration of TFF) was able to more closely recapitulate TFF-EVs' effect. TFF-EVs showed highest uptake by microscopy and flow cytometry quantification. Curiously, the second most-uptaken sample on microscopy was TSEC add-back, while on flow cytometry, TSEC protein fraction was second to TFF EVs.

### Conclusions
TFF+SEC is a scalable approach that allows us to effectively concentrate/purify/separate HPL-EVs and proteins, making it feasible to evaluate the effects of different HPL components, isolated or combined. HPL-TFF-EV samples but not soluble factors were highly efficient in promoting skin organoid assembly and inhibiting PHA-induced T-cell proliferation; SEC further separated EVs from functional corona proteins. We plan to further evaluate the mode of action and molecular mechanism of HPL-EV and their associated corona proteins.

PARACELSUS
MEDIZINISCHE PRIVATUNIVERSITÄT

Klinikum Nürnberg
wir sind für Sie da!

# Mid-term survival of geriatric patients with septic arthritis of the knee and the influence of risk factors on survival

N. Haag[1], PD Dr. med. M. Geßlein [1,2], Dr. med. univ. J. Rüther[2], Dr. med. univ. M. Willauschus[2], Univ.-Prof. Dr. med. H. J. Bail[1,2]

[1]Paracelsus Medical University, Nuremberg, Germany; [2]Department of Traumatology and Orthopedics, Klinikum Nuremberg, Germany;

## Abstract

Septic arthritis is common in older patients and directly related to joint surgery or hematogenous distribution from an unknown origin. Frequent causes are gram-positive bacteria. This study aimed to evaluate the effect of risk factors like implants, synovial sample cultures, and ASA PS Classification on survival.

Included were 133 older patients, >60 years, with septic monoarthritis. The existence of implants, synovial sample cultures, and ASA PS Classification was drawn retrospectively from medical records. Survival data were obtained from medical records and public obituaries. We used Kaplan-Meyer-Survival-Curves to estimate the probability of survival the Log rank-test to compare survival rates after five years.

Mean in age was 74.9 years (SD ± 9.2), follow up–rate was 74.4%, mean follow-up was 1481.3 days (SD ± 1393.8).

Mean survival in patients with implants (51.9%) was 2112.5 days (95%-CI 1600.0 – 2625.0); in patients without implants, 3256.0 days (95%-CI 2684.3 – 3827.7). A significant difference in survival was found between the groups (p = 0.015). Mean survival in patients with a positive synovial sample culture was 2541.2 days (95%-CI 2051.4–3031.1), without a positive synovial sample culture, 2759.5 days (95%-CI 2170.3 – 3348.6). No significant difference was detected between the groups (p = 0.08). Mean survival in patients with ASA II was 4324.1 days (95%-CI 3633.4 – 5014.7), with ASA III was 2438.4 days (95%-CI 1959.5 – 2917.4), with ASA IV was 1533.8 days (95%-CI 797.0 – 2270.5). A significant difference in survival was found between the three groups (p<0.001).

Older adults diagnosed with septic monoarthritis showed a significant reduction in survival when medical implants were present or higher ASA PS Classification. Synovial sample cultures revealed no significant impact on survival.

## Introduction

Septic arthritis, an infection of the joint, is frequently caused by gram-positive strains deriving from human skin like Staphylococcus aureus and involves mostly large joints such as the knee, hip, and shoulder[1]. Causes appear to be direct inoculation of bacteria after joint surgery or hematogenous infection with delayed onset. A peek in prevalence is found in children, and the elderly. Major risk factors for septic arthritis are older age, medical implants, microbiological colonization, joint disease, and joint surgery. This study evaluates the impact of risk factors on survival of older adults with septic monoarthritis.

Implants provide surfaces for biofilm formation and could therefore be a potential source of infection.

The characteristics of some bacteria can compromise the immune system of patients more than others and cause poorer outcomes.

ASA Physical Status Classification is a widely used and proven classification system for patients going into surgery. In this study it provides a guide for the validity of the data.

## Objectives

- The overall survival of older adults with acute septic monoarthritis of the knee undergoing arthroscopic surgery and evaluate possible risk factors to reduce survival.
- The impact from medical implants on survival
- The impact of a positive synovial sample culture on survival
- The impact of high ASA PS Classification at the time of surgery on survival

## Methods

- Retrospective study using medical records at Klinikum Nuremberg
- Included data:
  age, gender, affected joint, existence and site of medical implants, date of admission, follow-up in days, date of death, ASA PS Classification at the time of surgery, microbiological analysis of the joint aspirate, number of joint surgeries
- Survival data were obtained from medical records and public obituaries
- Kaplan-Meyer-Survival-Curves were used to estimate the probability of survival
- The Log-Rank test was used to compare survival rates after five years
- The p-value was considered significant with values p ≤ 0.05

## Results

| | Total number | Mean survival [days ± SD ] | 5-year survival | P-value |
|---|---|---|---|---|
| Study population | 133 (100%) | 2742.4 ± 209.9 | 47% | - |
| Implants | 69 (51.9%) | 2112.5 ± 261.5 | 39% | 0.015 |
| No Implants | 64 (48.1%) | 3255.9 ± 291.7 | 58% | |
| PSSC | 91 (68.4%) | 2541.2 ± 250.0 | 44% | 0.08 |
| No PSSC | 42 (31.6%) | 2759.5 ± 300.6 | 59% | |
| ASA II | 25 (18.8%) | 4324.1 ± 352.4 | 83% | <0.001 |
| ASA III | 76 (57.1%) | 2438.4 ± 244.4 | 45% | |
| ASA IV | 32 (24.1%) | 1533.8 ± 375.9 | 25% | |

SD = Standard deviation; PSSC = Positive synovial sample culture; ASA = American Society of Anaesthesiology Physical Status Classification

Patient age ranged from 60 years to 96 years (mean 74.9 years, SD ± 9.2), with 48 (36.1%) being female and 85 (63.9%) male. Complete follow-up data could be obtained from all patients (five-year follow-up rate of 74.4%). The mean follow-up for all patients was 1481.3 days (SD ± 1393.8; range 0 – 5095 days).

**Figure 1-3: Cumulative 5-year survival probability of (1) patients with preexisting medical implants and patients without preexisting medical implants (p = 0.015), (2) patients with a positive culture result and patients without a positive synovial sample culture result (p = 0.08), (3) patients categorized in ASA PS Classification II-IV (p < 0.001).**

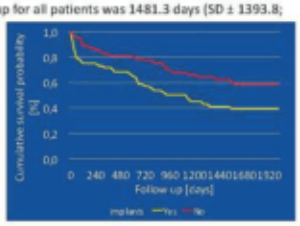


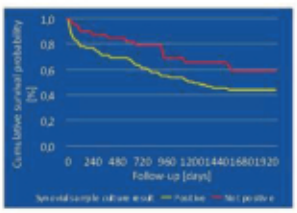


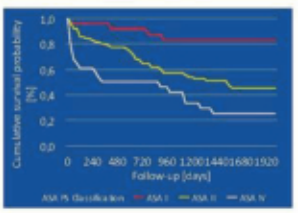


## Conclusions & Perspectives

Older adults diagnosed with septic monoarthritis showed a significant reduction in survival when medical implants or higher ASA PS Classification were present. Synovial sample cultures revealed no significant impact on survival.

Special care and immediate surgical treatment for those patients should be considered to improve outcomes and eventually decrease lethality.

## References and Acknowledgements

1. Mathews CJ, Weston VC, Jones A, Field M, Coakley G. Bacterial septic arthritis in adults. *Lancet*. 2010;375(9717):846-855.
2. Newman JH. Review of septic arthritis throughout the antibiotic era. *Annals of the Rheumatic Diseases*. 1976;35(3):198-205.
3. Otto M. Staphylococcal Biofilms. *Microbiol Spectr*. 2018;6(4):10.1128/microbiolspec.GPP1123-0023-2018.

I would like to express my deepest gratitude to Dr. med Markus Geßlein, Dr. med. univ. Johannes Rüther, and Dr. med. univ. Maximilian Willauschus for their guidance and profound belief in my work and abilities. And I would also like to thank my parents and Fritz for always cheering me on and having my back.

## Mid-term survival of geriatric patients with septic arthritis of the knee and the influence of risk factors on survival

Nina Pauline Haag[1], Markus Geßlein[1,2], Johannes Rüther[2], Maximilian Willauschus[2], Hermann Josef Bail[1,2]

[1]Paracelsus Medical University, Nuremberg, Germany; [2]Department of Traumatology and Orthopedics, Klinikum Nuremberg, Germany; Contact: nina.haag@stud.pmu.ac.at

### Objective
Septic arthritis is common in older adults and directly related to joint surgery or hematogenous distribution from an unknown origin. Frequent causes are gram-positive bacteria. This study aimed to evaluate the effect of risk factors like implants, positive synovial sample cultures results, and ASA PS Classification on survival.

### Methods
133 older adults, >60 years, with septic monoarthritis were included. The existence of implants, synovial sample cultures, and ASA PS Classification were drawn retrospectively from medical records. Survival data were obtained from medical records and public obituaries. We used Kaplan-Meyer-Survival-Curves to estimate the probability of survival, the Log rank-test to compare survival rates after five years.

### Results
Mean in age was 74.9 years (SD ± 9.2), 5-year follow-up–rate was 74.4%, mean follow-up was 1481.3 days (SD ± 1393.8). Mean survival in patients with implants (51.9%) was 2112.5 days (95%-CI 1600.0 – 2625.0); in patients without implants, 3256.0 days (95%-CI 2684.3 – 3827.7). A significant difference in survival was found between the groups ($p = 0.015$). Mean survival in patients with a positive synovial sample culture was 2541.2 days (95%-CI 2051.4–3031.1), without a positive synovial sample culture, 2759.5 days (95%-CI 2170.3 – 3348.6). No significant difference was detected between the groups ($p = 0.08$). Mean survival in patients with ASA II was 4324.1 days (95%-CI 3633.4 – 5014.7), with ASA III was 2438.4 days (95%-CI 1959.5 – 2917.4), with ASA IV was 1533.8 days (95%-CI 797.0 – 2270.5). A significant difference in survival was found between the three groups ($p<0.001$).

### Conclusions
Older adults diagnosed with septic monoarthritis showed a significant reduction in survival when medical implants or higher ASA PS Classification were present. Synovial sample cultures revealed no significant impact on survival.

UNIKLINIKUMSALZBURG

# Quantitative echocardiographic analysis of the right atrial size reflects the severity of histopathological confirmed fibrosis in patients undergoing cardiac surgery

Haslinger M[1], Paar V[1], Gharibeh S[1], Krombholz-Reindl P[2], Neuner M[3], Jirak P[1], Lichtenauer M[1], Granitz C[1], Föttinger F[1], Seitelberger R[2], Kirnbauer M[3], Hoppe UC[1], Dinges C[2], Motloch LJ[1].

[1]Department of Internal Medicine II, Paracelsus Medical University, Salzburg, Austria
[2]Department of Cardiac Surgery, Paracelsus Medical University, Salzburg, Austria
[3]Department of Anesthesiology, Perioperative Medicine and Intensive Care Medicine, Paracelsus Medical University, Salzburg, Austria

**Introduction:** Fibrotic remodeling is one of the main reasons for atrial dysfunction. Therefore, clinical assessment of this pathophysiological process might be a useful tool. Nevertheless, quantification of atrial fibrosis might be challenging in the daily clinical practice. Transthoracic echocardiography is a well evaluated tool for the assessment of cardiac function including the right atrium. However, if echocardiographic alterations might reflect histological and/or molecular remodeling processes, was not investigated yet.

**Methods:** To evaluate this issue, in a prospective pilot study we evaluated echocardiograms of 18 patients (male 66.6%; age 69.3±9.8 years) undergoing cardiac surgery with no previous history of atrial fibrillation. To investigate a potential association with histopathological findings, right atrial specimen were obtained during cardiac surgery in available patients. Furthermore, to evaluate potential associations with TNF-alpha dependent fibrotic pathways, SMAD-3 expression was assessed by western blot. Results were correlated with functional parameters assessed during echocardiography.

**Results:** Fibrotic area quantified by histological analyses was not correlated with right ventricular enddiastolic diameter or TAPSE. However, we found a positive correlation with quantitative indicators of right atrial size including right atrial area (mean=18.2±3.1cm², r=0.78, p=0.02) and right atrial volume (mean=52.7±15.0ml, r=0.77, p=0.03), while the strongest correlation was observed with right atrial volume index (mean=27.9±9.3ml/m², r=0.81, p=0.02). There was no correlation with the expression of SMAD-3 indicating no associations with TNF-Alpha dependent pathways.

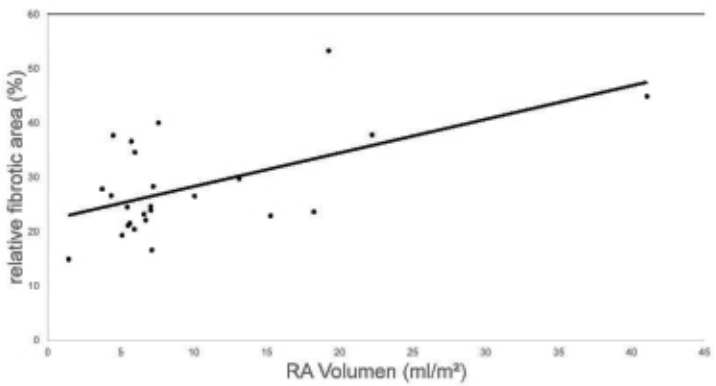


**Conclusion:** Quantitative echocardiographic parameters of the right atrial size are strong predictors of the histological stage of right atrial fibrosis. Further investigations need to evaluate potential associations between alterations of atrial parameters observed during echocardiography and responsible fibrognetic pathways

Contact: Department of Internal Medicine II, Paracelsus Medical University, Salzburg, Austria
Dr. M. Haslinger, mi.haslinger@salk.at

UNIKLINIKUM SALZBURG - Paracelsus Medizinische Universität | Gemeinnützige Salzburger Landeskliniken Betriebsges.m.b.H.

## Quantitative echocardiographic analysis of the right atrial size reflects the severity of histopathological confirmed fibrosis in patients undergoing cardiac surgery

Michael Haslinger[1], Vera Paar[1], Sarah Gharibeh[1], Philipp Krombholz-Reindl[2], Matthias Neuner[3], Peter Jirak[1], Michael Lichtenauer[1], Christina Granitz[1], Fabian Föttinger[1], Rainald Seitelberger[2], Michael Kirnbauer[3], Uta C Hoppe[1], Christian Dinges[2], Lukas J Motloch[1]

[1]Department of Internal Medicine II, Paracelsus Medical University, Salzburg, Austria; [2]Department of Cardiac Surgery, Paracelsus Medical University, Salzburg, Austria; [3]Department of Anesthesiology, Perioperative Medicine and Intensive Care Medicine, Paracelsus Medical University, Salzburg, Austria; Contact: mi.haslinger@salk.at

### Objective
Fibrotic remodeling is one of the main reasons for atrial dysfunction. Therefore, clinical assessment of this pathophysiological process might be a useful tool. Nevertheless, quantification of atrial fibrosis might be challenging in the daily clinical practice. Transthoracic echocardiography is a well evaluated tool for the assessment of cardiac function including the right atrium. However, if echocardiographic alterations might reflect histological and/or molecular remodeling processes, was not investigated yet.

### Methods
To evaluate this issue, in a prospective pilot study we evaluated echocardiograms of 18 patients (male 66.6%; age 69.3±9.8 years) undergoing cardiac surgery with no previous history of atrial fibrillation. To investigate a potential association with histopathological findings, right atrial specimen were obtained during cardiac surgery in available patients. Furthermore, to evaluate potential associations with TNF-alpha dependent fibrotic pathways, SMAD-3 expression was assessed by western blot. Results were correlated with functional parameters assessed during echocardiography.

### Results
Fibrotic area quantified by histological analyses was not correlated with right ventricular enddiastolic diameter or TAPSE. However, we found a positive correlation with quantitative indicators of right atrial size including right atrial area (mean=18.2±3.1cm2, r=0.78, p=0.02) and right atrial volume (mean=52.7±15.0ml, r=0.77, p=0.03), while the strongest correlation was observed with right atrial volume index (mean=27.9±9.3ml/m2, r=0.81, p=0.02). There was no correlation with the expression of SMAD-3 indicating no associations with TNF-Alpha dependent pathways.

### Conclusions
Quantitative echocardiographic parameters of the right atrial size are strong predictors of the histological stage of right atrial fibrosis. Further investigations need to evaluate potential associations between alterations of atrial parameters observed during echocardiography and responsible fibrognetic pathways

PARACELSUS
MEDIZINISCHE PRIVATUNIVERSITÄT

# Hypotonicity Sensitizes Biliary Tract Cancer Cells to Cisplatin Cytotoxicity

Katharina Helm[1], Julia Preishuber[1], Christian Mayr[1], Dino Bekric[1], Michael Kittl[1], Daniela Schuster[4], Philipp Schuster[4], Markus Ritter[1,2,3] and Martin Jakab[1]

[1]Paracelsus Medical University, Center for Physiology, Pathophysiology and Biophysics, Institute for Physiology and Pathophysiology – Salzburg, Strubergasse 22, 5020 Salzburg, Austria; [2]Ludwig Boltzmann Institute for Arthritis and Rehabilitation, Strubergasse 22, 5020 Salzburg, Austria | [3]Gastein Research Institute, Paracelsus Medical University, Strubergasse 22, 5020 Salzburg, Austria; [4]Institute of Pharmacy, Pharmaceutical and Medicinal Chemistry, Strubergasse 15, 5020 Salzburg, Austria

**Author for correspondence: Martin Jakab**, Email: martin.jakab@pmu.ac.at

## Background and Aims

Biliary tract cancer (BTC) is a group of malignancies of epithelial bile duct cells with dismal prognosis due to a lack of effective therapies. A major reason for poor treatment outcome is the development of chemoresistance towards common therapies like cisplatin. The cytotoxicity of cisplatin results from its accumulation and activation in the cytoplasm of the target cell, followed by DNA-interaction and induction of apoptosis. Tumor cells counteract these effects e.g., by diminished cisplatin uptake and activation, enhanced extrusion, or resistance to apoptosis. Cl⁻ loss via volume-regulated anion ($Cl^-$) channels (VRAC) under normotonic conditions termed apoptotic volume decrease (AVD) is an early event of apoptosis and prerequisite for successive steps. A specific VRAC subunit composition of leucine-rich repeat containing 8 family members LRRC8A+D has can serve as a cisplatin uptake pathway. This study investigates the role of VRAC in BTC cisplatin sensitivity.

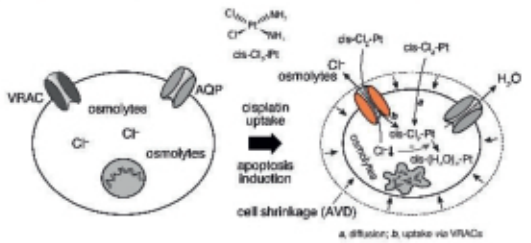


**Figure 1:** Possible cisplatin uptake-pathway: AQP, aquaporin; cis-$Cl_2$-Pt, cis-dichloro-diammine-platinum (cisplatin); cis-$(H_2O)_2$-Pt, hydrated (activated) cisplatin; VRAC, volume-regulated anion channel; +, possible facilitation of cisplatin activation

## Methods

Expression of LRRC8 subunits on the mRNA and protein level was tested by RT-qPCR and Western blot, respectively. VRAC currents were measured using whole-cell patch clamp. Cell viability (cytotoxicity) was assessed using Resazurin assays.

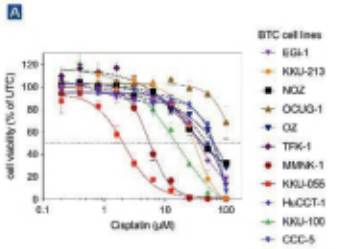


**Figure 2A:** Results of cell viability measurements using Resazurin with a panel of BTC cell lines and cisplatin concentrations from 0.2–100 µM after 72 h of treatment. $LD_{50}$ values for cisplatin ranged from 2.0 µM in KKU-055 cells to 150 µM in OCUG-1 cells. (UTC, untreated controls)

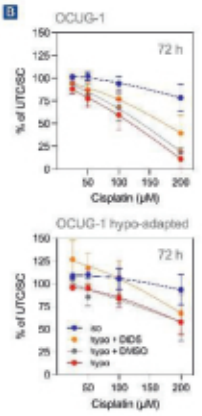


**Figure 2B:** Results of viability measurements in OCUG-1 cells. The sensitivity to 25, 50, 100 and 200 µM cisplatin over 72 h was increased, when cells were concomitantly exposed to a hypotonic medium (~60 mOsm/kg) compared to cells under isotonic conditions. This effect was partly reversed by the VRAC inhibitor DIDS (upper panel). In OCUG-1 cells chronically cultured in hypotonic medium (OCUG-1 hypo-adapted) the cisplatin sensitivity over 72 h was less stimulated by hypotonicity as compared to cells cultured under normal isotonic conditions (lower panel). (UTC, untreated controls; SC, solvent controls)

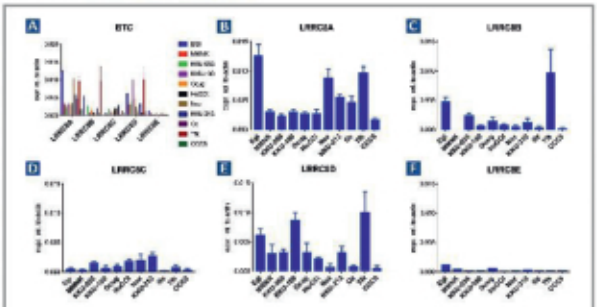


**Figure 3:** Results of RT-qPCR analysis obtained from BTC cell lines showing the expression levels of LRRC8 subunits (LRRC8A–E). All LRRC8 subunits are expressed on the mRNA level with cell type-specific differences. On average, subunits A and D are most abundantly expressed. In **(A)** all cell lines and expression levels relative to actin for all subunits are shown. **(B)–(F)** show the same expression data in separate diagrams for each LRRC8 subunit.

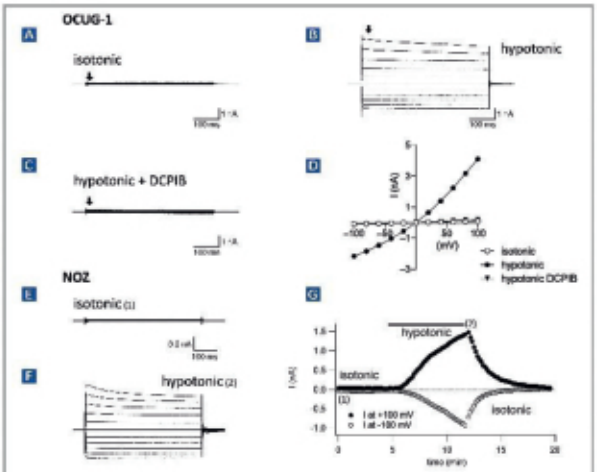


**Figure 4:** Patch clamp recordings of whole-cell VRAC $Cl^-$ currents in an OCUG-1 cell **(A)–(D)** and a NOZ cell **(E)–(G)** under isotonic conditions **(A)** and **(E)**, after stimulation with hypotonic solution **(B)** and **(F)** and subsequent blocking with the VRAC inhibitor DCPIB **(C)** and **(D)**. Currents were elicited by 500-ms voltage steps from –100 to +100 mV at 20-mV increments. The holding potential between steps was 0 mV. **(D)** Current-voltage relations obtained from the tracings shown in (A)–(C) at the points indicated by arrows. **(G)** Time-course of reversible VRAC activation under hypotonic and deactivation under isotonic conditions. (1) and (2) indicate the time points when currents shown in (E) and (F) were recorded. VRAC currents showed typical features such as outward rectification, current inactivation at constant membrane potentials > +60 mV and inhibition by the $Cl^-$ channel blocker DCPIB.

## Conclusions

Our data suggest that VSOR channels play a role in cisplatin uptake by BTC cells and that opening of VSOR channels under hypotonic conditions fosters cisplatin cytotoxicity. On the contrary, loss of VRAC function might favor chemoresistance.

## References

> Jentsch TJ: VRACs and other ion channels and transporters in the regulation of cell volume and beyond. Nat Rev Mol Cell Biol 2016;17(5):293-307. doi: 10.1038/nrm.2016.29
> Hoffmann EK, et al. Role of volume-regulated and calcium-activated anion channels in cell volume homeostasis, cancer and drug resistance. Channels (Austin) 2015;9:380-396. doi: 10.1080/19336950.2015.1089807
> Lee EL, et al. Impaired Activity of Volume-Sensitive Cl Channel Is Involved in Cisplatin Resistance of Cancer Cells. J Cell Physiol 2007;211:513-521. doi: 10.1002/jcp.20961
> Marin JJG, et al. Chemoresistance and chemosensitization in cholangiocarcinoma. Biochim Biophys Acta 2017;(10.1016/j.bbadis.2017.06.005. doi: 10.1016/j.bbadis.2017.06.005
> Ranki S, et al. Epidemiology of biliary tract cancers: an update. Ann Oncol 2009;20:146-159. doi: 10.1093/annonc/mdn588
> Voss FK, et al. Identification of LRRC8 heteromers as an essential component of the volume-regulated anion channel VRAC. Science 2014;344:634-638. doi: 10.1126/science.1252826
> Planells-Cases R, et al. Subunit composition of VRAC channels determines substrate specificity and cellular resistance to Pt-based anti-cancer drugs. EMBO J 2015;34(24), 2993-3008. doi: 10.15252/embj.201593488

## Hypotonicity Sensitizes Biliary Tract Cancer Cells to Cisplatin Cytotoxicity

Katharina Helm[1], Julia Preishuber[1], Christian Mayr[1], Dino Bekric[1], Michael Kittl[1], Daniela Schuster[4], Philipp Schuster[4], Markus Ritter[1,2,3], Martin Jakab[1]

[1]Paracelsus Medical University, Center for Physiology, Pathophysiology and Biophysics, Institute for Physiology and Pathophysiology – Salzburg; [2]Ludwig Boltzmann Institute for Arthritis and Rehabilitation; [3]Gastein Research Institute, Paracelsus Medical University; [4]Institute of Pharmacy, Pharmaceutical and Medicinal Chemistry, Paracelsus Medical University; Contact: martin.jakab@pmu.ac.at

### Objective
Biliary tract cancer (BTC) is a group of malignancies of epithelial bile duct cells with dismal prognosis due to a lack of effective therapies. A major reason for poor treatment outcome is the development of chemoresistance towards common therapies like cisplatin. The cytotoxicity of cisplatin results from its accumulation and activation in the cytoplasm of the target cell, followed by DNA-interaction and induction of apoptosis. Tumor cells counteract these effects e.g., by diminished cisplatin uptake and activation, enhanced extrusion, or resistance to apoptosis. $Cl^-$ loss via volume-regulated anion ($Cl^-$) channels (VRAC) under normotonic conditions termed apoptotic volume decrease (AVD) is an early event of apoptosis and prerequisite for successive steps. A specific VRAC subunit composition of leucine-rich repeat containing 8 family members LRRC8A+D has can serve as a cisplatin uptake pathway (1). This study investigates the role of VRAC in BTC cisplatin sensitivity.

### Methods
Expression of LRRC8 subunits on the mRNA and protein level was tested by RT-qPCR and Western blot, respectively. VRAC currents were measured using whole-cell patch clamp. Cell viability (cytotoxicity) was assessed using Resazurin assays.

### Results
Using a comprehensive panel of 11 BTC cell lines, we determined the dose- and time-dependent cytotoxic effect of cisplatin. $LD_{50}$ values for cisplatin ranged from 2.0 $\mu$M in KKU-055 cells to 150 $\mu$M in OCUG-1 cells. All LRRC8 isoforms A–E were expressed in BTC cells on the mRNA level with highest expression levels on average of isoforms A and D. LRRC8A and D expression was confirmed on the protein level. VRAC $Cl^-$ currents were measured in OCUG-1 and NOZ cells and showed typical features such as outward rectification, current inactivation at constant membrane potentials > +60 mV and inhibition by the $Cl^-$ channel blocker DCPIB. In OCUG-1 cells with the highest cisplatin-resistance, the sensitivity to 25, 50, 100 and 200 $\mu$M cisplatin over 72 h was increased, when cells were concomitantly exposed to a hypotonic medium (–60 mOsm/kg) compared to cells under isotonic conditions. This effect was partly reversed by the VRAC inhibitor DIDS. In OCUG-1 cells chronically cultured in hypotonic medium (hypo-adapted cells) the cisplatin sensitivity over 72 h was less enhanced by hypotonicity as compared to cells cultured under normal isotonic conditions. Next steps will be testing for differential expression of LRRC8 subunits, measurement of VRAC currents and intracellular cisplatin accumulation in iso- versus hypo-adapted cells.

### Conclusions
Our data suggest that VRAC $Cl^-$ channels play a role in cisplatin uptake by BTC cells and that opening of VRACs under hypotonic conditions fosters cisplatin cytotoxicity. On the contrary, loss of VRAC function might favor chemoresistance.

### Acknowledgements
This project is supported by the PMU-FFF grant E-17/26/137-JAK to M.J.

### References
1. Planells-Cases R, et al. Subunit composition of VRAC channels determines substrate specificity and cellular resistance to Pt-based anti-cancer drugs. EMBO J 2015;34(24), 2993-3008. doi: 10.15252/embj.201592409

# THE ENHANCER LANDSCAPE PREDETERMINES SKELETAL REGENERATION CAPACITY OF BONE MARROW STROMAL CELLS

Hochmann S.[1], Ou K.[2], Poupardin R.[1], Mittermeir M.[1], Riminucci M.[3], Textor M.[4], Ellinghaus A.[4], Salaheddine A.[5], Elminger J.[4], Polánsky-Biskup J.[2], Duda G.[4], Schmidt-Bleek K.[4], Geissler S.[4], Strunk D.[1]

[1]Experimental and Clinical Cell Therapy Institute (SCI), Spinal Cord Injury and Tissue Regeneration Center, Paracelsus Medical University, Salzburg, Austria
[2]BIH, Charité Universitätsmedizin Berlin, Germany; [3]Department of Molecular Medicine, Sapienza University of Rome, Italy
[4]Julius Wolff Institute & Berlin-Brandenburg Center for Regenerative Therapies, Charité - Universitätsmedizin Berlin, Germany
[5]RD Development & Disease, Max Planck Institute for Molecular Genetics & Institute for Medical and Human Genetics, Berlin, Germany
sarah.hochmann@pmu.ac.at

Novel therapies for non-healing fractures, representing up to 10% of all fractures or millions of patients worldwide annually, are urgently needed (Qazi et al., 2015). BM stromal cells have been demonstrated to completely re-establish bone and marrow cavity in several patients after long bone fracture (Marcacci et al., 2007; Quarto et al., 2001). Introduction of a tempting mesengenic differentiation concept, based on hypothetic mesenchymal stromal/stem cell multipotency, resulted in a multiplication of experimental and clinical studies testing the safety and efficacy of bone regeneration by mainly extra-skeletal stromal cells from various tissues, including WAT and UC as easily accessible sources, with so far limited success (Salhotra et al., 2020).

Bone regeneration may occur via endochondral ossification of a hyaline cartilage template or direct intramembranous ossification within the fracture region depending on the anatomic site of defect. This complexity is enhanced further due to different embryonic origin of the skeletal components during development. The appendicular skeleton including limbs, pectoral and pelvic girdle is formed from lateral plate mesoderm, the skull, vertebrae, sternum and ribs from paraxial mesoderm, and face bones from neural crest. Specialized chondrocytes cover the articular surfaces in all joints (Wagley, 2016).

More than a million patients treated with mostly un-manipulated hematopoietic stem/progenitor cells are making 'bone marrow transplantation' a role model for successful cell-based regenerative therapies (Gratwohl et al., 2015). This medical success story has been extended recently by establishing *ex vivo* gene therapy strategies for inherited blood diseases and chimeric antigen receptor T cell-based immunotherapies (Rafiq et al., 2020; Wolintzan et al., 2020). Progress of successful cell-based replacement strategies towards non-hematopoietic tissue has been limited so far, mainly restricted to skin epidermis, cornea and autologous cartilage implantation (Hirsch et al., 2017; Makris et al., 2015; Pellegrini et al., 2018; Sochacki et al., 2020; Soh et al., 2020).

## Graphical Abstract

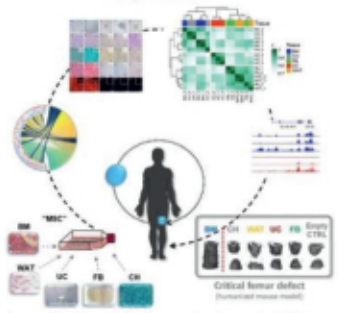


**Graphical Abstract: No identical stromal cells.** Direct comparison of MSC combined with stringent molecular, functional and morphological analysis substantiate the selection of chondro-/osteo-competent stromal progenitors for actual skeletal regeneration. Clinically relevant cell sources of MSC were compared for their skeletal gene expression signature *in vitro* and for their chondrogenic competence in a 3 D cartilage organoid assay. Further, complete regeneration of critical size femur defects in NSG mice was only observed with pretibial human BM-derived scaffold-free cartilage organoid transplants after four weeks *in vivo*, despite maintained presence of human cells in all transplants.

## Histological Examination

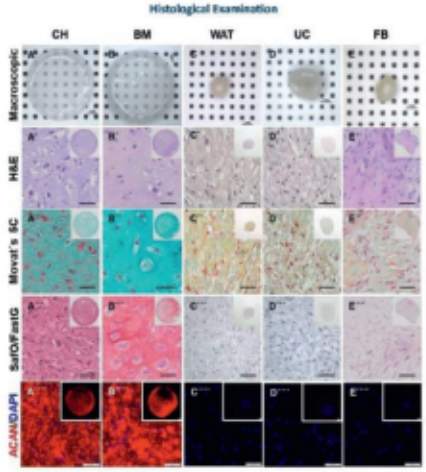


**Figure 2: Cartilage disk organoid formation by 3D chondrogenesis.** (A-E) Macroscopic picture of cartilage disks and contracted microspheres. (A'-E') Hematoxylin eosin (H&E) staining. (A''-E'') Movat's pentachrome (Movat's 5C) staining showing proteoglycan in blue as stained by the Alcian blue component. (A'''-E''') The Safranin O / Fast Green (SafOFastG) matrix staining allowed to determine the Bom score value of the tissue engineered cartilage samples. (A''''-E'''') Aggrecan (ACAN) and DAPI stainings. (A-E) Scale bar 1 mm. (A'''''-E''''') Scale bar 50 µm.

## Histological Examination of Bone Transplants

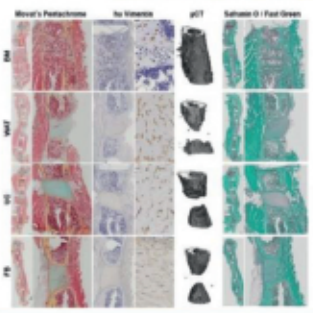


**Figure 6: Stromal cell derived disks transplanted in critical size femur fracture after 28 days of regeneration.** Movat's pentachrome stainings illustrate regeneration of critical size femur fraction only in transplanted animals receiving a transplant originating from fetal-derived cells. Hu Vimentin stainings confirm the human origin of transplants. pOT data show fully regenerated bone structures only in skeletal derived cartilage transplant. Safranin O / Fast Green staining reveals that the tissue engineered cartilage template was fully remodeled to bone structures after 28 days of regeneration due to the lack of the red colored Safranin staining.

## Global Footprint of Stromal Identities

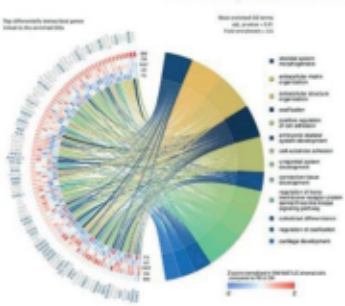

**Figure 1: Global footprint of stromal identities.** Chord plot of gene ontology (GO) term categories most significantly regulated in bone marrow (BM) stromal cells compared to white adipose tissue (WAT), umbilical cord (UC), fibroblast (FB) datasets, connected to the corresponding genes. Differential expression was conducted in a linear mixed model analysis on 346 datasets normalized with 3 Yugene approach. 366 up-regulated genes in BM compared to at least two other cell sources (WAT, UC or FB; adjusted p-value < 0.05) was selected for GO enrichment analysis. The most significant GO terms (adjusted p-value < 0.01, fold enrichment > 3.5, minimum GO term size ≥ 12 genes) are shown on the right in descending order from most to least significant. Corresponding significantly differentially expressed genes are shown on the left together with the Z-score-normalized expression values, derived from the Yugene normalized values, represented in the different sources (in blue-to-red tones: blue, earlier regenerative and mid, environment), in the order of BM expression Z score. A clear enrichment for bone and skeletal genes was found in BM compared to other sources. Chondrocyte (CH) data shown for comparison (chondrogenic potential phenotype).

## Shape and Weight Predicts Quality

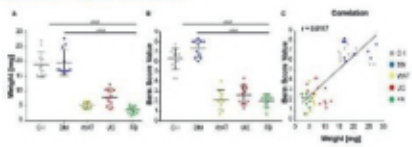


**Figure 3: Weight predicts quality of four-week engineered 3D cartilage disk organoids.** (A) Weights of cartilage disks from skeletal origin differ significantly from other stromal cell sources. (B) Bom Score Values of cartilage disks from skeletal origin differ significantly from other stromal cell sources. (C) Correlation of Bom score and weights predicts the quality of tissue engineered cartilage organoid (**** p≤0.0001, n = 6).

## Structural and Regulator Gene Expression Time Course Analysis

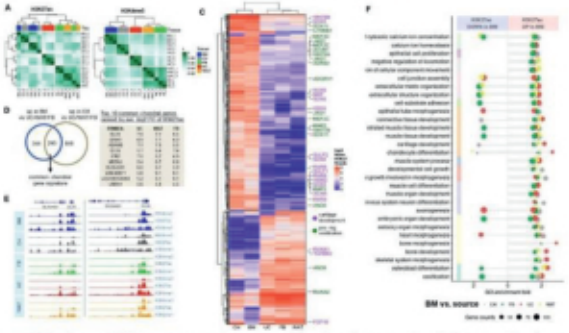


**Figure 4: Global analysis revealed differences in active regulatory regions, which predispose bone marrow stromal cells to superior bone formation.** (A,B) Pearson's correlation plot of log2 reads per kilobase million (RPKM) values of (A) H3K27ac peaks and of (B) H3K4me3 peaks demonstrate that bone marrow (BM) stromal cells and chondrocytes (CH) complex cluster regarding their origin from marrow niches. (C) Heatmap of significantly differentially enriched peaks (log2-fold change ≥ 2, false discovery rate (FDR) < 0.05) in BM vs umbilical cord, white adipose tissue stromal cells and fibroblasts (UC/WAT/FB, respectively) and in CH vs UC/FB/WAT. Genes involved in cartilage development and positive regulation of ossification are highlighted. (D) Common chondral signatures in BM and CH compared to UC/WAT/FB, respectively, and top 10 common chondral genes, ranked by mean log2-fold change of H3K27ac in BM vs UC/FB/WAT. (E) Genome browser views of Meteorc mark H3K27ac, H3K4me1, H3K4me3 enrichment on DLX5 and SOX9 loci. (F) Gene ontology enrichment analysis covering H3K27ac significantly increased ("up") or decreased ("down") in BM vs. all other tissues. Peaks "up" in BM" mapped to genes involved in vasculature, microbial, differentiation, and skeletal system morphogenesis, suggesting that these genes are more transcriptionally active or undifferentiated BM compared to other cell types.

## Selectively Accessible Enhancers for Ossification and Osteoblast Differentiation

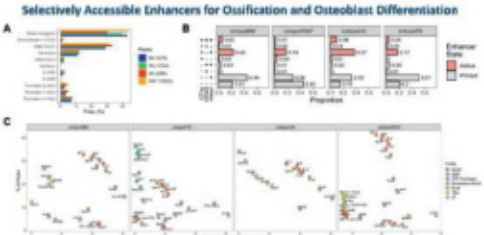


**Figure 5. Selectively accessible enhancers in undifferentiated bone marrow (BM) stromal cells are important for ossification and osteoblast differentiation.** (A) Unique tissue-specific peaks obtained by assay for transposase-accessible chromatin sequencing (ATAC-seq) and considered as enhancers, mapped primarily to intragenic and intronic regions. (B) Unique ATAC-seq peaks primarily overlapped with enhancer mark H3K4me1 (> 60% of total unique peaks in all cell types), of which ~ 30 – 40% are active (H3K27ac +). (C) Unbiased motif enrichment analysis identified tissue-specific GATA for umbilical cord (UC) stromal cells and bHLH family for fibroblasts (FB) and common bZIP family) transcription factor motifs in unique ATACseq peaks. Transcription factor families were color-coded.

These results support the notion that a natural skeletal regeneration potential appears to be restricted to skeletal stem/progenitor cells and their mature progeny. The data favor chondrocytes for cartilage and BM-MSPC for bone regeneration. Clinical trials testing non-skeletal cells (e.g. WAT, UC) for skeletal regeneration require with particular caution regarding efficacy and safety. Predictive potency assays will facilitate selecting the 'right' cells for each patient.

The authors declare no conflict of interest.

## THE ENHANCER LANDSCAPE PREDETERMINES SKELETAL REGENERATION CAPACITY OF BONE MARROW STROMAL CELLS

Sarah Hochmann[1], Kristy Ou[2], Rodolphe Poupardin[1], Michaela Mittermeir[1], Mara Riminucci[3], Martin Textor[4], Agnes Ellinghaus[4], Ali Salaheddine[5], Juri Elminger[4], Julia Polánsky-Biskup[2], Georg Duda[4], Katharina Schmidt-Bleek[4], Sven Geissler[4], Dirk Strunk[1]

[1]Experimental and Clinical Cell Therapy Institute (ExCT), Spinal Cord Injury and Tissue Regeneration Center, Paracelsus Medical University, Salzburg, Austria; [2]BIH, Charite Universitätsmedizin Berlin, Germany; [3]Department of Molecular Medicine, Sapienza University of Rome, Italy; [4]4Julius Wolff Institute & Berlin-Brandenburg Center for Regenerative Therapies, Charité - Universitätsmedizin Berlin , Germany; [5]RG Development & Disease, Max Planck Institute for Molecular Genetics & Institute for Medical and Human Genetics, Berlin, Germay; Contact: sarah.hochmann@pmu.ac.at

### Objective

Healing non-union long bone fractures by cell therapy requires prospective selection of functional transplants to benefit millions of patients worldwide. We compared clinically relevant stromal cells from adult human bone marrow (BM), white adipose tissue (WAT) and umbilical cord (UC) to mature chondrocytes (CH) and skin fibroblasts (FB) for gene expression signature, 3D cartilage organoidogenesis, epigenomic landscape and in vivo fracture healing.

### Results

Comprehensive gene expression meta-analysis revealed significant over-representation of skeletal-related genes in BM and CH, correlating with cartilage formation. Relevant osteochondral transcription factors were expressed in all stromal populations, indicating additional molecular players being decisive during endochondral bone regeneration. We found an underlying epigenetic landscape pre-determining bone regeneration. Transcription factor binding sites of common transcription factor families including Runt and bZIP were selectively accessible in enhancers and promoters of ossification-related genes in BM. Complete regeneration of critical size femur defects in a humanized mouse model was observed only with prebuild human BM-derived scaffold-free cartilage organoid transplants.

### Conclusions

These results support the notion that skeletal regeneration competence is predetermined in skeletal-derived progenitors due to a selective epigenetic landscape enabling common transcription factors to act on genes involved in ossification.

# In-Hospital thrombocytopenia following TAVI – Predictors and Outcomes

Stine Horna [1,2], Ferdinand Vogt [3,4], Miroslaw Ledwon[1], Dennis Eckner[3], Jürgen Jessl [3], Theodor Fischlein[1], Francesco Pollari [1]

1) Cardiac Surgery, Klinikum Nürnberg - Paracelsus Medical University, Nuremberg, Germany;
2) Faculty of Medicine, Paracelsus Medical University, Nuremberg, Germany;
3) Cardiology, Paracelsus Medical University, Klinikum Nürnberg, Nuremberg, Germany;
4) Cardiac Surgery, Artemed Klinikum München Süd, Munich, Germany

**OBJECTIVE**

Transcatheter aortic valve implantation (TAVI) is an attractive treatment for patients with aortic valve stenosis. Nevertheless, postoperative thrombocytopenia is regularly observed. The reasons and impact for this phenomenon are unknown at so far.

We aimed to assess incidence, risk factors and outcomes of thrombocytopenia following TAVI.

**METHODS**

- Retrospective analysis of all consecutive patients threathed between 2009 and 2018
- Patients with prior thrombocytopenia were excluded
- Platelet count was corrected for hematocrit (CPC) to exclude possible bias by hemodilution
- Endpoints were in-hospital thrombocytopenia:
  - mild thrombocytopenia ("MT") defined as a CPC<100000/µl
  - severe thrombocytopenia ("ST") defined as a CPC<50000/µl
- Outcomes were compared with no-thrombocytopenia group (NoT)
- Multivariate logistic regression was used to determine the baseline variables associated with the outcomes.

**RESULTS**

997 patients were analyzed. MT and ST were observed in 28.1% and 2.6%, respectively. MT patients were more frequent female (p=0.002), otherwise we did not observe any baseline differences (mean age NoT 81.7, MT 82, ST 82.9 years; mean platelet count NoT 247.2, MT 172.8, ST 170.9 000/µl).

In both MT and ST group, the lowest CPC was found on the 3rd and 4th postoperative day. MT was uniformly distributed in all prosthesis group (self expandable=31.6%; balloon expandable=26.6%). ST was observed mainly in balloon expandable group (3.0%). Only one person in the self expandable group had ST (0.37%).

On the logistic regression, the preoperative hematocrit, the preoperative number of platelets, the access and paroxysmal atrial fibrillation were found to be significant predictors of MT. ST was associated with preoperative platelet count, transapical access and the use of a balloon expandable prosthesis.

Following clinical outcomes were recorded: incidence of life-threating and major bleeding (NoT 14.2%, MT 20.8%, ST 56.3%), median length of hospital stay (NoT 8, MT 10, ST 14 days), in hospital mortality (NoT 4%, MT 0.3%, ST 18.7%) and resolved significance in comparison with NoT (p<0.05).

**CONCLUSIONS**

- **Both MT and ST following TAVI are associated with a worse clinical outcome.**
- **According to our analysis, MT is frequent, and occurs uniformly in all prosthesis groups.**
- **ST is less common but more frequent with the use of a balloon expandable prostheses.**
- **A low baseline platelets count and transapical access are associated with both MT and ST.**

© Paracelsus Medizinische Privatuniversität Nürnberg | Universitätsstr. 21-25 | Nürnberg

## In-Hospital thrombocytopenia following TAVI – Predictors and Outcomes

Stine Horna[1,2], Dr. Dr. Ferdinand Vogt[1,4], Dr. Miroslaw Ledwon[1], Dr. Dennis Eckner[3], Dr. Jürgen Jessl[3], Prof. Dr. Theodor Fischlein[1], PD Dr. Francesco Pollari, Ph.D.[1]

[1]Department of Cardiac Surgery, Klinikum Nürnberg - Paracelsus Medical University, Nuremberg, Germany; [2]Faculty of Medicine, Paracelsus Medical University, Nuremberg, Germany; [3]Department of Cardiology, Paracelsus Medical University, Klinikum Nürnberg, Nuremberg, Germany; [4]Department of Cardiac Surgery, Artemed Klinikum München Süd, Munich, Germany; Contact: stine.horna@stud.pmu.ac.at

### Objective
Transcatheter aortic valve implantation (TAVI) is an attractive treatment for patients with aortic valve stenosis. Nevertheless, postoperative thrombocytopenia is regularly observed. The reasons and impact for this phenomenon are unknown at so far. We aimed to assess incidence, risk factors and outcomes of thrombocytopenia following TAVI.

### Methods
Transcatheter aortic valve implantation (TAVI) is an attractive treatment for patients with aortic valve stenosis. Nevertheless, postoperative thrombocytopenia is regularly observed. The reasons and impact for this phenomenon are unknown at so far. We aimed to assess incidence, risk factors and outcomes of thrombocytopenia following TAVI.

### Results
907 patients were analyzed. MT and ST were observed in 28.1% and 2.6%, respectively. MT patients were more frequent female ($p=0.002$), otherwise we did not observe any baseline differences (mean age NoT 81.7, MT 82, ST 82.9 years; mean platelet count NoT 247.2, MT 172.9, ST 176.9 000/$\mu$l).
In both MT and ST group, the lowest CPC was found on the 3rd and 4th postoperative day. MT was uniformly distributed in all prosthesis group (self-expandable=31.6%; balloon-expandable=26.6%). ST was observed mainly in balloon-expandable group (3.6%). Only one person in the self-expandable group had ST (0.37%).
On the logistic regression, the preoperative hematocrit, the preoperative number of platelets, the access and paroxysmal atrial fibrillation were found to be significant predictors of MT. ST was associated with preoperative platelet count, transapical access and the use of a balloon expandable prosthesis.
Following clinical outcomes were recorded: incidence of life-threating and major bleeding (NoT 14.2%, MT 20.8%, ST 58.3%), median length of hospital stay (NoT 8, MT 10, ST 14 days), in-hospital mortality (NoT 4%, MT 6.3%, ST 16.7%) and reached significance in comparison with NoT ($p<0.05$).

### Conclusions
Both MT and ST following TAVI are associated with a worse clinical outcome. According to our analysis, MT is frequent, and occurs uniformly in all prostheses groups. ST is less common but more frequent with the use of a balloon expandable prostheses. A low baseline platelets count and transapical access are associated with both MT and ST.

# Do you know if your patient can cross the traffic light during the green period? – a propective observational study

Inga Jarosch[1,2], Sophia Leidinger[1], Tessa Schneeberger[1,2], Jan Wiederhold[1], Rainer Gloeckl[1,2], Daniela Leidl[1,2], Andreas R. Koczulla[1,2], Klaus Kenn[1,2]

[1] Klinik für Innere Medizin, Schwerpunkt Pneumologie, Schön Klinik Berchtesgadener Land, Schönau am Königssee, Germany
[2] Universities of Marburg, Philipps-University Marburg, Member of the German Center for Lung Research (DZL), Universities Giessen and Marburg Lung Center, GIMLC, Marburg, Germany

## BACKGROUND

In many countries, a minimum speed of 1.2 m/sec is necessary to cross a traffic light during the green period. Patients with chronic obstructive pulmonary disease (COPD) or interstitial lung diseases (ILD) frequently suffer from severe exercise-induced breathlessness and impaired exercise capacity which result in a reduced gait speed. In a retrospective analysis, only 10.7% of COPD patients reached the target speed of 1.2m/sec[1] and by implication, 89.3% of these patients were not able to cross a traffic light during the green period, safely.

Therefore, the primary aim of our study was to investigate the effects of pulmonary rehabilitation (PR) on walking speed in patients who initially do not reach the critical threshold of 1.2 m/sec.

## METHODS

48 subjects with severe COPD or interstitial lung disease (ILD) who participated in a 3-week inpatient comprehensive PR program were consecutively included in this prospective observational trial. Only patients with a walking speed <1.2 m/sec (measured during 4m gait speed test) performed post PR assessments and were considered for final analysis (n=40).

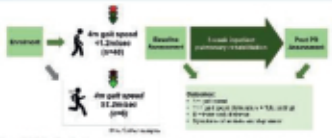


Figure 1: Study flow chart

**Primary outcome** was the change in 4m gait speed assessed from pre to post PR.



**Figure 2:** 4m gait speed test

As **secondary outcomes**, walking speed was measured via 3 different tests:

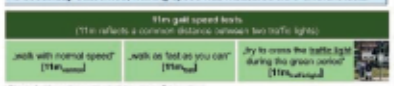


Figure 3: 11m gait speed tests (laboratory + free setting)

## RESULTS

In 40 out of 48 patients, the walking speed was below 1.2m/sec (87%).

**Primary outcome:**

- Walking speed significantly increased by +0.16m/sec (p<0.001) in the 4m gait speed test.

**Secondary outcomes:**

- Interestingly, the baseline speed was comparable in 11m_twilight and 11m_brisk but significantly slower compared to 11m_fast.
- Speed was improved following PR in all three 11m gait speed tests. however, the change in 11m_walk&talk speed did not reach statistical significance (p=0.057)(**Fig. 4**).

Table 1: Baseline Characteristics. Values are mean (SD) unless otherwise noted.

| | n=48 |
|---|---|
| Disease aetiology (ratio COPD/ILD) | 7/1 |
| Age | 67 (7) |
| BMI, kg/m² | 25.4 (5.8) |
| FEV1, %pred | 40.0 (16.8) |
| FVC, %pred | 68.1 (19.2) |
| DLCO, %pred. | 27.6 (8.7) |
| $paO_2$, mmHg | 64.8 (10.2) |
| $paCO_2$, mmHg | 38.3 (3.8) |
| LTOT, n (%) | 34 (70.8) |
| Lung-related hospitalizations during the previous year, n of patients (%) | 27 (67.5) |
| Falls during the previous year, n of patients (%) | 7 (17.5) |
| 6-min/6 min distance, m | 297 (111) |
| SpO2-nadir during the 6MWT, % | 84 (7) |
| HADS anxiety score, pts. | 6.8 (4.4) |
| HADS depression score, pts. | 6.8 (4.3) |

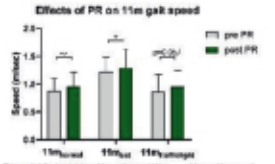


Figure 4: Effects of PR on 11m gait speed (11m_normal, 11m_fast, 11m_twilight)

Table 2: Physiological parameters at the end of the walk tests 11m_normal and 11m_twilight at discharge

| | 11m_normal | 11m_twilight | Mean difference (95%CI) | p value |
|---|---|---|---|---|
| Borg dyspnea, pts. | 2.6 (1.2) | 3.6 (1.2) | -1.1 (-2.3 to 0.3) | **0.012** |
| $SpO_2$, % | 94 (4) | 90 (7) | -3.2 (-0.8 to -5.6) | 0.089 |
| Heart rate, b/min | 92 (16) | 136 (15) | +16.1 (6.2 to 21.9) | **0.022** |




Figure 5: Post PR speed measured by gait speed tests 11m_normal (A) and 11m_twilight (B), categorized according to the cut-off (1.2m/sec).

## CONCLUSIONS

- PR improves walking speed in patients with severe COPD or ILD.
- Patients seem to choose their individual normal but not fast speed to cross a traffic light. However, post-exercise physiological parameter may indicate higher exertion levels during real life setting compared to a laboratory test.
- Post PR, 20-22% of patients gained the skill to cross the traffic light during the green period which might reduce an important barrier in patients daily life activity.

## Do you know if your patient can cross the traffic light during the green period? – a prospective observational study

Inga Jarosch[1,2], Sophia Leidinger[1], Tessa Schneeberger[1,2], Jian Wiederhold[1], Rainer Gloeckl[1,2], Daniela Leitl[1,2], Rembert Koczulla[1,2], Klaus Kenn[1,2]

[1]Institute for Pulmonary Rehabilitation Research, Schoen Klinik Berchtesgadener Land, Schoenau am Koenigssee, Germany; [2]Pulmonary Rehabilitation, Philipps-University of Marburg, German Center for Lung Research (DZL), University Giessen/Marburg Lung Center (UGMLC), Marburg, Germany; Contact: ijarosch@schoen-klinik.de

### Objective
In many countries, a minimum speed of 1.2 m/sec is necessary to cross a traffic light during the green period. In a retrospective analysis, only 10.7% of COPD patients reached this target speed (1).
Primary aim was to investigate the effects of pulmonary rehabilitation (PR) on walking speed in patients who initially do not reach the critical threshold of 1.2m/sec.

### Methods
46 subjects with severe COPD or interstitial lung disease (ILD), participating in a 3-week inpatient comprehensive PR were consecutively included in this trial. Only patients with a walking speed <1.2m/sec performed post PR assessments and were considered for final analysis. Primary outcome was the change in 4m gait speed assessed from pre to post PR. As a secondary outcome, gait speed was measured in a laboratory as well as in a real life setting on a distance of 11m which reflects a common distance between 2 traffic lights.

### Results
28 subjects with COPD (67±6years, FEV1: 33±8%pred.) and 18 subjects with ILD (67±8years, FVC: 50±15%pred.) performed baseline assessment. 6 patients out of 46 (13%) reached a speed of ≥1.2m/sec. In 40 patients, walking speed increased by +0.16m/sec (95%CI [0.09 to 0.23] $p<0.0001$) in the 4m gait speed test and by +0.10m/sec (95%CI [0.04 to 0.16] $p<0.001$) in the 11m gait speed test during PR. In 25% of patients (n=10), PR resulted in an increase of walking speed above the threshold of 1.2m/sec.

### Conclusions
PR improves walking speed in patients with severe COPD or ILD. After PR, one out of four patients gained the skill to cross the traffic light during the green period which might reduce an important barrier in patients daily life activity.

### References
1. Nolan et al. Thorax 2018;73(2):191-192.

# C - reactive protein is a promising indicator of ventricular arrhythmias in pacemaker patients

Peter Jirak1, Bernhard Wernly1, Lynne Hinterbuchner1, Vera Paar1, Laureu Hauptmann1, Daniela Kojcic1, Albert Topf1, Uta C Hoppe1, Michael Lichtenauer1, Kilian Hüfler2, Christiana Schernthaner1, Lukas Jarosław Motloch1

1 Clinic of Interna Medicine II, Department of Cardiology, Paracelsus Medical University of Salzburg, Austria
2 University Clinic of Anaesthesiology, Perioperative Medicine and General Intensive Care, Paracelsus Medical University of Salzburg, Austria

**Background:** Ventricular tachyarrhythmias are the main reason for sudden cardiac death to date. Accordingly, tools for risk stratification for ventricular arrhythmias are paramount. Non-sustained ventricular tachycardia (nsVT) represents a predictor of malignant rhythm disorders. Recently, low grade chronic inflammation was shown to predict ventricular arrhythmic events in high risk patients. This study aims to investigate, if inflammatory markers may predict higher arrhythmia burden in a low risk population.

**Methods:** We prospectively analyzed ventricular arrhythmia burden in pacemaker records of 166 patients (age 79.2 9.3; male 60.2%, 38 with coronary artery disease (CAD)) with preserved ejection fraction (left ventricular ejection fraction≥50%) during a annually pacemaker follow up in a single center. To evaluate potential predictive factors, associations of laboratory values including inflammatory markers (CRP and interleukin 6) with occurrence of nsVT was evaluated using logistic regression. Sensitivity analysis in patients with and without established CAD was performed.

**Results:** The cumulative incidence of nsVT was 12.7%. Concentrations of BNP (OR 1.00 95%CI 0.99-1.01; p=0.46), troponin (OR 0.98 95%CI 0.95-1.02; p=0.43) or interleukin-6 (OR 1.03 95%CI 0.99-1.07; p=0.16) were not associated with the occurrence of nsVTs. However, the concentration of CRP was associated with increased odds of nsVT (OR 1.26 95%CI 0.97-1.64; p=0.09) in trend. In sensitivity analysis in CAD patients, CRP was associated with increased likelihood of nsVT (OR 3.89 95%CI 1.14-13.29; p=0.03), whereas in patients without CAD there was no association between CRP and rates of nsVTs (OR 1.16 95%CI 0.88-1.54; p=0.30).

**Conclusion:** Our study shows that inflammatory markers like CRP may be promising predictors of rhythm disorders CAD patients. While CRP was associated with increased odds for nsVTs in pacemaker patients with CAD, IL-6 did not show a significant correlation. This might be based on a more volatile expression of IL-6 while CRP represents a more stable parameter for inflammation.

166 pacemaker patients with EF>50%
CAD in 38 patients



12,7% of patients displayed nsVTs

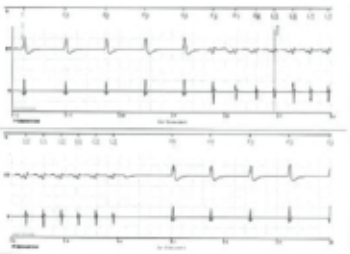

| | CAD | vs. | non-CAD |
|---|---|---|---|
| pBNP | p=ns | | p=ns |
| Troponin | p=ns | | p=ns |
| Interleukin 6 | p=ns | | p=ns |
| CRP | **p=0,03** | | p=0,30 |

Correlation of CRP and nsVTs in patients with CAD

Contact: Dr. Peter Jirak - p.jirak@salk.at - University Hospital Salzburg - Paracelsus Medical University Salzburg - Department of Internal Medicine II
Conflict of interest: The authors declare that they have no conflict of interest concerning this project
Acknowledgements: Moritz Mima

## C - reactive protein is a promising indicator of ventricular arrhythmias in pacemaker patients

Peter Jirak[1], Bernhard Wernly[2], Lynne Hinterbuchner[1], Vera Paar[1], Laurenz Hauptmann[1], Dzeneta Fejzic[1], Albert Topf[1], Uta Hoppe[1], Michael Lichtenauer[1], Kilian Höfer[2], Christiana Schernthaner[1], Lukas Motloch[1]

[1]UK für Innere Medizin II - Uniklinikum Salzburg; [2]UK für Anästhesie - Uniklinikum Salzburg; Contact: p.jirak@salk.at

### Objective
Ventricular tachyarrhythmias are the main reason for sudden cardiac death to date. Accordingly, tools for risk stratification for ventricular arrhythmias are paramount. Non-sustained ventricular tachycardia (nsVT) represents a predictor of malignant rhythm disorders. Recently, low grade chronic inflammation was shown to predict ventricular arrhythmic events in high risk patients. This study aims to investigate, if inflammatory markers may predict higher arrhythmia burden in a low risk population.

### Methods
We prospectively analyzed ventricular arrhythmia burden in pacemaker records of 166 patients (age 79.2 9.3; male 60.2%, 38 with coronary artery disease (CAD)) with preserved ejection fraction (left ventricular ejection fraction ≥50%) during a annually pacemaker follow up in a single center. To evaluate potential predictive factors, associations of laboratory values including inflammatory markers (CRP and interleukin 6) with occurrence of nsVT was evaluated using logistic regression. Sensitivity analysis in patients with and without established CAD was performed.

### Results
The cumulative incidence of nsVT was 12.7%. Concentrations of BNP (OR 1.00 95%CI 0.99-1.01; p=0.46), troponin (OR 0.98 95%CI 0.95-1.02; p=0.43) or interleukin-6 (OR 1.03 95%CI 0.99-1.07; p=0.16) were not associated with the occurrence of nsVTs. However, the concentration of CRP was associated with increased odds of nsVT (OR 1.26 95%CI 0.97-1.64; p=0.09) in trend. In sensitivity analysis in CAD patients, CRP was associated with increased likelihood of nsVT (OR 3.89 95%CI 1.14-13.29; p=0.03), whereas in patients without CAD there was no association between CRP and rates of nsVTs (OR 1.16 95%CI 0.88-1.54; p=0.30).

### Conclusions
Our study shows that inflammatory markers like CRP may be promising predictors of rhythm disorders CAD patients. While CRP was associated with increased odds for nsVTs in pacemaker patients with CAD, IL-6 did not show a significant correlation. This might be based on a more volatile expression of IL-6 while CRP represents a more stable parameter for inflammation.

## Higher incidence of stroke in severe COVID-19 is not associated with a higher burden of arrhythmias: Comparison to other types of severe pneumonia

*Peter Jirak, Zornitsa Shomanova, Dominyka Butkiene, Robert Larbig, Daniel Dankl, Nino Frank, Clemens Seelmaier, Michael Lichtenauer, Bernhard Strohmer, Jan Sackarnd, Uta C. Hoppe, Jürgen Sindermann, Holger Reinecke, Gerrit Frommeyer, Rudin Pistulli, Lukas J. Motloch*

ÖKG Österreichische Kardiologische Gesellschaft

- 120 ICU-patients requiring mechanical (NIV/intubation) ventilation - 60 COVID vs. 60 non-COVID
- Persistent/Permanent AF excluded
- Matched by paroxysmal AF, age, gender, heart failure, CAD, arterial hypertension and valvular heart disease

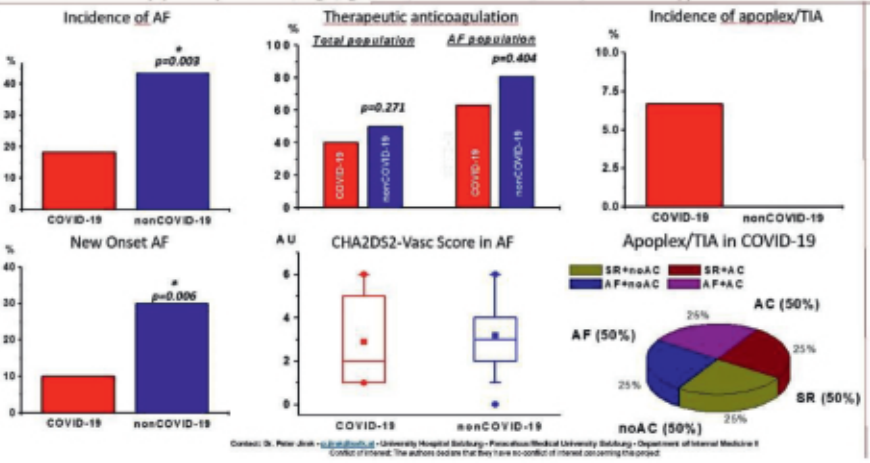


- Atrial fibrillation was less frequent in COVID-19
- Similar CHAD2S2-VASc Scores but higher rates of stroke and other thromboembolic in COVID-19 patients
- Stroke occurred regardless of anticoagulation and was unrelated to the presence of arrhythmias in COVID-19 patients

Kliniken Maria Hilf Mönchengladbach
UKM Universitätsklinikum Münster
UNIKLINIKUM SALZBURG

## Higher incidence of stroke in severe COVID 19 is not associated with a higher burden of arrhythmias: Comparison to other types of severe pneumonia

Peter Jirak[1], Zornitsa Shomanova[2], Robert Larbig[3], Daniel Dankl[4], Nino Frank[4], Clemens Seelmaier[1], Dominyka Butkiene[3], Michael Lichtenauer[1], Bernhard Strohmer[1], Jan Sackarnd[2], Uta Hoppe[1], Jürgen Sindermann[2], Holger Reinecker[2], Gerrit Frommeyer[5], Rudin Pistulli[2], Lukas Motloch[1]

[1]UK für Innere Medizin II - Uniklinikum Salzburg; [2]UK für Kardiologie I - Universitätsklinikum Münster; [3]Krankenhaus Mariahilf Mönchengladbach; [4]UK für Anästhesie - Uniklinikum Salzburg; [5]UK für Kardiologie II - Universitätsklinikum Münster; Contact: p.jirak@salk.at

### Objective
Thromboembolic events, including stroke, are typical complications of COVID-19. Whether arrhythmias, frequently described in severe COVID-19, are disease-specific and thus promote strokes is unclear. We investigated the occurrence of arrhythmias, and stroke during rhythm monitoring in critically ill COVID-19, compared to severe pneumonias of other origin.

### Methods
Recruited were 120 critically ill patients requiring mechanical ventilation in three European tertiary hospitals, including n=60 COVID-19, matched according to risk factors for occurrence of arrhythmias to n=60 patients from a retrospective consecutive cohort of severe pneumonias of other origin.

### Results
Arrhythmias, mainly atrial fibrillation (AF), were frequent in COVID-19. However, when compared to nonCOVID-19, no difference was observed with respect to ventricular tachycardias (VT) and relevant bradyarrhythmias (VT 10.0 vs. 8.4 %, p=ns and asystole 5.0 vs. 3.3%, p=ns) with consequent similar rates of cardiopulmonary resuscitation (6.7 vs. 10.0% p=ns). AF was even more common in nonCOVID-19 (AF 18.3 vs. 43.3%, p=0.003; newly onset AF 10.0 vs. 30.0%, p=0.006) which resulted in higher need for electrical cardioversion (6.7 vs. 20.0%, p=0.029). Despite these findings and comparable rates of therapeutic anticoagulation (TAC), the incidence of stroke was higher in COVID-19 (6.7.% vs. 0.0, p=0.042). These events happened also in absence of AF (50%) and with TAC (50%).

### Conclusions
Arrhythmias were common in severe COVID-19, consisting mainly of AF, yet less frequent than in matched pneumonias of other origin. A contrasting higher incidence of stroke independent of arrhythmias observed also with TAC, seems to be an arrhythmia-unrelated disease-specific feature of COVID-19.

# The Geriatric Patient in the Emergency Department – The Role of Imaging in Patient Care Management

M.T. Jurca, C. Eckrich, M.M. Lell, J. Welker, M. Gosch, P. Manava

Institute of Radiology and Nuclear Medicine, Paracelsus Medical University, Nuremberg

Klinikum Nürnberg

Older adults in the Emergency Department (ED) make an important percentage of all ED visits from which about 30 to 50% of them go on to get hospitalized [1–2] In the ED, it could be challenging to distinguish between chronic and acute symptoms and many generally have multiple comorbidities and complications, often associated with functional disabilities, like impaired cognition and mobility, making diagnosis and effective treatment challenging. Radiological examinations such as X-ray and ultrasound are considered to be critical in the ED management, [3] because symptoms, not clearly expressed may be unveiled using medical imaging.

## OBJECTIVE

To explore:

- the role of imaging in primary diagnosis of older adults in the ED
- Comparing clinical diagnosis with radiological findings utilizing ultrasound, conventional chest and abdominal radiography

## METHODS

- Selection of participants that fulfilled the criteria (71 and older) was accomplished using the hospital information system.
- The study cohort (127 participants) received at least two of the following examinations: abdominal ultrasound, chest radiography and abdominal radiography.
- Initial clinical diagnosis before imaging was correlated with the radiological diagnosis and the radiological diagnosis with the final diagnosis at hospital discharge.
- Dementia and immobility were seperately taken into account.
- The data was numerically quantified and organized in a Microsoft Excel 2016 (Microstoft Corporation, Albuquerque, New Mexico) spreadsheet.
- Data analysis was performed with SPSS Statistics 25 (IBM Corporation, Armonk, New-York).



Figure 1: Age distribution of study chort.

| Chest X-Ray | Suspected Diagnosis | | Findings | |
|---|---|---|---|---|
| | Frequency | % | Frequency | % |
| Consolidation/Pneumonia | 27 | 21.6 | 26 | 18.2 |
| Pleural effusion | 1 | 0.8 | 9 | 6.3 |
| Cardiac decompensation | 9 | 6.2 | 9 | 6.2 |
| Tumor | 3 | 2.7 | 2 | 1.8 |
| Pneumothorax | 1 | 0.8 | | |
| No pathological findings | | | 49 | 45.7 |
| Cardiomegaly | | | 7 | 5.3 |
| Increased bronchovascular markings | | | 13 | 11.8 |
| Hernia | | | 2 | 1.8 |
| COPD | 1 | 0.8 | | |
| Unclear | 68 | 61.8 | | |
| Total | 113 | 100 | 113 | 100 |

Table 1. suspected diagnosis and findings chest X-Ray

| Abdominal X-Ray | Suspected Diagnosis | | Findings | |
|---|---|---|---|---|
| | Frequency | % | Frequency | % |
| Ileus | 32 | 29.3 | 8 | 7.3 |
| Pneumoperitoneum | 5 | 6.3 | | |
| Disruption of intestinal motility | | | 20 | 18.3 |
| Subileus | | | 8 | 7.3 |
| Obstipation | 5 | 6.3 | 49 | 45 |
| No pathological findings | | | 14 | 12.8 |
| Meteorism | | | 9 | 8.3 |
| Unclear | 67 | 46 | | |
| Degenerative findings | | | 1 | 0.9 |
| Total | 109 | 100 | 109 | 100 |

Table 2. Suspected Diagnosis and Findings, Abdominal X-Ray

| Abdominal Ultrasound | Suspected diagnosis | | Findings | |
|---|---|---|---|---|
| | Frequency | Percent | Frequency | Percent |
| Cholecystitis | 7 | 5.6 | 12 | 9.7 |
| Disturbance/Obstruction, thickening | 4 | 3.2 | 3 | 2.4 |
| Constipation | | | 2 | 1.6 |
| Pancreatitis | 2 | 1.6 | | |
| Ileus | 11 | 8.9 | 8 | 6.5 |
| Urinary retention | 2 | 1.6 | 4 | 3.2 |
| Unclear | 69 | 55.2 | 6 | 4.8 |
| No pathological findings | | | 25 | 21 |
| Ileus | 3 | 1.6 | 5 | 4.0 |
| Hernia | | | 5 | 4 |
| Free fluid | 6 | 4.8 | 10 | 8.1 |
| Feces | 12 | 9.7 | | |
| Cholestasis | 13 | 8.1 | 25 | 20.2 |
| Meteorism | | | 16 | 12.9 |
| Cirrhosis | 2 | 1.6 | | |
| Persistent fluid collection (hematoma, seroma, abscess) | | | 1 | 0.8 |
| Total | 124 | 100 | 124 | 100 |

Table 3. Suspected Diagnosis and Findings in Abdominal Ultrasound.

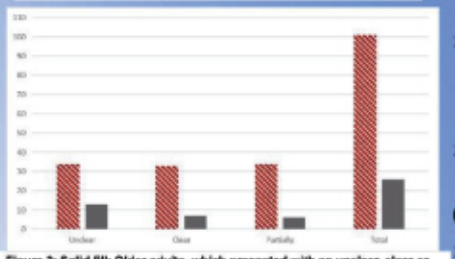

Figure 2: Solid fill: Older adults, which presented with an unclear, clear or partially clear clinical diagnosis in the ED in which radiology did not confirm the final diagnosis at discharge. Diagonal stripes: Older adults with an unclear, clear of partially clear clinical diagnosis, which has been confirmed/established using imaging methods (ultrasound, chest and abdominal radiography) and shows consensus with the final diagnosis at discharge.

REFERENCES

[1] Aminzadeh et al. Older adults in the emergency department: A systematic review of patterns of use, adverse outcomes, and effectiveness of interventions. Ann Emerg Med.
[2] Lo AX et al. Factors Associated with Hospital Admission for Older Adults Receiving Care in U.S. Emergency Departments. Journals Gerontol - Ser A Biol Sci Med Sci. 2017;72(8)
[3] Fusco et al. Older adults in Emergency Department: management by clinical severity at triage. Ann Ig. 2014;26(5).

## RESULTS

- Mean age of the patients was 83.7 years (range 71-97, median age 84 years). The data showed a Gaussian age distribution (Figure 1)
- 110 patients received a chest film: 61.8% had no clear working diagnosis established prior to imaging and in 48 patients (43.2 %) no pathology was detected on the film (Table 1).
- The second most common cause for chest radiography was the possibility of consolidation or pneumonia in 24.5%, of which 18.2 % had a positive radiological finding (Table 1)
- The most common cause of abdominal complaints was constipation and this was present in 49 of 109 (45%) of patients, the second most common was a disruption of intestinal motility with 18.3 %. However, the most common working diagnosis for abdominal film was ileus with 29.3%, which was confirmed in 7.3 % of the abdominal X-rays (Table 2)
- In sonography 66 patients (53.2%) had an unclear working diagnosis. After the examination, 26 patients (20.5%) had no pathological findings, 25 patients (19.7%) cholecystitis and in 16 patients (12.9%) meteorism (Table 3).
- No significant correlation could be found with a Pearson-Chi-Square value of 0.295, a Likelihood-Quotient of 0.301 and a Linear-by-Linear Association of 0.140
- In 86 of 127 cases, the radiological findings showed a positive consensus with the final diagnosis at discharge and in 16 cases there was no consensus.
- Radiology correctly assessed part of the final diagnosis in 24 of 127 cases.

## CONCLUSIONS

- Initial diagnosis based on radiography and ultrasound highly correlates with final diagnosis and these relatively inexpensive and ubiquitously available imaging tests still have a meaningful impact on management and diagnosis findings especially in older adults with functional impairment and atypical presentation of symptoms.

## The Geriatric Patient in the Emergency Department – The Role of Imaging in Patient Care Management

Maria Teodora Jurca[1], Caroline Eckrich, Michael Lell, Jan Welker, Markus Gosch, Panagiota Manava

[1]Institute of Radiology and Nuclear Medicine, Paracelsus Medical University, Nuremberg, Germany; Contact: mariateodora.jurca@klinikum-nuernberg.de

### Objective
Older adults generally have multiple comorbidities and complications, often associated with functional disabilities, like impaired cognition and mobility, making diagnosis and effective treatment challenging. Demographic changes led to an increasing number of older adults presenting in the emergency department (ED). In this study, the objective was to investigate the role of imaging in primary diagnosis of older adults in the ED.

### Methods
127 older adults (mean age 83.7 years, SD 5.9), presented in ED and received a combination of radiological imaging (abdominal ultrasound, chest and abdominal radiography) were included in the cohort. Patients were divided into three groups according to the level of confidence of working diagnosis. The suspected diagnosis in the ED, imaging findings and final diagnosis at discharge were analyzed.

### Results
37 patients (29.1%) received two and 90 patients (70.9%) received all three examinations. 20.5 % had an accompanying diagnosis of dementia. Consensus between the initial radiological diagnosis and the final diagnosis at discharge was found in 67.7% (n=86) of patients, partial consensus in 19.7% (n= 25) and lack of consensus in 12.6% (n=16). Imaging played a significant role in establishing final diagnosis, in 72.3% of primarily unclear (n=34 of 47), in 82.5% of clear (n=33 of 40), and in 85% partially clear clinical diagnosis (n=34 of 40).

### Conclusions
Our analysis showed that initial diagnosis based on radiography and ultrasound highly correlates with final diagnosis and these relatively inexpensive and ubiquitously available imaging tests still have a meaningful impact on management and diagnosis findings especially in older adults with functional impairment and atypical presentation of symptoms.

### References
1. Aminzadeh F, Dalziel WB. Older adults in the emergency department: A systematic review of patterns of use, adverse outcomes, and effectiveness of interventions. Ann Emerg Med. 2002;39(3):238-247. doi:10.1067/mem.2002.121523
2. Lo AX, Flood KL, Biese K, Platts-Mills TF, Donnelly JP, Carpenter CR. Factors Associated with Hospital Admission for Older Adults Receiving Care in U.S. Emergency Departments. Journals Gerontol - Ser A Biol Sci Med Sci. 2017;72(8):1105-1109. doi:10.1093/gerona/glw207
3. Fusco M, Buja A, Furlan P, et al. Older adults in Emergency Department: management by clinical severity at triage. Ann Ig. 2014;26(5):409-417. doi:10.7416/ai.2014.2000

# Nursing Development Center (NDC) – Perspectives on safety culture in acute care from health care professionals

K. Kaiser, L. Ebner, I. Gnass, D. Langegger, N. Nestler & M. Glarcher
Institute of Nursing Science and Practice, Paracelsus Medical University, Salzburg, AUSTRIA
Contact: karin.kaiser@pmu.ac.at

## Objective

Patient safety climate, as a measurable component of safety culture, is a widely used element in evaluating improvement initiatives and conducting quality assessment in health care. A high safety climate provides the foundation for safe patient care [1].

**The aim of this study was to explore health care professionals' perspectives of safety climate in Austrian hospitals and to identify areas for quality improvement.**

## Methods

A cross-sectional, descriptive, exploratory survey was conducted in physicians, therapists, nurses, and midwives working in eight hospitals from one hospital operator in Austria. Data were collected online via Lime Survey from September to October 2019 using the Swiss version of the Safety Climate Survey (SCS). The internationally used, validated SCS contains 28 items, which can be rated on a five-point Likert scale. Higher values in the assessment correspond to a more positive safety climate [1, 2, 3]. The measurement of the percentage of 'problematic responses' (PPR) was also conducted, and refers to the number of individuals that scored low level (≤2) of reported safety climate [1]. The results were analyzed using descriptive and inferential statistics in IBM SPSS.27.

## Results

Out of 5,160 eligible staff, 1,315 health care professionals (25.5%) completed the survey (female 78.6%). The mean age was 42.2 [SD ± 10.26] years, 191 (17.9%) respondents hold a managerial position, and 487 (44.1%) had a work experience > 20 years. Differences in the perception of the safety climate can be found between individual hospitals. Safety climate was rated significantly higher form older employees and staff in managerial position. No differences were determined by gender of the self-assigned specialist area. Participants with more than 20 years of professional experience assessed the safety climate significantly higher than those with five to ten years. Nurses and midwives rated the safety climate significantly lower than physicians and therapists. PPR at item level demonstrates percentages higher than 10% in 17 out of 28 items, especially in the domains of communication and hospital errors, related with patient harm.




Sample of health care professionals (n = 1,130)

## Mean item and PPR

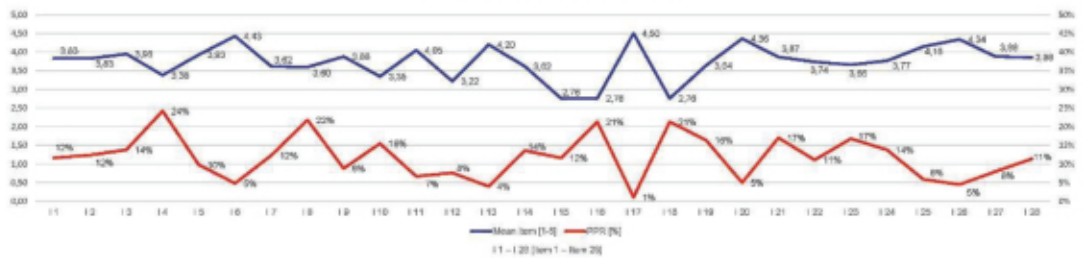

## Conclusion

PPR values above 10%, indicating a low safety climate, refer to the hospital's managerial staff. The direct work environment in terms of safety climate was rated more positively by respondents. The higher values are evident in the areas of interprofessional communication for safety concerns and safety precautions by managerial staff. Health care professionals' different perspective of safety climate and the calculation of the PPR clearly indicate that action is needed to strengthen health communication, reduce, and minimize hospital errors. To subsequently derive evidence-based interventions, a literature review will be conducted, and interventions to strengthen the safety climate will be implemented.

## References

[1] Gehring, K., Mascherek, A. C., Bezzola, P. & Schwappach, D. L. (2015). Safety climate in Swiss hospital units: Swiss version of the Safety Climate Survey. *J Eval Clin Pract, 21*(2), 332-338. doi: 10.1111/jep.12326

[2] Sexton, J. B., Helmreich, R. L., Neilands, T. B., Rowan, K., Vella, K., Boyden, J., ... Thomas, E. J. (2006). The Safety Attitudes Questionnaire: psychometric properties, benchmarking data, and emerging research. *BMC Health Serv Res, 6*, 44. doi: 10.1186/1472-6963-6-44

[3] Shleynberg, G., Sexton, B. J. & Thomas, E. (2013). Test retest reliability of the safety climate scale. In T. U. o. T. C. o. E. f. P. S. R. a. Practice. (Hrsg.), (Vol. 01-05). Texas: Technical Report

www.pmu.ac.at/pflege.htm

## Nursing Development Center - Perspectives on safety culture in acute care from health care professionals

Karin Kaiser[1], Lisa Ebner[1], Irmela Gnass[1], Doris Langegger[1], Nadja Nestler[1], Manela Glarcher[1]

[1]Institute of Nursing Science and Practice, Paracelsus Medical University, Salzburg, Austria; Contact: karin.kaiser@pmu.ac.at

### Objective
Patient safety climate, as a measurable component of safety culture, is a widely used element in evaluating improvement initiatives and conducting quality assessment in health care. A high safety climate provides the foundation for safe patient care [1]. The aim of this study was to explore health care professionals' perspectives of safety climate in Austrian hospitals and to identify areas for quality improvement.

### Methods
A cross-sectional, descriptive, exploratory survey was conducted in physicians, therapists, nurses, and midwives working in eight hospitals from one hospital operator in Austria. Data were collected online via Lime Survey from September to October 2019 using the Swiss version of the Safety Climate Survey (SCS). The internationally used, validated SCS contains 28 items, which can be rated on a five-point Likert scale. Higher values in the assessment correspond to a more positive safety climate [1, 2, 3]. The measurement of the percentage of 'problematic responses' (PPR) was also conducted, and refers to the number of individuals that scored low level ($\leq 2$) of reported safety climate [1]. The results were analyzed using descriptive and inferential statistics in IBM SPSS.27.

### Results
Out of 5,160 eligible staff, 1,315 health care professionals (25.5%) completed the survey (female 78.6%). The mean age was 42.2 [SD $\pm$ 10.26] years, 191 (17.9%) respondents hold a managerial position, and 487 (44.1%) had a work experience $>$ 20 years. Differences in the perception of the safety climate can be found between individual hospitals. Safety climate was rated significantly higher form older employees and staff in managerial position. No differences were determined by gender of the self-assigned specialist area. Participants with more than 20 years of professional experience assessed the safety climate significantly higher than those with five to ten years. Nurses and midwives rated the safety climate significantly lower than physicians and therapists. PPR at item level demonstrates percentages higher than 10% in 17 out of 28 items, especially in the domains of communication and hospital errors, related with patient harm.

### Conclusions
PPR values above 10%, indicating a low safety climate, refer to the hospital's managerial staff. The direct work environment in terms of safety climate was rated more positively by respondents. The higher values are evident in the areas of interprofessional communication for safety concerns and safety precautions by managerial staff. Health care professionals' different perspective of safety climate and the calculation of the PPR clearly indicate that action is needed to strengthen health communication, reduce, and minimize hospital errors. To subsequently derive evidence-based interventions, a literature review will be conducted, and interventions to strengthen the safety climate will be implemented.

### References
1. Gehring, K., Mascherek, A. C., Bezzola, P. & Schwappach, D. L. (2015). Safety climate in Swiss hospital units: Swiss version of the Safety Climate Survey. J Eval Clin Pract, 21(2), 332-338. doi: 10.1111/jep.12326
2. Sexton, J. B., Helmreich, R. L., Neilands, T. B., Rowan, K., Vella, K., Boyden, J., ... Thomas, E. J. (2006). The Safety Attitudes Questionnaire: psychometric properties, benchmarking data, and emerging research. BMC Health Serv Res, 6, 44. doi: 10.1186/1472-6963-6-44
3. Shteynberg, G., Sexton, B. J. & Thomas, E. (2013). Test retest reliability of the safety climate scale. In T. U. o. T. C. o. E. f. P. S. R. a. Practice. (Hrsg.), (Vol. 01-05). Texas: Technical Report

# Nitrerge Neuronen der menschlichen Aderhaut:

# Eine quantitative Studie

Stefanie Holzinger[1,2], Christian Platzl[2], Heidi Wolfmeier[2], Falk Schrödl[2], Alexandra Kaser-Eichberger[2]

1 Abschlussarbeit BSc Studium Pharmazie JG2018

2 Zentrum für Anatomie und Zellbiologie, Institut für Anatomie und Zellbiologie Salzburg, Paracelsus Medizinische Privatuniversität Salzburg

## Einleitung

Die Choroidea ist die mittlere der drei Schichten des hinteren Augenbechers, zwischen Sklera und Retina gelegen (siehe Abbildung 1). Zu ihren Funktionen gehört die Kontrolle des Augendrucks und des choroidalen Blutflusses. Ein Bestandteil der Choroidea sind die intrinsischen choroidalen Neuronen (ICN), deren Funktion bei der Aderhauthomöostase noch nicht vollständig verstanden ist. Durch den Nachweis des Enzyms neuronale Stickstoffmonoxidsynthase (nNOS) wurde gezeigt, dass einer der von ICN exprimierten Neurotransmitter Stickstoffmonoxid (NO) ist. (1)

**Ziel dieser Arbeit ist es, den Anteil an nitrergen ICN zu ermitteln. Hierzu wird die Anzahl der nNOS-exprimierenden Zellen mit der Gesamtanzahl der ICN verglichen.**

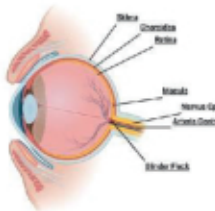


**Abbildung 1 Auge Querschnitt**
Die Abbildung zeigt ein menschliches Auge im Querschnitt. Im hinteren Augenabschnitt befinden sich die drei Schichten Retina, Choroidea und Sklera. Auch der blinde Fleck, Macula, Nervus opticus und Arteria centralis retinae sind dargestellt. (2)

## Material und Methoden

### Präparation, Schneiden und Immunohistochemie der Choroidea

Die Spenderaugen wurden fixiert und die Choroidea herauspräpariert. Mittels Cryotom wurden Gefrierschnitte der Choroidea angefertigt. Diese wurden für immunhistochemische Untersuchungen aufbereitet. Die Gesamtpopulation aller Neuronen wurde mittels des pan-neuronalen Markers Neurofilament 160/210 (NF) dargestellt und nitrerge Neurone mittels n-NOS identifiziert. Die ICN konnten so fluoreszenzmikroskopisch dargestellt und ihre Anzahl berechnet werden.

## Ergebnisse

### Fluoreszenzmikroskopie

nNOS-positive ICN (Abbildung 2) und nNOS-negative ICN (Abbildung 3)

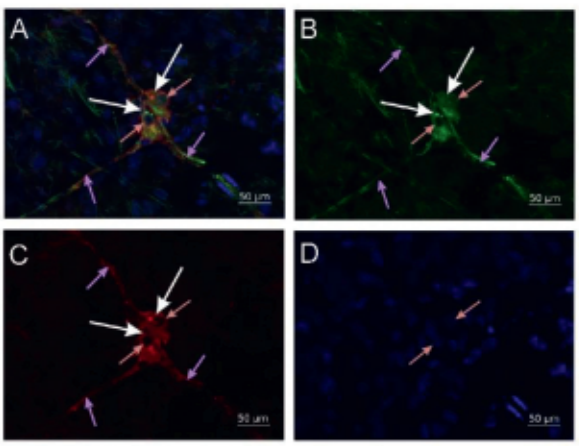


**Abbildung 2 nNOS-Positive ICN mit Nervenfasern**
Weiße Pfeile zeigen nNOS-positive ICN, drei Nervenfasern gehen von oder zu den ICN (violette Pfeile), die roten Pfeile zeigen die Zellkerne der ICN. A. Alle Lichtkanäle sind aktiviert, nNOS, Neurofilament, DAPI sind sichtbar. B. Die Neurofilament-positiven Nervenzellen sind in grün zu sehen. C. Die nNOS-positiven Nervenzellen sind rot dargestellt. D. Die Zellkerne fluoreszieren blau. (3)

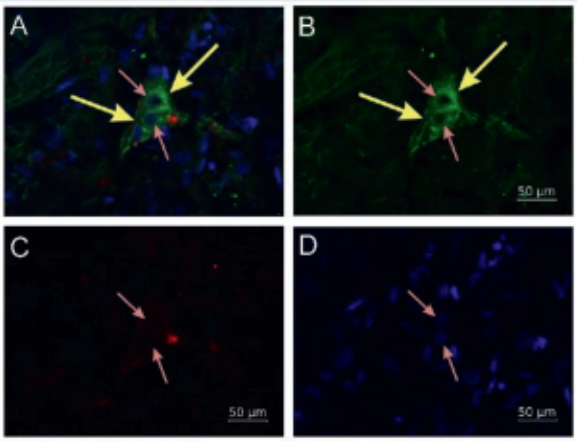


**Abbildung 3 nNOS-negative ICN**
Die beiden gelben Pfeile zeigen auf ICN, welche nNOS-negativ sind, die roten Pfeile markieren die Zellkerne. A. Alle Lichtkanäle sind aktiviert, nNOS, Neurofilament, DAPI sind sichtbar. B. Signal im grünen Kanal aufgrund NF- positiver Nervenzellen. C. Kein Signal im roten Kanal aufgrund fehlender nNOS Immunreaktivität. D. Die Zellkerne fluoreszieren blau. (3)

### Quantitative Auswertung

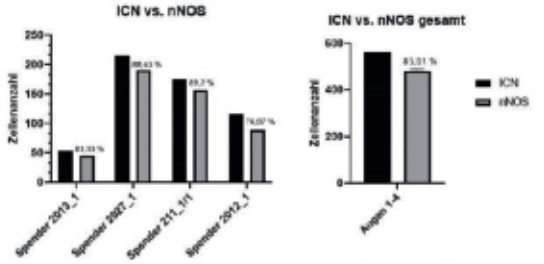


**Abbildung 4 ICN gesamt vs. nNOS**
Die schwarzen Balken stellen die Gesamtanzahl der ICN (entspricht der Anzahl der NF- positiven Neurone) dar. Die grauen Balken repräsentieren die Anzahl der nNOS-positiven ICN. Der Anteil der nNOS-positiven ICN an ICN gesamt ist in Prozent angegeben.

**Abbildung 5 ICN vs. nNOS gesamt**
Gesamtergebnis aller ausgezählten Choroideas. Insgesamt wurden 563 NF-positive (schwarz) und 482 nNOS-positive (grau) ICN gezählt, was einen Anteil von 85,81% der gesamt gezählten ICN ausmacht. Die Standardabweichung beträgt 6,05.

## Zusammenfassung

In dieser Arbeit wurde mittels Immunhistochemie das Verhältnis von nNOS-positiven ICN an der Gesamtpopulation von ICN in der menschlichen Aderhaut (n=4) untersucht. Die Färbungen konnten erfolgreich durchgeführt werden und waren mittels Fluoreszenzmikroskopie gut auswertbar. Die quantitative Analyse ergab, dass nicht alle, sondern lediglich 85,61 % der gezählten ICNs auch nNOS-positiv sind (siehe Abbildung 4 und 5). Die genaue Funktion der nNOS-positiven ICN ist noch nicht bekannt; weitere Forschungen ist nötig um ihre Rolle bei Augenerkrankungen wie z.B. der Myopie zu klären.

Diese Arbeit ist Teil der Abschlussarbeit BSc Studium Pharmazie JG2018

Danksagung

Vielen Dank an das Körperspendeprogramm des Instituts für Anatomie und Zellbiologie für die Bereitstellung der Spenderaugen. Ebenso richtet sich ein großer Dank an Priv.-Doz. Dr. Alexandra Kaser-Eichberger und Prof. Dr. med. Falk Schrödl für die fachliche Unterstützung und Ermöglichung des Projektes.

Literatur

*(1) NICKLA, D. L. & WALLMAN, J. 2010. The multifunctional choroid. Prog Retin Eye Res, 29, 144-68 (2) Abbildung erstellt in BioRender.com (3) Die Bilder wurden mit dem Programm ZEN lite 2021 und mit 20x Vergrößerung aufgenommen. Die Bilder zeigen die Choroidea von Spender 2027_1.*

## Nitrerge Neuronen der menschlichen Aderhaut: Eine quantitative Studie

Stefanie Holzinger[1,2], Christian Platzl[2], Heidi Wolfmeier[2], Falk Schrödl[2], Alexandra Kaser-Eichberger[2]

[1]Abschlussarbeit BSc Studium Pharmazie JG2018; [2]Zentrum für Anatomie und Zellbiologie, Institut für Anatomie und Zellbiologie Salzburg, Paracelsus Medizinische Privatuniversität Salzburg; Contact: alexandra.kaser@pmu.ac.at

### Objective
Die Choroidea ist die mittlere der drei Schichten des hinteren Augenbechers. Zu ihren Funktionen gehört unter anderem die Kontrolle des Augendrucks und des choroidalen Blutflusses. Ein Bestandteil der Choroidea sind die intrinsischen choroidalen Neurone (ICN), deren Funktion bei der Aderhauthomöostase noch nicht vollständig verstanden ist. Durch den Nachweis des Enzyms neuronale Stickstoffmonoxidsynthase (nNOS) wurde gezeigt, dass einer der von ICN exprimierten Neurotransmitter Stickstoffmonoxid ist.

### Methods
In dieser Studie wurde Immunhistochemie an dünnen gefrorenen Aderhautschnitten durchgeführt (n=4), um quantitative Daten von nNOS-exprimierenden ICN zu erhalten. Die quantitative Auswertung erfolgte am Fluoreszenzmikroskop, die Gesamtzahl aller ICN wurde dabei mittels des pan-neuronalen Markers Neurofilament160/200 ermittelt.

### Results
Die quantitative Analyse der immunhistochemischen Färbungen ergab, dass nicht alle, sondern lediglich 85,61 % der gezählten ICN auch nNOS-positiv sind.

### Conclusions
Die genaue Funktion der nNOS-positiven ICN ist noch nicht bekannt; weitere Forschungen sind nötig um ihre Rolle bei Augenerkrankungen wie z.B. der Myopie zu klären.

PARACELSUS
MEDIZINISCHE PRIVATUNIVERSITÄT

Ludwig Boltzmann Institut
Arthritis und Rehabilitation

# Low pH attenuates apoptosis by suppressing the volume-sensitive outwardly rectifying (VSOR) chloride current in chondrocytes

Michael Kittl[1], Martina Winklmayr[2], Julia Preishuber-Pflügl[1], Victoria Strobl[1,3] Martin Gaisberger[1,2,3], Markus Ritter[1,2,3] and Martin Jakab[1]

[1]Paracelsus Medical University, Center for Physiology, Pathophysiology and Biophysics, Institute for Physiology and Pathophysiology – Salzburg, Strubergasse 22, 5020 Salzburg, Austria

[2]Ludwig Boltzmann Institute for Arthritis and Rehabilitation, Strubergasse 22, 5020 Salzburg, Austria

[3]Gastein Research Institute, Paracelsus Medical University, Strubergasse 22, 5020 Salzburg, Austria

***BACKGROUND***

In a variety of physiological and pathophysiological conditions, cells are exposed to acidic environments. Severe synovial fluid acidification also occurs in a progressive state of osteoarthritis (OA) affecting chondrocytes. In prior studies extracellular acidification has been shown to protect cells from apoptosis but the underlying mechanisms still remain elusive. In the present study we demonstrated that the inhibition of $Cl^-$ currents plays a significant role in the antiapoptotic effect of acidification in human articular chondrocytes.

***METHODS***

Drug-induced apoptosis was analyzed after exposure to staurosporine by caspase 3/7 activity and by annexin-V/7-actinomycin D (7-AAD) staining, followed by flow cytometry. Cell viability, $Cl^-$ currents and the mean cell volume were determined using resazurin assays, the whole cell patch clamp technique, and the Coulter method, respectively.

## 1 pH–induced $Cl^-$ current inhibition

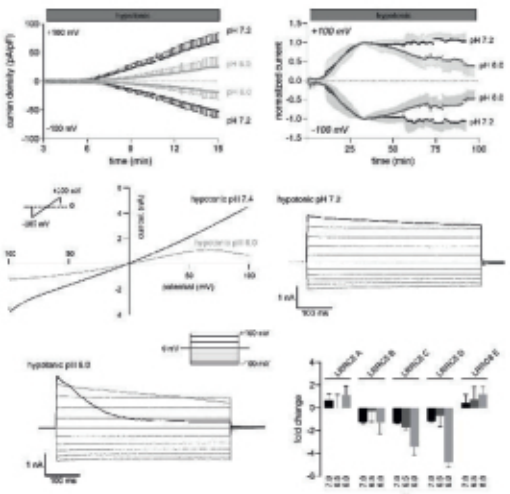

*$Cl^-$ current inhibition under acidic conditions*

In most cells including chondrocytes, cell swelling leads to the activation $Cl^-$currents, displaying a moderated time-dependent inactivation at high-positive potentials. Time-dependent inactivation was more pronounced shortly after exposing cells to an acidic pH of 8.0 and $ICl_{swell}$ slowly deactivated over time. In addition Q-rt PCR analysis revealed, that mRNA expression of two subunits of the VSOR channel, LRRC8C and D, was downregulated ~4fold under acidic conditions.

## 2 pH–induced impaired volume regulation

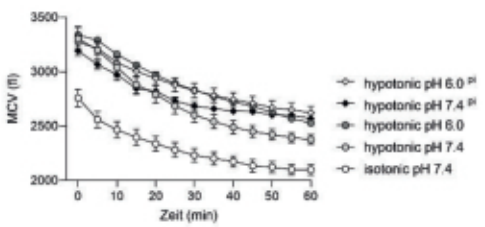


*Impaired volume regulation under acidic conditions*

VSOR currents are crucial for regulating the cell volume, by extruding $Cl^-$ ions or organic osmolytes to counteract osmotic cell swelling. Considering that VSOR currents are suppressed under acidic conditions we could demonstrate that the regulatory volume decrease (RVD) is impaired under hypotonic and acidic conditions.

## 3 Low pH protects chondrocytes against apoptosis

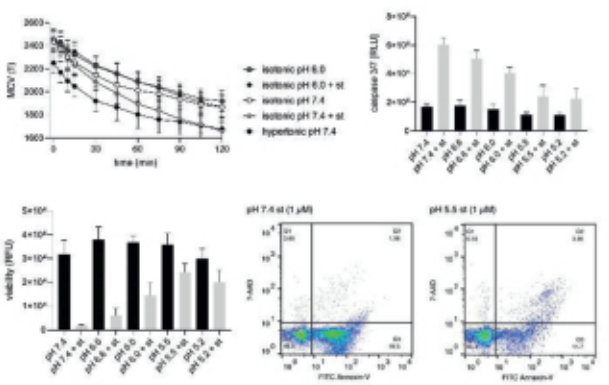

*Acidic preconditioning protects chondrocytes against staurosporine (st)-induced apoptosis*

Cell shrinkage is an early and crucial event in apoptosis, which is called apoptotic volume decrease (AVD). Similar to the RVD, VSOR $Cl^-$ currents are involved in AVD. Here, we could demonstrate that AVD is completely absent and apoptosis is diminished under acidic conditions. Interestingly, 5 h after the induction of apoptosis the decline in the living cell population (pH 7.4) was almost reversed under acidic conditions, indicating that extracellular acidification has a protective effect in human articular chondrocytes.

## 4 Putative model of the antiapoptotic effect of acidosis

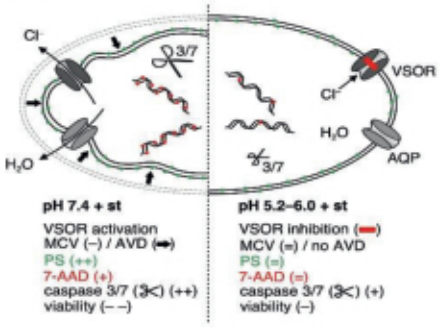


Under pH 7.4 (left side) staurosporine treatment leads to activation VSOR $Cl^-$channels to induce cell shrinkage (AVD), which is an initial step in the course of apoptosis, followed by phosphatidylserine (PS) exposure, caspase activation, DNA fragmentation, membrane blebbing and loss of membrane integrity evidenced by the 7-AAD uptake. Under acidic conditions (right side) VSOR channels are deactivated so that AVD is absent under isotonic conditions and consequently apoptosis is prevented in the presence of staurosporine (st).

***In summary, this study shows that VSOR $Cl^-$ channels are inhibited under acidic condition. Since $Cl^-$ channels are involved in various volume regulatory processes, like RVD and AVD, cell volume homeostasis and apoptosis are massively impaired by acidity. The maintenance of extracellular matrix production exclusively depends on the functional stability of chondrocytes. A comprised cell volume homeostasis and altered viability are, therefore, likely to promote articular cartilage degeneration and progression of osteoarthritis (OA).***

## Low pH attenuates apoptosis by suppressing the volume-sensitive outwardly rectifying (VSOR) chloride current in chondrocytes

Michael Kittl[1], Martina Winklmayr[2], Julia Preishuber-Pflügl[1], Victoria Strobl[1,3], Martin Gaisberger[1,2,3], Markus Ritter[1,2,3], Martin Jakab[1]

[1]Paracelsus Medical University, Center for Physiology, Pathophysiology and Biophysics, Institute for Physiology and Pathophysiology – Salzburg, Strubergasse 22, 5020 Salzburg, Austria; [2]Ludwig Boltzmann Institute for Arthritis and Rehabilitation, Strubergasse 22, 5020 Salzburg, Austria; [3]Gastein Research Institute, Paracelsus Medical University, Strubergasse 22, 5020 Salzburg, Austria; Contact: michael.kittl@pmu.ac.at

### Objective
In a variety of physiological and pathophysiological conditions, cells are exposed to acidic environments. Severe synovial fluid acidification also occurs in a progressive state of osteoarthritis (OA) affecting chondrocytes. In prior studies extracellular acidification has been shown to protect cells from apoptosis but the underlying mechanisms still remain elusive. In the present study we demonstrated that the inhibition of $Cl^-$ currents plays a significant role in the antiapoptotic effect of acidification in human articular chondrocytes.

### Methods
Drug-induced apoptosis was analyzed after exposure to staurosporine by caspase 3/7 activity and by annexin-V/7-actinomycin D (7-AAD) staining, followed by flow cytometry. Cell viability, Cl- currents and the mean cell volume were determined using resazurin assays, the whole cell patch clamp technique, and the Coulter method, respectively.

### Results
The results reveal that extracellular acidification decreases the caspase 3/7 activity, enhances the viability following staurosporine treatment and gradually deactivated the volume-sensitive outwardly rectifying (VSOR) $Cl^-$ current. Furthermore, the regulatory volume decrease (RVD) as well as the apoptotic volume decrease (ADV), which represents an early event during apoptosis, were no longer apparent under acidic conditions after hypotonicity-induced cell swelling and staurosporine-induced apoptosis, respectively. Similar to the effect of acidosis, the VSOR $Cl^-$ current inhibitor DIDS rescued chondrocytes from apoptotic cell death and suppressed AVD after induction of apoptosis with staurosporine.

### Conclusions
From these data, we conclude that the deactivation of VSOR Cl- currents impairs cell volume regulation under acidic conditions, which is likely to play an important role in the survivability of human articular chondrocytes.

### Acknowledgements
This project was supported by the research support funds of the Paracelsus Medical University, E-19/29/153-KIT to MK.

# Functional characterization of *Staphylococcus aureus* strains isolated from patients with epidermolysis bullosa

Christina Köchl[1], Birgit Tockner[1], Anna Kaufmann[1], Johannes Bischof[1], Petra Pjevac[2], Doglas Parise[3], Mariana Parise[3], Marisol Salgado Albarrán[3], Jan Baumbach[3], Lorena Tuchscherr de Hauschopp[4], Dirk Strunk[5], Roland Wagner[1,#], Julia Reichelt[1,§], Dagmar Achleitner[6], Jan M. Kern[6], Roland Lang[7], Johann W. Bauer[7], Josefina Piñon Hofbauer[1,*], Christina Guttmann-Gruber[1,*]

Affiliations: [1]EB House Austria, Research Program for Molecular Therapy of Ectodermoses, Department of Dermatology and Allergology, University Hospital of the Paracelsus Medical University, Salzburg, Austria; [2]Core Microbiome Facility of the Medical University of Vienna and the University of Vienna, Austria; [3]Department of Experimental Bioinformatics, TUM School of Life Sciences Weihenstephan, Technical University of Munich, Germany; [4]Institute of Medical Microbiology, University Hospital of Jena, Germany; [5]Experimental & Clinical Cell Therapy Institute, Spinal Cord Injury and Tissue Regeneration Center Salzburg (SCI-TReCS), PMU Salzburg, Austria; [6]Division of Medical Microbiology, University Hospital Salzburg (SALK), Salzburg, Austria; [7]Department of Dermatology and Allergology, University Hospital Salzburg, Paracelsus Medical University Salzburg, Austria; current address: [#]Department of Dermatology, Venereology and Allergy, Medical University of Innsbruck, Innsbruck, Austria; [§]Department of Dermatology and Allergology, University Hospital of the Paracelsus Medical University, Salzburg, Austria. *equally contributing authors

## BACKGROUND

Loss-of-function mutations in the gene *COL7A1* are responsible for the severe genetic mechano-bullous skin fragility disorder recessive dystrophic epidermolysis bullosa (RDEB)[1]. RDEB is characterised by persistent, non-healing wounds that are often massively infected, contributing to ongoing inflammation. Such wounds have a high risk of malignant transformation, and tumours carry a very poor prognosis for patients highlighting a link between persistent inflammation and cancer. The precise molecular mechanisms that contribute to tumourigenesis under these conditions are not completely understood. Whole exome sequencing and RNAseq analysis of RDEB tumors have previously revealed a predominance of mutational signatures associated with APOBEC, involved in innate immune defense, and an upregulation of pathways linked to inflammation and microbial infection.[2] Given the observation of reduced microbial diversity and an increased abundance of *Staphylococcus aureus* (*S. aureus*) at sites of chronic wounding in RDEB[3], the accumulating evidence underscores the impact of microbial infection on endogenous cellular mutagenic processes. The aim of this project is characterize *S. aureus* isolates sampled from RDEB wounds and assess their impact on host cell transcriptome and secretome.

## PROJECT AIMS *and* EXPERIMENTAL DESIGN




## RESULTS I: Comparison of bacterial genomes

We have established 15 *S. aureus* isolates from wounds of different RDEB patients. Phylogenetic tree analysis, based on homologies in 500 genes, revealed a broad clustering of isolates into two groups (group A, group B).

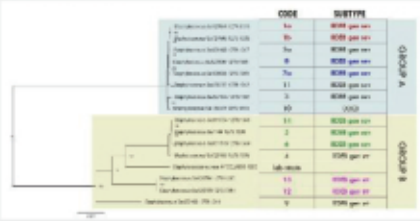


Colour code indicates *S. aureus* isolated from the same patient but different locations and time points.

## RESULTS II: Differential growth kinetics and gene expression

We observed minor but significant differences in bacterial growth kinetics and in expression of several quorum-sensing factors at stationary phase between the two groups.

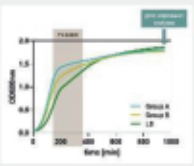

### Quorum sensing

the ability of bacteria to detect and to respond to cell population density by gene regulation

### Genes involved

- *agrA*: encodes two-component signal transduction systems downregulating surface proteins and upregulation of secreted proteases during growth
- *aur*: Aureolysin is a extracellular matrix metalloprotease contributing to virulence by e.g. cleaving host factors of the immune system.
- *sigB*: factor crucial for the establishment of long-term persistence in host




## RESULTS III: *S. aureus* strains exhibit differential hemolytic potential

Hemolysin is a ß-pore-forming toxin secreted by *S. aureus* leading to necrotic death of the target cell. Hemolytic activity of different *S. aureus* isolates was investigated by plating bacteria on blood agar plates and measuring hemolysis zone per colony forming unit (CFU) (A). In general, group B isolates demonstrated lower hemolytic activity, though this was not significant by this analyses (B). We also observed varying hemolytic potential of *S. aureus* isolates established from the same patient (Isolate 5,6, and 14) at different wound sites and time points (C).

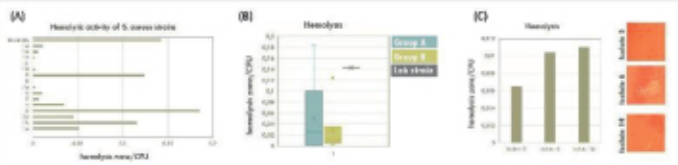


## RESULTS IV: *Live infection of keratinocytes with S. aureus impacts host cell gene expression and protease secretion*

The different *S. aureus* strains were labelled with FITC and further used for live infection of wild type keratinocytes (A). Trypsin-like protease activity was assessed in cell culture supernatants upon 2 hrs of infection. Notably, different *S. aureus* isolates established from the same patient (5, 6 and 14) exhibited different protease levels compared to the negative ctrl (n=3) (B). Furthermore, preliminary data confirmed upregulation of inflammatory markers CCL5 and CXCL10 (C), previously used as markers of successful infection[4].

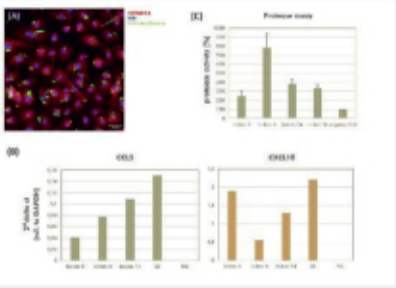


### Genes of interest

- **CCL5: chemokine**, involved in immunoregulatory and **inflammatory processes**, connected to esophageal SCC, previously demonstrated to be upregulated in infected skin cells[4]
- **CXCL10: anti-microbial chemokine**, stimulation of monocytes, natural killer cells and T-cell migration, previously demonstrated to be upregulated in infected skin cells[4]

## CONCLUSION and OUTLOOK

- *S. aureus* isolates differently impact transcriptome and secretome of host cells which might impact wound status (acute vs chronic).
- RNAseq analysis of bacterial isolates will provide further insight into expression of virulence genes and their contribution to disease pathology.

References

1. Fine JD et al. (2008) **J Am Acad Dermatol.** 58(6):931-50
2. Cho RJ et al. (2018) **Sci. Transl. Med.** 10(455) pii: eaas9668
3. Fuentes I et al. (2018) **J Invest Dermatol.** 138(11):2492-95
4. Tuchscherr L et al. (2010) **J Infect Dis.** 202(7):1031-40.

**This work is funded by DEBRA Austria and the Paracelsus Medical University Salzburg (PMU-FFF E-18/28/149/GGR).**

*Contact:* Josefina Piñón Hofbauer, PhD ✉ j.d.pinon@salk.at; Christina Guttmann-Gruber, PhD ✉ c.gruber@salk.at

## Functional characterization of Staphylococcus aureus strains isolated from patients with recessive dystrophic epidermolysis bullosa

Christina Köchl[1], Birgit Tockner[1], Anna Kaufmann[1], Johannes Bischof[1], Petra Pjevac[2], Doglas Parise[3], Marisol Parise[3], Marisol Salgado Albarran[3], Jan Baumbach[3], Lorena Tuchscherr de Hauschopp[4], Dirk Strunk[5], Roland Wagner[1,7], Julia Reichelt[1,8], Dagmar Achleitner[6], Jan M. Kern[6], Roland Lang[7], Johann W. Bauer[7], Josefina Pinon Hofbauer[1,9], Christina Guttmann-Gruber[1,9]

[1]EB House Austria, Research Program for Molecular Therapy of Genodermatoses, Department of Dermatology and Allergology, Paracelsus Medical University, Salzburg, Austria; [2]Joint Microbiome Facility of the Medical University of Vienna and the University of Vienna, Austria; [3]Department of Experimental Bioinformatics, Technical University of Munich, Germany; [4]Institute of Medical Microbiology, University Hospital of Jena, Germany; [5]Experimental & Clinical Cell Therapy Institute, Spinal Cord Injury and Tissue Regeneration Center Salzburg (SCI-TReCS), PMU Salzburg, Austria; [6]Division of Medical Microbiology, University Hospital Salzburg, Salzburg, Austria; [7]Department of Dermatology and Allergology, University Hospital Salzburg, Paracelsus Medical University, Salzburg, Austria; [8]current address: Department of Dermatology, Venereology and Allergy, Medical University of Innsbruck, Austria; [9]equally contributing; Contact: c.gruber@salk.at

### Objective
Recessive dystrophic epidermolysis bullosa (RDEB) is associated with the development of aggressive squamous cell carcinoma (SCC) constituting the main cause of premature death in patients. SCCs predominantly arise at sites of chronic wounding, inflammation and infection highlighting a link between these pathological conditions and malignant transformation. RNAseq analysis of RDEB tumors have previously revealed an upregulation of pathways linked to inflammation and microbial infection. Given the observation of reduced microbial diversity and an increased abundance of *Staphylococcus aureus (S. aureus)* at sites of chronic wounding in RDEB, we aimed to characterize *S. aureus* isolates sampled from RDEB wounds and assess their impact on host cell transcriptome and secretome.

### Methods
15 different *S. aureus* isolates were established from RDEB wounds and subjected to whole genome sequencing. Bacterial growth kinetics was monitored and haemolytic activity assessed by culturing on blood agar plates. *S. aureus* isolates were FITC-labelled and used to infect primary wild type keratinocytes at an MOI of 75. Internalization of bacteria was confirmed by immunofluorescence microscopy. We performed protease activity assays on the infection medium and monitored host cell transcriptomic changes by real time PCR.

### Results
Phylogenetic analysis revealed a broad clustering of *S. aureus* isolates into two groups. Applying this stratification to the analysis of the data, we could detect minor but significant differences in bacterial growth kinetics and in expression of several quorum-sensing factors between the two groups. Bcterial isolates also exhibited differences in haemolytic activity, pointing to their varying pathogenic potential. After live infection of keratinocytes with various bacterial isolates we observed differences in protease activity in infection medium. Notably, *S. aureus* strains established from different wounds of the same patient varied in their protease activity highlighting intra-patient wound-specific variances. Finally, preliminary data confirmed induction of inflammatory genes in infected cultures compared to controls, linking *S. aureus* infection with the induction of endogenous cellular mutagenic processes.

### Conclusions
Our data suggest that S. aureus isolates differently impact transcriptome and secretome of host cells which might contribute to wound status and impact subsequent malignant transformation. RNAseq analysis of bacterial isolates will provide further insight into expression of virulence factors and their contribution to disease pathology.

### Acknowledgements
Funded by DERBA Austria and Paracelsus Medical University Salzburg (E-18/28/149/GGR).

# Ophthalmological Surgeries with a Novel Ultrashort Pulse Laser Source

## The Project's Target:

The aim of the project is to improve ophthalmological surgeries by using ultrashort pulse (USP) lasers instead of standard nanosecond (ns) lasers. Due to the much shorter pulse widths of USP-lasers compared to standard nanosecond lasers by three orders of magnitude, microprocessing of human tissue can be achieved with much less pulse energy. As a result only a very small amount of heat is deposited in the tissue and acoustic shock waves are greatly reduced. This prevents the tissue from evaporating and tearing, and results in a far more precise and controllable tissue ablation. For this reason, the process is also known as cold material removal.
The ophthalmological surgeries – the laser iridotomy, the post-cataract treatment, the selective laser-trabeculoplasty and the cutting of the lens – are performed on porcine eyes, and subsequently characterized with light and scanning electron microscopy.
In addition, the laser-induced shock waves that occur during ablation are investigated to evaluate if they are harmful to the eye. For this purpose, the laser sources are focused in a water bath, and the shock waves are simultaneously imaged with a streak camera.

## Laser Iridotomy:

Three different laser sources are tested on porcine eyes and the ablations are evaluated using the scanning electron microscopy:

**1. Nanosecond laser**
$\tau_p \approx 10$ ns; $E_p \leq 600$ µJ

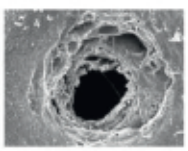

Frayed edges, torn tissue

x230
100 µm

**2. Standard USP laser**
$\tau_p \approx 12$ ps; $E_p \leq 220$ µJ

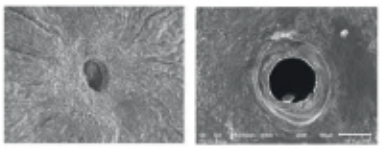

Deterministic ablation, round, flat edges, small

x230
100 µm

**3. Novel USP laser**
$\tau_p \geq 18$ ps; $E_p = 36$ µJ

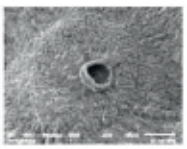

Round, small, sufficient quality

## Post Cataract Treatment:

It has been proven possible to cut the anterior lens capsule with a standard USP laser. The photography shows three capsulotomies (green arrows) on a porcine eye with different diameters. The photography is taken through a slit lamp.

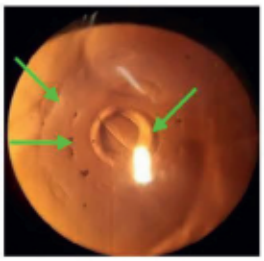

## Shock Waves:

Shock wave (1) visualization (real and false color image) of the standard USP laser source induced breakdown (2) in water. The target (3) is used to visualize the reflection (4) of the shock wave.

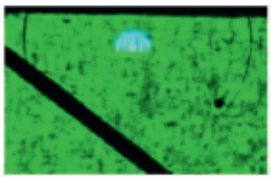

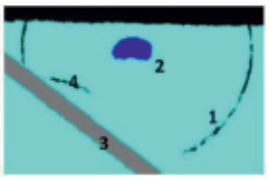


## Results:

Iridotomy: The ablation of the tissue is far more precise and deterministic with a USP laser than with a nanosecond laser source.
Post cataract treatment: The cutting of the lens tissue is possible with a USP laser source.
Shock waves: The visualization of the shock waves after the optical breakdown is possible.

## Further Steps:

The laser parameters required for the various ophthalmological surgeries must be adapted for the newly developed laser source.
The relative intensity of the acoustic shock waves from the various laser beam sources must be quantified.


Technische Hochschule Nürnberg

Michael Körber, M.Sc.
michael.koerber@th-nuernberg.de

Prof. Dr. sc. nat. Bernd Braun,
Prof. Dr. rer. nat. Manfred Kottcke,
Andreas Giese, M.Sc.,
Milan Fritsche, M.Sc.,
Jonathan Wenk

Klinikum Nürnberg

Prof. Dr. med. Josef Schmidbauer
Dr. med. Francesco Luciani

Montfort Laser GmbH

Dr. sc. nat. Daniel Kopf



This project has received funding from the Eurostars-2 joint programme with co-funding from the European Union Horizon 2020 research and innovation programme

## Ophthalmological Surgeries with a novel Ultrashort Pulse Laser Source

Michael Körber[1,2], Milan Fritsche[1], Andreas Giese[1], Daniel Kopf[3], Manfred Kottcke[1], Francesco Luciani[4], Josef Schmidbauer[2,4], Jonathan Wenk[1], Bernd Braun[1]

[1]Technische Hochschule Nürnberg Georg Simon Ohm, Nuremberg, Germany; [2]Paracelsus Medical University, Nuremberg, Germany; [3]Montfort Laser GmbH, Götzis, Austria; [4]Klinikum Nürnberg, Nuremberg, Germany; Contact: michael.koerber@th-nuernberg.de

### Objective

In laser-based ophthalmological surgeries Q-switched Nd:YAG lasers are the standard devices. Typically, these lasers have a pulse width of a few nanoseconds and a pulse energy of about one millijoule. Even though these lasers are well established, the use of ultrashort laser pulses leads to a significant improvement in accuracy, to a reduction of undesired side effects, and promises to open up new areas of laser-based surgeries. The objective of the project is the development and test of an ultrashort pulse laser source for various ophthalmological surgeries such as iridotomy, post cataract treatment and laser-trabeculoplasty with partly existing procedures and partly new methods. Furthermore, the accompanying shock waves produced by the laser spot during the surgeries are investigated to clarify, if they are harmful for the eye.

### Methods

The tests are carried out with three different laser sources: The first is a 20 W fiber coupled Nd:YAG nansecond laser with laser parameters comparable to those of standard ophthalmic laser sources. It emits laser pulses with a pulse length down to 10 nanoseconds and up to 0.6 millijoule (mJ). The others are ultrashort pulse laser sources. One of them is a state-of-the-art oscillator-amplifier-system with pulse widths of 10 ps and pulse energies of up to 200 microjoule ($\mu J$). The other one is a newly developed passively Q-switched microchip laser set-up. It emits pulses with a pulse width of about 20 picoseconds and a pulse energy of 36 $\mu J$. Here, the set-up is much more compact and simpler than the oscillator-amplifier-system. The ophthalmological surgeries are performed on porcine eyes. They were carried out and compared with all three laser sources. In particular, the surgery of the cornea, the iris, the eye lens, and the lens capsule are tested. The results are evaluated using both a scanning electron microscope and a high-resolution light microscope. The tests regarding the shock waves are carried out by focusing the laser beams in a water bath and simultaneously imaging the shock waves with a streak camera. The relative intensities of the acoustic waves generated by the different laser sources are measured and compared to each other.

### Results

Former and actual results of the research show a huge improvement for the laser-based surgeries by using ultrashort pulses instead of nanosecond pulses. The holes of the iridotomies are much smaller (one fifth) and of better qualities with regard to the cutting edges. A precise processing of the lens capsule is shown to be feasible as well as the cutting of the lens. For all surgeries so far tested the energy intake could be reduced to some tenth of microjoule per pulse instead of some millijoule. In addition, the measurement of the accompanying shock waves generated by the laser pulses are possible with the streak camera.

### Conclusions

The use of ultrashort laser pulses for ophthalmological surgeries like iridotomy, post cataract treatment and laser-trabeculoplasty shows a number of beneficial effects like lower heat load, more precise micro processing and more deterministic process parameters. The development of a new compact and simple laser source with pulse widths in the range of existing much more complex ultrashort pulse lasers systems promises a wide range of applications.

PARACELSUS MEDIZINISCHE PRIVATUNIVERSITÄT

Klinikum Nürnberg
wir sind für Sie da.

Contact: maria.kokozidou@pmu.ac.at
theodor.fischlein@klinikum-nuernberg.de

Science Get Together, 2021
Nuremberg, Germany

# The influence of various great saphenous vein graft storage solutions on the endothelium integrity

Maria Kokozidou[1], Tobias Braun[2], Julia Mladek[2], Gundula Schulze-Tanzil[1], Jurij Kalisnik[2], Philipp Krombolz-Reindl[3], Rainald Seitelberger[3], Theodor Fischlein[2]

[1] Institute for Anatomy, Paracelsus Medical University, Nuremberg, Germany
[2] Department of Cardiac Surgery (Cardiovascular Center), Klinikum Nürnberg, Paracelsus Medical University, Nuremberg, Germany
[3] Department of Cardiac-, Vascular- and Endovascular Surgery, University Clinics Salzburg, SALK, Salzburg

## Objective

Coronary bypass surgery mostly used graft is the great saphenous vein (GSV). Endothelial damage of the graft results in graft failure. Graft preservation and degree of endothelium denudation is very much dependent on the preservation solution of the graft prior to implantation. The aim of this study was to investigate the quality of the graft endothelium depending on the intraoperative preservation in Duragraft (−/- heparin), Custodiol, physiological NaCl, Ringer acetate, Biseko or normal cell culture medium.

## Methods

**a)** Primary human endothelial cells (hECs) were isolated from GSV (Ethic Commission No. 15073). Next day the cells were stimulated with either Duragraft (−/- heparin), Custodiol, physiological NaCl, Ringer acetate, Biseko or hECs growth medium (n=3 for each preservation medium, three independent experiments, each experiment in duplicate, with cells isolated from three different donors) for 1 h, 2 h, 4 h, 7 h and 18 h under static and dynamic conditions at room temperature. Cell vitality was documented via live/dead staining (LeTo) using a confocal laser scanning microscope (LSM) and analysed using ImageJ.

**b)** Three different vein samples were received from each vein graft that were treated with NaCl, Ringer or Biseko (n=3 for each). The first segment was taken directly after the GSV explantation, the second in the meantime between graft explantation and implantation and the third one was the rest of the venous segment right before the final cannulation of the graft. The samples were fixed in 4 % parafolmadehyde and were stained with Alcian blue.

## Results

All LeTo results were normalised against the cell confluence of the ECs when cultured in medium at time point 0. NaCl presented the lowest cell confluence at all time points in both, static and dynamic conditions. It was significantly lower ($p<0.05$) at 2 h and 18 h ($p<0.0001$) than Ringer in static conditions (figure 1A & B). In dynamic conditions NaCl presented again the lowest cell confluence and was significantly lower than medium at 2 h ($p<0.05$). In dynamic conditions Ringer was associated with significantly higher confluence at time point 4 h than NaCl ($p<0.001$), at time point 7 h than NaCl and Biseko (0.0001) and Custodiol with heparin ($p<0.01$), at time point 18 h than Duragraft ($p<0.05$), Duragraft with heparin ($p<0.001$), Custodiol, NaCl and Biseko ($p<0.0001$) (Figure 1 C, D). There was no significant difference in regard to cell confluence between Custodiol with or without heparin at all time points in both static and dynamic conditions.

The Alcian blue staining of the three different probes of each treated GSV graft revealed different grades of destruction of the sulphated glycosaminoglycans (sGAGs) that are essential elements of the endothelial glycocalyx (Figure 2). Nevertheless, no significant differences could be detected.

## Conclusion

Our results favour the use of Ringer's solution as an intraoperative storage solution for the GSV grafts in comparison to the least favoured of all NaCl and Duragraft and Custodiol gaining a position between the two. Biseko shows a relatively unstable performance.

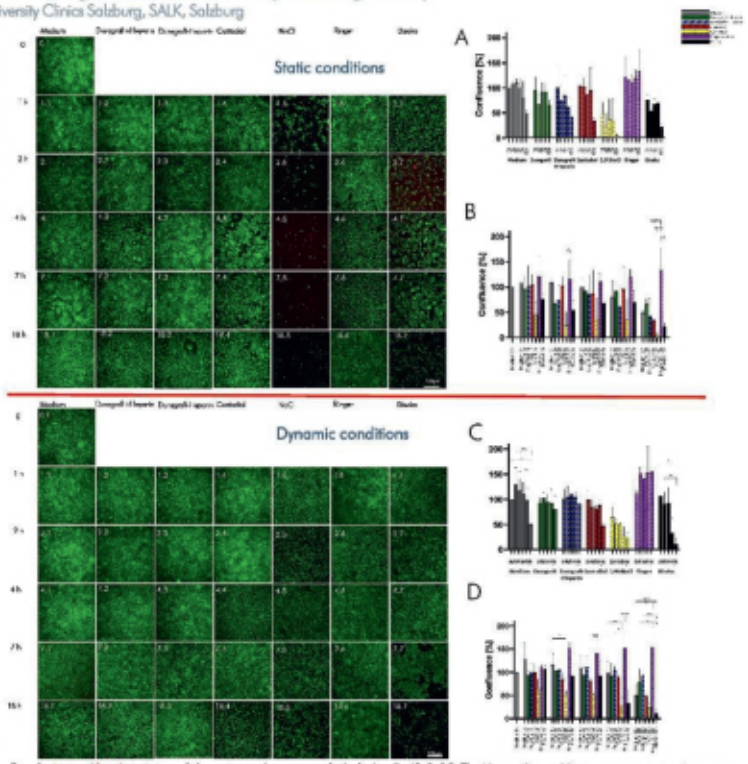


**Fig. 1: Living/dead staining of the primary human endothelial cells (0.0-18.7).** Above the red line: representative pictures under static conditions; below the red line: pictures under dynamic conditions. Images (0.0) are the starting point of the experiments (0 h), pictures 1.1–1.7 at 1 h, 2.1– 2.7 at 2 h, 4.1–4.7 at 4 h, 7.1–7.7 at 7 h and 18.1-18.7 at 18 h. The columns are ordered according to solutions (Duragraft with and without heparin, Custodiol, NaCl, Ringer, Biseko and Medium). Scale bar: 100 µm.
**Charts show cell confluence rates (%) depending on the solutions (A and B) and timepoints (C and D) compared.** A and C show stimulations under static conditions, B and D show stimulations under dynamic conditions. *Significant differences ($P<0,05$); **Significant differences ($P<0.01$); ***Significant differences ($P<0.001$); ****Significant differences ($P<0.0001$).

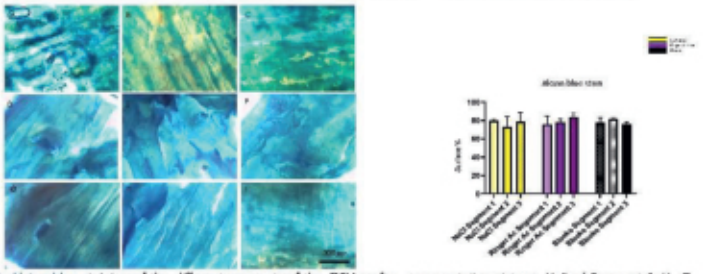


**Fig. 2: Alcian blue staining of the different segments of the GSV grafts:** representative pictures (A-I) of Segment 1 (A, D and G), Segment 2 (B, E and H) and Segment 3 (C, F and I), treated with NaCl (A-C), Ringer (D-F) and Biseko (G-I). Scale bar: 300 µm. **Charts show endothelial surface (%)** covered with sGAGs (blue), depending on the solutions (Ringer and NaCl) of the three different graft segments; there are no statistically significant differences, sGAGs: sulphated glycosaminoglycans.

This study was financed by Manfred Roth foundation and PMU FFF Research Fund .

## The influence of various great saphenous vein graft storage solutions on the

Maria Kokozidou[1], Tobias Braun[2], Julia Mladek[2], Gundula Schulze-Tanzil[1], Jurij Kalisnik[2], Philipp Krombolz-Reindl[3], Rainald Seitelberger[3], Theodor Fischlein[2]

[1]Institute of Anatomy, Paracelsus Medical University, Nuremberg, Germany; [2]Department of Cardiac Surgery (Cardiovascular Center), Klinikum Nürnberg, Paracelsus Medical University, Nuremberg, Germany; [3]Department of Cardiac-, Vascular- and Endovascular Surgery, University Clinics Salzburg, SALK, Salzburg; Contact: maria.kokozidou@pmu.ac.at

### Objective
The great saphenous vein (GSV) is the mostly used graft for coronary bypass surgery. Endothelial damage of the graft results in graft failure. Graft preservation and degree of endothelium denudation is very much dependent on the preservation solution of the graft prior to implantation. The aim of this study was to investigate the quality of the graft endothelium depending on the intraoperative preservation in Duragraft (+/- heparin), Custodiol, physiological NaCl, Ringer acetate, Biseko or endothelial cell culture medium.

### Methods
a) Primary human endothelial cells (hECs) were isolated from GSV (Ethic Commission No. 15073). In the next day the cells were stimulated with either Duragraft (+/- heparin), Custodiol, physiological NaCl, Ringer acetate, Biseko or hECs growth medium (n=3 for each preservation medium, each experiment in duplicate) for 1 h, 2 h, 4 h, 7 h and 18 h under static and dynamic conditions in room temperature. Cell vitality was documented via live/dead staining (LeTo) in a confocal laser scanning microscope (LSM) and analysed using ImageJ.
b) Three different vein samples were received from each vein graft that were treated with NaCl, Ringer or Biseko (n=3 for each). The first segment was taken directly after the GSV explantation, the second in the meantime between graft explantation and implantation and the third one was the rest of the venous segment right before final cannulation of the graft. The samples were fixed in 4 % paraformaldehyde and stained with Alcian blue.

### Results
All LeTo results were normalised against the cell confluence of the ECs when cultured in medium at time point 0. NaCl presented the lowest cell confluence at all-time points in both static and dynamic conditions. It was significantly lower ($p<0.05$) at 2 h and 18 h ($p<0.0001$) than Ringer in static conditions. In dynamic conditions NaCl presented again the lowest cell confluence and which was significantly lower than in medium at 2 h ($p<0.05$). In dynamic conditions Ringer was associated with significantly higher confluence at time point 4 h than NaCl ($p<0.001$), at time point 7 h than NaCl and Biseko (0.0001) and Custodiol with heparin ($p<0.01$), at time point 18 h than Duragraft ($p<0.05$), Duragraft with heparin ($p<0.001$), Custodiol, NaCl and Biseko ($p<0.0001$). There is no significant difference between Custodiol with or without heparin at all-time points in both static and dynamic conditions.
The Alcian blue staining of the three different probes of each treated GSV graft revealed different grades of destruction of the sulphated glycosaminoglycans (sGAGs) that are essential elements of the endothelial glycocalyx, nevertheless no significant differences were detectable.

### Conclusions
Our results favour the use of Ringer's solution as an intraoperative storage solution for the GSV grafts in comparison to the least favoured of all, NaCl and Duragraft and Custadiol gaining a position between the two. Biseko shows a relatively unstable performance at different time points.

### Acknowledgements
This study was financed by Manfred Roth foundation and PMU FFF Research Fund.

### References
1. no references

PARACELSUS MEDIZINISCHE PRIVATUNIVERSITÄT

Klinikum Nürnberg
Wir sind für Sie da!

# Individualized growth trajectories: Evaluation of growth outcomes in the California Perinatal Quality Care Collaborative (CPQCC)

**Pauline Kosmann[1], MK Quin[2], Hon Yiu So[3], Henry Chong Lee[2], Christoph Fusch[1], Niels Rochow[1]**

[1]Pediatrics, Paracelsus Medical University, Nuremberg, [2]Neonatology, Stanford School of Medicine, USA, [3]Statistics, University of Waterloo, Ontario, Canada

## BACKGROUND

This study is aims to analyze growth of preterm infants in California Perinatal Quality Care Collaborative (CPQCC) by using Individualized growth trajectories (GTC):

- GTC adjusts for birth weight, gestational age (GA) and sex.
- is based on normal physiology including postnatal weight loss
- and intrauterine growth rate adjusted for postnatal physiology
- and merges with World Health Organization growth standards at term age

Landau-Crangle, E. et. al. 2018, www.growthcalculator.org

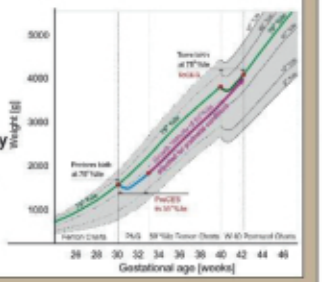


## OBJECTIVES

To evaluate growth of preterm infants under consideration of neonatal morbidities in a population-based cohort.

## METHODS

- Multicohort study using data from the CPQCC (144 California NICUs) during the years 2008-2018
- Inclusion criteria: GA 23 to 36+6/7 weeks
- Exclusion criteria: death or major malformation
- Calculation for each infant:
  - GTC weight at discharge
  - deviation (delta W) between GTC and actual discharge weight
  - weight gain from birth to discharge
- Regression analysis were performed to study the association of neonatal morbidities to delta W using R and SPSS.

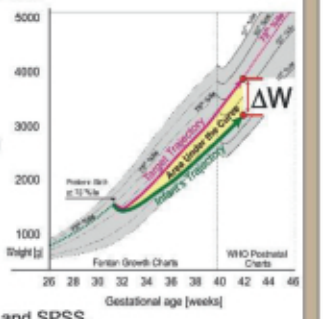


| Infants stratified by | Regression analyses adjusted for |
|---|---|
| Gestational age (GA) | Gestational age (GA) |
| Discharge postmenstrual age (PMA) | Discharge postmenstrual age (PMA) |
| Birth weight quintile group | Birth weight |
| | Sex |

## RESULTS

- This study included n=77,369 preterm infants

*Tab 1. Length of stay and growth of selected GA groups stratified for discharge PMA*

| GA (weeks) | Discharge during 34 to 37+6/7 Length of stay (days) | delta W (g) | weight gain (g/kg/d) | Discharge during 38 to 41 + 6/7 Length of stay (days) | delta W (g) | weight gain (g/kg/d) | Discharge during 42 to 45+6/7 Length of stay (days) | delta W (g) | weight gain (g/kg/d) |
|---|---|---|---|---|---|---|---|---|---|
| 23 | 92 ± 7 | -203 | 13 | 116 ± 8 | -266 | 13 | 140 ± 8 | -422 | 13 |
| 26 | 71 ± 7 | -132 | 13 | 93 ± 8 | -187 | 13 | 119 ± 8 | -405 | 12 |
| 29 | 48 ± 7 | -43 | 13 | 70 ± 8 | -81 | 13 | 98 ± 8 | -368 | 12 |
| 32 | 26 ± 7 | 6 | 10 | 48 ± 7 | -10 | 12 | 78 ± 8 | -236 | 11 |
| 35 | 10 ± 4 | -19 | -1 | 24 ± 7 | -02 | 8 | 56 ± 8 | -230 | 8 |

## RESULTS

- **Delta W was higher in more immature infants and those who were discharged at later PMA**
- **Infants with higher birth weights for the same gestational age had higher delta W compared to infants with lower birth weight (Fig 1).**
- **Infants with higher birth weights for the same gestational age showed higher gain velocity than infants with lower birth weight (Fig 2).**

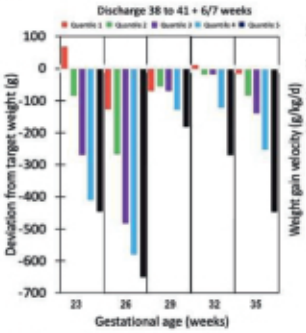


*Figure 1. Deviation from target weight (delta W) stratified for GA and 5 birth weight quantiles of selected GA groups*

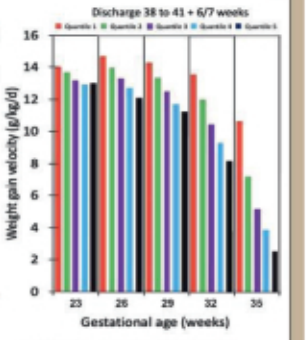


*Figure 2. Weight gain from birth to discharge stratified for GA and 5 birth weight quantiles of selected GA groups*

- Breast milk fed infants deviated on average by 22g from GTC
- Disease-free infants had significantly smaller delta W (p<0.001)
- Neonatal morbidities were significantly related to a higher delta W (p<0.001) → higher mean difference between target weight and actual weight

*Tab. 2. Average deviation from the GTC at discharge for neonatal morbidities*

| | |
|---|---|
| 391g | necrotizing enterocolitis surgery |
| 148g | retinopathy of prematurity |
| 126g | late onset sepsis |
| 78g | patent ductus arteriosus |
| 21g | chronic lung disease |

## CONCLUSION

- A considerable number of preterm infants with GA < 28 weeks have a delta W greater than 200g, indicating further need for optimizing growth.
- Healthy preterm infants showed less deviation from the GTC, and morbidities were associated with higher delta W.
- The larger deviation deviation from GTC in infants born with higher birth weight could be explained by systematic error in the interpretation of current growth charts
  → This finding urges the use of individualized growth trajectories for preterm infants..

Niels Rochow, MD, PhD, Pediatrics, Paracelsus Medical University, niels.rochow@klinikum-nuernberg.de

## Individualized growth trajectories: Evaluation of growth outcomes in the California Perinatal Quality Care Collaborative (CPQCC)

Pauline Kosmann[1], MK Quin[2], Hon Yiu So[3], Henry Chong Lee[2], Christoph Fusch[1], Niels Rochow[1]

[1]Department of Pediatrics, Paracelsus Medical University, Nuremberg; [2]Neonatology, Stanford School of Medicine, USA; [3]Statistics, University of Waterloo, Ontario, Canada; Contact: nielsrochow@gmail.com

### Objective

Individualized growth trajectory (GTC) is a concept which provides neonatologist an individual growth curve for a preterm infant from birth through the first years of life.[1] The curve is individually adjusted for birth weight, gestational age (GA) and sex. It is based on normal physiology including postnatal weight loss, intrauterine growth rate adjusted for postnatal physiology and merges with World Health Organization growth standards at term age.
Objective of this study is to evaluate growth of preterm infants under consideration of neonatal morbidities in a population-based cohort.

### Methods

Multicohort study using data from the CPQCC which includes 144 California NICUs during the years 2008-2018. Inclusion criteria were GA: 23 to 36+6/7 weeks. Exclusion criteria were death or major malformation. For each infant, GTC weight at discharge, the deviation (delta W) between GTC and actual discharge weight, and weight gain from birth to discharge were calculated. Infants were stratified by GA, by postmenstrual age (PMA) at discharge, and by birth weight quintile groups for each week. Regression analysis adjusted for birth weight, GA, PMA at discharge and sex were performed to study the association of neonatal morbidities to delta W using R and SPSS.

### Results

This study included n=77,369 preterm infants (Tab 1). More immature infants and those who were discharged at later PMA showed higher delta W (Tab 2). Infants with higher birth weights for the same GA had higher delta W compared to infants at lower quintiles (Fig 1). A similar finding was shown for weight gain data (Fig. 2).
Breast milk fed infants deviated on average by 22g from GTC. Disease-free infants had significantly smaller delta W ($p<0.001$). Neonatal morbidities were significantly related to a higher mean difference between target weight and actual weight (delta W, $p<0.001$): necrotizing enterocolitis surgery by 391g, retinopathy of prematurity by 148g, late onset sepsis by 126g, patent ductus arteriosus by 78g, and chronic lung disease by 21g.

### Conclusions

A considerable number of preterm infants with GA < 28 weeks have a delta W greater than 200g, indicating further need for optimizing growth.
In particularly, infants born within the higher birth weight quintiles may need more catch-up than current approaches to meet desired GTC targets. It could be hypothesized that current growth charts lead infants with higher birth weight to a lower postnatal trajectory compared to GTC.

### References

1. Landau-Crangle et. al. 2018, www.growthcalculator.org

# Mesoderm induction improves human induced pluripotent stem cell-derived megakaryocyte differentiation and platelet production

Linda Krisch[1,2], Gabriele Brachtl[1], Sarah Hochmann[1], André Cronemberger Andrade[1], Patricia Ebner-Peking[1], Michaela Oeller[2], Katharina Schallmoser[2], and Dirk Strunk[1]

[1]Cell Therapy Institute, Spinal Cord Injury and Tissue Regeneration Center Salzburg (SCI-TReCS), Paracelsus Medical University (PMU), 5020 Salzburg, Austria
[2]Department of Transfusion Medicine and SCI-TReCS, Paracelsus Medical University (PMU), 5020 Salzburg, Austria

linda.krisch@pmu.ac.at

## Introduction

Several protocols have been established to obtain megakaryocytes (MK) and platelets in vitro from induced pluripotent stem cells (iPSC) with limited efficiency. We have previously observed that initial mesoderm induction improved endothelial and mesenchymal stromal differentiation. We therefore hypothesized that an additional mesoderm induction step prior to hemogenic endothelial cell (HEC) differentiation, might also improve MK progenitor (MKP) production, resulting in an increased platelet output. We further asked if defined basic media compositions affect the final megakaryocyte maturation process. In an iterative process, we compared HEC induction efficiency, MKP production and platelet counts of two independent human iPSC lines with or without initial mesoderm induction.

## Mesoderm induction improves HEC differentiation and MKP production from iPSC

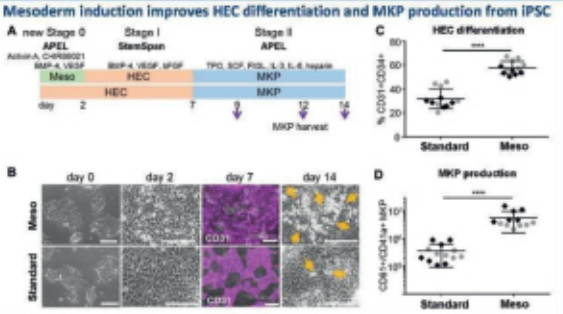


Figure 1 (A) Experiment outline of iPSC differentiation toward megakaryocyte progenitors (MKP, purple arrows) via hemogenic endothelial cells (HEC) without (Standard) or with initial 2 day (stage II) mesoderm induction (Meso). (B) Cell morphology during differentiation from iPSC to MKP. In situ reporter staining was performed on day 7 highlighting HEC (purple). On day 14, an increased amount of round-shaped floating cells (indicated by orange arrows) was observed in cultures after mesoderm induction. Scale bar: 200 µm. (C) A significant increase of CD31+/CD34+ cells and (D) the total count of CD61+/CD41a+ MKP was detected by flow cytometry after mesoderm induction compared to standard conditions on day 7 (at the end of stage I; p < 0.0001) and at the end of stage II (p < 0.0001). Results from iPSC clones UCB144-C12-C (grey circles) and BIH001-A (black diamonds). C and D.

## Expansion and maturation of iPSC-derived MK in different media conditions

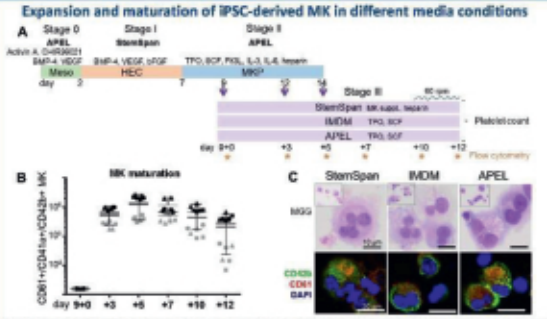


Figure 2 (A) Experimental outline using the improved mesoderm induction conditions (Meso). Megakaryocyte progenitors (MKP, purple arrows) were harvested and matured into megakaryocytes (MK) in stage III for up to 12 days in three different media (StemSpan, IMDM or APEL). From day 9+0, MK were cultured under dynamic conditions, as indicated by the wavy line. (B) The total amount of maturing CD61+/CD41a+/CD42b+ MK revealed no significant differences after culture in the three media (StemSpan, hexagons; IMDM, squares; APEL, triangles; symbol color depicts two independent iPSC clones (UCB144-C12-C, grey and BIH001-A, black; p > 0.05). (C) May-Grünwald Giemsa stain of maturating MK at d9+7 (MGG; top row). Characteristic MK immunophenotype (CD42b (green), CD61 (red) and DAPI (nuclei blue); bottom row).

## Mesoderm induction improves platelet production from iPSC

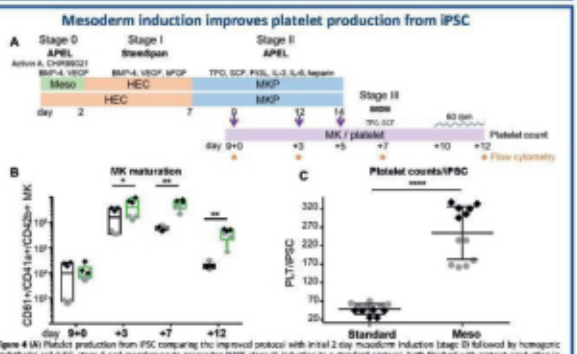


Figure 4 (A) Platelet production from iPSC comparing the improved protocol with initial 2 day mesoderm induction (stage II) followed by hemogenic endothelial cell (HEC, stage I) and megakaryocyte progenitor (MKP, stage II) induction to a standard protocol, both finished with platelet production in IMDM supplemented with TPO and SCF (stage III). (B) The total amount of CD61+/CD41a+/CD42b+ MK was significantly increased on day 9+3 (p = 0.0181), day 9+7 (p = 0.0031) and day 9+12 (p = 0.0062) after mesoderm induction (Meso, green bars) compared to standard conditions (black bars). (C) Platelet counts on day 9+12, normalized to input iPSC, were significantly increased after mesoderm induction (p < 0.0001). Results from two independent iPSC clones (UCB144-C12-C, grey circles, and BIH001-A, black diamonds).

## Platelet release of iPSC-derived MK in different media conditions

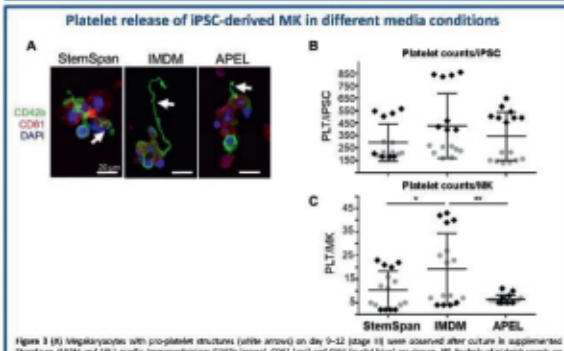


Figure 3 (A) Megakaryocytes with pro-platelet structures (white arrows) on day 9+12 (stage III) were observed after culture in supplemented StemSpan, IMDM and APEL media. Immunofluorescence (CD42b (green), CD61 (red) and DAPI (nuclei blue) are shown. (B) Analysis of platelet counts on day 9+12 (stage III) after culture in supplemented APEL, IMDM, and StemSpan media. Comparable platelet counts per input iPSC (p > 0.05) were found in all media conditions. (C) Platelet counts calculated per input megakaryocyte were significantly increased after culture in supplemented IMDM medium, compared to StemSpan (p = 0.046) and APEL (p = 0.022) media. Results from two independent iPSC clones (UCB144-C12-C, grey circles, and BIH001-A, black diamonds).

## Detection of coagulation- and angiogenesis-related proteins in adult and iPSC-derived platelets

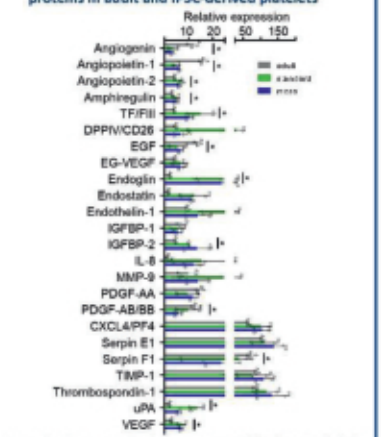


Figure 5. Analysis of angiogenesis-related protein expression in adult and iPSC-derived platelets harvested at d9+12. Coagulation- and angiogenesis-related proteins were significantly increased (Angiopoietin 2, p < 0.0001; Amphiregulin, p = 0.0002; Tissue Factor, p = 0.0009; Endoglin, p < 0.0001; Endostatin, p < 0.0001; sFRP2, p = 0.0004; VEGF, p < 0.0001) or decreased (Angiogenin, p < 0.0001; Angiopoietin 1, p = 0.0006; EGF, p < 0.0001; PDGF AB/BB, p = 0.0014; Serpin F1, p = 0.0001) in iPSC-derived (standard, green bars; meso, blue bars) compared to adult platelets (grey bars, open triangles). Platelets harvested from iPSC without and with initial mesoderm induction showed comparable expression patterns (p > 0.05). Results from two independent iPSC clones (UCB144-C12-C, open circles and BIH001-A, open diamonds).

## Summary/Conclusion

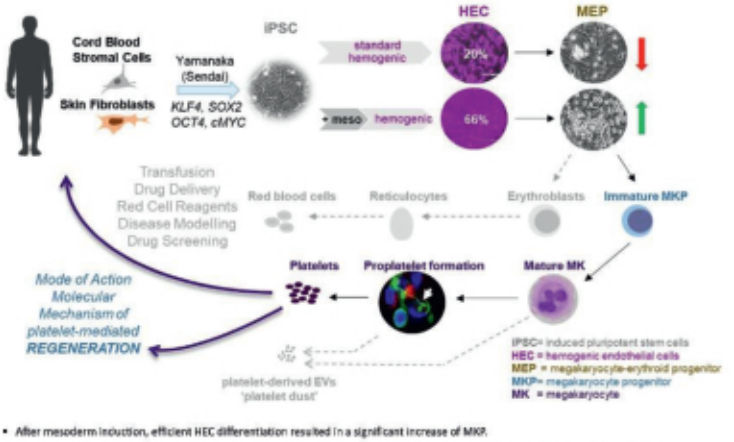


- After mesoderm induction, efficient HEC differentiation resulted in a significant increase of MKP.
- MKP differentiated into mature MK releasing comparable platelet amounts per input iPSC under all three media conditions tested.
- After mesoderm induction the number of platelets produced per input iPSC was five-fold increased compared to standard conditions.
- Coagulation- and angiogenesis-related proteins were significantly increased or decreased in iPSC-derived compared to adult platelets.
- Based on our improved protocol, efficient iPSC-platelet production will enable identification of molecular mechanisms of platelet-mediated regeneration and pave the way towards providing sufficient amounts of functional platelets for clinical application.

## Mesoderm induction improves human induced pluripotent stem cell-derived megakaryocyte differentiation and platelet production

Linda Krisch[1,2], Gabriele Brachtl[1], Sarah Hochmann[1], André Cronemberger Andrade[1], Patricia Ebner-Peking[1], Michaela Oeller[2], Katharina Schallmoser[2], Dirk Strunk[1]

[1]Cell Therapy Institute, Spinal Cord Injury and Tissue Regeneration Center Salzburg (SCI-TReCS), Paracelsus Medical University, Salzburg, Austria; [2]Department of Transfusion Medicine and SCI-TReCS, Paracelsus Medical University, Salzburg, Austria; Contact: linda.krisch@pmu.ac.at

### Objective
Several protocols have been established to obtain megakaryocytes (MK) and platelets in vitro from induced pluripotent stem cells (iPSC) with limited efficiency. We have previously observed that initial mesoderm induction improved endothelial and mesenchymal stromal differentiation. We therefore hypothesized that an additional mesoderm induction step by bone morphogenetic protein 4 (BMP4), activin A, vascular endothelial growth factor (VEGF) and the GSK-3β kinase inhibitor CHIR99021 priming, prior to hemogenic endothelial cell (HEC) differentiation, might also improve MK progenitor (MKP) production, resulting in an increased platelet output. We further asked if defined basic media compositions affect the final megakaryocyte maturation process.

### Methods
In an iterative process, we first compared HEC induction of two independent human iPSC lines with or without initial mesoderm induction. In a final validation phase, we compared standard conditions without and improved conditions including mesoderm induction, for their platelet production capacity. The function of iPSC-derived platelets derived from standard and mesoderm conditions was compared to adult platelets by measurement of pro-coagulant activity in rotational thromboelastometry and by analysis of angiogenesis-related protein expression.

### Results
We found significantly more efficient HEC differentiation after mesoderm induction resulting in a significant increase of MKPs. MKPs likewise differentiated into mature MKs releasing comparable platelet amounts per input iPSC under all three media conditions tested. Compared to standard conditions, we found a five-fold increase in the number of platelets produced per input iPSC after mesoderm induction (49 ± 14 versus 255 ± 72). Finally, we could show that coagulation- and angiogenesis-related proteins were significantly increased (Angiopoietin 2, Amphiregulin, Tissue Factor, Endoglin, Endostatin, IGFBP2, VEGF) or decreased (Angiogenin, Angiopoietin 1, EGF, PDGF-AB/BB, Serpin F1) in iPSC-derived compared to adult platelets.

### Conclusions
Based on our improved protocol, more efficient iPSC-platelet production will enable identification of molecular mechanisms of platelet-mediated regeneration and pave the way towards providing sufficient amounts of functional platelets for clinical application.

UNIKLINIKUMSALZBURG

# Sarcopenia is an independent predictor for mortality and morbidity in coronary bypass surgery

P.Krombholz-Reindl[1] / A. Winkler[1] / A.Vötsch[1] / J.Steindl[1] / C.Schernthaner[2] / W.Hitzl[3] / R.Seitelberger[1] / R.Gottardi[4]

DEPARTMENT OF CARDIAC SURGERY, VASCULAR SURGERY AND ENDOVASCULAR SURGERY[1], DEPARTMENT OF CARDIOLOGY[2], DEPARTMENT OF OPHTALMOLOGY AND OPTOMETRY[3] PMU SALZBURG, AUSTRIA,
MEDICLIN HEART CENTER, LAHR, GERMANY[4]

## Introduction

The aim of the study was to investigate the potential role of preoperative measurement of thoracic muscle density as a marker for sarcopenia and frailty in patients undergoing coronary bypass surgery.

## Methods

Preoperative CT derived measurements of cross–sectional area and muscle density (Hounsfield units) of 480 consecutive patients undergoing coronary bypass surgery between January 2017 and December 2019 were retrospectively analysed.

The pectoral, intercostal, interspinal, latissimus dorsi and serratus muscles were measured at the level of the 4th thoracic vertebra, the erector spinae muscle at the level of the 12th vertebra on the axial slices on native scans.

The lower quartile of muscle density measurements were defined as sarcopenia. Sarcopenic versus non-sarcopenic patients were compared regarding the 30-day mortality and perioperative morbidity.

## Results

Sarcopenic patients had a significant higher 30 day mortality (4,2% vs. 1,1% p<0.05), more major neurologic events (23,5% vs. 8,6% p<0.01), higher rates of reintubation (8,4% vs. 1,9% p<0.01), acute kidney injury requiring hemodialysis (4,2% vs. 0,6% p<0.01), wound infection (8,4% vs. 1,9% p<0.01) and postoperative atrial fibrillation (37% vs. 18,3% p<0,01). Sarcopenic patients were older (71,5 years vs. 67,6 years p<0.01) but there were no differences regarding preoperative comorbidities (diabetes, chronic obstructive lung disease, hyperlipidemia, peripheral and cerebral vascular disease), preoperative medication, mean Euroscore II and operative characteristics (aortic cross clamp time and perfusion time).

## Conclusion

In our series, preoperative low thoracic muscle density was associated with an increase in perioperative mortality and morbidity in patients undergoing coronary bypass surgery. Measurement of thoracic muscle density is an easy and useful parameter in preoperative risk assessment.

| | Sarcopenic (n=119) | Non-sarcopenic (n=360) | p-value |
|---|---|---|---|
| age (years) | 71,5± 7,8 | 67,6± 9,2 | **p<0.001** |
| male | 63% | 85,3% | **p<0.001** |
| hypertension | 95,8% | 88,3% | p=0.019 |
| smoking | 37,8% | 44,2% | p=0.240 |
| hyperlipidaemia | 87,4% | 88,6% | p=0.742 |
| cAVK | 26,9% | 18,6% | p=0.06 |
| prior stroke | 6,7% | 9,7% | p=0.361 |
| pAVK | 15,1% | 11,4% | p=0.333 |
| diabetes | 38,7% | 33,1% | p=0.268 |
| COPD | 4,6% | 6,7% | p=0.399 |
| kidney failure (mean preOP creatinin mg/dl) | 1,09± 0,6 | 1,07 ± 0,6 | p=0.849 |
| prior myocardial infarction | 31,9% | 34,7% | p=0.655 |
| atrial fibrillation | 11,7% | 7,5% | p=0.184 |
| Euroscore II | 2,6± 2 | 2,7 ± 3,4 | **p=0.852** |

FIG.1 shows baseline characteristics between the groups.

| | Sarcopenic (n=119) | Non-sarcopenic (n=360) | p-value |
|---|---|---|---|
| perfusion-time (min) | 93,5 ± 40,3 | 91,3 ± 43,8 | p=0.597 |
| aortic cross-clamp time (min) | 50,5 ± 23,6 | 49,3 ± 25,2 | p=0.630 |
| on-pump surgery | 93,3% | 91,1% | p=0.567 |
| no. of distal ITA (mean) | 1,3 ± 0,8 | 1,4 ± 0,8 | p=0.273 |
| no. of distal art. graft (mean) | 1,55 ± 0,9 | 1,7 ± 0,9 | p=0.749 |
| no. of distal venous graft (mean) | 1,5 ± 1,1 | 1,2 ± 1,1 | **p=0.020** |

FIG.2 shows operative characteristics between the groups.

| | Sarcopenic n=119 | Non-sarcopenic n=360 | p-value |
|---|---|---|---|
| 30-day mortality | 4,2% | 1,1% | **p<0.05** |
| Major neurologic event (stroke, TIA, severe delir) | 23,5% | 8,6% | **p<0.01** |
| Rate of reintubation | 8,4% | 1,9% | **p<0.01** |
| Acute kidney injury requiring hemodialysis | 4,2% | 0,6% | **p<0.01** |
| Wound infection | 8,4% | 1,9% | **p<0.01** |
| Atrial fibrillation (new onset) | 37% | 18,3% | **p<0.01** |

FIG.3 shows the primary endpoint (30day-mortality) and important clinical outcomes between the groups.

**Contact: Department of Cardiac Surgery, Vascular Surgery and Endovascular Surgery, Landeskrankenhaus Salzburg**
**Ass. Dr. Philipp Krombholz-Reindl, p.krombholz-reindl@salk.at**

## Sarcopenia is an independent predictor for mortality and morbidity in coronary bypass surgery

Philipp Krombholz-Reindl[1], Andreas Winkler[1], Andreas Vötsch[1], Johannes Steindl[1], Christiana Schernthaner[2], Wolfgang Hitzl[3], Rainald Seitelberger[1], Roman Gottardi[4]

[1]Department of Cardiac Surgery, Vascular Surgery and Endovascular Surgery, Paracelsus Medical University, Salzburg, Austria; [2]Department of Cardiology, Paracelsus Medical University, Salzburg, Austria; [3]Department of Ophtalmology and Optometry, Paracelsus Medical University, Salzburg, Austria; [4]Mediclin Heart Center, Lahr, Germany; Contact: p.krombholz-reindl@salk.at

### Objective
The aim of the study was to investigate the potential role of preoperative measurement of thoracic muscle density as a marker for sarcopenia and frailty in patients undergoing coronary bypass surgery.

### Methods
Preoperative CT derived measurements of cross–sectional area and muscle density (Hounsfield units) of 480 consecutive patients undergoing coronary bypass surgery between January 2017 and December 2019 were retrospectively analysed.
The pectoral, intercostal, interspinal, latissimus dorsi and serratus muscles were measured at the level of the 4th thoracic vertebra, the erector spinae muscle at the level of the 12th vertebra on the axial slices on native scans.
The lower quartile of muscle density measurements were defined as sarcopenia. Sarcopenic versus non-sarcopenic patients were compared regarding the 30-day mortality and perioperative morbidity

### Results
Sarcopenic patients had a significant higher 30 day mortality (4,2% vs. 1,1% $p<0.05$), more major neurologic events (23,5% vs. 8,6% $p<0.01$), higher rates of reintubation (8,4% vs. 1,9% $p<0.01$), acute kidney injury requiring hemodialysis (4,2% vs. 0,6% $p<0.01$), wound infection (8,4% vs. 1,9% $p<0.01$) and postoperative atrial fibrillation (37% vs. 18,3% $p<0,01$). Sarcopenic patients were older (71,5 years vs. 67,6 years $p<0.01$) but there were no differences regarding preoperative comorbidities (diabetes, chronic obstructive lung disease, hyperlipidemia, peripheral and cerebral vascular disease), preoperative medication, mean Euroscore II and operative characteristics (aortic cross clamp time and perfusion time).

### Conclusions
In our series, preoperative low thoracic muscle density was associated with an increase in perioperative mortality and morbidity in patients undergoing coronary bypass surgery. Measurement of thoracic muscle density is an easy and useful parameter in preoperative risk assessment.

### References
1. No references

# The relationship of intraspinal to extraspinal disorders in nonidiopathic scoliosis

F. Landauer, K. Trieb

Department of Orthopaedic and Trauma Surgery, Paracelsus Medical University Salzburg

Objective

The outcome of scoliosis corset treatment is influenced by the cause of scoliosis. Idiopathic scoliosis must be differentiated from intraspinal and extraspinal pathologies, which are grouped together as non-idiopathic scoliosis.

A differential history and MRI of the spine should increase the number of non-idiopathic scolioses and modify brace treatment.

Methods

In this retrospective study, 1416 patients with scoliosis were examined after exclusion of obvious neurological diseases. After spine radiography, patients with abnormal lumbar and cervicothoracic curves were offered MRI. Scoliosis-related diagnoses were divided into intraspinal and extraspinal disorders. These data are compared with a previous study without free availability of MRI (n=285).

Results

In the current study, 22.2% (n=315) of patients were diagnosed with non-idiopathic scoliosis; in contrast to our previous study, only 19.3% could be deduced.

Intraspinal disorders 74% (n=233): the most common cause of non-idiopathic scoliosis with intraspinal disorder is malformation 56.2% (n=131). Lumbosacral transition disorder (Castellvi II-IV) accounted for 18.5% (n=43). 31 of the cases could only be confirmed by MRI and 15 patients complain of pain. Spondylolysis/spondylolisthesis could be found in 5.6% (n=13) of patients with pain. In 10.3% (n=24) a wedge vertebra (Cobb angle >10°) could be diagnosed as the vertebral crest. Syringomyelia was diagnosed in 5.2% (n=12) patients. Intraspinal malformation (tumor, neurofibromatosis, eosinophilic granuloma, etc.) was diagnosed in 2.6% (n=6).

Extraspinal disorders 26% (n=82): in 42.7% (n=35) of patients with extraspinal disorder, a syndrome could be identified as the most probable cause (Prader-Willi syndrome, Marfan syndrome, Ehlers-Danlos syndrome, Down syndrome, etc.). Hormonal imbalance, growth hormone treatment as a probable cause of scoliosis was clustered in 14.6% (n=12). Thoracic surgery in early childhood was registered in 23.2% (n=19). Other various diagnoses responsible for scoliosis were found in 19.5% (n=16) such as neurofibromatsis (without intraspinal lesion), CRMO-chronc repetitive multilocal osteomyelitis, spondyloepiphyseal dysplasia or Mazabroud syndrome.

Conclusions

A detailed history and MRI scan are critical to the diagnosis of scoliosis. The availability of MRI increases the number of non-idiopathic (symptomatic) scolioses. Consequently, the results are important for the indication and goal of brace treatment.

## The relationship of intraspinal to extraspinal disorders in nonidiopathic scoliosis

Franz Landauer[1], Klemens Trieb[1]

[1]Department of Orthopaedic and Trauma Surgery, Paracelsus Medical University Salzburg, Austria; Contact: F.landauer@salk.at

### Objective
The outcome of scoliosis corset treatment is influenced by the cause of scoliosis. Idiopathic scoliosis must be differentiated from intraspinal and extraspinal pathologies, which are grouped together as non-idiopathic scoliosis. A differential history and MRI of the spine should increase the number of non-idiopathic scolioses and modify brace treatment.

### Methods
In this retrospective study, 1416 patients with scoliosis were examined after exclusion of obvious neurological diseases. After spine radiography, patients with abnormal lumbar and cervicothoracic curves were offered MRI. Scoliosis-related diagnoses were divided into intraspinal and extraspinal disorders. These data are compared with a previous study without free availability of MRI (n=285).

### Results
In the current study, 22.2% (n=315) of patients were diagnosed with non-idiopathic scoliosis; in contrast to our previous study, only 19.3% could be deduced.
Intraspinal disorders 74% (n=233): the most common cause of non-idiopathic scoliosis with intraspinal disorder is malformation 56.2% (n=131). Lumbosacral transition disorder (Castellvi II-IV) accounted for 18.5% (n=43). 31 of the cases could only be confirmed by MRI and 15 patients complain of pain. Spondylolysis/spondylolisthesis could be found in 5.6% (n=13) of patients with pain. In 10.3% (n=24) a wedge vertebra (Cobb angle >10°) could be diagnosed as the vertebral crest. Syringomyelia was diagnosed in 5.2% (n=12) patients. Intraspinal malformation (tumor, neurofibromatosis, eosinophilic granuloma, etc.) was diagnosed in 2.6% (n=6).
Extraspinal disorders 26% (n=82): in 42.7% (n=35) of patients with extraspinal disorder, a syndrome could be identified as the most probable cause (Prader-Willi syndrome, Marfan syndrome, Ehlers-Danlos syndrome, Down syndrome, etc.). Hormonal imbalance, growth hormone treatment as a probable cause of scoliosis was clustered in 14.6% (n=12). Thoracic surgery in early childhood was registered in 23.2% (n=19). Other various diagnoses responsible for scoliosis were found in 19.5% (n=16) such as neurofibromatsis (without intraspinal lesion), CRMO-chronc repetitive multilocal osteomyelitis, spondyloepiphyseal dysplasia or Mazabroud syndrome.

### Conclusions
A detailed history and MRI scan are critical to the diagnosis of scoliosis. The availability of MRI increases the number of non-idiopathic (symptomatic) scolioses. Consequently, the results are important for the indication and goal of brace treatment.

The incidence of lumbo sacral transitional vertebra in scoliosis

Franz Landauer, Klemens Trieb

Department of Orthopaedic and Trauma Surgery, Paracelsus Medical University Salzburg

Objectives: Euler's buckling mode theory states that the curvature of a flexible column depends on how it is fixed. This leads to the hypothesis that lumbar transition disorders result in a particular form of scoliosis. Therefore, in the presence of a lumbo sacral transitional vertebra (LSTV), correction of lumbar scoliosis should follow a consistent curvature pattern.

Methods: In this retrospective study, 85 patients (63 female and 22 male) with known LSTV were followed-up from MRI or CT images. The MRI and CT images were assigned according to the Castellvi classification. 22 patients were not included because of scoliosis less than 20° Cobb angle. 63 patients aged 10-45 years with scoliosis over 20° Cobb angle already in adolescence were followed up. Curvature was differentiated into lumbar, thoracolumbar, and thoracic curves and compared in relation to the Castellvi classification. Corset treatment and lumbar pain were queried in the medical history.

Results: Castellvi classification showed the following distribution: IA n=2, IIA n=41, IIB n=16, IIIA n=11, IIIB n=11, IV n=4 patients.

The curve shape was different with thoracolumbar 33, lumbar 17 and thoracic in 13 patients. 41 of the patients complained of low back pain.

Corset treatment was performed in 20 patients given indication, Cobb angle was 35.3+/-12.5° at baseline, 8 of them developed more than 5° Cobb angle and 2 reached indication for scoliosis surgery (>45° Cobb angle). The remaining 43 patients had no indication for brace treatment (too old) or refused it. Another 3 patients had an appointment because of low back pain after scoliosis surgery several years ago and undiagnosed LSTV. 2 patients were diagnosed with LSTV and required surgery for low back pain. Only 1 patient with a thoracic curve had severe low back pain. The incidence of LSTV in our patient population was 6% (85/1416).

High concordance was found with the asymmetric shape of LSTV (n=63) and the orientation of the curve (e.g., LSTV with left deviation and left convex lumbar or thoracolumbar curve and vice versa). Only 3 cases showed bilateral malformation in lumbar curves. Thoracic curves always had bilateral malformation.

Conclusions: Patients with lumbar and thoracolumbar scoliosis and low back pain are suspicious for LSTV. MRI in all three levels is necessary to detect LSTV. The indication for brace treatment without this clarification should be critically evaluated.

## The incidence of lumbo sacral transitional vertebra in scoliosis

Franz Landauer[1], Klemens Trieb[1]

[1]Department of Orthopaedic and Trauma Surgery, Paracelsus Medical University Salzburg, Austria; Contact: f.landauer@alk.at

### Objective
Euler's buckling mode theory states that the curvature of a flexible column depends on how it is fixed. This leads to the hypothesis that lumbar transition disorders result in a particular form of scoliosis. Therefore, in the presence of a lumbo sacral transitional vertebra (LSTV), correction of lumbar scoliosis should follow a consistent curvature pattern.

### Methods
In this retrospective study, 85 patients (63 female and 22 male) with known LSTV were followed-up from MRI or CT images. The MRI and CT images were assigned according to the Castellvi classification. 22 patients were not included because of scoliosis less than 20° Cobb angle. 63 patients aged 10-45 years with scoliosis over 20° Cobb angle already in adolescence were followed up. Curvature was differentiated into lumbar, thoracolumbar, and thoracic curves and compared in relation to the Castellvi classification. Corset treatment and lumbar pain were queried in the medical history.

### Results
Castellvi classification showed the following distribution: IA n=2, IIA n=41, IIB n=16, IIIA n=11, IIIB n=11, IV n=4 patients.
The curve shape was different with thoracolumbar 33, lumbar 17 and thoracic in 13 patients. 41 of the patients complained of low back pain.
Corset treatment was performed in 20 patients given indication, Cobb angle was 35.3+/-12.5° at baseline, 8 of them developed more than 5° Cobb angle and 2 reached indication for scoliosis surgery (>45° Cobb angle). The remaining 43 patients had no indication for brace treatment (too old) or refused it. Another 3 patients had an appointment because of low back pain after scoliosis surgery several years ago and undiagnosed LSTV. 2 patients were diagnosed with LSTV and required surgery for low back pain. Only 1 patient with a thoracic curve had severe low back pain. The incidence of LSTV in our patient population was 6% (85/1416).
High concordance was found with the asymmetric shape of LSTV (n=63) and the orientation of the curve (e.g., LSTV with left deviation and left convex lumbar or thoracolumbar curve and vice versa). Only 3 cases showed bilateral malformation in lumbar curves. Thoracic curves always had bilateral malformation.

### Conclusions
Patients with lumbar and thoracolumbar scoliosis and low back pain are suspicious for LSTV. MRI in all three levels is necessary to detect LSTV. The indication for brace treatment without this clarification should be critically evaluated.

# Upregulation of mitotic bookmarking transcription factors may induce enhanced proliferation of human stromal cells by human platelet lysate

S. Laner-Plamberger[1,2*], M. Oeller[1,2*], C. Mrazek[3], A. Hartl[4], E. Rohde[1,2], D. Strunk[2,5] & K. Schallmoser[1,2]

[1] Department of Transfusion Medicine,
[2] Spinal Cord Injury and Tissue Regeneration Center Salzburg,
[3] Department of Laboratory Medicine, [4] Institute of Biomedicine, [5] Cell Therapy Institute
Paracelsus Medical University, Salzburg, Austria
[*] equal contribution

PARACELSUS MEDIZINISCHE PRIVATUNIVERSITÄT — UNIKLINIKUM SALZBURG

## Objective

Due to abundant growth factors, pooled human platelet lysate (pHPL) is an efficient human alternative for fetal bovine serum (FBS) significantly enhancing stromal cell (STC) proliferation. However, the lack of standardized production hampers the comparability of pHPL-products (*Schallmoser K et al., Trends Biotechnol. 2020*) and the effect of pHPL-based factors on cellular behaviour is still not fully understood. In this study, three different pHPL-preparations for cultivation of STCs from three different sources (bone marrow, white adipose tissue and umbilical cord) were compared with FBS: Standard pHPL-medium, fibrinogen-depleted serum-converted pHPLS- and mechanically fibrinogen-depleted pHPL-medium. Media were analyzed for biochemical parameters and growth factor/cytokine content. Stromal cells cultured in different pHPL media and FBS were compared regarding immunophenotype, *in vitro* differentiation potential, proliferation and clonogenic capacity. Furthermore, the mRNA expression levels of the transcription factors SOX2, cMYC, NANOG, OCT4 and KLF4, also known as mitotic bookmarking factors, were investigated in all pHPL- compared to FBS-media. As these factors are supposed to enable a quick re-entry to the cell cycle, this may explain the superiority of human platelet factors for efficient STC proliferation compared to FBS, pathing the way for new chemically defined ideal cell culture media for stromal cell based medicinal products (*Laner-Plamberger et al., J Transl Med. 2019*).

## 1. Experimental Setup

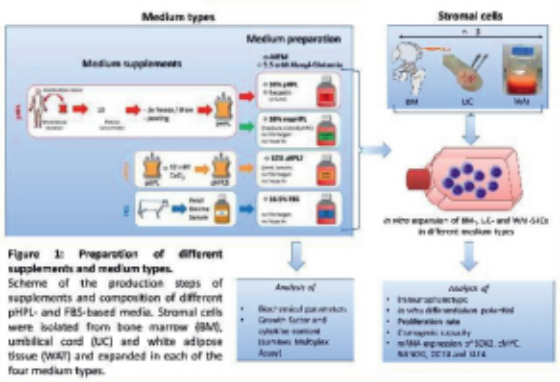


**Figure 1: Preparation of different supplements and medium types.** Scheme of the production steps of supplements and composition of different pHPL- and FBS-based media. Stromal cells were isolated from bone marrow (BM), umbilical cord (UC) and white adipose tissue (WAT) and expanded in each of the four medium types.

## 2. Biochemical and Growth Factor/Cytokine Analysis of HPL-based Media

| Table 1 | Supplements | | | | Medium | Medium supplemented with | | | |
|---|---|---|---|---|---|---|---|---|---|
| | pHPL | pHPLS | FBS | Standard blood values | α-MEM | pHPL (10%) | pHPLS (10%) | mcpHPL (10%) | FBS (10.5%) |
| pH | | | | | | | | | |
| Osmolality [mosmol/kg] | | | | | | | | | |
| Total Protein [g/dl] | | | | | | | | | |
| Albumin [g/L] | | | | | | | | | |
| Glucose [mg/dL] | | | | | | | | | |
| Fibrinogen [mg/dl] | | | | | | | | | |
| Triglyceride [mg/dl] | | | | | | | | | |
| Cholesterol [mg/dl] | | | | | | | | | |
| $Na^+$ [mmol/L] | | | | | | | | | |
| $K^+$ [mmol/L] | | | | | | | | | |
| Ca [mmol/L] | | | | | | | | | |
| $Ca^{2+}$ [mmol/L] | | | | | | | | | |
| $Mg^{2+}$ [mmol/L] | | | | | | | | | |
| $Fe^{2+}$ [µmol/L] | | | | | | | | | |

**Table 1: Biochemical analysis of supplements and medium types.** All pHPL preparations showed significantly increased levels for total protein, albumin, glucose, cholesterol and $Na^+$ compared to FBS, while $K^+$ and $Fe^{2+}$ were significantly reduced. Parameter concentrations tested in pHPL, pHPLS (10 lots each) and FBS (6 lots) compared to standard human blood values as well as basic α-MEM and α-MEM supplemented with 10% pHPL, pHPLs and mcpHPL or 10.5% FBS are compared in the table shown. Data are shown as mean ± SD; n.d., not detected. pHPL vs. pHPLS: $^{\#\#\#}p < 0.001$; pHPL or pHPLS vs. FBS: $^{*}p < 0.05$, $^{***}p < 0.001$; Media: pHPL-media vs. FBS-medium: $^{*}p < 0.05$, $^{**}p < 0.01$ and $^{***}p < 0.001$.

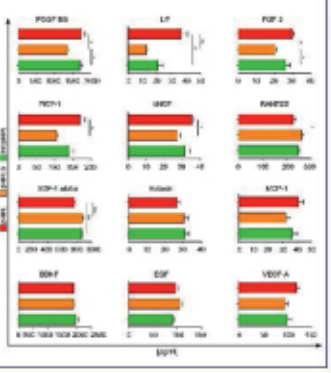


**Figure 2: Fibrinogen depletion impacts growth factor and cytokine content.** Concentration of cytokines and growth factors in pHPL-, pHPLS- and mcpHPL-supplemented medium analyzed by multiplex analysis. Data are shown as mean of three individual pHPL batches measured in duplicates ± SD ($^{*}p < 0.05$, $^{**}p < 0.01$, $^{***}p < 0.001$ compared to pHPL medium).

## 3. Immunophenotype and *in vitro* Differentiation Potential of Stromal Cells Are Independent of Culture Conditions

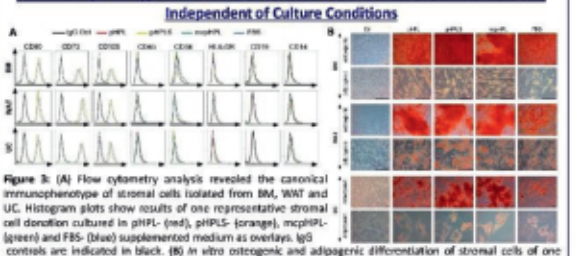


**Figure 3:** (**A**) Flow cytometry analysis revealed the canonical immunophenotype of stromal cells isolated from BM, WAT and UC. Histogram plots show results of one representative stromal cell donation cultured in pHPL- (red), pHPLS- (orange), mcpHPL- (green) and FBS- (blue) supplemented medium as overlays. IgG controls are indicated in black. (**B**) *In vitro* osteogenic and adipogenic differentiation of stromal cells of one representative donor in different culture media are shown. Total magnification 40x for osteogenic differentiation and corresponding control (staining: Alizarin Red), 200x for adipogenic differentiation and control (staining: Sudan III). Scale bars: 100 µm.

## 4. Proliferation Capacity Is Enhanced for Different Stromal Cells in pHPL-based Media Compared to FBS-supplemented Medium

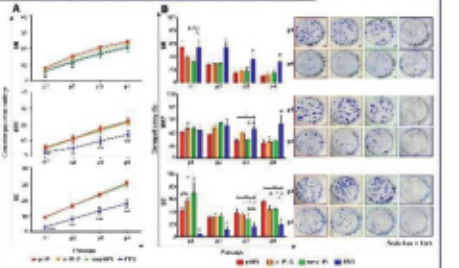


**Figure 4:** (**A**) Proliferative capacity of stromal cells expanded in either pHPL- (red), pHPLS- (orange) or mcpHPL- (green) compared to FBS- (blue) medium. UC- and WAT-STCs showed significantly enhanced proliferation. Data are shown as cumulative population doublings (cPD) of three independent donations for each tissue source tested in duplicates ± SD ($^{*}p < 0.05$ comparing pHPL/pHPLS to FBS-supplementation; $^{*}p < 0.05$, $^{**}p < 0.01$, $^{***}p < 0.001$, all pHPL-media compared to FBS-supplementation). (**B**) Cloning efficiency (%) of BM-, WAT- and UC-STCs over four passages in different pHPL- and FBS-supplemented media. Clonogenicity was comparable to FBS in BM- and WAT-STCs and enhanced in UC-derived STCs cultured with HPL. Data are presented as mean of triplicates ± SD ($^{*}p < 0.05$, $^{**}p < 0.01$, $^{***}p < 0.001$, $^{\#}p < 0.05$ in comparison to all other groups). Representative photographs of colony forming units are shown for p1 and p4.

## 5. mRNA Expression of Mitotic Bookmarking Factors SOX2, KLF4 and cMYC Is Augmented in pHPL-based Culture Conditions

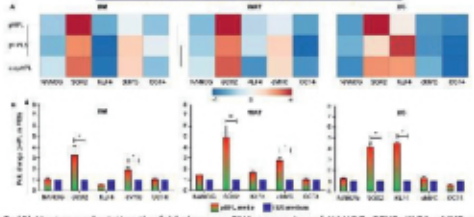


**Figure 5:** (**A**) Heat map depicting the fold change mRNA expression of NANOG, SOX2, KLF4, cMYC and OCT4 in stromal cells cultivated in pHPL-, pHPLS- and mcpHPL-based medium with red color indicating up- and blue color downregulation compared to FBS medium. (**B**) mRNA expression in BM-, WAT- and UC-derived stromal cells cultured in pHPL-based media (summarized as red/orange/green bar) compared to FBS (blue bar). Data shown are mean fold change values of three individual donors measured in duplicates ($^{*}p < 0.05$, $^{**}p < 0.01$).

## 6. Summary & Conclusion

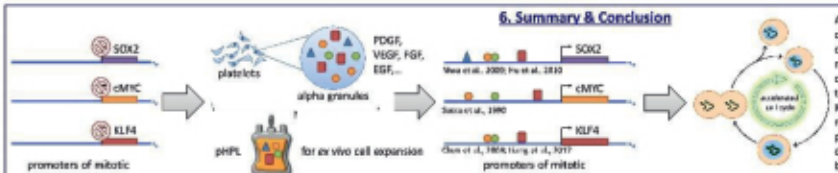


Although fibrinogen depletion of pHPL affected the growth factor concentration of the supplemented media, cell proliferation, clonogenicity and *in vitro* differentiation of stromal cells was well maintained. Irrespective of the preparation mode, pHPL-based culture media significantly enhanced the mRNA expression of the transcription and mitotic bookmarking factors SOX2, cMYC and KLF4. HPL-borne growth factors may stimulate the expression of mitotic bookmarking factors, thereby allocating a growth promoting stimulus. Our data indicate, that the supportive effect of pHPL for stromal cell proliferation might in part be explained by the enhanced expression of mitotic bookmarking factors that allow an accelerated re-entry to the cell cycle.

s.laner-plamberger@salk.at

## Upregulation of mitotic bookmarking transcription factors may induce enhanced proliferation of human stromal cells by human platelet lysate

Sandra Laner-Plamberger[1,2], Michaela Oeller[1,2], Cornelia Mrazek[3], Arnulf Hartl[4], Eva Rohde[1,2], Dirk Strunk[5], Katharina Schallmoser[1,2]

[1]Department of Transfusion Medicine, Paracelsus Medical University, Salzburg, Austria; [2]Spinal Cord Injury and Tissue Regeneration Center Salzburg, Paracelsus Medical University, Salzburg, Austria; [3]Department of Laboratory Medicine, Paracelsus Medical University, Salzburg, Austria; [4]Institute of Ecomedicine, Paracelsus Medical University, Salzburg, Austria; [5]Cell Therapy Institute, Paracelsus Medical University, Salzburg, Austria; Contact: s.laner-plamberger@salk.at

### Objective
For clinical cell manufacturing pooled human platelet lysate (pHPL) is increasingly used as efficient alternative for fetal bovine serum (FBS). However, the effect of platelet derived factors on stromal cell biology is still not fully understood and the lack of standardized production may hamper comparability of cell products.
Aim of this study was to compare the biochemical composition of FBS, pHPL and supplemented media and to analyse the influence on human stromal cells from different source tissues. Furthermore, the mRNA expression of distinct mitotic bookmarking factors involved in cell cycle progression was investigated.

### Methods
Biochemical parameters and growth factor/cytokine content of FBS, three different pHPL preparations (standard pHPL, fibrinogen-depleted serum-converted pHPLS and mechanically fibrinogen-depleted pHPL-medium) and supplemented media were compared. Immunophenotype, proliferation rates, colony forming capacity and trilineage in vitro differentiation potential were determined for stromal cells from bone marrow (BM), white adipose tissue (WAT) and umbilical cord (UC). RTQ-PCR was used to investigate the expression levels of selected target genes (cMYC, SOX2 and KLF4), known to act as mitotic bookmarking factors.

### Results
While total protein, glucose, cholesterol and Na+ were significantly elevated in pHPL preparations, $K^+$ and $Fe^{3+}$ levels were significantly higher in FBS. Multiplex analysis of pHPL-based media revealed maintenance of growth factors and cytokines after fibrinogen-depletion. All pHPL-based media significantly enhanced cell proliferation and clonogenicity compared to FBS, while immunophenotype and in vitro differentiation potential were unaffected. Compared to FBS, the expression of SOX2 was significantly higher in all stromal cell types after pHPL-culture, whereas we observed a significant increase of cMYC expression in BM- and WAT-stromal cells, and of KLF4 expression in UC-stromal cells.

### Conclusions
The characterization of varying pHPL preparations may help to standardize animal serum-free culture media used for stromal cell-based products. Compared to FBS, all pHPL-supplemented media significantly increased the cell proliferation rate, and enhanced the expression of the mitotic bookmarking factors SOX2, cMYC and KLF4, enabling an accelerated re-entry to the cell cycle (1).

### References
1. Laner-Plamberger S., Oeller M. et al., J Transl Med. 2019 Dec 30;17(1):432

PARACELSUS MEDIZINISCHE PRIVATUNIVERSITÄT

Klinikum Nürnberg
wir sind für Sie da!

# Individualized target fortification of breast milk with protein, carbohydrates, and fat for preterm infants - Neurodevelopmental outcomes

**Nicolas Leier[1], Niels Rochow[1,2], Gerhard Fusch[2], Hon Yiu So[3], Salhab el Helou[2], Christoph Fusch[1,2]**

[1]Pediatrics, Paracelsus Medical University, Nuremberg; [2]Pediatrics, McMaster University, Hamilton, Canada; [3]Statistics, University of Waterloo, Canada

## INTRODUCTION

- Premature infants spend most of last trimester ex-utero - a time crucial for the growth and maturation of the brain.
- It has been shown that improved substrate delivery leads to a higher growth rate and improved neurodevelopment.
- Standard Fortification (SF) adds a fixed dose of commercial fortifier to breast milk aiming to meet nutritional requirements of the fast-growing preterm infants.
- However, it had been shown that breast milk has high natural variation leading to growth restriction in more than 50 % preterm infants receiving SF.
- Target Fortification (TFO) measures all three macronutrients of the breast milk and adds modular protein, lipids, and carbohydrates after adding a standard fortifier.
- Thereby it assures that preterm infants receive a diet according to ESPGHAN recommendations instead of feeding milk of random composition.




## OBJECTIVES

- To investigate the impact of TFO on neurodevelopmental outcome at 18-month follow-up compared to SF.

## METHODS

- This follow-up study of a prospective, single-center, double-blind RCT with n=103 preterm infants <30 weeks of gestation assessed the neurodevelopmental outcome of 69 preterm infants at 18 months corrected age.
- They were fed either standard or target fortified breast milk during 21 days of intervention to be completed prior to 36 weeks postmenstrual age (PMA).
- The control group received standard fortification (SF), the intervention group received TFO with individual addition of modular carbs, protein and fat based on breast milk analysis done three times per week.
- The neurodevelopmental outcome was evaluated with the Bayley Scales of Infant Development-III (BSID-III) at 18 months.

## RESULTS

- 69 preterm infants received a BSID-III assessment.
- The TFO intervention group had a significantly higher average intake of fat, lactose and protein and a significantly higher protein-to-energy ratio.
- The neurodevelopmental assessment with Bayley-III at 18 months showed higher cognitive, language and motor scores in the intervention group compared to the control group but did not reach 0.05 significance level (Tab 1).
- The number of infants with low BSID-III scores (<85) was less in the TFO group (n=3) compared to the SF group (n=8).

## RESULTS

Tab. 1: Neurodevelopmental outcomes

| Bayley Score | Control (n=35) | Intervention (n=34) | Mean difference [95% CI] | p-value |
|---|---|---|---|---|
| **Cognitive** | 95.7 ± 13.0 | 99.3 ± 11.6 | 3.6 [-9.5, 2.4] | .235 |
| **Language** | 87.4 ± 16.7 | 90.1 ± 14.8 | 2.7 [-10.7, 5.2] | .497 |
| - receptive | 92.3 ± 15.3 | 93.9 ± 16.3 | 1.6 [-9.5, 6.3] | .694 |
| - expressive | 84.8 ± 14.6 | 88.3 ± 10.7 | 3.4 [-9.9, 3.0] | .289 |
| **Motor** | 93.0 ± 12.8 | 94.8 ± 9.2 | 1.8 [-7.2, 3.6] | .501 |
| - fine | 97.3 ± 11.0 | 98.4 ± 10.6 | 1.1 [-6.4, 4.2] | .676 |
| - gross | 89.2 ± 12.9 | 92.2 ± 9.4 | 3.0 [-8.5, 2.5] | .286 |

- Subgroup analysis showed differences between short- and long-term outcomes.

**Short-term outcome:**

- Infants of mothers with low protein in the native breast milk in the control group showed lowest weight at 36 weeks PMA.

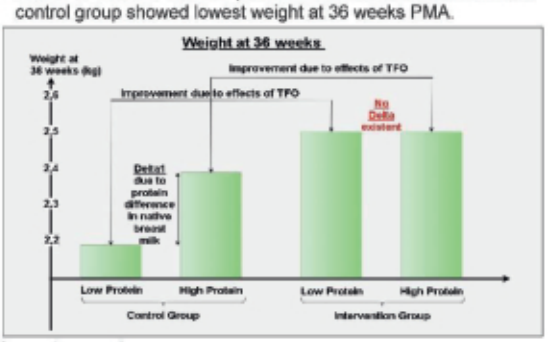


**Long-term outcome:**

- Infants of mothers with low protein content had lower neurodevelopmental outcome.

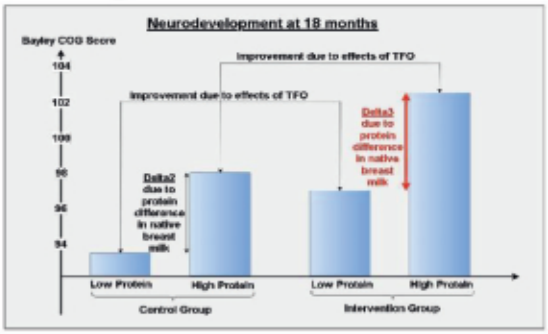


## CONCLUSION

- A trend towards improved neurodevelopment can be assumed, despite results not being statistically significant.
- TFO seems to reduce the number of infants at risk for severe neurodevelopmental impairment.
- Post discharge fortification may improve neurodevelopment.
- Multicenter studies are needed to increase the statistical power.

Christoph Fusch, MD, PhD, Pediatrics, Paracelsus Medical University, christoph.fusch@klinikum-nuernberg.de

## Individualized target fortification of breast milk with protein, carbohydrates, and fat for preterm infants - Neurodevelopmental outcomes

Nicolas Leier[1], Niels Rochow[1,2], Gerhard Fusch[2], Hon Yiu So[3], Salhab el Helou[2], Christoph Fusch[1,2]

[1]Pediatrics, Paracelsus Medical University, Nuremberg; [2]Pediatrics, McMaster University, Hamilton, Canada; [3]Statistics, University of Waterloo, Canada; Contact: nicolas.leier1@gmail.com

### Objective
To investigate the impact of Target Fortification (TFO) on neurodevelopmental outcome at 18-month follow-up compared to Standard Fortification (SF) in preterm infants.

### Methods
This follow-up study of a prospective, single-center, double-blind RCT with n=103 preterm infants <30 weeks of gestation assessed the neurodevelopmental outcome of 69 preterm infants at 18 months corrected age. They were fed either standard or target fortified breast milk during 21 days of intervention to be completed prior to 36 weeks postmenstrual age (PMA). The control group received standard fortification, the intervention group received TFO with individual addition of modular carbs, protein and fat based on breast milk analysis done three times per week. The neurodevelopmental outcome was evaluated with the Bayley Scales of Infant Development-III (BSID-III) at 18 months.

### Results
69 preterm infants received a BSID-III assessment. The TFO intervention group had a significantly higher average intake of fat, lactose and protein and a significantly higher protein-to-energy ratio. The neurodevelopmental assessment with Bayley-III at 18 months showed higher cognitive, language and motor scores in the intervention group compared to the control group but did not reach 0.05 significance level. The number of infants with low BSID-III scores (<85) was less in the TFO group (n=3) compared to the SF group (n=8). Subgroup analysis showed differences between short-and long-term outcomes. Short-term outcome: Infants of mothers with low protein in the native breast milk in the control group showed lowest weight at 36 weeks PMA. Long-term outcome: Infants of mothers with low protein content in the control and in the intervention group had lower neurodevelopmental outcomes than infants of mothers with high protein content in the native breast milk.

### Conclusions
- A trend towards improved neurodevelopment can be assumed, despite results not being statistically significant.
- TFO seems to reduce the number of infants at risk for severe neurodevelopmental impairment.
- Post discharge fortification may improve neurodevelopment.
- Multicenter studies are needed to increase the statistical power.

Klinikum Nürnberg
PARACELSUS MEDIZINISCHE PRIVATUNIVERSITÄT

# Intraoperative hemoadsorption reduces sepsis-related death in all-comers undergoing surgery for infective left-sided endocarditis

S Leiler[1], JM Kalisnik[1], H Mamdooh[1], T Bertsch[2], J Zibert[3], J Sirch[1], M Fittkau[1], Theodor Fischlein[1]

[1] Department of Cardiac Surgery - Paracelsus Medical University Nuremberg, Germany
[2] Institute of Clinical Chemistry, Laboratory Medicine and Transfusion Medicine - Paracelsus Medical University Nuremberg, Germany
[3] Faculty of Health Sciences – University of Ljubljana, Slovenia

**Introduction:** Cardiac surgery in patients with infective endocarditis (IE) is associated with high mortality up to 50%. Most patients with IE are affected by a systemic inflammatory response caused by the disease itself as well as the artificial cardiopulmonary bypass (CPB). Postoperative septic multi-organ failure remains an important factor of mortality, even after curative successful surgery. Hemoadsorption (HA) therapy may improve surgical outcomes by reducing the circulating cytokines.

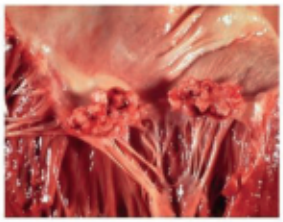

Fig. 1 Infective Endocarditis

**Objective:**

- to assess the efficacy of intraoperative HA in the clinical outcome in patients with left-sided IE of the native or prosthetic valve

**Methods:** 195 patients with confirmed left-sided acute infective (IE) of the native or prosthetic valve and urgent indication for surgery were enrolled in the study. All patients underwent surgery consisting of extensive debridement and predominantly replacement of the affected valve(s) between January 2015 and March 2021. Two cohorts were generated according to the actual standard of care at the department in retrospective, sequential design. The first cohort included 101 patients who underwent surgery without intraoperative HA. The second cohort consisted of 94 patients where HA took place and CytoSorb (Cytosorbents, Monmouth Junction, NJ) adsorber cartridge was installed into the CPB for its entire duration. The end points were the incidence of postoperative sepsis, sepsis-associated death, 3-day and 30-day mortality. Furthermore, postoperative laboratory values were evaluated.

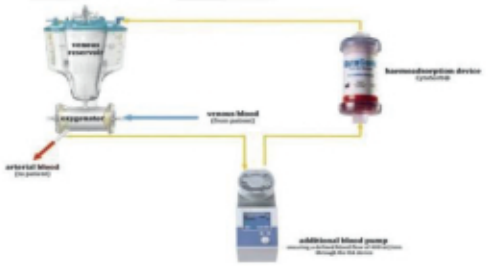

Fig. 2 Integration of the haemoadsorption filter into the cardiopulmonary bypass (CPB) circuit: oxygenated blood is taken from the oxygenator of the CPB, and an additional blood pump ensures a defined blood flow of 500 mL/min through the adsorber to the venous reservoir of the CPB.

**Results:**

| Parameter | HA_NO n=101 | HA_YES n=94 | p-value |
|---|---|---|---|
| Age (years ) | 69 (57.0; 76.0) | 68 (57.2;75.0) | 0.622 |
| Sex distribution (% male) | 81 | 75 | 1.000 |
| EuroSCORE II | 8.4 (3.5;19.7) | 9.9 (5.2;21.8) | 0.540 |
| Leucocytes preoperatively ($x10^{-6}$/mcL) | 9.0 (7.2;13,5) | 8.3 (6.2;12.9) | 0.156 |
| Platelets preoperatively ($x10^{-3}$/mcL) | 237 (164;300) | 236 (164;298) | 0.903 |
| CRP* preoperatively (mg/dl) | 5.9 (3.0;10.8) | 5.9 (2.2;10.3) | 0.577 |
| Hb* preoperatively (g/dl) | 10.2 (9.1;11.3) | 10.1 (9.1;11.5) | 0.856 |
| LDH* preoperatively | 292 (237;370) | 292 (253;414) | 0.626 |
| Endocarditis of 2 valves (%) | 14 | 10 | 0.263 |
| Periprosthetic Endocarditis (%) | 28 | 41 | 0.149 |

| Parameter | HA_NO n=101 | HA_YES n=94 | p-value |
|---|---|---|---|
| **Sepsis related death (%)** | **20** | **7,5** | **0.021** |
| 3-day mortality (%) | 13.9 | 6.4 | 0.138 |
| 30-day mortality (%) | 20.8 | 13.8 | 0.275 |
| **Hb at arrival to ICU (g/dl)** | **10.2 (9.2;11.0)** | **10.9 (10.1;11.8)** | **0.001** |
| **Hb: POD 1 (g/dl)** | **9.2 (8.5;9.9)** | **9.7 (8.7;10.2)** | **0.044** |
| **CRP: POD 1 (mg/dl)** | **9.8 (7.0;15.1)** | **8.8 (5.0;11.9)** | **0.019** |
| **Leucocytes: POD 2 ($x10^{-6}$/mcL)** | **11.7 (8.7;15.0)** | **9.8 (7.4;14.0)** | **0.033** |
| **Thrombocytes: POD 1 ($x10^{-3}$/mcL)** | **177 (125;236)** | **141 (114;204)** | **0.021** |
| **Thrombocytes: POD 2 ($x10^{-3}$/mcL)** | **168 (124;225)** | **134 (102;196)** | **0.041** |

The results are reported as Median (lower; upper quartile) in non-normally distributed and as Mean (± Standard Deviation) in normally distributed data. *CRP: C-reactive protein; Hb: Haemoglobin; LDH: Lactic dehydrogenase; POD: postoperative day

**Conclusions:** Treatment was well tolerated and safe. Intraoperative HA reduced sepsis related death, CRP and leucocyte levels after IE surgery. Trends towards reduced 3- and 30-day mortality have been observed, however without reaching statistical significance. The net-effect of significantly higher early haemoglobin concentrations parallelly with decreased thrombocyte counts seem not to have affected the clinical outcomes across the groups. Finally, the data suggest that intraoperative HA improves surgical outcomes in all-comers for left-sided IE.

© Paracelsus Medizinische Privatuniversität Nürnberg – Universitätsklinik für Herzchirurgie

## Intraoperative hemoadsorption reduces sepsis-related death in all-comers undergoing surgery for infective left-sided endocarditis

Špela Leiler[1], Jurij M Kališnik[1], Hazem Mamdooh[1], Thomas Bertsch[2], Janez Žibert[3], Joachim Sirch[1], Matthias Fittkau[1], Theodor Fischlein[1]

[1]Department of Cardiac Surgery - Paracelsus Medical University, Nuremberg, Germany; [2]Institute of Clinical Chemistry, Laboratory Medicine and Transfusion Medicine - Paracelsus Medical University, Nuremberg, Germany; [3]Faculty of Health Sciences – University of Ljubljana, Slovenia; Contact: spela.leiler@klinikum-nuernerg.de

### Objective
Cardiac surgery in patients with infective endocarditis (IE) is associated with high mortality up to 50%. Most patients with IE are affected by a systemic inflammatory response caused by the disease itself as well as the artificial cardiopulmonary bypass (CPB). Postoperative septic multi-organ failure remains an important factor of mortality, even after curative successful surgery. Hemoadsorption (HA) therapy may improve surgical outcomes by reducing the circulating cytokines. The objective of this study was to assess the efficacy of intraoperative HA in patients with left-sided IE, including prosthetic valve endocarditis.

### Methods
195 patients with confirmed left-sided acute IE of the native valve or prosthetic valve and urgent indication for surgery were enrolled in the study. All patients underwent cardiac surgery consisting of extensive debridement and predominantly replacement of the affected valve(s) between January 2015 and March 2021. Two cohorts were generated according to the actual standard of care at the department in retrospective, sequential design. The first cohort (Control) included 101 patients who underwent surgery without intraoperative HA. The second cohort (HA) consisted of 94 patients where HA has been applied with CytoSorb (Cytosorbents, Monmouth Junction, NJ) adsorber cartridge having had been installed into the CPB for its entire duration. The end points were the incidence of sepsis related death, 3- and 30-day mortality. In addition, routine postoperative laboratory values were evaluated.

### Results
Patients' preoperative characteristics, such as age, comorbidities and laboratory values were comparable between the two groups. Sepsis related death was more common in the control group (HA vs. control: 7,5 vs. 20%, p = 0.021). 3-day and 30-day mortality did not reach statistical significance, however trends in differences between the 2 groups could be observed (HA vs. control: 6,4 vs. 13,9%, p= 0.138) and (HA vs. control: 20,8 vs. 13,8%, p = 0.275) respectively. CRP concentration was higher in the control group; 9,8 and 8,8 g/dl in the HA group, p= 0,019. Leucocyte count was significantly higher in the control group on the second postoperative day (HA vs. Control: 9,8 vs. 11,7 x10-6/mcL), p= 0,033). Platelet count was higher in the control group 177 vs. 141 x10-3/mcL (p= 0,021) and haemoglobin concentration was lower in the control group (HA vs. Control: 10,2 vs. 10,9 g/dL, p= 0,001) on the first postoperative day.

### Conclusions
Treatment was well tolerated and safe. Intraoperative HA reduced sepsis related death, CRP and leucocyte levels after IE surgery. Trends towards reduced 3- and 30-day mortality have been observed, however without reaching statistical significance. The net-effect of significantly higher early haemoglobin concentrations parallelly with decreased thrombocyte counts seemingly has not affected clinical outcomes across the groups. To sum up, our data suggest that intraoperative hemoadsorption improves surgical outcomes in all-comers for left-sided IE.

# Serum levels of GFAP and NfL are related to the neurological impairment and spinal edema after spinal cord injury

Iris Leister [1,2,3,4], Ludwig Aigner [1,2,3,4,5,*], Barbara Altendorfer [3,4], Doris Maier [1,2], Orpheus Mach [1,2], Christof Wutte [6,7], Andreas Grillhösl [8], Angel Arevalo-Martin [9], Daniel Garcia-Ovejero [9], Lukas Grassner [1,2,3,4,10]

PARACELSUS MEDIZINISCHE PRIVATUNIVERSITÄT · ParaMove · BGU Murnau Berufsgenossenschaftliche Unfallklinik Murnau, SCI Research Unit · HOSPITAL NACIONAL DE PARAPLÉJICOS Toledo

## Background

Neurological examination in the very acute phase after spinal cord injury (SCI) is often impossible and severely confounded by pharmacological sedation, or concomitant injuries. Therefore, diagnostic biomarkers that objectively characterize injury severity, or the mere presence of SCI are urgently needed to facilitate clinical decision-making in the very early post-injury phase.

This study aims to determine if serum markers of neural origin are related to i) presence and severity of SCI, and ii) magnetic resonance imaging (MRI) parameters in the very acute post-injury phase.

## Methods

We performed a secondary analysis of serological parameters, as well as MRI findings in patients with SCI (n=38) who were initially included in a prospective clinical trial at a level I trauma center in Bavaria (SCI and Trauma Center Murnau, Germany). Patients with cervical or thoracic injury independent of injury completeness were included in the initial trial. Blood samples were collected between days 1-4 post-injury. Serum protein levels of Glial Fibrillary Acidic Protein (GFAP), Neuron-Specific Enolase (NSE), and Neurofilament light protein (NfL) were determined using R-Plex Assays (Meso Scale Discovery). A group of 41 age- and sex-matched healthy individuals served as control group. In the group of individuals with SCI, pre-operative sagittal and axial T2-weighted and sagittal T1-weighted MRI scans were available for 21 patients.

### Biomarkers: differences and cut-offs

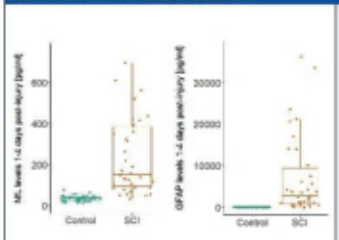


Significant differences in serum concentration of NfL and GFAP between the SCI group and the control group:

**NfL:** MD = 299.04 pg/ml (p<0.003)
SCI: 352.68 (577.3) vs. Control: 33.64 (14) pg/ml

**GFAP:** MD = 9188.72 pg/ml (p=0.003)
SCI: 9225.02 (17924.19) vs. Control: 36.3 (18.96) pg/ml

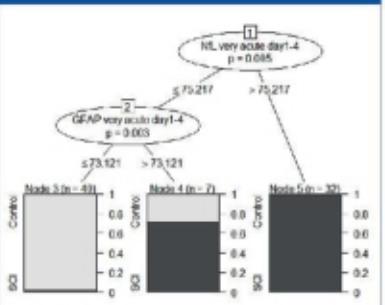


Unbiased recursive partitioning URP-CTREE first node: NfL concentration in pg/ml; second node: GFAP concentration in pg/ml; three terminal nodes (3, 4, 5) for the endpoint distribution SCI vs. healthy controls; n, sample size; p, significance level.

### Correlations with MRI findings

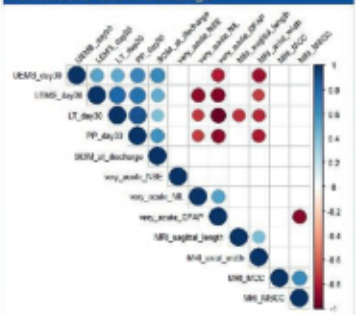


Correlation matrix: significant Pearson's correlation coefficients; significance level p<0.05. The maximum spinal cord compression (MSCC) correlates significantly inversely with the serum concentration of GFAP in the very acute post-injury phase.

## Findings and Interpretation

**Results:** Serum markers of neural origin are different among individuals who sustained traumatic SCI depending on injury severity by means of ISNCSCI sub-scores, and the extent of spinal swelling according to MRI in the very acute post-injury phase. Serum levels of NfL and GFAP can differentiate between individuals with SCI and healthy controls within the first four days post-SCI. Those quantitative markers are of particular value in individuals who are not able to participate in a clinical assessment within the first days post-injury.

**Conclusions:** Serum proteins NfL and GFAP qualify as biomarkers to detect the presence and severity of SCI in the acute post-injury phase, where the reliability of clinical exams is limited.

**Author's Affiliations:**
1 ParaMove, SCI Research Unit, BG Trauma Center Murnau, Murnau, Germany and Paracelsus Medical University, Salzburg, Austria
2 Spinal Cord Injury Center, Clinical Research Unit, BG Trauma Center Murnau, Murnau, Germany
3 Institute of Molecular Regenerative Medicine, Paracelsus Medical University, Salzburg, Austria
4 Spinal Cord Injury and Tissue Regeneration Center Salzburg (SCI-TReCS), Paracelsus Medical University, Salzburg, Austria
5 Austrian Cluster for Tissue Regeneration
6 Department of Neurosurgery, BG Trauma Center Murnau, Murnau, Germany
7 Institute of Biomechanics, BG Trauma Center Murnau, Germany, and Paracelsus Medical University, Salzburg, Austria
8 Department of Radiology, Neuroradiology and Interventional Radiology, BG Trauma Center Murnau, Murnau, Germany
9 Laboratory of Neuroinflammation, Hospital Nacional de Parapléjicos, SESCAM, Toledo, Spain
10 Department of Neurosurgery, Medical University Innsbruck, Innsbruck, Austria

*** Correspondence:**
Univ.-Prof. Dr. Ludwig Aigner
Institute of Molecular Regenerative Medicine
Spinal Cord Injury and Tissue Regeneration Center Salzburg
Paracelsus Medical University
Strubergasse 22
5020 Salzburg, Austria
e-Mail: ludwig.aigner@pmu.ac.at

## Serum levels of GFAP and NfL are related to the neurological impairment and spinal edema after traumatic spinal cord injury

Iris Leister[1,2,3,4], Ludwig Aigner[1,2,3,4,5,*], Barbara Altendorfer[3,4], Doris Maier[1,2], Orpheus Mach[1,2], Christof Wutte[6,7], Andreas Grillhösl[8], Angel Arevalo-Martin[9], Daniel Garcia-Ovejero[9], Lukas Grassner[1,2,3,4,10]

[1]ParaMove, SCI Research Unit, BG Trauma Center Murnau, Murnau, Germany, and Paracelsus Medical University, Salzburg, Austria; [2]Spinal Cord Injury Center, Clinical Research Unit, BG Trauma Center Murnau, Murnau, Germany; [3]Institute of Molecular Regenerative Medicine, Paracelsus Medical University, Salzburg, Austria; [4]Spinal Cord Injury and Tissue Regeneration Center Salzburg (SCI-TReCS), Paracelsus Medical University, Salzburg, Austria; [5]Austrian Cluster for Tissue Regeneration; [6]Department of Neurosurgery, BG Trauma Center Murnau, Murnau, Germany; [7]Institute of Biomechanics, BG Trauma Center Murnau, Germany, and Paracelsus Medical University, Salzburg, Austria; [8]Department of Radiology, Neuroradiology and Interventional Radiology, BG Trauma Center Murnau, Murnau, Germany; [9]Laboratory of Neuroinflammation, Hospital Nacional de Paraplejicos, SESCAM, Toledo, Spain; [10]Department of Neurosurgery, Medical University Innsbruck, Innsbruck, Austria; Contact: iris.leister@pmu.ac.at

### Objective
Neurological examination in the very acute phase after spinal cord injury (SCI) is often impossible and severely confounded by pharmacological sedation, or concomitant injuries. Therefore, diagnostic biomarkers that objectively characterize injury severity, or the mere presence of SCI are urgently needed to facilitate clinical decision-making in the very early post-injury phase.
This study aims to determine if serum markers of neural origin are related to i) presence and severity of SCI, and ii) magnetic resonance imaging (MRI) parameters in the very acute post-injury phase.

### Methods
We performed a secondary analysis of serological parameters, as well as MRI findings in patients with SCI (n=38) who were initially included in a prospective clinical trial at a level I trauma center in Bavaria (Trauma Center Murnau, Germany). Patients with cervical or thoracic injury independent of injury completeness were included in the initial trial. Blood samples were collected between days 1-4 post-injury. A serum tube was collected, aliquoted, and stored at −80◦C. Serum protein levels of Glial Fibrillary Acidic Protein (GFAP), Neuron-Specific Enolase (NSE), and Neurofilament light protein (NfL) were determined using R-Plex Assays (Meso Scale Discovery). A group of 41 age- and sex-matched healthy individuals served as control group. In the group of individuals with SCI, pre-operative sagittal and axial T2-weighted and sagittal T1-weighted MRI scans were available for 21 patients.

### Results
Serum markers of neural origin are different among individuals who sustained traumatic SCI depending on injury severity, and the extent of the lesion according to MRI in the very acute injury phase (1-4 days post-SCI). Also, serum concentrations of NfL and GFAP can differentiate between individuals with SCI and healthy controls within the first four days post-injury. Those quantitative markers are of particular value in individuals who are not able to participate in a clinical assessment due to pharmacological sedation, or concomitant injuries.

### Conclusions
Serum proteins NfL and GFAP qualify as diagnostic biomarkers for the presence and severity of SCI in the acute post-injury phase, where the reliability of clinical exams is limited.

# Benefits of pulmonary rehabilitation in COVID-19 - a prospective observational cohort study -

Daniela Leitl[1,2], Rainer Gloeckl[1,2], Inga Jarosch[1,2], Tessa Schneeberger[1,2], Christoph Nell[3], Nikola Stenzel[4], Claus F. Vogelmeier[5], Klaus Kenn[1,2], Andreas R. Koczulla[1, 2]

[1] Department of Pulmonary Rehabilitation, Philipps-University of Marburg, Member of the German Center for Lung Research (DZL), Marburg, Germany
[2] Institut for Pulmonary Rehabilitation Research, Schoen Klinik Berchtesgadener Land – Schoenau am Koenigssee, Germany
[3] Department of Pulmonology, Philipps-University Marburg, Germany
[4] Psychologische Hochschule Berlin (PHB), Berlin
[5] Department of Medicine, Pulmonary and Critical Care Medicine, University Medical Centre Giessen and Marburg, Philipps-Universität Marburg, Germany. Member of the German Center for Lung Research (DZL), Marburg, Germany
[6] Teaching hospital, Paracelsus Medical University, Salzburg, Austria

## Background

The new Corona-Virus disease (COVID-19) can result in a large variety of chronic health issues like impaired lung function, reduced exercise performance, and diminished quality of life. Our study aimed to investigate the efficacy, feasibility, and safety of pulmonary rehabilitation (PR) in COVID-19 patients and to compare outcomes between patients with a mild/moderate and a severe/critical course of the disease.

## Methods

Patients in the post-acute phase of a mild to critical course of COVID-19 admitted to a comprehensive three-week inpatient PR were included in this prospective, observational cohort study. Several measures of exercise performance (6-minute walk distance, 6MWD), lung function (forced vital capacity, FVC), and quality of life (36 question short-form health survey, SF-36) were assessed before and after PR. In a subgroup of patients with severe / critical COVID-19 an endurance shuttle walk test was performed before and after PR.

Tabelle 1. Baseline Charakteristika

| | mild / moderate COVID-19 | severe / critical COVID-19 |
|---|---|---|
| n | 24 | 26 |
| Age, yrs | 52 [47 - 56] | 66 [60 - 71] |
| Sex, female (%) | 20 (83%) | 8 (31%) |
| Duration of Hospitalization, d | NA | 37 [18 - 60] |
| O2-therapy during hospitalization, n (%) | 0 (0%) | 24 (92%) |
| Duration between first positive PCR-test and PR admission, d | 178 [127 – 217] | 61 [40 – 108] |
| Comorbidities prior to COVID-19, n | 2 [2-4] | 3 [3 - 5] |
| FVC, %/pred. | 80.0 [59.2 - 90.9] | 75.1 [59.8 - 90.6] |
| 6MWD, m | 509 [426 - 539] | 344 [244 - 392] |

## Results

Fifty patients were included in the study (24 with mild/moderate and 26 with severe/critical COVID-19). On admission, patients had a reduced 6MWD (mild: 509m [426-539]; severe: 344m [244-392]), an impaired FVC (mild: 80% [59-91]; severe: 75% [60-91]) and a low SF-36 mental health score (mild: 49pts [37-54]; severe: 39pts [30-53]). Patients attended a median of 100% [94-100] of all provided PR sessions. At discharge, patients in both subgroups improved in 6MWD (mild/moderate: +48m [35-113m]; severe/critical: +124m [75-145m], both p<0.001), FVC (mild/moderate: +7.7% [1.0-17.8], p=0.002; severe/critical: +11.3% [1.0-16.9], p<0.001) and SF-36 mental component (mild/moderate +5.6pts [1.4-9.2], p=0.071; severe/critical: +14.4pts [-0.6-24.5], p<0.001). At discharge the ESWT duration improved from 460sec to 1200sec (p=0.001) with 14 patients (54%) reaching the test duration maximum of 20 minutes.

No adverse event was observed.

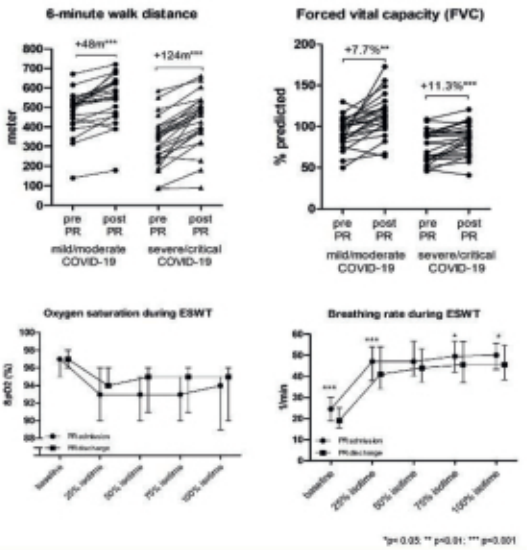


## Conclusion

Our study shows that PR is effective, feasible, and safe to improve exercise performance, lung function, and quality of life in patients with persistent impairments due to a mild to critical course of COVID-19.

Published: Gloeckl, R., Leitl, D., Jarosch, I., Schneeberger, T., Nell, C., Stenzel, N., ... & Koczulla, A. R. (2021). Benefits of pulmonary rehabilitation in COVID-19–a prospective observational cohort study. ERJ Open Research.

## Benefits of pulmonary rehabilitation in COVID-19 a prospective observational cohort study

Daniela Leitl[1, 2], Rainer Glöckl[1, 2], Inga Jarosch[1, 2], Tessa Schneeberger[1, 2], Christoph Nell[3], Nikola Stenzel[4], Claus F. Vogelmeier[5], Klaus Kenn[1, 2], Andreas R. Koczulla[1, 2, 6]

[1]Department of Pulmonary Rehabilitation, Philipps-University of Marburg, Member of the German Center for Lung Research (DZL), Marburg, Germany; [2]Institute for Pulmonary Rehabilitation Research, Schön Klinik Berchtesgadener Land – Schönau am Königssee; Germany; [3]Department of Pulmonology, Philipps-University Marburg, Germany; [4]Psychologische Hochschule Berlin (PHB), Berlin; [5]Department of Medicine, Pulmonary and Critical Care Medicine, University Medical Centre Giessen and Marburg, Philipps-Universität Marburg, Germany. Member of the German Center for Lung Research (DZL), Marburg, Germany; [6]Teaching hospital, Paracelsus Medical University, Salzburg, Austria; Contact: dleitl@schoen-klinik.de

### Objective
The new Corona-Virus disease (COVID-19) can result in a large variety of chronic health issues like impaired lung function, reduced exercise performance, and diminished quality of life [1, 2]. Our study aimed to investigate the efficacy, feasibility, and safety of pulmonary rehabilitation (PR) in COVID-19 patients and to compare outcomes between patients with a mild/moderate and a severe/critical course of the disease.

### Methods
Patients in the post-acute phase of a mild to critical course of COVID-19 admitted to a comprehensive three-week inpatient PR were included in this prospective, observational cohort study. Several measures of exercise performance (6-minute walk distance, 6MWD), lung function (forced vital capacity, FVC), and quality of life (36 question short-form health survey, SF-36) were assessed before and after PR. In a subgroup of patients with severe / critical COVID-19 an endurance shuttle walk test was performed before and after PR.

### Results
Fifty patients were included in the study (24 with mild/moderate and 26 with severe/critical COVID-19). On admission, patients had a reduced 6MWD (mild: 509m [426-539]; severe: 344m [244-392]), an impaired FVC (mild: 80% [59-91]; severe: 75% [60-91]) and a low SF-36 mental health score (mild: 49pts [37-54]; severe: 39pts [30-53]). Patients attended a median of 100% [94-100] of all provided PR sessions. At discharge, patients in both subgroups improved in 6MWD (mild/moderate: +48m [35-113m]; severe/critical: +124m [75-145m], both $p<0.001$), FVC (mild/moderate: +7.7% [1.0-17.8], $p=0.002$; severe/critical: +11.3% [1.0-16.9], $p<0.001$) and SF-36 mental component (mild/moderate +5.6pts [1.4-9.2], $p=0.071$; severe/critical: +14.4pts [-0.6-24.5], $p<0.001$). At discharge the ESWT duration improved from 460sec to 1200sec ($p=0.001$) with 14 patients (54%) reaching the test duration maximum of 20 minutes. No adverse event was observed.

### Conclusions
Our study shows that PR is effective, feasible, and safe to improve exercise performance, lung function, and quality of life in patients with persistent impairments due to a mild to critical course of COVID-19.

### References
1. Huang, C., et al., 6-month consequences of COVID-19 in patients discharged from hospital: a cohort study. Lancet, 2021. 397(10270): p. 220-232.
2. Goertz, Y.M.J., et al., Persistent symptoms 3 months after a SARS-CoV-2 infection: the post-COVID-19 syndrome? ERJ open research, 2020. 6(4).

# Maladjustment of pressure settings of a Codman-Hakim programmable shunt valve by electromagnetic door locks – A case report

Christiane Licht [1] Kneginja Richter [1,2]

1 University Clinic for Psychiatry and Psychotherapy Paracelsus Medical University Nuernberg, Germany

2 Technical University for applied Sciences Georg Simon Ohm Nuernberg, Germany

Klinikum Nürnberg

Wir sind für Sie da!

## Backround

Hydrocephalus is caused by the progressive accumulation of cerebral spinal fluid (CSF) within the intracranial space, resulting in the abnormal expansion of cerebral ventricles and, consequently, in brain damage. The standard treatment of hydrocephalus in children and adults is implantation of a shunt.

In this study, we present a patient from Forensic Psychiatry who had the pressure settings of an implanted Codman-Hakim programmable shunt valve changed when walking through an electromagnetically controlled doorway on a hospital ward.

## Shunt valve



Johnson & Johnson product description Codman-Hakim shunt valve

## Scetch of a Codman-Hakim shunt valve

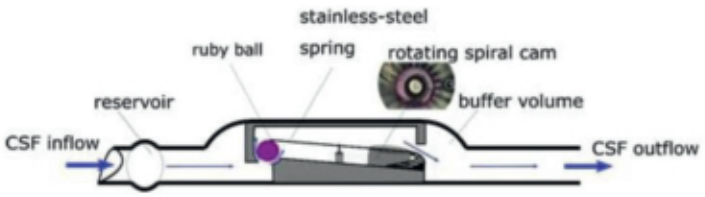


The Codman-Hakim valve is a programmable CSF shunt with an opening pressure between 30 and 200 mm H2O. The valve relies on a special ball-in-cone system. A spherical ruby ball is pressed against a conical valve seat by a stainless-steel spring. Atop the spring sits a rotating spiral cam. If the pressure difference across the valve exceeds a predefined popping pressure, the ball rises from the seat to vent CSF. To provide a larger valve orifice, the ball moves further away from the seat if the flow rate through the valve increases.

## Rotating spiral cam

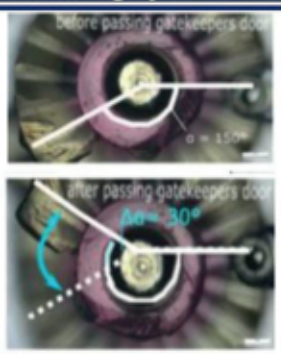


Before and after passing a door the angle of the spiral cam was measured using an optical microscope.

## Case description

A 53-year old man presented with triventricular hydrocephalus and was treated with a left ventriculo-peritoneal Codman-Hakim programmable shunt valve which was initially set to 60 mm H2O. During the patient's hospitalization in Forensic Psychiatry the valve pressure setting changed minimum 6 times randomly during despite frequent reprogramming and surveillance.

Because of the strict absence of other external electromagnetic devices, it was concluded that the valve's altered pressure setting must have been caused by some other device present on the ward. Thus, the electromagnetic door locks of the hospital ward were suspected as the cause of the changed pressure settings.

To evaluate interactions between the Codman Hakim valve and the doors a similar Codman Hakim shunt valve was held up at patient's face level while walking through different doors in the hospital ward.

## Findings and outlook

We found that the electromagnetic locking mechanism of common hospital doors had a strong enough magnetic field to unintentionally change the patient's shunt setting.

The described case and our internal testing suggest that even weak magnetic fields may lead to significant changes in the cam setting of Codman-Hakim shunt valves.

Therefore, even common household items may interfere with different shunt valves. Because our everyday life involves more and more electronic and technological advances, the number of potentially interfering devices is very likely to increase.

Both low-intensity and strong magnetic fields carry the risk of interacting with the pressure settings of shunt valves, a problem that both patients and medical professionals should be made aware of.

PARACELSUS
MEDIZINISCHE PRIVATUNIVERSITÄT

## Maladjustment of pressure settings of a Codman-Hakim programmable shunt valve by electromagnetic door locks – A case report

Christiane Licht[1], Kneginja Richter[1, 2]

[1]University Clinic for Psychiatry and Psychotherapy Paracelsus Medical University Nuernberg, Germany; [2]Technical University for applied Sciences Georg Simon Ohm Nuernberg, Germany; Contact: christiane.licht@klinikum-nuernberg.de

### Objective
Maladjustments and failures of programmable ventriculo-peritoneal shunts have been reported in cases in which patients have encountered powerful electromagnetic fields, e.g. MRI.
By the means of a case this study shows an easy maladjustment of a Codman-Hakim programmable valve also by small magnetic fields from everyday life.

### Methods
Pressure settings of a patient's valve changed randomly, presumably by walking though electromagnetically controlled doors of a hospital ward.
With a test dummy changes of pressure setting were tracked.

### Results
Both - pressure settings of the patient's Codman-Hakim programmable valve as well as pressure settings of a new valve - were unwanted modified simply by walking through common doors in a hospital ward.

### Conclusions
Thus already weak magnetic fields (< 200 mT) might cause changes in the pressure settings of programmable shunt valves and therefore lead to maladjustment. Patients should be informed and pay attention of using everyday life's devices, like rod magnets or mobile phones.

# Repetitive Transcranial Magnetic Stimulation for Catatonia – a case report

Christiane Licht [1], Eva Alt [1], Sarah Fuchs, [1] Axel Ruttmann [1], Kneginja Richter [1, 2, 3], Thomas Hillemacher [1]

1 University Clinic for Psychiatry and Psychotherapy, Paracelsus Medical University, Nürnberg, Germany

2 Technical University for applied Sciences, Georg Simon Ohm Nürnberg, Germany

3 Labour for Neurostimulation and Chronobiology, University Clinic for Psychiatry and Psychotherapy, Paracelsus Medical University Nürnberg, Germany

Klinikum Nürnberg
Wir sind für Sie da!

## Backround

Catatonia is a potentially life-threatening condition that is often presented with a large variety of metabolic, neurologic, psychiatric, and toxic conditions. Often it is accompanied by stupor, exhaustion, and if left untreated, often leads to respiratory failure, collapse, and death (1 - 3).

Currently, pathophysiology and etiology remain widely unknown.

Although, no uniform therapy method has yet been brought forward, a treatment with benzodiazepines and electroconvulsive therapy (ECT) are the most widely studied treatment methods - and therefore recommended in national and international guidelines.

However, treatments with benzodiazepines, antipsychotics, or zolpidem are often not entirely satisfactory. Sometimes also ECT is - due to the necessary anesthesia - not generally available or sometimes medically contraindicated, and often associated with constraint and ethical difficulties (4).

Evidence from few case reports suggests the use of newer non-invasive neurostimulation techniques like repetitive transcranial magnetic stimulation (rTMS) or transcranial direct current stimulation (tDCS) to treat catatonia.

Until today, rTMS has been little explored for catatonia. Here, we are reporting a case of a 55-year-old female patient with known paranoid schizophrenia, who developed strong catatonic symptoms and was successfully treated with rTMS.

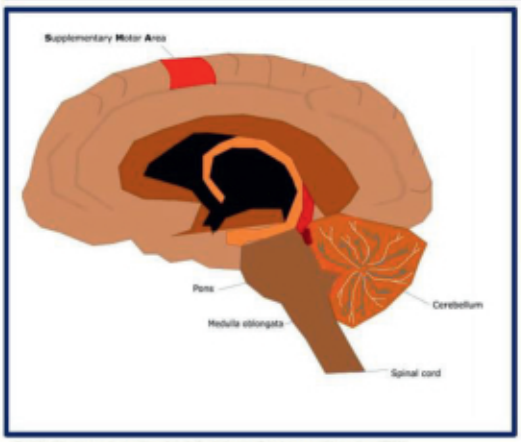


Scetch of the human brain with point of stimulation the Supplemenary Motor Area (SMA)



rTMS treatment in the Laboratory for Neurostimulation

## Treatment parameters



MagVenture magnetic 8-shaped coil Cool B65

Following the published rTMS guidelines and study protocol of Walther (5, 6), we targeted the motor system via the left supplementary motor area (SMA). Before each session, the resting motor threshold (RMT) was determined to identify the individual stimulation intensity. Each stimulation was delivered by a MagVenture device with an 8-shaped coil (cool-B65 butterfly-shaped coil, Medtronic).

The patient received a total of three successful treatments and a single continuous session with 1000 pulses each. The SMA was localized by moving the coil 3 cm anterior from the leg motor area along the midline, which is expected to stimulate bilateral SMA. The handle of the coil was pointing backwards along the midline.

With intensity of 110% RMT, at an angle of 45°, 25 stimulus series with 40 pulses per series, and a pulse width for 25 ms with a frequency of 1 Hz the patient was stimulated. This already led to a spectacular improvement after only the first low-frequency session.

## Findings and Outlook

For the first time since her admission, Ms. L. woke up in the morning, walked to the floor, and started to talk!

The distinctive catatonic symptoms - such as immobility, mutism, and fixed gaze - were already significantly reduced after the first 24 hours of the first session of rTMS.

At least even a feeding without a gastric tube was possible again!

In the light of the present case, our findings show a new opportunity in the use of rTMS for patients who do not respond to benzodiazepines or ECT.

Additionally, rTMS might be an option in patients who respond to ECT but need long-term treatment to control their catatonic symptoms.

Further clinical trials are needed to determine an evidence-based evaluation of the potential risks and benefits of rTMS for catatonia.

## References

1. Walther, S. & Stüb, W. Catatonia. CNS Spectr. 21, 341–348 (2016).
2. Pelzer, A. C. M., van der Heijden, F. M. M. A. & den Boer, E. Systematic review of catatonia treatment. Neuropsychiatr. Dis. Treat. 14, 317–326 (2018).
3. Walther, S., Stegmayer, K., Wilson, J. E. & Heckers, S. Structure and neural mechanisms of catatonia. The Lancet Psychiatry 6, 610–619 (2019).
4. Hansbauer, M. et al. rTMS and tDCS for the treatment of catatonia : A systematic review. Schizophr. Res. (2020) doi:10.1016/j.schres.2020.05.020.
5. Walther, S. et al. Inhibitory Repetitive Transcranial Magnetic Stimulation to Treat Psychomotor Slowing: A Transdiagnostic, Mechanism-Based Randomized Double-Blind Controlled Trial. Schizophr. Bull. Open 1, (2020).
6. Lefaucheur, J. P. et al. Evidence-based guidelines on the therapeutic use of repetitive transcranial magnetic stimulation (rTMS). Clin. Neurophysiol. 125, 2150–2206 (2014).

PARACELSUS
MEDIZINISCHE PRIVATUNIVERSITÄT

## Repetitive Transcranial Magnetic Stimulation for Catatonia – a case report

Christiane Licht[1], Eva Alt[1], Sarah Fuchs[1], Axel Ruttmann[1], Keginja Richter[1, 2, 3], Thomas Hillemacher[1]

[1]University Clinic for Psychiatry and Psychotherapy, Paracelsus Medical University, Nürnberg, Germany; [2]Technical University for applied Sciences, Georg Simon Ohm Nürnberg, Germany; [3]Labour for Neurostimulation and Chronobiology, University Clinic for Psychiatry and Psychotherapy, Paracelsus Medical University Nürnberg, Germany; Contact: christiane.licht@klinikum-nuernberg.de

### Objective

Catatonia is a potentially life-threatening condition that is often presented with a large variety of metabolic, neurologic, psychiatric, and toxic conditions. Often it is accompanied by stupor, exhaustion, and if left untreated, often leads to respiratory failure, collapse, and death.
Currently, pathophysiology and etiology remain widely unknown!
However, treatments with benzodiazepines, antipsychotics, or zolpidem are often not entirely satisfactory. Sometimes also ECT is - due to the necessary anesthesia - not generally available or sometimes medically contraindicated, and often associated with constraint and ethical difficulties.

### Methods

Evidence from few case reports suggests the use of newer non-invasive neurostimulation techniques like repetitive transcranial magnetic stimulation (rTMS) or transcranial direct current stimulation (tDCS) to treat catatonia.
Until today, rTMS has been little explored for catatonia. Here, we are reporting a case of a 55-year-old female patient with known paranoid schizophrenia, who developed strong catatonic symptoms and was successfully treated with rTMS.

### Results

For the first time since her admission, Ms. L. woke up in the morning, walked to the floor, and started to talk!
The distinctive catatonic symptoms - such as immobility, mutism, and fixed gaze - were already significantly reduced after the first 24 hours of the first session of rTMS.
At least even a feeding without a gastric tube was possible again!

### Conclusions

In the light of the present case, our findings show a new opportunity in the use of rTMS for patients who do not respond to benzodiazepines or ECT.
Additionally, rTMS might be an option in patients who respond to ECT but need long-term treatment to control their catatonic symptoms.
Further clinical trials are needed to determine an evidence-based evaluation of the potential risks and benefits of rTMS for catatonia.

### References

1. Walther, S. & Strik, W. Catatonia. CNS Spectr. 21, 341–348 (2016).
2. Pelzer, A. C. M., van der Heijden, F. M. M. A. & den Boer, E. Systematic review of catatonia treatment. Neuropsychiatr. Dis. Treat. 14, 317–326 (2018).
3. Walther, S., Stegmayer, K., Wilson, J. E. & Heckers, S. Structure and neural mechanisms of catatonia. The Lancet Psychiatry 6, 610–619 (2019).
4. Hansbauer, M. et al. rTMS and tDCS for the treatment of catatonia : A systematic review. Schizophr. Res. (2020) doi:10.1016/j.schres.2020.05.028.
5. Walther, S. et al. Inhibitory Repetitive Transcranial Magnetic Stimulation to Treat Psychomotor Slowing: A Transdiagnostic, Mechanism-Based Randomized Double-Blind Controlled Trial. Schizophr. Bull. Open 1, (2020).
6. Lefaucheur, J. P. et al. Evidence-based guidelines on the therapeutic use of repetitive transcranial magnetic stimulation (rTMS). Clin. Neurophysiol. 125, 2150–2206 (2014).

# Central Nervous System Manifestation of a mantle cell lymphoma at the resection site of a meningioma: a case report

Liebert A., Kerry G., Hähnel S., Voit-Hoehne H.-L., Steiner H.-H.

Klinikum Nürnberg

## Case description:

This case describes an unusual secondary lymphoma spread to an intracranial meningioma resection site. To our knowledge, there is no previously documented case of such coincidence.

A 58 years old male underwent a tumor resection of a right-sided parietal meningioma WHO I° in August 2015.

In July 2018 a recurrent tumor was removed (Image 1). A Simpson Grade I resection was achieved and a postoperative cranial CT scan did not indicate any tumor residuum. The histopathological examination of the tumor resulted in the diagnosis of an atypical meningioma WHO II°. Based on this diagnosis, the patient was advised to undergo radiotherapy. In September 2018, cranial imaging demonstrated a cystic transformation of the resection site with strong circular enhancement with contact to the previously conducted dural reconstruction with collagen matrix (Images 2 A, B). We performed surgery again in which the cerebral tissue did not appear to be pathological. Nevertheless the histopathological examination demonstrated a perivascular infiltration by a non-Hodgkins-B-cell lymphoma, a classical mantle cell lymphoma.

After obtaining the diagnosis, staging by CT scans of the chest and abdomen as well as flow cytometry of a bone marrow aspirate classified the mantle cell lymphoma as stage IV A according to Ann Arbor Staging Classification. The CT scans demonstrated enlarged lymph nodes at multiple locations, moderate splenomegaly was also demonstrated. The cytology of the bone marrow was physiological. In the flow cytometry, a bone marrow infiltration was demonstrated by the presence of CD5+/ CD20+/CD23+ cells. An iliac crest trephine displayed diffuse bone marrow infiltration with suppression of hematopoiesis. Systemic chemotherapy with R-CHOP/R-DHAP and successive high dose therapy with stem cell transplantation as well as radiotherapy for the meningeal focus were recommended.

Five months after the last surgery, but before the recommended chemotherapy and radiotherapy, an MRI scan demonstrated regressions of the edema as well as of the contrast medium enhanced areas (Image 3 A, B).

## Discussion:

The simultaneous appearance of meningioma and lymphoma in the CNS is rare. Nevertheless, multiple cases were reported [1]. This is not surprising due to the high frequency of meningiomas and their long symptom-free growth period. The CNS involvement by mantle cell lymphoma is less common. A multicenter study by Chesh et al., including 1396 patients with treated mantle cell lymphoma, demonstrated only 4.1% of mantle cell lymphomas present in the CNS and only 0.9% of the patients demonstrated CNS involvement at the time of the diagnosis [2]. The way of lymphoma cells to the CNS is not entirely clarified, hematogenous or direct spread from bone marrow infiltration has been hypothesized [3].

## Conclusion:

To our knowledge, this is the first case with a secondary spread by a primary extracerebral lymphoma to a meningioma resection site in the world medical literature. One possible cause of the manifestation in the tumor resection site may be a direct migration of lymphoma cells from the skull bone marrow while performing the craniotomy. Another hypothesis is that the surgery and the healing process triggered the lymphoma.

**References:**

[1] Gordon AA, Fallon KE, Riley RD. Meningioma interdigitated with primary central nervous system B cell lymphoma: A case report and literature review. Surg Neurol Int 13 Dec 2011;2:181

[2] C. Y. Chesh, A. George, E. Gibl et al. Central nervous system involvement in mantle cell lymphoma: clinical features, prognostic factors and outcomes from the European Mantle Cell Lymphoma Network. Annals of Oncology, Volume 24, Issue 8, August 2013, Pages 2119–2123.

[3] Lenkt LJ, Dawson DM, Rosenthal DS, Mahoney WC. CNS involvement in the non-Hodgkin's lymphomas. Cancer. 1980;45(3):545.

- *August 2015*
  Tumor resection
  Meningioma WHO I°
- *July 2018*
  Tumor resection of a recurrent atypical Meningioma WHO II° (Image 1, axial MRI scan T1 with Gd)
- *September 2018*
  Surgery of cystic lesion in resection site
  Histology: CNS manifestation by a classical mantle cell lymphoma
  (Image 2 A, B, axial and coronal MRI scan T1 with Gd)
- *February 2019*
  Before therapy
  (Image 3 A, B, axial MRI scan T1 with Gd and FLAIR)

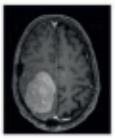

Image 1

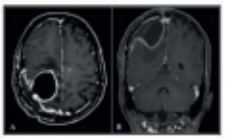

Image 2 A, B

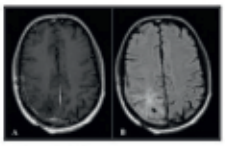

Image 3 A, B

Paracelsus Medizinische Privatuniversität | Universitätsklinik für Neurochirurgie | Klinikum Nürnberg | Adrian Liebert | adrian.liebert@klinikum-nuernberg.de

## Central Nervous System Manifestation of a mantle cell lymphoma at the resection site of a meningioma: a case report

Adrian Liebert[1], Ghassan Kerry[1], Stefan Hähnel[3], Heinz-Leonhard Voit-Hoehne[2], Hans-Herbert Steiner[1]

[1]Department of Neurosurgery, Paracelsus Medical University, Nuremberg, Germany; [2]Department of Neuroradiology, Paracelsus Medical University, Nuremberg, Germany; [3]Department of Neuroradiology, University Hospital Heidelberg, Heidelberg, Germany; Contact: adrian.liebert@klinikum-nuernberg.de

### Objective
Previous cases of simultaneous appearance of meningioma and CNS lymphoma are described in the literature. However, to our knowledge, this is the first case with the secondary spread of extracerebral lymphoma to a resection site that has been reported in the world medical literature.

### Methods
We present a case of a male patient with this unkown coincidence.

### Results
A male patient underwent two tumor resections for a meningioma. Approximately two months after the second surgery the patient's clinical status worsened and a CT scan was performed. Due to an increase in cerebral edema, cranial imaging was completed with an MRI scan. The imaging was rather ambiguous about the etiology of the edema. For this reason, we performed another surgery. Histopathological examination revealed infiltration of a mantle cell lymphoma, which was not diagnosed before in this patient.

### Conclusions
The simultaneous appearance of meningioma and lymphoma in the CNS is rare. Nevertheless, multiple cases were reported [1]. This is not surprising due to the high frequency of meningiomas and their long symptom free growth period. The CNS involvement by mantle cell lymphoma is less common. A multicenter study by Cheah et al., including 1396 patients with treated mantle cell lymphoma, demonstrated only 4.1% of mantle cell lymphomas present in the CNS and only 0.9% of the patients demonstrated CNS involvement at the time of the diagnosis [2]. The way of lymphoma cells to the CNS is not entirely clarified; hematogenous or direct spread from bone marrow infiltration has been hypothesized [3].
One possible cause of the manifestation in the tumor resection site may be a direct migration of lymphoma cells from the skull bone marrow while performing the craniotomy. Another hypothesis is that the surgery and the healing process triggered the lymphoma.

### References
1. Gordon AS, Fallon KE, Riley KO. Meningioma interdigitated with primary central nervous system B cell lymphoma : A case report and literature review. Surg Neurol Int 13 Dec 2011;2:181
2. C. Y. Cheah , A. George, E. Giné et al. Central nervous system involvement in mantle cell lymphoma : clinical features , prognostic factors and outcomes from the European Mantle Cell Lymphoma Network. Annals of Oncology , Volume 24, Issue 8, August 2013, Pages 2119 2123.
3. Levitt LJ, Dawson DM, Rosenthal DS, Moloney WC. CNS involvement in the non Hodgkin' s lymphomas . Cancer. 1980;45(3):

PARACELSUS
MEDIZINISCHE PRIVATUNIVERSITÄT

Klinikum Nürnberg
wir sind für Sie da!

# Effect of long COVID -19 on respiratory burst of neutrophils.


Sebastian Lobmann[1], Gustavo Chaves[1], Golo-Sung Haarmeyer[4] , Jörg Steinmann[2], Thomas Bertsch[3], Joachim H. Ficker[4], Boris Musset[1]

[1]Institute of Physiology, Pathophysiology and Biophysics, Klinikum Nuremberg Medical School, Paracelsus Medical University Nuremberg, 90419 Nuremberg, Germany
[2]Institute of Clinical Hygiene, Medical Microbiology and Clinical Infectiology, Klinikum Nuremberg Medical School, Paracelsus Medical University Nuremberg, 90419 Nuremberg, Germany
[3]Institute of Clinical Chemistry, Laboratory Medicine and Transfusion Medicine - Central Laboratory, Klinikum Nuremberg Medical School, Paracelsus Medical University Nuremberg, 90419 Nuremberg, Germany
[4]Department of Respiratory Medicine, Allergology and Sleep Medicine, Paracelsus Medical University, General Hospital Nuremberg, Paracelsus Medical Private University Nuremberg, 90419 Nuremberg, Germany

Contact: sebastian.lobmann@stud.pmu.ac.at


## Objective

At the Institute[1], we previously studied the respiratory burst of human phagocytes from healthy volunteers.
Currently, there are increased reports of mucormycosis associated with and following COVID-19 infections from India, because neutrophils play an important role in the defense against fungi (1), we were interested whether it would be possible to detect differences in the respiratory burst of neutrophils from healthy volunteers and long covid patients.

## Methods

We trigger an immune response of the cells with PMA. Since hydrogen peroxide is a product of the respiratory burst, we can quantify the respiratory burst by hydrogen peroxide production. We determine the hydrogen peroxide using the AmplexRed method in a fluorescence essay.
Long COVID patients were defined as non-infectious patients with a Horowitz score of less than 200.
For the long COVID patients, no extra blood samples were taken, but in coordination with the intensive care unit and the central laboratory, the blood samples from the routine tests were not discarded, but the unused volume in the monovettes were forwarded to us.
For the isolation of the neutrophils we used the density centrifugation or the MACSxpress Whole Blood kit.
We tested diphenyleneiodonium chloride (DPI) and Carbonyl cyanide 3-chlorophenylhydrazone (CCCP) as two different inhibitors for the respiratory burst.
DPI inhibit the NADPH oxidase.
CCCP suppresses the expression of few electron transport chain proteins.It is also Protonophore and uncoupler of oxidative phosphorylation in mitochondria.

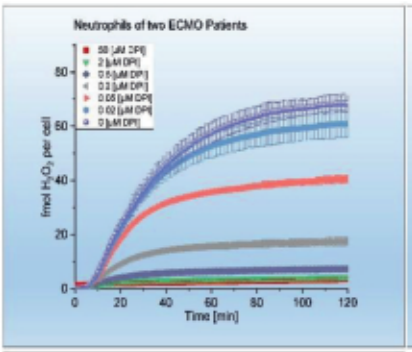


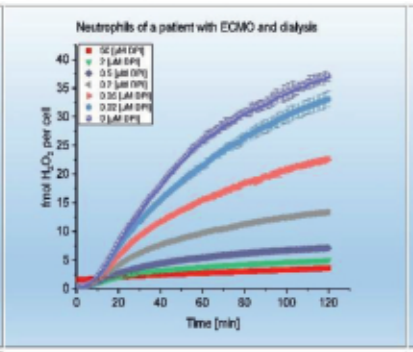


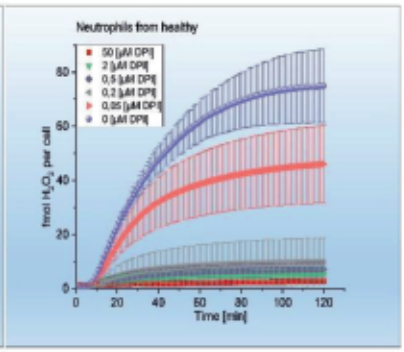


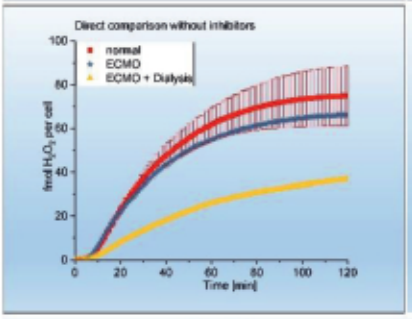


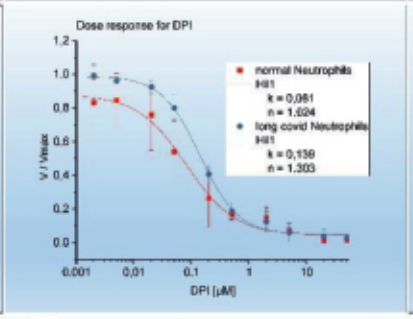


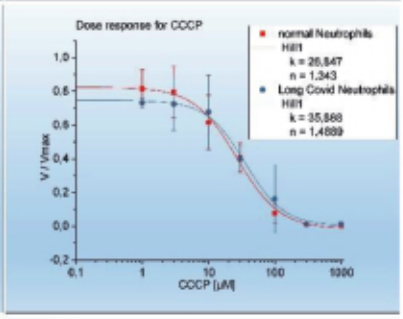


## Results

In the sample of the patient with dialysis and ECMO there is a clear difference to the healthy subjects. This patient was also the most critical.
No clear trend can currently be seen in the other samples.
The $IC_{50}$ for DPI remains within the expected range for both ECMO only and ECMO plus dialysis samples.
For the $IC_{50}$ of CCCP, it seems to be similar between healthy and the long covid as well.

## Conclusions

Because the $IC_{50}$ for DPI and CCCP are comparable, it suggests that the basic mode of action of the inhibitors is not affected and the mechanisms of respiratory burst are not fundamentally altered.
Since we have singly studied neutrophils from three COVID-19 patients so far, these are preliminary experiments and should be validated in further experiments.
In the patient with ECMO and dialysis, it is not clear whether the change in respiratory burst in neutrophils is due to COVID-19 or the connected devices.

## References


1.Desai, Jigar V., and Michail S. Lionakis. "The role of neutrophils in host defense against invasive fungal infections." Current clinical microbiology reports 5.3 (2018): 181-189.


## Outlook

Previous experiments have shown that eosinophils have the best signal-to-noise ratio and the absolute productions of hydrogen peroxide is less variability than neutrophils. However, the whole blood isolation kit for eosinophils did not work at all in our experiments. For density centrifugation with column, we have up to now used significantly more blood than we had available for these experiments. Therefore, we used the Neutrophil Whole Blood Isolation Kit, as we could safely isolate sufficient cells for the experiments with this kit.
The effect of dexamethasone and other drugs on the respiratory burst of neutrophils could also be considered.

## Effect of long COVID-19 on respiratory burst of neutrophils.

Sebastian Lobmann[1], Gustavo Chaves[1], Golo-Sung Haarmeyer[4], Jörg Steinmann[2], Thomas Bertsch[3], Joachim H. Ficker[4], Boris Musset[1]

[1]Institute of Physiology, Pathophysiology and Biophysics, Klinikum Nuremberg Medical School, Paracelsus Medical University Nuremberg, 90419 Nuremberg, Germany; [2]Institute of Clinical Hygiene, Medical Microbiology and Clinical Infectiology, Klinikum Nuremberg Medical School, Paracelsus Medical University Nuremberg, 90419 Nuremberg, Germany; [3]Institute of Clinical Chemistry, Laboratory Medicine and Transfusion Medicine - Central Laboratory, Klinikum Nuremberg Medical School, Paracelsus Medical University Nuremberg, 90419 Nuremberg, Germany; [4]Department of Respiratory Medicine, Allergology and Sleep Medicine, Paracelsus Medical University, General Hospital Nuremberg, Paracelsus Medical Private University Nuremberg, 90419 Nuremberg, Germany; Contact: sebastian.lobmann@stud.pmu.ac.at

### Objective

At the Institute1, we previously studied the respiratory burst of human phagocytes from healthy volunteers.
Currently, there are increased reports of mucormycosis associated with and following COVID-19 infections from India, because neutrophils play an important role in the defense against fungi (1), we were interested whether it would be possible to detect differences in the respiratory burst of neutrophils from healthy volunteers and long COVID patients.

### Methods

We trigger an immune response of the cells with PMA. Since hydrogen peroxide is a product of the respiratory burst, we can quantify the respiratory burst by hydrogen peroxide production. We determine the hydrogen peroxide using the AmplexRed method in a fluorescence essay.
Long COVID patients were defined as non-infectious patients with a Horowitz score of less than 200.
For the long COVID patients, no extra blood samples were taken, but in coordination with the intensive care unit and the central laboratory, the blood samples from the routine tests were not discarded, but the unused volume in the monovettes were forwarded to us.
For the isolation of the neutrophils we used the density centrifugation or the MACSxpress Whole Blood kit.
We tested diphenyleneiodonium chloride (DPI) and Carbonyl cyanide 3-chlorophenylhydrazone (CCCP) as two different inhibitors for the respiratory burst.

### Results

In the sample of the patient with dialysis and ECMO there is a clear difference to the healthy subjects. This patient was also the most critical.
No clear trend can currently be seen in the other samples.
The IC50 for DPI remains within the expected range for both ECMO only and ECMO plus dialysis samples.
For the IC50 of CCCP, it seems to be similar between healthy and the long COVID as well.

### Conclusions

Because the IC50 for DPI and CCCP are comparable, it suggests that the basic mode of action of the inhibitors is not affected and the mechanisms of respiratory burst are not fundamentally altered.
Since we have singly studied neutrophils from three COVID-19 patients so far, these are preliminary experiments and should be validated in further experiments.
In the patient with ECMO and dialysis, it is not clear whether the change in respiratory burst in neutrophils is due to COVID-19 or the connected devices.

### References

1. Desai, Jigar V., and Michail S. Lionakis. "The role of neutrophils in host defense against invasive fungal infections." Current clinical microbiology reports 5.3 (2018): 181-189.

TECHNISCHE HOCHSCHULE NÜRNBERG
GEORG SIMON OHM

# Cytosolic Mineralocorticoid Receptor interacts differentially with other Proteins depending on Ligand

Miriam Weber[1], Ralf Lösel[2]

[1]Dept. of Clinical Pharmacology Mannheim, University of Heidelberg, and [2]Dept of Applied Chemistry, Technische Hochschule Nürnberg; Contact: ralf.loesel@th-nuernberg.de

## Objective

The Mineralocorticoid Receptor (MR) has attracted considerable interest, as its activation has been shown to pose an independent risk factor for cardiovascular disease. Consequently, antagonists at the MR such as spironolactone are used to prevent progression. MR, like other nuclear receptors, may be located in the nucleus regulating transcription or outside the nucleus, where it may exert nongenomic effects. While the differential recruitment of transcriptional cofactors in the nucleus have been shown for many nuclear receptors, little is known about the interaction of MR in the cytosol. This study addresses MR-interacting proteins and the effect of various ligands.

## Methods

The coding sequence of human MR was cloned into vectors pEXPR-IBA-103 and -105, thus creating proteins with OneStrepTag fused to the N-terminus or the C-terminus, respectively. Both constructs were functional in transactivation assays (MMTV-Luc).
HEK293T cells were transfected with the constructs and the cells were scraped off 24 hrs later. Suspended cells were stimulated with steroid for 5 min at 37°C, then cooled and lysed. The cleared lysate was passed over a StrepTactin column and the protein complexes were eluted using HABA. Proteins were separated by one dimensional SDS PAGE, bands were stained, excised and digested using trypsin. The peptides thus obtained were used for protein identification by MALDI (peptide mass fingerprinting) using a BIFLEX or UltraFlex instrument.

## Results

MR residing in the cytosol interacts with a considerable number of other proteins (cf fig. 2 and table 1). The abundance of some proteins vary with the ligand that is present. Band 1 in fig.1, propionyl-CoA carboxylase β precursor, could be a nonspecific result as its α chain contains biotin, however this does not explain the differential interaction observed.

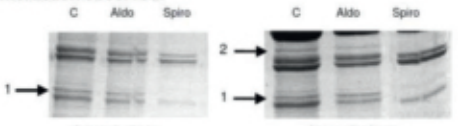


Figure 1. Proteins that are differentially recruited to the MR complex. The arrows indicate two proteins that are strikingly different in the spiro-occupied MR compared to aldosterone-occupied or non-liganded MR

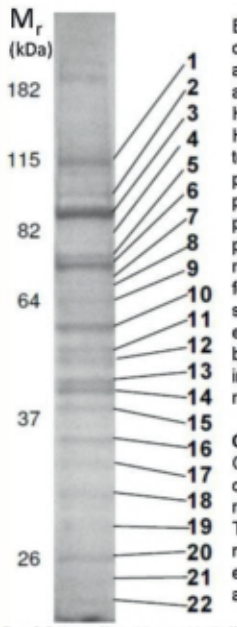


Figure 2: Gel image of the proteins comprising the MR complex (MR with N-terminal tag) separated by SDS gel electrophoresis and stained nonspecifically. Numbers on the right hand side indicate the proteins identified by MS (see table 1).

Band 2 in fig. 1, clearly visible only with the construct labeled at the N-terminus, was identified as GRP78 (also called BiP or HSPA5), a member of the HSP70 family. It is not possible to distinguish between the precursor and the mature protein (as we did not find peptides from aa 1-49), the peptide bearing the KDEL retention signal was consistently found, indicating that GRP78 should reside in the endoplasmic reticulum. MR has been reported to be located also in or at the endoplasmic reticulum in the kidney.

## Conclusions

Our data indicate that the cytosolic form of MR also responds to the kind of ligand. This is in line with the rapid, non-genomic action of MR elicited by both agonists and antagonists.

Table 1: Proteins identified from the 1D gel in fig. 2. * indicates proteins reported to frequently interact in a nonspecific manner; + indicates a Swiss-Prot entry.

| Band # 1D Gel | GenBank Accession No. | Protein | molecular mass [kDa] calc'd | gel | matching peptides | sequence coverage [%] |
|---|---|---|---|---|---|---|
| 1 | AAA59571 | Mineralocorticoid receptor | 106,5 | 130 | 52 | 35 |
| 2 | P13639 | Elongation factor 2 | 96,4 | 92 | 33 | 38 |
| 3 | P08238 | HSP 90 β (HSPB2)* | 83,4 | 85 | 33 | 24 |
| 3 | P07900 | HSP 90 α (HSPB1)* | 85,0 | 85 | 34 | 23 |
| 4 | P11021 | 78 kDa glucose-regulated protein precursor (GRP78)* | 72,2 | 75 | 33 | 24 |
| 5 | M11717 | 75 kDa glucose-regulated protein, mitochondrial precursor (HSPA9)* | 70,5 | 70 | 18 | 17 |
| 6 | BC017275 | HSPA8* | 64,8 | 70 | 8 | 17 |
| 7 | AAC50088 | HSNC IP5 | 60,9 | 66 | 7 | 17 |
| 8 | P05165 | Propionyl-CoA carboxylase β chain precursor | 58,8 | 58 | 35 | 43 |
| 9 | BAD96744 | Tubulin α3 * | 50,5 | 55 | 8 | 29 |
| 10 | CAA61893 | Tubulin β * | 49,1 | 52 | 9 | 29 |
| 11 | P68732 | Alpha-Enolase | 47,0 | 47 | 9 | 35 |
| 12 | BC007949 | Elongation factor 1 γ | 50,2 | 46 | 33 | 33 |
| 13 | M19449 | Creatin kinase chain B | 42,9 | 43 | 9 | 22 |
| 14 | Q96EB1 | Actin γ* | 40,5 | 42 | 6 | 24 |
| 15 | NP_002286 | Ribosomal Protein RS 4HX* | 32,9 | 39 | 10 | 48 |
| 16 | P04075 | Fructose-bisphosphate aldolase A | 39,7 | 36 | 8 | 37 |
| 17 | P04406 | Glyceraldehyde 3-phosphate dehydrogenase | 36,0 | 35 | 9 | 38 |
| 18 | Q04071 | L-Lactate dehydrogenase | 36,9 | 32 | 7 | 22 |
| 19 | 1433E_HUMAN* | Protein 14-3-3 ε | 26,7 | 28 | 6 | 27 |
| 20 | BC008748 | Protein-L-isoaspartate O-methyl transferase | 24,8 | 25 | 32 | 50 |
| 21 | P27822 | Transgelin-2 | 22,4 | 20 | 8 | 53 |
| 22 | AAA19537 | p23 | 19,0 | 18 | 7 | 45 |

## Cytosolic Mineralocorticoid Receptor interacts differentially with other Proteins depending on Ligand

Miriam Weber[1], Ralf Lösel[2]

[1]Department of Clinical Pharmacology, University Hospital Mannheim, Mannheim, Germany; [2]Department of Applied Chemistry, Technische Hochschule Nürnberg, Nurmeberg, Germany; Contact: ralf.loesel@th-nuernberg.de

### Objective

The Mineralocorticoid Receptor (MR) has attracted considerable interest, as its activation has been shown to pose an independent risk factor for cardiovascular disease. Consequently, antagonists at the MR such as spironolactone are used to prevent progression. MR, like other nuclear receptors, may be located in the nucleus regulating transcription or outside the nucleus, where it may exert nongenomic effects. While the differential recruitment of transcriptional cofactors in the nucleus have been shown for many nuclear receptors, little is known about the interaction of MR in the cytosol. This study aim to identify MR-interacting proteins and the effect of various ligands on the interaction.

### Methods

The coding sequence of human MR was cloned into vectors pEXPR-IBA-103 and -105, thus creating proteins with OneStrepTag fused to the N-terminus or the C-terminus, respectively. Both constructs were functional in transactivation assays (MMTV-Luc).

HEK293T cells were transfected with the constructs. 24 hrs later, cells were stimulated with steroid for 5 min at 37°C, then cooled and lysed. The cleared lysate was passed over an affinty column to siolate the MR and the proteins complexes to it.

Proteins were separated by one dimensional SDS PAGE, bands were stained, excised and digested using trypsin.

The peptides thus obtained were used for protein identification by MALDI (peptide mass fingerprinting) using a BIFLEX or UltraFlex instrument.

### Results

21 Proteins that interact with the cytosolic form of MR were identified. The abundance of some proteins vary with the ligand that is present (aldosterone, spironolactone, or none), most remarkably

-propionyl-CoA carboxylase β precursor, which could be a nonspecific result as its α chain contains biotin, however this does not explain the differential interaction observed.

-GRP78 (also called BiP or HSPA5), a member of the HSP70 family. It is not possible to distinguish between the precursor and the mature protein (as we did not find peptides from aa 1-49), the peptide bearing the KDEL retention signal was consistently found, indicating that GRP78 should reside in the endoplasmic reticulum. MR has been reported to be located also in or at the endoplasmic reticulum in the kidney.

### Conclusions

Our data indicate that the cytosolic form of MR also responds to the kind of ligand that is bound. This is in line with the rapid, non-genomic action of MR elicited by both agonists and antagonists.

PARACELSUS MEDIZINISCHE PRIVATUNIVERSITÄT

Klinikum Nürnberg
Wir sind für Sie da!

# Integration of body composition assessments for preterm infants into clinical routine

L. Lücke, K. Knab, S. Schäfer, J. Zimmermann, A. Szakacs-Fusch, J. Kolaric, N. Rochow, C. Fusch

Department of Pediatrics, Paracelsus Medical University, Nuremberg

## INTRODUCTION

- Age-appropriate body composition (BC) significantly impacts neurological outcomes in preterm infants while preventing risk for possible metabolic diseases and obesity.
- Air displacement plethysmography (PeaPod) is an established standard method, however only available in neonates without respiratory support.
- Recently released Bioimpedance Analysis (BIA) device allows BC assessments in early postnatal period, however still has to be validated.
- The aim of this study is to integrate BC assessments of PeaPod and BIA into clinical routine as tools for nutritional status analysis in preterm infants.

## OBJECTIVES

- To analyze required workload of weekly PeaPod assessments.
- To assess the applicability of PeaPod measurements of preterm infants born for groups of different gestational ages (GA).
- To assess whether growth trajectories from BC measurements are parallel to previously designed reference curves (McMaster PeaPod Study).
- To study feasibility of BIA during early postnatal period and to compare BIA with PeaPod results.

## STUDY DESIGN AND METHODS

- Retrospective analysis of weekly routine BC assessments using the PeaPod in clinically stable infants without respiratory support.
- Additional BIA measurements were performed daily during the first week of life. Subgroup analysis was performed comparing BIA and PeaPod (*Fig. 1*).
- Age-specific percentiles for percent fat mass (FM%), fat mass (FM), and fat-free mass (FFM) in preterm and term infants were calculated from available literature using R.

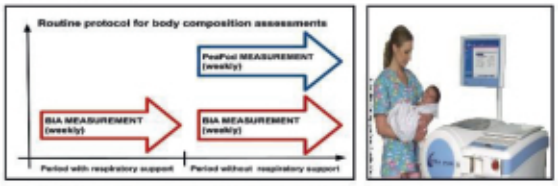


***Fig. 1:*** *Routine protocol for body composition assessments*

## RESULTS

- BC data was collected from January until May 2021 in 115 preterm infants at the University Children's Hospital Nuremberg. The first PeaPod measurement was in the GA group <28 weeks at significantly higher postmenstrual age (PMA) and week of life (WOL) (*Table 1*).

| Gestational age at birth | >28 weeks | 28-32+6/7 wk | >32 weeks | All subjects (<37 weeks) |
|---|---|---|---|---|
| Number of subjects | 10 | 18 | 87 | 115 |
| WOL at first PeaPod test | 11 | 5 | 1 | 2.5 |
| PMA at first PeaPod test | 37 | 35 | 35 | 35.5 |
| Number of tests before discharge | 3 | 2 | 1.5 | 2 |

***Table 1:*** *Frequency of PeaPod assessments in clinical routine per group of GA*

- On average 11 (7-15) weekly PeaPod tests were performed (Total N=214).
- Time required per assessment (including dressing, undressing, weighting, calibration and measurement time) was 15 minutes. Mean total work time required on test day was 165 (105-225) minutes for both, operator and nurse.
- Individual trajectories of PeaPod results for FM and FFM align parallel to reference curves, however follow different percentiles (*Fig. 2 A and B*).
- When results from BIA and Peapod are compared, individual growth trajectories merge with an offset for FM of 60 ±130 g, FFM of 70 ± 140 g and FM% of 2 ± 4 % (*Fig. 2 A, B, C*).

## RESULTS

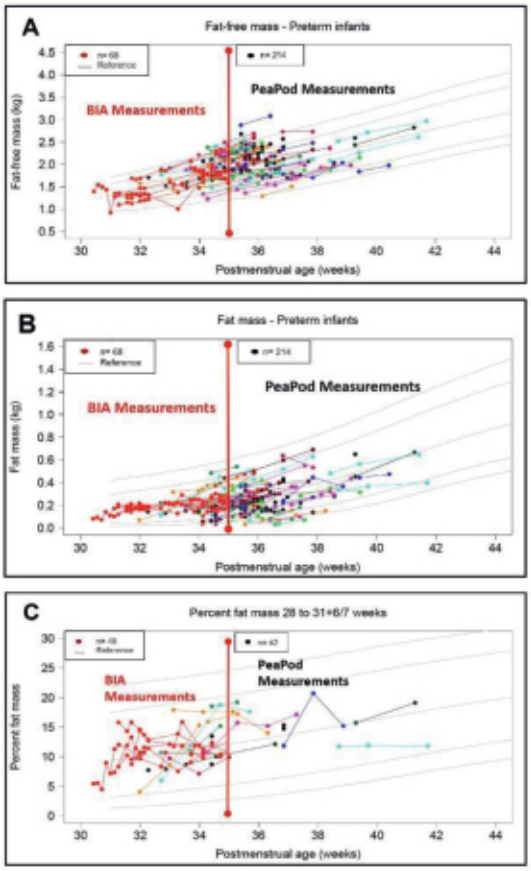


***Fig. 2:*** *BC measurements for postmenstrual age measured with BIA (left, red color) and PeaPod (right, different color for each individual) Panel A: FFM; Panel B: FM; Panel C: FM%; 28 to 31+6/7 weeks GA*

## CONCLUSION

- We have successfully integrated PeaPod BC assessments into clinical routine with reasonable workload.
- Individual BC growth trajectories present individual variability of BC prediction which indicates differing nutritional statuses.
- PeaPod assessments are possible in clinically stable infants. PeaPod measurements are initiated at later WOL and PMA in infants with lower GA. Here, BIA could be used as complement method when PeaPod is not applicable. The observed offset however indicates that further validation would be needed for BIA.
- The established routine allows us, as a leading center for nutrition, growth and development for preterm infants to improve BC development. It opens possibilities for further studies and individual nutritional modification in preterm infants.

Christoph Fusch, MD, PhD, Pediatrics, Paracelsus Medical University, christoph.fusch@klinikum-nuernberg.de

## Integration of body composition assessments for preterm infants into clinical routine

Lennart Lücke[1], Katja Knab[1], Stefan Schäfer[1], Jasper Zimmermann[1], Adel Szakacs-Fusch[1], Julijana Kolaric[1], Niels Rochow[1], Christoph Fusch[1]

[1]Department of Pediatrics, Paracelsus Medical University, Nuremberg, Germany; Contact: lennart.luecke@stud.uni-due.de

### Objective
Air displacement plethysmography (ADP) is a promising method to assess body composition (BC) and the nutritional status in preterm infants. This study aims to analyze the required workload of weekly body composition assessments in preterm infants using the PeaPod device (ADP). Further we aim to assess the applicability of PeaPod measurements of preterm infants born for different groups of gestational ages (GA) and to assess whether growth trajectories from BC measurements are according to previously designed reference charts. This study investigates whether BC results from Bioimpedance Analysis (BIA) are comparable with PeaPod results during the early postnatal period.

### Methods
Retrospective analysis of weekly routine PeaPod assessments were performed in clinically stable infants without respiratory support. Subgroup analysis is performed in infants with additional BIA measurements during the first week of life and then weekly. Age-specific percentiles for percent fat mass (FM%), fat mass (FM), and fat-free mass (FFM) in preterm and term infants were calculated from available literature using R.

### Results
BC data was collected from January until May 2021 in 115 preterm infants GA at birth <37 weeks at the University Children's Hospital Nuremberg. BC tests were performed at higher weeks of life in group <28 GA (11) when compared with group >32 (1). Number of tests before discharge was highest in <28 GA group (3) when compared with a 28-31+6/7 (2) and >32 GA (1.5). 11 (7-15) weekly PeaPod measurements were performed. Time required per assessment (including dressing,undressing, weighting, calibration and measurement time) was 15 minutes. Mean total work time required on test day was 180 (105-225) minutes for both, operator and nurse. Individual trajectories of PeaPod results for FM and FFM align parallel to reference charts. When results from BIA and Peapod are compared, individual growth trajectories merge with an offset of 14±70 g, 11 ± 70 g and 5 ±3 % for FM, FFM and FM%.

### Conclusions
PeaPod BC assessments were successfully integrated into clinical routine with reasonable workload. PeaPod assessments are possible in clinically stable infants. This status is reached later in infants born with low GA. Individual BC growth trajectories suggest BC growth parallel to developed BC reference charts. BIA method could potentially be used as a complement method when PeaPod is not applicable. The observed offset however indicates that further validation would be needed for the BIA method.

# A new exploratory score for determining the prognostic value of MRI in patients with status epilepticus

Machegger L[1], Bosque Varela P[2,3], Zimmermann G[4], Oellerer A[1], Steinbacher J[1], McCoy M[2], Pfaff J[1], Trinka E[2,3], Kuchukhidze G[2,3]

[1] University Institute of Neuroradiology, Christian Doppler Klinik, Paracelsus Medical University of Salzburg, Austria

[2] Department of Neurology, Christian Doppler Klinik, Affiliated Member of the European Reference Network EpiCARE, and Centre for Cognitive Neuroscience, Paracelsus Medical University of Salzburg, Austria

[3] Neuroscience Institute, Christian Doppler Klinik, Salzburg, Austria

[4] Team Biostatistics and Big Medical Data, Intelligent Data Analytics Lab, Paracelsus Medical University of Salzburg, Austria

**Background**: Status epilepticus (SE) is a neurological emergency frequently associated with peri-ictal MRI abnormalities (PMA). PMA commonly include diffusion restriction, hyperperfusion and high signal in T2-weighted images (including FLAIR). PMA can be completely reversible or persistent. It can be followed by permanent alterations such as cortical laminar necrosis, mesial temporal sclerosis and focal brain atrophy. We aimed to determine a prognostic value of PMA for the outcome of SE.

**Methods:** We prospectively recruited 268 patients with SE between February 2019 and January 2021. 145/268 (54%) patients underwent MRI within 48 h after the onset of SE. Patients with hypoxic brain injury (n=6) were excluded. An MRI score based on three aspects: 1) location 2) size and 3) distribution of PMA was used. Alterations in different MRI sequences were considered as separate lesions and were divided into cortical and subcortical. Each location scored 1 point; large lesions - 2 points; in case of presence of both cortical and subcortical lesions the sum was multiplied by 2. An example is given in fig 1 (Total MRI score = 3+3+3+3 = 12 x 2 (since there are neocortical lesions: insula and subcortical lesion: hippocampus.) = 24). This score was correlated with other SE-outcome scores, days spent at intensive care unit (ICU) and admission on ICU.

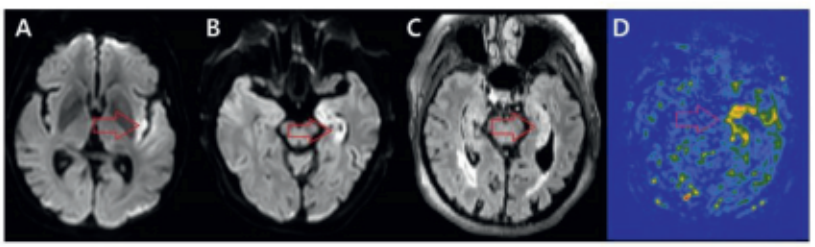


Fig 1. This patient had a total of 4 lesions: DWI restriction in left insula (picture A), DWI restriction in left hippocampus (picture B), hyperintensity in FLAIR in left hippocampus (picture C), hyperperfusion in left hippocampus (picture D).

**Results:** PMA was observed in 53/145 (37%) of patients (51% female; mean 61.7 age 65 years, range 19-93 years). The mean value on an MRI score was 12.6 (range 1-104). Mean values (with range) of other prognostic scores were: STESS (2.7, 0-6); mSTESS (3.2; 0-7); EMSE (45.6; 7-124) and END-IT (2.3; 0-5). Mean days spent on ICU were 5.7 (range 0-45); see fig 2.

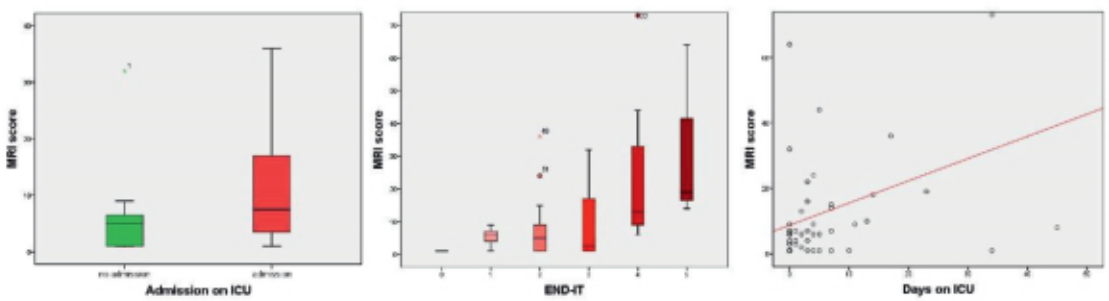


Fig 2. There were moderate positive correlations of MRI score with a need of admission on ICU (r= 0.299, p=0.031), END-IT (r= 0.410, p=0.003) and days spent on ICU (r= 0.374, p=0.006).

**Conclusions:** Our new exploratory MRI score correlates with an unfavorable functional outcome in patients with SE, the need of admission on ICU and a prolonged treatment there.

## A new exploratory score for determining the prognostic value of MRI in patients with status epilepticus

Lukas Machegger[1], Pilar Bosque Varela[2,3], Georg Zimmermann[4], Andreas Oellerer[1], Jürgen Steinbacher[1], Mark McCoy[2], Johannes Pfaff[1], Eugen Trinka[2,3], Giorgi Kuchukhidze[2,3]

[1]University Institute of Neuroradiology, Christian Doppler Klinik, Salzburg, Austria; [2]Department of Neurology, Christian Doppler Klinik, Affiliated Member of the European Reference Network EpiCARE, and Centre for Cognitive Neuroscience, Paracelsus Medical University of Salzburg, Austria; [3]Neuroscience Institute, Christian Doppler Klinik, Salzburg, Austria; [4]Team Biostatistics and Big Medical Data, Intelligent Data Analytics Lab, Paracelsus Medical University of Salzburg, Austria; Contact: l.machegger@salk.at

### Objective
Status epilepticus (SE) is a neurological emergency frequently associated with peri-ictal MRI abnormalities (PMA). PMA commonly include diffusion restriction, hyperperfusion and high signal in T2-weighted images (including FLAIR). PMA can be completely reversible or persistent. It can be followed by permanent alterations such as cortical laminar necrosis, mesial temporal sclerosis and focal brain atrophy. We aimed to determine a prognostic value of PMA for the outcome of SE.

### Methods
We prospectively recruited 268 patients with SE between February 2019 and January 2021. 145/268 (54%) patients underwent MRI within 48 h after the onset of SE. Patients with hypoxic brain injury (n=6) were excluded. An MRI score based on three aspects: 1) location 2) size and 3) distribution of PMA was used. Alterations in different MRI sequences were considered as separate lesions and were divided into cortical and subcortical. Each location scored 1 point; large lesions - 2 points; in case of presence of both cortical and subcortical lesions the sum was multiplied by 2. This score was correlated with other SE-outcome scores, days spent at intensive care unit (ICU) and admission to ICU.

### Results
PMA was observed in 53/145 (37%) of patients (51% female; mean 61.7 age 65 years, range 19-93 years). The mean value on an MRI score was 12.6 (range 1-104). Mean values (with range) of other prognostic scores were: STESS (2.7, 0-6); mSTESS (3.2; 0-7); EMSE (45.6; 7-124) and END-IT (2.3; 0-5). Mean days spent in ICU were 5.7 (range 0-45). There were moderate positive correlations of MRI score with a need of admission to ICU ($r= 0.299$, $p=0.031$), days spent in ICU ($r= 0.374$, $p=0.006$) and END-IT ($r= 0.410$, $p=0.003$).

### Conclusions
Our new exploratory MRI score correlates with an unfavorable functional outcome in patients with SE, the need of admission to ICU and a prolonged treatment there.

# First description of non-obstructing cerebral aqueduct cysts seen in Normal pressure hydrocephalus patients

Machegger L[1], Steinbacher J[1], Klausner F[1], Oellerer A[1], Pfaff J[1], Kuchukhidze G[2,3], Trinka E[2,3], McCoy M[2]

[1] University Institute of Neuroradiology, Christian Doppler Klinik, Paracelsus Medical University of Salzburg, Austria

[2] Department of Neurology, Christian Doppler Klinik, Affiliated Member of the European Reference Network EpiCARE, and Centre for Cognitive Neuroscience, Paracelsus Medical University of Salzburg, Austria

[3] Neuroscience Institute, Christian Doppler Klinik, Salzburg, Austria

**Background**: Normal pressure hydrocephalus (NPH) also described as the symptomatic communicating hydrocephalus (CH), is clinically characterized by the triad of dementia, gait disturbance and urinary incontinence in elderly individuals. Diagnosing CH or NPH is challenging, as it may be difficult to separate it from other neurodegenerative diseases. In addition to a morphological change such as the dilatation of the cerebral aqueduct, called the "trumpet sign", rare findings as aqueduct cysts may also underline the presence of an increased absolute stroke volume.

**Methods:** We retrospectively identified 193 patients clinically suspicious for NPH at our institution between March 2016 and November 2019. These patients underwent MRI with CSF Drive, a heavily T2 weighted sequence for visualization of CSF and a CSF PCA sequence for the purpose of visualizing the CSF flow within the aqueduct. Furthermore, quantitative CSF-velocity imaging of the cerebral aqueduct for measuring the aqueductal lumen area and CSF velocity was performed.

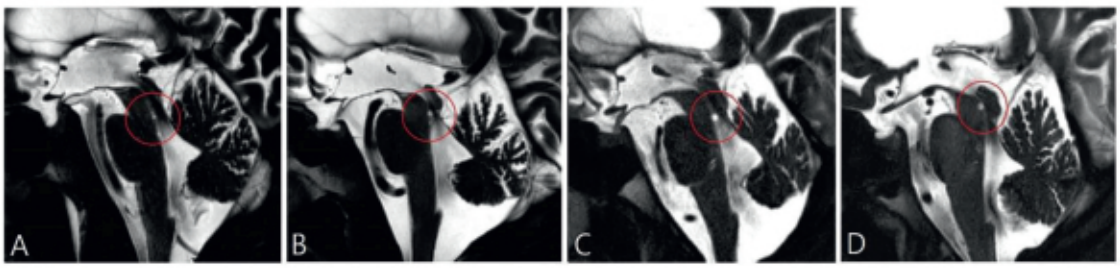


Fig 1. Four examples of cerebral aqueduct cysts in NPH patients with exaggerated flow void due to elevated absolute stroke volume.

**Results:** Cerebral aqueduct cysts were observed in 13/193 (6.7%) of patients (38.5% female; median age 71 years, range 58-80 years). The median absolute stroke volume in milliliters for patients with cysts was 0.430 (range 0.130-1.050) compared to without 0.120 (range 0.000-1.040), for forward flow volume 0.210 (range 0.060-0.510) compared to 0.120 (range 0.000-0.650) and for backward flow volume 0.225 (range 0.060-0.530) compared to 0.120 (range 0.000-0.470). There were moderate positive correlations of absolute stroke volume (r= 0.205, p=0.006), forward flow volume (r= 0.208, p=0.005) and backward flow volume (r= 0.204, p=0.006).

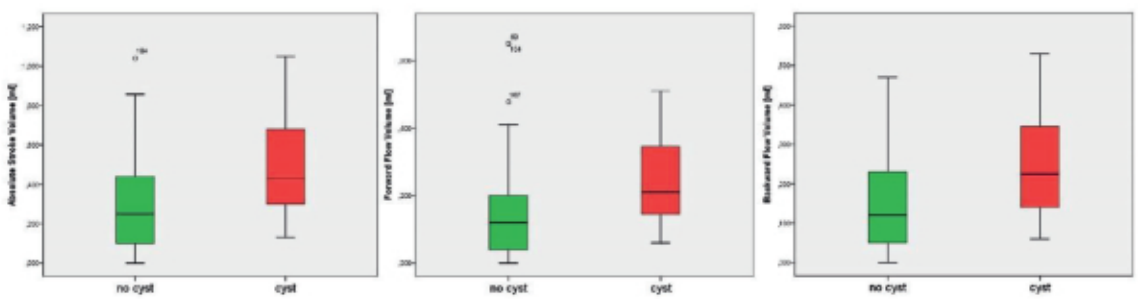


Fig 2. There were moderate positive correlations of absolute stroke volume (r= 0.205, p=0.006), forward flow volume (r= 0.208, p=0.005) and backward flow volume (r= 0.204, p=0.006).

**Conclusions:** The occurrence of non-obstructing cerebral aqueduct cysts is associated with increased absolute stroke volume in patients with long standing communicating hydrocephalus such as in normal pressure hydrocephalus.

## First description of non-obstructing cerebral aqueduct cysts seen in Normal pressure hydrocephalus patients

Lukas Machegger[1], Jürgen Steinbacher[1], Fritz Klausner[1], Andreas Oellerer[1], Johannes Pfaff[1], Giorgi Kuchukhidze[2,3], Eugen Trinka[2,3], Mark McCoy[2]

[1]University Institute of Neuroradiology, Christian Doppler Klinik, Paracelsus Medical University of Salzburg, Austria; [2]Department of Neurology, Christian Doppler Klinik, Affiliated Member of the European Reference Network EpiCARE, and Centre for Cognitive Neuroscience, Paracelsus Medical University of Salzburg, Austria; [3]Neuroscience Institute, Christian Doppler Klinik, Salzburg, Austria; Contact: l.machegger@salk.at

### Objective
Normal pressure hydrocephalus (NPH) also described as the symptomatic communicating hydrocephalus (CH), is clinically characterized by the triad of dementia, gait disturbance and urinary incontinence in elderly individuals. Diagnosing CH or NPH is challenging, as it may be difficult to separate it from other neurodegenerative diseases. In addition to a morphological change such as the dilatation of the cerebral aqueduct, called the "trumpet sign", rare findings as aqueduct cysts may also underline the presence of an increased absolute stroke volume.

### Methods
We retrospectively identified 193 patients clinically suspicious for NPH at our institution between March 2016 and November 2019. These patients underwent MRI with CSF Drive, a heavily T2 weighted sequence for visualization of CSF and a CSF PCA sequence for the purpose of visualizing the CSF flow within the aqueduct. Furthermore, quantitative CSF-velocity imaging of the cerebral aqueduct for measuring the aqueductal lumen area and CSF velocity was performed.

### Results
Cerebral aqueduct cysts were observed in 13/193 (6.7%) of patients (38.5% female; median age 71 years, range 58-80 years). The median absolute stroke volume in milliliters for patients with cysts was 0.430 (range 0.130-1.050) compared to without 0.120 (range 0.000-1.040), for forward flow volume 0.210 (range 0.060-0.510) compared to 0.120 (range 0.000-0.650) and for backward flow volume 0.225 (range 0.060-0.530) compared to 0.120 (range 0.000-0.470). There were moderate positive correlations of absolute stroke volume ($r = 0.205$, $p=0.006$), forward flow volume ($r = 0.208$, $p=0.005$) and backward flow volume ($r = 0.204$, $p=0.006$).

### Conclusions
The occurrence of non-obstructing cerebral aqueduct cysts is associated with increased absolute stroke volume in patients with long standing communicating hydrocephalus such as in normal pressure hydrocephalus.

PARACELSUS
MEDIZINISCHE PRIVATUNIVERSITÄT

Klinikum Nürnberg
Wir sind für Sie da!

# Results from the 10 years follow-up following sutureless aortic valve replacement: survival and hemodynamic outcomes

H. Mamdooh[1], F. Pollari[1], F. Jiven-Jetzelsberger[1], I. Großmann[1], F. Vogt[1], T. Fischlein[1]

*1) Cardiac Surgery, Paracelsus Medical University – Klinikum Nürnberg, Nuremberg, Germany; Contact: Hazem.Mamdooh@klinikum-nuernberg.de.*

## OBJECTIVE

Surgical aortic valve replacement with a sutureless prosthesis (Su-AVR, Figure 1) was introduced in last decade as an attractive alternative to conventional AVR especially in elderly and high-risk patients or in candidates for a minimal invasive approach[1]. However, data regarding long-term outcomes and prosthesis durability are still lacking.

We aimed to investigate the survival and hemodynamic outcomes in a long-term follow-up.



Fig.1. Aa sutureless aortic valve prosthesis "Perceval" (LivaNova, Saluggia, Italy)

Fig.2. Left: a patient that underwent an isolated AVR through a miniaturotomy. Right: draw showing the anatomical relations of this minimally invasive access.



Fig.3. Classification of valve prosthesis degeneration according to ESC guidelines.

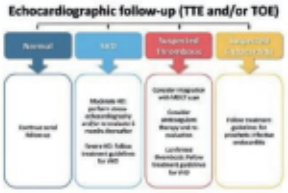


## METHODS

- 605 patients who underwent successfully Su-AVR between 2010 and January 2021 were screened
- *Excluded patients who underwent Su-AVR because of reAVR (29) and active endocarditis (5) --> 570 were suitable for analysis*
- All isolated Su-AVR were performed through a mini-J sternotomy (Figure 2)
- A follow-up including a transthoracic echocardiography was performed (according to ESC guidelines 2017, Figure 3) [2]

## RESULTS

Mean age was 76.5±5.2 years, 52% were female, 4% were in dialysis, 8.3% had a prior cardiac surgery, mean logistic Euroscore was 14%±12, mean Euroscore II 3.7%±4. 35% underwent a combined procedure such as a concomitant CABG (n=145) or an intervention on the mitral valve (n=14). Overall 30 days mortality was 3.3%, and 2% for isolated Su-AVR. Mean Follow-up = 2.5 years ± 2.3. Incidence of paravalvular leaks (PVL) >mild was 0% at 1 year and remained stable; 2.9% (2 over 68 patients) showed a moderate PVL after 10 years. Reintervention rate, Re-AVR or TAVI, due to structural deterioration was: 0.17% after 1 year, 1% after 3 years, 5.7% after 5 years, 5.8% after 10 years. 7 patients experienced a prosthetic valve endocarditis (PVE) at follow-up (1.2%). Of these, 4 patients had an early PVE (2, 4, 5 and 10 months after implantation), and 3 patients a late PVE (1 case after 3 years and 2 cases after 5 years).

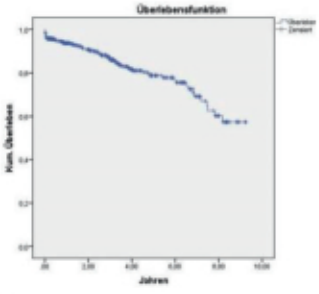


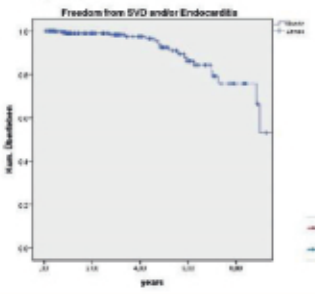


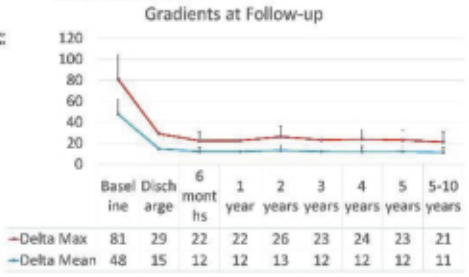


| | Baseline | Discharge | 6 months | 1 year | 2 years | 3 years | 4 years | 5 years | 5-10 years |
|---|---|---|---|---|---|---|---|---|---|
| Delta Max | 81 | 29 | 22 | 22 | 26 | 23 | 24 | 23 | 21 |
| Delta Mean | 48 | 15 | 12 | 12 | 13 | 12 | 12 | 12 | 11 |

## CONCLUSION

- The sutureless prosthesis shows a good hemodynamic performance also in the long-term follow-up.
- The incidence of endocarditis was low and prosthesis degeneration is comparable to standard bioprosthesis.
- Both Re-AVR and TAVI-in-Sutureless are possible solutions in case of degeneration.
- **Our findings supports a sutureless solution in candidates for bioprostheses at intermediate risk with a life-expectancy up to 10 years.**




References

1. Pollari F, et al. Better short-term outcome by using sutureless valves: a propensity-matched score analysis. Ann Thorac Surg. 2014 Aug;98(2):611-6; discussion 616-7. doi: 10.1016/j.athoracsur.2014.04.072.
2. European Heart Journal (2017) 38, 3382–3390

© Paracelsus Medizinische Privatuniversität Nürnberg – Universitätsklinik für Herzchirurgie

## Results from the 10 years follow-up following sutureless aortic valve replacement: survival and hemodynamic outcomes

Hazem Mamdooh[1], Francesco Pollari[1], Fatima Jiven-Jetzelsberger[1], Irena Großmann[1], Ferdinand Vogt[1], Theodor Fischlein[1]

[1]Cardiac surgery, Klinikum Nürnberg - Paracelsus Medical University; Contact: Hazem.Mamdooh@klinikum-nuernberg.de

### Objective

Surgical aortic valve replacement with a sutureless prosthesis (Su-AVR) was introduced in last decade as an attractive alternative to conventional AVR especially in elderly and high-risk patients or in candidates for a minimal invasive approach [1]. However, data regarding long-term outcomes and prosthesis durability are still lacking.

### Methods

We retrospectively analyzed 605 patients who underwent successfully AVR with a sutureless prosthesis in our center between 2010 and january 2021. Indication for Su-AVR was severe aortic valve stenosis or degenerated aortic valve prosthesis in high- or intermediate risk patients. All isolated Su-AVR were performed through a mini-J sternotomy. A follow-up including a transthoracic echocardiography , according to ESC guidelines [2], was performed in our institutional outpatient's ward.

### Results

Mean age was 76.5±5.2 years, 52% were female, 4% were in dialysis, 8.3% had a prior cardiac surgery, mean logistic Euroscore was 14%±12, mean Euroscore II 3.7%±4. 35% underwent a combined procedure such as a concomitant CABG (n=145) or an intervention on the mitral valve (n=14). Overall
30 days mortality was 3.3%, and 2% for isolated Su-AVR. Following mean gradients were observed: 12±4.4mmHg at 1st year; 12.9±5.1 at 2nd year; 12.1±6 mmHg at 3rd year; 12±5.6 mmHg at 4th year; 16.8±15 at 5th year; 13.6±13 at 10th year.
Incidence of paravalvular leaks (PVL) >mild was 0% at 1 year and remained stable; 2.9% (2 over 68 patients) showed a moderate PVL after 10 years. Reintervention rate, Re-AVR or TAVI, due to structural deterioration was: 0.17% after 1 year, 1% after 3 years, 5.7% after 5 years, 5.8% after 10 years. 7 patients experienced a prosthetic valve endocarditis (PVE) at follow-up (1.2%). Of these, 4 patients had an early PVE (2, 4, 5 and 10 months after implantation), and 3 patients a late PVE (1 case after 3 years and 2 cases after 5 years).

### Conclusions

Clinical outcomes and hemodynamic performance of sutureless AVR were excellent. Incidence of prosthesis degeneration and endocarditis were low in this long term follow up.

### References

1. Better short-term outcome by using sutureless valves: a propensity-matched score analysis. Pollari F, Santarpino G, Dell'Aquila AM, Gazdag L, Alnahas H, Vogt F, Pfeiffer S, Fischlein T. Ann Thorac Surg. 2014 Aug;98(2):611-6; discussion 616-7. doi: 10.1016/j.athoracsur.2014.04.072. Epub 2014 Jun 10.
2. European Heart Journal (2017) 38, 3382–3390

# Determinants of Hyperglucagonemia in Pediatric Non-alcoholic Fatty Liver Disease

K. Maruszczak[1,2], K. C. Radzikowski[1], S. Schütz[1,2], P. Bergsten[3], H. Mannell[3], Anders Forslund[4], K. Mörwald[1,2], H. Mangge[5], D. Weghuber[1,2,*]

[1]Department of Pediatrics, Paracelsus Private Medical School, Salzburg, Austria;
[2]Obesity Research Unit, University Hospital Salzburg, Paracelsus Medical University, Salzburg, Austria
[3]Department of Medical Cell Biology, University Uppsala, Uppsala, Sweden
[4]Department of Women's and Children's Health, University Uppsala, Uppsala, Sweden
[5]Clinical Institute for Medical and Chemical Laboratory Diagnosis, Medical University Graz, Graz, Austria
*Correspondence: Daniel Weghuber d.weghuber@salk.at

## OBJECTIVE

Over the years, non-alcoholic fatty liver (NAFLD) disease has progressed to become the most frequent chronic liver disease in children and adolescents. The full pathology is not yet known, but disease progression leads to cirrhosis and hepatocellular carcinoma. Risk factors included hypercaloric diet, obesity, insulin resistance and genetics. Hyperglucagonemia appears to be a pathophysiological consequence of hepatic steatosis, thus, **the aim of the study is that hepatic fat accumulation leads to increased insulin resistance and impaired glucagon metabolism leading to hyperglucagonemia in pediatric NAFLD.**

## METHODS

- 132 children and adolescents between 10 and 18 years, with varying degrees of obesity, were included in the study.
- Using Magnetic Resonance Imaging (MRI) average liver fat was determined, and patients were stratified as NAFLD (≥5% liver fat content) and non-NAFLD (≤5%).
- All patients underwent a standardized oral glucose tolerance test (OGTT).
- Additionally, anthropometric parameters (height, weight, BMI, waist circumference, hip circumference) such as lab data including lipid profile (triglycerides, HDL, LDL), liver function parameters (ALT, AST), uric acid, glucose metabolism (fasting insulin and glucagon, HbA1c, glucose 120 min) and indices evaluating insulin resistance (HIRI, SPISE, HOMA-IR, WBISI) were measured.
- Statistical analysis: NAFLD groups were matched 1:1 according to nearest neighbor algorithm for BMI-SDS. Non-parametric Wilcoxon rank sum tests were applied for unpaired samples. Investigations of dependencies were assessed using univariate regression models. For the NAFLD subgroup evaluation a correlation analysis was done, following a mixed method approach for modelling the predictors.

**Table 1.** Baseline characteristics of the study population and comparison of NAFLD and non-NAFLD patients matched for BMI-SDS

| | Study population (N = 132*) | NAFLD (N = 66) | Non-NAFLD (N = 66) | p-value |
|---|---|---|---|---|
| **CLINICAL FEATURES** | | | | |
| Age (years) | 14.09 ± 2.34 | 14.38 ± 2.33 | 14.03 ± 2.48 | 0.69 |
| Tanner stage* | I: 10 (7.6%)<br>II-IV: 83 (62.9%)<br>V: 30 (22.7%)<br>n.a.: 9 (6.8%) | I: 7 (10.1%)<br>II-IV: 42 (63.6%)<br>V: 13 (19.6%)<br>n.a.: 4 (6.1%) | I: 3 (4.5%)<br>II-IV: 41 (62.1%)<br>V: 17(25.8%)<br>n.a.: 5 (7.6%) | |
| BMI (kg/m²) | 31.53 ± 6.86 | 32.38 ± 4.61 | 32.05 ± 4.98 | 0.74 |
| BMI-SDS | 2.67 ± 1.12 | 2.84 ± 0.51 | 2.77 ± 0.49 | 0.38 |
| SBMI (kg/m²) | 33.96 ± 5.83 | 34.93 ± 3.52 | 34.63 ± 3.51 | 0.57 |
| Waist circumference (cm) | 101.95 ± 17.48 | 105.30 ± 13.26 | 103.89 ± 12.85 | 0.77 |
| Hip circumference (cm) | 107.91 ± 14.99 | 107.88 ± 11.57 | 110.45 ± 12.76 | 0.16 |
| Waist-to-hip-ratio | 0.94 ± 0.09 | 0.98 ± 0.09 | 0.94 ± 0.08 | 0.02 |
| BP systolic (mmHg) | 120.53 ± 11.57 | 121.51 ± 12.19 | 121.28 ± 10.55 | 0.99 |
| **BODY FAT COMPOSITION** | | | | |
| Total body fat (%) | 42.50 ± 5.87 | 41.30 ± 6.42 | 41.54 ± 4.69 | 0.87 |
| MRI VAT volume (cm³) | 1483.46 ± 703.24 | 1753.67 ± 662.31 | 1382.27 ± 433.62 | 0.00 |
| MRI SAT volume (cm³) | 8332.09 ± 2789.08 | 8867.25 ± 3068.33 | 8625.70 ± 2127.87 | 0.99 |
| MRI liver fat content (%) | 9.38 ± 10.26 | 15.59 ± 10.95 | 3.17 ± 0.87 | 0.00 |
| **GLUCOSE METABOLISM** | | | | |
| Fasting glucose (mmol/l) | 5.15 ± 1.27 | 5.25 ± 2.81 | 5.01 ± 0.60 | 0.54 |
| OGTT 120 min. glucose (mmol/l) | 6.72 ± 2.16 | 7.16 ± 2.89 | 6.41 ± 1.39 | 0.22 |
| Fasting insulin (µU/ml) | 111.85 ± 80.79 | 129.49 ± 99.40 | 104.03 ± 66.58 | 0.08 |
| HbA1c (mmol/mol) | 35.81 ± 7.09 | 37.47 ± 11.95 | 34.77 ± 2.93 | 0.15 |
| Fasting glucagon (µU/ml) | 11.84 ± 6.69 | 14.30 ± 8.54 | 10.38 ± 3.68 | 0.01 |
| SPISE | 5.47 ± 2.43 | 4.80 ± 1.34 | 5.12 ± 1.34 | 0.22 |
| WBISI | 5.47 ± 4.33 | 4.14 ± 2.83 | 4.89 ± 2.05 | 0.10 |
| HIRI | 47661.88 ± 36967.22 | 52958.30 ± 29584.58 | 45451.40 ± 21246.58 | 0.46 |
| HOMA-IR | 3.75 ± 2.51 | 4.41 ± 2.82 | 3.32 ± 1.84 | 0.06 |
| **LIPID PROFILE** | | | | |
| Total cholesterol (mmol/l) | 4.12 ± 0.76 | 4.30 ± 0.87 | 4.13 ± 0.66 | 0.24 |
| LDL cholesterol (mmol/l) | 2.48 ± 0.68 | 2.66 ± 0.79 | 2.40 ± 0.61 | 0.08 |
| HDL cholesterol (mmol/l) | 1.28 ± 0.32 | 1.19 ± 0.24 | 1.28 ± 0.37 | 0.32 |
| Triglycerides (mmol/l) | 1.17 ± 0.68 | 1.37 ± 0.73 | 1.05 ± 0.51 | 0.01 |
| Adiponectin (µg/ml) | 7.72 ± 3.07 | 7.12 ± 2.89 | 8.39 ± 3.17 | 0.11 |
| Leptin (ng/ml) | 35.18 ± 22.40 | 31.87 ± 15.67 | 37.45 ± 28.26 | 0.87 |
| **LIVER FUNCTION** | | | | |
| AST (µkat/l) | 0.53 ± 0.31 | 0.64 ± 0.44 | 0.45 ± 0.23 | 0.00 |
| ALT (µkat/l) | 0.66 ± 0.64 | 0.80 ± 0.79 | 0.57 ± 0.29 | 0.00 |
| GGT (µkat/l) | 0.37 ± 0.28 | 0.49 ± 0.42 | 0.29 ± 0.11 | 0.00 |
| Uric acid (µmol/l) | 349.68 ± 81.32 | 365.77 ± 87.34 | 330.38 ± 91.39 | 0.06 |

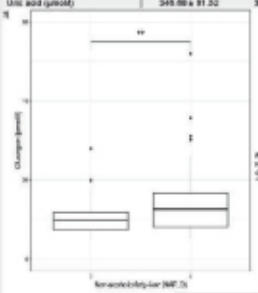


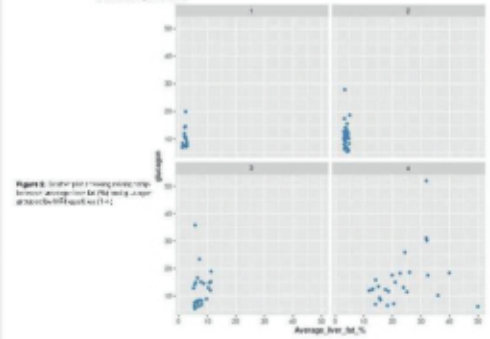


**Table 2.** Multivariate regression analysis with standardized coefficients, determinants of hyperglucagonemia (NAFLD, n = 21)

| Model 1 | Coefficient | Standard Error | p-value |
|---|---|---|---|
| Average liver fat, % | 0.097620 | 0.136 | 0.477 |
| VAT, cm² | 0.000894 | 0.002 | 0.017 |
| HIRI | 0.000167 | 0.00005 | 0.083 |
| **Model 2** | | | |
| Average liver fat, % | 0.18 | 0.10 | 0.073 |
| HOMA-IR | 0.14 | 0.07 | 1 |
| Fasting insulin | 0.07 | 0.04 | 0.211 |

## RESULTS

- Children and adolescents with NAFLD had significantly higher fasting glucagon values compared to the non-NAFLD cohort (p=0.0079), figure 1.
- In the study population univariate analysis of fasting glucagon was associated with BMI-SDS (p<0.01), BMI (kg/m²) (p=0.073), visceral adipose tissue volume (VAT) (p<0.001), average liver fat content (p<0.001), fasting insulin concentration (p<0.001), triglycerides (p<0.001) and HDL (p=0.034).
- This correlation equally applied to all insulin indices HOMA-IR, WBSI, HIRI (all p<0.001) and SPISE (p<0.002).
- The MRI quartiles showed that the fourth cut-off had the highest correlation between average liver fat and glucagon (cut-offs: 25% = 2.91%, 50% 5.11%, 75% = 11.73%) matched for BMI-SDS.
- Two models were done in a stepwise multiple regression analysis for the NAFLD subgroup analysis showing that HIRI (p=0.001) and VAT volume (p=0.006) are the best predictors for hyperglucagonemia in pediatrics.

### Conclusion

Children and adolescents with NAFLD have significantly higher fasting plasma glucagon values, which can best be predicted by the insulin index HIRI and visceral adipose tissue, showing that metabolically the hepatic resistance is a leading cause for hyperglucagonemia.

**ACKNOWLEDGEMENT & FUNDING**

European Union's Seventh Framework Programme (FP7/2007–2013) under grant agreement number 279153 (Beta-JUDO). In addition, support for the study was received from the Regional Research Council in Uppsala, Sweden, the Swedish Diabetes Foundation, the Swedish Society for Diabetology, Swedish Research Council (2016-01040).

## Determinants of hyperglucagonemia in pediatric non-alcoholic fatty liver disease

Katharina Maruszczak[1, 2]

[1]Department of Pediatrics, University Hospital Salzburg, Division of Gastroenterology, Hepatology and Nutrition, Paracelsus Medical University, Salzburg, Austria; [2]Obesity Research Unit, University Hospital Salzburg, Paracelsus Medical University, Salzburg, Austria; [3]Department of Medical Cell Biology, University Uppsala, Uppsala, Sweden; [4]Department of Women's and Children's Health, University Uppsala, Uppsala, Sweden; [5]Clinical Institute for Medical and Chemical Laboratory Diagnosis, Medical University Graz, Graz, Austria; Contact: k.maruszczak@salk.at

### Objective
Over the years, non-alcoholic fatty liver (NAFLD) disease has progressed to become the most frequent chronic liver disease in children and adolescents. The full pathology is not yet known, but disease progression leads to cirrhosis and hepatocellular carcinoma. Risk factors included hypercaloric diet, obesity, insulin resistance and genetics. Hyperglucagonemia appears to be a pathophysiological consequence of hepatic steatosis, thus, the aim of the study is that hepatic fat accumulation leads to increased insulin resistance and impaired glucagon metabolism leading to hyperglucagonemia in pediatric NAFLD.

### Methods
132 children and adolescents between 10 and 18 years, with varying degrees of obesity, were included in the study. Using Magnetic Resonance Imaging (MRI) average liver fat was determined, and patients were stratified as NAFLD (>5% liver fat content) and non-NAFLD (<5%). All patients underwent a standardized oral glucose tolerance test (OGTT). Additionally, anthropometric parameters (height, weight, BMI, waist circumference, hip circumference) such as lab data including lipid profile (triglycerides, HDL, LDL), liver function parameters (ALT, AST), uric acid, glucose metabolism (fasting insulin and glucagon, HbA1c, glucose 120 min) and indices evaluating insulin resistance (HIRI, SPISE, HOMA-IR, WBISI) were measured.

### Results
Children and adolescents with NAFLD had significantly higher fasting glucagon values compared to the non-NAFLD cohort ($p=0.0079$). In the NAFLD cohort univariate analysis of fasting glucagon was associated with BMI-SDS ($p<0.01$), BMI (kg/m$^2$) ($p=0.073$), visceral adipose tissue volume (VAT) ($p<0.001$), average liver fat content ($p<0.001$), fasting insulin concentration ($p<0.001$), triglycerides ($p<0.001$) and HDL ($p=0.034$). This correlation equally applied to all insulin indices HOMA-IR, WBSI, HIRI (all $p<0.001$) and SPISE ($p<0.002$). Multivariate analysis ($r^2/R^2$ adjusted 0.557/0.509) for the same subgroup identified HIRI ($p=0.001$), VAT volume ($p=0.006$) and average liver fat content ($p=0.477$) as the best predictors for hyperglucagonemia.

### Conclusions
Children and adolescents with NAFLD have significantly higher fasting plasma glucagon values, which can best be predicted by the insulin index HIRI and visceral adipose tissue.

# Glucagon, NAFLD and Amino Acids – an Evidence Map

Katharina Maruszczak[1,2], Pia Koren[1], Konrad Radzikowski[1], Gabriel Torbahn[3], Daniel Weghuber[1,2]

[1]Department of Pediatrics, University Hospital Salzburg, Division of Gastroenterology, Hepatology and Nutrition, Paracelsus Medical University, Salzburg, Austria,
[2]Obesity Research Unit, University Hospital Salzburg, Paracelsus Medical University, Salzburg, Austria,
[3]Department of Pediatrics, Paracelsus Medical University, Nürnberg, Germany

## OBJECTIVES

- Comorbidities of obesity cause variations in distinct metabolic pathways, such as hepatic fat accumulation which leads to non-alcoholic fatty liver disease (NAFLD)
- Aim of this evidence map is to systematically evaluate the present literature and to identify research gaps on the glucagon induced amino acid turnover and its metabolic interaction with NAFLD.

## METHODS

- Systematic literature search in three electronic databases (Medline, Embase, Web of Science).
- Screening of titles/abstracts and full-texts by two independent reviewers.
- Eligibility criteria:
  - Patients: e.g. non-diabetic patients, NAFLD, with or without obesity, increased liver enzymes, fasting amino acids, fasting glucagon
  - Studies: Quantitative studies of either humans or animals and required to contain at least two of the three main research areas, these being glucagon, amino acid metabolism and NAFLD
  - No restriction on geographical location or language
- Data was extracted independently by two reviewers.
- Conflicts were resolved by discussion or a third reviewer.

## RESULTS

- Twenty-nine references were finally included (see Fig. 1).
- The publication years dated back until 1965 and showed a great increase from 2014 to 2020 (see Fig. 2).
- Only 1 study focused on adolescents, all other studies were carried out among adults.
- The most common comorbidity was obesity.
- In total there were 13 animal studies and 16 human studies.
- Study designs in human experiments: case-control studies (n=10), cross-sectional studies (n=4), RCT (n=1) and experimental studies (n=1)
- The hyperinsulinemic-euglycemic clamp and the oral glucose tolerance test were the most used experimental methods to evaluate metabolic changes.
- Metabolic pathways in focus are displayed in Fig. 3.

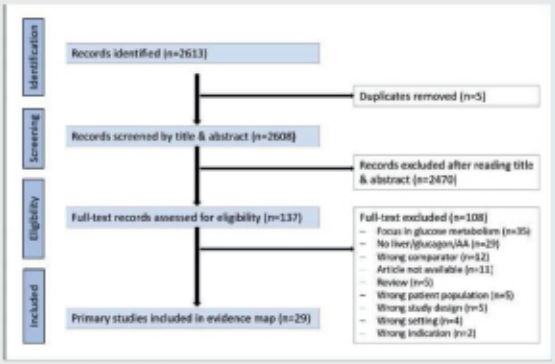


Fig. 1: PRISMA flow-chart

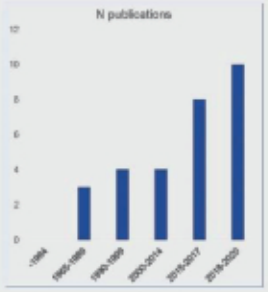


Fig. 2: Publication frequency of studies on glucagon, amino acids and NAFLD

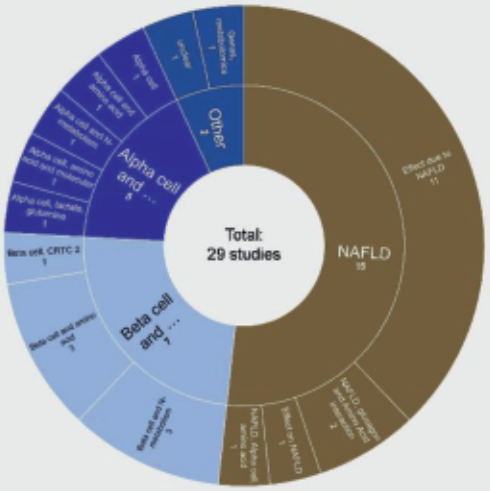


Fig. 3: Sunburst chart of metabolic pathways in focus

## CONCLUSION

**Research assessing the interaction of NAFLD, glucagon and the amino acid metabolisms in human studies are sparse and completely lacking in pediatrics. Furthermore, longitudinal studies such as studies focusing on hyperglucagonemia independent of diabetes but related to NAFLD present an unambiguous research gap.**

## Glucagon, NAFLD and Amino acids- an Evidence map

Katharina Maruszczak[1, 2]

[1]Department of Pediatrics, University Hospital Salzburg, Division of Gastroenterology, Hepatology and Nutrition, Paracelsus Medical University, Salzburg, Austria; [2]Obesity Research Unit, University Hospital Salzburg, Paracelsus Medical University, Salzburg, Austria; [3]Department of Pediatrics, Paracelsus Medical University, Nuernberg, Germany; Contact: k.maruszczak@salk.at

### Objective
Health systems are not only confronted with the growing worldwide childhood obesity epidemic, but also associated comorbidities. These subsequently cause variations in distinct metabolic pathways, such as hepatic fat accumulation, which leads to non-alcoholic fatty liver disease (NAFLD). The aim of this evidence map is to systematically evaluate the literature and to identify research gaps on the glucagon induced amino acid turnover and its metabolic interaction with NAFLD.

### Methods
A systematic literature search was conducted in April 2020 to identify research using three electronic databases. Two independent reviewers screened titles and abstracts, according to prespecified eligibility criteria, as well as full-text articles. Quantitative studies of either humans or animals, at all age, were included. Studies were required to contain at least two of the main research areas, being glucagon, amino acid metabolism and NAFLD. Data was independently extracted by two reviewers and summarized according to study design, publication year, comorbidities, age, sex, sample size, intervention, study duration and control group. Conflicts were resolved by discussion or a third reviewer.

### Results
Twenty-nine references were finally included. The publication years dated back until 1965 and showed a great increase from 2012 to 2020. All studies were carried out among adults, only 1 study focused on adolescents. The most common comorbidity was obesity. In total there were 13 animal studies and 16 human studies. The study designs in the human experiments differed immensely. The hyperinsulinemic-euglycemic clamp and the oral glucose tolerance test were the most used experimental methods to evaluate metabolic changes. Thirteen studies focused on metabolic effects due to NAFLD, however only 2 studies focused on the interaction of NAFLD, glucagon and the amino acid metabolism, both being non-human studies. The other 14 studies focused on metabolomics, beta cell function or just on one topic of the research area and not as an interaction on one another.

### Conclusions
Research on the interaction of NAFLD, glucagon and the amino acid metabolisms in human studies is sparse and completely lacking in pediatrics. Furthermore, longitudinal studies such as studies focusing on hyperglucagonemia independent of diabetes but related to NAFLD present an unambiguous research gap.

# Pathogenicity assessment of pendrin (SLC26A4) variant p.L117F

Arnoldas Matulevicius[1], Karen B. Avraham[2], Antonio Sarikas[1], Silvia Dossena[1]

[1]Institute of Pharmacology and Toxicology, Paracelsus Medical University, Salzburg, Austria
[2]Department of Human Molecular Genetics and Biochemistry, Sackler Faculty of Medicine, Tel Aviv, Israel

## Background and Objective

- Pendrin (SLC26A4) is an anion exchanger encoded by the *SLC26A4* gene.
- *SLC26A4* mutations result in inherited hearing loss characterized by malformations of the inner ear.
- p.L117F is the most common variant of *SLC26A4* gene in the deaf Jewish Ashkenazi population and has been reported in homozygosis in multiple individuals with hearing loss (K.B. Avraham Lab internal data).
- Nevertheless, two independent reports described a lack of functional impairment for this variant, therefore its clinical significance cannot be determined with certainty [1,2].
- To solve this contradiction and reach a conclusive pathogenicity assignment or exclusion for the p.L117F pendrin variant, we characterized its ion transport activity, transcript and protein expression levels as well as subcellular localization in cell-based assays and compared these molecular features to those of wild type pendrin.

## Methods

- Wild type and p.L117F pendrin variants were cloned in mammalian expression vectors and expressed in HEK293 Phoenix and HeLa cells.
- Ion transport function of pendrin variants was evaluated by quantitative measurement of iodide/chloride exchange using a fluorometric method based on the iodide sensitivity of an EYFP variant (EYFP p.H148Q, I152L) (3,4) (**Figure 1**).

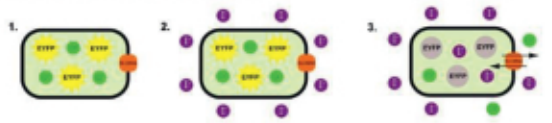


**Figure 1. Schematic principle of functional assay of iodide exchange.** (1) Cells co-expressing SLC26A4 (orange) and the iodide-sensitive EYFP isoform (yellow). (2) Iodide addition to the extracellular environment. (3) Flux of iodide toward cytosol through SLC26A4 in exchange for chloride, resulting in fluorescence decrease of the iodide-sensitive EYFP isoform

- Messenger RNA expression levels were assessed by real-time RT-qPCR.
- Subcellular localization was assessed by co-localization of the fusion protein pendrin-EYFP with appropriate markers of the plasma membrane (PM) and endoplasmic reticulum (ER) (5,6).
- Protein expression levels were assessed by quantitative imaging.

## Results

- There was no significant difference in mRNA expression levels between wild type pendrin and its variant p.L117F (**Figure 2**).
- Determination of subcellular localization of proteins showed that, similarly to wild type pendrin, pendrin p.L117F was efficiently transposed to the PM (**Figure 3**).
- However, co-localization with the ER denoted that a small but significant fraction of pendrin p.L117F was retained in this subcellular compartment (**Figure 4**).
- The protein expression levels of pendrin p.L117F were significantly reduced compared to those of the WT (43% reduction, $p<0.05$, n=20, one-way ANOVA with Bonferroni's multiple comparison test) (**Figure 5**).
- In parallel, the ion transport function of this variant was affected (42% reduction, $p<0.001$, n=24, one-way ANOVA with Bonferroni's multiple comparison test), but not completely abrogated (**Figure 6**).
- Treatment of cells transfected with pendrin p.L117F with an inhibitor of the ubiquitin proteasome system (10 µM carfilzomib for 16 hours) significantly increased pendrin p.L117F protein expression levels (153.5±14.3%, n=20, $p<0.001$) when compared to cells exposed to the vehicle (0.1% DMSO) (**Figure 5B**).
- This effect was paralleled with a significant rescue of the ion transport function (41.6±2.5%, n=24, $p<0.01$) to wild type levels (**Figure 6**).

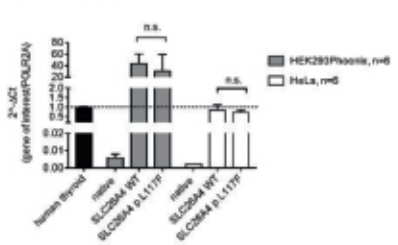


**Figure 2. Messenger RNA levels of wild type pendrin and its variant p.L117F measured by RT-qPCR.** HEK293 Phoenix and HeLa cells were transiently transfected with vectors coding for the wild type (WT) and p.L117F SLC26A4 variants, and the expression levels of the transcript of interest were determined after 48 and 72 hours, respectively. Ct values of *SLC26A4* were normalized for those of the housekeeping transcript *POLR2A* and expressed as fold-change compared to *SLC26A4* expression in human thyroid. Statistical differences between data sets were verified by the unpaired, two-tailed Student's t test. n.s. = $p>0.05$, n indicates the number of independent cell cultures, 2 technical replicates of each sample were assessed.

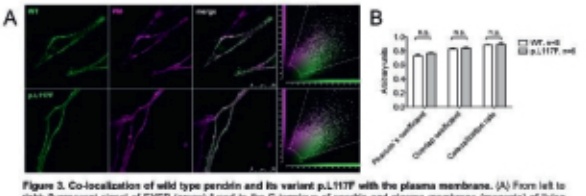


**Figure 3. Co-localization of wild type pendrin and its variant p.L117F with the plasma membrane.** (A) From left to right: fluorescent signal of EYFP (green) fused to the C-terminus of pendrin and plasma membrane (magenta) of living HeLa cells 72 hours after transfection, corresponding merge image and scatter plot. Scale bar: 25 µm; (B) Pearson's correlation coefficient, overlap coefficient and co-localization rate referred to the co-localization of wild type (WT) and p.L117F pendrin variants with the plasma membrane. n.s. = $p>0.05$ compared to wild type, n=6, unpaired, two-tailed Student's t test. (n) refers to the number of cells from 3 independent subcultures.

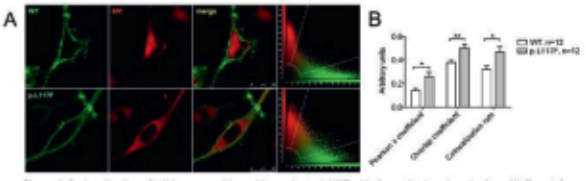


**Figure 4. Co-localization of wild type pendrin and its variant p.L117F with the endoplasmic reticulum.** (A) From left to right: fluorescent signal of EYFP (green) fused to the C-terminus of pendrin and endoplasmic reticulum (red) of living HeLa cells 72 hours after transfection, corresponding merge image and scatter plot. Scale bar: 25 µm; (B) Pearson's correlation coefficient, overlap coefficient and co-localization rate referred to the co-localization of wild type (WT) and p.L117F pendrin variants with the endoplasmic reticulum. * = $p<0.05$, ** = $p<0.01$ compared to wild type, n=12, unpaired, two-tailed Student's t test. (n) refers to the number of cells from 3 independent subcultures.

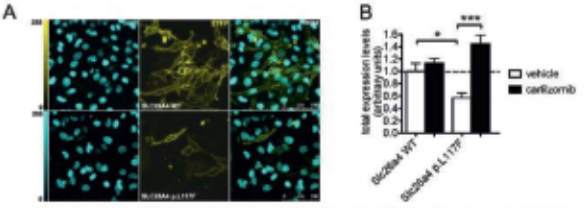


**Figure 5. Expression levels of wild type and p.L117F pendrin with and without treatment with an inhibitor of the ubiquitin proteasome system.** (A) From left to right: fluorescent signal of nuclear DAPI (cyan), EYFP (yellow) fused to the C-terminus of pendrin and corresponding merge image of HeLa cells 72 hours after transfection. Scale bar: 100 µm; (B) Cells transfected with pendrin variants were treated with 10 µM carfilzomib or the vehicle (0.1% DMSO) for 16 hours. Values are expressed as fluorescence intensity (levels of grey) normalized for the cell density represented by DAPI fluorescence. *** = $p<0.001$, * = $p<0.05$, n=20, one-way ANOVA with Bonferroni's multiple comparison test. (n) refers to the number of cells from 3 independent subcultures.

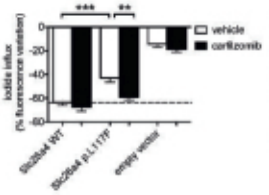


**Figure 6. Function of wild type and p.L117F pendrin with and without treatment with an inhibitor of the ubiquitin proteasome system.** Cells transfected with pendrin variants and the iodide-sensitive EYFP were treated with 10 µM carfilzomib or the vehicle (0.1% DMSO) for 16 hours. Histograms represent the intracellular fluorescence decrease over the experimental period (19 sec.) measured after injection of iodide in the extracellular bath. *** = $p<0.001$, ** = $p<0.01$, n=24, one-way ANOVA with Bonferroni's multiple comparison test. (n) refers to the number of independent fluorescence readings from 4 independent experiments.

## Conclusions

- **The alteration of ion transport function and protein expression as well as the partial retention of pendrin p.L117F in the ER are consistent with a pathogenic potential of this variant.**
- **The reduction of protein expression in the absence of differences in transcript levels points to an accelerated degradation of pendrin p.L117F compared to the wild type.**
- **The correct targeting of a substantial pool of this protein variant to the plasma membrane, together with a significant residual ion transport function may have led to incorrect pathogenicity exclusion in former studies.**
- **The substantial increase in protein levels and ion transport function induced by carfilzomib strongly suggest that pendrin p.L117F protein levels are regulated by the ubiquitin proteasome system and further indicate that targeting this degradation pathway may represent a novel therapeutic strategy for hearing loss linked to pendrin dysfunction.**

## References

1.Taylor JP, Metcalfe RA, Watson PF, Weetman AP, Trembath RC. Mutations of the PDS gene, encoding pendrin, are associated with protein mislocalization and loss of iodide efflux: implications for thyroid dysfunction in Pendred syndrome. J Clin Endocrinol Metab. 2002;87(4):1778-1784.
2.Wasano K, Takahashi S, Rosenberg SK, et al. Systematic quantification of the anion transport function of pendrin (SLC26A4) and its disease-associated variants. Hum Mutat. 2020;41(1):316-331.
3.Dossena S, Rodighiero S, Vezzoli V, et al. Fast fluorometric method for measuring pendrin (SLC26A4) Cl-/I- transport activity. Cell Physiol Biochem. 2006;18(1-3):67-74.
4.Pera A, Dossena S, Rodighiero S, et al. Functional assessment of allelic variants in the SLC26A4 gene involved in Pendred syndrome and nonsyndromic EVA. Proc Natl Acad Sci U S A. 2008;105(47):18608-18613.
5.de Moraes VCS, Bernardinelli E, Zocal N, et al. Reduction of Cellular Expression Levels Is a Common Feature of Functionally Affected Pendrin (SLC26A4) Protein Variants. Mol Med. 2016;22:41-53.
6.Roesch S, Bernardinelli E, Nofziger C, et al. Functional Testing of SLC26A4 Variants-Clinical and Molecular Analysis of a Cohort with Enlarged Vestibular Aqueduct from Austria. Int J Mol Sci. 2018;19(1):209.

## Pathogenicity assessment of pendrin (SLC26A4) variant p.L117F

Arnoldas Matulevicius[1], Karen B. Avraham[2], Antonio Sarikas[1], Silvia Dossena[1]

[1]Institute of Pharmacology and Toxicology, Paracelsus Medical University, Salzburg, Austria; [2]Department of Human Molecular Genetics and Biochemistry, Sackler Faculty of Medicine, Tel Aviv, Israel; Contact: arnoldas.matulevicius@gmail.com

### Objective
Pendrin (SLC26A4) is an anion exchanger encoded by the SLC26A4 gene. SLC26A4 mutations result in inherited hearing loss characterized by malformations of the inner ear. p.L117F is the most common variant of SLC26A4 gene in the deaf Jewish Ashkenazi population and has been reported in homozygosis in multiple individuals with hearing loss (K.B. Avraham Lab internal data). Nevertheless, two independent reports described a lack of functional impairment for this variant, therefore its clinical significance cannot be determined with certainty. To solve this contradiction and reach a conclusive pathogenicity assignment or exclusion for the p.L117F pendrin variant, we characterized its ion transport activity, transcript and protein expression levels as well as subcellular localization in cell-based assays and compared these molecular features to those of wild type pendrin.

### Methods
Wild type (WT) and p.L117F pendrin variants were cloned in mammalian expression vectors and expressed in HEK293 Phoenix and HeLa cells. Ion transport function of pendrin variants was evaluated by quantitative measurement of iodide/chloride exchange using a fluorometric method based on the iodide sensitivity of an EYFP variant (EYFP p.H148Q, I152L). Messenger RNA expression levels were assessed by real-time RT-qPCR. Subcellular localization was assessed by co-localization of the fusion protein pendrin-EYFP with appropriate markers of the plasma membrane (PM) and endoplasmic reticulum (ER). Protein expression levels were assessed by quantitative imaging.

### Results
There was no significant difference in mRNA expression levels between wild type pendrin and its variant p.L117F. Determination of subcellular localization of proteins showed that, similarly to wild type pendrin, pendrin p.L117F was efficiently transposed to the PM. However, co-localization with the ER denoted that a small but significant fraction of pendrin p.L117F was retained in this subcellular compartment. The protein expression levels of pendrin p.L117F were significantly reduced compared to those of the WT (43% reduction). In parallel, the ion transport function of this variant was affected (42% reduction), but not completely abrogated. Treatment of cells transfected with p.L117F with an inhibitor of the ubiquitin proteasome system (10 $\mu$M carfilzomib for 16 hours) significantly increased p.L117F protein expression levels (153.5±14.3%, n=20, $p<0.001$) when compared to cells exposed to the vehicle (0.1% DMSO). This effect was paralleled with a significant rescue of the ion transport function (41.6±2.5%, n=24, $p<0.01$) to WT levels.

### Conclusions
The alteration of ion transport function and protein expression as well as the partial retention of pendrin p.L117F in the ER are consistent with a pathogenic potential of this variant. The reduction of protein expression in the absence of differences in transcript levels points to an accelerated degradation of pendrin p.L117F compared to the wild type. The correct targeting of a substantial pool of this protein variant to the plasma membrane, together with a significant residual ion transport function may have led to incorrect pathogenicity exclusion in former studies. The substantial increase in protein levels and ion transport function induced by carfilzomib strongly suggest that pendrin p.L117F protein levels are regulated by the ubiquitin proteasome system and further indicate that targeting this degradation pathway may represent a novel therapeutic strategy for hearing loss linked to pendrin dysfunction.

# Biliary tract cancer cells are highly sensitive towards the HDAC class I inhibitor romidepsin

Christian Mayr[1,2], Tobias Kiesslich[1,2], Sara Erber[1], Dino Bekric[1], Markus Ritter[1], Tarkan Jäger[3], Paul Winkelmann[4], Marlena Beyreis[1], Heidemarie Dobias[1], Bettina Neumayr[4], Eckhard Klieser[4], and Daniel Neureiter[4]

[1]Institute of Physiology and Pathophysiology; [2]Department of Internal Medicine I, [3]Department of Surgery, [4]Institute of Pathology; all at Salzburger Landeskliniken (SALK), Salzburg, Austria

**Author for correspondence: Christian Mayr**, Email: christian.mayr@pmu.ac.at

## Objective

Biliary tract cancer (BTC) is a deadly disease with dismal outcome and limited therapeutic options. It is well-known that besides somatic mutations, epigenetic (de)regulation contributes to BTC development and progression. Hence, targeting epigenetic regulators represents an interesting approach. Histone deacetylases (HDACs) are a group of enzymes that deacetylate lysine residues of histones, thereby generally causing epigenetic silencing of target genes. HDACs can be grouped in four classes (I, II a and b, III, and IV), where mechanistically, HDAC classes I, II a and b and IV are referred to as ‚classical HDACs'. Although a contribution of aberrant HDAC activity in BTC has already been demonstrated, data are still sparse.

In this study we therefore aim for a comprehensive investigation of HDAC inhibition as a viable anti-BTC strategy. Using a comprehensive panel of human BTC cell lines, we analyzed the expression of HDACs as well as the cytotoxic effect of a panel of HDAC inhibitors (targeting different HDAC classes). We furthermore evaluate for the first time the potential of the clinically relevant HDAC class I inhibitor romidepsin (currently > 90 clinical trials; clinicaltrials.gov) in BTC.

## Methods

HDAC expression was measured via real-time PCR and immunohistochemistry. Cytotoxic effects of complete HDAC inhibitors were evaluated using the resazurin assay. The mode of cytotoxicity of romidepsin was analyzed by a RealTime-Glo™ Annexin V Apoptosis and Necrosis Assay combined with the environmental control function of a Spark multimode reader. The epigenetic effect of romidepsin was evaluated by Western Blot and a HDAC activity assay (HDAC-Glo™ I/II Assay and Screening System). HDAC1/2 expression in BTC patient samples was analysed by immunohistochemistry and correlated with clinical parameters. The effect of combined cisplatin/romidepsin treatment was measured using the resazurin assay.

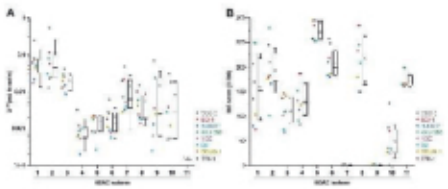

## Results 1: HDACs are expressed in BTC cells

mRNA and protein expression of HDACs in BTC cell lines. In general, HDACs show a cell line-dependent expression. Interestingly, we found no correlation between expression patterns of mRNA and protein levels. HDACs 1-3 show high expression, whereas HDACs 4-6 and HDACs 7-10 show low and medium expression, respectively. HDAC 11 was not detectable in BTC cells.

## Results 2: BTC cells show different sensitivites towards HDAC inhibitors

(A, B) In our study we used two pan-inhibitors (belinostat, vorinostat), and four class-specific HDAC inhibitors (mocetinostat, romidepsin, tubastatin A, UMK-235). Romidepsin (a class I inhibitor) was most efficient in BTC cells, reflected by $IC_{50}$ values in nM range and hence, was chosen for further investigation.

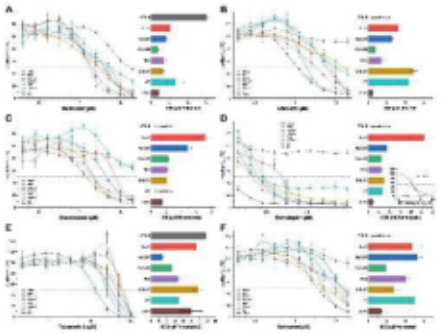

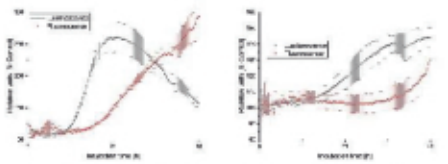

## Results 3: Romidepsin causes apoptosis in BTC cells

Romidepsin (5 nM) causes apoptosis and secondary necrosis in BTC cells (RealTime-Glo™ Annexin V Apoptosis and Necrosis Assay): Luminescence signal represents Annexin V binding, fluorescence signal represents loss of membrane integrity.

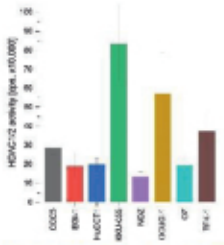

## Results 4: HDAC1/2 activity in BTC cells

Since BTC cells were most sensitive to the HDAC class I (1/2) inhibitor romidepsin, we measured HDAC1/2 activity in our BTC in vitro model.

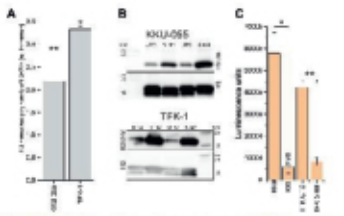

## Results 5: Romidepsin reduces HDAC activity

(A,B) Treatment with romidepsin (5 nM) causes increase of acetylation of histone 3 at lysone 9 (H3K9ac) after 24 hours
(C) Romidepsin (5 nM) reduces HDAC (I/II) activity

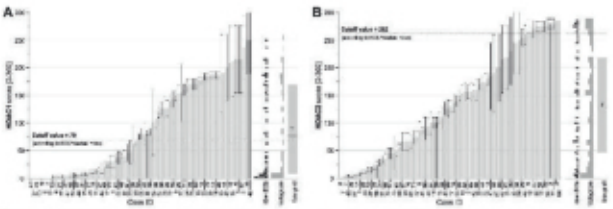

## Results 6: Analysis of HDAC1/2 expression in n = 78 BTC patient samples.

top: HDAC1/2 are heterogeneously expressed in BTC patient samples. Compared to adjacent non-tumor tissue, HDAC1/2 are often overexpressed in tumor areas (data not shown).
bottoms: high HDAC2 expression is correlated with reduced survival time. In contrast, HDAC1 expression was correlated with better survival (data not shown).

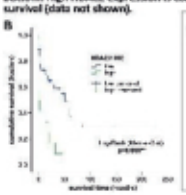

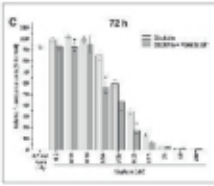

## Results 7: Romidepsin augments the cytotoxicity of cisplatin

Addition of a sub-lethal dose of romidepsin (0.5 nM) augments the cytotoxic effect of cisplatin in KKU-055 cells after 24 h, 48 h and 72 h, respectively (shown are the results after 72 h).
This effect was also seen, when cells were ‚primed' with romidepsin before addition of cisplatin.
Interestingly, these effects were exclusive for KKU-055 cells as no such augmentation was seen in other cell lines.

## Conclusion

**We here demonstrate that HDAC inhibition might be a viable anti-BTC strategy. We show that the HDAC class I inhibitor romidepsin has a strong cytotoxic and epigenetic effect in BTC cells. Furthermore, we found that HDAC1/2 are (over-)expressed in BTC patient samples and that high HDAC2 expression is significantly associated with reduced survival time.**

**Furthermore, we found that romidepsin has the potential to augment the cytotoxic effect of cisplatin, although this effect was seen on only one of the tested cell lines.**

## HDAC Screening identifies the HDAC Class I Inhibitor Romidepsin as a promising Epigenetic Drug for Biliary Tract Cancer

Christian Mayr[1,2], Tobias Kiesslich[1,2], Sara Erber[1], Dino Bekric[1], Heidemarie Dobias[1], Marlena Beyreis[1], Markus Ritter[1,3], Tarkan Jäger[4], Bettina Neumayer[5,6], Paul Winkelmann[5,6], Eckhard Klieser[5,6], Daniel Neureiter[5,6]

[1]Center for Physiology, Pathophysiology and Biophysics - Salzburg and Nuremberg, Institute for Physiology and Pathophysiology - Salzburg, Paracelsus Medical University; [2]Department of Internal Medicine I, University Clinics Salzburg, Paracelsus Medical University; [3]Ludwig Boltzmann Institute for Arthritis und Rehabilitation, Paracelsus Medical University; [4]Department of Surgery, University Clinics Salzburg, Paracelsus Medical University; [5]Institute of Pathology, University Clinics Salzburg, Paracelsus Medical University; [6]Cancer Cluster Salzburg; Contact: christian.mayr@pmu.ac.at

### Objective
Biliary tract cancer (BTC) is a fatal disease with limited therapeutic options. Inhibition of histone deacetylases (HDACs) represents an effective anti-cancer approach. Data regarding HDAC and BTC are sparse but promising. There, we performed a comprehensive investigation of HDAC expression and pharmacological HDAC inhibition in a BTC in vitro model.

### Methods
Expression of HDACs in BTC cells was measured via quantitative real-time PCR and immunohistochemistry. Cytotoxicity of HDAC pan-inhibitors (belinostat, vorinostat) and HDAC inhibitors targeting different HDAC classes (mocetinostat, romidepsin, LMK-235, tubastatin A) was analyzed using the resazurin assay. HDAC1/2 activity was measured via the HDAC-Glo I/II Assay and Screening System (Promega). Mode of cytotoxicity of romidepsin was evaluated via a time-resolved resazurin assay and the RealTime-Glo Annexin V Apoptosis and Necrosis Assay (Promega). Changes in H3K9Ac levels were measured to investigate the epigenetic effect of romidepsin. Combinatory treatment of romidepsin and cisplatin was evaluated via the resazurin assay and changes of IC50-values. Expression of HDAC1/2 in n = 78 BTC patient samples was done via immunohistochemistry. Appropriate statistical tests were used to correlate HDAC1/2 expression with clinicopathological data.

### Results
HDAC profiling revealed a heterogeneous expression of HDACs across the studied cell lines (n = 8). Furthermore, we found that BTC cells show different sensitivities towards the used HDAC inhibitors. The HDAC class I inhibitor romidepsin showed significant cytotoxicity in the (low) nM-range and was therefore chosen for further investigation. We found that romidepsin causes apoptosis and secondary necrosis and significantly reduces HDAC activity in BTC cells. Furthermore, we observed that sub-lethal concentrations of romidepsin augmented the toxic effect of the standard chemotherapeutic cisplatin. We also measured HDAC1 and 2 expression in BTC patients. HDAC1 expression correlated with tumor localization and tumor grading. Moreover, patients with high expression of HDAC2 had a significant shorter overall survival time.

### Conclusions
Our results demonstrate that the HDAC class I inhibitor romidepsin is a promising anti-BTC substance. In addition, we show that HDAC1 and 2 are expressed in BTC patient samples and associate with clinical parameters.

### References
1. No references

# Standardized single incision laparoscopy for resection in liver segments 7 and 8: retrospective analysis from a center



**Christof Mittermair**[1], Hannes Hell[1], Martin Grünbart[1], Tobias Hell[1] and Helmut Weiss[1]
1 Saint John of God Hospital, Salzburg, Austria, Department of Surgery
2 Department of Mathematics, University of Innsbruck, Austria

### Introduction

- Despite continuous improvements in minimally invasive liver surgery and growing evidence for its superiority compared to the open approach, resections in segments 7 and 8 remain challenging due to limited accessibility
- The angle for resections from the umbilicus is not ideal and different paths via different trocar positions in standard laparoscopy may reduce reachability of targets in these posterior segments
- The single incision laparoscopic (SIL) access via only one small subcostal incision may compensate these drawbacks and facilitate minimally invasive resections in posterior segments

### Material and Methods

- We retrospectively analysed a prospective data collection
- All relevant pre- intra- and postoperative data is available.
- All resections planned as SIL liver resections in segments 7 and 8 were included
- Extended resections including other segments were excluded from this analysis
- Data is given as mean, standard deviation (SD) and range

### Results 1: Patients' demographics

| | Total (n=17) | |
|---|---|---|
| | Mean (SD) | Range |
| Age (y) | 63 (11,87) | 41-87 |
| Femal gender | 5 | |
| BMI (kg/m2) | 28 (3,44) | 22,2-35,2 |
| ASA Score | 3 (0,78) | 1-3 |

SD: Standard Deviation
BMI: Body Mass Index
ASA: American Society of Anesthesiologists

### Results 2: Procedural details

| | Total (n=17) | |
|---|---|---|
| | Mean (SD) | Range |
| Duration (Minutes) | 115,65 (50,90) | 26-185 |
| Blood lost (ml) | 347,65 (760,73) | 0-3000 |
| Skin incision (cm) | 4,53 (1,26) | 2,5-7,5 |

### Results 3: operative details

- 12 metastases, 5 primary liver tumours
- Three conversions to open surgery (two due to cardiac decompensation and one due to anatomical uncertainty)
- Additional trocar in two patients
- Three concomitant procedures (two minimally invasive colon resections, one incisional hernia in the lower abdomen)
- Radiofrequency precoagulation was sufficient in all but one patient (use of two additional staplers)

### Results 4: postoperative outcome

- 100% R0 resections
- No mortality within 90 days
- Four complications (all Clavien Dindo 3a)
  - Two abscesses near the resection area drained radiologically
  - Two pleural effusions were punctured
- Length of hospital stay = 11±7,15 days (range 5-30 days)

### Exposure of segment 7



### Conclusion

- SIL resections of lesions located in liver segment 7 and 8 via the subcostal approach provide a superior reachability and feasibility.
- All pathologies could be resected completely
- No excessive mobilization of the right liver is required
- All minimally invasive standard resection techniques can be applied
- The rate of postoperative complications is comparable to standard minimally invasive liver resections

### Incision and scar



## Standardized single incision laparoscopy for resection in liver segments 7 and 8: retrospective analysis from a center

Christof Mittermair[1], Hannes Hoi[1], Martin Grünbart[1], Tobias Hell[2], Helmut Weiss[1]

[1]Department of Surgery, Saint John of God Hospital, Salzburg, Austria (Teaching Hospital of the Paracelsus Medical University); [2]Department of Mathematics, University of Innsbruck, Austria; Contact: christof.mittermair@bbsalz.at

### Objective
Minimally invasive liver resections have gained wide acceptance in the field of surgery over the past few years. Feasibility and safety have been demonstrated for multiple indications and the superiority in terms of morbidity could be confirmed. However, lesions in Segment 7 and 8 still represent a challenge due to limited accessibility via standard laparoscopy. Single incision laparoscopy (SIL) via a subcostal incision potentially abolishes the drawback due to a better angle from only one gateway. This study aims at analyzing the benefits of this method in a single institution.

### Methods
Consecutive cases of liver resections in segments 7 and 8 via a subcostal incision, performed between 2010 and 2019 were analyzed retrospectively. Indications, operative and perioperative outcome were evaluated.

### Results
17 Patients with pathologies restricted only to liver segments 7 and 8 were treated by means of SIL. 14 resections (82,4%) could be completed minimally invasive, additional trocars were necessary in two patients (11,8%). Three patients (17,6%) were converted to open surgery due to cardiac decompensation (n=2) or unclear anatomic situation (n=1). The rate of R0 resections was 100% and no intraoperative adverse event was witnessed. Mortality was zero and morbidity yielded at 23,5% (n=4; two liver abscesses were drained radiologically and two pleural effusion required puncture)

### Conclusions
SIL resections of lesions located in liver segment 7 and 8 via the subcostal approach provide a superior reachability and feasibility. Within these selected cases, only one resection had to be converted due to a surgical reason. Morbidity and mortality were within an expectable range.

# Bestehende therapeutische Antikoagulation und OP-Indikation bei symptomatischer Varikose – Chance oder Widerspruch?

Millenhoff C[1]- Millenhoff CI[1], Schürger G[1], Maurer A[1], Weigel C[2]
[1] Gelenk- u. Gefäßzentrum Mittelfranken, Akademische Lehrpraxis der Paracelsus Medizinische Privatuniversität Nürnberg; Schwabach, Deutschland
[2] AGU – Praxis für Anaesthesie, Schwabach,Deutschland

PARACELSUS MEDIZINISCHE PRIVATUNIVERSITÄT

GGZ Gelenk- und Gefäßzentrum Mittelfranken MVZ GbR

## Einleitung

Die operative Sanierung der symptomatischen Varikose steht insbesondere bei Patienten mit voller Antikoagulation (AK), je nach Gerinnungsmanagement, im Spannungsfeld zwischen erhöhtem perioperativen Blutungsrisiko und dem Risiko der Thromboembolie. Ein Pausieren oder ein Wechsel auf Heparin für die Zeit der OP (Bridge-Schema) steht immer wieder zur Diskussion. Am Beispiel kardiologisch erkrankter Patienten unter therapeutischer AK sollen die Chancen und Risiken des endovenösen Behandlungsansatzes ohne AK-Veränderung und seines Outcome beleuchtet werden.

**Primärmorbidität**

| | |
|---|---|
| ARE | 3x |
| VHF | 3x |

## Material und Methode

In Zeitraum von 11/2019 bis 12/2020 behandelten wir 11 Patienten (13 Beine) mit symptomatischer Varikose (C2-C5r) und erheblicher Comorbidität (ASA 3) im Alter von 78,1 +/- 10,2 Jahren unter ambulanten Bedingungen mittels endovenöser Lasertherapie (EVLT), oder endovenöser Desobliteration (EVD) unter voller AK (Phenprocoumon/Apixaban/Rivaroxaban).
Behandelt wurden die endovenös erreichbaren Gefäße, auf eine kleinstolige Sotenasotohairese verzichteten wir. Anaesthesiologisch erfolgte teils eine Tumeszenzanaesthesie, teils eine Lokalanaesthesie (ggf. begleitet von einer milden Analgosedierung); auf eine Intubationsnarkose verzichteten wir. Als Zielkriterium wurden perioperative Blutungskomplikationen, das Auftreten von Komplikationen im Zusammenhang mit der cardialen Grunderkrankung, sowie insbesondere der primärer Zielgefäßverschluß festgelegt.

**genutzte AK**

| | | |
|---|---|---|
| Eliquis | Apixaban | 5x |
| Marcumar | Phenprocoumon | 4x |
| Xarelto | Rivaroxaban | 1x |

**Comorbidität**

| | | |
|---|---|---|
| Cardiopath. | KHK/r, Hypertonie/Diabetes | 9x |
| ZNS | | 2x |
| Vascular | pAVK/Ödeme | 2x |
| Neurolog. | M.Parkinson/r, Polyneuropathie | 2x |

**gewählte Technik**

| | | |
|---|---|---|
| Invo-Medical | 1470nm Laser; 3Fibern | 7x |
| Nollert | Linearis Laser; 1470nm | 3x |
| Balton | Fotolaser | 3x |

**CEAP-Einteilung**

| | |
|---|---|
| C2 | 6 |
| C3 | 1 |
| C4 | 3 |
| C5 | 1 |
| C6 | 2 |

## Ergebnis

Bei einer mittleren Behandlungsstrecke von 57,2 cm +/- 20,3 und einer OP-Zeit von 34,6 min +/- 11,2 konnten wir 11 von 13 behandelte Venensystemen primär verschließen (84,6%), an einem Bein ergänzten wir sekundär eine lokale Sklerotherapie, an einem weiteren mittels lokaler Unterbindung. Es kam zu keiner relevanten/therapiepflichtigen Nachblutung oder Thromberbolie. Klinisch stellte sich eine erhebliche Befundbesserung ein, alle Ulcerationen heilten ab. Zusätzlich war keine Verschlechterung der Comorbidität zu verzeichnen. Die Nachbeobachtungszeit betrug 115d +/-71.

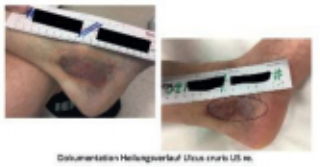

Dokumentation Heilungsverlauf Ulcus cruris US re.

## Schlussfolgerung

Eine indizierte Operation der symptomatischen Varikose bei relevant kardial erkrankten Patienten unter therapeutischer AK kann mit endovenösen Techniken und Konzentration auf die endovenös behandelbaren Venenaogenesis mit guten klinischen Erfolg und ohne erhöhte perioperative Blutungsrate, wie auch ohne Auftreten von Komplikationen in den Comorbiditäten und ihrer Therapie durchgeführt werden.
Mit der etablierten Technik der EVLT, aber auch dem innovativen Ansatz der EVD, eröffnen sich weitere bedenkenswerte Behandlungsoptionen bei Risikopatienten. Größere Fallzahlen zur genaueren Beurteilung sind wünschenswert.

**Verschlussrate Zielgefäß**

| | | |
|---|---|---|
| primär verschlossen | 11 | 84,60% |
| sekundär Unterbindung nötig | 2 | 15,40% |

## Bestehende therapeutische Antikoagulation und OP-Indikation bei symptomatischer Varikose – Chance oder Widerspruch?

Christian Möllenhoff[1], Clemens Möllenhoff[1], Gabriele Schürger[2], Alexander Maurer[1], Carla Weigel[1]

[1]Gelenk- u. Gefäßzentrum Mittelfranken, Akademische Lehrpraxis der Paracelsus Medizinische Privatuniversität Nürnberg; Schwabach, Deutschland; [2]AOZ – Praxis für Anaesthesie; Schwabach, Deutschland; Contact: moellenhoff@venenlaserzentrum.de

### Objective
Die operative Sanierung der symptomatischen Varikose steht insbesondere bei Patienten mit voller Antikoagulation (AK), je nach Gerinnungsmanagement, im Spannungsfeld zwischen erhöhtem perioperativen Blutungsrisiko und dem Risiko der Thrombembolie. Ein Pausieren oder ein Wechsel auf Heparin für die Zeit der OP (Bridge-Schema) steht immer wieder zur Diskussion
Am Beispiel kardiologisch erkrankter Patienten unter therapeutischer AK sollen die Chancen und Risiken des endovenösen Behandlungsansatzes ohne AK-Veränderung und seines Outcome beleuchtet werden.

### Methods
Im Zeitraum von 11/2019 bis 12/2020 behandelten wir 11 Patienten (13 Beine) mit symptomatischer Varikose (C2-C6r) und erheblicher Comorbidität (ASA 3) im Alter von 78,1 +/- 10,2 Jahren unter ambulanten Bedingungen mittels endovenöser Lasertherapie (EVLT), oder endovenöser Desobliteration (EVD) unter voller AK (Phenprocoumon/Apixaban/Rivaroxaban).
Behandelt wurden die endovenös erreichbaren Gefäße, auf eine kleinteilige Seitenastexhairese verzichteten wir. Anaesthesiologisch erfolgte teils eine Tumeszenzanaesthesie, teils eine Lokalanaesthesie (ggf. begleitet von einer milden Analgosedierung); auf eine Intubationsnarkose verzichteten wir. Als Zielkriterium wurden perioperative Blutungskomplikationen, das Auftreten von Komplikationen im Zusammenhang mit der cardialen Grunderkrankung, sowie insbesondere der primärer Zielgefäßverschluß festgelegt.

### Results
Bei einer mittleren Behandlungsstrecke von 57,2 cm +/- 20,3 und einer OP-Zeit von 24,6 min +/- 11,2 konnten wir 11 von 13 behandelte Venensystemen primär verschließen (84,6%), an einem Bein ergänzten wir sekundär eine lokale Sklerotherapie, an einem weiteren mittels lokaler Unterbindung. Es kam zu keiner relevanten/therapiepflichtigen Nachblutung oder Thrombembolie. Klinisch stellte sich eine erhebliche Befundbesserung ein, alle Ulcerationen heilten ab. Zusätzlich war keine Verschlechterung der Comorbidität zu verzeichnen. Die Nachbeobachtungszeit betrug 127d +/-63.

### Conclusions
Eine indizierte Operation der symptomatischen Varikose bei relevant kardial erkrankten Patienten unter therapeutischer AK kann mit endovenösen Techniken und Konzentration auf die endovenös behandelbaren Venensegmente mit gutem klinischen Erfolg und ohne erhöhte perioperative Blutungsrate, wie auch ohne Auftreten von Komplikationen in den Comorbiditäten und ihrer Therapie durchgeführt werden.
Mit der etablierten Technik der EVLT, aber auch dem innovativen Ansatz der EVD, eröffnen sich weitere bedenkenswerte Behandlungsoptionen bei Risikopatienten. Größere Fallzahlen zur genaueren Beurteilung sind wünschenswert

### References
1. Perioperative Bridging Anticoagulation in Patients with Atrial Fibrillation; BRIDGE-Investigators;N Engl J Med 2015; 373:823-833 DOI: 10.1056/NEJMoa1501035

# A protocol to evaluate and validate implant internal forces and moments

Mischa Mühling[1,2], Sabrina Sandriesser[1,2], Peter Augat[1,2]
[1] Institute for Biomechanics, BG Unfallklinik Murnau, Germany
[2] Institute for Biomechanics, Paracelsus Medical University Salzburg, Austria

BGU Murnau
Berufsgenossenschaftliche Unfallklinik Murnau

## Introduction

Implants are used in a wide range of fractured bones. For different fractures there are different implants like locking plates, compression plates and intramedullary nails. The manufacturers develop new models in order to face different fracture scenarios or improve the existing implants. Commonly new implants are tested and approved with respect to their corresponding predecessor products. There is limited knowledge about the internal forces and moments acting on the implants while implanted in the human body. Therefore, mechanical requirements for new implants are limited to the experience about the predecessor products.

**Aim of this study is to evaluate and validate implant internal forces and moments and translate the complex physiological loading case into a simplified 3 or 4 point bending loading case of the implant.**

## Material and Methods

### Choosing loading scenario:

The first step of the study is defining the loading scenario for the corresponding bone. In our case the femur was chosen due to the fact that the forces are well known by experimental measurements. The loading case for our scenario was chosen to be the heel strike force while walking (250% bodyweight) which is likely occuring at freshly operated patients with femur fractures [1]. Due to the fact, that the chosen artificial femur is corresponding to a 91 kg human the maximum load was chosen to be 2500 N.

### Verification of the loading on intact Femur

To verify the loads acting on the human femur we used the Bone's Mechanostat theory from 2003 by Frost [2]. The load is considered physiological when the loaded bones strain response is in the range of the described bone's thresholds of "modelling" or "operational microdamage". Therefore, an experimental test setup for an intact femur was created. An artificial femur (Sawbones Europe AB, Malmö, Swoden) was distally embedded and fixated in a cardanic joint. The load was applied proximally on the femur head by a cylindrical load applicator replicating a human hip joint. A spray pattern was applied on the surface of the model and left to thoroughly dry before mechanical testing. Strains on the surface of the femur were analyzed using a 3D optical measurement system (ARAMIS 5M, GOM GmbH, 139 Braunschweig, Germany). Strains on the spray pattern were checked to be in the physiological bone's thresholds.



### Implantation of the osteosynthesis

To guarantee for adequate construct alignment the osteosynthesis was first implanted by an experienced surgeon on the intact bone, followed by subsequent fracture creation. For fixation a 14 hole locking plate (AxSOS Recon, 222 mm, Stryker, Kalamazoo, USA) was used and symmetrically configured with 6 screws. The femur was osteotomized at the position of highest strains observed in the preceding tests. A 15 mm fracture gap was induced 111 mm distally of the trochanter perpendicular to the axial direction of the shaft using an oscillating saw. Strains were tracked using the previous setup with an additional high accuracy setup on the bridging length of the implant. The physical model was loaded by 100 N to stay in the linear elastic region of the construct.



### Validation and calculation of implant internal loads

A static structural finite element model was created in ANSYS Mechanical (21 R1, ANSYS, Canonsburg, USA) according to the fractured physical model. The contacts between screw and bone, screw and plate were modelled as bonded, while there was no contact between bone and plate, representing a locking screw system. Mechanical internal forces were calculated by creating several surfaces over the length of the implant with a 5 mm step and using those as cutting positions. The model was validated using the tracked movement of the whole construct while the calculation of the internal forces was validated by using the specific movement of the plate (high accuracy volume).



## Results

### Verification of the loading on intact Femur

The maximum principle strains at 2500 N loading remains good between 0.1 and 0.4 % on the intact femur. This values are in agreement with corresponding experiments on human cadaveric femora [3,4] and in the described thresholds of Frost.

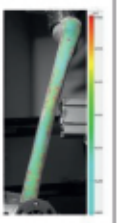

### Validation and calculation of implant internal loading

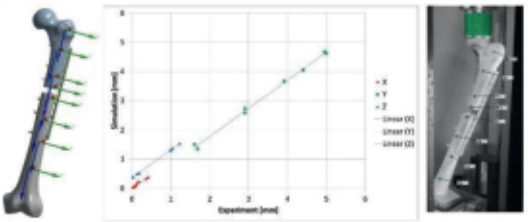


The movement of the whole construct at 100 N loading ranged from 0 to 5 mm and was well predicted by the FE-model. The principle strain on the plate in the working area matched well with the FE model indicating that internal loading is valid.

The internal moment in the plate calculated by the FE-model showed a maximum plateauing at 9.5 Nm between screws 2 and 3 and between screws 4 and 5. The internal moment in the working length remained at 7 Nm.

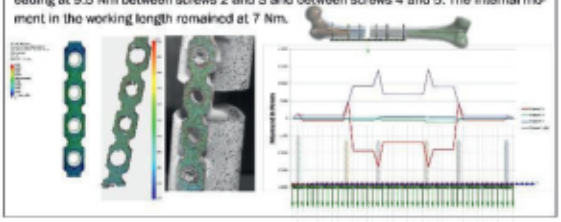

## Conclusion

In this study we presented a protocol by the example of locked plated femur shaft fracture to evaluate and validate implant internal forces and moments.

It included the identification and verification of loads acting on the corresponding bone, calculation of implant internal loading using finite element analysis and validation of the internal loading. The FE-models showed good correlation with the experimental data of the whole construct and the accurate measurement of the plate over the fracture gap. The identification of the loads can be obtained by musculoskeletal simulation when no experimental data is available. The loads will be verified as presented and thus, can be used just as good as measured data.

The presented protocol can be used to identify the internal loads of several different implants. The obtained information about the physiological situation of implants can be used to optimize the design of the implants.

Literature:
[1] Dennis et al. 2015, J Soft Dec Surg, e0130538
[2] Frost, H.M. 2003, Bone's mechanostat: A 2003 update, Anat. Rec., 275A: 1081-1101.
[3] Duda S et al. 2011, Clinical Biomechanics (Bristol, Avon), 26(4):411-414
[4] Grassi L et al. 2014, J Biomech Eng, 2014;136(11)

Kontakt:
Mischa Mühling, M. Sc.
E-Mail: mischa.muehling@murnau.de
Telefon: +49 8841 48-3867
Fax: +49 8841 48-4373

BG Kliniken Murnau,
Institut für Medizinische Forschung und Biomechanik
Prof.-Küntscher-Str. 8
82418 Murnau am Staffelsee
www.bgu-murnau.de

Paracelsus Science Day Salzburg 2021 - Virtual Science Seminar

## A protocol to evaluate and validate implant internal forces and moments

Mischa Mühling[1,2], Sabrina Sandriesser[1,2], Peter Augat[1,2]

[1]Institute for Biomechanics, BG Unfallklinik Murnau, Germany; [2]Institute for Biomechanics, Paracelsus Medical University Salzburg, Austria; Contact: mischa.muehling@bgu-murnau.de

### Objective

Implants are used in a wide range of fractured bones. For different fractures there are different implants like locking plates, compression plates and intramedullary nails. The manufacturers develop new models in order to face different fracture scenarios or improve the existing implants. Commonly new implants are tested and approved with respect to their corresponding predecessor products. There is limited knowledge about the internal forces and moments acting on the implants while implanted in the human body. Therefore, mechanical requirements for new implants are limited to the experience about the predecessor products.
Aim of this study is to evaluate and validate implant internal forces and moments and translate the complex physiological loading case into a simplified 3 or 4 point bending loading case of the implant.

### Methods

The physiological load for a heel strike on a femur was identified and verified by using an experimental test on an artificial femur. The surface strains occurring at the femur had to be in the thresholds of "modelling" or "operational microdamage" purposed by Frosts Bone's Mechanostat theory. A 15 mm femur shaft fracture was induced and fixed with a 14 hole locking plate and 6 locking screws. It was loaded proximally with 100 N to stay in the linear elastic region of the construct. Based on this experiment a finite element model was created and validated. The valid model was used to calculate internal forces and moments of the implant to achieve a detailed insight into the physiological loading and therefore, be able to replicate this in a 3- or 4-point bending situation.

### Results

The maximum principle strains at 2500 N loading remains good between 0.1 and 0.4 % on the intact femur. This values are in agreement with corresponding experiments on human cadaveric femora and in the described thresholds of Frost. The movement of the whole construct at 100 N loading ranged from 0 to 5 mm and was well predicted by the FE-model. The principle strain on the plate in the working area matched well with the FE model indicating that internal loading is valid. The internal moment in the plate calculated by the FE-model showed a maximum plateauing at 9.5 Nm between screws 2 and 3 and between screws 4 and 5. The internal moment in the working length remained at 7 Nm.

### Conclusions

In this study we presented a protocol by the example of locked plated femur shaft fracture to evaluate and validate implant internal forces and moments. It included the identification and verification of loads acting on the corresponding bone, calculation of implant internal loading using finite element analysis and validation of the internal loading. The FE-models showed good correlation with the experimental data of the whole construct and the accurate measurement of the plate over the fracture gap. The identification of the loads can be obtained by musculoskeletal simulation when no experimental data is available. The loads will be verified as presented and thus, can be used just as good as measured data. The presented protocol can be used to identify the internal loads of several different implants. The obtained information about the physiological situation of implants can be used to optimize the design of the implants.

### References

1. Damm et al. 2015, PLoS ONE 10(3): e0120438
2. Frost, H.M. 2003, Bone's mechanostat: A 2003 update. Anat. Rec., 275A: 1081-1101.
3. Eberle S et al. 2011, Clinical Biomechanics (Bristol, Avon) vol. 26,4 (2011): 410-4
4. Grassi L et al. 2014, J Biomech Eng. 2014;136(11)

PARACELSUS
MEDIZINISCHE PRIVATUNIVERSITÄT

Klinikum Nürnberg
Wir sind für Sie da!

# Burnout and resilience among hospital staff during the COVID-19 pandemic: cross-sectional results from the international Cope-Corona study

Müller, MM*, Stein, B, Baillès, E, Blanch, J, Conti, C, Dunne, PJ, Fadgyas Stanculete, M, Farré, JM, Font, E, Forner Puntonet, M, Fritzsche, K, Gayán, E, Guagnano, MT, König, S, Lanzara, R, Lobo, A, Nejatisafa, A-A, Obach, A, Offiah, G, Parramon, G, Peri, JM, Rosa, I, Rousaud, A, Schuster, SK, Torres, X, Waller, C

*Department of Psychosomatic Medicine and Psychotherapy, Paracelsus Medical University, General Hospital Nuremberg, Contact: markus.mueller@klinikum-nuernberg.de

Cope-Corona

## Abstract

Objective: The COVID-19 pandemic has had an enormous impact on hospital staff. The aim of this study was to understand what individual and organizational factors are related to stress and burnout as a reaction to the pandemic.
Methods: An online survey was distributed to hospital staff in seven countries (Germany, Andorra, Ireland, Spain, Italy, Romania, Iran) in summer 2020. Burnout was measured with two items. A set of variables was used to measure individual, coronavirus-related, and work-related factors, as well as demographics and occupational characteristics.
Results: In total, 2097 respondents answered more than 50 per cent of the survey (73.3 % women). Staff from a wide range of functions responded (MD, nurses, medical-technical personnel, administration, and many others). Burnout (d = 0.45, 95% CI: 0.35 to 0.54) was higher for staff working directly with infected patients, while Perceived Stress was not (d = 0.06, 95% CI: -0.03 to 0.14).
Multiple regression analyses revealed that the individual factors self-compassion, resilience and sense of coherence, as well as the organizational factors support at the workplace, support in private life, and health and safety at the workplace could protect against perceived stress and burnout. Higher risk perception and contact with COVID-19 patients was a potentially aggravating factor for burnout.
Conclusion: Burnout can be a problematic consequence of the COVID-19 pandemic. A supportive work environment, the availability of protective equipment, but also an organizational climate that promotes self-compassion and sense of coherence can help foster resilience against staff burnout. The individual factors can be a target of training, while the organizational factors can be a target of organizational development.




- International consortium based in Nuremberg with partners in Ireland, Andorra, Spain, Italy, Poland, Romania, Iran, and China
- With the support of the European Association for Psychosomatic Medicine (EAPM)

## Assessment Points in Time




This poster focuses on T1

## Theoretical Model

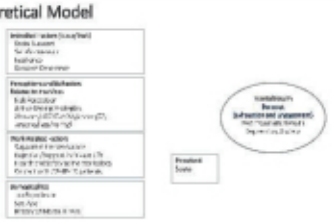

The theoretical model is based on the Job-Demands Resources Model (Demerouti et al., 2001) and includes individual and work-related factors as well as perceptions and behaviors related to the virus

## Methods

- Inclusion of all responders with at least **50% percent response**
- **Exclusion of multiple responses** using self generated code
- **Cross-sectional analyses** at T1
- **T-test and ANOVAs** for comparisons
- **Bonferroni corrections** for multiple comparisons
- **Multiple regression analyses** for model testing

## Participants at T1

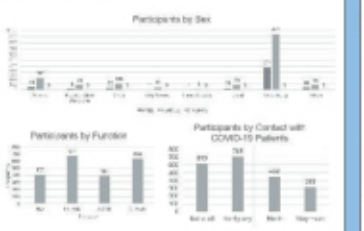


## How safe and supported does staff feel at the workplace?

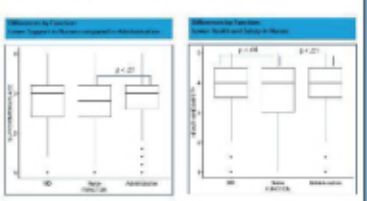

## Perceived Stress, Burnout, and Support at the Workplace in Relation to Contact with COVID-19 Patients

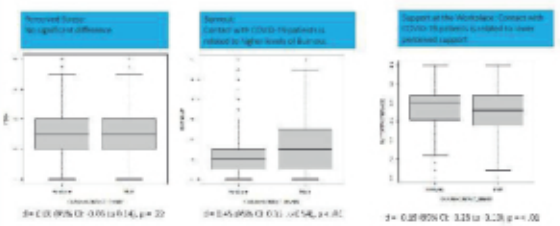

## Protective (+) and Aggravating (-) Factors

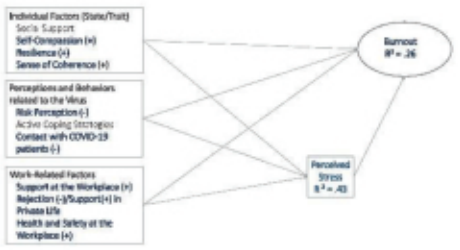


## Conclusions

- Higher levels of burnout especially with a lot of contact with COVID-19 patients.
- Important protective factors to guard against stress and burnout:
- Individual factors such as self-compassion, resilience and sense of coherence.
- Work-related factors such as support at work and the feeling of being able to stay healthy at work.
- Individual factors can be specifically trained.
- Work-related factors could be improved by improving cooperation within and between teams, transparent communication and the availability of protective equipment.

## Acknowledgements

This research project is made possible by the contributions and commitment of all participating centers.
Thank you to EAPM, namely Jordi Blanch (President) and Josef Winter (Administrator) for making this research collaboration possible.
No external funding is available for this project.
The authors declare that there are no conflicts of interest.
The study is registered at https://osf.io/zuw4m

EAPM Cope-Corona

**References**

Demerouti, E., Bakker, A. B., Nachreiner, F., & Schaufeli, W. B. (2001). The job demands-resources model of burnout. Journal of Applied Psychology, 86(3), 499–512. doi: 10.1037/0021-9010.86.3.499

## Burnout and resilience among hospital staff during the COVID-19 pandemic: cross-sectional results from the international Cope-Corona study

Markus M Müller[1, 2], Barbara Stein[1], Eva Baillès[3], Jordi Blanch[4, 5], Chiara Conti[6], Pádraic Dunne[7], Mihaela Fadgyas Stanculete[8], Josep Maria Farré[9], E Font[4], Mireia Forner Puntonet[10], Kurt Fritzsche[11], Elena Gayán[9], Maria Teresa Guagnano[12], Sarah König[2], Roberta Lanzara[13], Antonio Lobo[14, 15, 16], Ali-Akbar Nejatisafa[17], Amadeu Obach[4], Gozie Offiah[18], Gemma Parramon[10], Josep Maria Peri[4], Ilenia Rosa[13], Araceli Rousaud[4], Sara Katharina Schuster[2], Xavier Torres[4], Waller Christiane[1]

[1]Paracelsus Medizinische Privatuniversität, Klinikum Nürnberg, Klinik für Psychosomatische Medizin und Psychotherapie, Nürnberg, Deutschland; [2]Katholische Universität Eichstätt-Ingolstadt, Sozial- und Organisationspsychologie, Eichstätt, Deutschland; [3]Hospital Nostra Senyora de Meritxell, Servei de Salut Mental, Escaldes-Engordany, Andorra; [4]Hospital Clínic de Barcelona, Servei de Psiquiatria i Psicologia, Barcelona, Spanien; [5]University of Barcelona, Barcelona, Spanien; [6]Università degli Studi G. d'Annunzio Chieti e Pescara, Dept. of Psychological, Health and Territorial Sciences, Chieti-Pescara, Italien; [7]Royal College of Surgeons in Ireland, University of Medicine and Health Sciences, Centre Of Positive Psychology and Health, Dublin, Irland; [8]University of Medicine and Pharmacy Iuliu Hatieganu, Cluj-Napoca, Rumänien; [9]Dexeus University Hospital, Department of Psychiatry Psychology and Psychosomatics, Barcelona, Spanien; [10]Hospital Universitari Vall d'Hebron, Department of Psychiatry, Barcelona, Catalonia, Spain; [11]Universitätsklinikum Freiburg, Klinik für Psychosomatische Medizin und Psychotherapie, Freiburg, Deutschland; [12]Università degli Studi G. d'Annunzio Chieti e Pescara, Department of Internal Medicine, Chieti-Pescara, Italien; [13]'Sapienza' University of Rome, Department of Dynamic and Clinical Psychology, Rom, Italien; [14]Universidad de Zaragoza, Departamento de Medicina y Psiquiatría, Zaragoza, Spanien; [15]Instituto de Investigación Sanitaria Aragón, Zaragoza, Spanien; [16]CIBERSAM, Madrid, Spanien; [17]Tehran University of Medical Sciences, Psychosomatic Research Center, Department of Psychiatry, Tehran, Iran; [18]Royal College of Surgeons in Ireland, University of Medicine and Health Sciences, Dublin, Irland; Contact: markus.mueller@klinikum-nuemberg.de

### Objective
The COVID-19 pandemic has had an enormous impact on hospital staff. The aim of this study was to understand what individual and organizational factors are related to stress and burnout as a reaction to the pandemic.

### Methods
An online survey was distributed to hospital staff in seven countries (Germany, Andorra, Ireland, Spain, Italy, Romania, Iran) in summer 2020. Burnout was measured with two items. A set of variables was used to measure individual, coronavirus-related, and work-related factors, as well as demographics and occupational characteristics.

### Results
In total, 2097 respondents answered more than 50 per cent of the survey (73.3 % women). Staff from a wide range of functions responded (MD, nurses, medical-technical personnel, administration, and many others). Burnout (d = 0.45, 95% CI: 0.35 to 0.54) was higher for staff working directly with infected patients, while Perceived Stress was not (d = 0.06, 95% CI: -0.03 to 0.14).
Multiple regression analyses revealed that the individual factors self-compassion, resilience and sense of coherence, as well as the organizational factors support at the workplace, support in private life, and health and safety at the workplace could protect against perceived stress and burnout. Higher risk perception and contact with COVID-19 patients was a potentially aggravating factor for burnout.

### Conclusions
Burnout can be a problematic consequence of the COVID-19 pandemic. A supportive work environment, the availability of protective equipment, but also an organizational climate that promotes self-compassion and sense of coherence can help foster resilience against staff burnout. The individual factors can be a target of training, while the organizational factors can be a target of organizational development.

# Coagulation potential of SARS CoV-2 target cells and their extracellular vesicles

Katharina Muigg[1], Micheela Olle[2], Nicole Meeding[1] Eva Klinglmayer[1], Katharina Schallmoser[1], Nicole Meisner-Kober [1] Dirk Strunk[1]
[1]Experimental and Clinical Cell Therapy Institute, Spinal Cord Injury and Tissue Regeneration Center Salzburg (SCI-TReCS), Paracelsus Medical University,Salzburg,Austria.
[2]Department of Blood Group Serology and Transfusion Medicine, Paracelsus Medical University, Salzburg, Austria.
[3]Department of Chemical Biology and Biological Therapeutics, University of Salzburg

## Background

A large number of Covid-19 patients, suffer from microembolism or thrombotic events (20-30%), however the physiological reason remains to date, not elucidated. This PhD project will focus on the potential imbalance of pro- and anticoagulatory proteins on cells and their extracellular vesicles (EVs) upon viral infection. The cytokine storm relating from recruited immune cells may also alter pro- and anticoagulatory proteins (tissue factor (TF), thrombomodulin (TM) and endothelial protein C receptor (EPCR)) on cells and their EVs influencing distant cells and subsequently alter the cell mediated coagulation initiation.

**1**

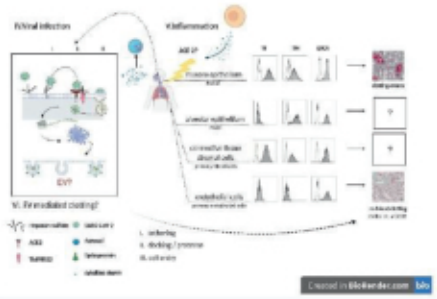

Created in BioRender.com

**Overview about the PhD project**

**I-IV. Viral infection**
SARS CoV-2 enters the cell via ACE-2 receptor and utilizes the host cellular maschinery in order to generate new viral particles. In parallel EV particles share similar assembling as the viral particles

**V. Inflammation**
Upon viral infection, immune cells are mobilized in order to combat the pathogen invasion. The proximate secreted pro-inflammatory cytokines can recruit more immune cells and amplify the cytokine storm.

**VI. EV mediated clotting**
EVs from infected cells transport via the recycled membrane procoagulatory proteins, resulting in an imbalanced pro and anticoagulatory state on cells

**2**

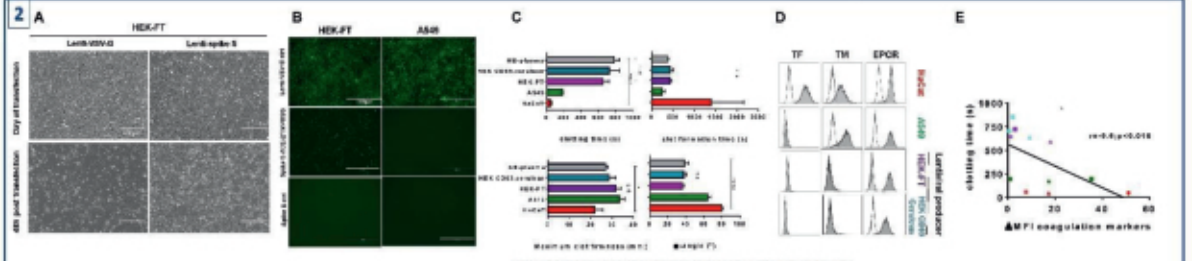


**Establishing pseudotyped lentiviral particles in HEK-FT cells and viral transduction of target cells**

**A)** Transduction of 1.4x10⁵ HEK-FT cells with gag/pol pseudotyped either with VSV-G (transduction efficiency) or SpikeS. After 48h supernatant, containing lentiviral particles was transvered and sterilfiltered. **B)** The lung epithelial carcinoma cell line A549 and HEK-FT were co-transfected with plasmid containing ACE2/TMPRSS, prior to infection with pseudotyped spikeS lentivirus. The glycoprotein VSV-G was served in this experiment as a transduction efficiency control and show >80% GFP expression.

**Clotting potential varies among different cell types and lentiviral producer cells**

**C)** Evaluation of clotting capacity of different cell types via rotational thromboelastometry (ROTEM) show the highest clotting time for the cell line HaCaT, followed by A549,but no clotting with HEK-FT and HEK CD63-cenilase compared with human plasma . Data from three technical replicates . Statistical analysis was performed using student's t-test, unpaired.

**D)** Pro- and anticoagulatory proteins vary on different cell types assed via FCM. The protein EPCR was found on all cell types, while TF was expressed on HaCaT and TM on the latter and A549. **E)** shows is the significant correlation between mean fluorescence intensity of TF,TM and EPCR and the clotting time (s) of epithelial and lentiviral producer cells; statistical analysis was performed using a pearson correlation ($p<0.05$)

**3**

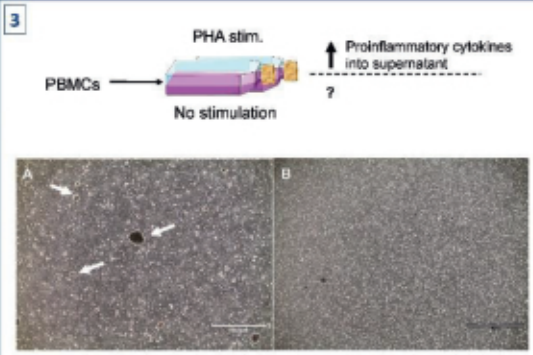


**Treatment with PHA triggers PBMCs to proliferate and show cell aggregation after 4 days**

**A)** Morphological changes during cultivation of 50x10⁶ PBMC after treatment with PHA on d4 were observed. Upon treatment, cells were aggregating and potentially secreting proinflammatory cytokines into the media **B)** PBMC without PHA treatment are shown. The cells bear a different cell morphology compared with the treated cells. (A+B) data from 10 pooled PBMC donors are shown

**4**

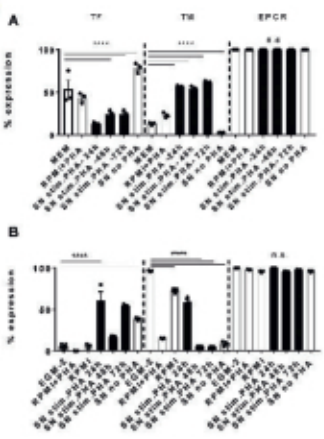


**A) Impact of PBMC stimulated vs. non stimulated supernatant on coagulation markers of human derived skin fibroblasts (hdFB).**

Treatment with stimulated SN of PBMCs show a highly significant decrease of TF in a time dependent manner, whereas non treated supernatant revealed an unexpected upregulation. The anticoagulatory protein TM was upregulated, upon treatment with stimulated SN, while non stimulated show the opposite. EPCR remain over time, not altered.
Three technical replicates are shown, statistical analysis of FCM data was performed using an unpaired ANOVA test ($p<0.05$); ±SEM

**B) Human endothelial colony forming cells (ECFC) respond differently to stimulated vs. non stimulated PHA SN.**

TF was induced over time, while TM show the highest decrease after 48 and 72h. As already shown for dHDF, EPCR was not altered. Three technical replicates are shown, statistical analysis of FCM data was performed using as unpaired ANOVA test($p<0.05$); ±SEM

**5 CONCLUSION and OUTLOOK**

Preliminary data indicate regulation of pro- and anticoagulatory proteins on epithelial and endothelial potential CoV-2 target cells, respectively. Evaluation of clotting capacity of epithelial cells and lentiviral competent cells are correlated with coagulation related proteins. Future experiments, will show the combined effect of inflammation and SARS CoV-2 pseudotype virus infection on coagulation proteins. These data, might provide mechanistic explanation in the context of microembolism and thormbotic events in Covid-19 patients.

Cell Therapy Institute, PMU Salzburg
katharina.muigg, katharina.muigg@pmu.ac.at

## Coagulation potential of SARS CoV-2 target cells and their extracellular vesicles

Katharina Muigg, Michaela Öller[2], Nicole Maedig[1], Eva Klinglmayer[3], Katharina Schallmoser[2], Nicole Meisner-Kober[3]

[1]Experimental and Clinical Cell Therapy Institute, Spinal Cord Injury and Tissue Regeneration Center Salzburg (SCI-TReCS), Paracelsus Medical University, Salzburg, Austria; [2]Department of Blood Group Serology and Transfusion Medicine, Paracelsus Medical; [3]Department of Chemical Biology and Biological Therapeutics, University of Salzburg; Contact: katharina.muigg@pmu.ac.at

### Objective
A large number of Covid-19 patients, suffer from microembolism (20-30%) or thrombotic events, however the physiological reason has been to date, not elucidated. This PhD project will focus on the potential imbalance of pro- and anticoagulatory proteins on cells and their extracellular vesicles (EVs) upon viral infection. The cytokine storm relating from recruited immune cells may also alter pro- and anticoagulatory proteins on cells and their EVs influencing distant cells and subsequently alter the cell mediated coagulation initiation.

### Results
Evaluation of clotting capacity of different cell types via rotational thromboelastometry (ROTEM) showed the highest clotting time for the cell line HaCaT, followed by A549, but no clotting with HEK-FT and HEK CD63-cerulean when compared with human plasma ($n=3;p<0.05$). Significant correlation between mean fluorescence intensity of TF, TM and EPCR and the clotting time (s) of epithelial and lentiviral producer cells was observed; ($p<0.05$). Moreover, human dermally derived fibroblasts (hdFB) show a highly significant decrease of TF in a time dependent manner treatment after stimulation with SN of PBMCs, whereas untreated supernatant revealed an unexpected upregulation. In human endothelial colony forming cells (ECFC) TF was induced over time, while TM show the highest decrease after 48 and 72h ($n=3$; $p<0.05$).

### Conclusions
Preliminary data indicate regulation of pro- and anticoagulatory proteins on epithelial and endothelial potential SARS CoV-2 target cells, respectively. Evaluation of clotting capacity of epithelial cells and lentiviral competent cells are correlated with coagulation related proteins. Future experiments, will show the combined effect of inflammation and SARS CoV-2 pseudotype virus infection on coagulation proteins. These data, might provide mechanistic explanation in the context of microembolism and thormbotic events in Covid-19 patients

# Benchmark test of flow sensors for the Sophie ventilator regarding dead space

**Linda Mur**

Paracelsus Medical University, Salzburg, Austria

Despite numerous improvements in respiratory support, ventilator-induced lung injury contributes as a notable factor to morbidity and mortality in preterm infants.[1]

Since recognized that high tidal volumes can lead to the development of volutrauma and pulmonary edema[2], clinicians seek new methods to reduce tidal volume as far as possible.

## OBJECTIVE

To explore:

- Classification of a new Neo pneumotachograph (PNT) in comparison to the other three flow sensors (A, B, Double PNT)
- how to keep the dead space as small as possible
- how relevant additional dead space created by a built-in $CO_2$ sampling device is

## METHODS

- experimental setup (Figure 1)
- continuous flow ventilator Sophie, connected to a pneumotachograph and a 50 ml lung, simulating a 1000 g infant
- four different flow sensors from Stephan GmbH with various adapters (dead space minimizer, adapter for closed suction) and Microstream $CO_2$ sampling were tested
- flooding the lung with $CO_2$ and measuring the $CO_2$ elimination time using a capnograph
- The measurements were carried out twenty times with each combination
- Mean elimination times (±SD) were compared (Figure 2)

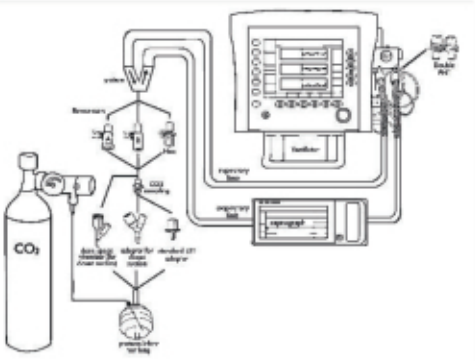


**Figure 1: experimental setup**

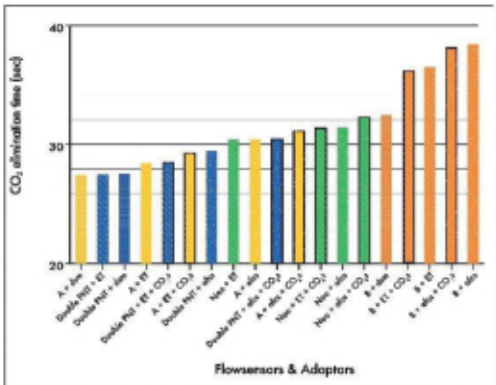


**Figure 2: The $CO_2$ elimination time in seconds for the various flow sensors with adapters, ETT standard adapter for endotracheal tube, dsm dead space minimizer, afcs adapter for closed suction, $CO_2$s $CO_2$ sampling**

**ACKNOWLEDGEMENT**

Assoc. Prof. Dr. Martin Wald (planning of investigation and spending support)

**REFERENCES**

[1] Auten RL et al, Clin Perinatol 2001;28:505-15

[2] Dreyfuss et al. Am Rev Respir Dis. 1988;137:1159-64

## RESULTS

- The Neo flow sensor can be classified with a dead space larger than A but smaller than B
- $CO_2$ elimination time significantly lower in PNT A and Double PNT than in Neo PNT and PNT B
- $CO_2$ elimination time with dead space minimizer was significantly shorter than without dead space minimizer for PNT A 27.4 s (± 0.05 s) with vs. 28.4 s (± 0.05 s) without, PNT B 32.44 s (± 0.06 s) and 36.46 s (± 0.13 s), and Double PNT 27.5 s (± 0.05 s) and 27.48 s (± 0.08 s)
- Using the Microstream CO2 sampling mean elimination time was 29.27 s (± 0.1 s) for the A PNT, 36.1 s (± 0.05 s) for B PNT, 28.47 s (± 0.05 s) for Double PNT and 31.29 s (±0.07 s) for the Neo PNT
- The $CO_2$ sampling achieved a significantly lower $CO_2$ elimination time with PNT B, whether used with the ETT standard adapter or adapter for closed suction
- Use of $CO_2$ sampling in the other flow sensor leads to an increase in $CO_2$ elimination time. (A: 2.98%, Neo PNT: 2.98%, Double PNT 3.48%)

## CONCLUSIONS

- $CO_2$ elimination time was significantly lower with the dead space minimizer for A PNT and B PNT, not significant for Double PNT and not assessable for Neo PNT
- use of dead space minimizers in extremely preterm infants might reduce the occurrence of volutrauma
- $CO_2$ sampling leads to a slight increase in dead space, but the effect does not seem to be so great that a justified use in premature infants can also be considered

## Benchmark test of flow sensors for the Sophie ventilator regarding dead space

Linda Mur[1]

[1]Paracelsus Medical University, Salzburg, Austria; Contact: linda.mur@stud.pmu.ac.at

### Objective

Flow sensors are placed directly in front of the endotracheal tube when ventilating premature infants. In this position, they increase the instrumental dead space. Higher tidal volumes are required to overcome the dead space, increasing the risk of ventilator-induced lung injury. In an experimental setup, the dead space of several flow sensors with different dead space and various adapters were tested how to keep the dead space as small as possible.

### Methods

The experiment was conducted with the continuous flow ventilator Sophie, connected to a pneumotachograph and a test lung, simulating a 1000 g infant. Four different flow sensors from Stephan GmbH with various adapters and Microstream $CO_2$ sampling were tested: A, B, Double, and the new Neo pneumotachograph for preterm infants. The dead space could be determined by flooding the lung with $CO_2$ and measuring the $CO_2$ elimination time using a capnograph. The measurements were carried out twenty times with each combination. Mean elimination times (±SD) were compared.

### Results

Mean $CO_2$ elimination time was 27.4 s (± 0.05 s) with and 28.4 s (± 0.05 s) without the dead space minimizer for the A Sensor, 32.4 s (± 0.06 s) and 36.5 s (± 0.13 s) for the B Sensor, 27.5 s (± 0.05 s) and 27.5 s (± 0.08 s) for the Double Sensor and 30.4 (± 0.15 s) without for the Neo Sensor because it is not compatible with it. If no dead space minimizer was installed, the standard adapter for the endotracheal tube was used as a reference. Using the Microstream $CO_2$ sampling, mean elimination time was 29.3 s (± 0.1 s) for the A, 36.1 s (±0.05 s) for B, 28.5 s (± 0.05 s) for Double and 31.3 s (±0.07 s) for the Neo pneumotachograph.

### Conclusions

CO2 elimination time was significantly lower with the dead space minimizer for A and B Sensor, not significant for Double, and not assessable for Neo pneumotachograph. CO2 sampling leads to a slight increase in dead space, which is relevant for extremely preterm infants. However, the effect does not appear to be so great that a justified use can be considered.

# Benchmark test of flow sensors for the Sophie ventilator regarding condensation susceptibility

**Linda Mur**

Paracelsus Medical University, Salzburg, Austria

Targeted patient-ventilator synchrony has become the standard of care in newborn intensive care.[1,2]

The potential disadvantage of this flow-targeted ventilation form is the use of a flow sensor (pneumotachograph) attached to the airway y-piece. Through the formation of condensation, the resistance increases causing the respirator to measure an incorrect flow.[3]

Correct measurement of the tidal volume is essential concerning adequate ventilation and the prevention of lung damage due to excessive tidal volume.[4]

Crucial for this study were the observations that pneumotachographs provide inconclusive tidal volume values over a longer period without triggering an alarm.

## OBJECTIVE

To explore:

- whether three commercially used flow sensors deliver consistent values over a long period
- how far we can trust the measured values from flow sensors
- how much flow sensors are prone to condensation water and how they react to it

## METHODS

- experimental setup
- continuous flow ventilator Sophie, connected to a pneumotachograph and a 50 ml lung, simulating a 1000 g infant
- three current neonatal flow sensors from Stephan GmbH were tested
- tidal volume was recorded by the ventilator every two seconds and saved in logfiles, which were compared
- The measurements were carried out five times with each pneumotachograph, tested for two hours

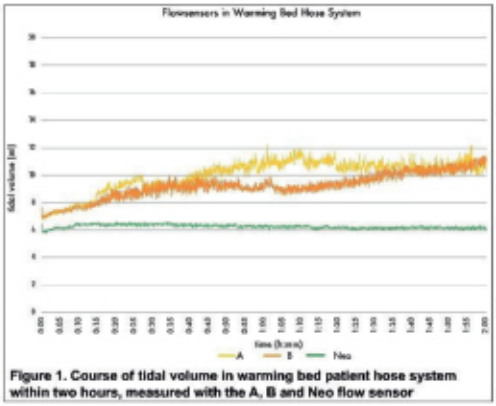


**Figure 1. Course of tidal volume in warming bed patient hose system within two hours, measured with the A, B and Neo flow sensor**

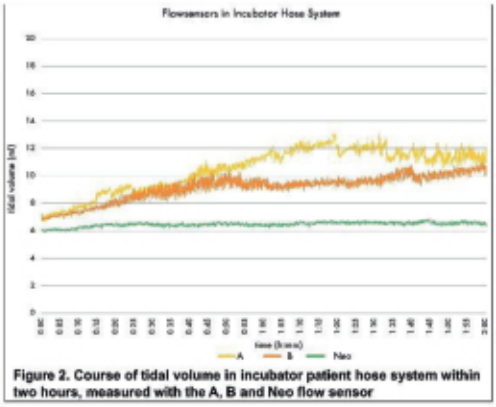


**Figure 2. Course of tidal volume in incubator patient hose system within two hours, measured with the A, B and Neo flow sensor**

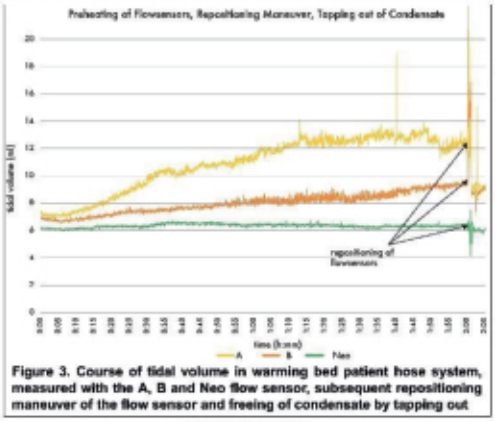


**Figure 3. Course of tidal volume in warming bed patient hose system, measured with the A, B and Neo flow sensor, subsequent repositioning maneuver of the flow sensor and freeing of condensate by tapping out**

- Three trials: with warming bed patient hose system, incubator patient hose system, and preheating of flow sensor
- Tapping out of condensate, if they are able to show the initially measured values again

## RESULTS

- The measured data revealed a deviation of 0.5 ml tidal volume after a short time (<10 min) in A and B flow sensor (Figure 1)
- Neo flow sensor was able to keep a constant measurement of tidal volume over two hours
- greater range of variations between the A and B flow sensors in incubator patient hose system (Figure 2)
- preheated flow sensors assume a higher initial value compared to the other two runs, but drops to the known initial value after a few minutes
- A and B flow sensors showed substantial deviations in the measured tidal volume during the repositioning maneuver, whereas the Neo flow sensor showed only minor deviations
- After tapping out, the Neo Flow sensor showed the initially measured values again, but the A and B sensor could not be reset to the original values (Figure 3)

## CONCLUSIONS

- Condensation water considerably influences the pneumotachograph's measurements
- Through the increasing differential pressure in pneumotachographs, the measured tidal volume values are incorrectly high
- the measured data should not be trusted
- In guaranteed volume ventilation, this reduces the peak inspiratory pressure and hypoventilation occurs

**ACKNOWLEDGEMENT**

Assoc. Prof. Dr. Martin Wald (planning of investigation and spending support)

**REFERENCES**

[1] Keyber et al. Intensive Care Med. 2017;43:1764-1780
[2] Dimitriou et al. Acta Paediatr. Apr 2001;90:445-7
[3] Pfitzner Anaesthesia 1977;32:343-52
[4] Dreyfuss et al. Am Rev Respir Dis. 1988;137:1159-64

## Benchmark test of flow sensors for the Sophie ventilator regarding condensation susceptibility

Linda Mur[1]

[1]Paracelsus Medical University, Salzburg, Austria; Contact: linda.mur@stud.pmu.ac.at

### Objective
Measuring the correct tidal volume is playing an increasingly important role in mechanical ventilation of extremely preterm infants. Companies have developed several flow sensors based on a pressure differential. Condensation in the pneumotachograph can compromise the measurement accuracy that leads to hypoventilation of the infant. In an experimental study, three commercially used flow sensors were compared to determine how much they are affected by condensation and whether they provide consistent values over a long period.

### Methods
The measurements were carried out five times with each pneumotachograph, tested for two hours. The experiment was conducted with the continuous flow ventilator Sophie (Stephan GmbH) connected to a pneumotachograph and a test lung, simulating a 1000 g preterm infant. Three pneumotachographs (A, B, Neo PNT) were exposed to simulated ventilation for two hours. The tidal volume measured by the flow sensors every two seconds was recorded by the Sophie Respirator and saved in log files. Based on these files, the progress of the tidal volume over time was compared. Each trial was repeated five times with identical settings.

### Results
The measurement data showed an increase in the measured tidal volume of 0.5 ml for two flow sensors after 10 minutes and 4ml after two hours. The third sensor was able to maintain a constant measurement of tidal volume over two hours.

### Conclusions
Condensation can significantly affect the measurements of the pneumotachograph. The measured tidal volume values may be incorrectly high due to the increasing differential pressure in pneumotachographs. Therefore, the measured values may also be questioned.

HOCHSCHULE
WEIHENSTEPHAN-TRIESDORF
UNIVERSITY OF APPLIED SCIENCES

# Effects of Angocin® on Microbacteria

L. Ebert, S. Schmelzer and L. Nausch*
Department of Agriculture, Food and Nutrition; University of Applied Sciences Weihenstephan-Triesdorf,
*Contact: lydia.nausch@hswt.de

**Objective:** According to the World Health Organisation (WHO), a total of 10 million deaths are predicted to be caused by antibiotic resistancies up until the year 2050 (1-3). Alternative approaches against bacterial infections are needed, e.g. therapies of plant-based extracts that inhibit growth in microbacteria, or combined therapies of common antibiotics and plant-based drugs. In this preliminary study, we investigate the antibiotic effect of (low dose) **Angocin®**, a plant-based product used to treat urinary bladder infection (Angocin® Anti-Infekt N, Repha GmbH, Biologische Arzneimittel).

**Methods:** Serial dilutions of different bacterial strains (*Escherichia coli* E4107, *Escherichia coli* E4104 (tetracyclin (TET) resistent), *Enterobacter cloacae subsp. dissolvens*) were plated on a mixture of Angocin®/ CASO-Agar (Carl-Roth® GmbH) and incubated for 24 h at 37°C. Colony forming units (cfu) were analysed in presence of Angocin® and compared to control growth conditions (no supplements added) and tetratcyclin (0.25 mg/ plate) added.

**Results:**

*Figure 1: Bacterial growth and Colony Forming Units under control conditions*

| Bacterial Strains | Serial Dilutions of Bacteria $10^{0}$ | $10^{-3}$ | $10^{-5}$ | $10^{-8}$ |
|---|---|---|---|---|
| *E4104* | confluent | confluent | > 300 | 4 |
| *E4107* | confluent | confluent | > 300 | 35 |
| *E.cloacae* | confluent | confluent | confluent | 11 |

*Figure 2: Bacterial growth and Colony Forming Units in presence of 0,25 mg Tetracyclin per plate*

| Bacterial Strains | Serial Dilutions of Bacteria $10^{0}$ | $10^{-3}$ | $10^{-5}$ | $10^{-8}$ |
|---|---|---|---|---|
| *E4104* | confluent | confluent | > 300 | 2 |
| *E4107* | 0 | 0 | 0 | 0 |
| *E.cloacae* | 0 | 0 | 0 | 0 |

*Figure 3: Bacterial growth and Colony Forming Units in presence of ¼ pill of Angocin® (44,44mg nasturtium, 17,77mg horse-radish root) per plate*

| Bacterial Strain | Serial Dilutions of Bacteria $10^{0}$ | $10^{-3}$ | $10^{-5}$ | $10^{-8}$ |
|---|---|---|---|---|
| *E4104* | confluent | 0 | 0 | 0 |
| *E4107* | 0 | 0 | 0 | 0 |
| *E.cloacae* | confluent | confluent | > 300 | 12 |

Figure 4: Bacterial Growth of E4104 at $10^{0}$ dilution on control agar medium without supplements (left) compared to bacterial growth on agar medium with Angocin® (right)

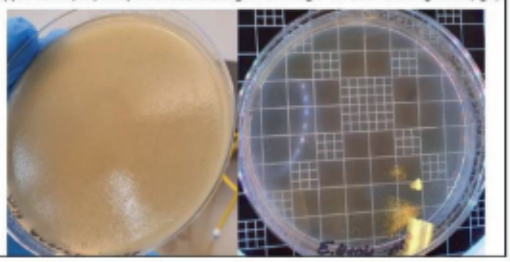

Confluent bacterial growth on CASO-Agar-Plates without any further supplements demonstrates viability of bacterial strains (Fig. 1). Low concentrations of Angocin® (1/4 pill, equivalent to 44.4 mg nasturtium and 17.8 mg horse-radish root) reduced growth of *E.coli* E4107 completely (Fig. 3), comparable to 0.25 mg Tetracyclin per plate (Fig. 2). Bacterial strain *E.coli* E4104 is resistant against tetracyclin and was therefore not reduced in growth by addition of TET to growth medium (Fig. 2). However, addition of Angocin® suppressed growth of *E.coli* E4104 from dilutions $10^{-3}$ on (Fig 3). Growth of E.cloacae was inhibited by Tet (Fig. 2), but not by low-dose Angocin® (Fig. 3).

**Conclusions:** Nearly complete inhibition of bacterial growth of *E.coli* E4107 and of *E.coli* E4104 in presence of low-dose Angocin® indicates the potential of mustard oil glycosides, the active components of nasturtium and horse-radish root, as alternative therapy against bacterial infections. It is noteworthy, that very low concentrations of Angocin® (1/4 pill) had a major impact on bacterial growth of *E. coli*. Confluent growth of *E. cloacae* in presence of Angocin® may be due to the low dose of Angocin® applied. Further studies are needed, to investigate the dose-dependency of bacterial growth in regard to varying concentrations of Agocin®.

(1)O'Neill, J. Tackling drug-resistant infections globally: final report and recommendations. (The Review On Antimicrobial Resistance, 2016).
(2)Sprenger, M. & Fukuda, K. New mechanisms, new worries. Science 351, 1263–1264 (2016).
(3)Kupferschmidt, K. Resistance fighters. Science 352, 758–761 (2016).

## Effects of Angocin® on Microbacteria

Lena Ebert[1], Sebastian Schmelzer[1], Lydia Nausch[1]

[1]Department of Agriculture, Food and Nutrition; University of Applied Sciences Weihenstephan-Triesdorf; Contact: lydia.nausch@hswt.de

### Objective

According to the World Health Organisation (WHO), a total of 10 million deaths are predicted to be caused by antibiotic resistancies up until the year 2050 (1-3). Alternative approaches against bacterial infections are needed, e.g. therapies of plant-based extracts that inhibit growth in microbacteria, or combined therapies of common antibiotics and plant-based drugs. In this preliminary study, we investigate the antibiotic effect of (low dose) Angocin®, a plant-based product used to treat urinary bladder infection (Angocin® Anti-Infekt N, Repha GmbH, Biologische Arzneimittel).

### Methods

Serial dilutions of different bacterial strains (*Escherichia coli* E4107, *Escherichia coli* E4104 (tetracyclin (TET) resistent), *Enterobacter cloacae subsp. dissolvens*) were plated on a mixture of Angocin®/ CASO-Agar (Carl-Roth® GmbH) and incubated for 24 h at 37°C. Colony forming units (cfu) were analysed in presence of Angocin® and compared to control growth conditions (no supplements added) and tetratcyclin (0.25 mg/ plate) added.

### Results

Confluent bacterial growth on CASO-Agar-Plates without any further supplements demonstrates viability of bacterial strains. Low concentrations of Angocin® (1/4 pill, equivalent to 44.4 mg nasturtium and 17.8 mg horse-radish root) reduced growth of E.coli E4107 completely, comparable to 0.25 mg Tetracyclin per plate. Bacterial strain E.coli E4104 is resistant against tetracyclin and was therefore not reduced in growth by addition of TET to growth medium. However, addition of Angocin® suppressed growth of E.coli E4104 from dilutions $10^{-3}$ on. Growth of E.cloacae was inhibited by Tet, but not by low-dose Angocin®.

### Conclusions

Nearly complete inhibition of bacterial growth of E.coli E4107 and of E.coli E4104 in presence of low-dose Angocin® indicates the potential of mustard oil glycosides, the active components of nasturtium and horse-radish root, as alternative therapy against bacterial infections. It is noteworthy, that very low concentrations of Angocin® (1/4 pill) had a major impact on bacterial growth of E. coli. Confluent growth of E. cloacae in presence of Angocin® may be due to the low dose of Angocin® applied. Further studies are needed, to investigate the dose-dependency of bacterial growth in regard to varying concentrations of Agocin®.

### References

1. O'Neill, J. Tackling drug-resistant infections globally: final report and recommendations. (The Review On Antimicrobial Resistance, 2016)
2. Sprenger, M. & Fukuda, K. New mechanisms, new worries. Science 351, 1263–1264 (2016)
3. Kupferschmidt, K. Resistance fighters. Science 352, 758–761 (2016)

bartelt
IHR LABOR-KOMPLETTAUSSTATTER
Chemikalien · Geräte · Service · Software

Unser Service
für Ihren Erfolg.

**Als Familienunternehmen und Labor-Experte in Ihrer Nähe legen wir besonderen Wert auf persönliche Betreuung. Wir beraten Sie gerne und finden gemeinsam die optimale Lösung für Ihren individuellen Bedarf!**

Wir planen mit Ihnen Ihr Labor und bieten hochwertige Geräte von namhaften Herstellern wie z.B. ***Asecos, Binder, Hettich, Kojair, Lauda, Liebherr, Memmert, Thermo Fisher Scientific, Systec, Vacuubrand, Zeiss*** und viele mehr. Erstklassige **Labor- und Biochemikalien** und diverse **Verbrauchsgüter** gehören ebenfalls zu unserem umfangreichen Sortiment. Profitieren Sie von unserem Service durch fachkundige und engagierte Mitarbeiter, sowie von unseren schnellen und flexiblen Lieferzeiten. Egal ob **Inbetriebnahme, Einschulung, Reparatur oder Wartung,** als Laborkomplettausstatter stehen wir Ihnen jederzeit gerne zur Verfügung und halten Sie auf dem neuesten Stand.

Ihr Ansprechpartner →

**BARTELT GmbH**
**Neufeldweg 42,**
**8010 Graz, Austria**

**+43 (0)316/47 53 28-0**
**office@bartelt.at**
**www.bartelt.at**

ONLINESHOP
WWW.BARTELT.AT

ResearchConnect is a specialist funding database built for and designed by the international research community.

Contact our expert team to learn how you could access more funding.

myresearchconnect.com

Streamlining access to funding for research institutions and universities worldwide.

Idox. Do more.

idox

# *Kompetenz für das Labor*

Unser Lieferprogramm umfaßt :
Laborhilfsmittel und Arbeitsschutz, Chemikalien, Laborgeräte
bzw. Laborzubehör und Laboreinrichtungen

**Jetzt gratis Katalog anfordern unter www.lactan.at!**



LACTAN
Chemikalien und Laborgeräte

CARL ROTH®

8020 Graz, Puchstraße 85 | Tel.: 0316/323692-0 | Fax: 0316/382160
info@lactan.at | www.lactan.at

# Targeting Neuroblastoma with Food Additives

**Michael Novak, Sepideh Aminzadeh-Gohari, Daniela D Weber, Barbara Kofler, Luca Catalano**

RESEARCH PROGRAM FOR RECEPTOR BIOCHEMISTRY AND TUMOR METABOLISM, DEPARTMENT OF PEDIATRICS,
UNIVERSITY HOSPITAL OF THE PARACELSUS MEDICAL UNIVERSITY, SALZBURG, AUSTRIA.

## INTRODUCTION

Neuroblastoma represents the third most common form of childhood cancer, 7 % of all tumors between birth and the age of 14 and even the most common diagnosed type of cancer within the first year of life. [1] Despite the excellent survival rate for stage 1 and stage 2 neuroblastoma patients (99 % & 93 %), overall survival for high-risk stages remains very low (40-50 %). [2] As there already exists some indication that the use of certain food additives, e.g. Resveratrol, Spermidine, 2´4´-Dimethoxychalcone, Mannose, Hydroxycitrate and Lipoic Acid have negative effects on cancer cell growth. The first aim of the study was to elucidate the most potent anti-proliferative compound for MYCN-amplified and non-MYCN-amplified neuroblastoma cells. Furthermore, we hypothesized, that combining each substance could result in additive or synergistic effects on cell proliferation of neuroblastoma cells but spare potential toxic effects on human non-cancer cells.

## METHODS

- The four neuroblastoma cell lines SK-N-BE(2)(MYCN-amplified), SH-SY5Y, GI-ME-N and Kelly (MYCN-amplified) as well as Human Dermal Fibroblasts (HDF) and HEK293(human embryonic kidney cells) were seeded in 96-well plates in quadruplicates.
- 24h after seeding, cells were treated with single-, double- or triple-combinations of food additives.
- 72h after treatment, a crystal violet assay was performed to determine cell proliferation.

## RESULTS

- 10 µM Spermidine and 10 µM 2´4´-Dimethoxychalcone had the best anti-proliferative effect in single-compound treatments as they reduced cell proliferation by 76 % and 72 %, respectively (Fig. 1 and Fig.2).
- Most triple-combination treatments showed an additive effect on certain cell lines but a specific combination that targets all four to a similar extend could not be identified. As the overall aim to identify a combination of food additives that targets all of the individual neuroblastoma cell lines was not fulfilled, we decided to use those combinations that target the most treatment resistant MYCN-amplified SK-N-BE(2) neuroblastoma cell line. The combination of Mannose, 2´4´-Dimethoxychalcone and Spermidine had the highest anti-proliferative effect on the SK-NBE(2) cell line (Fig.3).
- One combination of food additives was toxic on non-cancerous human cells. The combination of Resveratrol and 2´4´-Dimethoxychalconeresulted in a reduction of HEK293 cell proliferation of about 46 %. (Fig. 4)

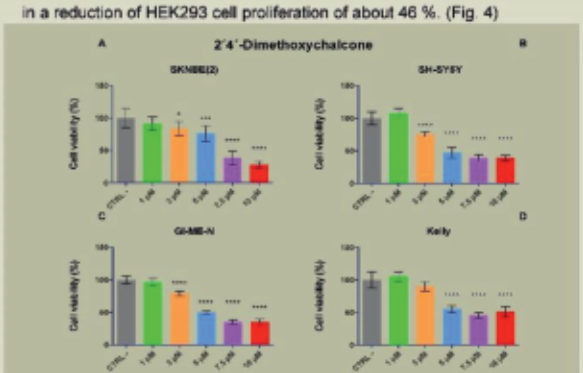


**Fig. 1: Effect on the relative viability of NB cells treated with 2´4´-Dimethoxychalcone (1 µM to 10 µM) compared to vehicle (CTRL).** After 3 days treatment the viability of the cells was evaluated by the Cristal violet assay. Values represent mean ± SD (n= 2 for each cell line). For statistical analysis one-way ANOVA followed by Dunnett's Multiple Comparison Test; *p<0.0240, **p<0.0034, ***p<0.0001 compared to CTRL.

**FUNDING**
FWF P 31228-B33

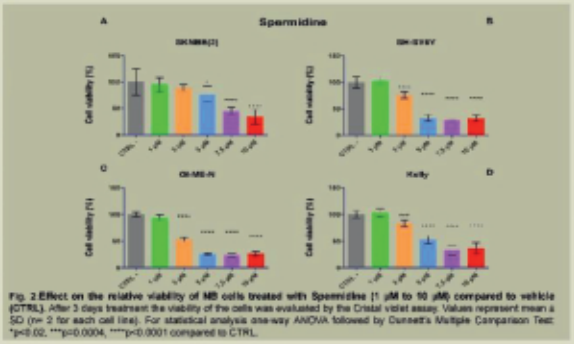


**Fig. 2 Effect on the relative viability of NB cells treated with Spermidine (1 µM to 10 µM) compared to vehicle (CTRL).** After 3 days treatment the viability of the cells was evaluated by the Cristal violet assay. Values represent mean ± SD (n= 2 for each cell line). For statistical analysis one-way ANOVA followed by Dunnett's Multiple Comparison Test; *p<0.02, ***p<0.0004, ****p<0.0001 compared to CTRL.

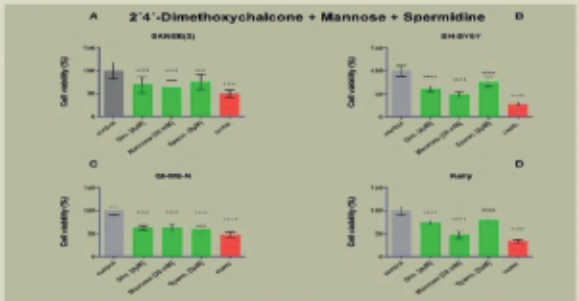


**Fig. 3: Effect on the relative viability of NB cells treated with 2´4´-Dimethoxychalcone (4µM), Mannose (20mM) and Spermidine (5 µM to 10 µM) compared to vehicle (CTRL).** After 3 days treatment the viability of the cells was evaluated by the Cristal violet assay. Values represent mean ± SD (n= 3 for each cell line). For statistical analysis one-way ANOVA followed by Dunnett's Multiple Comparison Test; ***p<0.0002; ****p<0.0001 compared to CTRL.

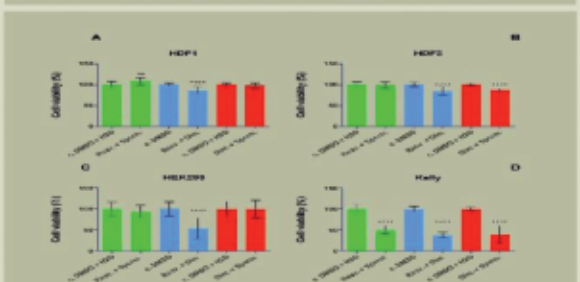


**Fig. 4: The effect of combination treatments of 20 µM Resveratrol, 4 µM 2´4´-Dimethoxychalcone and 5 µM Spermidine on (A) HDF1, (B) HDF2, (C) HEK293, (D) Kelly cells.** Values represent mean ± SD. For statistical analysis one-way ANOVA followed by Dunnett's Multiple Comparison Test;, Two (HEK293 and Kelly) and three (HDF1/2) replicates. ** p ≤ 0.01; **** p ≤ 0.0001.

## CONCLUSION

- The combination of Mannose, 2´4´-Dimethoxychalcone and Spermidine could be the best choice for further *in vitro* and *in vivo* experiments as it showed an additive reduction in cell viability compared to the single-substance treatment in the cell lines SH-SY5Y, GI-ME-N and Kelly and had the highest impact in cell proliferation of the most treatment-resistant SK-N-BE(2) cell line.
- Furthermore, this combination does not include a combination of Resveratrol and 2´4´-Dimethoxychalconee, which appeared to be toxic on HEK293 cells.
- The present study will be the basis for further *in vivo* studies with these food compounds as an adjunct therapy to cytotoxic, radiation and antibody therapies.

**REFERENCES**

[1] Ward et al. 2014: Childhood and adolescent cancer statistics
[2] Whittle et al. 2017: Overview and recent advances in the treatment of neuroblastoma

Contact: l.catalano@salk.at

## Targeting Neuroblastoma with Food Additives

Michael Novak Novak[1], Sepideh Aminzadeh-Gohari[1], Daniela Weber[1], Barbara Kofler[1], Luca Catalano[1]

[1]Research Program for Receptor Biochemistry and Tumor Metabolism, Department of Pediatrics,University Hospital of the Paracelsus Medical University, Salzburg, Austria.; Contact: l.catalano@salk.at

### Objective

Neuroblastoma is the most frequent type of cancer within the first year of life and represents the most diagnosed embryonal derived cancer among all age groups. After being diagnosed, curation and survival mostly depend on age of the patient and clinical as well as biological characteristics of the tumor. Albeit stage 1 and stage 2 of the disease with localized tumors can be cured with surgical resection in over 90% of cases, high-risk disease patients, which are frequently characterized by MYCN amplification, often rely on very aggressive treatment schedules with a survival rate of only 40-50%.

### Methods

The four neuroblastoma cell lines SK-N-BE(2), SH-SY5Y, GI-ME-N and Kelly were seeded in quadruplicates into 96-well plates and treated with Resveratrol, Spermidine, 2´4´-Dimethoxychalcone, Mannose, Hydroxycitrate and Lipoic Acid. 72h after treatment, a crystal violet assay was performed to elucidate the effect of the compounds on the cell proliferation. Furthermore, Human Dermal Fibroblasts (HDF1/2 cells) and Human Embryonic Kidney cells (HEK293) were also treated with compound combinations to elucidate toxic effects of the food additives used.

### Results

All compounds decreased dose-dependently the cell proliferation of the neuroblastoma cell lines. The strongest individual effect was observed with Spermidine and 2´4´-Dimethoxychalcone. Even though their strong individual effects on neuroblastoma cell viability, the treatment with the combination of Spermidine and 2´4´-Dimethoxychalcone did not result in an synergistic or additive effect.
Triple-combination treatments revealed that the combination of Mannose, 2´4´-Dimethoxychalcone and Spermidine was most effective against the treatment resistant MYCN amplified SK-N-BE(2) cell line.

### Conclusions

As the treatment with Mannose, 2´4´-Dimethoxychalcone and Spermidine together not only targets best the most treatment-resistant SK-N-BE(2) cell line, without showing major toxicity to non-cancer cells, this combination of food additives might be the best choice to use for further in vitro experiments. The present study will be the basis for further in vivo studies with these food compounds as an adjunct therapy to cytotoxic, radiation and antibody therapies.

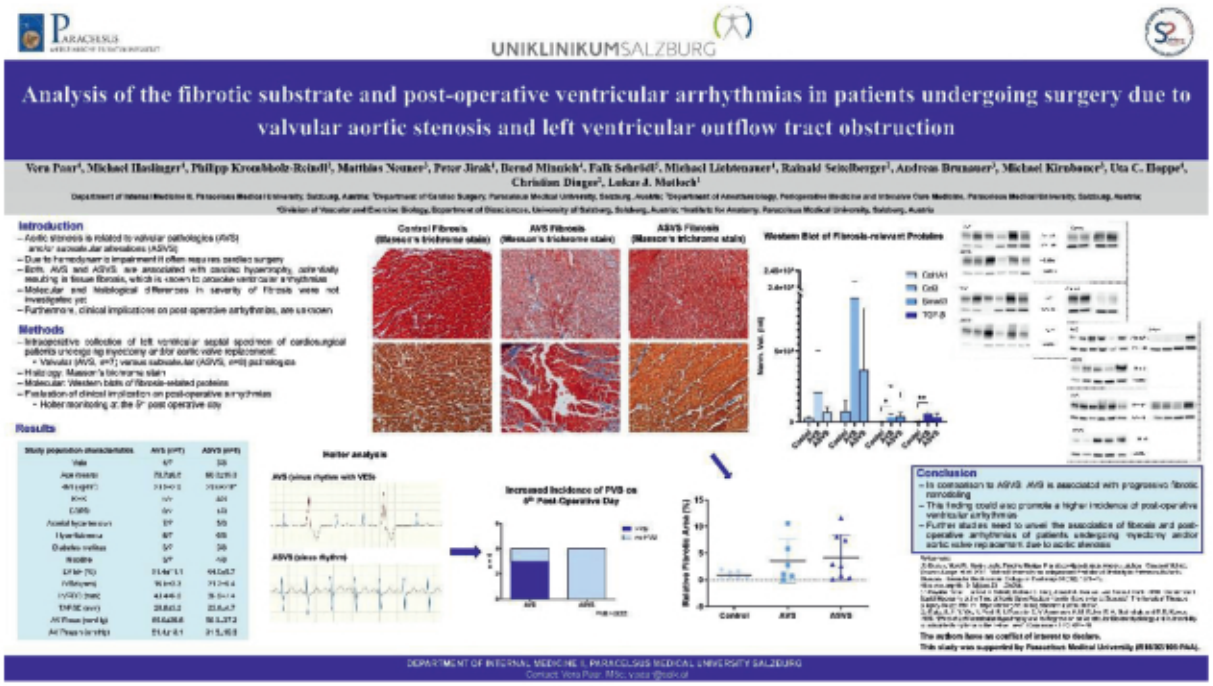
UNIKLINIKUMSALZBURG
Analysis of the fibrotic substrate and post-operative ventricular arrhythmias in patients undergoing surgery due to valvular aortic stenosis and left ventricular outflow tract obstruction
Introduction
Methods
Results
Conclusion
DEPARTMENT OF INTERNAL MEDICINE II, PARACELSUS MEDICAL UNIVERSITY SALZBURG

## Analysis of the fibrotic substrate and post-operative ventricular arrhythmias in patients undergoing surgery due to valvular aortic stenosis and left ventricular outflow tract obstruction

Vera Paar[1], Michael Haslinger[1], Philipp Krombholz-Reindl[2], Matthias Neuner[3], Peter Jirak[1], Bernd Minnich[4], Falk Schrödl[5], Michael Lichtenauer[1], Rainald Seitelberger[2], Andreas Brunauer[3], Michael Kirnbauer[3], Uta C. Hoppe[1], Lukas J. Motloch[1]

[1]Department of Internal Medicine II, Paracelsus Medical University, Salzburg, Austria; [2]Department of Cardiac Surgery, Paracelsus Medical University, Salzburg, Austria; [3]Department of Anesthesiology, Perioperative Medicine and Intensive Care Medicine, Paracelsus Medical University, Salzburg, Austria; [4]Division of Vascular and Exercise Biology, Department of Biosciences, University of Salzburg, Salzburg, Austria; [5]Institute for Anatomy, Paracelsus Medical University, Salzburg, Austria; Contact: v.paar@salk.at

### Objective

Valvular pathologies and/or subvalvular alterations are the two major pathologies of aortic stenosis and often require cardiac surgery. Both manifestations are associated with cardiac hypertrophy that potentially results in tissue fibrosis (1). However, molecular and histological differences in the severity of fibrosis in both etiologies were not investigated yet. Furthermore, clinical implications on post-operative arrhythmias, which potentially might depend on fibrosis, are unknown.

### Methods

To investigate this issue, we analyzed left ventricular septal specimen of cardiosurgical patients undergoing myectomy and/or aortic valve replacement due to valvular (AVS, n=7) vs. subvalvular (ASVS, n=8) pathologies by histological and molecular analyses. Additionally, to evaluate clinical implication on post-operative arrhythmias, 48 h rhythm monitoring, as well as Holter monitoring at the 5th post-operative day, were investigated. Healthy post-mortem septal cardiac specimen served as a control group.

### Results

While echocardiographic parameters were similar in both pathology groups, such as left ventricular ejection fraction (AVS: 61.4±11.1% vs. ASVS: 64.0±5.7%, p=0.58), peak trans-aortic velocity at rest (AVS: 4.6±0.8 m/s, vs. ASVS: 3.6±1.4 m/s, p=0.12), and intraventricular septum diastolic (AVS: 16.0±3.3 mm vs. ASVS: 21.4±6.4 mm, p=0.06), we observed a higher incidence of premature ventricular extra-beats on the fifth post-operative days in AVS. Histological analyses revealed that in both pathologies there is a trend towards a higher fibrotic burden in comparison to healthy control tissue (AVS: p=0.13, ASVS: p=0.07). This was confirmed by a higher presence of Smad3 and TGF-β1. However, there were no differences concerning histologically determined fibrosis (AVS: 3.5±4.1% vs. ASVS: 4.2±4.3%, p=0.75), as well as in the protein levels analyzed by western blot.

### Conclusions

In comparison to healthy control tissue, AVS and ASVS are associated with progressive fibrotic remodeling, though without differences between AVS and ASVS. While this finding could also promote a higher incidence of post-operative ventricular arrhythmias in cardiosurgical patients it does not seem to contribute to a higher arrhythmogenicity in AVS. Further studies need to investigate the association of fibrosis and post-operative arrhythmias in cardiosurgical patients.

### Acknowledgements

This study was supported by Paracelsus Medical University (R18/02/106-PAA).

### References

1. Dweck, Marc R., Sanjiv Joshi, Timothy Murigu, Francisco Alpendurada, Andrew Jabbour, Giovanni Melina, Winston Banya, et al. 2011. 'Midwall Fibrosis Is an Independent Predictor of Mortality in Patients with Aortic Stenosis'. Journal of the American College of Cardiology 58 (12): 1271–79. https://doi.org/10.1016/j.jacc.2011.03.064.

PARACELSUS
MEDIZINISCHE PRIVATUNIVERSITÄT

Klinikum Nürnberg
wir sind für Sie da!

# Externe Validation zweier aktueller MRT-basierter Risikokalkulatoren zur Diagnostik des Prostatakarzinoms

BEST student POSTER

Anna-Lena Petersmann[1], Prof. Dr. Sascha Pahernik[2], PD Dr. Florian Distler[3]

[1]Paracelsus Medizinische Privatuniversität, Nürnberg; [2]Klinik für Urologie, Paracelsus Medizinische Privatuniversität, Nürnberg; [3]Klinik für Urologie, Paracelsus Medizinische Privatuniversität, Nürnberg; Deutschland;
Kontakt: anna.petersmann@stud.pmu.ac.at

## ZUSAMMENFASSUNG

Die Diagnostik eines signifikanten Prostatakarzinoms (sPC) wird durch Überdiagnostik und unnötig durchgeführte Biopsien erschwert. Risikokalkulatoren (RC) wurden entwickelt, um diese Probleme zu dezimieren und eine individuelle Risiko-Prognose zugeben. Diese Nomogramme wurden unlängst um die Ergebnisse aus mpMRTs erweitert und benötigen deshalb weiterer externer Validierung. Zwei dieser Modelle wurden in dieser Arbeit miteinander verglichen. Das MRI-ERSPC-RC-3/4-Modell und das Risikomodell von van Leeuwen.

Im Zeitraum von Dezember 2016 bis September 2019 wurden 265 Patienten mit einem klinisch suspekten Befund eines Prostatakarzinoms erfasst. Jeder dieser Patienten erhielt ein mpMRT, in welchem die Läsionen mittels PI-RADS v. 2.1 klassifiziert wurden, und darauffolgend eine MRT/TRUS-Fusionsbiopsie. Alle histologischen Präparate wurden von Uropathologen analysiert und nach dem ISUP-System eingestuft. Alle Karzinome mit einem ISUP Grad ≥ 2 wurden als signifikante Prostatakarzinome (sPC) klassifiziert. Die statistische Auswertung erfolgte durch Vergleich der AUCs, Kalibrierungskurven und Decision-Curves.

Bei 123 (=46,4%) lag ein sPC vor. Die AUCs der ROC-Analyse ergab keinen signifikanten Unterschied; p=0,178. Die Kalibrierungskurve zeigte für das MRI-ERSPC-RC-3/4 Modell einen nahezu idealen Kurvenverlauf (intercept 0,07; slope 0,94) im Vergleich zum van Leeuwen Modell: (Intercept -1,03; slope 0,70). Die Decision Curves zeigten für einen Schwellenwert von 15% einen Net-Benefit von Δ0,1314 für das van Leeuwen-Modell für die gesamte Kohorte im Vergleich zum MRI-ERSPC-RC-3/4 Modell. Wird ein Risiko-Schwellenwert von 15% gewählt, würden mit dem van Leeuwen Modell 24% aller Biopsien vermieden vs. 14% durch das MRI-ERSPC-3/4-RC-Modell. Man übersähe 6% bzw. 5% aller sPC.

## ROC-KURVEN

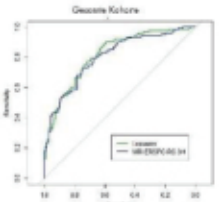

## EINGESPARTE BIOPSIEN VS. ÜBERSEHENE sPC

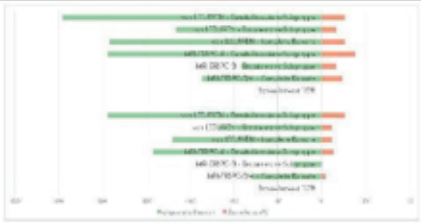

## KALIBRIERUNGSKURVEN

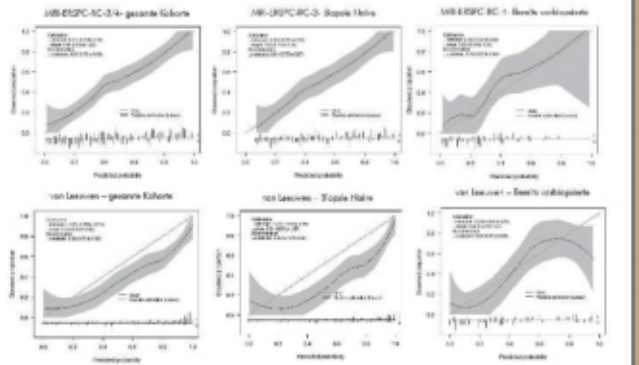

## DECISION CURVES

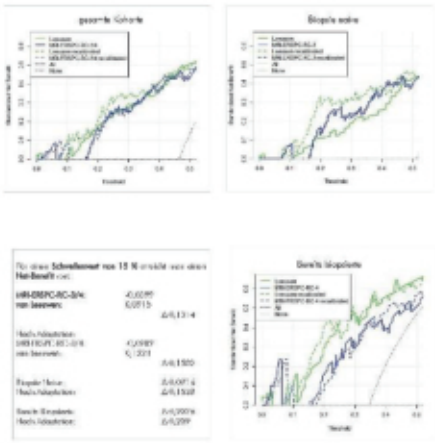

## SCHLUSSFOLGERUNG

Beide Risikomodelle liefern solide Ergebnisse. Trotz eingesparter Biopsien werden kaum signifikante Prostatakarzinome übersehen. Das van Leeuwen Modell lässt eine bessere Balance zwischen eingesparten Biopsien und übersehenen sPC bei niedrigen Schwellenwerten bis 15 % vermuten. Die bessere Gesamtkalibrierung kann jedoch das MRI-ERSPC-RC-3/4-Risikomodell vorweisen.

## REFERENZEN

- Prediction of High-grade Prostate Cancer Following Multiparametric Magnetic Resonance Imaging: Improving the Rotterdam European Randomized Study of Screening for Prostate Cancer Risk Calculators, Alberts AR et al., European Urology 75, 310 – 318, 2019
- A multiparametric magnetic resonance imaging-based risk model to determine the risk of significant prostate cancer prior to biopsy, van Leeuwen PJ, et al., BJU International 120, 774 – 781, 2017

## Externe Validation zweier aktueller MRT-basierter Risikokalkulatoren zur Diagnostik des Prostatakarzinoms

Anna-Lena Petersmann[1], Sascha Pahernik[2], Florian Distler[2]

[1]Paracelsus Medizinische Privatuniversität, Nürnberg; [2]Klinik für Urologie, Paracelsus Medizinische Privatuniversität, Nürnberg; Contact: anna.petersmann@stud.pmu.ac.at

### Objective

Die Diagnostik eines signifikanten Prostatakarzinoms (sPC) wird durch Überdiagnostik und unnötig durchgeführter Biopsien erschwert. Risikokalkulatoren (RC) wurden entwickelt, um diese Probleme zu dezimieren und eine individuelle Risiko-Prognose zugeben. Diese Nomogramme wurden unlängst um die Ergebnisse aus mpMRTs erweitert und benötigen deshalb weiterer externer Validierung. Zwei dieser Modelle wurden in dieser Arbeit miteinander verglichen. Das MRI-ERSPC-RC- 3/4-Modell (1) und das Risikomodell von van Leeuwen (2).

### Methods

Im Zeitraum von Dezember 2016 bis September 2019 wurden 265 Patienten mit einem klinisch suspekten Befund eines Prostatakarzinoms erfasst. Jeder dieser Patienten erhielt ein mpMRT, in welchem die Läsionen mittels PI-RADS v. 2.1 klassifiziert wurden, und darauffolgend eine MRT/TRUS-Fusionsbiopsie. Alle histologischen Präparate wurden von Uropathologen analysiert und nach dem ISUP-System eingestuft. Alle Karzinome mit einem ISUP Grad $\geq 2$ wurden als signifikante Prostatakarzinome (sPC) klassifiziert. Die statistische Auswertung erfolgte durch Vergleich der AUCs, Kalibrierungskurven und Decision-Curves.

### Results

Bei 123 (=46,4%) lag ein sPC vor. Die AUCs der ROC-Analyse ergab keinen signifikanten Unterschied; p=0,178. Die Kalibrierungskurve zeigte für das MRI-ERSPC-RC-3/4 Modell einen nahezu idealen Kurvenverlauf (intercept 0,07; slope 0,94) im Vergleich zum van Leeuwen Modell: (Intercept -1,03; slope 0,70). Die Decision Curves zeigten für einen Schwellenwert von 15% einen Net-Benefit von $\Delta$0,1314 für das van Leeuwen-Modell für die gesamte Kohorte im Vergleich zum MRI-ERSPC-RC-3/4 Modell. Wird ein Risiko-Schwellenwert von 15% gewählt, würden mit dem van Leeuwen Modell 24% aller Biopsien vermieden vs. 14% durch das MRI-ERSPC-3/4-RC-Modell. Man übersähe 6% bzw. 5% aller sPC.

### Conclusions

Beide Risikomodelle liefern solide Ergebnisse. Trotz eingesparter Biopsien werden kaum signifikante Prostatakarzinome übersehen. Das van Leeuwen Modell(2) lässt eine bessere Balance zwischen eingesparten Biopsien und übersehenen sPC bei niedrigen Schwellenwerten bis 15 % vermuten. Die bessere Gesamtkalibrierung kann jedoch das MRI-ERSPC-RC-3/4-Risikomodell(1) vorweisen.

### References

1. Prediction of High-grade Prostate Cancer Following Multiparametric Magnetic Resonance Imaging: Improving the Rotterdam European Randomized Study of Screening for Prostate Cancer Risk Calculators, Alberts AR et al., European Urology 75, 310 – 318, 2019
2. A multiparametric magnetic resonance imaging-based risk model to determine the risk of significant prostate cancer prior to biopsy, van Leeuwen PJ, et al., BJU International 120, 774 – 781, 2017

# Efficient CRISPR/Cas9n-mediated repair of a *COL17A1* mutation

Igor Petković[1], Johannes Bischof[3], Bernadette Liemberger[1], Oliver Patrick March[1], Julia Reichelt[1], Heide-Marie Binder[2], Dirk Strunk[2], Johann Wolfgang Bauer[1,3], Thomas Kocher[1], Ulrich Koller[1]

[1]EB House Austria, Research Program for Molecular Therapy of Genodermatoses, Department of Dermatology and Allergology, University Hospital of the Paracelsus Medical University Salzburg, 5020 Salzburg, Austria
[2]Cell Therapy Institute, SCI-TReCS, Paracelsus Medical University, 5020 Salzburg, Austria
[3]Department of Dermatology and Allergology, University Hospital of the Paracelsus Medical University Salzburg, 5020 Salzburg, Austria

## Introduction

Type XVII collagen is a component of hemidesmosomes that connects basal keratinocytes with the lamina lucida of the basal membrane zone (BMZ) between epidermis and dermis of the skin. Mutations in the *COL17A* lead to junctional epidermolysis bullosa (JEB), a skin disorder characterized by epidermal detachment from the basal membrane.[1] To minimize off-target events, a double nicking strategy by using the Cas9 nickase variant (D10A) has been shown as a good alternative without impairing on-target efficiency.[2] Homology directed repair (HDR) based CRISPR/Cas9 approach is a versatile tool for precise mutation correction.[3] In this study, we compared the HDR correction efficiency with both wild-type Cas9 and Cas9 nickase.

## Methods

sgRNAs and Cas9/Cas9n protein were delivered into the collagen type XVII (C17) deficient immortalized JEB keratinocytes as a ribonucleoprotein complex (RNP) via electroporation. As a repair template for HDR, symmetric or asymmetric single stranded oligonucleotides were used (ssODN). sgRNA1 was designed to specifically target the mutation (c.3898delTC) in *COL17A1* **(Fig. 1).**




**Figure 1.** Schematic of CRISPR/HDR targeting strategy. While wild-type Cas9 cuts both strands (A), the D10A mutated form of Cas9 (Cas9n) cuts only the target strand (B), therefore two sgRNAs are necessary to make a double-strand break (DSB).

## Results

NGS analysis revealed 59% and 23% correction efficiency via HDR approach in C17 deficient immortalized JEB keratinocytes treated with the Cas9/sgRNA1 and Cas9n/sgRNA1+2, both with symmetric ssODN, respectively **(Fig. 2).** Western blot and sqRT-PCR analysis revealed a high level of C17 restoration at the protein and RNA level. Flow cytometric analysis indicated a restoration efficiency of >58% in cells treated with Cas9/sgRNA1 and symmetric ssODN **(Fig. 3).** These results are supported by the immunofluorescence analysis of C17 deficient JEB keratinocytes. Immunofluorescence staining of skin equivalents revealed correct localization of C17 in BMZ **(Fig. 4).**

## Conclusion

As a precise and efficient approach, the homology directed repair has an enormous potential in the treatment of rare genetic diseases. We demonstrated that via HDR a high gene correction efficiency is achieved without a need for selection of corrected cells. The higher efficiency of precise editing was achieved in cells treated with the wild-type Cas9 compared to Cas9 nickase. However, the drawback of wild-type Cas9 is a greater propensity for off-target events.

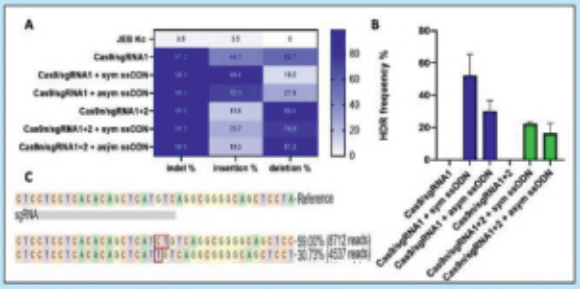


**Figure 2.** NGS Analysis of indel frequency (A) and HDR efficiency (B) in cells nucleofected with sgRNA, Cas9/Cas9n, and 2 different ssODNs. Schematic representation of correct TC insertion in the JEB keratinocytes nucleofected with Cas9/sgRNA1 combined with symmetric oligonucleotide.

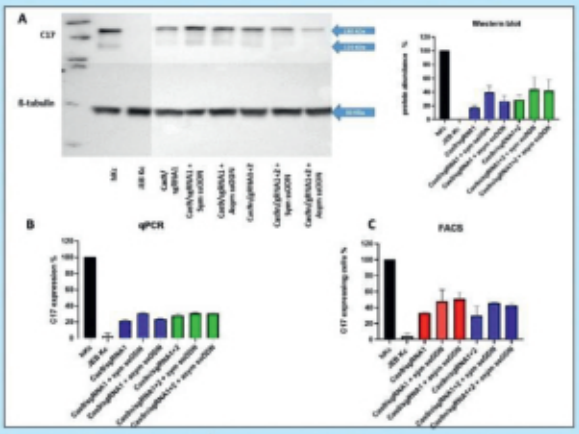


**Figure 3.** (A) Western blot analysis of cell lysate revealed type XVII collagen restoration with expression levels around 40% compared to the wild-type control. β-tubulin served as a loading control. (B) The relative gene expression level of restored *COL17A1* was confirmed via sqRT-PCR. (C) Flow cytometric analysis using a C17-specific antibody revealed a repair efficiency of >40% in the JEB keratinocytes treated with Cas9/sgRNA1 or Cas9n/sgRNA1+2 with symmetric or asymmetric ssODN.

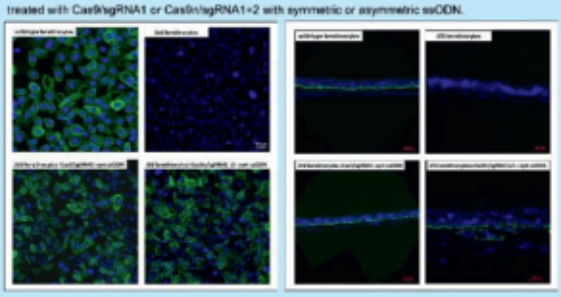

**Figure 4.** Immunofluorescence staining showing C17 (green) restoration in JEB keratinocytes treated with Cas9/sgRNA1 or Cas9n/sgRNA1+2 with symmetric ssODN. Wild-type keratinocytes and JEB keratinocytes served as a positive and negative control, respectively (left panel). Correct disposition of C17 within skin equivalents expanded from JEB keratinocytes treated with Cas9/sgRNA1 or Cas9n/sgRNA1+2 with symmetric ssODN was revealed via immunofluorescence staining (right panel). Nuclei stained with DAPI (blue).

## References

1 March OP, Reichelt J, Koller U. Gene editing for skin diseases: designer nucleases as tools for gene therapy of skin fragility disorders. Exp Physiol. 2017 Mar 7. doi: 10.1113/EP088044.
2 Ran FA, Hsu PD, Lin CY, Gootenberg JS, Konermann S, Trevino AE, Scott DA, Inoue A, Matoba S, Zhang Y, et al. Double nicking by RNA-guided CRISPR Cas9 for enhanced genome editing specificity. Cell. 2013;154(6):1380-9.
3 Kocher T, Bischof J, Haas SA, March OP, Liemberger B, Hainzl S, Ilmer J, Hoog A, Mayrg K, Binder H-M, Klausegger A, Strunk D, Bauer JW, Cathomen T, Koller U. A non-viral and selection-free COL7A1 HDR approach with improved safety profile for dystrophic epidermolysis bullosa. Molecular Therapy: Nucleic Acid (2021). doi: https://doi.org/10.1016/j.omtn.2021.05.015.

**The work was funded by DEBRA Austria, the Austrian Science Fund (FWF) P 32769-B, and Paracelsus Medical University (PMU-FFF) (A-20/02/041-KOU)**

LABORATORY FOR MOLECULAR THERAPY, EB HOUSE AUSTRIA
IGOR PETKOVIC, i.petkovic@salk.at

## Efficient CRISPR/Cas9n-mediated repair of a COL17A1 mutation

Igor Petkovic[1], Johannes Bischof[1], Bernadette Liemberger[1], Oliver Patrick March[1], Julia Reichelt[1], Heide-Marie Binder[2], Dirk Strunk[2], Johann Wolfgang Bauer[1,3], Thomas Kocher[1], Ulrich Koller[1]

[1]EB House Austria, Research Program for Molecular Therapy of Genodermatoses, Department of Dermatology and Allergology, University Hospital of the Paracelsus Medical University Salzburg, 5020 Salzburg, Austria; [2]Cell Therapy Institute, SCI-TReCS, Paracelsus Medical University, 5020 Salzburg, Austria; [3]Department of Dermatology and Allergology, University Hospital of the Paracelsus Medical University Salzburg, 5020 Salzburg, Austria; Contact: i.petkovic@salk.at

### Objective
Junctional epidermolysis bullosa (JEB) is an autosomal recessive skin disorder associated with mutations in the genes LAMA3, LAMB3, LAMC2, ITGA3, ITGA3, ITGB4 and COL17A1, which encode dermal-epidermal junction proteins within the skin. Type XVII collagen, encoded by COL17A1, is a transmembrane protein that connects basal keratinocytes with the lamina lucida of the basal membrane zone (BMZ) between the epidermis and dermis of the skin.

### Methods
In this study, we employed homology directed repair CRISPR/Cas9-based strategies to precisely correct a mutation within exon 52 of COL17A1 in JEB keratinocytes. We compared the efficacy of double-strand breaks or paired nicks induced by the wild-type Cas9 or Cas9n, followed by homology directed repair with symmetric or asymmetric single-stranded oligonucleotides that served as repair templates.

### Results
Wild-type Cas9 ribonucleoproteins delivered together with HDR oligonucleotides resulted in a high homologous recombination efficiency of 59%, while via double nicking an editing efficiency of 23% was achieved as revealed by next generation sequencing. Highly efficient type XVII collagen restoration was also confirmed at RNA, protein and cellular level. Furthermore, the correct localization of type XVII collagen was detectable within the basal membrane zone of generated skin equivalents.

### Conclusions
The proposed approach could serve as a good strategy for precise COL17A1 editing and a potential clinical application for JEB. We demonstrated that via HDR a high gene correction efficiency is achieved without a need for selection of corrected cells. The higher efficiency of precise editing was achieved in cells treated with the wild-type Cas9 compared to Cas9 nickase. However, the drawback of wild-type Cas9 is a greater propensity for off-target events.

### Acknowledgements
The work was funded by DEBRA Austria, the Austrian Science Fund (FWF) P 32769-B, and Paracelsus Medical University (PMU-FFF) (A-20/02/041-KOU)

# Retrospective analysis of excipients in drug therapy of premature infants and its potential impact on patient safety

M. Pintar-Hödl[1], I. Öfinger[1], L. Auer-Hackenberg[2], M. Wald[2], J. Pachmayr[2]

[1]Institute of Pharmacy, Paracelsus Medical University, Salzburg, Austria
[2]Department of Neonatology, University Hospital Salzburg, Austria

## Objective

Excipients in drug therapy of pediatric population may impact patient safety due to the immature metabolic system and the limited capability to clear compounds from the systemic circulation. Major concern arises with multi drug therapy when excipients may accumulate from different drugs or interact with active pharmaceutical ingredients.

In this study we assessed excipient exposure in drug therapy of neonates and analysed the impact on patient safety by conducting a literature based pharmacokinetic analysis. Our aim was to determine exposure to critical excipients in drug therapy of premature infants and recommend how to avoid potential adverse drug effects caused by excipient exposure.

## Study design

A retrospective data analysis was performed, on records of very low birth weight neonates (< 1500 grams) from the Neonatal Intensive Care Unit (NICU) at University hospital Salzburg. Hospitalized between January 1, 2018 and December 31, 2018. All medicinal products administered oral and intravenous were recorded. Drug products with critical excipients administered intravenous were selected and excipient exposure was analyzed in a subset of 51 patients. Daily excipient exposure was calculated based on data provided in the respective Summary of Product Characteristics. Excipient exposure levels were compared with thresholds given in guidelines published by the European Medicines Agency (EMA).

## Results

In 51 screened preterm infants, exposure values for benzoates range between 0.43 - 3.33 mg/day. Values of propylene glycol range between 0.05 - 183.7 mg/day. Values of ethanol range between 0.42 - 127.9 mg/day. Values of benzyl alcohol values range between 2.09 - 3.14 mg/day. Propylene glycol was administered to patients with Lorazepam, Dexamethasone and Phenobarbital at NICU. Propylene glycol levels exceeded the EMA recommended threshold of 1mg/kg/day in 10 patients out of 51 screened preterm neonates up to 13-fold higher than recommended. Ethanol administered with Alprostadil and Phenobarbital was exceeding EMA thresholds in 3 patients out of 51 with levels up to 21-fold higher than recommended. Benzyl alcohol present in Lorazepam was above the EMA threshold in 2 patients.

### „Overdose" of excipients in 10 patients out of 51 Vermont Oxford Network patients

**(Total number of Vermont Oxford Network patients in 2018 = 71)**

| Patient | Weight (Grams) | Excipient | Max. Patient Exposure (mg/kg/d) | Threshold/EMA (mg/kg/d) |
|---|---|---|---|---|
| 3 | 1388 | Propylen glycol | 132.4 | 1 |
| | | Benzyl alcohol | 3.1 | 0 |
| | | Ethanol | 6.6 | 6 |
| 4 | 938 | Propylen glycol | 41.0 | 1 |
| 5 | 783 | Propylen glycol | 45.3 | 1 |
| 7 | 752 | Propylen glycol | 23.7 | 1 |
| 8 | 1018 | Propylen glycol | 34.4 | 1 |
| 10 | 1108 | Ethanol | 8.3 | 6 |
| | 1763 | Propylen glycol | 34.5 | 1 |
| 12 | 1014 | Ethanol | 126.1 | 6 |
| 28 | 1213 | Propylen glycol | 68.8 | 1 |
| | | Benzyl alcohol | 1.0 | 0 |
| 29 | 897 | Propylen glycol | 43.0 | 1 |
| 42 | 633 | Propylen glycol | 55.3 | 1 |

**The 10 most frequent co-administered drugs:**




## Conclusion

Excipients were "overdosed" in 10 out of 51 Vermont Oxford Network patients at NICU Salzburg state hospital in 2018.

Despite existing guidelines for excipients and their compliance for the individual medicinal product, there is exposure to excipients in premature infants which is far above the recommended threshold levels, as established by the European Medicines Agency. This represents a risk for pediatric patients and indicates a clear need for rising the awareness on patient exposure to excipients and try to avoid "overdosing" to ensure patient safety.

### Active Substance Excipient Interactions

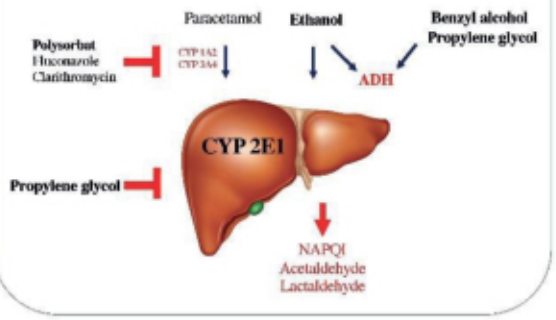

## Retrospective analysis of excipients in drug therapy of premature infants and its potential impact on patient safety

Dr. Monika Pintar-Hitzl[1], BSc. Isabel Ölinger[1], Dr. Lorenz Auer-Hackenberg[2], Assoc. Prof. Dr. Martin Wald[2], Univ.-Prof. Dr. Johanna Pachmayr[1]

[1]Institute of Pharmacy, Paracelsus Medical University, Salzburg, Austria; [2]Department of Neonatology, University Hospital Salzburg, Austria; Contact: monika.pintar@pmu.ac.at

### Objective
Excipients in drug therapy of pediatric population may impact patient safety due to the immature metabolic system and the limited capability to clear compounds from the systemic circulation. Major concern arises with multi drug therapy when excipients may accumulate from different drugs or interact with active pharmaceutical ingredients.
In this study we assessed excipient exposure in drug therapy of neonates and analysed the impact on patient safety by conducting a literature based pharmacokinetic analysis. Our aim was to determine exposure to critical excipients in drug therapy of premature infants and recommend how to avoid potential adverse drug effects caused by excipient exposure.

### Methods
A retrospective data analysis was performed, on records of very low birth weight neonates (< 1500 grams) from the Neonatal Intensive Care Unit (NICU) at Salzburg state hospital. Hospitalized between January 1, 2018 and December 31, 2018. All medicinal products administered oral and intravenous were recorded. Drug products with critical excipients administered intravenous were selected and excipient exposure was analyzed in a subset of 51 patients. Daily excipient exposure was calculated based on data provided in the respective Summary of Product Characteristics. Excipient exposure levels were compared with thresholds given in guidelines published by the European Medicines Agency (EMA).

### Results
In 51 screened preterm infants, exposure values for benzoates range between 0.43 - 3.33 mg/day. Values of propylene glycol range between 0.05 - 183.7 mg/day. Values of ethanol range between 0.42 - 127.9 mg/day. Values of benzyl alcohol values range between 2.09 - 3.14 mg/day. Propylene glycol was administered to patients with Lorazepam, Dexamethasone and Phenobarbital at NICU. Propylene glycol levels exceeded the EMA recommended threshold of 1mg/kg/day in 10 patients out of 51 screened preterm neonates up to 13-fold higher than recommended. Ethanol administered with Alprostadil and Phenobarbital was exceeding EMA thresholds in 3 patients out of 51 with levels up to 21-fold higher than recommended. Benzyl alcohol present in Lorazepam was above the EMA threshold in 2 patients.

### Conclusions
Excipients were "overdosed" in 10 out of 51 Vermont Oxford Network patients at NICU Salzburg state hospital in 2018.
Despite existing guidelines for excipients and their compliance for the individual medicinal product, there is exposure to excipients in premature infants which is far above the recommended threshold levels, as established by the European Medicines Agency. This represents a risk for pediatric patients and indicates a clear need for rising the awareness on patient exposure to excipients and try to avoid "overdosing" to ensure patient safety.

# ADHERENCE TO MINIMAL EXPERIMENTAL REQUIREMENTS FOR DEFINING EXTRACELLULAR VESICLES AND THEIR FUNCTIONS: A SYSTEMATIC REVIEW

Poupardin Rodolphe[1*], Wolf Martin, Strunk Dirk[1]

rodolphe.poupardin@pmu.ac.at

[1] Experimental and Clinical Cell Therapy Institute (EXCCT), Spinal Cord Injury and Tissue Regeneration Center, Paracelsus Medical University, Salzburg, Austria

## BACKGROUND:

- Extracellular vesicles (EVs) are nanometer-sized membrane-enclosed particles secreted via several mechanisms by virtually all cells. They are thought to be loaded with lipids, proteins, and various nucleic acid species of the source cell.
- Nano-sized lipoproteins or protein aggregates have overlapping characteristics with EVs concerning size or density, making proper selection of appropriate EV purification and characterization methods a key to draw concise conclusions (Fig 1).
- Minimal Information for Studies of Extracellular Vesicles (MISEV) [1, 2] guidelines suggest protocols and steps to follow for documenting specific EV-associated functional activities

**In this context, we conducted an unbiased review using a text mining approach to assess adherence to MISEV criteria**

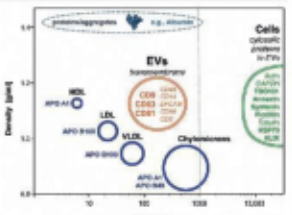


**Fig. 1: Size and density distribution of extracellular vesicles (EVs) and common contaminating particles and their molecular markers.** Diagram showing the overlap between different lipoprotein fractions (blue) extracellular vesicles (orange), protein aggregates (grey) and cells (green) in size (x axis, logarithmic) and density (y-axis). In addition, representative molecular markers found to be most used in our analysis and which were recommended in MISEV2018 as universal markers for identification of extracellular vesicles (orange, bold).

## METHODS:

- **Dataset acquisition:** Publications were selected in PubMed using the *RISMed* R package. We searched for manuscripts containing the keywords "extracellular vesicles" or "vesicles" together with "exosomes" in the title or abstract or papers with the major Mesh terms "extracellular vesicles" or "exosomes" (without looking at the child terms (non-explosive search)).
- **Keyword search** using regular expressions (regex), only in Material & Methods and Results part to detect methods used for isolation and characterization of EVs. To check for significant trends over time, linear regression analysis was conducted using R. Finally, we investigated whether the quality of identification and characterization of EVs in the manuscripts correlated with the number of citations.

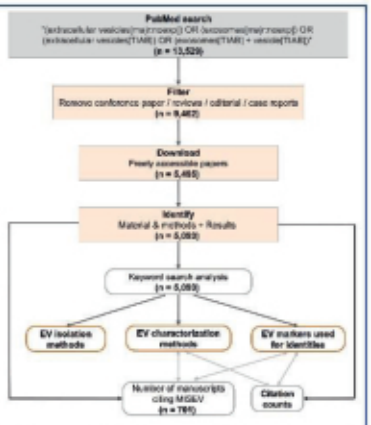


**Fig. 2: Dataset selection and approach used to investigate the compliance of the EV field to MISEV guidelines.** Research was conducted in PubMed (grey box) and then filtering steps were applied to keep unique records, remove conference / reviews / editorials / case reports. The keyword search was conducted in open access papers where material and methods and/or result sections were found. In parallel, we also extracted citation counts and the list of papers citing MISEV guidelines [1 2] for the 5,093 selected publications.

## RESULTS:

### The EV field is expanding at a fast pace

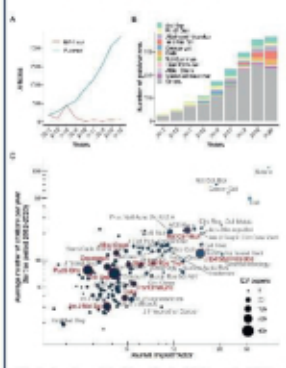

### Isolation methods used for EV preparation

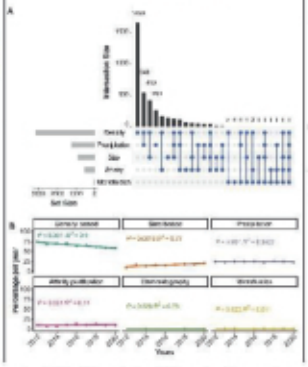

### Methods used for EV characterization

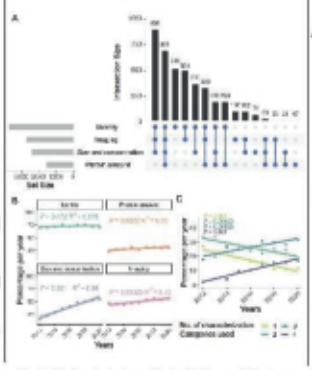

### Markers used to check EV purity

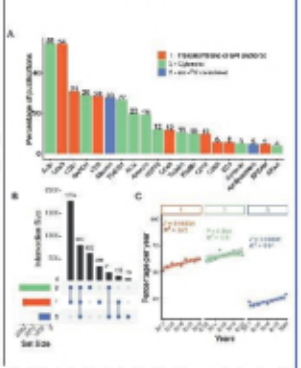

**Fig. 3: Overview of the EV publication field growth.** (A) Steep increase of EV manuscripts. The red line shows the number of EV manuscripts submitted to the EV-track database. (B) Bar plot showing the year of publication for the 5,093 selected EV papers. The 10 journals with the highest number of EV related publications (top 10) are shown in different colors as indicated. (C) Dot plot showing the relation between journal impact factor and average number of citations for 5,093 selected EV papers between 2012 and 2020. The dot size indicates the number of EV papers found per journal. The top 10 journals identified in Fig. 2B are highlighted in red.

**Fig. 4: EV isolation methods.** (A) The upset plot shows on the left the counts (set size) of the different methods ranked from the most used on the top (density-based isolation) to the least used on the bottom (microfluidics). Intersection size shows the number of publications found for each combination ranked in descending order. The dot chart corresponding to the upper histogram shows the most used combinations of isolation methods. (B) Percentage of papers using the different methods during each year.

**Fig. 5: EV characterization methods.** (A) The upset plots shows on the left the set size counts of the different methods ranked from the most used on the top (identity) to the least used on the bottom (protein amount). The upper histogram (in descending order) and the dot chart show the most used combinations for characterizing EVs. (B) Percentage of papers using the different methods for each year. (C) Percentage of EV manuscripts using a combination of characterization methods (identity, protein amount, size and concentration, imaging, omic-scale indicated by legend).

**Fig. 6: Analysis of proteins linked to EVs or contaminants.** (A) Most used marker proteins ordered according to the frequency of use displayed with a color code and using the category as defined by the MISEV2018 criteria (category 1: **Transmembrane or GPI-anchored** proteins associated to plasma membrane and/or endosomes; category 2: **Cytosolic** proteins recovered in EVs; category 3: Major components of non-EV co-isolated structures). (B) The upset plot shows on the left the set size counts of the different marker categories (left bars, color code as in A) ranked from the most used on the top to the least on the bottom. The upper histogram (in descending order) and the dot chart show the most used combinations of marker proteins for characterizing EVs. (C) Percentage of manuscripts per year using marker proteins from categories 1 - 3 to characterize their EV preparations over the years (2012 - 2020).

### Impact of the MISEV guidelines on the EV community

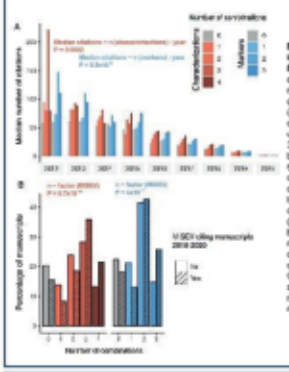

**Fig. 7: Impact of EV characterization and identification accuracy on citation frequency plus MISEV-based marker category reporting trends.** (A) Median number of citations per year for the different combinations of characterization methods (from 0 to 4 characterization categories combined in orange-red) and marker proteins used for EV preparation characterization (0 to 3 marker categories combined (light blue-blue). Linear regression analysis revealed a significant association between the number of characterization categories and median citation numbers ($P = 0.0052$) and between the number of marker categories and median citation numbers ($P = 6.6 \times 10^{-4}$), respectively. (B) Percentage of manuscripts citing (dashed bars) or not citing MISEV (non dashed bars) regarding the number of characterization categories used (red bars) or the different combinations of marker proteins (blue bars). Only manuscripts published between 2015 and 2020 were used for the analysis (724 manuscripts citing MISEV vs 3,678 manuscripts not citing MISEV).

## OUTLOOK AND CONCLUSIONS:

- The EV field is prospering at a fast pace leaping from 160 records in 2012 to 2,309 records/year until the end of 2020 (Fig3).
- In this context, we conducted an unbiased review of 5,096 accessible papers published in the EV research field in a broad range of journals between 2012 and 2020 (Fig 2).
- Publications from 810 journals were selected including 205 journals containing at least five EV-related manuscripts. Most manuscripts were found in 'Scientific Reports' (439), 'PLoS One' (284) and 'Journal of Extracellular Vesicles' (JEV; 247) (Fig 3)
- We found that most studies (1,659 / 5,093; 33.2%) used a single density-based isolation technique. The combination of density-based and precipitation methods was the second most frequently applied strategy (548 / 5,093; 10.8% of the manuscripts). (Fig 4)
- In our systematic analysis, we found that the awareness of investigators to better characterize their EV preparations using a combination of several methods was significantly rising. (Fig 5)
- The majority of studies still applied only one method for EV purification with few significant changes over the past years. (Fig 5)
- The three most frequently used markers for category one (**Transmembrane or GPI-anchored proteins**) were tetraspanins CD63, CD81, CD9. Actin, GAPDH and TSG101 were used most frequently for category two (**Cytosolic proteins**) and albumin as well as apolipoproteins for category three (**non-EV co-isolated**). Marker combinations revealed that 34.9% of studies used a combination of category one and two, and 15.9% used the combination of three categories. Finally, a significant increase of testing category one and category three marker determination in EV preparations was evident over time (Fig 6)
- Studies citing the MISEV position statements used significantly more methods for EV characterization and multiple markers to determine EV identity and purity indicating the impact of the guidelines in the EV community. (Fig 7)
- A precise characterization of EV preparations with multiple methods and marker categories also resulted in a significantly higher number of citations. (Fig 7)

## REFERENCES

1) J. Lötvall, et al; JEV. 2014; https://doi.org/10.3402/jev.v3.26913.
2) C. Théryet al; JEV. 2018; https://doi.org/10.1080/20013078.2018.1535750.

bioRxiv THE PREPRINT SERVER FOR BIOLOGY

Adherence to minimal experimental requirements for defining extracellular vesicles and their functions: a systematic review
Poupardin R, Wolf M., Strunk D.
doi: https://doi.org/10.1101/2021.04.23.441166

## Adherence to minimal experimental requirements for defining extracellular vesicles and their functions: a systematic review.

Rodolphe Poupardin[1], Martin Wolf[1], Dirk Strunk[1]

[1]Cell Therapy Institute, Spinal Cord Injury and Tissue Regeneration Center Salzburg (SCI-TReCS), Paracelsus Medical University (PMU), Salzburg, Austria; Contact: rodolphe.poupardin@pmu.ac.at

### Objective
Extracellular vesicles (EVs) are nanometer-sized membrane-enclosed particles secreted via several mechanisms by virtually all cells. Rigorous measures are required to cope with the advance of EV research, from 183 to 2,309 studies/year, between 2012-2020. The 'MISEV' guidelines requested standardizing methods, thereby assuring and improving EV research quality. We investigated how EV research improved over time.

### Methods
We conducted an unbiased review using a text mining approach to assess adherence to MISEV criteria over the period 2012-2020 and analyzed the methodology used for EV isolation and characterization. We also investigated whether the quality of identification and characterization of EVs in the manuscripts correlated with the number of citations.

### Results
We found a significant improvement over the years particularly regarding EV characterization where recent papers used a higher number of methods and EV markers to check for quantity and purity. Interestingly, we also found that EV papers using more methods and EV markers were cited more frequently. Papers citing MISEV criteria were more prone to use a higher number of characterization methods.

### Conclusions
This was the first unbiased study to monitor the global quality of research. Studies citing the MISEV position statements used significantly more methods for EV characterization and multiple markers to determine EV identity and purity indicating the impact of the guidelines in the EV community. We therefore established a concise checklist summarizing MISEV criteria to support EV researchers towards reaching the highest standards in the field.

# Galanin is a modulator of phagocytosis in the human monocytic cell line THP-1

Andrea Ramspacher[1], Andreas Koller[1,2], Susanne M. Brunner[1,2], Barbara Kofler[1]

[1]RESEARCH PROGRAM FOR RECEPTOR BIOCHEMISTRY AND TUMOR METABOLISM, DEPARTMENT OF PEDIATRICS, PARACELSUS MEDICAL UNIVERSITY, SALZBURG, AUSTRIA;
[2]RESEARCH PROGRAM FOR EXPERIMENTAL OPHTHALMOLOGY, DEPARTMENT OF OPHTHALMOLOGY AND OPTOMETRY, PARACELSUS MEDICAL UNIVERSITY SALZBURG, AUSTRIA.

## INTRODUCTION

The immune-endocrine cross talk comprises mainly signal molecules, which originate in the central nervous system but exert their functions in inflammatory processes, orchestrating and shaping responses of the innate and humoral immunity. Many regulatory peptides, secreted by neuronal cells, were already shown to modulate immune cell functions[1]. The regulatory neuropeptide galanin is broadly distributed in the central and peripheral nervous system but also in non-neuronal tissues. It exerts its diverse physiological functions via three G-protein-coupled receptors ($GAL_{1-3}$-R)[2]. Another neuropeptide, that can activate galanin receptors is spexin. It binds with high affinity to $GAL_2$-R and $GAL_3$-R, but not $GAL_1$-R[3]. In previous studies, we demonstrated that galanin modulates and shapes the basic process of cytokine and chemokine expression in human monocytes and macrophages[4,5]. Another function of these myeloid cells is their phagocytic activity, which is an important defense mechanism against invading pathogens. We hypothesized that galanin is also capable of shaping the phagocytic activity of monocytes and macrophages.

## METHODS

First, mRNA expression of the galanin system components was examined in monocytic THP-1 and phorbol 12-myristate 13-acetate (PMA)-differentiated macrophage-like THP-1 cells. Prior to the phagocytosis experiment, THP-1 monocytes and macrophages were treated with either galanin, scrambled galanin or spexin (10 - 1000 nM) for 24 hours. Phagocytic activity of monocytic THP-1 and PMA-differentiated THP-1 cells was determined by incubating cells with opsonized *E. coli* BioParticles and with untreated *E. coli* BioParticles (100 particles/cell),respectively for 20 minutes at 37° C and after fixation, analyzed by flow cytometry.

## RESULTS

- In both THP-1 cell types, monocytes and macrophages, we detected galanin, $GAL_1$-R and $GAL_2$-R mRNA expression, which was the highest among the three receptors. $GAL_3$-R was only detectable in monocytic THP-1 cells (Figure 1).
- Exposure to exogenous galanin before incubation with *E. coli* particles caused a significant, dose-dependent attenuation of phagocytic activity in THP-1 monocytes. With 100 nM galanin, a decrease of phagocytosis of 15 - 20% was observed. Treatment with scrambled galanin did not induce an effect on phagocytic activity. Spexin-treated THP-1 monocytes also exhibited a dose-dependent decrease in phagocytic activity. However, the attenuating effect of spexin was not as distinct as seen with galanin (Figure 2).
- Galanin-treated THP-1 macrophages showed a significant decrease of phagocytic activity after treatment with 10 nM and 100 nM galanin. Treatment with scrambled galanin did not lead to any changes in the phagocytic capacity of THP-1-derived macrophages. Only high concentrations of spexin (300 and 1000 nM) marginally attenuated the phagocytic activity (Figure 3).

## CONCLUSION

These findings indicate that galanin is capable of modulating phagocytosis in THP-1 monocytes and macrophages. Treatment with spexin had a weaker effect than galanin treatment, which may indicate that the modulation of phagocytosis by galanin is directed at least in part via $GAL_2$-R, which is less expressed in THP-1 macrophages compared to THP-1 monocytes.

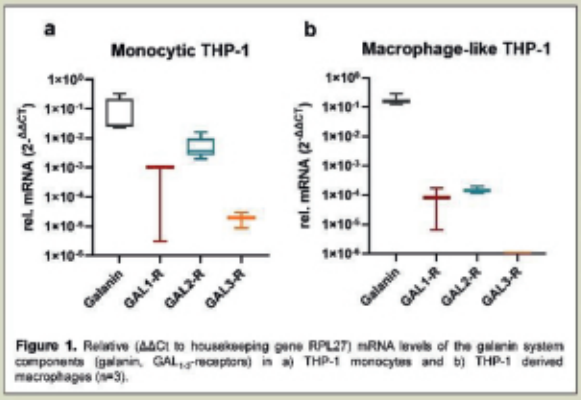


**Figure 1.** Relative (ΔΔCt to housekeeping gene RPL27) mRNA levels of the galanin system components (galanin, $GAL_{1-3}$-receptors) in a) THP-1 monocytes and b) THP-1 derived macrophages (n=3).

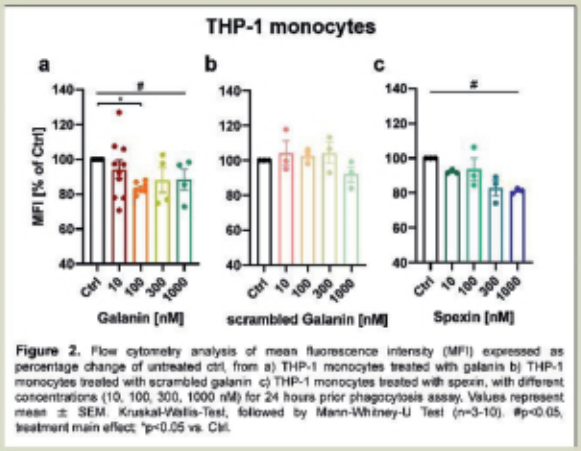


**Figure 2.** Flow cytometry analysis of mean fluorescence intensity (MFI) expressed as percentage change of untreated ctrl, from a) THP-1 monocytes treated with galanin b) THP-1 monocytes treated with scrambled galanin c) THP-1 monocytes treated with spexin, with different concentrations (10, 100, 300, 1000 nM) for 24 hours prior phagocytosis assay. Values represent mean ± SEM. Kruskal-Wallis-Test, followed by Mann-Whitney-U Test (n=3-10). #p<0.05, treatment main effect; *p<0.05 vs. Ctrl.

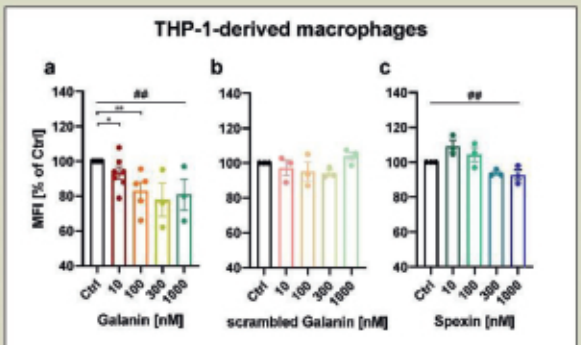


**Figure 3.** Flow cytometry analysis of mean fluorescence intensity (MFI) expressed as percentage change of untreated ctrl, from a) THP-1-derived macrophages treated with galanin b) THP-1-derived macrophages treated with scrambled galanin c) THP-1-derived macrophages treated with spexin, with different concentrations (10, 100, 300, 1000 nM) for 24 hours prior phagocytosis assay. Values represent mean ± SEM. Kruskal-Wallis-Test, followed by Mann-Whitney-U Test (n=3-10). ##p<0.01 treatment main effect; *p<0.05, **p<0.01 vs. Ctrl.

**References**
[1]Butts et al., 2008; Cell Immunol 252(1-2):7-15. [2]Lang et al. 2015; Pharmacol Rev 67(1):118-175 [3]Kim et al., 2014; Endocrinology 155(5):1864-73. [4]Ramspacher et al., 2019; Ann N Y Acad Sci 1-11. [5]Koller et al., 2019; Sci Rep 9:7237

Contact: a.ramspacher@salk.at

This study is supported by the Austrian Research Fund (FWF: P 32403) and the Paracelsus Medical University Salzburg (PMU-FFF: R-17/01/088-KOL)

## Galanin is a modulator of phagocytosis in the human monocytic cell line THP-1

Andrea Ramspacher[1], Andreas Koller[1,2], Susanne M. Brunner[1,2], Barbara Kofler[1]

[1]Research Program for Receptor Biochemistry and Tumor Metabolism, Department of Pediatrics, Paracelsus Medical University, Salzburg, Austria; [2]Research Program for Experimental Ophthalmology, Department of Ophthalmology and Optometry, Paracelsus Medical University, Salzburg, Austria; Contact: a.ramspacher@salk.at

### Objective

The immune-endocrine cross talk comprises mainly signal molecules, which originate in the central nervous system but exert their functions in inflammatory processes, orchestrating and shaping responses of the innate and humoral immunity. Many regulatory peptides, secreted by neuronal cells, were already shown to modulate immune cell functions. The regulatory neuropeptide galanin is broadly distributed in the nervous system but also in non-neuronal tissues. It exerts its diverse physiological functions via three G-protein-coupled receptors ($GAL_{1-3}$-R). Another neuropeptide, spexin, also binds with high affinity to $GAL_2$-R and $GAL_3$-R, but not $GAL_1$-R. In previous studies, we demonstrated that galanin modulates the basic process of cytokine/chemokine expression in human monocytes and macrophages. Another function of these myeloid cells is their ability to phagocytose foreign pathogens. We hypothesized that galanin is also capable of shaping the phagocytic activity of monocytes and macrophages.

### Methods

First, mRNA expression of the galanin system components was examined in monocytic THP-1 and phorbol 12-myristate 13-acetate (PMA)-differentiated macrophage-like THP-1 cells. Prior to the phagocytosis experiment, THP-1 monocytes and macrophages were treated with either galanin (GAL), scrambled galanin (sGAL) or spexin (SPX)(10 - 1000 nM) for 24 hours. Phagocytic activity of monocytic THP-1 cells and PMA-differentiated THP-1 cells was determined by incubating cells with opsonized/untreated *E. coli* BioParticles (100 particles/cell) for 20 minutes at 37°C and subsequently analyzed by flow cytometry.

### Results

• In both THP-1 monocytes and macrophages, we detected GAL, $GAL_1$-R and $GAL_2$-R mRNA expression, which was the highest among the three receptors. $GAL_3$-R was only detectable in monocytic THP-1 cells.

• Treatment with exogenous GAL before incubation with *E. coli* particles caused a significant, dose-dependent attenuation of phagocytic activity in THP-1 monocytes. With 100 nM GAL, a decrease of phagocytic activity of 15 - 20% was detected. Treatment with sGAL did not induce an effect on phagocytic activity. SPX-treated THP-1 monocytes also exhibited a dose-dependent decrease in phagocytic activity. However, the attenuating effect of SPX was not as distinct as seen with GAL.

• GAL-treated THP-1 macrophages also showed a dose-dependent decrease of phagocytic activity. Treatment with sGAL did not lead to any changes in the phagocytosis capacity of these cells. Only high concentrations of SPX (300 and 1000 nM) marginally attenuated the phagocytic activity.

### Conclusions

These findings indicate that GAL is capable of modulating phagocytosis in THP-1 monocytes and macrophages. Treatment with SPX had a weaker effect than treatment with GAL, which may indicate that the modulation of phagocytosis by GAL is directed at least in part via $GAL_2$-R, which is less expressed in THP-1 macrophages compared to monocytes.

### Acknowledgements

This study is supported by the Austrian Research Fund (FWF: P 32403) and the Paracelsus Medical University Salzburg (PMU-FFF: R-17/01/086-KOL).

# Role of Kir2.1 channels in an oxidative stress-related model of aging neuroglia

Alessia Remigante[1,2], Rossana Morabito[2], Angela Marino[2], Antonio Sarikas[3], Michael Pusch[1] and Silvia Dossena[3]

[1]Biophysics Institute, National Research Council, Genoa, Italy
[2]Department of Chemical, Biological, Pharmaceutical and Environmental Sciences, University of Messina, Italy
[3]Institute of Pharmacology and Toxicology, Paracelsus Medical University, Salzburg, Austria

## Objective

- Epilepsy is a chronic disease of the brain and its prevalence increases with age. Strikingly, about 50% of all epilepsy cases diagnosed in elderly patients (> 65 years) are idiopathic (1).
- Metabolic changes, including the production of reactive oxygen species, may contribute to epilepsy development (2).
- The neuronal glia plays a crucial role in epilepsy by controlling neuronal hyperexcitability.
- One of the key roles of glial cells is the spatial buffering of extracellular $K^+$ ions that are released by excited neurons and transported through glial inwardly rectifying potassium (Kir) channels from extracellular regions of high $K^+$ to those of low $K^+$ to inhibit epileptogenesis (**Figure 1**) (3). However, whether Kir channels can be the target of oxidative stress during aging is not known.
- Among experimental oxidative stress-related aging models, exposure to D-galactose (D-gal) is considered the most similar to natural aging (4).
- In the present study, we investigated the effect of D-gal-induced aging on Kir channel function in glioblastoma U87-MG cells.

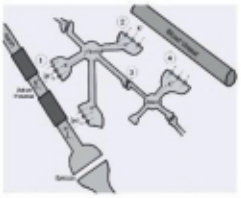

**Figure 1. Model of $K^+$ spatial buffering.** Potassium released during action potential propagation is taken up by astrocytes processes at nodes of Ranvier and synapses via strongly rectifying Kir channels, i.e. homomeric Kir2.1 channels, heteromeric Kir4.1/2.1 and Kir4.1/Kir5.1 channels. Potassium is extruded from glia at sites of low $K^+$ activity via weakly rectifying Kir4.1 homomeric channels. Taken from (3).

## Methods

- RT-qPCR was utilized to identify the isoform(s) of Kir channels expressed in glioblastoma U87-MG cells.
- In addition, cell viability and oxidative stress following exposure of cells for 24 hours to 30 or 100 mM D-gal have been assessed by the MTT colorimetric assay and estimation of thiobarbituric acid reactive substances (TBARS) levels – a marker of lipid peroxidation – as well as membrane total sulfhydryl (SH) groups, respectively.
- The membrane $K^+$ conductance was measured by the patch-clamp technique in whole-cell configuration. As Kir channels are sensitive to $Ba^{2+}$, all currents have been subtracted of the $Ba^{2+}$-insensitive component.
- To obtain equal osmolarity, equimolar amounts of mannitol were used as the control for D-gal.
- The oxidizing agent TBH70X (1 mM) was used as an alternative to D-gal for inducing oxidative stress.

## Results

- Screening of all 15 known isoforms of Kir channels by RT-qPCR revealed that the predominant transcript expressed in U87-MG cells corresponds to the Kir2.1 channel (**Figure 2**).
- Among other Kir channels known to be expressed in neuronal glia, Kir4.1 was 26-fold less expressed and other Kir2 members as well as Kir5.1 were virtually absent.

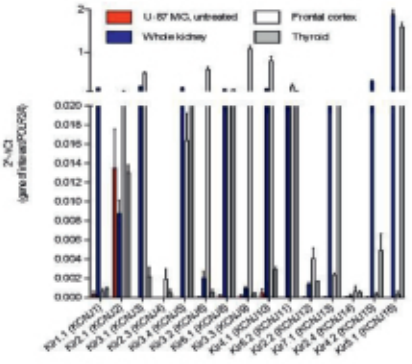


**Figure 2. Kir transcript expression in U87-MG cells.** One ug total RNA from three independent subcultures was reverse transcribed and probed for expression of the transcripts of all 15 known Kir isoforms by qPCR on the RotorGene (QIAGENE) platform. Human whole kidney, frontal cortex and thyroid served as positive controls.

- D-gal (30 and 100 mM) or TBH70X had no obvious cytotoxicity, but 100 mM D-gal or TBH70X activated oxidative stress pathways, namely significantly enhanced TBARS levels and reduced the abundance of membrane SH groups (**Figure 3 A-B-C**).

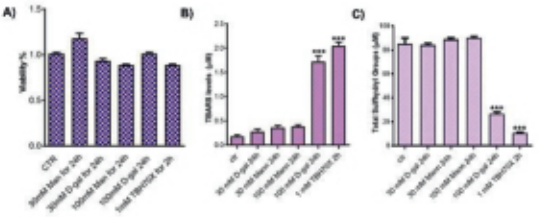


**Figure 3.** *In vitro* effects of increasing concentrations of D-gal (30 and 100 mM) for 24 hours, and 1 mM TBH70X for 2 hours on **A)** cell viability (MTT assay), **B)** thiobarbituric acid reactive substance (TBARS) and **C)** total sulfhydryl groups. *** p<0.001 versus control, 30mM D-gal, 30-100 mM Mannitol, and 1 mM TBH70X as determined by one way ANOVA followed by Bonferroni's post hoc test (n=3).

- Interestingly, 100 mM D-Gal exposure was associated with a pronounced decrease of $Ba^{2+}$-sensitive inwardly rectifying $K^+$ currents, most likely mediated by Kir2.1 (**Figure 4 B**) ($p<0.05$, n=5).
- Importantly, 30 mM D-gal and 30-100 mM mannitol failed to elicit oxidative stress and, accordingly, had no significant effect on the $Ba^{2+}$-sensitive $K^+$ current (n=5) (**Figure 4 A**) .

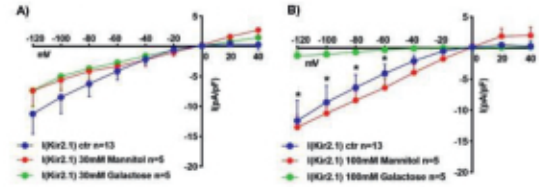


**Figure 4. D-gal inhibits Kir2.1 channel function.** The voltage protocol consisted of voltage steps from -120 to 40 mV in 20 mV increments from a holding potential of -60 mV. The duration of the voltage steps was 400 ms. **A)** Treatment with 30 mM D-gal for 24 hours did not suppress the Kir2.1current **B)** Treatment with 100 mM D-gal for 24 hours suppressed the Kir2.1current. Kir2.1 currents were isolated from the total currents by subtracting currents measured in the same cell after application of 2 mM $BaCl_2$, an efficient blocker of Kir2.1. *p<0.05, unpaired Student's t-test. (n) refers to the number of cells.

- Exposure of cells for 5 minutes or pre-incubation for 2 hours with 1 mM TBH70X significantly reduced the $Ba^{2+}$-sensitive $K^+$ currents compared to control, thus supporting the concept that the activity of Kir2.1 is highly sensitive to oxidative stress (**Figure 5 A-B**).

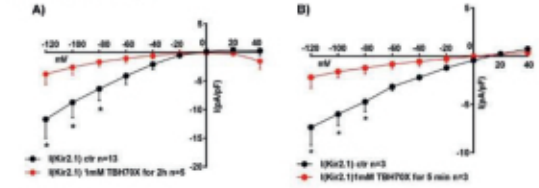


**Figure 5. Oxidation due to TBH70X application inhibits Kir2.1 channels.** Whole cell current was studied in U87-MG cells endogenously expressing Kir2.1. The voltage protocol consisted of voltage steps from -120 to 40 mV in 20 mV increments from a holding potential of -60 mV. The duration of the voltage steps was 400 ms. Exposure to 1 mM TBH70X for 5 minutes or 2 hours inhibited the Kir2.1 current (**A-B**). *p<0.05, unpaired Student's t-test. (n) refers to the number of cells.

## Conclusions

- These findings reveal a novel Kir2.1 channel modulation that is likely to occur in oxidative stress.
- We suggest that inhibition of Kir2.1 in neuronal glia may alter the extracellular $K^+$ buffering and contribute to oxidative stress-related neuronal hyperexcitability and epileptogenesis during aging.

## References

1. Beghi E., Giussani G. Aging and the Epidemiology of Epilepsy. Neuroepidemiology. 2018;51(3-4):216-223.
2. Ponsiia MD, Kaiazok K, Menezes R. Oxidative stress in neurodegenerative diseases and ageing. Child Mod Coll Longev. 2012;2012:796380. Hibino H, Inanobe A, Furutani K, Murakami S, Findlay I, Kurachi Y. Inwardly rectifying potassium channels: their structure, function, and physiological roles. Physiol Rev. 2010 Jan;90(1):291-366.
3. Butt AM, Kalsi A. Inwardly rectifying potassium channels (Kir) in central nervous system glia: a special role for Kir4.1 in glial functions. J Cell Mol Med. 2006 Jan-Mar;10(1):33-44.
4. Azman KF, Zakaria R. D-Galactose-induced accelerated aging model: an overview. Biogerontology. 2019 Dec;20(6):763-782.

## Role of Kir2.1 channels in an oxidative stress-related model of aging neuroglia

Alessia Remigante[1,2], Rossana Morabito[1], Angela Marino[1], Antonio Sarikas[3], Michael Pusch[2], Silvia Dossena[3]; Contact: aremigante@unime.it

[1]Dept. of Chemical, Biological, Pharmaceutical and Environmental Sciences, University of Messina, Italy; [2]Biophysics Institute, National Research Council, Genoa, Italy; [3]Institute of Pharmacology and Toxicology, Paracelsus Medical University, Salzburg, Austria

### Objective

Epilepsy is a chronic disease of the brain and its prevalence increases with age. Strikingly, about 50% of all epilepsy cases diagnosed in elderly patients are idiopathic[1]. Metabolic changes, including the production of ROS species, may contribute to epilepsy development. The neuronal glia plays a crucial role in epilepsy by controlling neuronal hyperexcitability. One of the key roles of glial cells is the spatial buffering of extracellular $K^+$ ions that are released by excited neurons and transported through glial inwardly rectifying potassium (Kir) channels from extracellular regions of high $K^+$ to those of low $K^+$ to inhibit epileptogenesis. However, whether Kir channels can be the target of oxidative stress (OS) during aging is not known. Among experimental OS-related aging models, exposure to D-galactose (D-gal) is considered the most similar to natural aging. In the present study, we investigated the effect of D-gal-induced aging on Kir channel function in glioblastoma U87-MG cells.

### Methods

RT-qPCR was utilized to identify the isoform(s) of Kir channels expressed in U87-MG cells. In addition, cell viability and OS following exposure of cells for 24h to 30/100mM D-gal have been assessed by the MTT colorimetric assay and estimation of thiobarbituric acid reactive substances, as well as membrane total sulfhydryl (-SH) groups, respectively. The membrane $K^+$ conductance was measured by the patch-clamp technique. As Kir channels are sensitive to $Ba^{2+}$, all currents have been subtracted of the $Ba^{2+}$ insensitive component. To obtain equal osmolarity, equimolar amounts of Mannitol were used as the control for D-gal. The oxidizing agent TBH70X was used as an alternative to D-gal for inducing OS.

### Results

Screening of all 15 known isoforms of Kir channels by RT-qPCR revealed that the predominant transcript expressed in U87-MG cells corresponds to the Kir2.1 channel. Among other Kir channels known to be expressed in neuronal glia, Kir4.1 was 26-fold less expressed and other Kir2 members as well as Kir5.1 were virtually absent. D-gal (30-100mM) or TBH70X had no obvious cytotoxicity, but 100mM D-gal or TBH70X activated OS pathways, namely significantly enhanced TBARS levels and reduced the abundance of membrane SH groups. Interestingly, 100mM D-Gal exposure was associated with a pronounced decrease of $Ba^{2+}$-sensitive inwardly rectifying $K^+$ currents, most likely mediated by Kir2.1. Importantly, 30mM D-gal and 30-100mM Mannitol failed to elicit OS and, accordingly, had no significant effect on the $Ba^{2+}$-sensitive $K^+$ current. Exposure of cells for 5 min or pre-incubation for 2h with 1mM TBH70X significantly reduced the $Ba^{2+}$-sensitive $K^+$ currents compared to control, thus supporting the concept that the Kir2.1 activity is highly sensitive to OS.

### Conclusions

These findings reveal a novel Kir2.1 channel modulation that is likely to occur in OS. We suggest that inhibition of Kir2.1 in neuronal glia may alter the extracellular $K^+$ buffering and contribute to OS-related neuronal hyperexcitabilty and epileptogenesis during aging.

### References

1. Beghi E, Giussani G. Aging and the Epidemiology of Epilepsy. Neuroepidemiology. 2018;51(3-4):216-223.

# Health-related quality of life in patients with traumatic spinal cord injury – A longitudinal study

Nora Renz[1,2], Georg Zimmermann[3,4,8], Stephanie Aschauer-Wallner[2], Herbert Resch[2] on behalf of the ASCIS study group, Kerstin Schwenker[1,2,7], Eugen Trinka[1,2,6,7] and Yvonne Höller[5]

[1]Department of Neurology, Christian Doppler University Hospital, Centre for Cognitive Neuroscience, Paracelsus Medical University, Salzburg, Austria. [2]Spinal Cord Injury and Tissue Regeneration Center, Paracelsus Medical University, Salzburg, Austria. [3]Team Biostatistics and Big Medical Data, IDA Lab Salzburg, Paracelsus Medical University, Salzburg, Austria. [4]Department of Mathematics, Paris Lodron University, Salzburg, Austria. [5]Department of Psychology, University of Akureyri, Akureyri, Iceland. [6]Neuroscience Institute, Christian Doppler University Hospital, Centre for Cognitive Neuroscience, Paracelsus Medical University, Salzburg, Austria. [7]Karl Landsteiner Institute for Neurorehabilitation and Space Neurology, Salzburg, Austria. [8]Department of Research and Innovation, Paracelsus Medical University, Salzburg, Austria. Contact: nora.renz@pmu.ac.at

## BACKGROUND:

- Traumatic Spinal Cord Injury (tSCI) is a condition with extensive impact on an individual's life and in particular on the health-related quality of life (HRQoL).[1]
- HRQoL is described as self-reported, subjectively experienced health in addition to objectively measured health parameters[2] and it includes the functioning of a person in their life with emphasis on "perceived wellbeing in physical, mental and social domains of health"[3].
- Longitudinal data for SCI patients is rarely available and very inhomogeneous.

## STUDY AIM:

- The aim of this study was to assess the HRQoL of patients suffering from tSCI and to identify the relative contributions of different factors such as age, gender, level of injury, neurological category, pain and functional status at the 1-year and the 2-3-year follow-up investigation.

## METHODS:

- **Procedure and Participants**
  - A total of 78 patients were extracted from the Austrian spinal cord injury study (ASCIS)[4] database for this analysis.
  - Longitudinal design: 1-year follow-up and 2-3-year follow-up investigation (different groups with overlapping participants; independent analysis and comparison in a narrative way)
  - Statistical analyses : nonparametric ANOVA-type tests which measure the "relative effect" (a measure of tendency towards larger values)

Table 1: (Socio-demographic and injury-related) Characteristics of study participants

| Parameters | Group 1 (N = 59): 1-year investigation | Group 2 (N = 46): 2-3-year investigation |
|---|---|---|
| **Gender, n (%)** | | |
| Male | 44 (77.2%) | 34 (73.9%) |
| Female | 13 (22.8%) | 12 (26.1%) |
| Total | 57 (100%) | 46 (100%) |
| **Age, ⌀ ± SD (years)** | | |
| Male | 48.6 ± 16.6 | 50.8 ± 17.1 |
| Female | 53.6 ± 20.7 | 49.3 ± 24.2 |
| Total | 52.0 ± 18.7 | 50.3 ± 19.3 |
| **Neurological category, n (%)** | | |
| Ventilator dependent | 0 | 0 |
| C1-C8; AIS A, B, C | 7 (12.3%) | 6 (13.0%) |
| T1-S5; AIS A, B, C | 9 (15.8%) | 10 (21.7%) |
| AIS D | 30 (52.6%) | 21 (45.7%) |
| AIS E | 5 (8.8%) | 4 (8.7%) |
| N/A | 6 (10.5%) | 5 (10.9%) |

- **Measurements**
  - **SF-36 v1 und v2:** HRQoL
  - **VAS Score:** the amount of current pain
  - **SCIM Score:** the ability to perform basic activities of daily living independently
  - **ASIA Score, injury height, type of lesion:** neurological status
  - **demographic variables:** gender, age

## RESULTS:

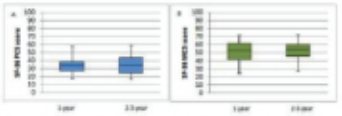

Figure 1: SF-36 MCS score (A) and PCS score (B) 1 year and 2-3 years investigation in comparison. PCS = physical health component summary, MCS = mental health component summary.

### 1-year follow-up: HRQoL

MCS = mental HRQoL PCS = physical HRQoL

Table 2: Results of the 1-year investigation

| Variable | Category | Mental health component summary (MCS) | | | | | Physical health component summary (PCS) | | | | |
|---|---|---|---|---|---|---|---|---|---|---|---|
| | | Per (CI 95%) | statistic | df1 | df2 | p | Per (CI 95%) | statistic | df1 | df2 | p |
| Age | >=50 (n=34) | 48.1 (43.7-52) | 3.65 | 1.62 | 96.49 | .033* | 42.5 (37.7-47) | 1.45 | 1.93 | 92.83 | .237 |
| | 40-49 (n=18) | 43.1 (37.7-48) | | | | | 44.1 (38.7-49) | | | | |
| | <40 (n=24) | 44.1 (39.2-49) | | | | | 49.1 (44.3-53) | | | | |
| Vent. cases | no (n=52) | 46.5 (42.9-50) | 6.01 | 1 | 69.93 | .016* | 45.1 (41.5-48) | 3.64 | 1 | 84.43 | .059* |
| | yes (n=12) | 40.4 (32.4-48) | | | | | 38.1 (32.1-44) | | | | |
| SCIM i.v. management | >=16 (n=43) | 46.1 (42.5-50) | .4 | 1 | 69.43 | .752 | 44.7 (41.1-48) | 0.68 | 1 | 91.56 | .0.413 |
| | <16 (n=14) | 43.1 (37.1-49) | | | | | 43.1 (37.1-49) | | | | |
| SCIM mobility I | >=40 (n=43) | 46.1 (42.5-50) | .01 | 1 | 94.36 | .913 | 44.1 (40.5-47) | 0.43 | 1 | 97.20 | .0.513 |
| | <40 (n=28) | 46.1 (42.1-50) | | | | | 44.1 (39.7-48) | | | | |
| SCIM mobility II | >=40 (n=43) | 47.1 (43.2-50) | 3.66 | 1 | 69.83 | .119 | 46.1 (42.2-49) | 10.42 | 1 | 89.08 | .0.044* |
| | <40 (n=12) | 39.1 (34.1-44) | | | | | 39.1 (34.1-44) | | | | |
| SCIM self-care | >=20 (n=28) | 47.1 (43.2-50) | .77 | 1 | 51.04 | .384 | 47.1 (42.1-52) | 17.02 | 1 | 49.18 | .0.001* |
| | <20 (n=27) | 39.1 (34.5-44) | | | | | 39.1 (34.5-44) | | | | |
| SCIM total score | >=61 (n=43) | 46.1 (42.5-50) | .06 | 1 | 93.88 | .779 | 46.1 (42.5-50) | 11.61 | 1 | 93.06 | .0.001* |
| | <61 (n=14) | 43.1 (35.5-51) | | | | | 43.1 (35.5-51) | | | | |

Factors

Abbreviations: AIS, American Spinal Injury Association Impairment Scale; MCS, mental health component summary (SF-36); PCS, physical health component summary (SF-36); SCIM, Spinal Cord Independence measure III; mobility I, mobility (indoors and outdoors); mobility II, mobility (room and toilet); i.v. management, respiration and sphincter management.

*p<.05; **p<.01; ***p<.001.

### 2-3-year follow-up: HRQoL

MCS = mental HRQoL PCS = physical HRQoL

Table 3: Results of the 2-3-year investigation

| Variable | Category | mental health component summary (MCS) | | | | | physical health component summary (PCS) | | | | |
|---|---|---|---|---|---|---|---|---|---|---|---|
| | | Per (CI 95%) | statistic | df1 | df2 | p | Per (CI 95%) | statistic | df1 | df2 | p |
| level of injury | cervical (N=23) | 50 (45-55) | 1.84 | 1.90 | 85.54 | .163 | 44 (41-48) | 12.04 | 1.68 | 94.68 | .0.001*** |
| | thoracic (n=16) | 51 (39-63) | | | | | 36 (27-45) | | | | |
| | lumbar (n=7) | 48 (40-55) | | | | | 54 (46-61) | | | | |
| neurological category | C1-C8; AIS A, B, C (n=8) | 40 (29-50) | .59 | 1.92 | 15.13 | .565 | 33 (25-41) | 12.91 | 2.41 | 25.23 | .0.001*** |
| | T1-S5; AIS A, B, C (n=15) | 51 (41.6, 60.4) | | | | | 46 (36, 55) | | | | |
| | AIS D (n=23) | 48 (43-54) | | | | | 54 (46-61) | | | | |
| | AIS E (n=6) | 48.63 (-Inf-Inf) | 48 (33-64) | | | | 61 (70-88) | | | | |
| pain score | >= 2 (n=19) | 40 (34-72) | 9.92 | 1 | 28.11 | .004** | 44 (39-49) | 9.26 | 1 | 21.09 | .002 |
| | <2 (n=27) | 57 (36-78) | | | | | 49 (-50-50) | | | | |
| SCIM i.v. management | >=16 (n=24) | 50 (43-61) | .23 | 1 | 36.51 | .634 | 46 (39-53) | 70.23 | 1 | 38.27 | .0.001*** |
| | <16 (n=11) | 48 (39-57) | | | | | 73 (65-74) | | | | |
| SCIM mobility I | >=20 (n=23) | 50 (44-62) | .47 | 1 | 33.63 | .499 | 51 (27-28) | 35.51 | 1 | 42.51 | .0.001*** |
| | <20 (n=12) | 47 (38-56) | | | | | 43 (42-73) | | | | |
| SCIM mobility II | >=20 (n=22) | 51 (49-62) | .02 | 1 | 22.19 | .881 | 39 (28-35) | 72.99 | 1 | 21.95 | .0.001*** |
| | <20 (n=13) | 48 (38-48) | | | | | 73 (65-74) | | | | |
| SCIM self-care | >=20 (n=20) | 48 (39-57) | .05 | 1 | 27.43 | .799 | 39 (28-35) | 76.11 | 1 | 36.76 | .0.001*** |
| | <20 (n=15) | 50 (43-62) | | | | | 73 (65-74) | | | | |
| SCIM total score | >=61 (n=23) | 50 (44-60) | .23 | 1 | 49.03 | .631 | 39 (28-35) | 70.19 | 1 | 43.87 | .0.001*** |
| | <61 (n=12) | 48 (40-56) | | | | | 73 (65-74) | | | | |

Factors

Abbreviations: AIS, American Spinal Injury Association Impairment Scale; MCS, mental health component summary (SF-36); PCS, physical health component summary (SF-36); SCIM, Spinal Cord Independence measure III; mobility I, mobility (indoors and outdoors); mobility II, mobility (room and toilet); i.v. management, respiration and sphincter management.

*p<.05; **p<.01; ***p<.001.

## CONCLUSIONS:

- Self-reported perceived pain is linked to higher mental HRQoL 1 year as well as 2-3 years after injury.
- Higher physical HRQoL is associated with better functional abilities 1 year as well as 2-3 years after injury.
- Mental and physical HRQoL remain stable from 1 year after injury to the 2-3 year after injury follow-up.

➢ These results are an implication for rehabilitation and long-term surveillance of recent SCI patients.

## LIMITATIONS:

- The small sample size and incomplete registry data, as well as selection bias of this registry are limitations of this study.

REFERENCES:

[1] Murray CJ, Vos T, Lozano R, Naghavi M, Flaxman AD, Michaud C, Ezzati M, Shibuya K, Salomon JA, Abdalla S, Aboyans V, Abraham J, Ackerman I, Aggarwal R, Ahn SY, Ali MK, Alvarado M, Anderson HR, Anderson LM, Andrews KG, Atkinson C, Baddour LM, Bahalim AN, Barker-Collo S, Barrero LH, Bartels DH, Basáñez MG, Baxter A, Bell ML, Benjamin EJ, Bennett D, Bernabé E, Bhalla K, Bhandari B, Bikbov B, Bin Abdulhak A, Birbeck G, Black JA, Blencowe H, Blore JD, Blyth F, Bolliger I, Bonaventure A, Boufous S, Bourne R, Boussinesq M, Braithwaite T, Brayne C, Bridgett L, Brooker S, Brooks P, Brugha TS, Bryan-Hancock C, Bucello C, Buchbinder R, Buckle G, Budke CM, Burch M, Burney P, Burstein R, Calabria B, Campbell B, Canter CJ, Carabin H, Carapetis J, Carmona L, Cella C, Charlson F, Chen H, Cheng AT, Chou D, Chugh SS, Coffeng LE, Colan SD, Colquhoun S, Colson KE, Condon J, Connor MD, Cooper LT, Corriere M, Cortinovis M, de Vaccaro KC, Couser W, Cowie BC, Criqui MH, Cross M, Dabhadkar KC, Dahodwala N, De Leo D, Degenhardt L, Delossantos A, Denenberg J, Des Jarlais DC, Dharmaratne SD, Dorsey ER, Driscoll T, Duber H, Ebel B, Erwin PJ, Espindola P, Ezzati M, Feigin V, Flaxman AD, Forouzanfar MH, Fowkes FG, Fransen R, Freeman MK, Gabbe BJ, Gabriel SE, Gakidou E, Ganatra HA, Garcia B, Gaspari F, Gillum RF, Gmel G, Gosselin R, Grainger R, Groeger J, Guillemin F, Gunnell D, Gupta R, Haagsma J, Hagan H, Halasa YA, Hall W, Haring D, Haro JM, Harrison JE, Havmoeller R, Hay RJ, Higashi H, Hill K, Hoen B, Hoffman H, Hotez PJ, Hoy D, Huang JJ, Ibeanusi SE, Jacobsen KH, James SL, Jarvis D, Jasrasaria R, Jayaraman S, Johns N, Jonas JB, Karthikeyan G, Kassebaum N, Kawakami N, Keren A, Khoo JP, King CH, Knowlton LM, Kobusingye O, Koranteng A, Krishnamurthi R, Laden F, Lalloo R, Laslett LL, Lathlean T, Leasher JL, Lee YY, Leigh J, Levinson D, Lim SS, Limb E, Lin JK, Lipnick M, Lipshultz SE, Liu W, Loane M, Ohno SL, Lyons R, Mabweijano J, MacIntyre MF, Malekzadeh R, Mallinger L, Manivannan S, Marcenes W, March L, Margolis DJ, Marks GB, Marks R, Matsumori A, Matzopoulos R, Mayosi BM, McAnulty JH, McDermott MM, McGill N, McGrath J, Medina-Mora ME, Meltzer M, Mensah GA, Merriman TR, Meyer AC, Miglioli V, Miller M, Miller TR, Mitchell PB, Mocumbi AO, Moffitt TE, Mokdad AA, Monasta L, Montico M, Moradi-Lakeh M, Moran A, Morawska L, Mori R, Murdoch ME, Mwaniki MK, Naidoo K, Nair MN, Naldi L, Narayan KM, Nelson PK, Nelson RG, Nevitt MC, Newton CR, Nolte S, Norman P, Norman R, O'Donnell M, O'Hanlon S, Olives C, Omer SB, Ortblad K, Osborne R, Ozgediz D, Pahari A, Pandian JD, Panozo Rivero A, Parry CD, Pascual-Marate F, Patel SN, Patton GC, Paul CL, Pavlin B, Pearce N, Pesudovs K, Peterson CB, Petzold M, Phillips MR, Pope D, Pope CA 3rd, Poulton R, Prabhakaran D, Prasad K, Qato D, Quanah R, Rafay A, Rai RS, Rana SM, Remuzzi G, Richardson K, Richardson M, Riley ID, Robinson M, Roca A, Rodriguez A, Rojas-Rueda D, Ronfani L, Rothenbacher D, Roy A, Sabin N, Safdi N, Sagar R, Sahathevan R, Salomon JA, Salvo D, Sampson U, Sanabria JR, Sanchez-Riera L, Santos IS, Satpathy M, Saunders JE, Sawhney M, Saylan MI, Scarborough P, Schmidt JC, Schneider IJ, Schöttker B, Schwebel DC, Scott JG, Seedat S, Sepanlou SG, Serdar B, Servan-El-Saiegh N, Shahraz S, Sharma R, Shen J, Shi P, Shiue I, Sibai AM, Singh D, Singh V, Skirbekk V, Sleet DA, Sliwa K, Soljak M, Softley A, Sorensen RJ, Soriano JB, Soshnikov S, Soyiri IN, Spencer CN, Stathopoulou V, Stein DJ, Stein MB, Stevens GA, Stewart LK, Steyerberg EW, Stolk WA, Stovner LJ, Subart M, Sur P, Sykes BL, Tabarés-Seisdedos R, Tan F, Tanne D, Tanner M, Tavakkoli M, Taylor HR, Taylor JA, Taylor S, Templin T, Tleyjeh IM, Tonelli M, Topor-Madry R, Torre AE, Tortolero Y, Tosetti A, Towbin JA, Tran BX, Truelsen T, Tsilimbaris M, Ubeda C, Undurraga EA, van der Werf MJ, van Os J, Vavilala MS, Venketasubramanian N, Wang M, Wang W, Warouw T, Watt K, Weatherall DJ, Weber MA, Weiderpass E, Weintraub RG, Whiteford HA, Wilkinson JD, Williams HC, Williams SR, Witt E, Wolfe F, Woolf AD, Wulf S, Yeh PH, Zaidi AK, Zheng ZJ, Zonies D, Lopez AD, AlMazroa MA, Memish ZA. The State of US Health, 1990-2010: Burden of Diseases, Injuries, and Risk Factors. JAMA. 2013 Aug 14;310(6):591-608. doi: 10.1001/jama.2013.13805. PMID: 23842577; PMCID: PMC4673766.

[2] Post M, Noreau L. Measurement and Modelling of Health-related Quality of Life. In: Kirshner J, Kopperdahl D, Quittek J, editors. Spiroergometry in Public Health. Sow Steps Academic Press; 2018. p. 195-205.

[3] Anderson Aaldres S, Wahlbrink O, Zagrer ..., et al. Is a Swiss Spinal Cord Injury Study: a registry for patients living with traumatic spinal cord injury. Spinal Cord Ser Cases. 2017;3:17078.

ACKNOWLEDGMENTS:

We thank the ASCIS network and all the participating local ASCIS sites, as well as Katharina Wahr for providing ASCIS datasets and for her assistance during analysis.

## Health-related quality of life in patients with traumatic spinal cord injury – A longitudinal study

Nora Renz[1,2], Georg Zimmermann[3,4,8], Stephanie Aschauer-Wallner[2], Herbert Resch[2], Kerstin Schwenker[1,2,7], Eugen Trinka[1,2,6,7], Yvonne Höller[5]

[1]Department of Neurology, Christian Doppler University Hospital, Centre for Cognitive Neuroscience, Paracelsus Medical University, Salzburg, Austria; [2]Spinal Cord Injury and Tissue Regeneration Center, Paracelsus Medical University, Salzburg, Austria; [3]Team Biostatistics and Big Medical Data, IDA Lab Salzburg, Paracelsus Medical University, Salzburg, Austria; [4]Department of Mathematics, Paris Lodron University, Salzburg, Austria; [5]Department of Psychology, University of Akureyri, Akureyri, Iceland; [6]Neuroscience Institute, Christian Doppler University Hospital, Centre for Cognitive Neuroscience, Paracelsus Medical University, Salzburg, Austria; [7]Karl Landsteiner Institute for Neurorehabilitation and Space Neurology, Salzburg, Austria; [8]Department of Research and Innovation, Paracelsus Medical University, Salzburg, Austria; Contact: nora.renz@pmu.ac.at

### Objective
Traumatic Spinal Cord Injury (tSCI) is a condition with extensive impact on an individual's life and in particular on the health-related quality of life (HRQoL), but so far longitudinal data are missing. The aim of this study was to assess the HRQoL of patients suffering from tSCI and to identify the relative contributions of different factors at the 1-year and the 2-3-year follow-up investigation.

### Methods
In this longitudinal study research data were extracted from the ASCIS (Austrian Spinal Cord Injury Study) database. 57 (77.2 % male, 22.8 % female) patients were followed-up 1 year after injury, and 46 (73.9 % male, 26.1 % female) patients 2-3 years after injury. The variables age, gender, level of injury, American Spinal Injury Association (ASIA) score were analyzed, as well as the variables pain using a Verbal Numeric Rating Scale (VNRS), the functional status and the ability of performing tasks of daily living surveyed by the Spinal Cord Independence Measure III (SCIM III) and HRQoL measured by the SF-36 or the SF-36 v2. Statistical analyses were conducted using nonparametric ANOVA-type tests.

### Results
Patients who reported a pain score greater 2 on the VNRS had a significantly lower SF-36 mental health component summary (MCS) score 1 year after injury ($ATS(1, 40.52) = 6.31$, $p = .016$ ) as well as 2-3 years after injury ($ATS(1, 26.11) = 9.32$, $p = .005$). Patients with a pain score greater 2 on the VNRS showed a significantly lower SF-36 PCS score ($ATS(1, 38.23) = 7.04$, $p = .012$). If the 'SCIM total score' was greater than 81, patients tended to have better scores on the SF-36 physical health component summary (PCS) scale 1 year after injury ($ATS(1, 49.05) = 17.61$, $p < .001$) and also 2-3 years after injury ($ATS(1, 43.87) = 78.39$, $p < .001$).

### Conclusions
These findings confirm that pain and functional abilities are relevant for HRQoL. Less pain and enhanced functional abilities lead to higher HRQoL, 1 year and 2-3 years after injury. HRQoL remains stable from 1 year to 2-3 years after injury.

# Online sleep counselling for shift workers is feasible and potentially effective

## Effects of online sleep counselling for shift workers

**Retzer**, Lukas[1,2]; Feil, Monika[2]; Zauter, Sigrid[2]; Lehmann, Robert[2]; Gräßel, Elmar[3]; Richter, Kneginja[1,2]
1: University Clinic for Psychiatry and Psychotherapy, Paracelsus Medical University, Nuremberg, Germany
2: Faculty for Social Sciences, Nuremberg Tech, Nuremberg, Germany
3: Center for Health Services Research in Medicine, University Hospital Erlangen, Germany

**INTRO**

- Many shift workers suffer from sleep disorders.
- Preventing and treating these issues with Cognitive Behavioral Therapy for Insomnia (CBT-I) can present a challenge in outpatient settings.
- We thus transferred elements from CBT-I to an online counselling setting.

**METHODS**

- Pilot study: N = 22; RCT: N = 18; Outpatient sample: N = 12
- Identical treatment principles and contents across groups
- Main outcome: Sleep efficiency (SE) calculated from sleep diaries
- Tested with t-Tests and rmANOVAS

**RESULTS**

- Significant improvements regarding SE in the pilot study (+ 7.2%; p = .001) and the outpatient sample (+ 7.2%; p = .03) (s. Fig. 1)
- RCT: Better SE-trajectory in the intervention group as compared to the control group (p < .001); however, no significant changes in SE in either group.

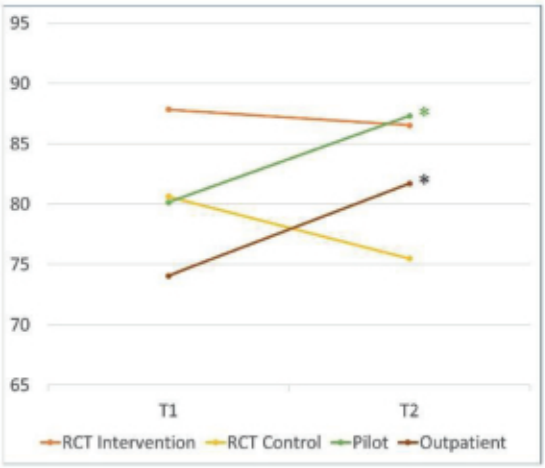


**Fig. 1: Sleep efficiencies (%) before (T1) and after (T2) treatment**
- Difference between RCT-I and RCT-C at T1 not significant
- Reasons: Small sample sizes, big standard deviations, "unhappy" randomization

**DISCUSSION**

- Online sleep counselling for shift workers, employing elements from CBT-I, is feasible and potentially effective.
- Verification of these results via an RCT is ongoing.

## Effects of online sleep counselling for shift workers

Lukas Retzer[1,2], Monika Feil[2], Sigrid Zauter[2], Robert Lehmann[2], Elmar Gräßel[3], Kneginja Richter[1,2]

[1]University Clinic for Psychiatry and Psychotherapy, Paracelsus Medical University, Nuremberg, Germany; [2]Faculty for Social Sciences, Nuremberg Tech, Nuremberg, Germany; [3]Center for Health Services Research in Medicine, University Hospital Erlangen, Germany; Contact: lukas.retzer@klinikum-nuernberg.de

### Objective
Shift work is connected to a number of health issues, most prominently sleep disorders, mainly because of the disruption in circadian rhythms it causes. Preventing and treating shiftwork-related sleep disorders with elements from Cognitive Behavioral Therapy for Insomnia (CBT-I) is possible in principle and potentially effective. However, reaching this target population, defined by irregular working hours, by way of regular face-to-face appointments can be challenging.

### Methods
Our group thus transferred CBT-I contents into an asynchronous online counselling setting, consisting of four text messages by specially trained psychologists, supplemented by a digital sleep diary and clinical questionnaires. This approach was tested in a non-controlled pilot study (n = 22)(1) and an ongoing randomized, clinical trial (RCT) with a waiting list control group (n = 17). Participants were recruited in collaborating companies where shift work is highly prevalent. We compare the data from the two online counselling trials with data from n = 12 shift workers who completed CBT-I treatment in our outpatient clinic. The main outcome is sleep efficiency, calculated from sleep diaries.

### Results
In the pilot study, sleep efficiency significantly increased by an average of 7.2% ($p = .001$), which is comparable in magnitude to the increase in our outpatient sample (7.7%; $p = .03$). In the RCT, we observed a significantly better development of sleep efficiency in the intervention group as compared to the control group ($p < .001$); however, at this point, there is no significant change in sleep efficiency to be reported in either group by itself.

### Conclusions
We report on the, to our knowledge, first online sleep counselling project for shift workers. Preliminary results show this approach to be feasible and potentially effective regarding sleep efficiency. An RCT to verify these results is ongoing.

### References
1. Peter, L., Reindl, R., Zauter, S., Hillemacher, T., & Richter, K. (2019). Effectiveness of an Online CBT-I Intervention and a Face-to-Face Treatment for Shift Work Sleep Disorder: A Comparison of Sleep Diary Data. International Journal of Environmental Research and Public Health, 16(17). https://doi.org/10.3390/ijerph16173081

# Functional recovery through intralesional application of extracellular vesicles in a rat model of traumatic spinal cord injury

Pasquale Romanelli[1,2], Lara Bieler[1], Patrick Heimel[3,8,10], Siniša Škokić[4], Dominika Jakubecova[1], Christina Kreutzer[1], Pia Zaunmair[1], Tomislav Smolčić[4], Bruno Benedetti[5], Eva Rohde[6,6,11], Mario Gimona[6,7,11], David Herchet[6,10], Marina Dobrivojević Radmilović[4,9], Sebastien Couillard-Despres[1,10]

Institute of Experimental Neuroregeneration, Spinal Cord Injury and Tissue Regeneration Centre Salzburg (SCI-TReCS), Paracelsus Medical University, Salzburg, Austria, 2 Innovacell AG, Innsbruck, Austria, 3 Core Facility Hard Tissue and Biomaterial Research, Karl Donath Laboratory, University Clinic of Dentistry, Medical University Vienna, 4 Croatian Institute for Brain Research, University of Zagreb School of Medicine, Zagreb, Croatia, 5 GMP Unit, Spinal Cord Injury & Tissue Regeneration Centre Salzburg (SCI-TReCS), Paracelsus Medical University, Salzburg, Austria, 6 Department of Transfusion Medicine, University Hospital, Salzburger Landeskliniken Gesmbh (SALK) and Paracelsus Medical University, Salzburg, Austria, 7 Research Program "Nanovesicular Therapies", Paracelsus Medical University, Salzburg, Austria, 8 Ludwig Boltzmann Institute for Experimental and Clinical Traumatology, AUVA Research Centre, Vienna, Austria, 9 Department of Histology and Embryology, University of Zagreb School of Medicine, Zagreb, Croatia, 10 Austrian Cluster for Tissue Regeneration, Vienna, Austria, 11 Transfer Centre for Extracellular Vesicle Theralytic Technologies (EV-TT), Salzburg, Austria

Local inflammation plays a pivotal role in the process of secondary damage after spinal cord injury. Acute intravenous application of extracellular vesicles (EVs) secreted by human umbilical cord mesenchymal stromal cells (hUC-MSCs) have been shown to dampen the induction of inflammatory processes following spinal cord injury. However, systemic application of EVs is associated with delayed delivery to the site of injury and the necessity for high doses to reach therapeutic levels

**Objective:**
In this project, we compared the impacts of a treatment based on EVs injected directly into the lesion site , to a treatment in which EVs were injected intravenously, for the functional regeneration and structural integrity following spinal cord injury (SCI).

**Methods:**
Spinal cord injury was performed in female Fisher 344 rats of 10 weeks of age through a 200kdyn contusion lesion at thoracic level 8 resulting in a moderate to severe incomplete SCI. The rats were randomly divided in treatment groups receiving acutely an intra parenchymal application of either vehicle, 1,5 x $10^9$ EVs or an intravenous application of 1,5 x $10^9$ EVs. Sham rats underwent the same surgical procedure but did not receive a contusion.
Histological analyses were performed 2 and 8 weeks after contusion. Locomotor recovery was assessed until 8 weeks after contusion. MRI, DTI and µCT analysis were performed ex vivo 8 weeks after injury

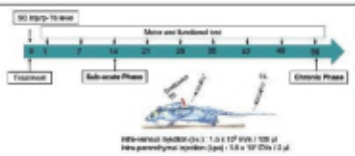


**Acute intralesional application of EVs improved functional recovery after SCI:**

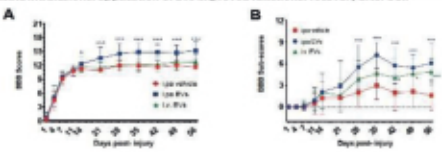


The motor function of hindlimbs was assessed using **(A)** the non-linear BBB-score scale (Basso et al. 1995), which ranges from (0) total paralysis to (21) normal locomotion. Rats moving freely within a 1 meter diameter arena were scored for 4 minutes by two observers blinded to group-belonging. On the first day post-SCI, hindlimbs of rats were nearly paralyzed. Over the following days, the mobility of joints and the walking pattern progressively recovered in all SCI groups. Strikingly, from the second week post-injury onward, the recovery of locomotion in i.pa. EV-treated rats was significantly more robust compared to the recovery following vehicle application. At 56 days post-injury, the BBB score reached 15.2 ± 1.9 in i.pa. EV-treated rats, which corresponds to a consistent forelimb – hindlimb coordination with predominant parallel paw placement at the initial floor contact. **(B)** BBB sub-scores (ranging from 0 to 13) were also calculated to quantify recovery based on toe clearance, paw position, trunk stability and tail use, independently of forelimb-hindlimb coordination (Popovich et al. 2012). Starting on 28 days post-injury, the BBB sub-score was significantly higher in rats that received i.pa. EV application, as compared to the vehicle-treated rats. Importantly, a greater degree of locomotor recovery was also detected from 42 days post-injury onward in rats treated with i.v. EVs, of vehicle-treated rats.

**Acute intralesional application of EVs quenched the inflammatory response after SCI**

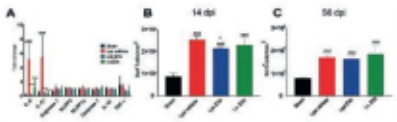


Statistical differences to sham group (#) and to vehicle group (*) using one-way ANOVA and Tukey post-hoc test

**(A)** We examined, 24 hours post-injury, the capacity of acute EV applications to install a milder inflammatory environment within the lesioned spinal cord. SCI provokes a strong upregulation of the expression of the pro-inflammatory cytokines IL-1β and IL-6 at the lesion site. Compared to vehicle-treated rats, the i.pa. application of EVs significantly reduced the induction of IL-1β and IL-6 expression by more than 90 % (p < 0.001). A similar reduction in IL-1β expression was also detected following the i.v. application of EVs. However, IL-6 expression was less efficiently suppressed by i.v. application of EVs and showed a reduction of approximately 77 %. **(B)** and **(C)** Lower density of microglia in the proximity of the lesion during the sub-acute phase after intralesional application of EVs. Representative immunodetection of Iba1 in the spinal cord of rats from **(D-F)** the sham group, and **(G-I)** from the i.pa. vehicle-treated tSCI group (2 mm rostral from the epicenter). Greater impact of intralesional application of EVs, as compared to intravenous, was also detected on scarring (not shown).

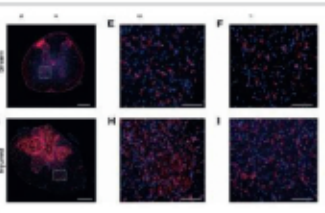


**Acute intralesional application of EVs reduced astrogliosis and scarring after tSCI**

During the sub-acute phase post-SCI, reactive astrocytes proliferate and build a fibroglial scar at the lesion site that acts as a physical barrier. Furthermore, astrocytes residing in the intact parenchyma proximal to the lesion become hypertrophic and upregulate the expression of glial fibrillary acidic protein (GFAP). The immunodetection of GFAP can therefore be used to monitor ongoing reactive gliosis. **(A-B)** Immunodetection of GFAP-expressing astrocytes (white) in the ventral horn of sham rats and i.pa. vehicle-treated tSCI rats at 14 days post-injury (3 mm rostral from lesion epicenter) Nuclear counterstain with DAPI (blue). Scale bar (A) = 100 µm. **(C)** Percentage of section area covered by GFAP at 14 days post-tSCI. At 14 days post-tSCI, examination in the perilesional area revealed that the percentage of area covered with GFAP had more than doubled in SCI rats that received the vehicle treatment, as compared to the sham group ($p < 0.001$). In contrast, EV treatment following SCI significantly lowered the accumulation of GFAP by approximately 35 %, compared to the vehicle treatment
Following SCI, non-cellular components, such as collagen, accumulate in the fibroglial scar and create an inhibitory environment for axonal sprouting. We assessed the impact of early EV applications on the accumulation of collagen I by immunodetection. **(D-E)** Immunodetection of collagen I (green) in the spinal cord of sham rats and i.pa. vehicle-treated rats at 14 days post-tSCI at the lesion epicenter. Scale bar (D) = 500 µm. **(F)** Percentage of section area covered by collagen I at 14 days post-tSCI. Analysis demonstrated that both administration routes of EVs reduced the deposition of collagen I, compared to rats treated with the vehicle

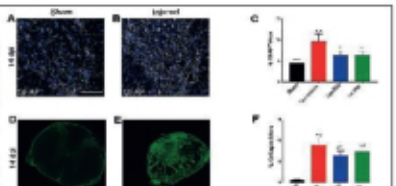


Statistical differences to sham group (#) and to vehicle group (*) using one-way ANOVA and Tukey post-hoc test

**Acute application of EVs improved structural outcomes after SCI**

Representative magnetic resonance (MRI) and micro-computed tomography (µCT) images of vehicle-treated rats at 56 days post-tSCI. Corresponding horizontal sections obtained with **(A)** T1-IR and T2 MRI sequences or **(B)** contrast agent-enhanced µCT. Arrows point to dense scar tissue in (A), arrowheads point to degenerating tracts in (A). Corresponding cross-sections obtained with **(C)** contrast agent-enhanced µCT and **(D)** immunohistology (GFAP in blue, NF-H in green and Iba1 in red) Arrows point to cysts in (C) and (D). A to C: red lines: cysts, yellow lines: damaged tissue and green lines: sample borders. Volumetric analysis did not reveal differences in tissue preservation, lesion size and cyst volume between the EVs and vehicle treatments. **(E)** Longitudinal fiber tracts rostral and caudal to the lesion epicenter detected by DTI. Statistical differences to vehicle group using two-way ANOVA and Tukey post-hoc test on tSCI groups: (***) $p < 0.001$. DTI analysis revealed a better structure preservation of the nerve tracts in the SCI groups treated with EVs.

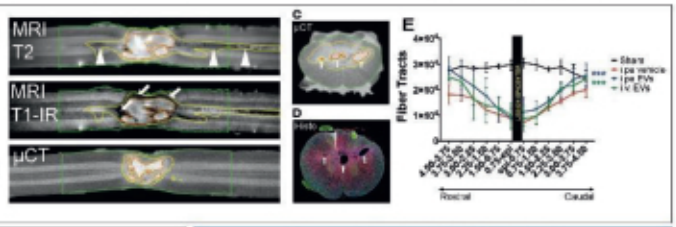


**Conclusion**

In conclusion, we demonstrated that the acute intralesional application of EVs via direct intra-parenchymal injection is more effective than the intravenous route to address the early processes of secondary damage in a rat model of tSCI. Furthermore, the intralesional treatment significantly improved the long term functional outcomes. Decades of research have indicated that treatment of spinal cord injury will require a manifold approach with different types of intervention for the different phases post-injury. Our observation demonstrates that EVs are particularly potent to address the processes of inflammation and scarring when applied very early and close to the site of injury. Moreover, an improvement of the lesion microenvironment and the additional structural sparing obtained with EV treatment constitute valuable assets for follow-up interventions aiming for endogenous axonal regeneration or involving cell therapies.

**ACKNOWLEDGMENTS and FUNDING**

The MRI scans were performed at the Laboratory for Regenerative Neuroscience – GloreLab, University of Zagreb, Croatia. This work has been supported by the Paracelsus Medical University Research Support Fund (PMU-FFF) R-19/01/117-ROM and the Austrian Agency for International Cooperation in Education and Research (OeAD-GmbH) HR02/2018. This work was also supported by Croatian-Austrian Scientific & Technological Cooperation grant 2018/2019, the Ministry of Science and Education of the Republic of Croatia. The study was supported by the Croatian Science Foundation projects BRADSCHEMIA (UIP-2017-05-8082) and RepairStroke (IP-06-2016-1990). We gratefully acknowledge financial support through the Project "EntryNov," from the State of Salzburg, Austria, and from Land Salzburg/WISS 2025/20/032-F1900731/KZP "EV-TT Bjork".

## Functional recovery through intralesional application of extracellular vesicles in a rat model of traumatic spinal cord injury.

Pasquale Romanelli[1,2], Lara Bieler[1], Patrick Heimel[3], Sinisa Skokic[4], Dominika Jakubecova[1], Christina Kreutzer[1], Pia Zaunmair[1], Tomislav Smolcic[4], Bruno Benedetti[1], Eva Rohde[5,6,8], Mario Gimona[5,7,8], David Hercher[3], Marina Dobrivojevic Radmilovic[4], Sebastien Couillard-Despres[1]

[1]Inst of Experimental Neuroregeneration, SCI-TReCS, Paracelsus Medical University, Salzburg; [2]Innovacell AG, Innsbruck; [3]Ludwig Boltzmann Institute for Experimental and Clinical Traumatology, AUVA Research Center, Vienna; [4]Croatian Institute for Brain Research, University of Zagreb School of Medicine, Zagreb, Croatia,; [5]GMP Unit, SCI-TReCS, Paracelsus Medical University, Salzburg; [6]Department of Transfusion Medicine, University Hospital, Salzburger Landeskliniken GesmbH (SALK) and Paracelsus Medical University, Salzburg; [7]Research Program "Nanovesicular Therapies", Paracelsus Medical University, Salzburg; [8]Transfer Centre for Extracellular Vesicle Theralytic Technologies (EV-TT), Salzburg; Contact: s.couillard-despres@pmu.ac.at

### Objective
Local inflammation plays a pivotal role in the process of secondary damage after spinal cord injury. Acute intravenous application of extracellular vesicles (EVs) secreted by human umbilical cord mesenchymal stromal cells (hUC-MSCs) have been shown to dampen the induction of inflammatory processes following spinal cord injury. In this project, we compared the impacts of a treatment based on EVs injected directly into the lesion site, to a treatment in which EVs were injected intravenously, for the functional regeneration and structural integrity following spinal cord injury (SCI).

### Methods
Spinal cord injury was performed in young adult female Fisher 344 rats through a 200 kdyn contusion lesion at thoracic level 8 resulting in a moderate to severe incomplete SCI. The rats were randomly divided in treatment groups receiving acutely an intra-parenchymal application of either vehicle or EVs, or an intravenous application of EVs. Sham rats underwent the same surgical procedure, but did not receive a contusion. Histological analyses were performed 2 and 8 weeks after contusion. Locomotor recovery was assessed until 8 weeks after contusion. MRI, DTI and μCT analysis were performed ex vivo 8 weeks after injury.

### Results
The acute intralesional application of EVs was found to significantly improved functional recovery after SCI, in particular the locomotion as assessed by the BBB score. In contrast, intravenous application of EVs had lower impact on the functional recovery. Moreover, intralesional application of EVs was also more potent to reduce the intensity of inflammatory processs and scarring occuring after injury in comparison to the intravenous EV application. Finally, the integrity of nerve tracts descending and ascending the spinal cord was higher in the rats that received EVs, as compared to rats that received vehicle, according to DTI measurements.

### Conclusions
In conclusion, we demonstrated that the acute intralesional application of EVs via direct intra-parenchymal injection is more effective than the intravenous route to address the early processes of secondary damage in a rat model of tSCI. Furthermore, the intralesional treatment significantly improved the long-term functional outcomes. Our observation demonstrates that EVs are particularly potent to address the processes of inflammation and scarring when applied very early and close to the site of injury.

### Acknowledgements
This work was supported by the PMU-FFF R-19/01/117-ROM and the OeAD-GmbH. We gratefully acknowledge financial support through the State of Salzburg.

# Immediate full weight-bearing with supplemental cerclage? A biomechanical study on the distal tibia

Sabrina Sandriesser[1], Stefan Förch[2], Edgar Mayr[2], Peter Augat[1]
[1] Institute for Biomechanics, BG Unfallklinik Murnau, Germany and Paracelsus Medical University Salzburg, Austria
[2] Department of Trauma, Orthopaedic, Plastic and Hand Surgery, University Hospital of Augsburg, Germany

BGU Murnau
Berufsgenossenschaftliche Unfallklinik Murnau

## Introduction

Tibia shaft fractures represent the most common fractures in long bones with a dominance of spiral fractures (34%) followed by oblique fractures (17%) [1]. As most fractures of the lower extremity, tibia shaft fractures require restrictions in weight-bearing immediately after surgery. Especially geriatric patients can hardly adhere to these partial weight-bearing recommendations [2]. To aim for early loading as tolerated the implant stability can be further augmented by cerclage wiring.

**The aim of this study was to investigate the stabilizing effect of supplemental cerclages in spiral fractures of the distal tibia treated by locked plating. It was postulated that different types of supplemental cerclage materials can reduce interfragmentary shear movements to clinically relevant amounts and allow for immediate full weight-bearing as tolerated compared to a solitary plate osteosynthesis.**

## Material and Methods

In the distal third of the shaft a reproducible spiral fracture was created in artificial composite tibiae (Sawbones) and instrumented with a metaphyseal locking plate (Figure 1a). The samples were tested with the solitary plate and in combination with different supplemental cerclages: one 1.7 mm cable cerclage closed by a crimp mechanism, two cable cerclages, a 1.5 mm double-looped wire cerclage closed by a twist bent downwards, and a 2 mm double-looped suture wire cerclage closed by a knot (Figure 1).

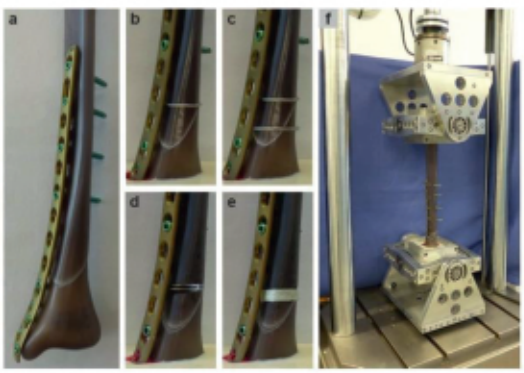


Figure 1: Frontal view of a spiral fracture of the distal tibia treated with a metaphyseal locking plate (a), and with supplemental cerclage configurations: one cable cerclage (b), two cable cerclages (c), a double-looped wire cerclage (d) and a double-looped suture wire cerclage. Mechanical setup in a servo-hydraulic test machine with cardan joints to avoid constraint forces (f).

To mount the samples on the servo-hydraulic test machine (Instron 8874), the proximal and distal ends of the tibia were embedded with the shaft aligned vertically in its anatomical axis. Prior the distal part of the plate was covered with modeling clay to avoid its coverage with embedding material.

Clinically relevant loads for 20 kg partial and 75 kg full weight-bearing were identified and the samples were tested under axial (200 N and 750 N), torsional (2 Nm and 7 Nm) and combined loading. Small adhesive marker points were fixed around the fracture zone to detect interfragmentary movements by a 3D motion tracking system (ARAMIS 5M). Beside construct stiffness, interfragmentary axial movements along the shaft axis and shear movements in horizontal plane were analyzed for differences between the respective cerclage groups and the solitary plate group.

## Results

With each supplemental cerclage axial construct stiffness significantly increased compared to the solitary plate group (980±350 N/mm; p≤0.012). By different types of supplemental cerclage materials interfragmentary movements were reduced to different amounts:

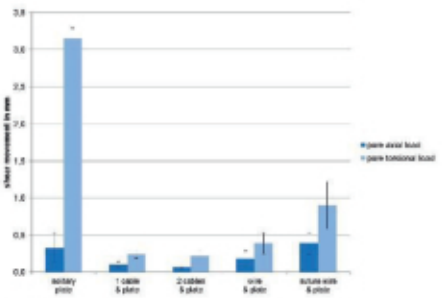


Figure 2: Interfragmentary shear movements in mm for the different test groups and cerclage configurations under pure axial and pure torsional applied loads.

- Under 750 N **pure axial loading** the solitary plate group experienced an axial movement of 0.9±0.2 mm, which was significantly reduced by each supplemental cerclage type (p≤0.012).
- Under 750 N **pure axial loading** shear movements of up to 0.3±0.2 mm were identified for the solitary plate group, which were comparable to supplemental wire and suture wire cerclages. Only both cable cerclage groups showed significantly reduced shear movements compared to the solitary plate group (p≤0.035) (Figure 2).
- Under 7 Nm **pure torsional loading** maximum shear movements of 3.2±0.1 mm were identified for the solitary plate group. With supplemental suture wire cerclages this movement was significantly reduced below 1 mm and for both cable cerclages as well as for wire cerclages a reduction below 0.5 mm was achieved (p≤0.012) (Figure 2).
- Under combined **axial and torsional loading**, the solitary plate group experienced shear movements of 0.6±0.1 mm under partial weight-bearing and 2.1±0.7 mm under full weight-bearing loads. With a supplemental cable cerclage the movement under full weight-bearing was reduced to 0.4±0.1 mm and was even significantly lower than the solitary plate group under partial weight-bearing (p=0.001).

## Discussion

This study demonstrates the substantial stabilizing effect of supplemental cerclages in locking plate fixation in a clinically relevant fracture model of the distal tibia. Although each of the applied cerclage type significantly reduced axial interfragmentary movement, a reduction in shear movements seems clinically and mechano-biologically more important to promote the fracture healing process [3]. Most reduction in shear movements was identified for the cable cerclage groups. Whether these findings can be transferred into the clinical routine has to be investigated in further clinical studies.

**From a biomechanical point of view immediate post-operative weight-bearing as tolerated seems possible, as the implant stability of the distal tibial locking plate is further augmented by supplemental cable cerclage wiring.**

Literature:
[1] Meier P. et al., Injury. 2013;44(4):484-91
[2] Kammerlander C. et al., J Bone Joint Surg Am. 2010;92(2):332-40
[3] Augat P. et al., J Orthop Res. 2003;21(6):1011-17

Contact:
Dipl.-Ing. Sabrina Sandriesser
E-Mail: sabrina.sandriesser@bgu-murnau.de
Telefon: +49 8841 48-4501
Fax: +49 8841 48-4273

BG Kliniken Murnau,
Institut der Medizinischen Universität Salzburg
Prof. A. Ulrich-Str. 3
82418 Murnau am Staffelsee
www.bgu-murnau.de

## Immediate full weight-bearing with supplemental cerclage? A biomechanical study on the distal tibia

Sabrina Sandriesser[1,2], Stefan Förch[3], Edgar Mayr[3], Peter Augat[1,2]

[1]Institute for Biomechanics, BG Unfallklinik Murnau, Germany; [2]Institute for Biomechanics, Paracelsus Medical University, Salzburg, Austria; [3]Department of Trauma, Orthopedic, Plastic and Hand Surgery, University Hospital of Augsburg, Germany; Contact: sabrina.sandriesser@bgu-murnau.de

### Objective
Most fractures of the lower extremity require restrictions in weight-bearing immediately after surgery. Especially geriatric patients can hardly adhere to recommended partial weight-bearing. To aim for early loading the implant stability can be augmented by cerclage wiring. The aim of this study was to investigate the stabilizing effect of supplemental cerclages in spiral fractures of the distal tibia treated by locked plating. It was postulated that different types of supplemental cerclage materials can reduce interfragmentary movements to clinically relevant amounts and the overall stability is superior to solitary plating.

### Methods
In the distal third of the shaft a reproducible spiral fracture was created in artificial composite tibiae (Sawbones) and instrumented with a metaphyseal locking plate. The samples were tested with the solitary plate and in combination with different supplemental cerclages: one cable cerclage closed by crimping, two cable cerclages, a double looped wire cerclage closed by twisting, and a double looped suture wire cerclage closed by a knot. Clinically relevant loads for post-operative partial and full weight-bearing were identified and the samples were tested under axial (200 N and 750 N), torsional (2 Nm and 7 Nm) and combined loading on a mechanical testing machine. Construct stiffness and interfragmentary movements were tracked by a motion tracking system (ARAMIS) and statistically analyzed.

### Results
With each supplemental cerclage axial construct stiffness significantly increased compared to the solitary plate group (980 ± 350 N/mm; $p \leq 0.012$). Under 750 N pure axial loading the solitary plate group experienced an axial movement of 0.9 ± 0.2 mm, which was significantly reduced by each supplemental cerclage ($p \leq 0.012$). Both cable cerclage groups showed significantly reduced shear movement compared to the solitary plate group ($p \leq 0.035$), while the wire and suture wire cerclages experienced comparable shear movements. Under pure torsional loading maximum shear movements of 3.2 ± 0.1 mm were identified for the solitary plate group. With supplemental suture wire cerclages this movement was significantly reduced below 1 mm and for both cable cerclages as well as for wire cerclages even below 0.5 mm ($p \leq 0.012$). By applying combined axial and torsional loading, the solitary plate group experienced shear movements of 0.6 ± 0.1 mm under partial weight-bearing and 2.1 ± 0.7 mm under full weight-bearing loads. With a supplemental cable cerclage the movement under full weight-bearing was reduced to 0.4 ± 0.1 mm and was even significantly lower than the solitary plate osteosynthesis under partial weight-bearing ($p = 0.001$).

### Conclusions
This study demonstrates the substantial stabilizing effect of supplemental cerclages in locking plate fixation in a clinically relevant fracture model of the distal tibia. Although each of the cerclage types significantly reduced axial interfragmentary movement, a reduction in shear movements seems clinically and mechano-biologically more important to promote fracture healing [3]. Most reduction in shear movements was identified for the cable cerclages. Whether these findings can be transferred into the clinical routine has to be investigated in further clinical studies. From a biomechanical point of view immediate post-operative weight-bearing as tolerated seems possible, as the implant stability of the distal tibial locking plate is further augmented by supplemental cable cerclage wiring.

# PRO- AND ANTIANGIOGENIC EFFECTS OF HUMAN TENDON CELLS DEPEND ON OXYGEN AVAILABILITY



Judit K. Schachinger[1,2], Christine Lehner[1,2], Herbert Tempfer[1,2] and Andreas Traweger[1,2]

[1]Institute of Tendon and Bone Regeneration, Paracelsus Medical University-Spinal Cord Injury & Tissue Regeneration Center Salzburg, 5020 Salzburg, Austria; [2]Austrian Cluster for Tissue Regeneration, Vienna, Austria

Tendons are hierarchically organized connective tissues that anatomically link muscle to bone and enable efficient energy transmission from muscle to the skeleton [1,2]. Healthy tendons harbor few cells, are rich in extracellular matrix (ECM) and have a low blood vessel density [3]. Injured tendons, however, are characterized by an excessive deposition of ECM, an increase in cell number and blood vessel ingrowth. It is assumed that pro- and antiangiogenic factors are well balanced in healthy tendon, maintaining low vascularization, and that this balance is lost in overused or injured tendon. Various proangiogenic factors such as Vascular Endothelial Growth Factor (VEGF) have been shown to be upregulated after tendon injury, whereas angiostatic mechanisms in healthy tendon remain poorly understood. [4].

## OBJECTIVE

- To establish a defined in vitro model allowing to study pro- and antiangiogenic mechanisms exerted by tendon cells under physiologic and pathologic conditions.

## METHODS

- Human semitendinosus tendon derived stem/ progenitor cells (TDSPC) and human adipose tissue derived stem cells (ADSC) were cultured under normoxic (19% $O_2$) and hypoxic conditions (5% $O_2$). Cell supernatants were tested in a human umbilical vein endothelial cell (HUVEC) based tube formation assay, allowing to assess their impact on angiogenesis- related cellular mechanisms. ADSCs were used as a control group to validate the model, since they are known to induce angiogenesis [5]. (Figure 1)

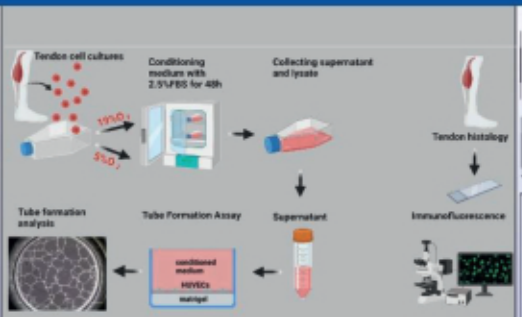


**Figure 1:** Workflow of cell culture, angiogenesis assay and Immunofluorescence analysis

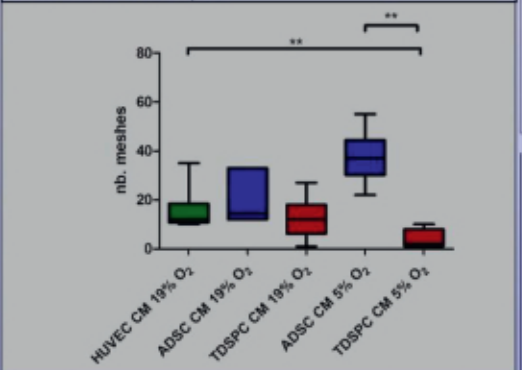


**Figure 2:** Quantification of HUVEC tube formation assay reveals that tendon stem/progenitor cell (TDSPC) derived conditioned medium (CM) cultivated at 5% $O_2$ significantly reduces the number of meshes, compared to proangiogenic adipose derived stem cell derived conditioned medium.

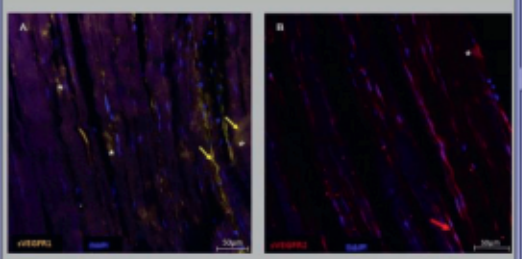

**Figure 3:** Both soluble VEGF receptor 1 (sVEGFR1) and soluble VEGF receptor 2 (sVEGFR2) are expressed in tendon cells (A, B, arrows). To some extent, expression is also detectable in the extracellular matrix (asterisks).

Created with BioRender.com

- By immunohistochemistry on cryosections of healthy human Semintendinosus tendons, the expression of soluble VEGFR 1 and 2, were examined, two factors known to exert angiostatic mechanisms in avascular tissues like the cornea [6].

## PRELIMINARY RESULTS

- TDSPCs conditioned medium (CM) generated at 5% $O_2$ significantly decreased the number of formed tubes compared to ADSC CM (5% $O_2$) and TDSPCs CM 19% $O_2$ ($p=0.005$). (Figure 2)

- Immunofluorescence analysis showed both sVEGFR1 and sVEGFR2 are expressed in all tendons analyzed (n=3), both in the tendon cells and in the extracellular matrix. (Figure 3)

## CONCLUSION & OUTLOOK

With this work we show that cultured tendon cells exert antiangiogenic mechanisms mediated by soluble factors. In future work, these factors will be further examined by mass spectrometry and mRNA sequencing. Moreover, potential changes of the balance between pro- and antiangiogenic factors will be examined by in vitro and ex vivo model of tendon disease.

For the first time, we show the expression of sVEGF receptors in tendon cells, proteins crucial for homeostasis in avascular ocular tissues like the cornea.

## REFERENCES

[1] Kirkendall DT., Scand J Med Sci Sports 1997; 7: 62-66

[2] Puhl et al., Scand J Med Sci Sports. 2005, 15, 211-22

[3] Kannus, P. Scand J Med Sci Sports; 2000 10: 312-20.

[4] Tempfer and Traweger, Front Physiol. 2015 Nov 18;6:330.

[5] Efimenko et al., Tsitologiia. 52, 144-54

[6] Komter et al., Advanced Drug Delivery Reviews 146 (2019), 170-189

## CONTACT

judit.schachinger@pmu.ac.at

## Pro- and antiangiogenic effects of human tendon cells depend on oxygen availability

Judit Schachinger[1,2], Herbert Tempfer[1,2], Christine Lehner[1,2], Andreas Traweger[1,2]

[1]Institute of Tendon and Bone Regeneration, Paracelsus Medical University-Spinal Cord Injury & Tissue Regeneration Center Salzburg, 5020 Salzburg, Austria;; [2]Austrian Cluster for Tissue Regeneration, Vienna, Austria; Contact: judit.schachinger@pmu.ac.at

### Objective

Tendons are hierarchically organized connective tissues that anatomically link muscle to bone and enable efficient energy transmission from muscle to the skeleton [1,2]. Healthy tendons harbor few cells, are rich in extracellular matrix (ECM) and have a low blood vessel density [3]. Injured tendons, however, are characterized by an excessive deposition of ECM, an increase in cell number and blood vessel ingrowth. It is assumed that pro- and antiangiogenic factors are well balanced in healthy tendon, maintaining low vascularization, and that this balance is lost in overused or injured tendon. Various proangiogenic factors such as Vascular Endothelial Growth Factor (VEGF) have been shown to be upregulated after tendon injury, whereas angiostatic mechanisms in healthy tendon remain poorly understood. [4]. The aim of this work is to establish a defined in vitro model allowing to study pro- and antiangiogenic mechanisms exerted by tendon cells under physiologic and pathologic conditions.

### Methods

Human semitendinosus tendon derived stem/ progenitor cells (TDSPC) and human adipose tissue derived stem cells (ADSC) were cultured under normoxic (19% O2) and hypoxic conditions (5% O2). Cell supernatants were tested in a human umbilical vein endothelial cell (HUVEC) based tube formation assay, allowing to assess their impact on angiogenesis- related cellular mechanisms. ADSCs were used as a control group to validate the model, since they are known to induce angiogenesis [5]. By immunohistochemistry on cryosections of healthy human semintendinosus tendons, the expression of soluble VEGFR 1 and 2, were examined, two factors known to exert angiostatic mechanisms in avascular tissues like the cornea [6].

### Results

TDSPCs conditioned medium (CM) generated at 5% O2 significantly decreased the number of formed tubes compared to ADSC CM (5% O2) and TDSPCs CM 19% O2 ($p=0.005$).
Immunofluorescence analysis showed both sVEGFR1 and sVEGFR2 are expressed in all tendons analyzed ($n=3$), both in the tendon cells and in the extracellular matrix.

### Conclusions

With this work we show that cultured tendon cells exert antiangiogenic mechanisms mediated by soluble factors. In future work, these factors will be further examined by mass spectrometry and mRNA sequencing. Moreover, potential changes of the balance between pro- and antiangiogenic factors will be examined by in vitro and ex vivo model of tendon disease. Moreover, for the first time we show the expression of sVEGF receptors in tendon cells, proteins crucial for homeostasis in ocular tissues like the cornea.

### References

1. Kirkendal et al., Scand J Med Sci Sports; 1997. 7: 62-6.
2. Pufe et al., Scand J Med Sci Sports; 2005. 15: 211-22
3. Kannus. P. Scand J Med Sci Sports; 2000 10: 312-20.
4. Tempfer and Traweger, Front Physiol. 2015 Nov 18;6:330.
5. Efimenko et al., Tsitologiia; 2015. 52, 144-54.
6. Kornter et al., Advanced Drug Delivery Reviews 146 (2019), 170-189

# Effects of an automatic oxygen system during walking in hypoxemic patients with severe COPD – a randomized controlled double-blind cross-over trial

T. Schneeberger[1,2], I. Jarosch[1,2], D. Leitl[1,2], R.Gloeckl[1,2], W. Hitzl[3,4,5], C.J. Dennis[6], T. Geyer[2], C-P. Criée[7], K. Kenn[1,2], AR. Koczulla[1,2,8]

[1]Institute for Pulmonary Rehabilitation Research, Schoen Klinik Berchtesgadener Land, Schoenau am Koenigssee, Germany
[2]Department of Pulmonary Rehabilitation, Philipps - University of Marburg, Marburg, German Center for Lung Research (DZL), Germany
[3]Paracelsus Medical University Salzburg, Research Office (Biostatistics), Salzburg, Austria
[4]Paracelsus Medical University Salzburg, Department of Ophthalmology and Optometry, Salzburg, Austria
[5]Paracelsus Medical University Salzburg, Research Program Experimental Ophthalmology and Glaucoma Research, Salzburg, Austria
[6]The University of Sydney, Faculty of Medicine and Health, Sydney, Australia
[7]Department of Sleep and Respiratory Medicine, Evangelical Hospital Goettingen-Weende, Bovenden, Germany
[8]Teaching hospital, Paracelsus Medical University, Salzburg, Austria

## Background

Hypoxemia during exercise is observed in people with COPD leading to treatment with supplemental oxygen ($O_2$) therapy. Usually, supplemental $O_2$ is delivered as a constant flow which might result in reduced oxygen saturation ($SpO_2$) during various $O_2$-demanding activities (e.g. walking). An automatic oxygen system (e.g. FreeO$_2$, OxyNov) automatically titrates $O_2$-flow to maintain patient $SpO_2$ to a predefined $SpO_2$-target. There is some evidence that automatic $O_2$-flows can be beneficial in comparison to a constant $O_2$-flow (standardized 2L/min[1] or resting flow-rate +1L/min[2]). However, it is unknown if an automatic oxygen system, with an $SpO_2$-target setting of 92%, compared to constant $O_2$-flows titrated for exercise as per the guidelines for oxygen therapy is beneficial. Further, it is unclear if there is an effect on exercising partial pressure of carbon dioxide ($PCO_2$) from the high $O_2$-flows (0 – 20L/min) possible with an automatic oxygen system.

## Objective

To investigate the effects of an automatic $O_2$-flow compared to a titrated constant $O_2$-flow (prescribed according to guidelines) on walking capacity in people with COPD.

## Methods

Fifty participants with COPD ($PO_2$<55mmHg at rest or during exercise) completed this prospective randomized controlled double-blind cross over trial (ClinicalTrials.gov:NCT03803384). Every participant performed, with a break of 24h between, 2 x Endurance Shuttle Walk Tests (ESWT) at 85% of max. walking pace with: (A) constant-$O_2$ ($ESWT_{constant}$) and (B) automatic $O_2$ ($SpO_2$-target=92%) ($ESWT_{automatic}$). Primary outcome was walking endurance time while secondary measures of $SpO_2$, heart rate (HR) and transcutaneous $PCO_2$ ($TcPCO_2$) were compared at isotime (end of shortest ESWT). Before and immediately at ESWT-termination blood gases were obtained and dyspnea rated via Borg-scale.

Lenoir T. et al. Respiratory care 2013; 61(11):1491-1496. [2]Vorstenbosch I., et al., Thorax 2013; 68(3):268-69

## Results

**Table 1. Baseline Characteristics**

| Parameters | COPD (n=50) |
|---|---|
| **Age**, yrs | 65 (8) |
| **sex** (male/female) | 27/23 |
| **$FEV_1$**, % pred. | 39.5 (8) |
| **TLC** % pred. | 137 (21.5) |
| **$PO_2$**, mmHg (rest, room air) | 54.7 (8) |
| **$PCO_2$**, mmHg (rest, room air) | 43.9 (8) |
| **LTOT use**, months | 53 (49) |

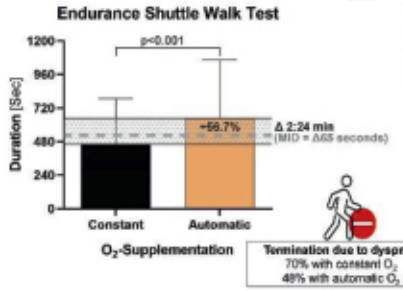


**Figure 1. Walking capacity during the endurance shuttle walk test. Dashed line=minimal important difference (MID) of an ESWT.**

**Termination due to dyspnea**
70% with constant $O_2$
48% with automatic $O_2$

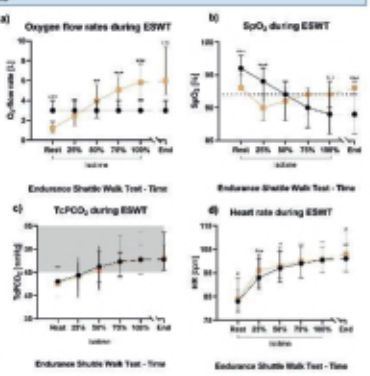


**Figure 2. a) Oxygen flow rates, b) oxygen saturation c) transcutaneous $PCO_2$ and d) heart rate during the endurance shuttle walk test.**

**Table 2. $PCO_2$ at end of endurance shuttle walk test**

| $PCO_2$ post ESWT, mmHg | | |
|---|---|---|
| constant | automatic | p-value |
| 50.5 (47, 54) | 50.5 (47, 55) | 0.41 |

## Conclusion

In hypoxemic patients with severe COPD the use of automatic $O_2$-flows to maintain an $SpO_2$ of 92% during exercise leads to improvements in walking endurance time, $SpO_2$ and dyspnea by a significant and clinically relevant amount. Also, despite higher $O_2$-flows with the automatic system, $PCO_2$ was not different between systems.

## Effects of an automatic oxygen system during walking in hypoxemic patients with severe COPD – a randomized controlled double-blind cross over trial

Tessa Schneeberger[1,2], Inga Jarosch[1,2], Daniela Leitl[1,2], Rainer Gloeckl[1,2], Wolfgang Hitzl[3,4,5], Clancy Dennis[6], Tatjana Geyer[1], Carl-Peter Criée[7], Klaus Kenn[1,2], Andreas Rembert Koczulla[1,2,8]

[1]Department of Pulmonary Rehabilitation, Philipps - University of Marburg, Marburg, German Center for Lung Research (DZL), Germany; [2]Institute for Pulmonary Rehabilitation Research, Schoen Klinik Berchtesgadener Land, Schoenau am Koenigssee, Germany; [3]Research Office (Biostatistics), Paracelsus Medical University, Salzburg, Austria; [4]Department of Ophthalmology and Optometry, Paracelsus Medical University, Salzburg, Austria; [5]Research Program Experimental Ophthalmology and Glaucoma Research, Paracelsus Medical University, Salzburg, Austria; [6]The University of Sydney, Faculty of medicine and health science, Sydney, Australia; [7]Department of Sleep and Respiratory Medicine, Evangelical Hospital Goettingen-Weende, Bovenden, Germany; [8]Teaching hospital, Paracelsus Medical University, Salzburg, Austria; Contact: TSchneeberger@schoen-klinik.de

### Objective

Hypoxemia during exercise is observed in people with COPD leading to treatment with supplemental oxygen ($O_2$) therapy. Usually, supplemental $O_2$ is delivered as a constant flow which might result in reduced oxygen saturation ($SpO_2$) during various $O_2$-demanding activities (e.g. walking). An automatic oxygen system (e.g. Free$O_2$, OxyNov) automatically titrates $O_2$-flow to maintain patient $SpO_2$ to a predefined $SpO_2$-target. There is some evidence that automatic $O_2$-flows can be beneficial in comparison to a constant $O_2$-flow (standardized 2L/min[1] or resting flow-rate +1L/min[2]). However, it is unknown if an automatic oxygen system, with an $SpO_2$-target setting of 92%, compared to constant $O_2$-flows titrated for exercise as per the guidelines for oxygen therapy is beneficial. Further, it is unclear if there is an effect on exercising partial pressure of carbon dioxide ($PCO_2$) from the high $O_2$-flows (0 – 20L/min) possible with an automatic oxygen system. Therefore, the primary aim of this study was to investigate the effects of an automatic $O_2$-flow compared to a titrated constant $O_2$-flow (prescribed according to guidelines) on walking capacity in people with COPD.

### Methods

Fifty participants with COPD ($PO_2$<55mmHg rest or exercise) completed this prospective randomized controlled double-blind cross over trial (ClinicalTrials.gov:NCT03803384). Every participant performed, with a break of 24h between, 2 Endurance Shuttle Walk Tests (ESWT) at 85% of max. walking pace with: (A) constant-$O_2$ ($ESWT_{constant}$) and (B) automatic $O_2$ (SpO2-target=92%) ($ESWT_{automatic}$). Primary outcome was walking endurance time while secondary measures of $SpO_2$, transcutaneous $PCO_2$ [TcPCO2], respiratory-rate [RR], heart rate [HR] were compared at isotime (end of shortest ESWT). Before and immediately at ESWT-termination blood gases were obtained and dyspnea rated via Borg-scale.

### Results

Participants (65±8years, $FEV_1$ 30.5±8%pred., $PO_2$ 54.7±6mmHg, $PCO_2$ 43.9±6mmHg, mean prescribed constant $O_2$-flow during exercise 3.0 [3.0, 4.0]L/min; median [upper, lower limit]) walked significantly longer in $ESWT_{automatic}$ in comparison to $ESWT_{constant}$ (522 [277, 1200]s vs. 333 [214, 581]s, p<0.001). During $ESWT_{automatic}$, $SpO_{2isotime}$ was significantly higher (92 [90, 94]% vs. 89 [86, 93]%, p<0.001) whereas $TcPCO_{2isotime}$, $RR_{isotime}$ and $HR_{isotime}$ were comparable between tests. At ESWT end, $PO_2$ ($ESWT_{automatic}$ 71 [64, 76]mmHg vs. $ESWT_{constant}$ 61 [55, 64]mmHg) and dyspnea significantly (each p<0.001) differed in favor of the automatic $O_2$-flow system while $PCO_2$ was comparable. The average automatic $O_2$-flow was 4.5 [3.2, 6.1]]L/min.

### Conclusions

In hypoxemic patients with severe COPD the use of automatic $O_2$-flows to maintain an $SpO_2$ of 92% during exercise leads to improvements in walking endurance time, $SpO_2$, $PO_2$ and dyspnea by a significant and clinically relevant amount. Also, despite higher $O_2$-flows with the automatic system, $PCO_2$ was not different between systems.

### References

1. Lellouche, F., et al., Respiratory care, 2016. 61(11):1456-1464.
2. Vivodtzev, I., et al., Thorax, 2019. 74(3):298-301.


MiA – Mentalisierung im Alter
Klinikum Nürnberg
Einleitung
Methode
Erste Zwischenergebnisse
Mentalisierung
Trauma und Mentalisierung
Material
Diskussion
Ausblick
Trauma

## MiA - Mentalisierung im Alter – Erste Ergebnisse einer laufenden Studie

Sophia Schneider[1,2], Christina Wunner[1,2], Mark Stemmler[2], Christiane Waller[1]

[1]Klinik für Psychosomatische Medizin und Psychotherapie, Klinikum Nürnberg; [2]Lehrstuhl für psychologische Diagnostik, Methodenlehre und Rechtspsychologie, Friedrich-Alexander Universität (FAU) Erlangen-Nürnberg; Contact: sophia.schneider2@klinikum-nuernberg.de

### Objective

Mentalisieren ist das Vergegenwärtigen eigener und fremder mentaler Zustände. Es spielt sowohl bei der Affektregulation als auch in sozialen Interaktionen eine bedeutsame Rolle. Die Fähigkeit zu Mentalisieren entwickelt sich in frühen Bindungsbeziehungen und kann durch traumatische Erfahrungen eingeschränkt werden.
Die vorliegende Studie behandelt die folgenden Fragestellungen: Wie ist die Mentalisierungsfähigkeit bei älteren Menschen ausgeprägt? Welchen Einfluss haben traumatische Erfahrungen auf die Mentalisierungsfähigkeit? Findet eine transgenerationale Weitergabe der Fähigkeit zu Mentalisieren statt in Abhängigkeit von der individuellen Stress- und Traumalast?

### Methods

Patient*innen (n=24 Alter: 60-89; M=79,8; SD=6,9) der Geriatrischen Tagesklinik (GTK) des Klinikums Nürnberg sowie jeweils ein Kind (n= 4; Alter: 51-64 M=56,0; SD=5,7) der Patientinnen füllten Fragebögen zur Erfassung von Mentalisierungsfähigkeit, traumatischen Erlebnissen, Angst, Depressivität und sozialer Unterstützung aus. Zudem wurde die Mentalisierungsfähigkeit mithilfe des Erwachsenenbindungsinterviews (Adult Attachment Interview; AAI) erfasst, welches anhand der Reflexiven Kompetenz-Skala ausgewertet wurde.

### Results

Die mittels AAI erhobene Mentalisierungsfähigkeit der Patient*innen war relativ niedrig.
Die selbst eingeschätzte und die im AAI erhobene Mentalisierungsfähigkeit korrelierten nicht signifikant.
Es zeigte sich ein signifikant positiver Zusammenhang zwischen Reflexionsfunktion und der posttraumatischen Symptomatik der Patient*innen.
Zwischen der Anzahl traumatischer Erlebnisse in der Biographie der Patient*innen sowie dem Ausmaß der Misshandlungs- und Vernachlässigungserfahrungen während der Kindheit und ihrer Mentalisierungsfähigkeit zeigte sich kein signifikanter Zusammenhang.
Die Daten der Kinder der Patientinnen konnten aufgrund der bisher geringen Stichprobengröße noch nicht ausgewertet werden.

### Conclusions

Die relativ niedrige im AAI gemessene Mentalisierungsfähigkeit der Patient*innen passt zu den Ergebnissen zahlreicher Studien zur Entwicklung des angrenzenden Theory of Mind-Konzeptes im Altersverlauf.
Der positive Zusammenhang zwischen posttraumatischen Symptomen und der Mentalisierungsfähigkeit steht allerdings im Widerspruch zu bisherigen Erkenntnissen zum Zusammenhang von Trauma und Mentalisierung.
Es ist zu beachten, dass die vorliegenden Ergebnisse auf einer kleinen vorläufigen Stichprobe beruhen. Weitreichende Schlussfolgerungen können somit zum aktuellen Zeitpunkt nicht gezogen werden.

### References

1. Fonagy, P., Target, M., Steele, H., & Steele, M. (1998). Reflective-functioning manual, version 5.0, for application to adult attachment interviews. London: University College London, 161-162.

# Augmentning tendon repair with SPARC

Bettina Schwemberger[1*], Severin Bittner[2*], Renate Gehwolf[1], Andrea Wagner[1], Andreas Traweger[1]

[1]Paracelsus Medical University Institute for Tendon and Bone Regeneration, Paracelsus Medical University, Spinal Cord Injury & Tissue Regeneration Center Salzburg, Austria
[2]Salzburg University of Applied Sciences, Campus Urstein, Puch, Austria
* contributed equally to this work

Andrea.Wagner@pmu.ac.at

Acknowledgements: This project is supported by the PMU-FFF (E-18/28/151-WAT)

PARACELSUS MEDIZINISCHE PRIVATUNIVERSITÄT

## INTRODUCTION

Among the most common musculoskeletal diseases are acute and chronic damage of tendons and ligaments. Due to their low regenerative capacity the treatment of these diseases proves to be difficult. Our recent studies of Achilles tendons of SPARC knockout mice showed a significant tendon phenotype with smaller tendon diameter and a disturbed collagen ratio as well as an increased amount of lipid droplets in the tenocytes [1,2]. SPARC is a matricellular protein with a bulk of functions not only in tendons. Amongst others it influences interactions between cells and the ECM as there are signal transduction processes, adhesion, morphology, proliferation, differentiation, migration and cell survival. The Secreted Protein Acidic and Rich in Cysteine (SPARC) is necessary for tendon maturation and homeostasis.

The overall objective of this ongoing study is to understand/describe the role of the matricellular protein SPARC in tendon healing.

## Graphical abstract

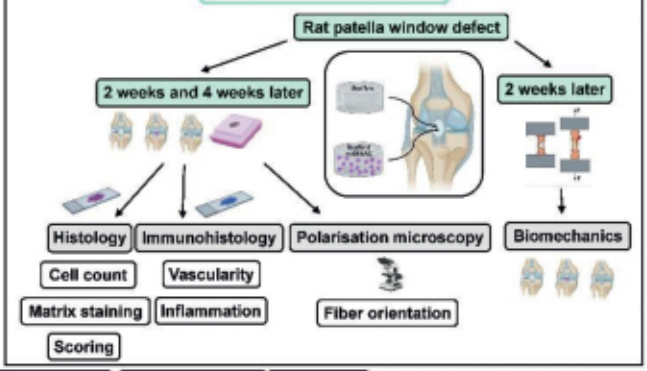


## PROJECT AIMS

1) Finding the optimal dose of rSPARC for tendon healing in a rat patella tendon window defect model treated with different doses of rSPARC protein (0, 0.1µg, 1µg and 5µg in Tisseel as vehicle). After a regeneration time of 2-8 weeks tendon samples will be analysed by histological examinations

2) The optimized dose identified in aim 1 will be used to investigate how the application of rSPARC will influence the functional outcome of tendon healing. Tendon repair processes will be analysed 2, 4, 6, and 8 weeks post-surgery for structural characteristics (e.g. histological examination, microCT, polarization microscopy), functionality (gait analysis and uniaxial tensile testings), and by gene expression analysis.

## Histology — Cell count

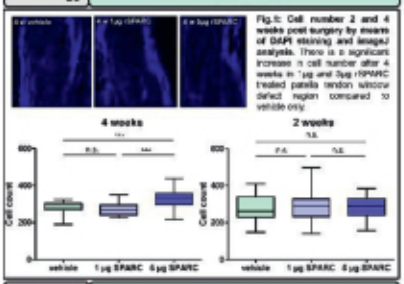


Fig.1: Cell number 2 and 4 weeks post surgery by means of DAPI staining and ImageJ analysis. There is a significant increase in cell number after 4 weeks in 1µg and 5µg rSPARC treated patella tendon window defect region compared to vehicle only.

## Immunohistology — Vascularity

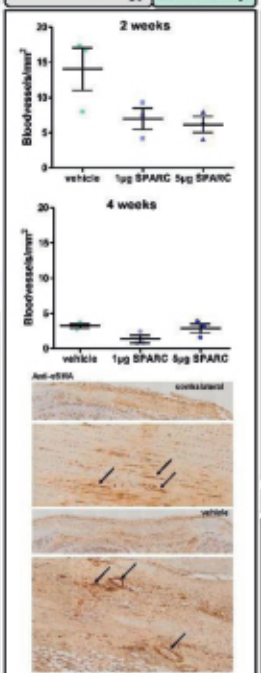


Fig.4: Anti αSMA staining for blood vessel counting. No significant differences in the number of blood vessels between the treatment groups was detected. Only a slight shift to lesser blood vessels was observed in the rSPARC treated groups. Arrows show blood vessels

## Polarisation microscopy — Fiber orientation

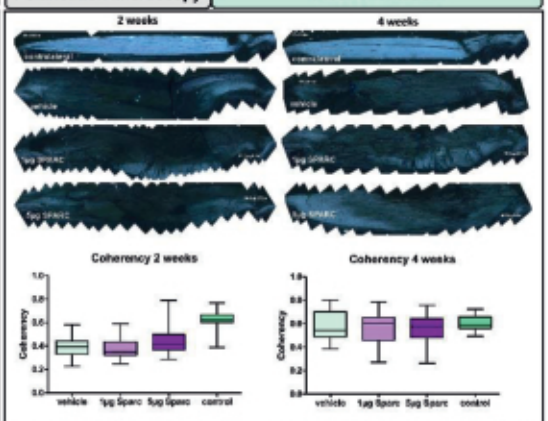


Fig.5: Fiber orientation represented by coherency. To define the fiber orientation we used the coherency as measure of the fiber parallelism. Coherency of mature tendon tissue is about 0.6 (see control). There are no significant differences in the coherency between the treatment groups detectable. But the parallel oriented collagen content in the defect region seemed to be more after 4 weeks post surgery in all treatment groups detected with polarised light.

## Histology — Matrix staining

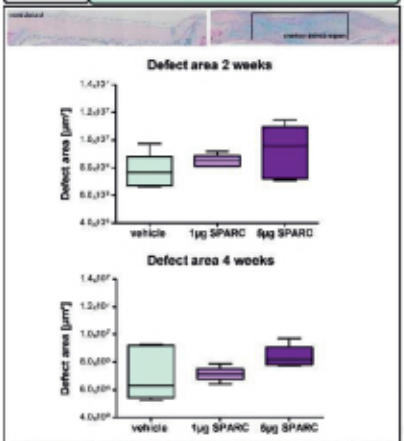


Fig.2: Matrix staining with Alcianblue to determine the defect area 2 and 4 weeks post surgery. There were no significant differences in the dimensions of the defect area between the treatment groups. In the 1µg rSPARC group after 2 weeks the variance of the area seems to be lesser.

## Biomechanics

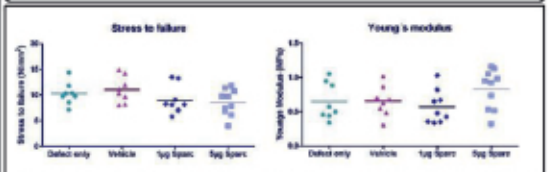


Fig.7: Biomechanics of the rat patella tendon 2 weeks post surgery. For the measurements we developed a new clamping tool for the biomechanical testing with the Zwick testing device. The results of the biomechanical testing showed no significant differences between the treatment groups neither in stress to failure nor in Young's modulus.

## Histology — Scoring

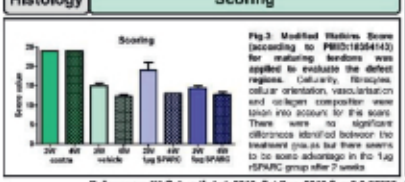


Fig.3: Modified Watkins Score (according to PMID:16364143) for maturing tendons was applied to evaluate the defect regions. Cellularity, fibroplasia, cellular orientation, vascularisation and collagen composition were taken into account for the score. There were no significant differences identified between the treatment groups but there seems to be some advantage in the 1µg rSPARC group after 2 weeks

## Immunohistology — Inflammation

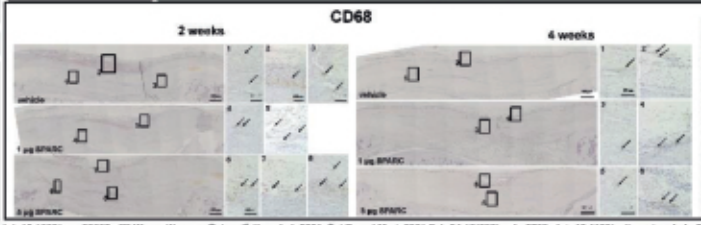


Fig.6: Immunohistological staining for the macrophage marker CD68. 2 weeks post surgery we found CD68 positive cells scattered nearly in the entire defect region. 4 weeks post surgery there were only some isolated macrophages in the center of the defect region detectable. Arrows show CD68 positive cells.

References: [1] Gehwolf et al. 2016, Sci Rep. 2016 Sep 2;6:32635. doi: 10.1038/srep32635. [2] Wang, Wagner, Gehwolf, Yan et al. 2021, Sci Transl Med. 2021 Feb 24;13(582):eabe5738. doi: 10.1126/scitranslmed.abe5738.

## Augmenting tendon repair with SPARC

Bettina Schwemberger[1], Severin Bittner[2], Renate Gehwolf[1], Andrea Wagner[1], Andreas Traweger[1]

[1]Paracelsus Medical University, Salzburg, Austria; [2]Salzburg University of Applied Sciences, Campus Urstein, Austria; Contact: b.schwemberger@pmu.ac.at

### Objective

Among the most common musculoskeletal diseases are acute and chronic damages of tendons and ligaments. Due to their low regenerative capacity the treatment of these diseases proves to be difficult. Our recent studies on Achilles tendons of Sparc knockout mice showed a significant tendon phenotype with smaller tendon diameter and a disturbed collagen ratio as well as an increased amount of lipid droplets in the tenocytes [1,2]. SPARC (Secreted Protein Acidic and Rich in Cysteine) is a matricellular protein with multiple functions not only in tendons. Amongst others, it influences interactions between cells and the matrix, signal transduction processes, cell adhesion, morphology, proliferation, differentiation, migration and cell survival, and it is necessary for tendon maturation and homeostasis.The overall objective of this ongoing study is to understand/describe the role of the matricellular protein SPARC in tendon healing.

### Methods

Twelve weeks old female Spargue dawley rats received a 2mm needle punch in the center of the patella tendon. The punch was filled with a Tisseel® fibrin clot as scaffold without and supplemented with 1$\mu$g and 5$\mu$g rSPARC protein (16 animals per group). A punch only group served as control. For histological examination 3 Patella tendons per group as well as their contralateral counterparts were fixed and embedded in paraffin 2 weeks post-surgery and 4 weeks post-surgery, respectively. For biomechanical testing 10 patella tendons per treatment group and the contralateral tendons were tested 2 weeks post-surgery. To determine the cell number in the defect areas a DAPI staining and for detection of the matrix of the defect region and for determination of the modified Watkins score a Alcianblue staining was performed. Immunohistological examination was done with anti αSMA (blood vessel staining) and anti CD68 (macrophage staining). Polarisation microscopy for analysis of collagen fiber orientation was done with unstained specimens

### Results

In our study we found an increased cellularity after treatment with rSPARC (1$\mu$g and 5$\mu$g) in rat patella tendon window defect 2 weeks post-surgery. Scoring of histological sections showed a tendency for an alignment of collagen fibers in the defect area similar to healthy tendon tissue. Two weeks post-surgery there are less blood vessels in the defect area when rSPARC was applied. No influence of rSPARC on the defect area size was observed and significant differences in the coherency of the collagen fibers were indeterminable. The biomechanical testing showed no functional improvement after rSPARC application.

### Conclusions

In 2 weeks post-surgery groups we find a positive effect in tendon repair by application of rSPARC protein, but this effect disappeared after 4 weeks. Therefore, in further studies we will test whether repetitive rSPARC protein applications during the regeneration process might have better effects.

### Acknowledgements

This project was supported by the PMU-FFF grant #E-18/28/151-WAT

### References

1. Gehwolf et al. 2016, Sci Rep. 2016 Sep 2;6:32635. doi: 10.1038/srep32635.
2. Wang, Wagner, Gehwolf, Yan et al. 2021, Sci Transl Med. 2021 Feb 24;13(582):eabe5738. doi: 10.1126/scitranslmed.abe5738.

# *IN VITRO* EVALUATION OF A NANOPARTICLE-BASED mRNA DELIVERY SYSTEM FOR TENDON TISSUE

Bettina Schwemberger[1], Lisa Sturm[1], Jaap Rip[2], Christian Plank[3], Sibylle Grad[4], Andreas Traweger[1]

[1] Institute of Tendon and Bone Regeneration, Spinal Cord Injury and Tissue Regeneration Centre Salzburg, Paracelsus Medical University, Salzburg, Austria
[2] 2BMed Therapeutics B.V. Drienerlolaan 5 - ZH252, 7522NB Enschede, The Netherlands
[3] ETHRIS GmbH, Semmelweisstrasse 3, 82152 Planegg, Germany
[4] Regenerative Orthopaedics, AO Research Institute Davos, Davos Platz, Switzerland

PARACELSUS MEDIZINISCHE PRIVATUNIVERSITÄT
UNIVERSITÄT SALZBURG

## INTRODUCTION

Osteoarthritis (OA) is the most common chronic joint condition, affecting >40 million Europeans. In 2017, the first OA gene therapy was approved and several more are in clinical development. All, however, use unsatisfactory (viral) delivery approaches, which result in suboptimal transfection in joint tissues. The aim of this Eurostars project is to develop a novel safe (non-viral) and effective mRNA therapy for OA, using unique in-joint injectable polymer-based nanoparticle carriers. This therapy aims at suppressing inflammation and support cartilage and tendon tissue regeneration. The present work shows the transfection optimization of tendon tissue using tdTomato mRNA.

## EXPERIMENTAL SETUP

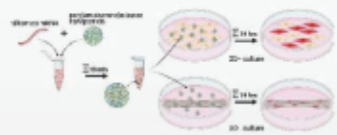

**Fig.1:** Poly(amidoamine)s-based nanoparticles (NPs) were complexed with tdTomato (tdTom) mRNA (2:50 w/w ratio). Increasing amounts of loaded NPs were used to determine the optimal mRNA delivery conditions for rat tendon derived stem/progenitor cells (rTDSPCs) in 2D culture, 3D tendon-like constructs and rat tail tendon fascicles. Transfection efficiency was analyzed using fluorescence microscopy and flow cytometry. Metabolic activity was determined using an AlamarBlue Assay.

## mRNA DELIVERY TO rTDSPCs (2D CULTURE)

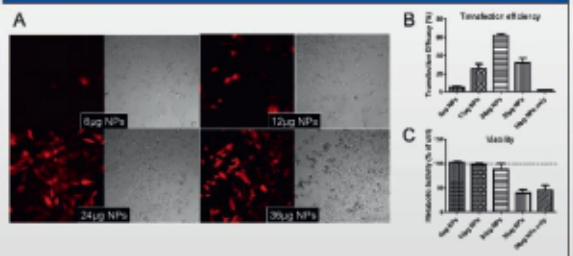


**Fig.2:** 2D culture of rTDSPCs showed a dose-dependent increase of transfection efficiency (seen with fluorescence microscopy **(A)** and flow cytometry **(B)**), reaching the highest efficiency (61.8 %) with 24 µg of loaded NPs. An amount of 36 µg NPs displayed cytotoxic effects on rTDSPCs, which can be seen through a change in cell morphology **(A)** and a decrease in metabolic activity to 39.4 % **(C)**.

## mRNA DELIVERY TO 3D TENDON-LIKE CONSTRUCTS

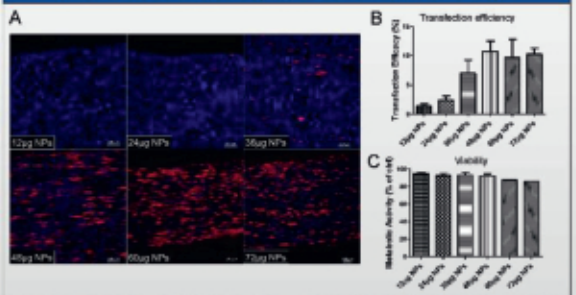


**Fig.3:** Treatment of 3D tendon-like constructs also revealed a dose-dependent increase in transfection rate, without significantly affecting cell viability. Optimal NP amount was between 48 to 60 µg. Unfortunately, NPs did not penetrate into deeper layers of the tissue, explaining the low transfection efficiency (%) measured by flow cytometry after digestion **(C)**.

## „FREE-FLOATING" RAT TAIL TENDON FASCICLES AS A PRO-INFLAMMATORY ORGANOTYPICAL MODEL

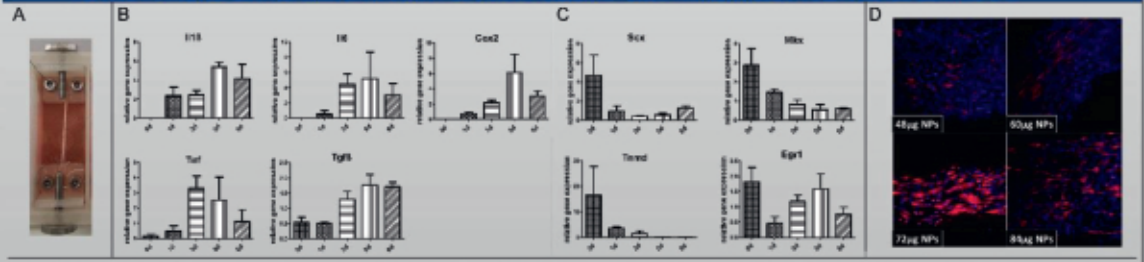


**Fig.4: (A)** Customized 3D-printed chambers were used to clamp and culture rat tail tendon (rTT) fascicles over a time period of 6 days without any mechanical load ("free floating"). **(B)** This *ex-vivo* model is suitable as an inflammatory organotypical model without the need of an extrinsic inflammatory stimulus, as the cultured fascicles showed an upregulation of pro-inflammatory cytokines (i.e. *Il1ß, Il6, Cox2, Tnf, Tgfß*) with the highest relative gene expression on day 5. **(C)** Tendon-related markers, like Scx, Mkx and Tnmd, showed a time-dependent decrease in expression, while Egr1 expression increased during culture with a decline on day 6. **(D)** rTT fascicles were transfected with tdTom loaded NPs on day 5. Again, there was a dose-dependent increase of tdTom positive cells, with an optimal transfection rate using 72 µg NPs. Again, only cells on the tissue surface were positive for tdTom.

## CONCLUSION

The poly(amidoamine)s-based NPs proved successful for mRNA delivery to tendon cells and tissue *in vitro*. With an increasing density of extracellular matrix (2D cell culture, 3D tendon-like constructs, rat tail tendon fascicles respectively), a higher amount of NPs needs to be applied to achieve acceptable transfection efficiencies. However, mRNA-loaded NPs do not penetrate into deeper tissue layers. "Free floating" rat tail tendon fascicles have been established as a promising pro-inflammatory organotypic culture model. Future experiments aim to demonstrate the anti-inflammatory and regenerative effects of therapeutic mRNAs (i.e. Il1RA, Il10 and Pdgfß) using this inflammatory *ex-vivo* model. Subsequently, the efficacy of the candidate mRNAs will be evaluated in an *in vivo* rat patellar tendon defect model.

This Eurostars project was funded by FFG – Project number 871708

# IN VITRO EVALUATION OF A NANOPARTICLE-BASED mRNA DELIVERY SYSTEM FOR TENDON TISSUE

Bettina Schwemberger[1], Lisa Sturm[1], Jaap Rip[2], Christian Plank[3], Sibylle Grad[4], Andreas Traweger[1]

[1]Institute of Tendon and Bone Regeneration, Spinal Cord Injury and Tissue Regeneration Centre Salzburg, Paracelsus Medical University, Salzburg, Austria; [2]20Med Therapeutics B.V. Drienerlolaan 5 - ZH252, 7522NB Enschede, The Netherlands; [3]ETHRIS GmbH, Semmelweisstrasse 3, 82152 Planegg, Germany; [4]Regenerative Orthopaedics, AO Research Institute Davos, Davos Platz, Switzerland; Contact: b.schwemberger@pmu.ac.at

## Objective

Osteoarthritis (OA) is the most common chronic joint condition, affecting >40 million Europeans. In 2017, the first OA gene therapy was approved and several more are in clinical development. The majority, however, use unsatisfactory (viral) delivery approaches, which result in suboptimal transfection in joint tissues. The aim of this Eurostars project is to develop a novel safe (non-viral) and effective mRNA therapy for OA. The present work shows the transfection optimization of tendon tissue with tdTomato mRNA.

## Methods

Poly(amidoamine)s-based nanoparticles (NPs) were complexed with tdTomato (tdTom) mRNA (2:50 w/w ratio). Increasing amounts of loaded NPs were used to determine the optimal mRNA delivery conditions for rat tendon derived stem/progenitor cells (rTDSPCs) in 2D culture, 3D tendon-like constructs and rat tail tendon fascicles. Transfection efficiency was analyzed using fluorescence microscopy and flow cytometry. Metabolic activity was determined using an AlamarBlue Assay.

## Results

2D culture of rTDSPCs showed a dose-dependent increase of transfection efficiency reaching the highest efficiency (61.8 %) using 24 µg loaded NPs, while an amount of 36 µg NPs displayed cytotoxic effects on rTDSPCs. 3D tendon-like constructs also showed a dose-dependent increase of tdTom positive cells (without significant effects on cell viability), with an optimal amount of mRNA-loaded NPs between 48 to 60 µg. To evaluate the efficiency of the NPs in an *ex vivo* tissue explant model, customized 3D-printed chambers were used to clamp and culture rat tail tendon (rTT) fascicles over a time period of 6 days without applying any mechanical load ("free floating"). This *ex vivo* model is known to mimic an inflammatory/degenerative state in tendon tissue without the need of an extrinsic inflammatory stimulus (e.g. recombinant Il1ß). As expected, cultured fascicles displayed an upregulation of pro-inflammatory cytokines (i.e. Il1ß, Il6, Cox2, Tnf, Tgfß) with the highest relative gene expression determined on day 5. Tendon-related markers, like Scx, Mkx and Tnmd, showed a time-dependent decrease in relative gene expression. rTT fascicles were then transfected with mRNA-tdTom loaded NPs on day 5. There was a dose-dependent increase in transfection, with an optimal dose of 72 µg NPs to achieve the best transfection rate. Unfortunately, NPs were not able to penetrate into deeper layers of the tissue (3D constructs and *ex vivo* culture), resulting in a transfection of cells on the tissue surface only.

## Conclusions

The poly(amidoamine)s-based NPs proved successful for mRNA delivery to tendon cells and tissue *in vitro*. However, with an increasing density of extracellular matrix (2D, 3D constructs, explanted tissue), a higher amount of NPs needed to be applied to achieve acceptable transfection rates. Further, only cells on the surface of the 3D construct or tendon tissue showed expression of the fluorescent reporter protein tdTom. Finally, "free floating" rat tail tendon fascicles have been established as a promising pro-inflammatory organotypic tissue explant model. Future experiments aim to prove the anti-inflammatory and regenerative effects of therapeutic mRNAs (i.e. Il1RA, Il10 and Pdgfß) using this inflammatory *ex vivo* model, with a subsequent *in vivo* study using a rat patellar tendon window defect model.

PARACELSUS
MEDIZINISCHE PRIVATUNIVERSITÄT

TECHNISCHE HOCHSCHULE NÜRNBERG
GEORG SIMON OHM

Kontakt: shijingjian55@126.com

Jingjian SHI

# Führt ein unbehandelter Diabetes mellitus Typ II zur Knorpeldegeneration? Untersuchungen *in situ* und im *in vitro* Arthrosemodell

**Jingjian Shi[1,2], Maria Kokozidou[1], Christian Werner[1], Clemens Gögele[1,3], Benjamin Kohl[4], Gundula Schulze-Tanzil[1]**

[1] Institut für Anatomie und Zellbiologie, Paracelsus Medizinische Privatuniversität, Nürnberg und Salzburg, Nürnberg, Deutschland
[2] Fakultät für Angewandte Chemie, Technische Hochschule Nürnberg Georg Simon Ohm, Nürnberg, Deutschland
[3] Fachbereich für Biowissenschaften, Paris Lodron Universität Salzburg, Salzburg, Österreich
[4] Klinik für Unfall- und Wiederherstellungschirurgie, Charité-Universitätsmedizin Berlin, Deutschland

## Fragestellung

Eine der häufigsten Begleiterkrankungen bei Osteoarthrose (OA), der häufigsten Gelenkerkrankung, stellt der Diabetes Mellitus Typ 2 (DMT2) dar. Dieser scheint an der Entstehung und Entwicklung einer OA beteiligt zu sein. Auf molekularer Ebene jedoch ist der genaue pathogenetische Zusammenhang zwischen OA und DMT2 nur unzureichend bekannt. In dieser Arbeit wird der Einfluss von DMT2 auf Knorpel durch Untersuchungen *in situ* im Kniegelenk und im *in vitro* Arthrosemodell beleuchtet.

## Material & Methoden

Organ- und Gelenkgewebe aus diabetischen Ratten (Zucker Diabetes Fatty [ZDF], fa/fa) und Kontrolltieren (fa/+) wurden histologisch aufgearbeitet **(Abb. 1-2)** und mit Score-Systemen histopathologisch beurteilt **(Abb. 1)**. In den *in vitro* Versuchen, wurden die Chondrozyten, die aus beiden Rattengruppen isoliert wurden, mit 10 ng/mL Tumor Nekrose Faktor (TNF)α für 3 Tage stimuliert um das entzündliche Milieu einer Arthrose nachzubilden. Die Vitalität (Lebend-Tot-Färbung, **Abb. 3**), Proliferation (CyQuant-) und metabolische Aktivität (Aamarblue-Assay, **Abb. 4**), Protein- sowie Genexpression (Immunmarkierungen und Real-time PCR, **Abb. 5-6**) wurden untersucht. Die Ergebnisse wurden mittels Grubbs-Test auf Ausreißer überprüft und mit t-Test und ANOVA (#/*p<0,05, ##/**p<0,01, ###/***p<0,001, ####/****p < 0,0001) analysiert.

## Ergebnisse & Diskussion

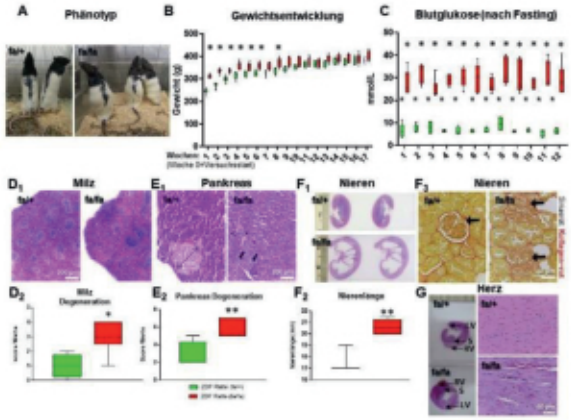


**Abbildung 1: ZDF Ratte als DMT2 Modell.** **A**: Im Vergleich zu den Kontrolltieren (fa/+) zeigen die diabetischen Tiere (fa/fa) einen adipösen Phänotyp. **B**: Gewichtsentwicklung: Die diabetischen Tiere (rot) sind schwerer als die Kontrollen (grün). Der Unterschied ist in den ersten Wochen signifikant. **C**: Die Blutglukosespiegel sind bei den diabetischen Tieren signifikant erhöht. $D_1$: Die diabetischen Tiere zeigen eine veränderte Milzhistologie (z.B. Disintegration der Follikelarchitektur). Die Veränderungen wurden mit einem Scoresystem ausgewertet ($D_2$). $E_1$, $E_2$: Das Pankreas der diabetischen Tiere weist Degenerationen auf (Doppelpfeil: Verkleinerung der Langerhans-Inseln und Pfeil: vakuoläre Degenerationen der Drüsenendstücke des exokrinen Teils). $F_1$, $F_2$, $F_3$: Es ist eine Nierendegeneration bei den Diabetikern erkennbar mit einer Schwellung und Zunahme an Kollagen in den Glomerula (Pfeil). **G**: Es ist eine Muskelhypertrophie und Kardiomyopathie des Herzens bei den diabetischen Tieren erkennbar mit Hyperämie, aufgelockerter Architektur der Kardiomyozyten und Fibroblastenzunahme. $D_1$, $E_1$, $F_1$, **G**: Hämatoxylin-Eosin-, **F3**: Sirusrot-Färbung. **G**: LV=linker Ventrikel, RV= rechter Ventrikel, S=Kammerseptum. Maßstab: 200 µm (D,E), 50 µm (F,G). ZDF, Zucker Diabetes Fatty.

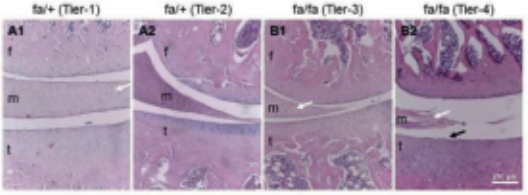


**Abbildung 2: Hämatoxylin-Eosin-Färbung der Gelenke.** (A1-2) Kniegelenk zweier nicht-diabetischer und (B1-2) diabetischer Tiere. f: Femur, m: Meniscus, t: Tibia. Gezeigt sind Frontalschnitte. Pfeile: schwarz – raue Knorpeloberfläche, weiss – Chondrozytenhypertrophie im Meniskus. Maßstab: 200 µm.

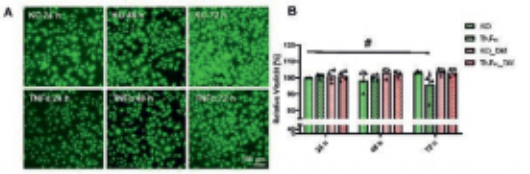


**Abbildung 3: Vitalität der Chondrozyten nach 24 h, 48 h und 72 h Stimulation mit TNFα.** Vitalität nicht diabetischer Chondrozyten (A, fa/+) und Auswertung mittels ImageJ Analyse (B). Grüne Zellen: vital, rote: tot. Maßstab: 100 µm. #p<0,05, one-way ANOVA.

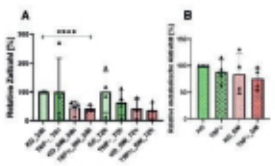


**Abbildung 4: Proliferation (24 und 72 h, A) und metabolische Aktivität (32 h, B) nach Stimulation mit TNFα in Chondrozyten der Kontroll- und diabetischen Tiere.** DM: Diabetes mellitus (fa/fa), KO: Kontrolle (fa/+), TNFα, Tumor Nekrose Faktor α.

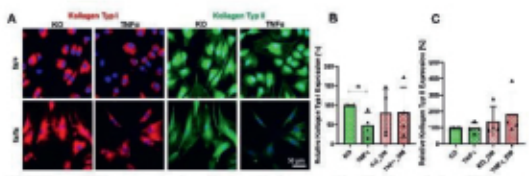


**Abbildung 5: Immunzytochemische Färbungen der Matrixproteine Kollagen Typ I und Typ II nach 24 h Kultur (A) und densitometrische Auswertung der Kollagen Typ I (B) und Typ II (C) Expression.** DM: Diabetes mellitus (fa/fa), KO: Kontrolle (fa/+), TNFα, Tumor Nekrose Faktor α. Rot: Kollagen Typ I, grün: Kollagen Typ II, blau: Zellkerne. Maßstab: 50 µm.

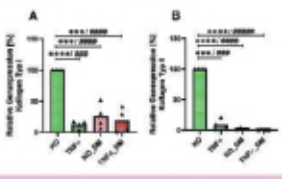


**Abbildung 6: Real-Time-PCR-Analyse der Genexpression von Kollagen Typ I (A) und Typ II (B) nach 48 h Stimulation mit TNFα.** DM: Diabetes mellitus (fa/fa), KO: Kontrolle (fa/+), TNFα, Tumor Nekrose Faktor α.

Im ZDF Modell wurden typische Folgeerscheinungen des DMT2 erfaßt. *In situ* konnte eine geringgradige Knorpeldegeneration bei einigen diabetischen Ratten gezeigt werden, wobei aber auch gelegentlich nicht-diabetische heterozygote Ratten, die die gleiche Protein-reiche Diät erhielten, Knorpelveränderungen im Kniegelenk aufwiesen. Kultivierte Chondrozyten von diabetischen Tieren zeigten tendenziell eine geringere Proliferation, reduzierte metabolische Aktivität und signifikant geringere Kollagen-Genexpression. In den Chondrozyten von Kontrolltieren verminderte TNFα nach 72 h signifikant die Vitalität sowie die Genexpression von Kollagen Typ I und Typ II. Chondrozyten diabetischer Spender zeigten dagegen tendenziell eine höhere Toleranz gegenüber TNFα. Aktuell werden *in situ* und *in vitro* Gelenke und Zellen weiterer Spendertiere untersucht und Zellkulturexperimente unter Hyperglykämie-Bedingungen durchgeführt.

Dieses Projekt wird durch die Förderung der Kerscher'schen-Stiftung ermöglicht.

## Führt ein unbehandelter Diabetes mellitus Typ II zur Knorpeldegeneration? Untersuchungen in situ und im in vitro Arthrosemodell

Jingjian Shi[1,2], Maria Kokozidou[1], Christian Werner[1], Clemens Gögele[1,3], Benjamin Kohl[4], Gundula Schulze-Tanzil[1]

[1]Institut für Anatomie und Zellbiologie, Paracelsus Medizinische Privatuniversität, Nürnberg; [2]Fakultät für Angewandte Chemie, Technische Hochschule Nürnberg Georg Simon Ohm, Nürnberg, Deutschland; [3]Fachbereich für Biowissenschaften, Paris Lodron Universität Salzburg, Salzburg, Österreich; [4]Klinik für Unfall- und Wiederherstellungschirurgie, Charité-Universitätsmedizin Berlin, Deutschland; Contact: shijingjian55@126.com

### Objective
Eine der häufigsten Begleiterkrankungen bei Osteoarthrose (OA), der häufigsten Gelenkerkrankung, stellt der Diabetes Mellitus Typ 2 (DMT2) dar. Dieser scheint an der Entstehung und Entwicklung einer OA beteiligt zu sein. Auf molekularer Ebene jedoch ist der genaue pathogenetische Zusammenhang zwischen OA und DMT2 nur unzureichend bekannt. In dieser Arbeit wird der Einfluss von DMT2 auf Knorpel durch Untersuchungen in situ im Kniegelenk und im in vitro Arthrosemodell beleuchtet.

### Methods
Organ- und Gelenkgewebe aus diabetischen Ratten (Zucker Diabetes Fatty [ZDF], fa/fa) und Kontrolltieren (fa/+) wurden histologisch aufgearbeitet (und mit Score-Systemen histopathologisch beurteilt. In den in vitro Versuchen, wurden die Chondrozyten, die aus beiden Rattengruppen isoliert wurden, mit 10 ng/mL Tumor Nekrose Faktor (TNF)α für 3 Tage stimuliert um das entzündliche Milieu einer Arthrose nachzubilden. Die Vitalität (Lebend-Tot-Färbung), Proliferation (CyQuant-) und metabolische Aktivität (Aamarblue-Assay), Protein- sowie Genexpression (Immunmarkierungen und Real-time PCR) wurden untersucht. Die Ergebnisse wurden mittels Grubbs-Test auf Ausreißer überprüft und mit t-Test und ANOVA (#/*$p<0,05$, ##/**$p<0,01$, ###/***$p<0,001$, ####/****$p < 0,0001$) analysiert.

### Results
In situ konnte bei der Untersuchung der Organe eine Nephropathie, Kardiomyopathie aber auch Veränderungen der Milzarchitektur im Rahmen des Diabetes bestätigt werden. In situ war auch eine geringgradige Knorpeldegeneration bei diabetischen Ratten aber auch einigen Kontrolltieren erkennbar. In vitro konnte TNFα die Vitalität der Chondrozyten tendenziell unterdrücken, die Proliferationsrate signifikant erniedrigen und die Genexpression von Kollagen Typ I und Typ II signifikant hemmen. Chondrozyten diabetischer Spender zeigten eine höhere Toleranz im Hinblick auf Vitalität und Proliferation zur TNFα Exposition und Hyperglykämie.

### Conclusions
Im ZDF Modell wurden typische Folgeerscheinungen des DMT2 erfaßt. In situ konnte eine geringgradige Knorpeldegeneration bei einigen diabetischen Ratten gezeigt werden, wobei aber auch gelegentlich nicht-diabetische heterozygote Ratten, die die gleiche Protein-reiche Diät erhielten, Knorpelveränderungen im Kniegelenk aufwiesen. In vitro können Unterschiede zwischen Chondrozyten diabetischer Spender im Vergleich zu den Kontrollen dargestellt werden. Aktuell werden in situ und in vitro Gelenke und Zellen weiterer Spendertiere untersucht und Zellkulturexperimente unter Hyperglykämie-Bedingungen durchgeführt.

### References
1. none

PARACELSUS
MEDIZINISCHE PRIVATUNIVERSITÄT

Klinikum Nürnberg
wir sind für Sie da.

Contact: sandeep.silawal@pmu.ac.at

Science Get Together 2021
Nuremberg, Germany

# Possible Interrelation between Complement and Prolactin Hormone Systems in Chondrocytes in Perspective of Osteoarthritis Pathogenesis

Sandeep Silawal [1], Miriam Wagner [1,3], Dominik Roth [1,3], Thomas Bertsch [2], Silke Schwarz [1], Maximilian Willauschus [1,4], Markus Geßlein [4], Jakob Triebel [2,#], Gundula Schulze-Tanzil [1,#]

1 Institute of Anatomy and Cell Biology, Paracelsus Medical University, Nuremberg, Prof. Ernst Nathan Str. 1, 90419 Nuremberg, Germany
2 Institute for Clinical Chemistry, Laboratory Medicine and Transfusion Medicine, Paracelsus Medical University, Prof. Ernst Nathan Str. 1, 90419 Nuremberg, Germany
3 Faculty of Applied Chemistry, Nuremberg Institute of Technology Georg Simon Ohm, Prinzregentenufer 47, 90489 Nuremberg, Germany
4 Department of Orthopedics and Traumatology, Paracelsus Medical University, Nuremberg General Hospital, Breslauer Str. 201, 90471 Nuremberg, Germany
# shared senior authorship

## Introduction

Both increased activity of the complement system (CS) and the role of the pituitary hormone prolactin (PRL) are implicated in osteoarthritis (OA) pathogenesis. Besides, Cathepsin D (CatD) activity is increased in the context of OA and can not only exert proteolytic but also non-proteolytic effects on cells. For the first time, a possible crosstalk between two separate humoral systems: the complement and the PRL hormone systems in chondrocytes are examined together.

## Methods

Primary human articular chondrocytes (hAC) were stimulated with complement protein C5 (10 µg /ml), PRL (25 ng/ml), CatD (100 ng/ml) or anaphylatoxin C5a (25 ng/ml) for 24 h or 72 h, while unstimulated cells served as controls. In addition, co-stimulations of C5 or PRL with CatD were carried out under the same conditions. The influence of the stimulants on cell viability and/or cell proliferation (CyQUANT® NF Cell Proliferation Assay) of hAC, the chondrosarcoma cell line OUMS-27 and endothelial cells of the human umbilical cord vein (HUVEC) were investigated. Gene expression analysis of C5a receptor (C5aR1), C5, complement regulatory protein CD59, PRL, PRL receptor (PRLR) and CatD were performed using real-time PCR. C5aR1 protein expression was detected using immunofluorescence labeling. The images of the stained cells were finally analysed using ImageJ. GraphPad Prism (Version 8.1.4) was used for the statistical analyses.

## Results

The stimulation of the hAC showed no significant impairment of the cell viability (Fig. 1). C5, C5a and PRL induced cell growth in OUMS-27 and HUVEC, but not in chondrocytes (Fig. 2). CatD as well as C5 significantly reduced the gene expression of CatD, C5aR1, C5 and CD59 (Fig. 3). PRL+CatD suppressed C5 gene expression as PRL+/-CatD suppressed CD59 gene expression significantly. PRLR gene expression was likewise impaired by C5, C5a and PRL+CatD stimulation (Fig. 3). On the protein level, CatD as well as C5a decreased C5aR1 synthesis (Fig. 4) in comparison to the control group.

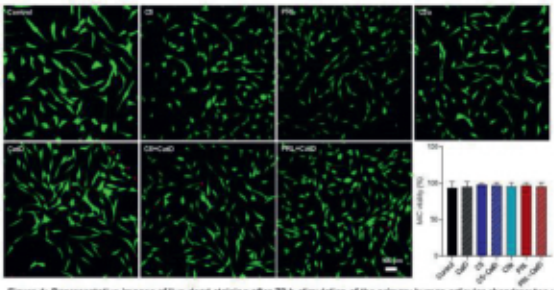

Figure 1: Representative images of live-dead staining after 72 h stimulation of the primary human articular chondrocytes with a graphical representation analyzed using ImageJ. Fluorescein diacetate (green: vital cells) and propidium iodide (red: dead cells). n = 3 independent experiments with chondrocytes from different donors. Mean with standard deviation. Values have been compared to the hypothetical value of 100% where all cells are vital after the experiment. Grubb's outlier test. Shapiro-Wilk test normal distribution. One sample t-test with significance in relation to control (*). Mixed effects analysis using post Hoc Tukey's multiple comparisons (*). Scale bar = 100 µm.

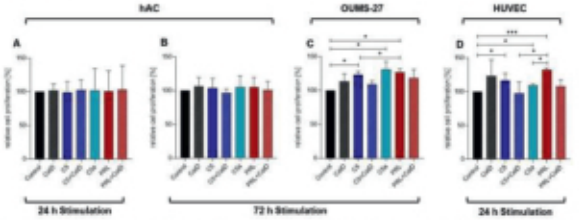


Figure 2: Relative cell proliferation in response to 24 h (A) and 72 h (B) stimulation of human articular chondrocytes, 72 h stimulation of OUMS-27 (C) and 24 h stimulation of HUVEC (D) assessed by CyQUANT® NF Cell Proliferation Assay. n = 3 (A), 5 (B), 3 (C), 5 (D) independent experiments with chondrocytes from different donors. Mean with standard deviation. Control has been normalized to 100. Grubb's outlier test. Shapiro-Wilk test normal distribution. One sample t-test with significance in relation to control (*). Mixed effects analysis using post Hoc Tukey's multiple comparisons (*). * = p ≤ 0.05; *** = p ≤ 0.001

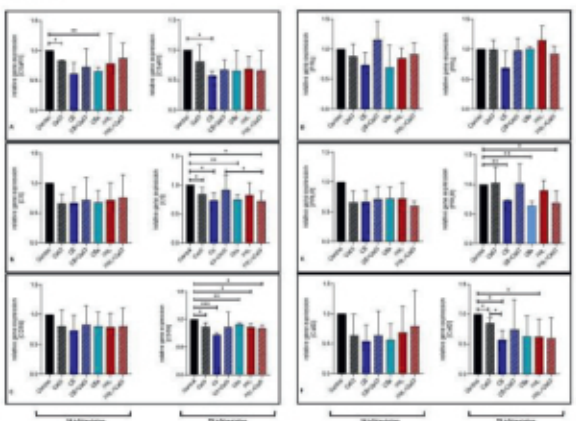

Figure 3: Relative chondrocytes gene expression of C5aR1 (A), C5 (B), CD59 (C), PRL (D), PRLR (E), CatD (F) after 24 h and 72 h of stimulation. n = 3 (24 h stimulation) and n = 5 (72 h stimulation) independent experiments with chondrocytes from different donors. Mean with standard deviation. Control has been normalized to 1. Grubb's outlier test. Shapiro-Wilk test normal distribution. One sample t-test with significance in relation to control (*). Mixed effects analysis using post Hoc Tukey's multiple comparisons (*). * = p ≤ 0.05; ** = p ≤ 0.01; *** = p ≤ 0.001.

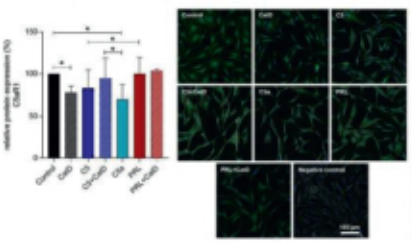

Figure 4: Chondrocytes protein expression of C5aR1 after 72 h of stimulation and negative control of the staining. n = 4 independent experiments with chondrocytes from different donors. A: Graphic representation of relative C5aR1 protein fluorescence intensity analyzed using ImageJ, mean with standard deviation. Control has been normalized to 100. Grubb's outlier test. Shapiro-Wilk test normal distribution. One sample t-test with significance in relation to control (*). Mixed effects analysis using post Hoc Tukey's multiple comparisons (*). * = p ≤ 0.05. B: representative images of chondrocytes immunolabeled with C5aR1 specific antibodies. Green (Alexa Fluor 488) = C5aR1, blue (DAPI) = cell nuclei, grey (Phalloidin Alexa 633) = Actin cytoskeleton. Scale bar = 100 µm.

## Conclusion

The significant suppression of the C5 gene expression under the influence of PRL+CatD and that of CD59 via PRL+/-CatD and conversely a suppression of the PRLR gene expression via C5 alone or C5a stimulation indicates an interrelation between the two mentioned systems. In addition, CatD and C5, in contrast to PRL, directly mediate a possible negative feedback of their own gene expression.

This study was supported by a research grant from the B. Braun foundation (BBST-D-16-00064)

## Possible Interrelation between Complement and Prolactin Hormone Systems in Chondrocytes in Perspective of Osteoarthritis Pathogenesis

Sandeep Silawal[1], Miriam Wagner[1,3], Dominik Roth[1,3], Thomas Bertsch[2], Silke Schwarz[1], Maximilian Willauschus[1,4], Markus Geßlein[4], Jakob Triebel[2], Gundula Schulze-Tanzil[1]

[1]Institute of Anatomy and Cell Biology, Paracelsus Medical University, Nuremberg, Prof. Ernst Nathan Str. 1, 90419 Nuremberg, Germany; [2]Institute for Clinical Chemistry, Laboratory Medicine and Transfusion Medicine, Paracelsus Medical University, Prof. Ernst Nathan Str. 1, 90419 Nuremberg, Germany; [3]Faculty of Applied Chemistry, Nuremberg Institute of Technology Georg Simon Ohm, Prinzregentenufer 47, 90489 Nuremberg, Germany; [4]Department of Orthopedics and Traumatology, Paracelsus Medical University, Nuremberg General Hospital, Breslauer Str. 201, 90471 Nuremberg, Germany; Contact: sandeep.silawal@pmu.ac.at

### Objective
Both increased activity of the complement system (CS) and the role of the pituitary hormone prolactin (PRL) are implicated in osteoarthritis (OA) pathogenesis. Besides, Cathepsin D (CatD) activity is increased in the context of OA and can not only exert proteolytic but also non-proteolytic effects on cells. For the first time, a possible crosstalk between two separate humoral systems: the complement and the PRL hormone systems in chondrocytes are examined together.

### Methods
Primary human articular chondrocytes (hAC) were stimulated with complement protein C5 (10 µg /ml), PRL (25 ng/ml), CatD (100 ng/ml) or anaphylatoxin C5a (25 ng/ml) for 24 h or 72 h, while unstimulated cells served as controls. In addition, co-stimulations of C5 or PRL with CatD were carried out under the same conditions. The influence of the stimulants on cell viability and/or cell proliferation (CyQUANT® NF Cell Proliferation Assay) of hAC, the chondrosarcoma cell line OUMS-27 and endothelial cells of the human umbilical cord vein (HUVEC) were investigated. Gene expression analysis of C5a receptor (C5aR1), C5, complement regulatory protein CD59, PRL, PRL receptor (PRLR) and CatD were performed using real-time PCR. C5aR1 protein expression was detected using immunofluorescence labeling. The images of the stained cells were finally analysed using ImageJ. GraphPad Prism (Version 8.1.4) was used for the statistical analyses.

### Results
The stimulation of the hAC showed no significant impairment of the cell viability. C5, C5a and PRL induced cell growth in OUMS-27 and HUVEC, but not in chondrocytes. CatD as well as C5 significantly reduced the gene expression of CatD, C5aR1, C5 and CD59. PRL+CatD suppressed C5 gene expression as PRL+/-CatD decreased CD59 gene expression significantly. PRLR gene expression was likewise impaired by C5, C5a and PRL+CatD stimulation. On the protein level, CatD as well as C5a suppressed C5aR1 synthesis in comparison to the control group.

### Conclusions
The significant suppression of the C5 gene expression under the influence of PRL+CatD and that of CD59 via PRL+/-CatD and conversely a suppression of the PRLR gene expression via C5 alone or C5a stimulation indicates an interrelation between the two mentioned systems. In addition, CatD and C5, in contrast to PRL, directly mediate a possible negative feedback of their own gene expression.

PARACELSUS
MEDIZINISCHE PRIVATUNIVERSITÄT

Klinikum Nürnberg
*wir sind für Sie da!*

University *of Ljubljana*
Faculty *of Computer and Information Science*

# "Die Bedeutung des interatrialen Blocks für das Auftreten von postoperativem Vorhofflimmern nach isoliertem Aortenklappenersatz und aortocoronarer Bypassoperation"

P Sluet[1], JM Kalisnik[1,2], V Günzler[1], L Kocet[3], J Zibert[3], J Sirch[2], M Fittkau[2], T Fischlein[1,2]

[1]Paracelsus Medizinische Privatuniversität Nürnberg, [2]Klinik für Herzchirurgie, Klinikum Nürnberg, [3]Fakultät für Informatik, Universität Ljubljana

Kontakt: Jurij.Kalisnik@klinikum-nuernberg.de

## Hintergrund

Nach herzchirurgischen Eingriffen ist das Vorhofflimmern eine häufige Komplikation und die häufigste Herzrhythmusstörung (1).
Es kann den postoperativen Verlauf negativ beeinflussen (2) und Krankenhausaufenthalte signifikant verlängern (3).
Ziel der Studie ist es zu untersuchen, ob präoperativ bestehende interatriale Blöcke (IAB) das Auftreten von postoperativem Vorhofflimmern begünstigen.

## Methodik

Es wurden retrospektiv 1155 Patienten am Klinikum Nürnberg untersucht, von denen 586 isoliert einen aortocoronaren Bypass und 567 isoliert einen chirurgischen Aortenklappenersatz erhalten haben. Die Operationen fanden im Zeitraum vom 01.01.2015 - 31.12.2019 statt. Die Patienten wurden anhand von prä- und postoperativ aufgezeichneten EKGs auf vorbestehende und postoperativ auftretende Herzrhythmus- und Überleitungsstörungen untersucht. Postoperativ aufgezeichnete EKGs sowie die Stationskurven wurden auf das Auftreten von Vorhofflimmern durchsucht.

## Ergebnis

Patienten mit einem vorbestehenden interatrialen Block weisen eine erhöhte Rate an postoperativem Vorhofflimmern auf. Dieser Zusammenhang zeigt sich bei Patienten, die sich einer Aortenklappen-OP unterzogen haben, nicht jedoch bei Bypassoperationen.
Das Vorhandensein von Bluthochdruck und einer Infarktanamnese zeigten sich als weitere Risikofaktoren.

## Klassifikation des IABs

| IAB-Typ | Merkmal |
|---|---|
| Partieller IAB (P-IAB) | - P-Welle > 120ms<br>- normalen oder bimodalen P-Wellen Morphologie in den Ableitungen II, III und AvF. (siehe Abbildung 1.1, 1.2) |
| Intermittierender IAB (I-IAB) | - Normal-EKG und Blockbild zeigen sich alternierend, z.T. im selben EKG. |
| Advanced IAB (A-IAB) | - P-Welle > 120ms<br>- biphasischen P-Wellen Morphologie in den Ableitungen II, III oder AvF. (siehe Abbildung 1.3) |

Tabelle 1, nach nach Boyés de Luna A, Martínez-Sellés M, Boyés-Genis A, Llesua R, Baranchuk A.
What every clinician should know about Boyés syndrome. Rev Esp Cardiol (Engl Ed). 2020

Pathophysiologie: Elektrophysiologisch beruht die erhöhte Überleitungszeit wahrscheinlich auf fibrotischen Veränderungen, die sich auf Region des Bachmann-Bündels konzentrieren (4).

## P-Wellen-Morphologie

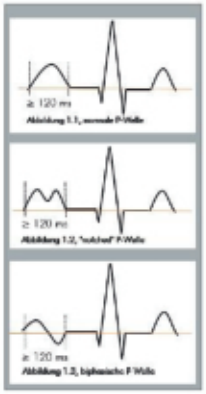


## Logistische Regression, AKE-Kohorte

| Variable | Odds ratio | 95% CI [lower, upper] | p-value | AUC [%] |
|---|---|---|---|---|
| Vorbest. IAB | 1.801 | [1.058, 3.067] | 0.030 | 64,7% |
| Infarktanamnese | 2.854 | [1.083, 7.519] | 0.034 | |
| Bluthochdruck | 2.670 | [1.319, 5.402] | 0.006 | |
| Bikuspide Aortenklappe | 0.549 | [0.351, 0.859] | 0.009 | |

Tabelle 2

## Schlussfolgerung

- Der IAB hat sich als Risikofaktor für poAF in der AVR-Kohorte bestätigt.
- Der IAB ist durch seine einfache Erhebbarkeit und einer objektiven Quantifizierbarkeit aufgrund seiner klaren Definitionskriterien ein unkompliziert und schnell zu erhebender Risikofaktor für den klinischen Alltag.
- Das alleiniges Auftreten bei AKE unterstreicht Notwendigkeit für Operationsadaptierte Risikobewertung.
- Weitere Studien für weitere Operationstypen sind vonnöten, um das Risikoprofil des IAB auszuschärfen.

## Literatur

1. Auer J, Weber T, Berent R, Ng CK, Lamm G, Eber B. Risk factors of postoperative atrial fibrillation after cardiac surgery. J Cardiol Surg. 2005;20(5):425-31
2. Greenberg JW, Lancaster TS, Schuessler RB, Melby SJ. Postoperative atrial fibrillation following cardiac surgery: a persistent complication. Eur J Cardiothorac Surg. 2017;52(4):665-72
3. Aranki SF, Shaw DP, Adams DH, Rizzo RJ, Couper GS, VanderVliet M, et al. Predictors of atrial fibrillation after coronary artery surgery. Current trends and impact on hospital resources. Circulation. 1996;94(3):390-7
4. Boyés de Luna A, Baranchuk A, Albero Escobar Richardo I, Massó van Roessel A, Martínez-Sellés M. Diagnosis of interatrial block. J Geriatr Cardiol. 2017;14(3):161-5.

## Die Bedeutung des interatrialen Blocks für das Auftreten von postoperativem Vorhofflimmern nach isoliertem Aortenklappenersatz und aortocoronarer Bypassoperation

Patrick Sluet[1], Jurij Matija Kalisnik[1,2], Valentin Günzler[1], Laura Kocet[3], Janez Žibert[3], Joachim Sirch[2], Matthias Fittkau[2], Theodor Fischlein[1,2]

[1]Paracelsus Medizinische Privatuniversität Nürnberg; [2]Klinik für Herzchirurgie, Klinikum Nürnberg; [3]Fakultät für Informatik, Universität Ljubljana; Contact: Patrick.Sluet@stud.pmu.ac.at

### Objective
After cardiac surgery, atrial fibrillation is the most common rhythm disturbance and can impair the postoperative course of the patient, as well as prolong the clinical stay. It is the aim of the study to investigate if preoperative interatrial blocks lead to a higher incidence of postoperative atrial fibrillation.

### Methods
In this study 1155 patients were examined. 586 patients received aortic valve replacement. 567 patients received coronary artery bypass grafting. All operations took place at Department for cardiac surgery, Paracelsus Medical University Hospital Nuremberg from 01.01.2015–31.12.2019. The Patients were screened for the occurrence of any heart rhythm disturbances pre- and postoperatively through analyses of pre- and postoperative obtained ECGs. Interatrial blocks have been identified with P-wave duration >120ms and sorted by p-wave morphology accordingly. Postoperatively acquired ECGs and patient clinical documentation have been screened for the appearance of atrial fibrillation.

### Results
Patients with a preexisting interatrial block show a higher rate of postoperative atrial fibrillation (OR 1,801, CI 1,058-3,062 p=0,030).
This is true for patients undergoing aortic valve replacement but not for patients undergoing aortocoronary bypass grafting. Advanced age (OR 1,065, KI 1,034 – 1,097, p=<0,001), a high EuroSCORE2 rating (OR 1,283, KI 1,106 – 1,488, p=0,001), hypertension (OR 2,670, KI 1,319 - 5,402, p=0,006) and history of infarction (OR 2,854, KI 1,083 - 7,519, p=0,034) have been identified as further risk factors.

### Conclusions
The interatrial block can be considered as a risk factor for the appearance of
postoperative atrial fibrillation. Beside well-established factors like age, hypertension, coronary artery disease, ischemia and fibrotic alterations of the atria, the IAB can be a valuable parameter in the clinical practice due to its easy, fast and reproducible obtainability.

PARACELSUS
MEDIZINISCHE PRIVATUNIVERSITÄT

Klinikum Nürnberg
Wir sind für Sie da!

# Case Report: Tertiäre Nebennierenrindeninsuffizienz bei zerebraler Metastasierung

**Claudius Söhn[1], Alexander Bott[1], Panagiota Manava[2]**

1) *Klinik für Innere Medizin 5 - Schwerpunkt Hämatologie und Onkologie, Universitätsklinik der Paracelsus Medizinischen Privatuniversität*
2) *Institut für Radiologie und Nuklearmedizin, Universitätsklinik der Paracelsus Medizinischen Privatuniversität*
*Kontakt: claudius.soehn@klinikum-nuernberg.de*

**Vorgeschichte**
Die Erstdiagnose eines kleinzelligen Bronchialkarzinom (SCLC) erfolgte 02/2020 bei einem 58-jährigen Patienten. Es bestand eine synchrone hepatische, lymphonoduläre und cerebrale Metastasierung. Unter der primären Immun-Chemotherapie mit Carboplatin, Etoposid und Atezolizumab kam es zu einem raschen Ansprechen aller – auch der cerebralen Manifestationen im Sinne einer kompletten Remission.
Eine prophylaktische Ganzhirnbestrahlung wurde zu Gunsten einer Nachsorge mittels cMRT nicht durchgeführt. Die Erhaltungstherapie mit Atezolizumab wurde fortgeführt.

**Verlauf**
Ende August 2020 kam es zu einer akuten Gangstörung und Allgemeinzustandsveränderung. TSH, ACTH- und Cortisol waren deutlich vermindert (Cortisol <1,0 µg/dl (6.02-18,4); ACTH 5,9 pg/ml (7,2 – 63,3)). Daher bestand der dringende Verdacht auf eine **Atezulizumab vermittelte-Autoimmun-Hypophysitis**. Der Patient präsentierte außer unspezifischer Schwäche keine Symptomatik einer adrenalen Insuffizienz. Ein CRH-Stimulationstest führte aber zu einem adäquaten Anstieg von ACTH und Cortisol. Dies spricht eindeutig gegen eine Hypophysen-Insuffizienz.

**Diagnose:**
Mittels MRT konnte ein Krankheitsprogress mit neuen spinalen und zerebralen Metastasen nachgewiesen werden. Im Hypothalamus zeigt sich eine 13 x 15 mm große Metastase (Abbildung a und b). Wir diagnostizierten eine **tertiäre Nebenniereninsuffizienz** im Rahmen der zerebralen Metastasierung.

**Therapie:**
- Substitution der betroffenen Hormone
- Einleitung einer Ganzhirn- und spinalen Bestrahlung

**Schlussfolgerung:**
Die Inzidenz der PD-1 / PD-L1-Antikörper vermittelten Hypophysitis wird mit 0,3 bis 3% angegeben (1). Metastasen im Bereich des Hypothalamus wurden in einer großen Fallserie bei < 1% der untersuchten Patienten gesehen (2).
Daher müssen neben der Immuntherapie-vermittelten Hypophysitis differentialdiagnostisch auch hypophysäre und hypothalamische Metastasen bedacht werden. In der Mehrzahl der Fälle sind diese Metastasen mit Mamma- oder Bronchial-Karzinomen assoziiert.

**Literatur:**
(1): Barroso-Sousa, Romualdo, et al. "Incidence of endocrine dysfunction following the use of different immune checkpoint inhibitor regimens: a systematic review and meta-analysis." *JAMA oncology* 4.2 (2018): 173-182.
(2): Janssen, Stefan, et al. "Prevalence of metastases within the hypothalamic-pituitary area in patients with brain metastases." *Radiation Oncology* 14.1 (2019): 1-6.

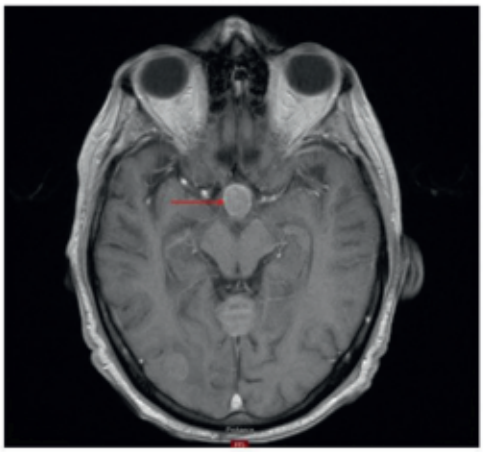

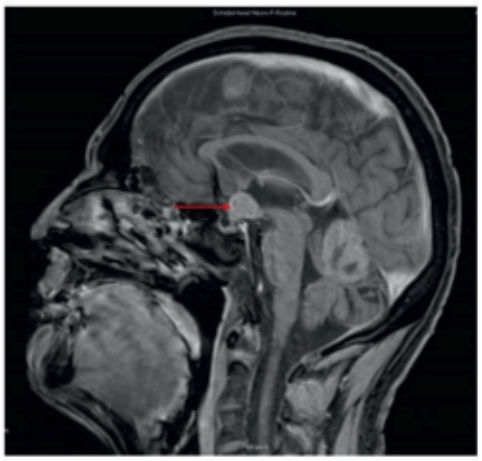

Abbildung a und b:
Kontrastmittel (KM)-anreichernde zerebrale Metastasen insbesondere am Hypothalamus (roter Pfeil) in axialer und sagittaler Ebene.

© Paracelsus Medizinische Privatuniversität | Nürnberg | Claudius Söhn

## Case Report: Tertiäre Nebennierenrindeninsuffizienz bei zerebraler Metastasierung

Claudius Söhn[1], Alexander Bott[1], Panagiota Manava[2]

[1]Klinik für Innere Medizin 5 - Schwerpunkt Hämatologie und Onkologie, Universitätsklinik der Paracelsus Medizinischen Privatuniversität, Nürnberg, Deutschland; [2]Institut für Radiologie und Nuklearmedizin, Universitätsklinik der Paracelsus Medizinischen Privatuniversität, Nürnberg, Deutschland; Contact: claudius.soehn@klinikum-nuernberg.de

### Objective

Die Erstdiagnose eines kleinzelligen Bronchialkarzinom (SCLC) erfolgte 02/2020 bei einem 58-jährigen Patienten. Es bestand eine synchrone hepatische, lymphonoduläre und cerebrale Metastasierung. Unter der primären Immun-Chemotherapie mit Carboplatin, Etoposid und Atezolizumab kam es zu einem raschen Ansprechen aller – auch der cerebralen Manifestationen im Sinne einer kompletten Remission. Eine prophylaktische Ganzhirnbestrahlung wurde zu Gunsten einer Nachsorge mittels cMRT nicht durchgeführt. Die Erhaltungstherapie mit Atezolizumab wurde fortgeführt.

### Methods

Ende August 2020 kam es zu einer akuten Gangstörung und Allgemeinzustandsveränderung. TSH, ACTH- und Cortisol waren deutlich vermindert (Cortisol <1,0 µg/dl (6.02-18,4); ACTH 5,9 pg/ml (7,2 – 63,3)). Daher bestand der dringende Verdacht auf eine Atezulizumab vermittelte Autoimmun-Hypophysitis. Der Patient präsentierte außer unspezifischer Schwäche keine Symptomatik einer adrenalen Insuffizienz. Ein CRH-Stimulationstest führte aber zu einem adäquaten Anstieg von ACTH und Cortisol. Dies spricht eindeutig gegen eine Hypophysen-Insuffizienz.

### Results

Mittels MRT konnte ein Krankheitsprogress mit neuen spinalen und zerebralen Metastasen nachgewiesen werden. Im Hypothalamus zeigt sich eine 13 x 15 mm große Metastase (Abbildung a und b). Wir diagnostizierten eine tertiäre Nebenniereninsuffizienz im Rahmen der zerebralen Metastasierung.
Therapie:

- Substitution der betroffenen Hormone
- Einleitung einer Ganzhirn- und spinalen Bestrahlung

### Conclusions

Die Inzidenz der PD-1 / PD-L1-Antikörper vermittelten Hypophysitis wird mit 0,3 bis 3% angegeben (1). Metastasen im Bereich des Hypothalamus wurden in einer großen Fallserie bei < 1% der untersuchten Patienten gesehen (2). Daher müssen neben der Immuntherapie-vermittelten Hypophysitis differentialdiagnostisch auch hypophysäre und hypothalamische Metastasen bedacht werden. In der Mehrzahl der Fälle sind diese Metastasen mit Mamma- oder Bronchial-Karzinomen assoziiert.

### References

1. Barroso-Sousa, Romualdo, et al. "Incidence of endocrine dysfunction following the use of different immune checkpoint inhibitor regimens: a systematic review and meta-analysis." JAMA oncology 4.2 (2018): 173-182.
2. Janssen, Stefan, et al. "Prevalence of metastases within the hypothalamic-pituitary area in patients with brain metastases." Radiation Oncology 14.1 (2019): 1-6.

# Prediction of Cardiac Surgery-Associated Acute Kidney Injury through Artificial Intelligence-Based Methods

FJ Stickl[1], JM Kalisnik[1,2], A Bauer[3], T Bertsch[1], S Konnoev[3], J Sirch[2], M Fittkau[2], T Fischlein[1,2]

[1]Paracelsus Medical University, Nuremberg, Germany; [2]Department of Cardiac Surgery, Nuremberg, Germany; [3]Julius Maximilian University, Würzburg, Germany.
Contact: Jurij.Kalisnik@Klinikum-nuernberg.de

## Introduction

Acute kidney injury is one of the most severe complications after cardiac surgery associated with prolonged hospitalization, intensive care unit stays, and mortality.[1] It is reported that cardiac surgery-associated acute kidney injury (CSA-AKI) occurs in up to 30 % of the patients.[2] To date, there are little therapeutic interventions (pharmacological or non-pharmacological) known to treat CSA-AKI, and the prevention of AKI associated with cardiac surgery remains critical. Many attempts have been made to develop risk-prediction models, mainly using logistic regression.

## Objective

- To predict the risk of CSA-AKI in the early postoperative period by utilizing an artificial intelligence-based machine learning approach
- To create a prediction model by using patient characteristics in combination with dynamic intra- and postoperative routine laboratory parameters
- To improve classical clinical scores' performance

## Methods

- Retrospective evaluation of 7354 patients undergoing cardiac surgery with cardiopulmonary bypass at Klinikum Nürnberg, Germany between April 2008 and October 2018
- CSA-AKI was defined according to 'Kidney Disease: Improving Global Outcomes' (KDIGO) criteria[3]
- Training and validation of two machine learning approaches ('Random Forests' and 'XGBoost') on 90% of the data to predict CSA-AKI within 24h after surgery
- Application of categorical variables for prediction of CSA-AKI including demographics, comorbidities, preoperative cardiac status, planned surgery, transfusion, intra-, and postoperative information, and postoperative assessment of kidney function
- The machine learning models' performances were compared using the area under the receiver operating characteristic curve (AUC)

## Results

- CSA-AKI was diagnosed in 1606 patients (21.8%).
- Patients developing CSA-AKI were older, more likely to have other comorbidities, and had worse in-hospital outcomes than patients without CSA-AKI
- The most significant variables have been identified and ranked according to relative relevance
- The first 15 pre-, intra-, and postoperative variables were used to build the model 'HemBP' (Table 2)
- 'HemBP' ('XGBoost' model) predicted the outcome of CSA-AKI the best (AUC 90.75%) (Table 1)

## XGBoost Model ‚HemBP'

| | Performance |
|---|---|
| AUC, % | 90.75 |
| Test Accuracy, % | 82.99 |
| Sensitivity, % | 80.91 |
| Specificity, % | 85.07 |
| Positive Predictive Value | 84.49 |
| Negative Predictive Value | 81.74 |
| Precision | 84.49 |

**Table 1 | Detailed performance matrix for ‚HemBP'.** AUC, area under the curve.

## Preoperative Patient Characteristics

| |
|---|
| Serum creatinine [mg/dL] (last value before surgery) |

## Intraoperative Patient Characteristics

| |
|---|
| Lowest hemoglobin [g/dL] value measured |
| Lowest blood pressure [mmHg] measured |
| Cardiopulmonary Bypass Time |
| Cross Clamp Time |
| Deepest temperature [°C] |

## Postoperative Patient Characteristics

| |
|---|
| eGFR CKD-epi [mL/min./1.73m²] arrival at ICU |
| ΔeGFR CKD-epi [mL/min./1.73m²] arrival at ICU |
| eGFR CKD-epi [mL/min./1.73m²] 6-18h postoperative |
| ΔeGFR CKD-epi [mL/min./1.73m²] 6-18h postoperative |
| Hemoglobin [g/dL] 0-6h postoperative |
| Hemoglobin [g/dL] 12-18h postoperative |
| Amount of blood in thoracic drainage 24h postoperative |
| Revision [yes/no] |

**Table 2 | Features building the 'XGBoost' model ‚HemBP'.**
The importance of the features, if multiple were available, is listed from high to low for each perioperative period.

## Conclusions & Perspectives

- This study is critical as 'HemBP' predicts CSA-AKI in the first 24h after surgery by using an artificial intelligence-based machine learning approach
- 'HemBP' forms a firm base for early CSA-AKI detection and opens possibility for timely therapeutic interventions
- The present platform enables us to design a web-based application for early CSA-AKI detection from the current 'HemBP' model for all cardiac surgery patients that will be easy applicable and can be used in the every-day clinical setting

## References

[1]The Multicenter Study of Perioperative Ischemia Research Group. Mangano et. Al. Ann Intern Med. 1998 Feb 1;128(3):194-203.
[2]Hoste EA, Cruz DN, Davenport A, et al. The Epidemiology of Cardiac Surgery-Associated Acute Kidney Injury. The International Journal of Artificial Organs. 2008;31(2):158-165.
[3]Kellum, J. A. et al. KDIGO-2012-AKI-Guideline. Kidney Int Suppl. 2012;2(1):1.

# PREDICTION OF CARDIAC SURGERY-ASSOCIATED ACUTE KIDNEY INJURY THROUGH ARTIFICIAL INTELLIGENCE-BASED METHODS

Franziska Josephine Stickl[1], Jurij Matija Kalisnik[1,2], Andree Bauer[3], Thomas Bertsch[4], Samuel Konnoev[3], Joachim Sirch[2], Matthias Fittkau[2], Theodor Fischlein[1,2]

[1]Paracelsus Medical University Nuremberg, Germany; [2]Department of Cardiac Surgery, Paracelsus Medical University Nuremberg, Germany; [3]Julius Maximilian University, Würzburg, Germany; [4]Institute of Laboratory and Transfusion Medicine, Paracelsus Medical University Nuremberg, Germany; Contact: franziska_stickl@yahoo.de

## Objective
Acute kidney injury is one of the most severe complications after open heart surgery associated with prolonged hospitalization, ICU stays, and mortality (1). It is reported that cardiac surgery-associated acute kidney injury (CSA-AKI) occurs in up to 30 % of the patients. Predicting the risk of cardiac surgery associated acute kidney injury (CSA-AKI) is critical, as to date, there are just little therapeutic interventions available. Past research focused on risk-prediction models using logistic regression that predominantly contain preoperative risk factors. The objective of the present study was to implement a model to reliably detect patients at risk of developing CSA-AKI in the early postoperative period.

## Methods
7354 patients undergoing cardiac surgery with CPB were evaluated at Klinikum Nürnberg between April 2008 and October 2018. CSA-AKI was defined according to 'Kidney Disease: Improving Global Outcomes' (KDIGO) criteria. Two machine learning approaches ('Random Forests' and 'XGBoost') were trained and validated on 90% of the data to predict CSA-AKI within 24 hours after surgery using different categorical variables. These included demographics, comorbidities, preoperative cardiac status, transfusion, and intra- and postoperative information, such as lowest intraoperative hemoglobin value and blood pressure, serum creatinine values, and thoracic drainage output.

## Results
CSA-AKI was diagnosed in 1606 patients (21.8 %). Patients developing CSA-AKI were older, more likely to have other comorbidities, and had worse in-hospital outcomes than patients without CSA-AKI. 'XGBoost' model 'HemBP' containing additional information on intraoperative hemoglobin value, blood pressure, and transfusion of blood products predicted the outcome of CSA-AKI the best (AUC 90.75 %).

## Conclusions
Model 'HemBP' was successfully implemented to detect CSA-AKI correctly in 83% of the patients within 24 hours after surgery. To our knowledge, it is the first prediction model using an artificial intelligence-based machine learning approach incorporating patient characteristics in combination with dynamic intra- and postoperative routine laboratory parameters. Model 'HemBP' forms a solid base for early CSA-AKI detection and opens possibility for timely therapeutical interventions. The present platform enables us to design a web-based application for CSA-AKI early detection from the current 'HemBP' model for all cardiac surgery patients that will be easy applicable and can be used in the every-day clinical setting.
Keywords: Acute kidney injury, cardiac surgery, CSA-AKI, machine learning, prediction models.

## References
1. The Multicenter Study of Perioperative Ischemia Research Group. Mangano et. Al. Ann Intern Med. 1998 Feb 1;128(3):194-203.

# The anti-asthmatic drug Montelukast improves motor coordination and balance in the Line 61 mouse model of Parkinson's disease

Katharina Strempfl[1,2,3], Michael S. Unger[1,2], Jörg Neddens[3], Stefanie Flunkert[3], Birgit Hutter-Paier[3], Nadine Palement[4], Horst Zerbe[4], Ludwig Aigner[1,2]

1: Institute of Molecular Regenerative Medicine, Paracelsus Medical University, Salzburg, Austria.
2: Spinal Cord Injury and Tissue Regeneration Center Salzburg (SCI-TReCS), Paracelsus Medical University, Salzburg, Austria.
3: QPS Austria GmbH, Grambach, Austria.
4: IntelgenX Corp., Saint-Laurent, QC H4S 1Y2, Canada

Contact: katharina.strempfl@pmu.ac.at

BEST PhD POSTER

## Background

Neuroinflammation caused by a dysregulated leukotriene (LT) signaling pathway may contribute to the pathogenesis of neurodegenerative diseases including Parkinson's disease (PD). LTs derive from arachidonic acid in a synthesis pathway involving the key enzyme 5-lipoxygenase (5-Lox) and its activator 5-lipoxygenase activating protein (FLAP) and evoke inflammatory responses by binding to specific LT receptors on target cells. Montelukast (MTK) is an anti-inflammatory drug originally approved for the treatment of asthma. MTK acts as a cysteinyl LT receptor antagonist and inhibits the actions of cysteinyl LTs by blocking cysteinyl leukotriene receptor 1 (CysLTR1) and G-protein-coupled receptor 17 (GPR17).

**This study aims to evaluate the potential of MTK as treatment option for PD, using the α-synuclein transgenic Line 61 mouse model.**

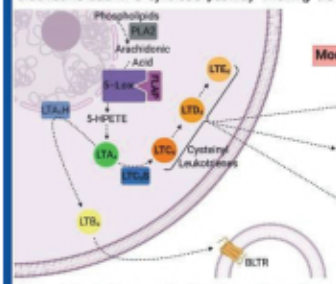


**Figure 1: Leukotriene synthesis and signaling pathway.** Created with BioRender.com
Abbreviations: 5-HPETE: 5-Hydroperoxyeicosatetraenoic acid, BLTR: Leukotriene $B_4$ receptor, $LTA_4H$: Leukotriene $A_4$ Hydrolase, $LTC_4S$: Leukotriene $C_4$ Synthase, PLA2: Phospholipase A2

## Methods

Starting at 2 weeks of age, 40 male Line 61 mice and 40 male non-transgenic (ntg) littermates were treated daily orally with either MTK or vehicle for 10 weeks. Behavioral tests were conducted at different time points of the treatment period to assess treatment effects on motor function, activity and anxiety.

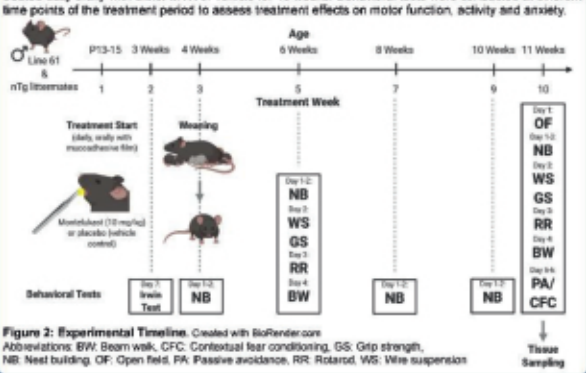


**Figure 2: Experimental Timeline.** Created with BioRender.com
Abbreviations: BW: Beam walk, CFC: Contextual fear conditioning, GS: Grip strength, NB: Nest building, OF: Open field, PA: Passive avoidance, RR: Rotarod, WS: Wire suspension

## MTK treatment improves motor coordination and balance

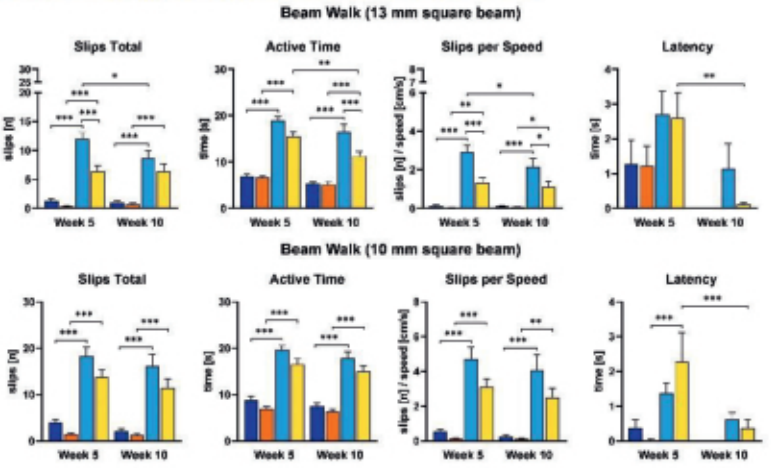


**Figure 3: Beam walk test performance of mice in treatment week 5 vs. week 10 on the 13 mm (top) and 10 mm (bottom) square beam:** The graphs show the total number of slips [n], the time mice needed to traverse the beam [s], the number of slips per speed [n/cm/s] and the latency before mice started to walk across the beam [s]. Data is displayed as group means (n=18-22) ± SEM per week. Three-way ANOVA followed by Bonferroni's multiple comparison test. *p<0.05, **p<0.01, ***p<0.001.

- In the **beam walk test** MTK treatment significantly reduced the number of slips (treatment week 5), the active time (treatment week 10) and the number of slips per speed (treatment week 5 and 10) on the 13 mm square beam in Line 61 mice compared to vehicle-treated Line 61 mice



- MTK-treated Line 61 mice performed better than vehicle-treated Line 61 mice on the 10 mm square beam
- A significant reduction of the latency to start to traverse the beams from treatment week 5 to 10 suggests an effect of MTK on motivation in Line 61 mice
- The **Rotarod test** shows a trend towards a higher latency to fall from the rotating rod in MTK-treated as compared to vehicle-treated Line 61 mice

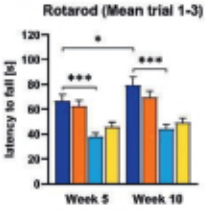


**Figure 4: Rotarod test mean results of treatment week 5 vs. week 10:** The graphs show the mean latency to fall [s] of 3 individual trials. Data is presented as group means (n=18-22) ± SEM per week. Three-way ANOVA followed by Bonferroni's multiple comparisons test. *p<0.01, ***p<0.001.

## Nesting behavior, muscle strength, activity, anxiety and emotional learning behavior were unchanged after MTK treatment

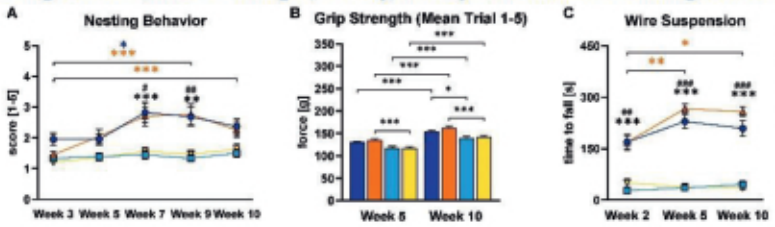


**Figure 5: Motor ability tests:** Scores obtained in the evaluation of the nesting behavior [1-5] in treatment weeks 3, 5, 7, 9 and 10 (A), the latency to fall off a wired grid [s] in the wire suspension test during treatment weeks 2, 5 and 7 (B) and the mean force [g] of 5 consecutive trials exerted on a grid with the fore paws in the grip strength test of treatment weeks 5 and 10 (C). Data is displayed as group means (n=18-22) ± SEM per week. Mixed-effects model with repeated measures (A,B) and three-way ANOVA (C) followed by Bonferroni's *post hoc* test. *p<0.05, **p<0.01, ***p<0.001.

#: ntg + MTK vs. Line 61 + MTK, *: ntg + vehicle vs. Line 61 + vehicle

- Throughout all groups, no significant differences could be observed in emotional learning behavior, activity and anxiety as assessed by the **open field**, **contextual fear conditioning** and **passive avoidance test** (data not shown)

## Conclusion

This study investigated the effects of a 10-week daily treatment with the anti-asthmatic drug MTK on the behavior of the Line 61 mouse model of PD. Significant genotype-related defects were detected in motor functions, but not in emotional learning, activity and anxiety. When comparing MTK-treated and vehicle-treated Line 61 animals, significant improvements were observed in the beam walk test already after 5 weeks of treatment. A non-significant trend towards an improved performance in the Rotarod test was observed. In contrast, both groups showed similar muscle strength results in the wire suspension and grip strength test. This suggests, that MTK treatment has an early beneficial effect on motor coordination and balance rather than on muscle strength itself. **In conclusion, these findings propose MTK as a possible treatment to alleviate motor impairments in PD.**

Outlook: Sampled brain tissue and gastrocnemius muscles will further be immunohistochemically and biochemically analyzed to investigate cellular and molecular changes to the brain after MTK treatment.

**Acknowledgements**

This work was supported by the FFG (project 867741) and the FWF (project P31362-B34).

## The anti-asthmatic drug Montelukast improves motor coordination and balance in the Line 61 mouse model of Parkinson's disease

Katharina Strempfl[1,2,3], Michael S. Unger[1,2], Jörg Neddens[3], Stefanie Flunkert[3], Birgit Hutter-Paier[3], Nadine Paiement[4], Horst Zerbe[4], Ludwig Aigner[1,2]

[1]Institute of Molecular Regenerative Medicine, Paracelsus Medical University, Salzburg, Austria; [2]Spinal Cord Injury and Tissue Regeneration Center Salzburg (SCI-TReCS), Paracelsus Medical University, Salzburg, Austria; [3]QPS Austria GmbH, Neuropharmacology, Grambach, Austria; [4]IntelgenX Corp., Saint-Laurent, QC H4S 1Y2, Canada; Contact: katharina.strempfl@qps.com

### Objective
Parkinson's disease (PD) is a neurodegenerative disorder affecting over seven million people worldwide. Its major hallmark is an abnormal aggregation of the α-synuclein protein (α-syn) in neurons and/or glial cells of the substantia nigra and the deep brainstem, impairing movement. The complex pathomechanisms underlying α-syn aggregation and neurodegeneration are still not fully understood and available treatment options are limited.
Neuroinflammation, which is mainly driven by microglia and is also caused by a dysregulated leukotriene signaling pathway, might play a critical role in evoking neurodegenerative conditions. A previous study showed that blocking of leukotriene signaling via the leukotriene receptor antagonist Montelukast (MTK) improved learning and memory deficits in the α-syn transgenic D-Line mouse model.
This study aims to evaluate whether MTK treatment can additionally alleviate motor symptoms in the α-syn transgenic Line 61 mouse model of PD.

### Methods
Male Line 61 mice and non-transgenic littermates were treated daily orally with 10 mg/kg MTK or placebo (vehicle) from 2 weeks of age for a total of 10 weeks. Behavioral tests for assessing motor functions, activity, anxiety and emotional learning were performed at different time points of the treatment period (2nd, 5th and 10th treatment week). Brains were collected for immunohistochemical and biochemical analyses of neuroinflammation markers and α-syn load.

### Results
Significant motor deficits were already observed in 4-weeks old Line 61 mice compared to age-matched non-transgenic littermates. In the beam walk test, motor coordination and balance were significantly improved in MTK-treated compared to vehicle-treated Line 61 mice. Additionally, moderate improvements of motor coordination were observed in MTK-treated Line 61 animals using the Rotarod test. Interestingly, muscle strength as well as activity, anxiety and emotional learning behavior of the mice were not affected by MTK treatment.
Immunohistochemical and transcriptome analyses of the brain for detailed investigation on the MTK-mediated molecular and cellular mechanisms are currently in progress.

### Conclusions
The results of this study demonstrate beneficial effects of Montelukast specifically on motor coordination and balance suggesting that Montelukast is a suitable drug for the treatment of motor impairments in Parkinson's disease and related neurodegenerative diseases.

# Low-Dose Radon Therapy in Atopic Dermatitis

V. Strobl[1,2], J. Fuchs[1,2,5], B. Hölzl[3], D. Meyersburg[4], V. Ahlgrimm-Siess[4], R. Tatarski[3], J. W. Bauer[4], M. Ritter [1,2,5], M. Gaisberger[1,2,3,#] & H. Dobias [1,2,#]

[1]Center for Physiology, Pathophysiology and Biophysics – Salzburg and Nuremberg, Austria and Germany, Institute for Physiology and Pathophysiology – Salzburg, Paracelsus Medical University, Austria; [2]Gastein Research Institute, Paracelsus Medical University, Salzburg, Austria; [3]Ludwig Boltzmann Institute for Arthritis and Rehabilitation, Paracelsus Medical University, Salzburg, Austria; [4]Department of Dermatology and Allergology, University Hospital of the Paracelsus Medical University – Salzburg, Austria; [5]Department of Internal Medicine – St. Veit im Pongau, Salzburger Landeskliniken (SALK) – Salzburg, Austria;

Contact: heidi.debias@pmu.ac.at, victoria.strobl@pmu.ac.at ; # equal contribution

## Objective

Low-Dose Radon Hyperthermia therapy (LDRnHT) has a long tradition in Europe and is a well-recognized treatment regimen for inflammatory diseases of the musculoskeletal system (e.g. rheumatoid arthritis) as well as for chronic disorders of the skin (e.g. psoriasis vulgaris) and the respiratory system (e.g. asthma bronchiale). Several clinical studies have demonstrated that LDRnHT can result in significant reduction of pain and enhancement of functionality, frequently accompanied by changes in various blood parameters.

Atopic dermatitis (AD) is an inflammatory skin disease that is mainly characterized by pruritus, dermal dryness and eczema. For some patients conventional therapy methods (anti-inflammatory medication, topic creams) are insufficient. These patients might benefit from LDRnHT. Several positive single person-based reports support this assumption, but clinical studies need to be conducted.

The purpose of this pilot study is to evaluate whether AD patients can evidently and sustainably benefit from LDRnHT.

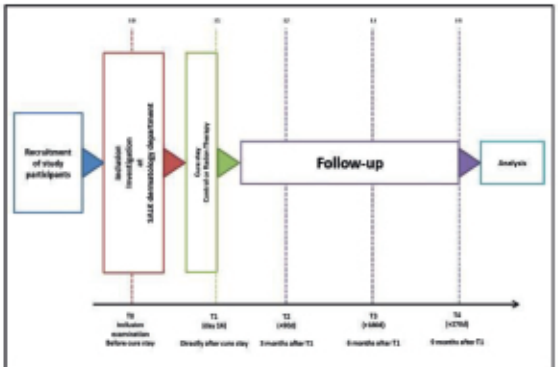


*Fig. 1: Study Schedule*

## Methods I

Patient recruitment started in spring 2017 and ended in summer 2020. All study participants had to pass an initial examination at the Department of Dermatology and Allergology at the University Hospital Salzburg, Austria. Patients enrolled were randomized into a control and an intervention group. Participants stayed in Bad Gastein for two weeks. For a schematic time table of the study, see Figure 1.

The intervention group received eight sessions of LDRnHT in the Gastein Healing Gallery (average radon activity = 44 kBq/m³; ambient temperature 37-41.5°C; air humidity ≥ 70%). The control group received sauna treatments with the same ambient temperature and humidity but without radon. Short-term modifications of skin condition, specific blood parameters, as well as quality of life (QoL), comparing the initial situation (T0) to immediate post-radon-therapy (T1) were assessed. Long-term effects were documented in follow-up examinations at three, six and nine months after T1 (T2/T3/T4, respectively; figure1). At every examination the skin condition was assessed by a dermatologist using the SCORing Atopic Dermatitis (SCORAD; range 0 – 103) rating tool, and blood samples and questionnaires were collected. Patients were asked to fill out the Patient Oriented SCORAD (PO-SCORAD, value range 0 – 103; figure 2) questionnaire using a computer or smartphone application, and the SKINDEX-29 tool to measure of the effect of the skin disease on quality of life. The EQ-5D-5L and VAS questionnaires were used to assess of Quality of Life (QoL). At T0 and T2, skin biopsies were taken for histological analyses. If the condition of a participant became worse, the dermatologist was authorized to assign a different therapy and end a patient's participation in the study.

Ethics approval: approved 25.01.2017, Ethikkommission Bundesland Salzburg E.-Nr. 2126

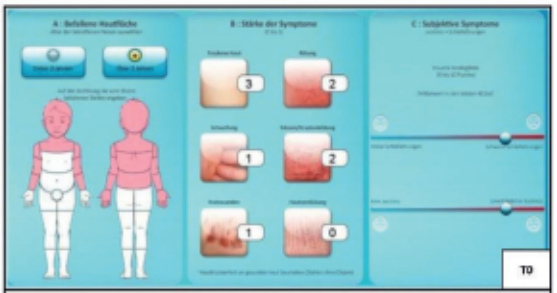


*Fig. 2: The PO-SCORAD software permits self-assessment of skin condition. Insomnia and pruritus are also incorporated in this tool. This graphic shows the initial skin condition (T0) of a study participant.*

## Methods II

Analysis and evaluation of blood samples will be conducted in the near future, primarily by FACS multiplex imaging. Several molecular blood parameters which are evidently involved in AD and inflammatory processes (e.g. CCL17/TARC, CCL22, IL-4, IL-13) shall be investigated. The focus will be on parameters that might indicate differences between patients responding and not responding to LDRnHT. Skin biopsies will be analysed at the GSI Helmholtz-Zentrum für Schwerionenforschung in Darmstadt, Germany. Statistical analysis of questionnaire data will be performed with appropriate measures.

## Results & Conclusion

34 patients were included in the study. 19 patients have completed the study program from T0 to T4. Five participants were not able to attend a cure stay due to the Covid-19 pandemic situation. Single-patient SCORAD and PO-SCORAD values over time are shown in figure 3. Some patients had missing SCORAD values at one or more time points and were excluded from analysis.

Short-term effects of LDRnHT therapy reflect in decreased SCORAD and PO-SCORAD values in the majority of patients at T1. AD patients might benefit more from LDRnHT in the future, considering its positive effect on other skin diseases e.g. *psoriasis vulgaris*. Nonetheless, AD is a disease with manifold aspects to be considered in therapy (e.g. concomitant allergies). There is a need for more clinical studies to gain further insight and possibly generate novel therapy concepts for AD, involving the potential of LDRnHT treatment in the Gastein Healing Gallery.

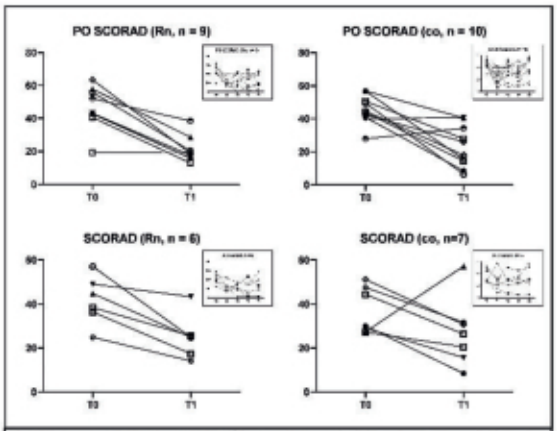


*Fig. 3: Single-patient SCORAD and PO-SCORAD values of intervention (Rn) and control group (co). Small boxes on the upper right show respective long-term values*

## Low-Dose Therapy in Atopic Dermatitis

Victoria Strobl[1,2], Julia Fuchs[1,2,3], Bertram Hölzl[5], Damian Meyersburg[4], Verena Ahlgrimm-Siess[4], Rafaella Tatarski[4], Johann Bauer[4], Markus Ritter[1,2,3], Martin Gaisberger[1,2,3], Heidemarie Dobias[1,2]

[1]Center for Physiology, Pathophysiology and Biophysics - Salzburg and Nuremberg, Austria and Germany, Institute for Physiology and Pathophysiology - Salzburg, Paracelsus Medical University, Austria; [2]Gastein Research Institute, Paracelsus Medical University, Salzburg, Austria; [3]Ludwig Boltzmann Institute for Arthritis and Rehabilitation, Paracelsus Medical University, Salzburg, Austria; [4]Department of Dermatology and Allergology, University Hospital of the Paracelsus Medical University - Salzburg, Austria; [5]Department of Internal Medicine - St. Veit im Pongau, Salzburger Landeskliniken (SALK) - Salzburg, Austria; Contact: victoria.strobl@pmu.ac.at

### Objective
Low-dose Radon Hyperthermia (LDRnHT) therapy is a well-recognized treatment method for inflammatory diseases in various compartments of the human body. Clinical studies demonstrated that LDRnHT- therapy can reduce pain, enhance functionality and positively shift crucial blood parameters. Atopic dermatitis (AD) is an inflammatory skin disease, mainly characterized by pruritus, dermal dryness and eczema. For some patients, conventional therapy methods are insufficient. These patients might benefit from LDRnHT. Many positive single reports from AD patients support this theory, but there are no clinical studies so far. The purpose of this pilot study is to evaluate whether AD patients can benefit from LDRnHT.

### Methods
Patient recruitment started in spring 2017 and ended in summer 2020. All study participants had to pass an initial examination at the Department of Dermatology and Allergology at the University Hospital Salzburg, Austria. Patients enrolled were randomized into a control and an intervention group. Participants stayed in Bad Gastein for two weeks. The intervention group received eight sessions of LDRnHT in the Gastein Healing Gallery (average radon activity ≈ 44 kBq/m3; ambient temperature 37-41.5°C; air humidity ≥ 70%). The control group received sauna treatments. Short-term modifications of skin condition, specific blood parameters, as well as quality of life (Qol), comparing the initial situation (T0) to immediate post-radon-therapy (T1) were assessed. Long-term effects were documented in follow-up examinations at three, six and nine months after T1 (T2/T3/T4, respectively;). At every examination the skin condition was assessed by a dermatologist using the SCORing Atopic Dermatitis (SCORAD; range 0 – 103) rating tool, and blood samples and questionnaires were collected. Patients were asked to fill out the Patient Oriented SCORAD (PO-SCORAD, value range 0 – 103;) and the SKINDEX-29 tool to measure of the effect of the skin disease on quality of life. The EQ-5D-5L and VAS questionnaires were used to assess of Quality of Life (Qol). At T0 and T2, skin biopsies were taken for histological analyses. If the condition of a participant became worse, the dermatologist was authorized to assign a different therapy and end a patient's participation in the study. Ethics approval: approved 25.01.2017, Ethikkommission Bundesland Salzburg E.-Nr. 2126

### Conclusions
Due to COVID-19, five of 34 patients included in the study could not attend a cure stay. 19 patients completed the full study program. Short-term effects of LDRnHT therapy reflect in decreased SCORAD and PO-SCORAD values in the majority of patients at T1. AD patients might benefit more from LDRnHT in the future, considering its positive effect on other skin diseases e.g. psoriasis vulgaris. Nonetheless, AD is a disease with manifold aspects to be considered in therapy (e.g. concomitant allergies). There is a need for more clinical studies to gain further insight and possibly generate novel therapy concepts for AD, involving the potential of LDRnHT treatment in the Gastein Healing Gallery.

PARACELSUS MEDIZINISCHE PRIVATUNIVERSITÄT

Klinikum Nürnberg
Wir sind für Sie da!

# Establishment of a fetal MRI method to measure the body composition for the development of fetal fat mass and fat-free mass trajectories

**David Surmann[1], Niels Rochow[1], Michael Noseworthy[2], Bryon DeFrance[3], Christoph Fusch[1]**

[1]Department of Pediatrics, Paracelsus Medical University, Nuremberg;
[2]Department of Pediatrics, [3]Department of Obstetrics and Gynecology, McMaster University, Hamilton

## INTRODUCTION

- It is recommended that preterm infants should develop like their healthy fetal counterparts which stay in utero until term age.
- To optimize nutrition, growth references for body composition of healthy fetuses would be needed.
- Available references for body composition (BC) are based on deceased newborns and may not reflect physiological growth.
- Postnatal growth charts based on preterms are no physiological reference.
- A non-invasive method to measure fetal body composition could be fetal MRI (fetMRI). Measurement of the body composition by MRI has been established for adults.
- The aim of this study is to develop a method to measure fetal body composition with MRI.

## OBJECTIVES

- To review literature for potential side effects of fetal MRI.
- To validate fetMRI as a method of acquiring body composition in utero.

## METHODS

- This validation study measured body composition in 10 subjects scheduled for c-section during the 37 to 40 week of gestation.
- FetMRI was performed up to 2 days prior to birth. Up to 3 days postnatally, a full body MRI (pMRI) scan as well as air displacement plethysmography (Peapod) was conducted on the newborn.
- Data was acquired at McMaster University, Hamilton, Canada.
- Dixon water suppressed sequences were segmented using 3D Slicer (v4.11) with semi-automatic package 'grow from seeds'.
- A calibration phantom *(Figure 1)* was developed with 0, 10, 20, 30, 40, 50 and 100% oil dissolved in sodium lauryl sulfate for MRI reference.
- Regression equations for relation between voxel intensity and percent fat mass (FM%) were established.
- Regression equation and volume were used to calculate BC.
- Imaging was conducted with 1.5T Siemens Symphony Tim MRI device.

## RESULTS

**Literature review:**

- We didn't identify studies which could show any harmful long-term effects on the human fetus related to the static magnetic field, pulsed radio frequency or time-varying magnetic gradient fields exposure (N= 1 review, 7 papers).
- Vena cava syndrome is a non-specific complication for MRI that should always be considered in longer examinations. This complication can be prevented by laying the pregnant woman into a left lateral side position.

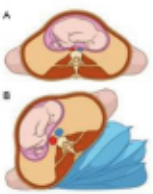


Fig. 1: Vena cava and aorta compression by the fetus (A) and relieved by tilting (B).

## RESULTS

**Phantom and development of regression analysis:**

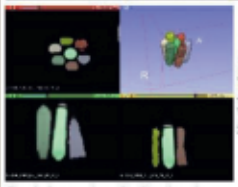

Fig. 2: Screenshot of calibration phantom

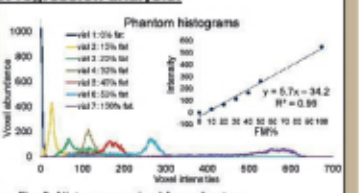


Fig. 3: Histograms gained from phantom segmentation

- N=10 newborns with gestational age 38 ± 2 weeks and birth weight of 3553 ± 360g.
- Repeatability of volume measurement was tested with 10 consecutive measurements of the same baby.

**Birth weight estimations:**

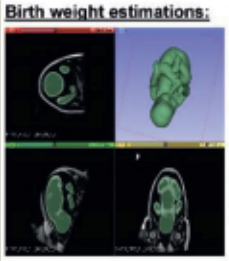

Fig. 4: Segmentation of baby (volume/ histogram)

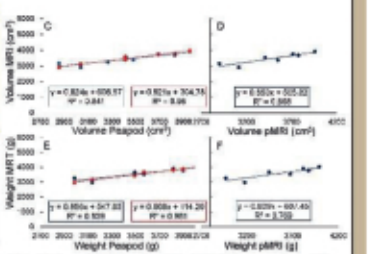


Fig. 5: Blue: fetMRI, red: pMRI, C&E Volume and weight correlation to Peapod, D&F correlation between pMRI & fetMRI

- Weight was calculated through the two compartments with it's specific densities of 0.9007 g/cm³ (fat) and 1.064 g/cm³ (fat free mass).
- Body weight was estimated using fetMRI and highly correlates with the birth weight $R^2$= 0.9.

**Evaluation of body composition:**

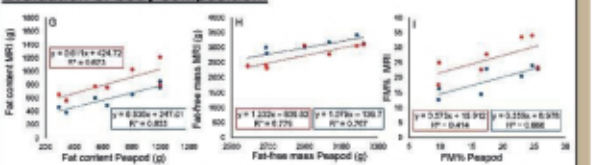


Fig. 6: Blue: fetMRI, red: pMRI, G: the absolute fat content, H: absolute fat-free mass, I: FM%

- Average deviation of FM% between fetMRI and Peapod was 2%.
- FM% of fetMRI and pMRI correlate with $R^2$ = 0.53.
- FetMRI and Peapod as well as pMRI and Peapod correlate with $R^2$ of 0.67 and 0.41, respectively.

## CONCLUSION

- Literature review showed that fetal MRI seems to be save for the human fetus.
- Fetal MRI could be used to assess fetal volume, weight and BC.
- In the future, fetal MRI will be employed to a longitudinal study during pregnancy to establish reference data for fetal body composition.

Christoph Fusch, MD, PhD, Pediatrics, Paracelsus Medical University, christoph.fusch@klinikum-nuernberg.de

## Establishment of a fetal MRI method to measure the body composition for the development of fetal fat mass and fat-free mass trajectories

David Surmann[1], Niels Rochow[1], Michael Noseworthy[2], Bryon DeFrance[3], Christoph Fusch[1]

[1]Department of Pediatrics, Paracelsus Medical University, Nuremberg, Germany; [2]Department of Pediatrics, McMaster University, Hamilton, Canada; [3]Department of Obstetrics and Gynecology, McMaster University, Hamilton, Canada; Contact: david.surmann@stud.pmu.ac.at

### Objective
Growth references for the body composition of healthy fetuses would be needed to optimize nutrition. Available references for body composition (BC) are based on deceased newborns and may not reflect physiological growth. Postnatal growth charts based on preterms are no physiological reference. A non-invasive method to measure fetal body composition could be fetal MRI (fetMRI). Measurement of the body composition by MRI has already been established for adults. The aim of this study is to develop a method to measure fetal body composition with MRI and to review literature analysing potential fetMRI risk.

### Methods
This validation study measured body composition in subjects scheduled for c-section during the 37 to 40 week of gestation. FetMRI was performed within 2 days prior to birth. Up to 3 days postnatally, a full body MRI (pMRI) scan and air displacement plethysmography (Peapod) was conducted. Data was acquired at McMaster University, Hamilton, Canada. Imaging was conducted with 1.5T Siemens Symphony Tim MRI device. Dixon water suppressed sequences were segmented using 3D Slicer (v4.11) with semi-automatic package 'grow from seeds'. A calibration phantom was developed with different tubes having 0, 10, 20, 30, 40, 50 and 100% oil dissolved in sodium lauryl sulfate. Regression equations for relation between voxel intensity and percent fat mass (FM%) were established. Regression equation and volume were used to calculate BC.

### Results
Newborns (n=10) with gestational age of 38±2 weeks and birth weight of 3630±360g had a body volume of 3440 $cm^2$. Percent fat mass of pMRI and PeaPod were related with $R^2$ = 46%. FetMRI and pMRI as well as fetMRI and PeaPod were related with $R^2$ of 86% and 67%, respectively. Body weight estimated using fMRI was highly correlated with birth weight $R^2$= 92%. The average deviation between percent fat mass between fetMRI and Peapod was 6%.
No study was identified which shows any harmful long-term effects on the human fetus related to magnetic resonance exposure. A preventable risk is the Vena cava syndrome that occurs from supine position during fetMRI.

### Conclusions
Literature review showed that fetal MRI seems to be save for the human fetus. FetMRI could be used to assess fetal volume, weight and body composition. In the future, fetMRI will be employed to a longitudinal study during pregnancy to establish reference data for fetal body composition.

# Virtual simulation versus hands-on training in Extracorporeal Life Support (ECLS) and ECMO

**Swol J[1], Baumgaertel M[1], Emmrich K[1], Butler K[1], Nietzold S[1], Sonntag S[2], Seiler H[3], Tallmann R[3], Ficker JH[1]**

[1]Department of Respiratory Medicine, Allergology and Sleep Medicine, Paracelsus Medical University, Nuremberg, Germany
[2]Virtonomy GmbH, Munich, Germany [3]Biomed Simulation Inc. San Diego, CA, USA

**Objective**: Extracorporeal membrane oxygenation (ECMO), also referred to as extracorporeal life support (ECLS), is designed to support cardiac and/or pulmonary function in case of organ failure.
Various simulation techniques have been developed to create practice situations for complex high risk and/or low frequency emergencies or procedures in ECLS. Additionally, ex-vivo ECLS models can be used investigating clinical issues related to oxygenator membrane properties, optimal blood flow velocities or other research questions. Regarding to COVID19 pandemic, new demands on teaching and training occurred and accelerated the development and deployment of virtual simulation technologies.

**Methods:** The ECMO simulation tools serve as an alternative to real patients and devices. Comparative studies involving virtual simulation versus hands-on training are indicated to inform evidence-based teaching in ECLS.

**Results:**
**Virtual reality** is a 3-D simulation that delivers a wide range of real-life scenarios to the user to allow them to interact with objects in a virtual environment, making it more effective than passive watching of video presentation. The desired digital simulation and learning platform may use artificial intelligence based on a database of imaging and pathological data, which covers all anatomical, pathological and geographical variability. The various benefits of virtual simulation in ECMO were identified as less expensive, intuitive to access, and independently located compared with non-digital simulations. Numerous risks, such as a mismatch of the cannulas in the event of unexpected anatomical variants or incorrect size determination, maybe significantly reduced.



**Medical simulation** offers numerous strategies for a comprehensive and practical training as well as safer patient care in the application of extracorporeal procedures. The simulation of an ex vivo ECLS system can be built with increasing complexity: Simple simulation of the system by connecting the cannulas to a tubing system provides a convenient visualization of the system is the first possible level, followed by cannulation mannequins with higher demands on the tubing system and an additional pumping system as circuit simulation. This simulator relies on scenarios similar to clinical practice in a controlled environment without any negative consequences due to errors (tubing connection to the cannulas, troubleshooting, oxygenator changing, or clotting). High-fidelity simulation allows both the detection of pathophysiological relationships by changing the device function and the simulation of the vital parameters of the patient. The advance stage includes a physiological algorithm, patient scenarios can be created that represent past and current patient courses and therapies.





**The water-filled ECLS circuit connected to the loop system for hands- on training**

**Conclusion**: Hands-on training and virtual reality may be used complimentary and not contrary in ECLS training, promoting experimental and reflexive learning and help to convey crisis management skills.

## Virtual simulation versus hands-on training in Extracorporeal Life Support (ECLS) and ECMO

Justyna Swol[1], Matthias Baumgaertel[1], Katrin Emmrich[1], Katrin Butler[1], Steffen Nietzold[1], Simon Sonntag[2], Hans Seiler[3], Richard Tallmann[3], Joachim H. Ficker[1]

[1]Department of Respiratory Medicine, Allergology and Sleep Medicine, Paracelsus Medical University, Nuremberg, Germany; [2]Virtonomy GmbH, Munich, Germany; [3]Biomed Simulation Inc. San Diego, CA, USA; Contact: jswol@icloud.com

### Objective
Extracorporeal membrane oxygenation (ECMO), also referred to as extracorporeal life support (ECLS), is designed to support cardiac and/or pulmonary function in case of organ failure. Various simulation techniques have been developed to create practice situations for complex high risk and/or low frequency emergencies or procedures in ECLS. Additionally, ex-vivo ECLS models can be used investigating clinical issues related to oxygenator membrane properties, optimal blood flow velocities or other research questions. Regarding to COVID19 pandemic, new demands on teaching and training occurred and accelerated the development and deployment of virtual simulation technologies.

### Methods
The ECMO simulation tools serve as an alternative to real patients and devices. Comparative studies involving virtual simulation versus hands-on training are indicated to inform evidence-based teaching in ECLS.

### Results
Thus, medical simulation offers numerous strategies for a comprehensive and practical training as well as safer patient care in the application of extracorporeal procedures. The simulation of an ex vivo ECLS system can be built with increasing complexity: Simple simulation of the system by connecting the cannulas to a tubing system provides a convenient visualization of the system is the first possible level, followed by cannulation mannequins with higher demands on the tubing system and an additional pumping system as circuit simulation. This simulator relies on scenarios similar to clinical practice in a controlled environment without any negative consequences due to errors (tubing connection to the cannulas, troubleshooting, oxygenator changing, or clotting). High-fidelity simulation allows both the detection of pathophysiological relationships by changing the device function and the simulation of the vital parameters of the patient. The advance stage includes a physiological algorithm, patient scenarios can be created that represent past and current patient courses and therapies.
Virtual reality is a 3-D simulation that delivers a wide range of real-life scenarios to the user to allow them to interact with objects in a virtual environment, making it more effective than passive watching of video presentation. The desired digital simulation and learning platform may use artificial intelligence based on a database of imaging and pathological data, which covers all anatomical, pathological and geographical variability. The various benefits of virtual simulation in ECMO were identified as less expensive, intuitive to access, and independently located compared with non-digital simulations. Numerous risks, such as a mismatch of the cannulas in the event of unexpected anatomical variants or incorrect size determination, maybe significantly reduced.

### Conclusions
Hands-on training and virtual reality may be used complimentary and not contrary in ECLS training, promoting experimental and reflexive learning and help to convey crisis management skills.

# Transcriptomic characterization of brain CD8⁺ T-cells identifies gene signature of tissue-resident memory T-cells in Alzheimer's disease transgenic mice

Unger MS.[1,2], Altendorfer B.[1,2], Poupardin R.[2,3], Hoog A.[2,3], Forster J.[1,2], Benedetti B.[2,4], Benedetti A.[2,4], Asslaber D.[5,6,7], Egle A.[5,6,7], Aigner L.[1,2,8],

[1]Institute of Molecular Regenerative Medicine, Paracelsus Medical University, Salzburg, Austria.
[2]Spinal Cord Injury and Tissue Regeneration Center Salzburg (SCI-TReCS), Paracelsus Medical University, Salzburg, Austria.
[3]Experimental and Clinical Cell Therapy Institute, Paracelsus Medical University, Salzburg, Austria.
[4]Institute of Experimental Neuroregeneration, Paracelsus Medical University, Salzburg, Austria.
[5]3rd Medical Department with Hematology and Medical Oncology, Oncologic Center, Paracelsus Medical University, Salzburg, Austria.
[6]Salzburg Cancer Research Institute with Laboratory of Immunological and Molecular Cancer Research and Center for Clinical Cancer and Immunology Trials, Salzburg, Austria.
[7]Cancer Cluster Salzburg, Salzburg, Austria.
[8]Austrian Cluster for Tissue Regeneration.
Contact: michael.unger@pmu.ac.at

SFB
PMU-FFF
E-20/32/169-UNG

## Objective

Neuroinflammation is a major contributor to disease progression in Alzheimer's disease (AD) and is characterized by the activity of brain resident glial cells, in particular microglia cells. However, there is increasing evidence that peripheral immune cells infiltrate the brain at certain stages of AD progression and shape disease pathology. In AD, that typically includes amyloid-beta plaque formation and microglia-mediated neuroinflammation, we recently demonstrated that a population of CD8⁺ T-cells starts to infiltrate into the AD-affected brain parenchyma (Unger M.S. et al., *Alzheimers Dement*, 2018; Unger M.S. et al., *J Neuroinflammation*, 2018). Additionally, a specific subpopulation of CD8⁺ T-cells is clonally expanded in the CSF of AD patients (Gate D. et al., Nature, 2020). Furthermore, studying the functional role of CD8⁺ T-cells in AD by experimentally ablating CD8⁺ T-cells in transgenic AD mice (APP-PS1), we demonstrated that CD8⁺ T-cells regulate neuronal- and synapse-related gene expression in the hippocampus (Unger M.S. et al., *Brain Behav Immun*, 2020). So far a detailed transcriptomic profile and phenotypic characterization of brain CD8⁺ T-cells in transgenic AD mice is missing. The herein presented data give new insights on the transcriptome of brain CD8⁺ T-cells, how they differ from blood CD8⁺ T-cells and demonstrate the presence of tissue-resident memory (Trm) CD8⁺ T-cells in the brain of transgenic AD mice. This might open the doors for immunotherapy as potential new treatment option for AD. (Images and data below are unpublished data or as otherwise indicated).

## 1. CD8⁺ Temra T-cells are elevated in the blood, negatively correlate with the cognitive scores and are clonally expanded in the CSF of AD patients

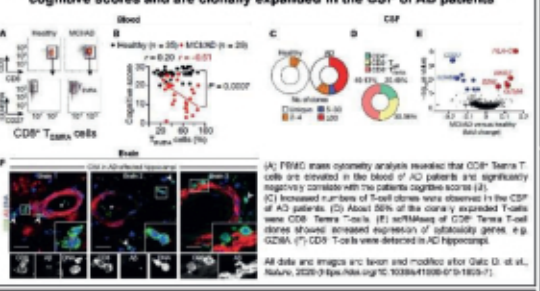


(A) FFPAD mass cytometry analysis revealed that CD8⁺ Temra T-cells are elevated in the blood of AD patients and significantly negatively correlate with the patients cognitive scores (*B*).
(C) Increased numbers of T-cell clones were observed in the CSF of AD patients. (D) About 56% of the clonally expanded T-cells were CD8⁺ Temra T-cells. (E) scRNAseq of CD8⁺ Temra T-cell clones showed increased expression of cytotoxicity genes, e.g. GZMA. (*) CD8⁺ T-cells were detected in AD hippocampi.

All data and images are taken and modified after Gate D. et al., Nature, 2020 (https://doi.org/10.1038/s41586-019-1895-7).

## 2. CD8⁺ T-cells infiltrate the brain of old and AD transgenic mice

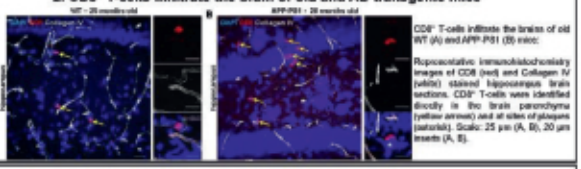


CD8⁺ T-cells infiltrate the brains of old WT (A) and APP-PS1 (B) mice:

Representative immunohistochemistry images of CD8 (red) and Collagen IV (white) stained hippocampus brain sections. CD8⁺ T-cells were identified directly in the brain parenchyma (yellow arrows) and at sites of plaques (asterisk). Scale: 25 µm (A, B), 20 µm inserts (A, B).

## 3. Experimental set-up of CD8⁺ T-cell isolation

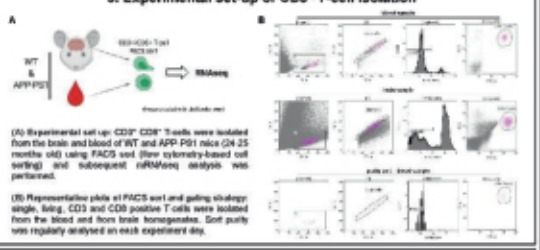


(A) Experimental set up: CD3⁺ CD8⁺ T-cells were isolated from the brain and blood of WT and APP-PS1 mice (24 25 months old) using FACS sort (flow cytometry-based cell sorting) and subsequent mRNAseq analysis was performed.

(B) Representative plots of FACS sort and gating strategy: single, living, CD3 and CD8 positive T-cells were isolated from the blood and from brain homogenates. Sort purity was regularly analysed on each experiment day.

## 4. Brain CD3⁺ CD8⁺ T-cells have a highly altered transcriptome compared to the blood

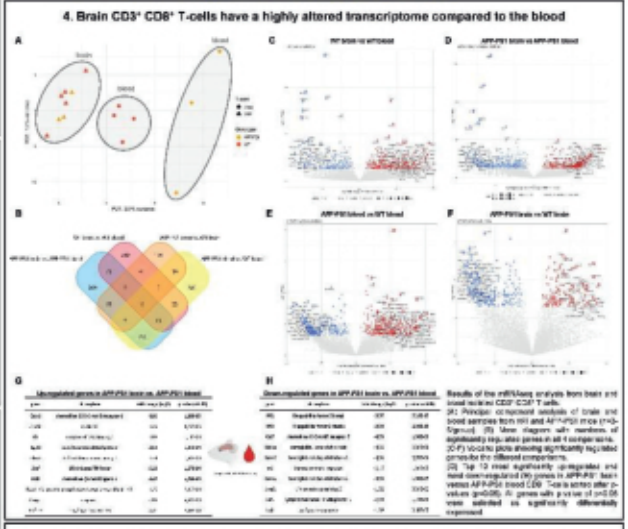


Results of the mRNAseq analysis from brain and blood isolated CD3⁺ CD8⁺ T-cells.
(A) Principal component analysis of brain and blood samples from old and APP-PS1 mice (n=3-5/group). (B) Venn diagram with numbers of significantly regulated genes in all 4 comparisons. (C-F) Volcano plots showing significantly regulated genes for the different comparisons.
(G) Top 12 most significantly up-regulated and most down-regulated (M) genes in APP-PS1 brain versus APP-PS1 blood (CD8⁺ T-cells sorted after in vivo). (H) Down-regulated genes in APP-PS1 brain vs. APP-PS1 blood (CD8⁺ T-cells sorted after in vivo). p-values p<0.05). A: genes with p-value of p<0.05 were selected as significantly differentially expressed.

## 5. Gene ontology enrichment & Kegg pathway analysis:

### Association with virus infection pathways in APP-PS1 brain CD3⁺ CD8⁺ T-cells

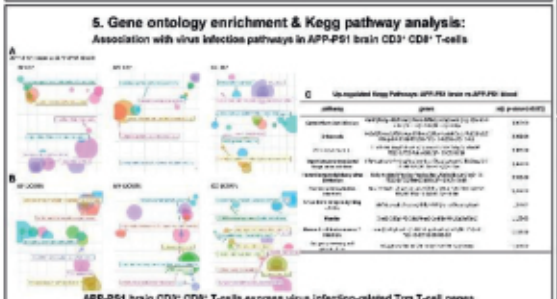


### APP-PS1 brain CD3⁺ CD8⁺ T-cells express virus infection-related Trm T-cell genes

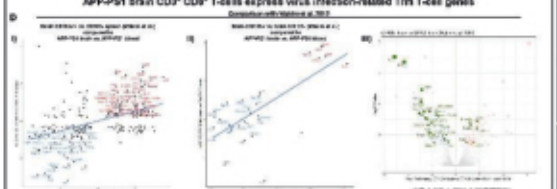

Gene ontology enrichment analysis of significantly regulated genes in CD3⁺ CD8⁺ T-cells from APP-PS1 brain versus APP-PS1 blood samples. (A) Over-represented GO terms (GO⁺) and under-represented GO terms (GO⁻) for biological processes (BP), molecular function (MF) and cellular components (CC). All genes with p-value of p<0.05 were selected for GO enrichment analysis. (B) List of Top 10 significantly up-regulated Kegg pathways and their corresponding genes in APP-PS1 brain vs. APP-PS1 blood CD8⁺ T-cells sorted after adjusted p-values (adj. p<0.05). (C) Venn plot showing gene similarity between brain CD8⁺ T-cells of virus infected mice (Wakim et al., *J Immunol*, 2012). 1.5kb significantly regulated genes that are shared (Trm) or is expressed in APP-PS1 brain CD8⁺ T-cells are brain CD8⁺ T-cells (CD103⁺ and CD103⁻) from the virus infection mouse model. (D Sign) Significantly regulated genes that are shared differentially expressed in APP-PS1 brain CD8⁺ T-cells and brain CD103⁺ CD8⁺ Trm T-cells. (E) Volcano plot showing overlapping genes of (D) in green. The most upreg genes between the sources leading to the top regulated genes and in/down the genes (IRF, TCF and Gzm).

## 6. Immunohistochemical characterization of brain CD8⁺ T-cells at sites of amyloid plaques

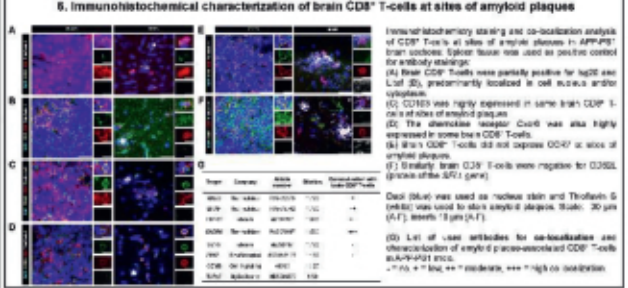


Immunohistochemistry staining and co-localization analysis of CD8⁺ T-cells at sites of amyloid plaques in APP-PS1 brain sections. Spleen tissue was used as positive control for antibody stainings.
(A) Brain CD8⁺ T-cells were partially positive for hg20 and Lsd (B), predominantly localized in cell nucleus and/or cytoplasm.
(C) CD103 was highly expressed in some brain CD8⁺ T-cells at sites of amyloid plaques.
(D) The chemokine receptor Cxcr6 was also highly expressed in some brain CD8⁺ T-cells.
(E) Brain CD8⁺ T-cells did not express GZMB at sites of amyloid plaques.
(F) Similarly, brain CD8⁺ T-cells were negative for GZMB (protein of the GZM gene).

Dapi (blue) was used as nuclear stain and Thioflavin S (white) was used to stain amyloid plaques. Scale: 30 µm (A-F'), inserts 10 µm (A-F').

(G) List of used antibodies for co-localization and characterization of amyloid plaque-associated CD8⁺ T-cells in APP-PS1 mice.
+/-: no, +: low, ++: moderate, +++: high co-localization.

## Outlook

- Flow cytometry analysis on T-cell subtypes (Tcm, Tem and Trm) in the brain (collab. A. Egle Lab).
- Defining the effects of CD8⁺ T-cells on neuronal function:

(A) in vivo CD8⁺ T-cell ablation experiments and electrophysiology (collab. B. Benedetti).

(B) different treatment windows: 3, 7, or 14 days.

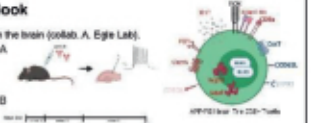


## Methods

In this study we isolated CD8⁺ T-cells from the brain and blood of old APP-PS1 and WT mice (24 months old) using flow cytometry-based cell sorting (FACS) and conducted detailed mRNAseq analysis (performed by Qiagen). We compared our transcriptomic data with gene microarray data of brain isolated tissue-resident memory (Trm) CD8⁺ T-cells derived from an acute virus infection mouse model (Wakim et al., *J Immunol*, 2012). Detailed immunohistochemical analysis and confocal microscopy of brain CD8⁺ T-cells was performed in APP-PS1 mice that were manually perfused and brain hemispheres were immersion fixed in 4% paraformaldehyde.

## Acknowledgements

The authors thank the flow cytometry and microscopy core facility of SCI-TReCS (Spinal Cord Injury and Tissue Regeneration Center Salzburg). Furthermore, we thank Pia Zaunmair and Ariane Benedetti for her help with the animal breeding. This work was supported by the FWF Special Research Program (SFB) F44 (F4413-B23) "Cell Signaling in Chronic CNS Disorders" and through funding by the PMU-FFF E-20/32/169-UNG

## Transcriptomic characterization of brain CD8+ T-cells identifies gene signature of tissue-resident memory T-cells in Alzheimer's disease transgenic mice.

Michael Stefan Unger[1,2], Barbara Altendorfer[1,2], Rodolphe Poupardin[2,3], Anna Hoog[2,3], Jennifer Forster[1,2], Bruno Benedetti[2,4], Ariane Benedetti[2,4], Daniela Asslaber[5,6], Alexander Egle[5,6], Ludwig Aigner[1,2,7]

[1]Institute of Molecular Regenerative Medicine, Paracelsus Medical University, Salzburg, Austria.; [2]Spinal Cord Injury and Tissue Regeneration Center Salzburg (SCI-TReCS), Paracelsus Medical University, Salzburg, Austria; [3]Experimental and Clinical Cell Therapy Institute, Paracelsus Medical University, Salzburg, Austria; [4]Institute of Experimental Neuroregeneration, Paracelsus Medical University, Salzburg, Austria; [5]IIIrd Medical Department with Hematology and Medical Oncology, Oncologic Center, Paracelsus Medical University, Salzburg, Austria.; [6]Salzburg Cancer Research Institute with Laboratory of Immunological and Molecular Cancer Research and Center for Clinical Cancer and Immunology Trials, Salzburg, Austria.; [7]Austrian Cluster for Tissue Regeneration.; Contact: michael.unger@pmu.ac.at

### Objective

Peripheral immune cell infiltration to the brain and its contribution to pathology is an important aspect in neurodegenerative diseases such as Alzheimer´s disease (AD). With AD progression, that typically includes amyloid-beta plaque formation and neuroinflammation, a population of CD8+ T-cells starts to infiltrate into the AD brain parenchyma. We recently demonstrated that CD8+ T-cells occur in the brain with increasing amyloid pathology and tightly associate with microglia and neuronal structures. A specific subpopulation of CD8+ T-cells is clonally expanded in the CSF of AD patients and by experimentally ablating CD8+ T-cells in transgenic AD mice (APP-PS1) we demonstrated that CD8+ T-cells regulate neuronal- and synapse-related gene expression in the hippocampus. So far a detailed transcriptomic profile and phenotypic characterization of brain CD8+ T-cells in transgenic AD mice is missing.

### Methods

In this study we isolated CD3+ CD8+ T-cells from the brain and blood of old APP-PS1 and WT mice (24-25 months old) using flow cytometry-based cell sorting and performed mRNAseq analysis. We compared our transcriptomic data with gene microarray data of brain isolated tissue-resident memory (Trm) CD8+ T-cells derived from an acute virus infection mouse model (Wakim et al., *J Immunol*, 2012). Additionally, detailed immunohistochemical analysis was performed on brain CD8+ T-cells in APP-PS1 mice.

### Results

Brain CD8+ T-cells from APP-PS1 animals had a more similar transcriptome to brain CD8+ T-cells from WT mice but substantially differed from blood circulating CD8+ T-cells. The genetic signature of brain CD8+ T-cells from APP-PS1 mice revealed the presence of Trm T-cells by specific regulation of core Trm T-cell genes. Gene ontology enrichment analysis on the significantly up-regulated genes showed an overrepresentation of biological processes as "response to virus" and "T-cell mediated immunity". KEGG pathway analysis on up-regulated genes in APP-PS1 brain derived CD8+ T-cells demonstrated up-regulated pathways for various "virus infections" and for "cellular senescence". In brain CD8+ T-cells from APP-PS1 mice we observed a highly overlapping gene signature with genes from brain Trm CD8+ T-cells derived from a virus infection mouse model. Additionally, we detected the presence of Trm CD8+ T-cells (CD103+ and Cxcr6+) at sites of amyloid plaques.

### Conclusions

Herein presented data give new insights on the transcriptome of brain CD8+ T-cells and demonstrate the presence of Trm CD8+ T-cells in the brain of transgenic AD mice. This might open the doors for immunotherapy as potential new treatment option for AD.

### Acknowledgements

This work is funded by the PMU-FFF E-20/32/169-UNG

PARACELSUS MEDIZINISCHE PRIVATUNIVERSITÄT

Klinikum Nürnberg
wir sind für Sie da.

Kontakt: vogtju71407@th-nuernberg.de

Virtueller Paracelsus Science Get Together, 02. Juli 2021

# *in vitro* Enthesisformation mittels Ko-Kultur auf einem triphasisch gestickten Träger für das Kreuzband Tissue Engineering

Julia Vogt[1,2], Clemens Gögele[2,3], Judith Hahn[4], Annette Breier[4], Michael Meyer[5], Michaela Schröpfer[5], Kerstin Schäfer-Eckart[6], Ralf Lösel[1], Gundula Schulze-Tanzil[2]

[1] Fakultät für Angewandte Chemie, Technische Hochschule Georg-Simon-Ohm, Nürnberg
[2] Institut für Anatomie und Zellbiologie, Paracelsus Medizinische Privatuniversität, Salzburg und Nürnberg, Nürnberg, Deutschland
[3] Fachbereich für Biowissenschaften, Paris Lodron Universität Salzburg, Österreich
[4] Leibniz Institut für Polymerforschung (IPF) Dresden, Deutschland
[5] FILK Freiberg Institute, Freiberg, Deutschland
[6] Klinik für Onkologie/Hämatologie, Klinikum Nürnberg Nord, Nürnberg, Deutschland

## Fragestellung

Ein vorderer Kreuzbandriss ist eine der häufigsten Bandverletzungen im Kniegelenk. Aufgrund der schlechten Heilung ist eine vordere Kreuzband-Rekonstruktion mit einer stabilen Verankerung, die durch eine sogenannte Enthesis vermittelt wird, erforderlich, die durch Tissue Engineering (TE) noch verbessert werden könnte.

**Das Ziel dieser Arbeit war es, das TE einer Enthesis, die die Knochenverankerung von Bändern vermittelt und mechanische Spannungen an der Integrationsstelle absorbiert, genauer zu untersuchen.**

## Material und Methoden

Zu diesem Zweck wurden lapine Kreuzbandzellen (LKBs) und osteogen differenzierte humane mesenchymale Stromazellen (hMSCs) auf einem triphasischen Scaffold kultiviert, das aus Poly(l-lactid-co-caprolacton) und Polymilchsäure gestickt war. Außerdem wurde der Einfluss eines Kollagenfadens auf Zellen als mögliche Zellbarriere, die die Vermischung der ko-kultivierten Zelltypen verhindern soll, untersucht **(Abb.1)**. Die Barrierescaffolds wurden mit LKB Sphäroiden besiedelt und deren Vitalität überprüft. Der Abstand der Zellen zur Barriere sowie die Auswachsrate der Zellen aus dem Sphäroid wurden bestimmt und mittels immunzytochemischer (Paxillin, filamentäres Aktin, Zellkerne) und histologischer Färbungen bestätigt **(Abb.2)**. Die funktionalisierten triphasischen Scaffolds bestehend aus Knochen-Knorpel- und Ligamentzone wurden mit unterschiedlichen Sphäroiden aus 14 Tage vorkultivierten LKBs und hMSCs, die 14 Tage lang osteogen differenziert und 14 Tage lang weiter kultiviert wurden, besiedelt **(Abb.3)**. Als Kontrollen wurden Sphäroide ohne längere Vorkultivierung oder Differenzierung zur Besiedlung verwendet. Ausgewertet wurde die Vitalität der Zellen **(Abb.4)**, der DNA- sowie der sulfatierte Glykosaminoglykan (sGAG) Gehalt und die relative Genexpression (qPCR) wurden quantitativ bestimmt **(Abb.5)**. Außerdem wurde eine immunzytochemische Färbung durchgeführt.

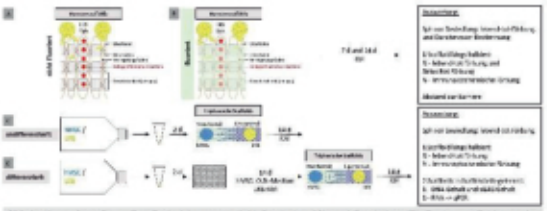

**Abb.1: Versuchsaufbau.** Zur Besiedelung von nicht fluorierten **(A)** und fluorierten **(B)** Barrierescaffolds wurden Sphäroide (Sph) aus lapine Kreuzbandfibroblasten (LKBs) hergestellt. Nach 7 und 14 Tagen (d) Kultivierung erfolgte die Auswertung. Zur Besiedelung der triphasischen Scaffolds wurden undifferenzierte **(C)** und differenzierte **(D)** humane mesenchymale Stromazellen (hMSCs) und LKBs genutzt. Nach 14 d Kultivierung erfolgte die Auswertung. KM: Kulturmedium, O.D.: osteogenes Differenzierungsmedium

## Ergebnisse und Diskussion

Die Funktionalisierung der Barrierescaffolds führte zu einer besseren Adhärenz der Sphäroide und Zellen an die Scaffoldfäden. Der Einfluss eines Kollagenfadens als Barriere für Zellen konnte nicht bestätigt werden. Im Vergleich zu den Sphäroiden aus LKBs hafteten die undifferenzierten und differenzierten hMSC Sphäroide besser an der Scaffoldoberfläche und wuchsen schneller. Der DNA Gehalt war im Knochenteil höher als im Ligamentteil und in den undifferenzierten Teilen höher als in den differenzierten. Der sGAG Gehalt war für die differenzierten Teile höher als für die undifferenzierten. Die Sphäroide auf den Scaffoldteilen hatten eine geringere Genexpression als die einzelnen Sphäroide. Die undifferenzierten hMSC Sphäroide zeigten eine höhere Genexpression von Kollagen Typ I, Kollagen Typ X und RUNX2 als die differenzierten hMSC Sphäroide. Die vorkultivierten LKB Sphäroide wiesen eine starke Genexpression von Kollagen Typ I und Tenascin C auf. Mohawk wurde nur von dem differenzierten Ligamentteil exprimiert.

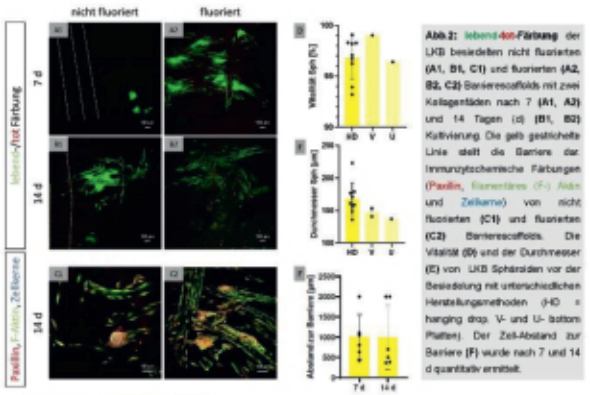


**Abb.2: lebend-/tot-Färbung** der LKB besiedelten nicht fluorierten **(A1, B1, C1)** und fluorierten **(A2, B2, C2)** Barrierescaffolds mit zwei Kollagenfäden nach 7 **(A1, A2)** und 14 Tagen (d) **(B1, B2)** Kultivierung. Die gelb gestrichelte Linie stellt die Barriere dar. Immunzytochemische Färbungen (Paxillin, filamentäres (F-) Aktin und Zellkerne) von nicht fluorierten **(C1)** und fluorierten **(C2)** Barrierescaffolds. Die Vitalität **(D)** und der Durchmesser **(E)** von LKB Sphäroiden vor der Besiedelung mit unterschiedlichen Herstellungsmethoden (HD = hanging drop, V- und U- bottom Platten). Der Zell-Abstand zur Barriere **(F)** wurde nach 7 und 14 d quantitativ ermittelt.

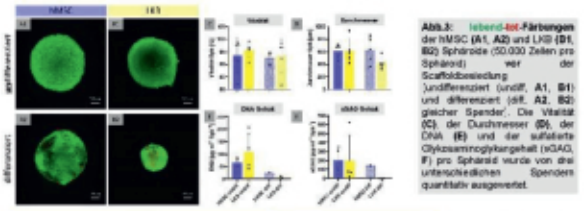


**Abb.3: lebend-/tot-Färbungen** der hMSC **(A1, A2)** und LKB **(B1, B2)** Sphäroide (50.000 Zellen pro Sphäroid) vor der Scaffoldbesiedlung ('undifferenziert (undiff, A1, B1) und differenziert (diff, A2, B2) gleicher Spender'. Die Vitalität **(C)**, der Durchmesser **(D)**, der DNA **(E)** und der sulfatierte Glykosaminoglykangehalt (sGAG, **F**) pro Sphäroid wurde von drei unterschiedlichen Spendern quantitativ ausgewertet.

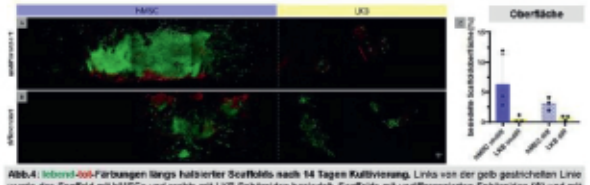


**Abb.4: lebend-/tot-Färbungen längs halbierter Scaffolds nach 14 Tagen Kultivierung.** Links von der gelb gestrichelten Linie wurde das Scaffold mit hMSCs und rechts mit LKB Sphäroiden besiedelt. Scaffolds mit undifferenzierten Sphäroiden **(A)** und mit 14 Tage osteogen-vordifferenzierte hMSC Sphäroide **(B)** wurden verglichen. Die besiedelte Scaffoldoberfläche **(C)** wurde quantitativ nach drei unabhängigen Versuchen ausgewertet.

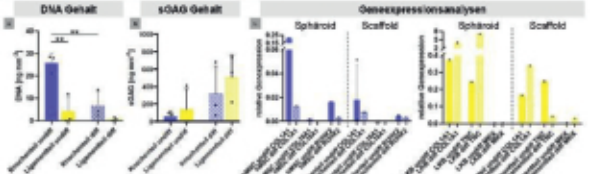


**Abb.5: Bestimmung des DNA Gehalt (A), des sulfatierten Glykosaminoglycan (sGAG) Gehalts (B) und der relativen Genexpression von Knochen- bzw. Ligament-assoziierten Matrixproteinen (C) und Transkriptionsfaktoren in den jeweiligen Scaffoldteilen bzw. von einzelnen Sphäroiden als Kontrolle.** COL1A1 = Kollagen Typ I, COL10A1 = Kollagen Typ X, RUNX2 = runt-related transcription factor-2, TNC = Tenascin C, MKX = Mohawk. Drei unabhängige Versuche ergaben signifikante Unterschiede nach einer one-way ANOVA Testung mit (**) für p<0,01.

## Schlussfolgerung und Ausblick

**Eine erfolgreiche zonale Besiedlung triphasischer Scaffolds unter Verwendung der Sphäroid-Methode ist innerhalb von 14 Tagen möglich und bietet einen neuen Ansatz für das Enthesis TE.**

Die Arbeiten sind assoziiert mit einem durch die Deutsche Forschungsgemeinschaft (SCHU1979/ 14-1) geförderten Projekt zum Tissue engineerten Kreuzbandersatz

## in vitro Enthesisformation mittels Ko-Kultur auf einem triphasisch gestickten Träger für das Kreuzband Tissue Engineering

Julia Vogt[1], Clemens Gögele[2,3], Judith Hahn[4], Annette Breier[4], Michael Meyer[5], Michaela Schröpfer[5], Kerstin Schäfer-Eckart[6], Ralf Lösel[1], Gundula Schulze-Tanzil[2]

[1]Fakultät für Angewandte Chemie, Technische Hochschule Georg-Simon-Ohm, Nürnberg; [2]Institut für Anatomie und Zellbiologie, Paracelsus Medizinische Privatuniversität, Salzburg und Nürnberg, Nürnberg, Deutschland; [3]Fachbereich für Biowissenschaften, Paris Lodron Universität Salzburg, Österreich; [4]Leibniz Institut für Polymerforschung (IPF) Dresden, Deutschland; [5]FILK Freiberg Institute, Freiberg, Deutschland;[6]Klinik für Onkologie/Hämatologie, Klinikum Nürnberg Nord, Nürnberg, Deutschland Contact: vogtju71407@th-nuernberg.de

### Objective
Ein vorderer Kreuzbandriss ist eine der häufigsten Bandverletzungen im Kniegelenk. Aufgrund der schlechten Heilung ist eine vordere Kreuzband-Rekonstruktion mit einer stabilen Verankerung, die durch eine sogenannte Enthesis vermittelt wird, erforderlich, die durch Tissue Engineering (TE) noch verbessert werden könnte. Das Ziel dieser Arbeit war es, das TE einer Enthesis, die die Knochenverankerung von Bändern vermittelt und mechanische Spannungen an der Integrationsstelle absorbiert, genauer zu untersuchen.

### Methods
Zu diesem Zweck wurden lapine Kreuzbandzellen (LKBs) und osteogen differenzierte humane mesenchymale Stromazellen (hMSCs) auf einem triphasischen Scaffold kultiviert, das aus Poly(l-lactid-co-caprolacton) und Polymilchsäure gestickt war. Außerdem wurde der Einfluss eines Kollagenfadens auf Zellen als mögliche Zellbarriere, die die Vermischung der ko-kultivierten Zelltypen verhindern soll, untersucht. Die Barrierescaffolds wurden mit LKB Sphäroiden besiedelt und deren Vitalität überprüft. Der Abstand der Zellen zur Barriere sowie die Auswachsrate der Zellen aus dem Sphäroid wurden bestimmt und mittels immunzytochemischer (Paxillin, filamentäres Aktin, Zellkerne) und histologischer Färbungen bestätigt. Die funktionalisierten triphasischen Scaffolds bestehend aus Knochen-Knorpel- und Ligamentzone wurden mit unterschiedlichen Sphäroiden aus 14 Tage vorkultivierten LKBs und hMSCs, die 14 Tage lang osteogen differenziert und 14 Tage lang weiter kultiviert wurden, besiedelt. Als Kontrollen wurden Sphäroide ohne längere Vorkultivierung oder Differenzierung zur Besiedlung verwendet. Ausgewertet wurde die Vitalität der Zellen, der DNA- sowie der sulfatierte Glykosaminoglykan (sGAG) Gehalt und die relative Genexpression (qPCR) wurden quantitativ bestimmt. Außerdem wurde eine immunzytochemische Färbung durchgeführt.

### Results
Die Funktionalisierung der Barrierescaffolds führte zu einer besseren Adhärenz der Sphäroide und Zellen an die Scaffoldfäden. Der Einfluss eines Kollagenfadens als Barriere für Zellen konnte nicht bestätigt werden. Im Vergleich zu den Sphäroiden aus LKBs hafteten die undifferenzierten und differenzierten hMSC Sphäroide besser an der Scaffoldoberfläche und wuchsen schneller. Der DNA Gehalt war im Knochenteil höher als im Ligamentteil und in den undifferenzierten Teilen höher als in den differenzierten. Der sGAG Gehalt war für die differenzierten Teile höher als für die undifferenzierten. Die Sphäroide auf den Scaffoldteilen hatten eine geringere Genexpression als die einzelnen Sphäroide. Die undifferenzierten hMSC Sphäroide zeigten eine höhere Genexpression von Kollagen Typ I, Kollagen Typ X und RUNX2 als die differenzierten hMSC Sphäroide. Die vorkultivierten LKB Sphäroide wiesen eine starke Genexpression von Kollagen Typ I und Tenascin C auf. Mohawk wurde nur von dem differenzierten Ligamentteil exprimiert.

### Conclusions
Eine erfolgreiche zonale Besiedlung triphasischer Scaffolds unter Verwendung der Sphäroid-Methode ist innerhalb von 14 Tagen möglich und bietet einen neuen Ansatz für das Enthesis TE.

PARACELSUS
MEDIZINISCHE PRIVATUNIVERSITÄT

Klinikum Nürnberg
Wir sind für Sie da!

# Spondylodiscitis – a retrospective analysis of hospitalized older patients

Alexandra Volp[1], Markus Gosch[2]

[1]Paracelsus Medical University, Nuremberg, Germany; [2]Department of Geriatrics, Paracelsus Medical University, Nuremberg, Germany;
Contact: alexandra.volp@stud.pmu.ac.at

## Abstract

**Background:** Spondylodiscitis is an infectious condition of the spine mostly observed in older adults and those with comorbidities. Mortality rates range from 2.0 – 12.6%. Elevated C-reactive protein (CRP) levels, a Charlson Comorbidity Index (CCI) of ≥ 2, and advanced age were described to be associated with higher mortality. The objective of this study was to evaluate outcome predictors in patients with spondylodiscitis.
**Material and Methods:** A total of 154 patients (mean age 74.6 years) were diagnosed with spondylodiscitis at Nuremberg General Hospital from 2014 – 2020. Among those, 51 patients died and/or received treatment in the intensive care unit (ICU), these were declared the negative outcome group. Based on CCI values, CRP peak levels, and the number of specialties involved in the treatment process, prediction equations were formulated. The prediction equations utilize these parameters to determine patients at higher risk of a negative outcome. Additionally, the influence of age on the negative outcome group was explored; patient age was plotted against the probability of a negative outcome.
**Results:** The statistical analysis showed a mortality rate of 15.6% in the study population. Negative outcome as a combination of fatalities and ICU treatment can be significantly predicted by elevated CRP peak levels and CCI values. A prediction equation which combines these parameters has a specificity of 87.8%. Adding the number of specialties involved in the treatment process, led to a specificity of 88.8%. Age was discovered to be inversely proportional to negative outcome probability. Patients in the age groups between 40 and 50 years presented with negative outcome rates of ≥ 50%. The negative outcome rates in patients of ≥ 80 years were ≤ 44%.
**Conclusion:** This study shows that higher CCI values, elevated CRP peak levels, and an increased number of specialties correlate with a higher probability of negative outcome in patients with spondylodiscitis. The CCI-CRP prediction equation allows for early detection of patients with elevated risk of being in the negative outcome group. Contrary to prior research, among this study population, patients of higher age showed a decreased probability of negative outcome.
**Keywords:** Spondylodiscitis Vertebral Osteomyelitis Outcome Prediction Spine Infection

## Introduction and background

Spondylodiscitis is a disease of mostly older adults[1]. A review of the literature revealed several factors that may influence outcome of patients. Most patients with spondylodiscitis suffer from several comorbidities.[2,3] Patients often present with increased C-reactive protein (CRP) levels and are of older age.[1]

## Study population and design

This retrospective study includes patients over the age of 18 that were hospitalized at Nuremberg General Hospital with the diagnosis of spondylodiscitis. Between December 2014 and January 2020, Nuremberg General Hospital had $N = 252$ patients hospitalized with this diagnosis. In this study 98 patients were excluded. Six patients were excluded due to missing documents, and 92 patients were excluded because their primary diagnosis was not made at Nuremberg General Hospital, or their primary therapy took place elsewhere. Overall, this study includes $N = 154$ patients, among them 54 women (35.1%) and 100 men (64.9%). The mean age at the time of hospitalization was 74.62 years ($SD = 13.51$) (range, 35.13 - 95.87).

## Outcome Analysis

The patient data was analyzed according to factors that may be relevant to the outcome in the study population and may help to make a prognosis. Based on a review of Loibl et al.,[3] the factors CCI, CRP, and Number of Specialties were subsequently analyzed for their relevance to the patient outcome. CCI values and CRP levels could be used as tools for early detection of patients with a possible negative outcome, whereas the number of specialties could rather serve as a retrospective means of quality analysis. The patient's death or treatment in the intensive care unit (ICU) were classified as negative outcomes. The negative outcome group contains 51 patients (33.1%, $N = 154$).

## Study aim

Finding a method to predict whether a patient will have a negative outcome due to this disease is the goal of this study. The results may provide clinicians with valuable information allowing for a more accurate prognosis of patients with spondylodiscitis.

## Results: CCI and CRP

Combined CCI and CRP peak values significantly predicted negative outcome, $F(1, 7) = 75.01$, $p < .001$.

$$P(neg.outcome) = .0354 + .0151 * |(CCI + 1) * 2.3 + CRP\left(\frac{mg}{dl}\right)|$$

The prediction equation can be reformulated to give a threshold CRP value at which point a patient would be considered at a high risk of a negative outcome.

$$CRP\left(\frac{mg}{dl}\right) = 35.0907 - 2.3 * CCI$$

## Results: CCI, CRP, and Number of Specialties

Combined weighted values of CCI, CRP, and the Number of Specialties showed a significant influence on the outcome $F(1, 7) = 69.10$, $p < .001$.

$$P(neg.outcome) = .015 * [|(CCI + 1) * 2.3 + CRP\left(\frac{mg}{dl}\right)| + .9 * S] - .103$$

## Results: Age

Patients in the age groups between 40 and 50 years presented with negative outcome probabilities of ≥ 50%. On the other hand, patients in the age groups of ≥ 80 years showed negative outcome rates between 19% and 44%.

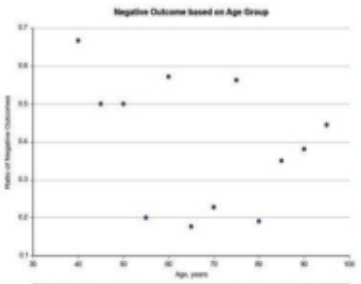

Figure 1: Ratio of Negative Outcomes based on Age

## Conclusions & Perspectives

The results of this study emphasize the predictive value of age, CCI values, CRP peak levels, and the number of specialties on negative outcome in patients with spondylodiscitis. Unexpectedly, high age seems to be inversely correlated with negative outcome. The singular parameters CCI and CRP peak levels significantly predict the negative outcome group. Higher statistical significance was achieved by combining these factors. The combined CCI-CRP prediction equation could be easily implemented into the clinical setting.
It appears that higher CCI values, CRP peak levels, and an increased number of specialties are associated with a higher probability of negative outcome in patients with spondylodiscitis.

## References

1 Jeong S-J, Choi S-W, Youm J-Y, Kim H-W, Ha H-G, Yi J-S. Microbiology and Epidemiology of Infectious Spinal Disease. *J Korean Neurosurg Soc*. 2014;56(1):21. doi:10.3340/jkns.2014.56.1.21
2 Zimmerli W. Vertebral Osteomyelitis. *N Engl J Med*. 2010;362(11):1022-1029. doi:10.1056/NEJMcp0910753
3 Loibl M, Stoyanov L, Doenitz C, et al. Outcome-related co-factors in 105 cases of vertebral osteomyelitis in a tertiary care hospital. *Infection*. 2014;42(3):503-510. doi:10.1007/s15010-013-0582-0
4 Locker GA, Easley KA, McHenry MC. Vertebral Osteomyelitis: Long-Term Outcome for 253 Patients from 7 Cleveland-Area Hospitals. :10.

## Spondylodiscitis – a retrospective analysis of hospitalized older patients

Markus Gosch[1], Alexandra Volp[2]

[1]Department of Geriatrics, Paracelsus Medical University, Nuremberg, Germany; [2]Paracelsus Medical University, Nuremberg, Germany; Contact: alexandra.volp@stud.pmu.ac.at

### Objective
Spondylodiscitis is an infectious condition of the spine mostly observed in older adults and those with comorbidities. Mortality rates range from 2.0 – 12.6%. Elevated C-reactive protein (CRP) levels, a Charlson Comorbidity Index (CCI) of ≥ 2, and advanced age were described to be associated with higher mortality. The objective of this study was to evaluate outcome predictors in patients with spondylodiscitis.

### Methods
A total of 154 patients (mean age 74.6 years) were diagnosed with spondylodiscitis at Nuremberg General Hospital from 2014 – 2020. Among those, 51 patients died and/or received treatment in the intensive care unit (ICU), these were declared the negative outcome group. Based on CCI values, CRP peak levels, and the number of specialties involved in the treatment process, prediction equations were formulated. The prediction equations utilize these parameters to determine patients at higher risk of a negative outcome. Additionally, the influence of age on the negative outcome group was explored; patient age was plotted against the probability of a negative outcome.

### Results
The statistical analysis showed a mortality rate of 15.6% in the study population. Negative outcome as a combination of fatalities and ICU treatment can be significantly predicted by elevated CRP peak levels and CCI values. A prediction equation which combines these parameters has a specificity of 87.8%. Adding the number of specialties involved in the treatment process, led to a specificity of 88.8%. Age was discovered to be inversely proportional to negative outcome probability. Patients in the age groups between 40 and 50 years presented with negative outcome rates of ≥ 50%. The negative outcome rates in patients of ≥ 80 years were ≤ 44%.

### Conclusions
This study shows that higher CCI values, elevated CRP peak levels, and an increased number of specialties correlate with a higher probability of negative outcome in patients with spondylodiscitis. The CCI-CRP prediction equation allows for early detection of patients with elevated risk of being in the negative outcome group. Contrary to prior research, among this study population, patients of higher age showed a decreased probability of negative outcome.

PARACELSUS
MEDIZINISCHE PRIVATUNIVERSITÄT

Klinikum Nürnberg
Wir sind für Sie da!

# Controlled and randomized study of the psychological effects of yoga during breast cancer therapy

Lea Sophie von Lutz

Department of Obstetrics and Gynecology, University Hospital Nuremberg, Paracelsus Medical University; Contact: lea.lutz@stud.pmu.ac.at

## ABSTRACT

According to the World Health Organization (WHO) breast cancer is one of the most common cancers among women worldwide, and the leading cause of cancer death in women worldwide.[1] In 2020 there was an estimated number of over two million new cases and an estimated number of deaths of nearly 700,000, whereas a decrease in mortality is noticed, which is most likely to be associated with improved therapy.

The treatment often extends over several months and bears a variety of psychological and physical burdens for the patients, which they have to deal with mostly on their own. Additionally, suffering from a life-threatening disease brings about a completely new situation with serious psychological problems for the patient. The patients experience a life-changing event and are forced to face up to their health situation.

In many areas the use of complementary and alternative medicine (CAM) has become more important over the years. It is commonly assumed that yoga has beneficial effects on somatic and mental health factors. In addition, the practice of yoga in cancer patients has few known side effects and is easily accessible as a cost-effective alternative in contrast to other procedures and is easily feasible at home.[2]

## OBJECTIVE

- primary objective of this thesis is to examine whether yoga lessons help the patients to achieve a greater contentment and to improve the quality of life during their medical treatment and thus to reduce the side effects of chemotherapy and radiation therapy
- the area of quality of life covers factors like fatigue, anxiety, depression, nausea, emesis, general state of health, polyneuropathy, quality of sleep and physical resilience
- questionnaires used: ZUF-8 and FACT-B

## MATERIAL AND METHODS

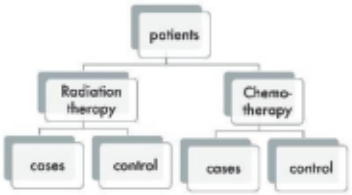


Fig. 1: Group organization

| | Radiation therapy | Chemo-therapy | Total |
|---|---|---|---|
| Cases | 20 | 19 | 39 |
| Control | 21 | 17 | 38 |
| Total | 41 | 36 | 77 |

Fig. 2: Study population




Fig. 3: Study timeline for the chemotherapy arm




Fig. 4: Study timeline for the radiation therapy arm

## RESULTS

- the two study arms were differentiated in their evaluation, because of different side effects and the different duration of therapies and yoga intervention: 6 months for patients with chemotherapy and approximately 6-8 weeks for the patients with radiation therapy
- in each study arm a significant improvement regarding quality of life was observed during the interventions when comparing case group and control group
- evaluation of the ZUF questionnaire revealed no discernible significance between the yoga group and the control group throughout the two arms, but the mean scores show a high overall value (maximum score 32)

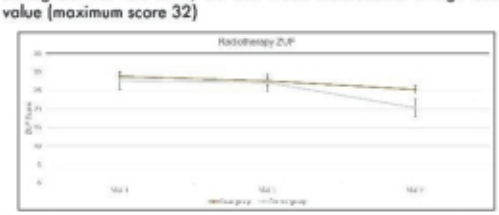


Fig. 5: ZUF mean score in the radiationtherapy arm with standard deviation

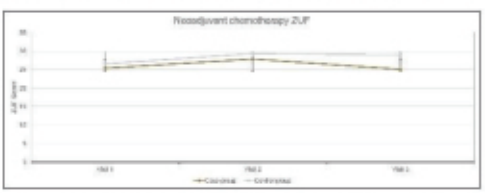


Fig. 6: ZUF mean score in the neoadjuvant chemotherapy arm with standard deviation

## CONCLUSION

- this controlled randomized trial of 120 women diagnosed with breast cancer compared a case group participating in yoga interventions with a control group receiving medical counseling sessions
- regarding quality of life through both study arms significant improvement was seen in the case group with yoga interventions compared with the control group, which received individual medical consultations
- contrary to what was expected, there was no significant improvement in patient satisfaction
- in accordance with the literature of already conducted studies, the assumption is confirmed that yoga is a useful complementary measure to conventional therapy in order to increase the quality of life of patients

## REFERENCES

- 1. Harbeck N, Gnant M. Breast cancer. Lancet. 03 2017;389(10074):1134-1150. doi:10.1016/S0140-6736(16)31891-8
- 2. Kaur G, Prakash G, Malhotra P, et al. Home-Based Yoga Program for the Patients Suffering from Malignant Lymphoma during Chemotherapy: A Feasibility Study. Int J Yoga. 2018 Sep-Dec 2018;11(3):249-254. doi:10.4103/ijoy.IJOY_17_18

## Controlled and randomized study of the psychological effects of yoga during breast cancer therapy

Lea Sophie von Lutz[1]

[1]Department of Obstetrics and Gynecology, University Hospital Nuremberg, Paracelsus Medical University; Contact: lea.lutz@stud.pmu.ac.at

### Objective
Prevalence as well as survival rates of breast cancer have increased significantly in recent years. Despite individual adjustments and improvements in therapy, patients still experience adverse physical and psychological side effects. The primary objective of the study focuses on the effect that the use of yoga as a complementary medical measure can have on the side effects of the therapy, in particular how the quality of life of patients and patients' satisfaction is influenced.

### Methods
A total of 77 patients with breast cancer were included in the study and divided into two arms according to their recommended therapy: radiation therapy or neoadjuvant chemotherapy. Afterwards, the groups were randomized into a yoga group and a consultation group. The assessment was performed prior to therapy, after completion of therapy, and six months after the end of therapy.

### Results
There were significant differences in the area of improvement in quality of life in both study arms when the case and control groups were compared. There were no significant differences in the improvement of patient satisfaction with the average values remaining at a consistently high level over the three assessment visits.

### Conclusions
Yoga intervention in the context of breast cancer proves to be useful to increase the quality of life during therapy. An accompanying complementary measure to conventional therapy should therefore be sought. A significant improvement of the patient satisfaction could not be proven, nevertheless both groups showed a high level of patient satisfaction.

### References
1. Lea Sophie von Lutz, Department of Obstetrics and Gynecology, University Hospital Nuremberg, Paracelsus Medical University

# Ketogenic diets reduce melanoma growth *in vivo* regardless of mutation status and metabolic signature

Daniela D Weber[1], Sepideh Aminzadeh-Gohari[1], Maheshwor Thapa[2], Anna-Sophia Redtenbacher[1], Luca Catalano[1], Tânia Capelôa[3], Thibaut Vazeille[3], Michael Emberger[4], Thomas K Felder[5], René G Feichtinger[1], Peter Koelblinger[6], Guido Dallmann[2], Pierre Sonveaux[3], Roland Lang[5], and Barbara Kofler[1]

[1]Research Program for Receptor Biochemistry and Tumor Metabolism, Dept. of Pediatrics, University Hospital of the Paracelsus Medical University, Salzburg, Austria; [2]biocrates life sciences ag, Innsbruck, Austria; [3]Institut de Recherche Expérimentale et Clinique (IREC), Université catholique de Louvain (UCLouvain), Brussels, Belgium; [4]Pathobiologie Salzburg, Salzburg, Austria; [5]Dept. of Laboratory Medicine, University Hospital of the Paracelsus Medical University, Salzburg, Austria; [6]Dept. of Dermatology and Allergology, University Hospital of the Paracelsus Medical University, Salzburg, Austria

## INTRODUCTION

Regarding energy production, many cancer cells strongly depend on glycolysis instead of oxidative phosphorylation (OXPHOS), rendering them susceptible to ketogenic diet (KD) [1]. KD is a high-fat, low-carbohydrate and adequate protein diet that reduces circulating glucose and, consequently, insulin and IGF-1 levels. Melanoma is a genetically (e.g. BRAF mutation status) and metabolically (e.g. OXPHOS activity level) heterogeneous solid tumor [2]. Thus, it remains unclear which genetic [3], metabolic, and immunological [4] factors contribute to the response to KDs. Therefore, we used various melanoma *in vivo* tumor models to determine whether the effect of KDs on melanoma progression depends on the oncogenic and metabolic signature as well as on a functional immune system.

## METHODS

Melanoma xenografts were established in immunodeficient CD-1 nude mice using BRAF mutant A375 and WM47, BRAF/NRAS wild-type WM3311, and NRAS mutant WM3000 cells varying in their glycolytic and respiratory capacity. Melanoma allografts were established in immunocompetent C57BL/6j syngeneic mice using highly metastatic B16-M4b cells [5]. Mice were equally assigned to control (CTRL) diet or KDs differing in their triglyceride composition (Table 1). The effects of KDs on tumor growth, metastasis, blood glucose as well as β-hydroxybutyrate (BHB) levels were evaluated. Metabolites in plasma and xenografts were analyzed using targeted metabolomics (MxP® Quant 500 + acylcarnitine assay, biocrates life sciences ag).

**Table 1. Composition and energy supply of the different diets.**

| Component (% per kg) | CTRL | LCT | LCT-MCT |
|---|---|---|---|
| Crude Protein | 18.1 | 8.1 | 8.1 |
| LCT | 7.1 | 74.6 | 49.8 |
| MCT® | 0 | 0 | 15 |
| MCT180 | 0 | 0 | 10 |
| Sugar | 6 | 1 | 1 |
| Starch | 51.2 | 0 | 0 |
| Crude fiber | 10 | 9.9 | 9.9 |
| Crude ash | 4.8 | 4.4 | 4.4 |

CTRL: amino diet, LCT: long chain triglyceride based KD, LCT (MCT®): long chain triglyceride based KD supplemented with C8 and C10 carbon medium chain triglycerides.

## RESULTS

→ KDs reduced the growth of melanoma xenografts regardless of the underlying mutational and metabolic signature compared to CTRL diet (Fig. 1a-d). KDs decreased blood glucose (Fig. 1e) and increased plasma BHB levels (Fig. 1f) in melanoma-bearing mice compared to mice fed a CTRL diet.

→ KDs trended to reduce the size of recurring tumors after surgical intervention. Moreover, KDs reduced the number of B16-M4b-bearing mice developing lung metastases (Fig. 2).

→ Targeted metabolomics revealed that KDs induce distinct alterations in amino acid related pathways such as lysine degradation, glycine, serine and threonine metabolism, arginine biosynthesis, and tryptophan metabolism. Moreover, KDs increased primary bile acid synthesis (Fig. 3).

→ KDs also affected plasma (Fig. 4) and tumor (Fig. 5) lipid profiles. In particular, KDs increased sphingomyelin synthesis, indicated by increased ratios of sphingomyelins to ceramides and phosphatidylcholines, respectively. KDs also altered the hydroxylation of sphingomyelins and acylcarnitines.

## CONCLUSION

Our data show that KDs can target melanoma growth regardless of its genetic and metabolic plasticity. The effect of KDs on melanoma progression was independent of the immune status of the mice, indicating that the effect of KDs on tumor proliferation does not entirely depend on an intact immune system as suggested recently [4]. Moreover, KDs affected different metabolic pathways simultaneously, which seems to create an unfavorable metabolic environment for melanoma cell proliferation, rendering the KD a promising adjunct to melanoma therapy.

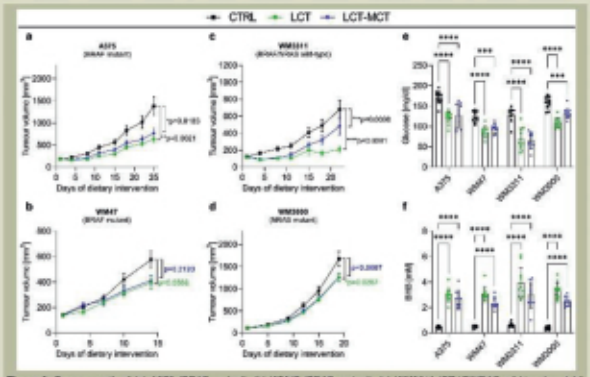


**Figure 1:** Tumor growth of (a) A375 (BRAF mutant), (b) WM47 (BRAF mutant), (c) WM3311 (BRAF/NRAS wild-type) and (d) WM3000 (NRAS mutant) melanoma xenografts. Mice were fed with control diet or different KDs. Mean ± SEM, the area under the growth curve (AUC) was calculated for every mouse and statistical significance between the AUC of CTRL and each KD group was evaluated using one-way ANOVA. (e) Blood glucose and (f) BHB levels of melanoma-bearing mice fed with CTRL diet or KDs. Mean ± SD, Two-Way ANOVA, *** p<0.001, **** p<0.0001. n = 10-13.

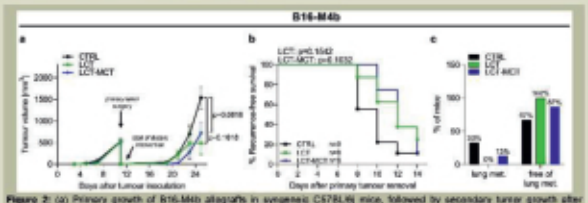


**Figure 2:** (a) Primary growth of B16-M4b allografts in syngeneic C57BL/6j mice, followed by secondary tumor growth after primary tumor removal. One day after surgery, mice were fed either CTRL diet or KDs. Mean ± SEM, the area under the growth curve (AUC) was calculated for every mouse and statistical significance between the AUC of CTRL and each KD group was evaluated using one-way ANOVA. (b) Recurrence-free survival of mice fed with CTRL diet or KDs. Kaplan-Meier survival curve, Log-rank (Mantel-Cox) test. (c) Percentage of mice presenting metastasis or no metastasis in the lungs of B16-M4b melanoma bearing mice after 14 days of dietary intervention. n = 8-9.

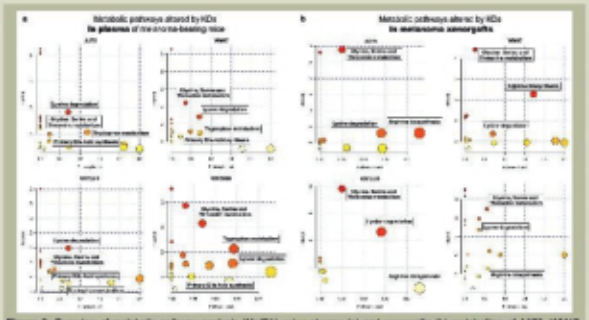


**Figure 3:** Overview of metabolic pathway analysis (MetPA) using plasma (a) and xenografts (b) metabolites of A375, WM47, WM3311, and WM3000 melanoma-bearing mice. Consistently altered pathways by KDs in plasma and xenografts are highlighted in the respective MetPA result overview, indicating matched pathways arranged by p-values from pathway enrichment analysis (Y-axis) and pathway impact values from pathway topology analysis (X-axis). Node color and radius are based on its p-value and pathway impact value, respectively.

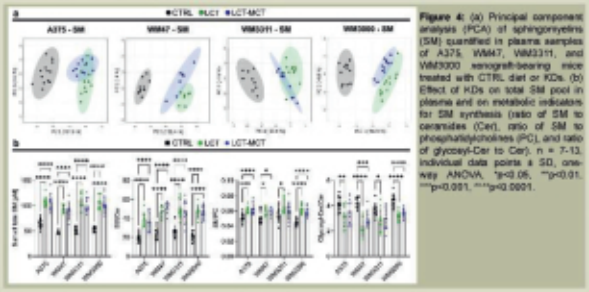


**Figure 4:** (a) Principal component analysis (PCA) of sphingomyelins (SM) quantified in plasma samples of A375, WM47, WM3311, and WM3000 xenograft-bearing mice treated with CTRL diet or KDs. (b) Effect of KDs on total SM pool in plasma and on metabolic indicators for SM synthesis (ratio of SM to ceramides (Cer), ratio of SM to phosphatidylcholines (PC), and ratio of glycosyl-Cer to Cer). n = 7-13, individual data points ± SD, one-way ANOVA, *p<0.05, **p<0.01, ***p<0.001, ****p<0.0001.

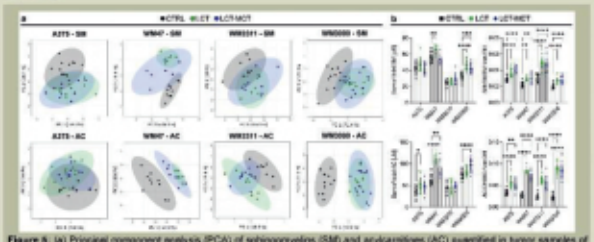


**Figure 5:** (a) Principal component analysis (PCA) of sphingomyelins (SM) and acylcarnitines (AC) quantified in tumor samples of A375, WM47, WM3311, and WM3000 xenograft-bearing mice treated with CTRL diet or KDs. (b) Effect of KDs on SM and AC pools and hydroxylation in tumor tissues. n = 7-13 per group, individual data points ± SD, one-way ANOVA, *p<0.05, **p<0.01, ***p<0.001, ****p<0.0001.

**REFERENCES**

[1] Weber DD et al., Mol Metab 2019
[2] Feichtinger RG et al., Exp Dermatol 2018
[3] Xia S et al, Cell Metab 2017
[4] Ferrere G et al, JCI Insight 2020
[5] Porporato PE et al., Cell Rep 2014

**FUNDING**

EU H2020-MSCA-ITN-2016-722605 TRANSMIT project, Paracelsus Medical University (E-17/25/132-LKK), grants from Roche and Pierre Fabre, Belgian Fonds National de la Recherche Scientifique (F.R.S.-FNRS, grants CDR #J.0135.18 and Télévie #7.4529.17) and Louvain Foundation.

contact: d.weber@salk.at

## Ketogenic diets reduce melanoma growth in vivo regardless of mutation status and metabolic signature

Daniela D Weber[1], Sepideh Aminzadeh-Gohari[1], Maheshwor Thapa[2], Anna-Sophia Redtenbacher[1], Luca Catalano[1], Tânia Capelôa[3], Thibaut Vazeille[3], Michael Emberger[4], Thomas K Felder[5], René G Feichtinger[1], Peter Koelblinger[6], Guido Dallmann[2], Pierre Sonveaux[3], Roland Lang[6], Barbara Kofler[1]

[1]Research Program for Receptor Biochemistry and Tumor Metabolism, Dept. of Pediatrics, Paracelsus Medical University, Salzburg, Austria; [2]biocrates life sciences ag, Innsbruck, Austria; [3]Institut de Recherche Expérimentale et Clinique (IREC), Université catholique de Louvain (UCLouvain), Brussels, Belgium; [4]Patholab Salzburg, Salzburg, Austria; [5]Dept. of Laboratory Medicine, Paracelsus Medical University, Salzburg, Austria; [6]Dept. of Dermatology and Allergology, Paracelsus Medical University, Salzburg, Austria; Contact: d.weber@salk.at

### Objective
The high dependency of many cancer cells on glycolysis instead of oxidative phosphorylation (OXPHOS) should render cancer cells susceptible to ketogenic diet (KD). KD is a high-fat, low-carbohydrate and adequate protein diet that reduces circulating glucose and, consequently, insulin and IGF-1 levels. Melanoma is a genetically and metabolically heterogeneous solid tumor. Our aim was to determine the effect of KDs, differing in their triglyceride composition, on transplanted melanomas with varying metabolic signatures and genetic backgrounds in mice.

### Methods
Melanoma xenografts were established using WM3311 (BRAF/NRAS wild-type; glycolysis high/OXPHOS high), WM47 (BRAF V600E mutant, glycolysis high/OXPHOS high), A375 (BRAF V600E mutant, glycolysis high/OXPHOS low) and WM3000 (NRAS Q61R mutant; glycolysis low/OXPHOS low) cells in CD-1 nude mice. Melanoma allografts were established in C57BL/6j immunocompetent mice using highly metastatic B16-M4b cells. Melanoma-bearing mice were fed with a control diet (CTRL) or KDs. Plasma and tumor metabolites were analyzed using the MxP® Quant 500 Kit combined with an acylcarnitine assay (biocrates life sciences ag).

### Results
KDs decreased growth of wild-type, BRAF mutant as well as NRAS mutant melanoma xenografts. KDs significantly increased the survival time of A375 and WM3000 melanoma-bearing mice compared to mice fed with CTRL diet. In the immunocompetent B16-M4b melanoma model, KDs trended to reduce the size of recurred tumors after surgical intervention and KDs reduced the number of mice developing lung metastases. Targeted metabolomics revealed that KDs induce distinct alterations in amino acid related pathways such as lysine degradation, glycine, serine and threonine metabolism, arginine biosynthesis, and tryptophan metabolism. Moreover, KDs increased primary bile acid synthesis. Plasma and tumor lipid profiles were also affected by KDs. In particular, KDs increased sphingomyelin synthesis as well as the hydroxylation of sphingomyelins and acylcarnitines.

### Conclusions
Taken together, our data show that KDs can target melanoma growth regardless of its genetic and metabolic plasticity. Moreover, KDs affect different metabolic pathways simultaneously, which seems to create an unfavorable metabolic environment for melanoma growth, rendering the KD a promising adjunct to melanoma therapy.

### Acknowledgements
This project was supported by grants from the EU H2020-MSCA-ITN-2016-722605 TRANSMIT project, the Paracelsus Medical University (E-17/25/132-LKK), Roche and Pierre Fabre, Belgian Fonds National de la Recherche Scientifique and the Louvain Foundation.

**Nicolas Weilgony[1], Ilka Flesner[1], Adel Szakacs-Fusch[2],Christoph Fusch[2], and Ronald Ebbert[1]**

1: Technische Hochschule Nürnberg Georg Simon Ohm, Faculty of Applied Chemistry, Nuremberg, Germany; 2: Klinik für Neugeborene, Kinder und Jugendliche; Universitätsklinik der Paracelsus Medizinischen Privatuniversität, Klinikum Nürnberg Süd

Contact: ronald.ebbert@th-nuernberg.de

# Analysing the Neonatal Microbiome by qPCR and Nanopore Sequencing

## Objective

The gut microbiome in infants is important for development and health, and perturbations of the microbiota can have drastic health consequences[1]. Preterm infants in general have less diverse gut microbiota, often require antibiosis and are at increased risk of sepsis and necrotizing enterocolitis (NEC)[2,3]. In infants, mode of delivery and nutrition are important factors determining early colonization[4]. We want to establish a methodology enabling identification of the complete neonatal microbiome by 3rd generation sequencing combined with absolute quantification by qPCR.

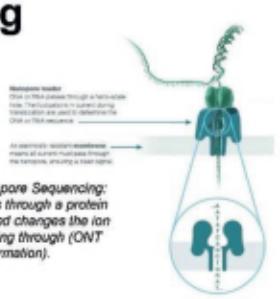

*FIG. 1 Nanopore Sequencing: DNA passes through a protein nanopore and changes the ion current flowing through (ONT product information).*

## Results

Stool samples of term and preterm infants were collected and DNA extracted. Different eu- and prokaryotic taxa are identified and quantified by quantitative PCR using group-specific primer pairs.

16S sequences of the DNA samples were amplified and sequencing libraries created using the "16S Barcoding Kit" supplied by Oxford Nanopore Technologies (ONT). Sequencing a commercial DNA standard, all species were found and quantification closely matched the theoretical content (FIG. 2). When DNA was extracted from a commercial cell standard, variations increased as expected, but all bacteria except *Bifidobacterium* were identified (FIG. 3). DNA from stool samples sequenced with the same kit yielded the same results, i.e. no Bifidobacteria, even when qPCR indicated their presence (FIG. 4, "16S" and "qPCR").

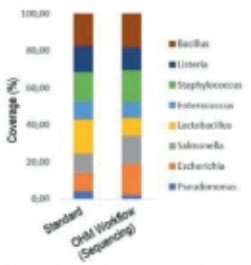


*FIG. 2 Comparison of sequencing results with the theoretical contents of a commercial DNA standard.*

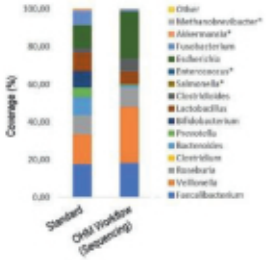


*FIG. 3 Comparison of sequencing results with the theoretical contents of a commercial cell standard.*

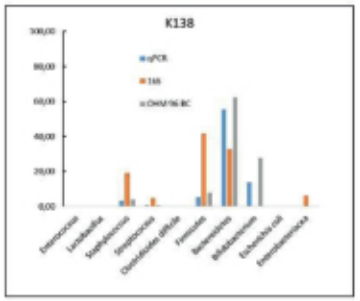


*FIG. 4 Results for one patient sample using group-specific qPCR reactions ("qPCR"), ONT sequencing with the 16S-Barcoding Kit ("16S") and with the newly developed method ("OHM 96 BC") to identify bacterial genera.*

Since Bifidobacteria are important members of a healthy neonatal microbiome, a different, truly universal protocol had to be established. We used alternative forward Primers and found one universal pair also amplifying Bifidobacteria (FIG. 4, "OHM 96 BC"). Using a protocol with a 2nd barcoding PCR, these Primers can be used to prepare sequencing libraries with up to 96 barcodes, effectively decreasing consumable costs.

Combining the data obtained by sequence analysis and qPCR and taking the copy number of 16S genes in different genera into account, relative abundances of 16S sequences in a sample can be transformed into absolute cell numbers (FIG. 5).

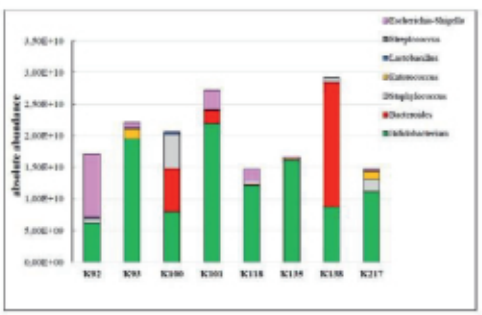


*FIG. 5 Absolute Abundances (cell numbers/ g of stool) of bacterial genera in different samples.*

## Conclusion

The combination of group-specific qPCR and new, truly universal 16S sequencing enables reliable analysis of the complete intestinal microbiome, e.g. to monitor influences of nutrition, medications or other factors.

## References

1 Neu, Josef (2013). Current pediatrics reports 1 (4), 215–221.
2 Cassir, Nadim et al. (2015): Clinical infectious diseases 61 (7), 1107–1115.
3 Wandro, Stephen et al. (2018): mSphere 3 (3).

**This project was generously supported by Staedtler Stiftung, Nürnberg**

STAEDTLER STIFTUNG

TECHNISCHE HOCHSCHULE NÜRNBERG GEORG SIMON OHM

Klinikum Nürnberg

## Analysing the Neonatal Microbiome by qPCR and Nanopore Sequencing

Nicolas Weilgony[1], Ilka Flesner[1], Adel Szakacs-Fusch[2], Christoph Fusch[2], Ronald Ebbert[1]

[1]Technische Hochschule Nürnberg Georg Simon Ohm, Faculty of Applied Chemistry, Nuremberg, Germany; [2]Klinik für Neugeborene, Kinder und Jugendliche; Klinikum Nürnberg Süd, Paracelsus Medical University, Nuremberg, Germany; Contact: ronald.ebbert@th-nuernberg.de

### Objective

The gut microbiome in infants is important for development and health, and perturbations of the microbiota can have drastic health consequences (1). Preterm infants in general have less diverse gut microbiota, often require antibiosis and are at increased risk of sepsis and necrotizing enterocolitis (2,3). We want to establish a methodology enabling identification of the complete neonatal microbiome by 3rd generation sequencing combined with absolute quantification by qPCR.

### Methods

Stool samples of term and preterm infants were collected and DNA extracted. Different eu- and prokaryotic taxa are identified and quantified by quantitative PCR using group-specific primer pairs. 16S sequences of the DNA samples were amplified and sequencing libraries created using the "16S Barcoding Kit" supplied by Oxford Nanopore Technologies (ONT).

### Results

Sequencing a commercial DNA standard, all species were found and quantification closely matched the theoretical content. When DNA was extracted from a commercial cell standard, variations increased as expected, but all bacteria except Bifidobacterium were identified. DNA from stool samples sequenced with the same kit yielded the same results, i.e. no Bifidobacteria, even when qPCR indicated their presence.

Since Bifidobacteria are important members of a healthy neonatal microbiome, a different, truly universal protocol had to be established. We used alternative forward Primers and found one universal pair also amplifying Bifidobacteria. Using a protocol with a 2nd barcoding PCR, these Primers can be used to prepare sequencing libraries with up to 96 barcodes, effectively decreasing consumable costs.

Combining the data obtained by sequence analysis and qPCR and taking the copy number of 16S genes in different genera into account, relative abundances of 16S sequences in a sample can be transformed into absolute cell numbers.

### Conclusions

The combination of group-specific qPCR and new, truly universal 16S sequencing enables reliable analysis of the complete intestinal microbiome, e.g. to monitor influences of nutrition, medications or other factors.

### References

1. Neu, Josef (2013): Current pediatrics reports 1 (4), 215–221.
2. Cassir, Nadim et al. (2015): Clinical infectious diseases 61 (7), 1107–1115
3. Wandro, Stephen et al. (2018): mSphere 3 (3).

BIOMÉRIEUX




**Seit mehr als 50 Jahren entwickelt und produziert bioMérieux *in vitro* Diagnostika zur Verbesserung der öffentlichen Gesundheit.**

Tägliches Ziel aller unserer Mitarbeiter ist es, Fachkräften im Gesundheitswesen erstklassige Lösungen anzubieten, die ihnen helfen, Patienten und Verbrauchern in aller Welt zu dienen – mit richtigen Entscheidungen zur richtigen Zeit!

**Denn dies ist der Kern einer verlässlichen Diagnostik!**

**www.biomerieux.de**



NEW ENGLAND BioLabs GmbH

be INSPIRED
drive DISCOVERY
stay GENUINE



Request the brand new
NEB Catalog &
Technical Reference
2021/22!



Discover immersive
AR content via the NEB AR App

Wishing you a happy and prosperous

**Paracelsus Science Get Together 2021,**

as well as continued success
for all your research endevours.

*Get your free NEB Catalog at:*
*www.neb-online.de/Katalog*

New England Biolabs
– Enzymes & Reagents for:

Sample Preparation for RNA Synthesis
Next-Gen-Seq DNA
Modification
Synthetic Biology qPCR & PCR
Nucleic Acid Purification Cloning &
RNA Competent Cells Assembly
Genome Editing Epigenetics Glycobiology
CRISPR/Cas Gene Expression
Protein Expression Genomics Cellular Analysis
Amplification

**Abteilung Innere Medizin**
Ärztliche Leitung: PD. Dr. med. Dane Wildner

**Krankenhäuser**
Nürnberger Land GmbH

# Perfusionsmuster eines hepatozellulären Karzinoms vom fibrolamellären Subtyp in der Kontrastmittelsonographie (CEUS)

Dane Wildner[1], Annette Kaiser[2], Malgorzata Jurga-Freytag[1], Thomas Golchert[1]

1 Abteilung Innere Medizin, Krankenhaus Lauf
2 Institut für Pathologie, Klinikum Nürnberg

## Hintergrund

Die Kontrastmittelsonographie (CEUS) ist eine etablierte Methode zur Abklärung fokaler Leberläsionen. Typische Perfusionsmuster ermöglichen eine Unterscheidung zwischen benignen und malignen Leberläsionen. Das hepatozelluläre Karzinom weist dabei im Vergleich zum umliegenden Leberparenchym ein irreguläres Hyperenhancement in der arteriellen Anflutung mit langsamem Wash-Out in der portalvenösen und Spätphase auf. Wir präsentierten den seltenen Fall eines HCCs vom fibrolamellären Subtyp mittels CEUS.

## Fallbericht

Ein 24-jähriger Patient stellt sich mit B-Symptomatik und unspezifischen Oberbauchschmerzen seit Dezember 2020 ambulant vor. Es sind keine Vorerkrankungen bekannt. Laborchemisch zeigt sich lediglich eine milde Anämie (Hb 11.4g/dl. N14-18) und eine diskrete Erhöhung von Gamma-GT (78U/l. N<60) und CRP (1.9mg/dl. N<0.5). Sonographisch stellt sich im linken Leberlappen eine inhomogene, scharf begrenzte Raumforderung mit arterialisierter Perfusion im Farbdoppler dar (Abb.1 a-d). Aufgrund einer HCC-verdächtigen Perfusion in CEUS (Abb.1 e-h) erfolgt die Punktion der Läsion. Es zeigt sich ein HCC vom fibrolamellären Subtyp mit eosinophilem Zytoplasma, ausgeprägter bindegewebiger Stromakomponente und umschriebenen bindegewebigen Kollagensepten (Abb. 2. a-d). Nach Komplettierung des Stagings (normale Tumormarker AFP, CEA, Ca19-9, β-HCG, PSA) wurde bei lokal fortgeschrittenem Befund der Leber und der Lymphknoten der oberen mesenterialen Gruppe ohne Fernmetastasen (Abb. 3) die Empfehlung zur weiteren Behandlung im Tumorboard diskutiert (primäre Resektion).

## Schlussfolgerung

Das HCC von fibrolamellären Subtyp weist trotz einer starken bindegewebigen Stromakomponente ein HCC-typisches Perfusionsmuster in der KM-Sonographie auf.

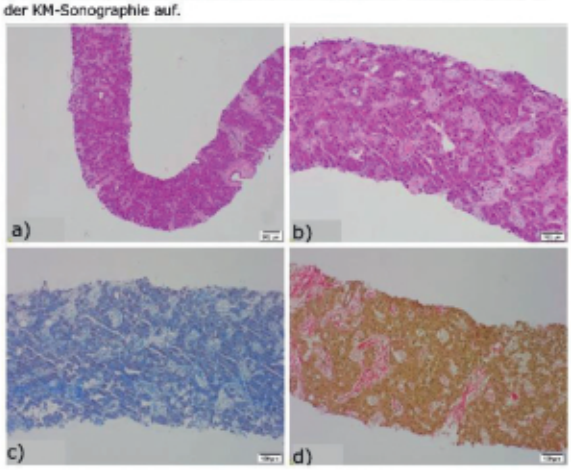


**Abbildung 2:** a)/b) HE-Färbung 10x/20x c) Ladewig-Färbung-starke Kollagenbildung 20x d) EVG-Färbung-elastische Fasern 20x

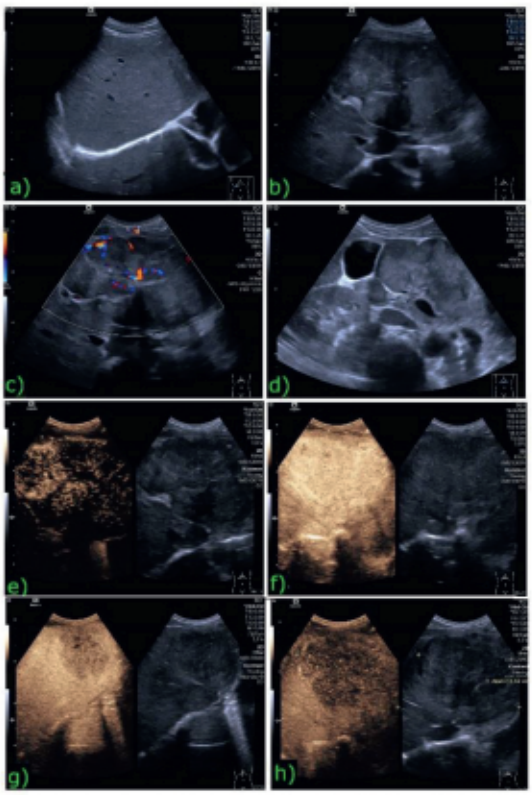


**Abbildung 1:** a)-d) B-Bild & Farbdoppler. Unauffälliges Leberparenchym, scharf begrenzte hypervaskularisierte Leberläsion. e)-h) HCC-typisches Perfusionsmuster in CEUS.

Phasen: e) arteriell f) & g) portalvenös h) Spätphase

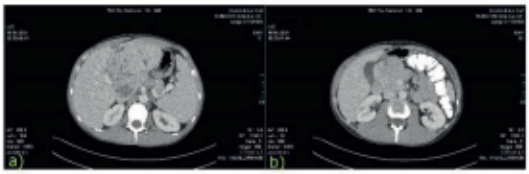


**Abbildung 3:** KM-CT Abdomen – portalvenöse Phase

**Literatur:**
1. Wildner D et al. Differentiation of malignant liver tumors by software-based perfusion quantification with DCEUS. DOI: 10.3233/CH-180378
2. Wildner D et al. DCE-US for the characterization of HCC and CCC. DOI: 10.1055/s-0034-1385170
3. Dietrich CF et al. Guidelines and GCP-Recommendations for CEUS in the Liver. DOI: 10.1055/a-1177-0530

## Kontakt

**PD Dr. med. Dane Wildner, Krankenhäuser Nürnberger Land – Standort Lauf, Abteilung Innere Medizin, Simonshoferstr. 55, 91207 Lauf an der Pegnitz Tel.: 09123/180-132. e-mail.: dane.wildner@kh-lauf.de**

## Perfusionsmuster eines hepatozellulären Karzinoms vom fibrolamellären Subtyp in der Kontrastmittelsonographie (CEUS)

Dane Wildner[1], Annette Kaiser[2], Malgorzata Jurga-Freytag[1], Thomas Golchert[1]

[1]Abteilung Innere Medizin, Krankenhaus Lauf; [2]Institut für Pathologie, Klinikum Nürnberg; Contact: dane.wildner@kh-lauf.de

### Objective

Die Kontrastmittelsonographie (CEUS) ist eine etablierte Methode zur Abklärung fokaler Leberläsionen. Typische Perfusionsmuster ermöglichen eine Unterscheidung zwischen benignen und malignen Leberläsionen. Das hepatozelluläre Karzinom weist dabei im Vergleich zum umliegenden Leberparenchym ein irreguläres Hyperenhancement in der arteriellen Anflutung mit langsamem Wash-Out in der portalvenösen und Spätphase auf. Wir präsentierten den seltenen Fall eines HCCs vom fibrolamellären Subtyp mittels CEUS.

### Methods

Ein 24-jähriger Patient stellt sich mit B-Symptomatik und unspezifischen Oberbauchschmerzen seit Dezember 2020 ambulant vor. Es sind keine Vorerkrankungen bekannt. Laborchemisch zeigt sich lediglich eine milde Anämie (Hb 11.4g/dl. N14-18) und eine diskrete Erhöhung von Gamma-GT (78U/l. N<60) und CRP (1.9mg/dl. N<0.5). Sonographisch stellt sich im linken Leberlappen eine inhomogene, scharf begrenzte Raumforderung mit arterialisierter Perfusion im Farbdoppler dar (Abb.1 a-d). Aufgrund einer HCC-verdächtigen Perfusion in CEUS (Abb.1 e-h) erfolgt die Punktion der Läsion. Es zeigt sich ein HCC vom fibrolamellären Subtyp mit eosinophilem Zytoplasma, ausgeprägter bindegewebiger Stromakomponente und umschriebenen bindegewebigen Kollagensepten (Abb. 2. a-d). Nach Komplettierung des Stagings (normale Tumormarker AFP, CEA, Ca19-9, b-HCG, PSA) wurde bei lokal fortgeschrittenem Befund der Leber und der Lymphknoten der oberen mesenterialen Gruppe ohne Fernmetastasen (Abb. 3) die Empfehlung zur weiteren Behandlung im Tumorboard diskutiert (primäre Resektion).

### Conclusions

Das HCC von fibrolamellären Subtyp weist trotz einer starken bindegewebigen Stromakomponente ein HCC-typisches Perfusionsmuster in der KM-Sonographie auf.

### References

1. Wildner D et al. Differentiation of malignant liver tumors by software-based perfusion quantification with DCEUS. DOI: 10.3233/CH-180378
2. Wildner D et al. DCE-US for the characterization of HCC and CCC. DOI: 10.1055/s-0034-1385170
3. Dietrich CF et al. Guidelines and GCP-Recommendations for CEUS in the Liver. DOI: 10.1055/a-1177-0530

# A DEEP-LEARNING-BASED TECHNIQUE FOR THE QUANTITATIVE ANALYSIS OF FEMOROTIBIAL OSTEOPHYTE AND BONE VOLUMES - DATA FROM THE OSTEOARTHRITIS INITIATIVE


Judit K. Schachinger[1,2], Susanne Maschek[1,3], Anna Wisser[1,2,3], David Fuerst[1,2,3], Akshay S. Chaudhari[4], Jana Kemnitz[1], Christian F. Baumgartner[5], Ender Konukoglu[5], Felix Eckstein[1,2,3], Wolfgang Wirth[1,2,3]

[1]Institute of Anatomy & Cell Biology, PMU Salzburg, Austria;
[2]Ludwig Boltzmann Institute for Arthritis & Rehabilitation, PMU Salzburg, Austria;
[3]Chondrometrics GmbH, Freilassing, Germany;
[4]Stanford University, Stanford, CA, USA;
[5]ETH, Zurich, Switzerland


Osteophytes (OPs) are prominent features in knee osteoarthritis (OA) and an important criterion for defining radiographic knee OA. They have also been suggested to be associated with pain and subsequent knee replacement [1,2]. Currently, most studies investigating the role of osteophytes rely on semi-quantitative scoring from X-rays or 3D MRI. A quantitative analysis of osteophytes from MRI may provide greater sensitivity to change than scoring-based methodologies, but requires segmentation, which is time-consuming when performed manually. Convolutional neural networks (CNNs) such as the U-Net have been previously applied for automated segmentation of articular cartilage and other joint tissues.

## OBJECTIVE

- To examine the agreement between fully automated, U-Net-based segmentation of distal femoral and proximal tibial osteophyte and bone volumes with manual expert segmentation, in knees with radiographic OA.

## METHODS

- The study included coronal FLASH MRI (Fig. 1) from 64 right knees with radiographic OA (KLG 2/3/4: n=36/19/9, each 32 women/men, age: 61±9y)
- Manual segmentation of the distal femur and proximal tibia (including OPs) performed by a single expert reader with the first readings quality-controlled by a second expert reader.
- U-Net trained using four labels (training/validation set n=36/14): femoral bone, femoral OPs, tibial bone, tibial OPs
- U-Net applied to automatically segment the femorotibial cartilages in n=14 knees (test set)
- Agreement between automated and manual segmentations evaluated using the Dice Similarity Coefficient (DSC), Hausdorff Distance (HD), and the Average Symmetric Surface Distance (ASSD)
- Computation of bone and OP volume from automated and manual segmentations

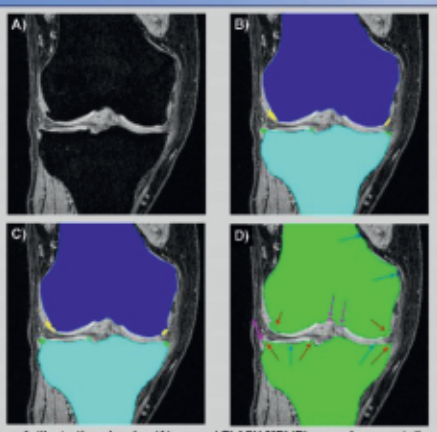


**Figure 1: Illustration showing (A) coronal FLASH MRI (B) manual segmentation of bone and osteophytes, (C) automated segmentation of bone (blue) and osteophytes (green, yellow), (D) agreement between automated and manual segmentation (green: consistent automated and manual segmentation, blue: only automated segm. (→), magenta: only manual segm. (→), red: different labels (→))**

**Table 1: Agreement between automated and manual segmentations**

| | Distal Femur | | Proximal Tibia | |
|---|---|---|---|---|
| | Bone | Osteophytes | Bone | Osteophytes |
| DSC | 0.98 ± 0.01 | 0.49 ± 0.12 | 0.99 ± 0.00 | 0.44 ± 0.11 |
| HD | 3.18 ± 2.15 | 11.10 ± 5.33 | 2.71 ± 2.15 | 8.01 ± 1.98 |
| ASSD | 0.10 ± 0.04 | 0.84 ± 0.64 | 0.06 ± 0.04 | 0.73 ± 0.32 |

Values reported as mean ± standard deviation. DSC: Dice Similarity Coefficient; HD: Hausdorff Distance (in mm); ASSD: Average Symmetric Surface Distance (in mm)

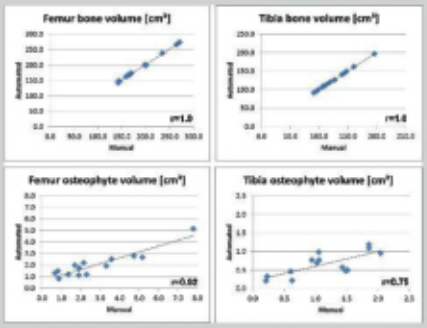


**Figure 2: Scatter plots illustrating the association between bone and osteophyte volumes computed from automated and manual segmentations**

**Table 2: Bone and osteophyte volume observed for automated and manual segmentations in radiographic OA knees**

| | Distal Femur | | Proximal Tibia | |
|---|---|---|---|---|
| | Bone | Osteophytes | Bone | Osteophytes |
| Automated | 190.2 ± 42.6 | 2.0 ± 1.1 | 125.7 ± 29.6 | 0.7 ± 0.3 |
| Manual | 187.6 ± 43.1 | 2.7 ± 2.0 | 125.2 ± 29.4 | 1.1 ± 0.6 |
| Difference | 2.6 ± 2.2 | -0.7 ± 1.1 | 0.5 ± 0.9 | -0.5 ± 0.4 |
| [95% CI] | [1.3, 3.8] | [-1.4, -0.1] | [0.0, 1.0] | [-0.7, -0.2] |
| (P-Value) | (0.001) | (0.026) | (0.056) | (0.001) |

Bone and osteophyte volumes reported in cm³ as mean ± standard deviation

## RESULTS

- High agreement observed between manual and automated bone segmentations (Table 1).
- Only moderate agreement observed between femoral/tibial OPs (Table 1).
- Bone volume highly correlated between segmentation methods (Fig. 2).
- Bone volume somewhat greater from automated than from manual segmentations (Table 2).
- Osteophyte volumes moderately to highly correlated between the fully automated vs. manual segmentation (Fig. 2).
- Osteophyte volume underestimated by the automated CNN segmentation, both in the distal femur and proximal tibia (Table 2)

## CONCLUSIONS

- Our results suggest that an automated, U-Net-based approach is capable of providing accurate segmentation of distal femoral and proximal tibial bone.
- In addition, the fully automated technology permits to obtain a reasonable estimate of femoral and tibial osteophyte volumes.
- The lower agreement observed for the osteophytes is most likely due to their smaller size and their variable shape and location. A greater number of manually segmented MRIs appears to be beneficial for adequate training of the U-Net.
- Future work will test whether the methodology is sensitive to longitudinal changes in osteophytes volumes over time, and to what extent such quantitative longitudinal measures relate to clinical outcomes, such as pain, function, or risk of knee replacement.

## REFERENCES


[1] Liu et al., Mod Rheumatol. 2017; 27(2):332-338.
[2] Zhu et al., Osteoarthritis Cartilage 2017;25(7):1064-92.


## FUNDING


Image analysis: PMU research fund (E-18/27/146-WIK)


## CONTACT


wolfgang.wirth@pmu.ac.at

## A DEEP-LEARNING-BASED TECHNIQUE FOR THE QUANTITATIVE ANALYSIS OF FEMOROTIBIAL OSTEOPHYTE AND BONE VOLUMES – DATA FROM THE OSTEOARTHRITIS INITIATIVE

Judit Schachinger[1], Susanne Maschek[2], Akshay Chaudhari[3], Jana Kemnitz[1], Christian Baumgartner[4], Ender Konukoglu[4], Felix Eckstein[1,5], Wolfgang Wirth[1,5]

[1]Department of Imaging and Functional Musculoskeletal Research, Institute of Anatomy and Cell Biology, Paracelsus Medical University, Salzburg, Austria; [2]Chondrometrics GmbH, Freilassing, Germany; [3]Stanford University, Stanford, CA, USA; [4]ETH Zürich, Zürich, Switzerland; [5]Ludwig Boltzmann Institute for Arthritis & Rehabilitation, PMU Salzburg, Austria; Contact: wolfgang.wirth@pmu.ac.at

### Objective
Osteophytes (OPs) are prominent features in knee osteoarthritis (OA) and have been suggested to be associated with pain. A quantitative analysis of osteophytes from MRI may provide greater sensitivity to change than current scoring-based methodologies, but requires segmentation, which is time-consuming when performed manually. The objective of the current work was to examine the agreement between fully automated, U-Net-based segmentation of distal femoral and proximal tibial osteophyte and bone volumes with that of expert manual segmentation, in knees with radiographic OA.

### Methods
The study included coronal FLASH MRIs from 64 right knees (36 KLG 2; 19 KLG, and 4 KLG4) from 64 Osteoarthritis Initiative (OAI) participants (n=32/32 women/men, age: 61±9y). Manual segmentations of all 64 knees were performed by a single expert reader, the first readings were quality-controlled by a second expert reader. 2D U-Nets were trained using 4 labels (femoral bone, femoral osteophytes, tibial bone, tibial osteophytes). The training/validation set included n=36/14 knees. The agreement between the fully automated and manual segmentation was evaluated in a test set of 14 knees using the Dice similarity coefficient (DSC) and by comparing bone and osteophyte volumes between methods.

### Results
The results showed very high agreement between manual and automated segmentations of the bones, with a DSC of 0.98±0.01 for the distal femur and 0.99±0.00 for the proximal tibia. The agreement observed for femoral/tibial osteophytes was notably lower, with DSCs of 0.49±0.12 and 0.44±0.11. Bone volumes were observed to be somewhat greater from automated than from manual segmentations for the distal femur (mean difference: 2.6 $cm^3$ / +1.4%, 95% CI: [1.3, 3.8 ] $cm^3$, p=0.001), whereas no statistically significant difference was observed for the proximal tibia (mean difference: 0.5 $cm^3$ / +0.4%, 95% CI: [0.0, 1.0] $cm^3$, p=0.06). Yet, correlation between automated vs. manually segmented bones was very high (r=1.00 for both the femur and tibia). The osteophyte volumes, in contrast, were underestimated by the automated CNN segmentation, both in the distal femur (mean difference: -0.7 $cm^3$ / -27%, 95% CI: [-1.4, -0.1]$cm^3$, p=0.03) as well as in the proximal tibia (mean difference: -0.5 $cm^3$ / -44%, 95% CI: [-0.7, -0.2 ]$cm^3$, p=0.001). Yet, osteophyte volumes were moderately to highly correlated between the fully automated vs. manual segmentation for both the femur (r=0.92) and the tibia (r=0.75).

### Conclusions
The results suggest that an automated, U-Net-based approach is capable of providing accurate analysis of distal femoral and proximal tibial bone volume. In addition, the fully automated technology permits to obtain a reasonable estimate of femoral and tibial osteophyte volumes. The lower agreement observed for the osteophytes is most likely due to their smaller size and their highly variable shape and location.

### Acknowledgements
Paracelsus Medical University research fund (PMU-FFF): E-18/27/146-WIK

# FULLY AUTOMATED CARTILAGE SEGMENTATION OF LATE STAGE OSTEOARTHRITIS (KLG4) KNEES USING DEEP LEARNING WITH U-NET ARCHITECTURES

Anna Wisser[1], Wolfgang Wirth[1,2], Akshay S. Chaudhari[3], David Fürst[1,2], Christian F. Baumgartner[4], Ender Konukoglu[4], Felix Eckstein[1,2]

[1]Institute of Anatomy & Cell Biology - Salzburg, PMU Salzburg, Austria
[2]Ludwig Boltzmann Institute for Arthritis & Rehabilitation, PMU Salzburg, Austria
[3]Stanford University, Stanford, CA, USA
[4]Department of Information Technology & Electrical Engineering, ETH, Zurich, Switzerland

We recently reported the agreement and accuracy of automated cartilage segmentation of knees with radiographic OA (compared with healthy ones) using convolutional neural network-based U-Net architecture (Wirth et al., 2021).

It was observed that automated cartilage segmentation overestimated femorotibial cartilage thickness analysis vs. manual segmentation, and that this effect was mainly apparent in KLG4 knees with denuded subchondral bone areas [dABs] (Wirth et al., 2021).

## OBJECTIVES

1. Examine whether a specific training model of KLG4 knees (n=26) shows better segmentation performance with less cartilage thickness overestimation than a larger, more general model of KLG 2-4 knees (n=86);
2. Explore whether a model trained with a larger set of KLG4 knees further improves performance.
3. Compare the relationship between overestimation of cartilage thickness & dABs.

## METHODS

For the automated segmentation of the KLG4 test set (n=6) 3 models were built using data from the Osteoarthritis Initiative (OAI). The small number of test data was due to it being a subset of a test-set from a previous study on KLG 2-4 knees that had both sagDESS and corFLASH segmentations (Wirth et al., 2021).

- First, U-Nets were trained/validated (n=86/18), using a general ROA model of ROA knees (37% KLG2, 33% KLG3, 30% KLG4).
- Next, a small, but specific KLG4 model was built (n=26/6), using only the subset of KLG4 knees with DESS MRI, from the above study.
- Finally, a larger KLG4-specific model was trained/validated in n=125/24 knees.

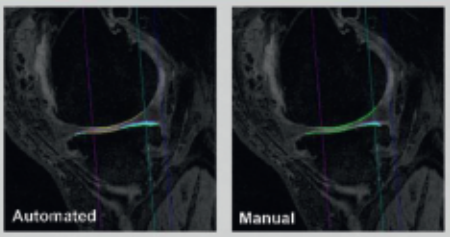


**Figure 1: Automated and manual segmentation of femorotibial cartilages in the same knee** (yellow = overlap of the cartilage surface [AC, magenta] and the bone interface [tAB, green])

**Table 1: Agreement between automated & manual (reference) segmentation of the KLG4 test set (n=6) using 3 different segmentation models**

| Anatomical region: | Mean Dice Similarity Coefficient (DSC) | | |
|---|---|---|---|
| Segmentation model → | KLG2-4 | KLG 4S | KLG 4L |
| MT | 0.82 (0.03) | 0.82 (0.03) | 0.84 (0.03) |
| cMF | 0.82 (0.03) | 0.82 (0.03) | 0.84 (0.03) |
| LT | 0.89 (0.02) | 0.88 (0.03) | 0.89 (0.03) |
| cLF | 0.88 (0.03) | 0.88 (0.03) | 0.90 (0.02) |
| Average | 0.85 | 0.85 | 0.87 |

„KLG2-4": general ROA model (n=86/17 for training/validation); „KLG4 S": small KLG-specific model (n=26/6); „KLG4 L": larger KLG-specific model (n=125/24);
"MT": medial tibia; "cMF": central medial femur; "LT": Lateral tibia; "cLF": central lateral femur

**Table 2: Systematic offset of cartilage thickness measurments between automated & manual (reference) segmentation of the KLG4 test set (n=6) for 3 different training and validation sets using DESS:**

| Anat. region: | | Cartilage thickness (mm) | | | Cartilage thickness (%) | | |
|---|---|---|---|---|---|---|---|
| Training/Validation set type → | | KLG2-4 | KLG 4S | KLG 4L | KLG2-4 | KLG 4S | KLG 4L |
| MT | Mean | 0.38 | 0.17 | 0.31 | 36 | 17 | 31 |
| | SD | 0.12 | 0.13 | 0.09 | 12 | 13 | 9 |
| cMF | Mean | 0.34 | 0.45 | 0.33 | 53 | 43 | 51 |
| | SD | 0.17 | 0.14 | 0.14 | 27 | 22 | 21 |
| LT | Mean | 0.12 | 0.06 | 0.14 | 7 | 6 | 8 |
| | SD | 0.08 | 0.13 | 0.08 | 5 | 8 | 4 |
| cLF | Mean | 0.13 | -0.01 | 0.13 | 7 | -1 | 7 |
| | SD | 0.15 | 0.15 | 0.08 | 8 | 8 | 4 |
| Average | Mean | 0.24 | 0.16 | 0.23 | 26 | 16 | 24 |

„KLG2-4": general ROA model (n=86/17 for training/validation); „KLG4 S": small KLG-specific model (n=26/6);
„KLG4 L": larger KLG-specific model (n=125/24);
"MT": medial tibia; "cMF": central medial femur; "LT": Lateral tibia; "cLF": central lateral femur

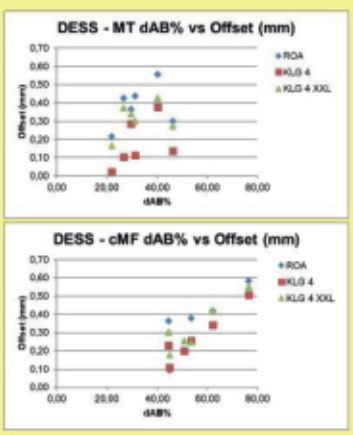


**Figure 2: Denuded area of subchondral bone (dAB) versus the cartilage thickness measurement offset (mm) between the automated vs. manual analysis in MT (top) and cMF (bottom)**

## RESULTS

- The mean Dice Similarity Coefficients (DSC) across all 4 femorotibial cartilages (TFTJ) were 0.85, 0.85 and 0.87 for the 3 training models (Table 1, Fig. 1).
- The systematic cartilage thickness overestimates by U-Net segmentation are shown in Table 2. The offsets were largest in the medial femur (cMF: Fig. 2).
- Pearson correlation coefficients between manual (reference) vs. automated (3 models) cartilage thickness analysis were r=0.85, 0.84 & 0.94 for the 3 models in the TFTJ, and r= 0.74, 0.87 & 0.92 in the cMF.
- The dABs involved 22% of the total (TFTJ) subchondral bone area in the test set, and 12%, 26% & 24% in the training sets. The largest dABs were observed in the cMF (56%), vs 33% in the MT (Fig. 2), and only 2%, in the cLF and in the LT.
- In the cMF, the correlations between overestimates of cartilage thickness and the dABs were r= 0.82, 0.95, and 0.92 for the 3 models, respectively (Fig. 2).

## CONCLUSIONS

- Overestimates of cartilage thickness by automated U-Net segmentation appear to be due to presence of dABs.
- A (small) KLG-4-specific training model reduced the cartilage thickness overestimate vs. manual segmentation and led to a stronger correlation of U-Net vs. manual analysis in the cMF.
- The larger KLG4-specific model did not achieve a reduction in the thickness overestimate vs. the general model, but substantially increased the correlation of automated vs. manual analysis.
- The results suggest that the specificity of the training model is important in automated cartilage thickness analysis.

**FUNDING & ACKNOWLEDGEMENTS:**
PMU research fund (E-18/27/149-WIK).

**REFERENCES**

Wirth et al. (2021): OARSI 2021 Abstract

**CONTACT** anna.wisser@sbg.ac.at

# FULLY AUTOMATED CARTILAGE SEGMENTATION OF LATE STAGE OSTEOARTHRITIS (KLG4) KNEES USING DEEP LEARNING WITH U-NET ARCHITECTURES – MODEL SPECIFICITY IS IMPORTANT

Anna Wisser[1], Wolfgang Wirth[1,4], Akshay Chaudhari[2], David Fürst[1,4], Christian F. Baumgartner[3], Ender Konukoglu[3], Felix Eckstein[1,4]

[1]Department for Imaging and Functional Musculoskeletal Research, Institute of Anatomy and Cell Biology - Salzburg, Center for Anatomy and Cell Biology, Paracelsus Medical University, Salzburg, Austria; [2]Stanford University, Stanford, CA, USA; [3]Department of Information Technology and Electrical Engineering, ETH Zurich, Switzerland; [4]Ludwig Boltzmann Institute for Arthritis & Rehabilitation, Paracelsus Medical University, Salzburg, Austria; Contact: anna.wisser@stud.pmu.ac.at

## Objective
The agreement and accuracy of automated cartilage segmentation of knees with radiographic osteoarthritis (ROA) using deep learning (DL) and convolutional neural network (CNN)-based U-Net architectures has recently been reported. It was observed that automated cartilage segmentation slightly overestimated cartilage thickness vs. manual segmentation, and that this effect was mainly apparent in KLG4 knees with denuded subchondral bone areas (dABs). The objective of the current study was to 1) examine whether a specific training model of KLG4 knees shows better segmentation performance with less cartilage thickness overestimation than a larger, more general model of KLG 2-4 knees; 2) explore whether a model trained with a larger set of KLG4 knees further improves performance; 3) compare the relationship between overestimation and denuded bone areas.

## Methods
The test set on which the automated segmentations were performed included 6 KLG4 knees from the Osteoarthritis Initiative (OAI) who had expert manual segmentation (reference) of the femorotibial cartilages from sagDESS MRI. Three models for automated image segmentation were built with a DL CNN U-Net architecture: A general ROA model (n=86/18 [training/validation]) using ROA knees with a wide range of KL grades (37% KLG2, 33% KLG3, 30% KLG4), a smaller and a larger KLG4-specific model (n=26/6; n=125/24).

## Results
A mean Dice Similarity Coefficient (DSC) across all 4 femorotibial cartilages (TFTJ) of 0.85 was observed for the general ROA and the small KLG4-specific model, 0.87 for the larger KLG4-specific model. The average systematic cartilage thickness overestimation by U-Net segmentation was 0.24mm (26%), 0.16mm (16%), 0.23mm (24%) for the three models, respectively. Offsets were largest in the medial femur (cMF: 53%, 43%, and 51%). Pearson's correlation between automated and manual cartilage thickness computations was r=0.85, 0.84, 0.94 for the three models in the TFTJ, and 0.74, 0.87, 0.92 in the cMF. The dABs involved 22% of the total (TFTJ) subchondral bone area in the test set, 12%, 26%, 24% in the training sets. The largest dABs were observed in the cMF (average 56%, vs 33% in the MT, 2%, in the cLF, and 2% in the LT). In the cMF, the correlations between overestimates of cartilage thickness, and the dABs were r= 0.82, 0.95, and 0.92 for the three models.

## Conclusions
Overestimation of cartilage thickness by automated U-Net segmentation in ROA knees appears to be due to the presence of dABs. A small KLG4-specific training model reduced the overestimation of cartilage thickness compared to a more general ROA model (KLG2-4) and also led to a stronger cartilage thickness correlation of U-Net vs. manual analysis, but only in the cMF. The larger KLG4-specific model did not reduce thickness overestimation, but increased the correlation of thickness measures in the cMF and the TFTJ. The results suggest that specificity of the training set is important in automated cartilage analysis.

## Acknowledgements
Paracelsus Medical University research fund (PMU-FFF): E-18/27/146-WIK

# Proteomic analysis reveals angiogenic and immunomodulatory function for placental stromal cell-derived extracellular vesicles

M. Wolf[1], B. Vári[1], C. Blöchl[2], AM. Raninger[1], R. Poupardin[1], CM. Beez[3], A. Hoog[1], G. Brachtl[1], E. Eminger[1], M. Oeller[4], A. Spittler[5], T. Heuser[6], A. Obermayer[7], M. Seifert[3], CG. Huber[2], K. Schallmoser[1], R. Ofir[7], Z. Aberman[7], HD. Volk[3], D. Strunk[1]

[1]Cell Therapy Institute, Spinal Cord Injury and Tissue Regeneration Center Salzburg (SCI-TReCS), Paracelsus Medical University (PMU), Salzburg, Austria
[2]Dept. of Biosciences, Paris Lodron University Salzburg
[3]BCRT & Institute of Medical Immunology, Charité – Universitätsmedizin Berlin, Germany
[4]Department of Transfusion Medicine and SCI-TReCS, PMU, Salzburg, Austria
[5]Christian Doppler Center of Translational Research, Medical University, Vienna
[6]Vienna Biocenter Core Facilities, Medical University, Vienna
[7]Pluristem Ltd., Haifa, Israel

martin.wolf@pmu.ac.at

## INTRODUCTION

Peripheral artery disease affects >10% of the European elderly population resulting in an increased risk for cardiovascular failures and death. Critical limb ischemia (CLI), as its final stage, often leads to amputation. Allogeneic placental expanded (PLX) stromal cells are currently evaluated in a clinical phase III trial as an advanced CLI therapy. In our study, we aim to identify the mode of action of this novel cell-based treatment. Therefore, we hypothesize that PLX-cell-derived extracellular vesicles (EVs) contribute to PLX-cell effectiveness. This project is part of **PACE "A multicenter phase III study using HLA-unmatched allogeneic placenta-derived stromal cells (PLX-PAD) for the treatment of severe critical limb ischemia accompanied by mechanistic studies".**

## HYPOTHESIS

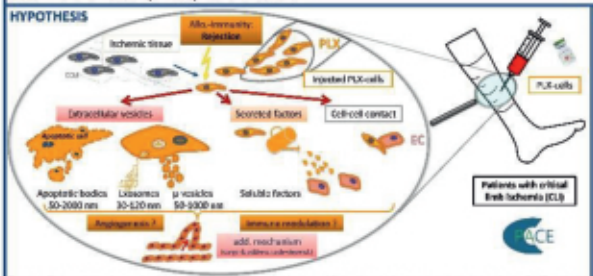


**Figure 1:** To investigate the mode of action and the molecular mechanism of PLX cells, which are currently evaluated in the PACE study for their application in CLI patients, we aim to investigate whether direct cell-cell contact of PLX cells with arteriogenous endothelial cells (ECs), secreted soluble factors or EVs facilitate angiogenic potential. We further plan to find out whether signals from the ischemic environment influence this effect.

## METHODS

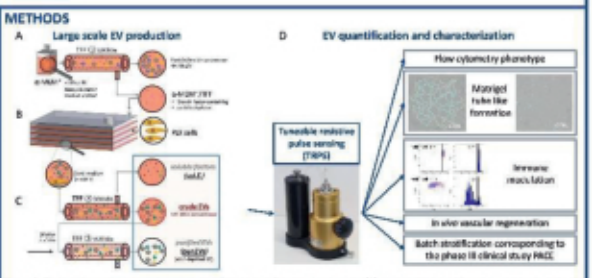


**Figure 2:** To be able to determine the potency of PLX-derived EVs, we developed a (A) standardized workflow for particle depletion in medium supplemented with pooled human platelet lysate (pHPL) via tangential flow filtration (TFF) (B) as well as subsequent large scale cell propagation and (C) EV purification protocols to separate soluble factors (sol.F) from crude EVs and purified (pur.) EVs. (D) The major goal of our project lies in the extensive characterization of EV functions to better understand their role in vascular regeneration.

## PRODUCTION AND PHENOTYPE OF PLX EVs

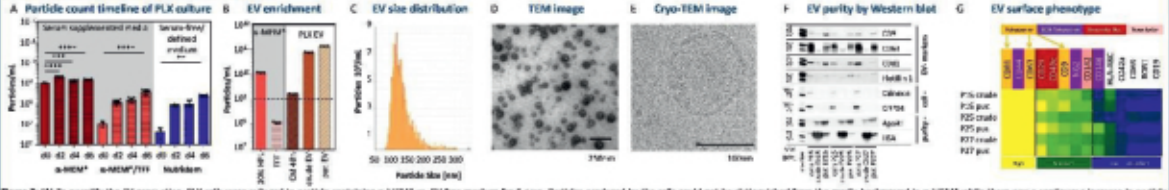


**Figure 3:** (A) To quantify the EV production, PLX cells were cultured in particle containing α-MEM* vs. EV free medium for 6 days. Particles produced by the cells could not be distinguished from the media background in α-MEM* while there was a continuous increase in particle depleted α-MEM* of chemically defined medium. (B) Particle numbers measured by TRPS show efficient enrichment of particles during the EV purification process with TFF. (C) The size distribution of PLX EV was measured by TRPS. (D) Both, negative contrast TEM picture and (E) cryo-TEM image show round structures of about 100 nm. The cryo-TEM image in addition shows a characteristic double membrane structure. (F) Western blot analysis of EV identity and purity markers according to MISEV 2018 criteria. (G) The surface marker phenotype of PLX-derived EVs was investigated by multiplex bead-based flow cytometry (FCV). Results are depicted in a Heatmap format for crude vs. pur. EVs derived from three independent PLX-donors.

## PROTEOMIC COMPARISON OF PLX SECRETOME FRACTIONS




**Figure 4:** (A) To analyze the protein content of the PLX-derived EVs and to compare it to their soluble factors we first used unlabeled proteomics. An overview of proteins identified in one ore more of the different secretome fractions is presented as Venn diagram. (B,C) To get a deeper insight into differentially expressed proteins we utilized tandem mass tag proteomics. With this approach we found proteins (ecalgrin) to EV specific GO terms almost exclusively in the pur. EV fraction. This result also can be seen as an internal control. In addition proteins associated with cell movement and angiogenesis where highly enriched in this fraction compared to the sol.F. Proteins associated with of the immune system regulation where more equally distributed. Never the less some inhibitory pathways of the immune responses like TGF-β were higher abundant in the pur.EV fraction as shown in a more in depth pathway analysis performed with the ingenuity database.

## ANGIOGENIC AND IMMUNE MODULATION POTENTIAL OF PLX CELLS AND PLX-DERIVED EVs

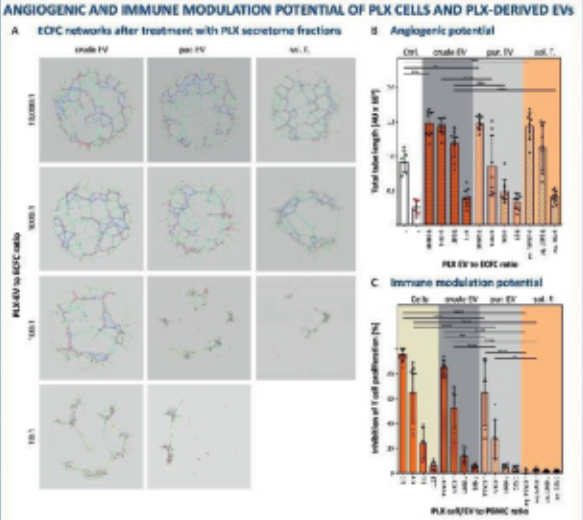


**Figure 5:** (A)The Angiogenic potential of PLX-derived EVs was analysed by in vitro matrigel-based tube-like structure formation assay. Total length of tube-like structures formed by endothelial colony forming cells (ECFC) after 12 h incubation were imaged using a life cell imaging station and were analyzed using Image J's Angiogenesis Analyzer plugin (Carpentier, 2012). (B) Statistical analysis of three independent donors measured in triplicates showed that crude EV concentrates have the highest tube-like structure supportive capacity at ratios between 10:1000:1 and 100:1, whereas this effect is significantly reduced at 1:100:1. (C) The immune modulation capacity of PLX cells was monitored on PHA-induced T cell proliferation. Compared to PLX cells, in general PLX-derived EVs showed a reduced (significant for the pur. EV) inhibition capacity of T cell proliferation. In contrast to the tube-like formation assay the soluble factors fraction did not show any effect in this assay.

## SUMMARY

- Placental expanded (PLX) stromal cells secrete extracellular vesicles (EVs) into their environment. These EVs can be purified and concentrated from culture supernatants for further analysis.
- PLX EVs show typical EV size distribution and shape, display EV-specific surface markers, such as tetraspanins and in addition show ECM interaction molecules, fibronectin receptor and tissue factor on their surface.
- Proteomic analysis revealed significant enrichment of proteins associated with angiogenesis, cell movement and negative regulation of immune responses in the EV fraction of the PLX secretome compared to soLF..
- PLX EVs show high angiogenic potential *in vitro* in a dose-dependant manner. Crude EVs show significantly higher angiogenic potential than pure EVs.
- PLX cells and their EVs exhibit immune modulation capacity which is significantly reduced for pure EVs.

## ACKNOWLEDGEMENTS

This work is part of a project that has received funding from the European Union's Horizon 2020 research and innovation program under grant agreement N°733008
PACE (A multicenter phase III study using HLA-unmatched allogeneic placenta-derived stromal cells (PLX-PAD) for the treatment of severe critical limb ischemia accompanied by mechanistic studies)

## Enhanced angiogenesis and wound healing in vivo induced by extracellular vesicles from therapeutic grade allogeneic human placental stromal cells

Martin Wolf[1], Rodolphe Poupardin[1], Constantin Blöchl[2], Andre Cronemberger Andrade[1], Fausto Gueths Gomes[3], Patrica Peking Ebner[1], Balazs Vari[1], Essi Eminger[1], Heide-Marie Binder[1], Anna M Raninger, Gabi Brachtl, Andreas Spittler[4], Thomas Heuser[5], Astrid Obermayer[2], Christian G Huber[2], Katharina Schallmoser[3], Hans-Dieter Volk[6], Dirk Strunk[1]

[1]Cell Therapy Institute, Spinal Cord Injury and Tissue Regeneration Center Salzburg (SCI-TReCS), Paracelsus Medical University (PMU), Salzburg, Austria; [2]Dept. of Biosciences, Paris Lodron University Salzburg; [3]Department of Transfusion Medicine and SCI-TReCS, PMU, Salzburg, Austria; [4]Anna Spiegel Center of Translational Research, Medical University, Vienna; [5]Vienna Biocenter Core Facilities, Medical University, Vienna; [6]BCRT & Institute of Medical Immunology, Charite - Univeritätsmedizin Berlin, Germany; Contact: martin.wolf@pmu.ac.at

### Objective
Cell therapy approaches using of the shelf allogeneic products have shown surprising results despite lack of engraftment of the transplanted cells. Their efficacy was so far considered to be mostly mediated by secreted trophic factors. We tested if extracellular vesicles (EVs) contribute to their mode of action. Here we provide evidence that EVs derived from therapeutic placental-expanded (PLX) stromal cells are potent inducers of angiogenesis and modulate immune cell proliferation in a dose-dependent manner.

### Methods
Crude EVs were enriched >100-fold from large volume PLX conditioned media via tangential flow filtration (TFF) as determined by tuneable resistive pulse sensing (TRPS). Additional TFF purification was devised to separate EVs from cell-secreted soluble factors. EV identity was confirmed by western blot, electron microscopy and super resolution microscopy. To identify the mode of action we compared isolated EV preparations with corresponding soluble factors via proteomic analysis, in vitro angiogenesis assay, stimulation capacity of Immune cells, and in vivo wound healing mouse model.

### Results
Surface marker profiling of tetraspanin-positive EVs identified expression of cell- and matrix-interacting adhesion molecules. Differential tandem mass tag proteomics comparing PLX-EVs to PLX-derived soluble factors revealed significant differential enrichment of 258 proteins in purified PLX-EVs involved in angiogenesis, cell movement and immune system signalling. At the functional level, PLX-EVs and cells in contrast to soluble factors inhibited T cell mitogenesis and showed different activation patterns of proliferation pathways in Monocytes and T cells. PLX-EVs and soluble factors displayed dose-dependent proangiogenic potential by enhancing tube-like structure formation in vitro as well as enhanced vessel density and wound healing in an in vivo mouse model.

### Conclusions
Our findings indicate that the mode of PLX action involves an EV-mediated proangiogenic function and immune response modulation that may help explaining clinical efficacy beyond presence of the transplanted allogeneic cells

# Does the "Gremlin/BMP-axis" modulate tendon inflammation?

Franziska Zabelt[1], Bettina Schwemberger[1], Rodolphe Poupardin[2], Renate Gehwolf[1], Andreas Traweger[1]

[1]Paracelsus Medical University, Tendon and Bone Regeneration, SCI-TReCS, Salzburg, Austria,
[2]Paracelsus Medical University, Experimental Cell Therapy, SCI-TReCS, Salzburg, Austria

Franziska.zabelt@pmu.ac.at

This project is funded by PMU-FFF Project E-20/32/167-GEH

## INTRODUCTION:

Tendon pathologies are multifaceted and are characterized by an overall decline in tendon function, often accompanied by pain. Bulk RNA sequencing identified the BMP antagonists Gremlin-1 and Gremlin-2 to be significantly upregulated by IL1ß. Both proteins have been described as efficient bone morphogenetic protein (BMP) antagonists involved in various processes during development but also in disease, e.g. fibrosis and inflammation. We therefore propose to decipher the role of Gremlin-1/-2 in modulating tendon inflammation via their interaction with BMPs.

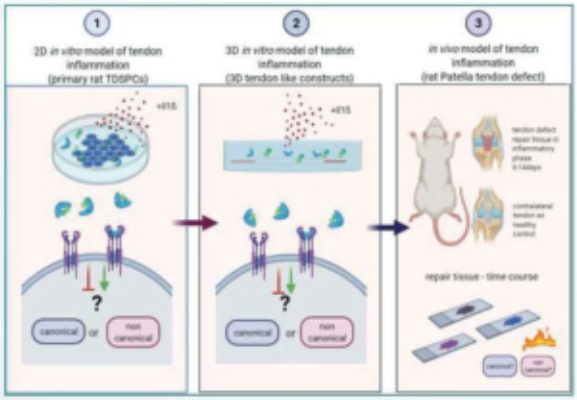


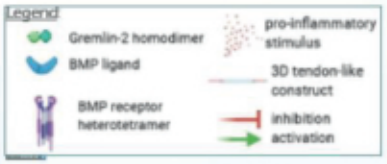


## METHODS

1. ➢ Identify Grem 1/2 interacting Bmps (by Co-IP, WB)
   - ➢ Characterize downstream signalling pathways (canonical, non-canonical) and related expression of e.g. profibrotic markers, inflammatory markers (by GX, WB, IF, luciferase reporter assays)
   - ➢ Lentiviral over-expression & knock-down of Grem 1/2 in tendon cells
2. ➢ Generate 3D tendon like constructs with Grem 1/2 over-expressing or under-expressing tendon cells
   - ➢ Analyse inflammatory responses of Grem 1/2 transduced inflamed 3D tendon-like constructs
3. ➢ Generate a longitudinal incision defect in the rat Patella tendon
   - ➢ Analyse tendon repair tissue of the early and late inflammatory phase for the Grem/Bmp-axis (by histology, IHC, IF, DUOLINK-PLA)

## AIM OF THE ON-GOING STUDY:

Tendon degeneration is characterized by manifold changes in the biology of tendons, a decline in overall function and an enhanced risk for injury. The role of inflammation for these detrimental processes is still insufficiently understood. Based on our finding that Gremlins are increased in inflammatory-primed 3D tendon constructs, we propose that the "Gremlin/BMP axis" plays an important role in tendinopathy. **Therefore, the overall objective of this study is to characterize the role of Gremlins in either promoting or attenuating tissue inflammation in tendons.**

## IL1β HEATMAP

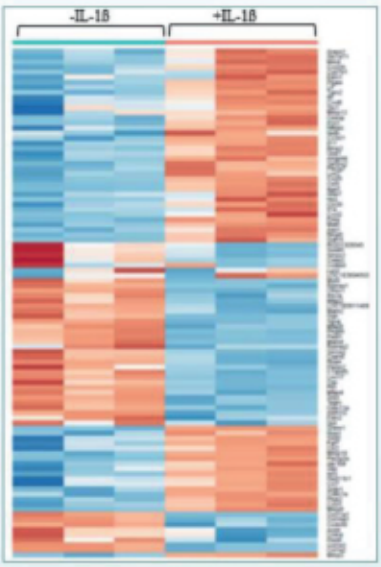


## FIRST RESULTS:

First immunofluorescence experiments as well as RT-qPCR results show that Grem2 is highly upregulated after IL1β, rGrem2 and rGrem1 stimulation (Figure 1) providing an established basis for further experiments.

## Il1β HEATMAP:

To better understand molecular mechanisms activated in tendons upon an inflammatory stimulus we performed a global transcriptome analysis of 3D-tendon like constructs treated with Interleukin-1ß. Bulk RNA-Sequencing analysis identified 3184 significant differentially expressed genes upon pro-inflammatory stimulation, the top 100 regulated genes are shown in the heat map. The strongest increase in mRNA expression was seen for the Bmp antagonist Gremlin-2, as well as an increase in the homologous Gremlin-1.

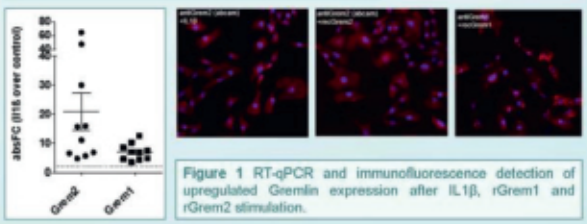


Figure 1 RT-qPCR and immunofluorescence detection of upregulated Gremlin expression after IL1β, rGrem1 and rGrem2 stimulation.

## Does the "Gremlin/BMP-axis" modulate tendon inflammation?

Franziska Zabelt[1], Bettina Schwemberger[1], Rodolphe Poupardin[2], Renate Gehwolf[1], Andreas Traweger[1]

[1]Paracelsus Medical University, Tendon and Bone Regeneration, SCI-TReCS, Salzburg, Austria; [2]Paracelsus Medical University, Experimental Cell Therapy, SCI-TReCS, Salzburg, Austria; Contact: franziska.zabelt@pmu.ac.at

### Objective
Tendon degeneration is defined by an array of changes in the biology of the tissue, a decline in overall function as well as an increased risk for injury. The role of inflammation in these destructive processes is still inadequately understood. Based on the findings that Gremlins are increased in inflammatory-primed 3D tendon-like constructs, we propose that the "Gremlin/BMP-axis" plays an essential role in the development of tendinopathy.

### Methods
To investigate the consequences of perturbing Gremlin expression in tendon cells, c-Myc-tagged rat Gremlin-1 and -2 cDNAs will be subcloned into the lentiviral transfection vector pLVX-EF1α-IRES-Puro. Subsequently, tendon stem and progenitor cells, which have been isolated and expanded from rat tendon tissue, will be transfected. In 2D in vitro cultures we will then investigate and characterize the molecular effects of the Grem/BMP-signalling axis on (i) the canonical (e.g. phosphorylation of R-Smads Smad1/5/8) and (ii) the non-canonical (e.g. phosphorylation of PI3K/AKT, MAPK) downstream signalling events in inflamed and untreated tendon cells by applying Western Blot analysis and immunofluorescence stainings. Further, gene expression analysis (RNA isolation, cDNA synthesis, and qPCR will be used to investigate the changes in tendon-related marker expression (e.g. Scleraxis, Tenomodulin, Mohawk, Egr-1, etc.) and extracellular matrix transcript levels (e.g. Collagen type I/III, Decorin, Biglycan, Tenascin C, etc.). After transfection of tendon cells, Western Blot analysis and immunofluorescence stainings will be applied to characterize the effects of Gremlin-1/-2 (over)expression on the protein level of the above listed tendon related markers or extracellular matrix proteins.

### Results
Preliminary immunofluorescence experiments as well as RT-qPCR results show that Gremlin-2 is highly upregulated after IL1β, rGremlin-2 and rGremlin-1 stimulation providing an established basis for further experiments.

### Conclusions
Our results will be the basis for 3D in vitro experiments, where these transfected tendon cells will be used to generate statically loaded 3D tendon like construct [1]. This will help to understand how Gremlin-1/-2 (over)expression will impact on tendon construct formation, matrix assembly, or the inflammatory response of tendons.

### Acknowledgements
This project is supported by PMU-FFF grant #E-20/32/167-GEH.

### References
1. Gehwolf R, Spitzer G, Wagner A, Lehner C, Weissenbacher N, Tempfer H, Traweger A (2019) 3D-Embedded Cell Cultures to Study Tendon Biology Methods Mol Biol 2045:155-165 doi:10.1007/7651_2019_208

## Klinische Bedeutung der Targeted axillary dissection (TAD) nach neoadjuvanter Chemotherapie bei Mammakarzinompatientinnen mit prätherapeutisch befallenen Lymphknoten und Konversion zu ycN0

Christine Zeder-Göß[1], Ralf Adamus[2], Frank E.-M. Gisbert[1], Thorsten Koch[1], Annette Linke[2], Simone Linsenbühler[1], Cosima Brucker[1]

[1]Klinik für Frauenheilkunde und Geburtshilfe, Paracelsus Medical University, Nuremberg, Germany; [2]Institut für Radiologie und Nuklearmedizin, Paracelsus Medical University, Nuremberg, Germany; Contact: christine.zeder-goess@klinikum-nuernberg.de

### Objective

Die komplette Ausräumung der axillären Lymphknoten (ALND – axilläre Lymphonodektomie) galt lange Zeit als Standardverfahren für die Therapie des Mammakarzinoms. Sie hatte sowohl therapeutische sowie diagnostische Funktion. Da die ALND mit einer hohen Morbidität verbunden ist, konnte sie erfreulicherweise bei primärer OP und unauffälligen Lymphknoten durch die schonendere Sentinel-Lymphknotenbiopsie (SLNB) ersetzt werden, ohne das krankheitsfreie Überleben oder das Gesamtüberleben zu beeinträchtigen (1). Bei Patientinnen, die eine neoadjuvante Chemotherapie erhalten und vor Therapiebeginn einen positiven Lymphknotenstatus aufweisen und unter Chemotherapie zu einem ycN0 Stadium konvertieren, ist die Sicherheit der SLNB nach Chemotherapie aufgrund einer zu hohen Falsch-Negativ-Rate (FNR) umstritten. Eine prospektive Registerstudie von Caudle et al. demonstrierte ein Verfahren (TAD), bei dem der prätherapeutisch befallene Lymphknoten durch Clip oder radioaktiven Tracer markiert wird. Für Patientinnen, bei denen der markierte Lymphknoten mit dem SLN entfernt wurde, betrug die FNR nur 1,4% (2). Diese Ergebnisse unterstützen die Hypothese, dass das Verfahren der TAD geeignet ist, die ungünstigen Erfolgsraten der SLNB zu optimieren und gleichzeitig die Morbidität zu reduzieren. Obwohl die TAD zunehmend eingesetzt wird, sind prospektiven Daten hierzu sehr limitiert und es gelten international unterschiedliche Empfehlungen (3). Die EUBREAST Studiengruppe initiierte eine internationale Registerstudie (AXSANA) bei der wichtige Daten zum operativen Vorgehen in der Axilla prospektiv erfasst und ausgewertet werden (4). Als ein teilnehmendes Studienzentrum möchten wir als Brustzentrum am Klinikum Nürnberg bei unseren Patientinnen mit einem klinischen LK-Befall die gezielte prätherapeutische LK-Markierung ab Juni 2021 einsetzen und eigene unizentrische prospektive Daten akquirieren.

### Methods

Bei Patientinnen mit klinisch eindeutig positiven und/oder histologisch gesicherten axillären Lymphknotenmetastasen wird vor neoadjuvanter Chemotherapie ein magnetischer Seed (Magseed®) in die entsprechenden Lymphknoten platziert. Nach Abschluss der Chemotherapie erhalten die Patientinnen zusätzlich zur Brust- eine axilläre Operation, wobei die genaue Op-Methode (ALND, TAD (= TLNB + SNB), TLNB, SNB) interdisziplinär präoperativ/intraoperativ vom Operateur entschieden werden kann. Die Op-Methode (inklusive Handling und Detektierbarkeit), die Pathologie der Lymphknoten und der klinische Verlauf der Patientinnen werden in einer prospektiven Datenbank erfasst.

### Results

Die Auswertung umfasst die Prognose der Patientinnen für die verschiedenen Op-Techniken (ALND, TAD, SLNB, TLNB), die Durchführbarkeit der Op-Methoden (Detektierbarkeit des SNB/TLNB, Zeitaufwand, Handling) sowie Erfassung der Rate an erfolgreichem Nodalstaging für die einzelnen Verfahren.

### Conclusions

Die Daten unserer Klinik sollen dazu beitragen, den klinischen Stellenwert der TAD und das Markierungsverfahren mittels magnetischem Seed genauer zu untersuchen und zu etablieren.

1. De Gournay et al. *Impact of sentinel node biopsy on long-term quality of life in breast cancer patients.* Br J Cancer. 2013
2. Caudle AS et al. *Improved Axillary Evaluation Following Neoadjuvant Therapy for Patients With Node-Positive Breast Cancer Using Selective Evaluation of Clipped Nodes: Implementation of Targeted Axillary Dissection.* J Clin Oncol. 2016
3. Gasparri ML et al. *What we learned in axillary management of breast cancer patients at the American society of clinical oncology (ASCO) 2020 virtual meeting? The EUBREAST point of view.* EClinicalMedicine. 2021
4. *AXSANA (AXillary Surgery After NeoAdjuvant Treatment): Prospektive, multizentrische Registerstudie zur Bewertung verschiedener leitlinienkonformer Operationsverfahren in der Axilla (Sentinel-Node Biopsie, Targeted Axillary Dissection, Axilladissektion) nach neoadjuvanter Chemotherapie* (Protokoll Deutsch_V5.1_2021-01-07)

## Klinische Bedeutung der Targeted axillary dissection (TAD) nach neoadjuvanter Chemotherapie bei Mammakarzinompatientinnen mit prätherapeutisch befallenen Lymphknoten und Konversion zu ycN0

Christine Zeder-Göß[1], Ralf Adamus[2], Frank E.-M. Gisbert[1], Thorsten Koch[1], Annette Linke[2], Simone Linsenbühler[1], Cosima Brucker[1]

[1]Klinik für Frauenheilkunde und Geburtshilfe, Paracelsus Medical University, Nuremberg, Germany; [2]Institut für Radiologie und Nuklearmedizin, Paracelsus Medical University, Nuremberg, Germany; Contact: christine.zeder-goess@klinikum-nuernberg.de

### Objective

Die komplette Ausräumung der axillären Lymphknoten (ALND – axilläre Lymphonodektomie) galt lange Zeit als Standardverfahren für die Therapie des Mammakarzinoms. Sie hatte sowohl therapeutische sowie diagnostische Funktion. Da die ALND mit einer hohen Morbidität verbunden ist, konnte sie erfreulicherweise bei primärer OP und unauffälligen Lymphknoten durch die schonendere Sentinel-Lymphknotenbiopsie (SLNB) ersetzt werden, ohne das krankheitsfreie Überleben oder das Gesamtüberleben zu beeinträchtigen. Bei Patientinnen, die eine neoadjuvante Chemotherapie erhalten und vor Therapiebeginn einen positiven Lymphknotenstatus aufweisen und unter Chemotherapie zu einem ycN0 Stadium konvertieren, ist die Sicherheit der SLNB nach Chemotherapie aufgrund einer zu hohen Falsch-Negativ-Rate (FNR) umstritten. Eine prospektive Registerstudie von Caudle et al. demonstrierte ein Verfahren (TAD), bei dem der prätherapeutisch befallene Lymphknoten durch Clip oder radioaktiven Tracer markiert wird. Für Patientinnen, bei denen der markierte Lymphknoten mit dem SLN entfernt wurde, betrug die FNR nur 1,4%. Diese Ergebnisse unterstützen die Hypothese, dass das Verfahren der TAD geeignet ist, die ungünstigen Erfolgsraten der SLNB zu optimieren und gleichzeitig die Morbidität zu reduzieren. Obwohl die TAD zunehmend eingesetzt wird, sind prospektiven Daten hierzu sehr limitiert und es gelten international unterschiedliche Empfehlungen. Die EUBREAST Studiengruppe initiierte eine internationale Registerstudie (AXSANA) bei der wichtige Daten zum operativen Vorgehen in der Axilla prospektiv erfasst und ausgewertet werden. Als ein teilnehmendes Studienzentrum möchten wir als Brustzentrum am Klinikum Nürnberg bei unseren Patientinnen mit einem klinischen LK-Befall die gezielte prätherapeutische LK-Markierung ab Juni 2021 einsetzen und eigene unizentrische prospektive Daten akquirieren.

### Methods

Bei Patientinnen mit klinisch eindeutig positiven und/oder histologisch gesicherten axillären Lymphknotenmetastasen wird vor neoadjuvanter Chemotherapie ein magnetischer Seed (Magseed®) in die entsprechenden Lymphknoten platziert. Nach Abschluss der Chemotherapie erhalten die Patientinnen zusätzlich zur Brust- eine axilläre Operation, wobei die genaue Op-Methode (ALND, TAD (= TLNB + SNB), TLNB, SNB) interdisziplinär präoperativ/intraoperativ vom Operateur entschieden werden kann. Die Op-Methode (inklusive Handling und Detektierbarkeit), die Pathologie der Lymphknoten und der klinische Verlauf der Patientinnen werden in einer prospektiven Datenbank erfasst.

### Results

Die Auswertung umfasst die Prognose der Patientinnen für die verschiedenen Op-Techniken (ALND, TAD, SLNB, TLNB), die Durchführbarkeit der Op-Methoden (Detektierbarkeit des SNB/TLNB, Zeitaufwand, Handling) sowie Erfassung der Rate an erfolgreichem Nodalstaging für die einzelnen Verfahren.

### Conclusions

Die Daten unserer Klinik sollen dazu beitragen, den klinischen Stellenwert der TAD und das Markierungsverfahren mittels magnetischem Seed genauer zu untersuchen und zu etablieren.

PARACELSUS MEDIZINISCHE PRIVATUNIVERSITÄT

DKG KREBSGESELLSCHAFT Zertifiziertes Lungenkrebs Zentrum

Klinikum Nürnberg Wir sind für Sie da!

# Clinically relevant prognostic biomarkers for immune-checkpoint inhibitor therapy in NSCLC

Gloria Zeitler[1,2], Joachim H. Ficker[1,2], Dieter Würflein[1,2], Fabian Reich[1,2], Wolfgang Brückl[1,2]

Affiliation: 1) Department of Internal Medicine 3, Lung Cancer Center, Klinikum Nuremberg, Nuremberg, Germany; 2) Paracelsus Medical University (PMU), Nuremberg, Germany; contact: gloria.zeitler@stud.pmu.ac.at

**Background:** We investigated the association of clinical and laboratory findings with response and treatment effects in immune-checkpoint inhibitor (ICI) treated advanced NSCLC patients. A smaller group out of this cohort treated with 1st line ICI therapy (pembrolizumab) was analyzed separately.

**Methods:** NSCLC patients receiving at least one dose of ICI therapy at the Lung Cancer Center Nuremberg between 2016 and 2019 were identified retrospectively. Factors associated with progression free survival or overall survival were assessed with Cox proportional hazard models. A prognostic score (Δ-Score) combining ΔLDH, ΔCRP and ΔG-GT was created and categorizes patients into prognostic subsets.

**Results:** Among 89 patients, 66.3% were men, median age was 68 years and 70.8% received pembrolizumab as 1st line treatment. For the whole cohort, median PFS and OS was 5 months and 11.2 months, respectively. Median PFS was 5.7 months and median OS was 12.7 months in the 1st line therapy cohort. On multivariate analysis, an increasing ΔLDH (p = 0.043), NLR < 5 (p = 0.045) and CRP-Q1 (≤ 7.7 mg/dL) (p = 0.033) were significantly associated with increased median PFS. CRP-Q1 was also associated with a greatly enhanced median OS for the whole cohort. A low Δ-Score reached a high level of significance in terms of PFS and showed a clear trend regarding OS.

**Conclusions:** Our results demonstrate that laboratory measurements are effective tools in the prediction of response and outcome in NSCLC patients treated by ICI. Further studies are warranted to confirm their prognostic significance in this patient population.

**Disclosure Statement:** The authors declare that there is no conflict of interest. This work was supported by an unrestricted grant from the W. Lutz Stiftung, Nuremberg to W.M.B. and J.H.F.

## Introduction

- In the recent years, the choice of standard therapeutic options for metastatic NSCLC patients has been expanded by immune-checkpoint-inhibitor (ICI) therapy either as monotherapy or in combination with chemotherapy, anti-angiogenic antibodies or with other forms of ICI.
- However, many mortality curves of the ICI therapy show an increased risk of death during the initial phase of ICI treatment. Reasons for this phenomenon may be primary resistance with hyper-progressive tumor growth as well as immune-related adverse events. Therefore, it is of utmost importance for the treating physician to reliably know whether the ICI will be beneficial for the individual NSCLC patient or not.
- The goal of this thesis is to identify one or even more biomarkers with a prognostic power for effects of treatment and response in NSCLC patients treated by ICI. This thesis focuses on factors that can be easily implemented in daily clinical practice and are determined prior to ICI therapy or during the initiation phase.

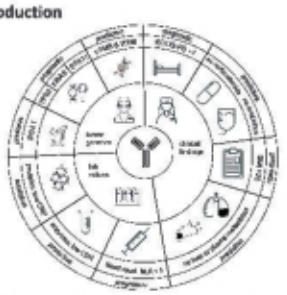

**Figure 1.** Clinically relevant positive prognostic and prediction markers for immunecheckpoint-inhibitor therapy in non-small cell lung cancer (NSCLC) reflecting the current state of science

## ICI therapy in palliative 1st and 2nd line treatment and its efficacy

| Characteristic | Whole ICI cohort (n=89) | ICI 1st line cohort (n=63) | ICI 2nd line cohort (n=26) | p-value |
|---|---|---|---|---|
| Gender | | | | |
| Male | 59 (66.3%) | 42 | 17 | 0.054 |
| Female | 30 (33.7%) | 21 | 9 | |
| Age (y) | 68 (36 - 86) | 68 | 68 | 0.948 |
| ECOG | | | | |
| 0 | 10 (11.2%) | 10 | 0 | 0.021 |
| 1 | 49 (55.1%) | 35 | 14 | |
| 2 | 25 (28.1%) | 16 | 9 | |
| 3 | 5 (5.6%) | 2 | 3 | |
| Histology | | | | |
| Adenocarcinoma | 58 (65.2%) | 43 | 15 | 0.884 |
| Squamous cell carcinoma | 25 (28.1%) | 18 | 7 | |
| Other | 6 (6.7%) | 2 | 4 | |
| Smoker | 68 (76.4%) | 51 | 17 | 0.014 |
| Pack years | 40 (0 - 90) | 40 | 40 | 0.814 |
| Peripheral lung | 71 (79.8%) | 51 | 20 | 0.504 |
| Pulmonary metastasis | 64 (71.9%) | 46 | 18 | 0.504 |
| Brain MTS | 14 (15.7%) | 9 | 5 | 0.504 |
| PD-L1 | 9 (10.1%) | 6 | 3 | >0.999 |
| PD-L1 [%] | 0 (0 - 90) | 0 | 0 | |
| PD-L1 [%] | 24 (27.0%) | 21 | 3 | |
| PD-L1 [%] | 48 (53.9%) | 36 | 12 | |
| PD-L1 [%] | 17 (19.1%) | 6 | 11 | |
| Driver Mutation | | | | |
| Positive | 10 (11.2%) | 10 | 0 | 0.098 |
| Total | 79 (88.8%) | 53 | 26 | |
| KRAS mutation | 38 (42.7%) | 28 | 10 | 0.814 |
| KRAS mutation | 35 (39.3%) | 25 | 10 | |
| Other mutation | 3 (3.4%) | 3 | 0 | |
| Systemic therapy prior | 26 (29.2%) | 0 | 26 | <0.001 |
| Platinum | 24 (27.0%) | 0 | 24 | <0.001 |
| Pemetrexed | 21 (23.6%) | 0 | 21 | <0.001 |
| Docetaxel | 3 (3.4%) | 0 | 3 | 0.031 |
| Gemcitabine | 1 (1.1%) | 0 | 1 | 0.331 |

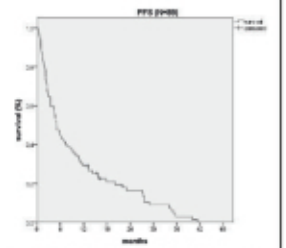


**Figure 2.** Kaplan-Meier survival curve of PFS and table with patient characteristics of the whole cohort

- Objective response rate (ORR) was 47.2% and disease control rate (DCR) was 53.9% for all 89 patients.
- In the whole cohort, the median duration of response (DOR) was 15.9 months (95% CI: 9.5-22.2), slightly higher in the 1st line therapy arm with median of 23 months (95% CI: 9.7-36.4).
- Median PFS in the whole ICI therapy cohort and in the 1st line group were 5 months (95% CI: 3.5-6.4) and 5,8 months (95% CI: 2.8-8.7), respectively.
- The median OS for the whole ICI cohort was 11.2 months (95% CI: 5.1-17.4), for the 1st line therapy group 12.7 months (95% CI: 0-33.8).

## Univariate and multivariate analysis of PFS in the whole cohort

| Laboratory finding | Median PFS | Univariate analysis | | Multivariate analysis | |
|---|---|---|---|---|---|
| | in months | HR (95% CI) | p-value < | HR (95% CI) | p-value < |
| NLR (n = 81) | | | | | |
| <5 | 6.1 | 1.98 (1.13-3.7) | **0.024** | 2.09 (1.02-4.29) | **0.043** |
| ≥5 | 2.9 | | | | |
| WBC, /µl (n = 82) | | | | | |
| Normal (≤ 10 000) | 5.8 | 1.06 (0.67-1.67) | 0.794 | | |
| Increased (> 10 000) | 4.6 | | | | |
| baseline CRP level, mg/dl (n = 82) | | | | | |
| Normal (< 0.5) | 6.9 | 1.69 (0.90-3.34) | 0.053 | | |
| Elevated (≥ 0.5) | 2.8 | | | | |
| ΔCRP level (n = 79) | | | | | |
| Decrease | 5.8 | 0.99 (0.94-1.06) | 0.972 | | |
| Increase | 4.3 | | | | |
| CRP-Quartile, mg/dl (n = 82) | | | | | |
| Q1 (≤ 7.7) | 6.1 | 2.14 (1.3-3.8) | **0.010** | 2.52 (1.06-5.99) | **0.033** |
| Q2 (> 7.7) | 1.9 | | | | |
| baseline LDH level, U/L (n = 82) | | | | | |
| Normal (≤ 248) | 5.7 | 0.76 (4.72-1.23) | 0.269 | | |
| Elevated (> 248) | 4.7 | | | | |
| ΔLDH (n = 69) | | | | | |
| Decrease | 4.6 | 0.54 (0.3-0.9) | **0.022** | 2.15 (1.03-4.53) | **0.043** |
| Increase | 10.7 | | | | |
| G-GT level, U/L (n = 82) | | | | | |
| Normal (≤ 60) | 7.6 | 1.69 (1.01-2.91) | **0.046** | | |
| Increased (> 60) | 4.3 | | | | |
| ΔG-GT (n = 66) | | | | | |
| Decrease | 10.1 | 2.06 (1.20-3.56) | **0.009** | 1.79 (0.79-3.65) | 0.179 |
| Increase | 4.3 | | | | |

## Score of Δ-parameters for PFS – whole cohort

The score of Δ-parameters (Δ-Score) combines the change between the first and second application of ICI therapy of LDH, CRP and G-GT and categorizes patients into prognostic subsets based on the following scoring system:

| Score of Δ-parameters | | |
|---|---|---|
| ΔLDH | normal or increased | 1 |
| | decreased | 2 |
| ΔCRP | normal or decreased | 1 |
| | increased | 2 |
| ΔG-GT | normal or decreased | 1 |
| | increased | 2 |
| | | Sum (3-6) |

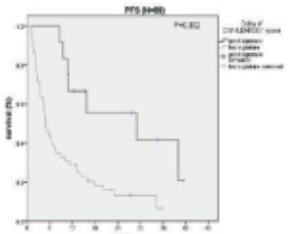


**Figure 3.** Kaplan-Meier survival curve of progression free survival in good vs. bad signature group of the whole cohort.

- Patients belonging to the good signature group (3 points reached) had a median PFS of 28.98 months compared to those in the bad signature group (>3 points reached) (4.96 months) (p-value < 0.020).
- Furthermore, every additional point reached is associated with worse median PFS (p-value = 0.026) in the scoring system (Δ-Score).

| Δ-Score | Median PFS | 95% CI | p-value |
|---|---|---|---|
| 3 | 28.98 | 9.0 - 60.0 | **0.026** |
| 4 | 5.1 | 3.3 - 6.8 | |
| 5 | 4.5 | 2.1 - 7.0 | |
| 6 | 1.6 | 0.0 - 4.1 | |
| good signature | 28.98 | 9.0 - 60.0 | **0.001** |
| bad signature | 4.96 | 3.5 - 6.4 | |

## Conclusions

In this study, we demonstrated that laboratory measurements are effective tools in the prediction of response and treatment outcomes in NSCLC patients. Especially NLR, CRP, and LDH effectively differentiate patients with good outcome. In addition, G-GT was identified as prognostic predictor in NSCLC patient treated with ICI therapy for the first time. Furthermore, a score created out of Δ levels of laboratory values discriminated patients with tremendous differences in PFS (and OS). More clinical studies and inclusion of translational researches e.g., molecular factors from liquid biopsies, will be needed to improve ICI treatment and select patients, who will benefit from ICI mono or combined therapies in NSCLC.

## References

- Reck M, Rodríguez-Abreu D, Robinson AG, Hui R, Csoszi T, Fülöp A, et al. Updated Analysis of KEYNOTE-024: Pembrolizumab Versus Platinum-Based Chemotherapy for Advanced Non-Small-Cell Lung Cancer With PD-L1 Tumor Proportion Score of 50% or Greater. J Clin Oncol. 2019;37(7):537-46.
- Gandhi L, Garassino MC. Pembrolizumab plus chemotherapy in lung cancer. Lancet Oncol. 2018;19(3):e113-e24.
- Zhang L, Li Y, Yan X, Wang B, Guo R, Yu G, et al. Immune-related adverse events of pembrolizumab monotherapy versus chemotherapy for non-small cell lung cancer patients treated with immune checkpoint inhibitors: a meta-analysis. Immunotherapy. 2018;10(8):669-76.
- Gadd J, Kelleher AD, Prince KM, Liebowitz D, Hengel S, Patterson S, et al. Effective Innate Cytokine Responses Predict Reduced HIV Load Set Point in Women Undergoing Acute Hepatitis C Virus Infection. The Journal of infectious diseases. 2017;215(1):29.
- Vilgelm AE, Richmond A. Chemokines Modulate Immune Surveillance in Tumorigenesis, Metastasis, and Response to Immunotherapy. Front Immunol. 2019;10:333.
- Jochems C, Hodge JW, Fantini M, Fujii R, Morillon YM, 2nd, Greiner JW, et al. An NK cell line (haNK) expressing high levels of granzyme and engineered to express the high affinity CD16 allele. Oncotarget. 2016;7(52):86359-73.
- Sanmamed MF, Perez-Gracia JL, Schalper KA, Fusco JP, Gonzalez A, Rodriguez-Ruiz ME, et al. Changes in serum interleukin-8 (IL-8) levels reflect and predict response to anti-PD-1 treatment in melanoma and non-small-cell lung cancer patients. Ann Oncol. 2017;28(8):1988-95.
- Sorensen, Anne Krarup, et al. "Clinically relevant prognostic and predictive markers for immunotherapy in patients with non-small cell lung cancer: analysis of PD-L1 expression and circulating tumor cells." BMC Cancer 2020 Dec 1;20(1):1059. doi: 10.1186/s12885-020-07516-0. PMID: 33272262; PMCID: PMC7713331.

## Clinically relevant prognostic biomarkers for immune-checkpoint inhibitor therapy in NSCLC

Gloria Zeitler[1], Fabian Reich[1], Joachim H. Ficker[1], Dieter Würflein[1], Wolfgang Brückl[1]

[1]Department of Internal Medicine 3, Paracelsus Medical University, Nuremberg, Germany; Contact: gloria.zeitler@stud.pmu.ac.at

### Objective
We investigated the association of clinical and laboratory findings with response and therapy effects in immune-checkpoint inhibitor (ICI) treated advanced NSCLC patients. A smaller group out of this cohort treated with 1st line ICI therapy (pembrolizumab) was analyzed separately.

### Methods
NSCLC patients receiving at least one dose of ICI therapy at the Lung Cancer Center Nuremberg between 2016 and 2019 were identified retrospectively. Factors associated with PFS or OS were assessed with Cox proportional hazard models. A prognostic score (Δ-Score) combining ΔLDH, ΔCRP and ΔG-GT was created and categorizes patients into prognostic subsets.

### Results
Among 89 patients, 66.3% were men, median age was 68 years and 70.8% received pembrolizumab as 1st line treatment. For the whole cohort, median PFS and OS was 5 months and 11.2 months, respectively. Median PFS was 5.7 months and median OS was 12.7 months in the 1st line therapy cohort. On multivariate analysis, an increasing ΔLDH ($p = 0.043$), NLR $< 5$ ($p = 0.045$) and CRP-Q1 ($\leq 7.7$ mg/dL) ($p = 0.033$) were significantly associated with increased median PFS. CRP-Q1 was also associated with a greatly enhanced median OS for the whole cohort. A low Δ-Score reached a high level of significance in terms of PFS and showed a clear trend regarding OS.

### Conclusions
Our results demonstrate that laboratory measurements are effective tools in the prediction of response and outcome in NSCLC patients treated by ICI. Further studies are warranted to confirm their prognostic significance in this patient population.

## Investigating the effect of β-cyclodextrin on dopamine D2 receptor ligand binding

Lukas Zell[1], Veronika Temml[1], Daniela Schuster[1]

[1]Institute of Pharmacy, Department of Pharmaceutical and Medicinal Chemistry, Paracelsus Medical University, Salzburg, Austria; Contact: lukas.zell@pmu.ac.at

### Objective

Evaluating the activities of compounds is essential for developing novel therapeutic strategies. Radioligand binding assays remain the main technique to investigate binding affinities, thus quantifying, e.g. compound-receptor interactions. However, fluorescent ligand-binding assays (homogenous time-resolved fluorescence, HTRF) are an emerging alternative. While general assay conditions like salt concentration, pH range, co-factors, incubation time, and receptor concentration are mostly pre-determined in commercially available assays, co-solvents, e.g. DMSO or PEG and solubility enhancer concentrations are customizable. While co-solvents are used to increase solubility of lipophilic compounds, most receptor binding assays are cell-based and solvents may interfere with membrane integrity, thus limiting the assay's applicability. However, solubility enhancing substances, e.g. cyclodextrins (CDs), have been shown to overcome limiting issues in FDA-approved formulations. Via the generation of inclusion complexes (ICs) compound solubility and plasma concentration are improved while solvent cytotoxicity is decreased simultaneously. Interestingly, CDs have not been investigated in vitro considering the simultaneous increase of solubility while not interfering with compound-receptor interactions. The dopamine receptor family, a major GPCR family, represents an interesting candidate for the investigation of ICs regarding such receptor interaction.

### Methods

This project aims at comparing dopamine D2 receptor ligands formulated with and without CDs, and subsequently quantifying their binding affinity utilizing a HTRF receptor-ligand binding assay. Therefore, the generation of ICs will be shown via equilibrium dialyis. The binding affinity of the generated ICs will be quantified and compared to the respective ligands formulated without the use of ICs utilizing a HTRF binding assay.

### Results

In this case study it could be shown, that CDs didn't interfere with receptor binding or exhibit cytotoxic effects, thus rendering CD-based ICs applicable for in vitro testing.

### Conclusions

Overcoming solubility issues of newly designed compounds via IC formulation is a promising strategy to significantly increase the applicability of HTRF-based cell-based compound-receptor binding assays.

## Establishment of a seminal platform for AI Development in a radiological-clinical context

Peter Zinterhof[1], Claus-Trutz Kastl[1]
[1]Institute of Radiology, Paracelsus Medical University, Salzburg, Austria;
Contact: p.zinterhof@salk.at

### Introduction

With respect to very dynamic developments in the field of Artificial Intelligence (AI) and Machine Learning (ML), Radiology benefits from usually very rich clinical datasets that encompass various imaging technologies, such as Computed Tomography, Magnetic Resonance Imaging, X-Ray, and others.
In order to harness these data for research in a clinical setting, we develop an integrated workflow, that covers virtually every step of the process. Beginning with data acquisition, research data management, tools for annotation and examination, we also provide easy methods for training artificial neural networks on premises. One of the main goals is to provide an open, extensible platform that can be developed over time and finds its way into daily routines of clinical radiologists.

### Methods

The development of an integrated workflow for AI-based research in Radiology has been embedded in an ongoing project of two PhD-students: One student is a trained physician, while the second a computer scientist with a background in high performance computing, as well as machine learning. This relatively broad spectrum of different scientific fields helps to create solutions that are sustainable.

In order to tackle possible data privacy issues as well as availability of suitable computational resources, an in-house AI-platform has been planned, procured, and established by the team. This platform currently offers 2 dedicated high-performance AI-workstations, one NVIDIA DGX-Station comprising 4 Volta-GPUs, as well as a custom-built 'development cube', which is based on two NVIDIA Ampere GPUs (RTX 3090). The platform thus sports more than 40.000 CUDA-cores, 176 GB of fast GPU-memory, as well as a total of 36 TB of local storage, that is shared with NFS4.
In compliance with general security protocols remote access is provided by means of 'VMware Horizon View' which allows access to a dedicated virtual machine on one of the workstations via the remote desktop protocol. The VM helps to decouple remote sessions from concurrent on-site use of the workstation. Another advantage of this setup is persistence of graphical user sessions.

### Results

The proposed workflow is both based on interactive tools, as well as batch processing that operate within a Linux environment. A queuing system (SLURM) is used to manage training runs of neural networks, as well as for harvesting specific datasets from a central PACS (Picture Archiving and Communication System).
The harvesting process is not restricted to download operations from the underlying PACS, but also provides meta-data extraction and filtering according to user-supplied key-words. Meta-data are automatically imported into a NoSQL-database system (MONGODB), which provides schema-free storage operations that effectively support extensibility and robustness. Additionally, all imaging data are redirected into HDF5-datasets, that are optimized for highly performant read/write access and serve as a basis for the creation of training/validation/testing datasets as required by common deep learning frameworks.
For improved use of the available research storage areas, original DICOM data can be discarded during the harvesting.
A Python-based graphical user interface provides instant access to HDF5-datasets, which serve for manual and AI-assisted annotation of data. DL-based super-resolution is employed for enhanced visualization capabilities of the tool and user-provided neural networks can also be integrated seamlessly in order to provide various assessments of a given dataset or patient study.

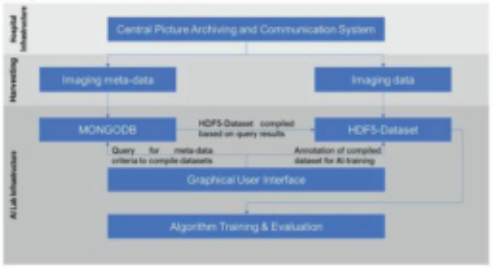


### Conclusion

We have demonstrated the development of a scalable and robust research platform for clinical projects in the nascent field of artificial intelligence. The setup offers latest technologies both in terms of AI-hardware and machine learning software frameworks. The main advantage if a carefully orchestrated set of technologies, that limit the complexities of administrative tasks, while fostering a vibrant research environment.

## Establishment of a seminal platform for AI Development in a radiological-clinical context

Peter Zinterhof[1], Claus-Trutz Kastl[1]

[1]Department/Institute of Radiology, Paracelsus Medical University, Salzburg, Austria; Contact: p.zinterhof@salk.at

### Objective

With respect to very dynamic developments in the field of Artificial Intelligence (AI) and Machine Learning (ML), Radiology benefits from usually very rich clinical datasets that encompass various imaging technologies, such as CT, MRI, X-Ray, and others.
In order to harness these data for research in a clinical setting, we develop an integrated workflow, that covers virtually every step of the process. Beginning with data acquisition, data management, tools for annotation and examination, we also provide easy methods for training artificial neural networks. One of the main goals is to provide an open, extensible platform to be developed over time and that can be integrated into the routines of clinicians.

### Methods

The development of an integrated workflow for AI-based research in Radiology has been embedded in an ongoing project of two PhD-students: One student is a trained physician, while the second a computer scientist with a background in high performance computing, as well as machine learning. In order to tackle possible data privacy issues as well as the availability of suitable computational resources, an in-house AI-platform has been planned, procured, and established by the team. This platform currently offers 2 dedicated high-performance AI-workstations, one NVIDIA DGX-Station comprising 4 Volta-GPUs, as well as a custom-built 'development cube', which is based on two NVIDIA Ampere GPUs (RTX 3090). The platform thus sports more than 40.000 CUDA-cores, 176 GB of fast GPU-memory, as well as a total of 36 TB of local storage, that is shared with NFS4.

### Results

The proposed workflow is both based on interactive tools, as well as batch processing that operate within a Linux environment. A queuing system (SLURM) is used to manage training runs of neural networks, as well as for harvesting specific datasets from a central PACS (Picture Archiving and Communication System).
The harvesting process is not restricted to download operations from the underlying PACS, but also provides meta-data extraction and filtering according to user-supplied key-words. Meta-data are automatically imported into a NoSQL-database system (MONGODB), which provides schema-free storage operations that effectively support extensibility and robustness. Additionally, all imaging data are redirected into HDF5-datasets, that are optimized for highly performant read/write access and serve as a basis for the creation of training/validation/testing datasets as required by common deep learning frameworks. For improved use of the available research storage areas, original DICOM data can be discarded during the harvesting.
A graphical user interface provides instant access to HDF5-datasets, which serve for manual and AI-assisted annotation of data. DL-based super-resolution is employed for enhanced visualization capabilities of the tool and user-provided neural networks can also be integrated easily in order to provide various assessments of a given dataset or patient study.

### Conclusions

We have demonstrated the development of a scalable and robust research platform for clinical projects in the nascent field of artificial intelligence. The setup offers latest technologies both in terms of AI-hardware and machine learning software frameworks. The main advantage if a carefully orchestrated set of technologies, that limit the complexities of administrative tasks, while fostering a vibrant research environment.

## Liste der beteiligten Einrichtungen

(in alphabetischer Reihenfolge)

- Berufsgenossenschaftliche Unfallklinik Murnau – Lehrkrankenhaus der PMU Salzburg
- Gelenk- und Gefäßzentrum Mittelfranken – Akademische Lehrpraxis der PMU Nürnberg
- Hochschule Weihenstefan-Triesdorf
- Krankenhaus der Barmherzigen Brüder Salzburg – Lehrkrankenhaus der PMU Salzburg
- Paracelsus Medizinische Privatuniversität Nürnberg / Klinikum Nürnberg
- Paracelsus Medizinische Privatuniversität Salzburg / Universitätsklinikum Salzburg
- Paris Lodron Universität Salzburg
- Schön Klinik Berchtesgadener Land – Lehrkrankenhaus der PMU Salzburg
- Technische Hochschule Nürnberg

# Verzeichnis aller Autor*innen

(fett gedruckt = Präsentator*in)


| Autor*in | Abstract Nr. |
|---|---|
| **A** | |
| Ablinger, Celina | **1**, 6, 31 |
| Achleitner, Dagmar | 61 |
| Achleitner, Melanie T. | **2** |
| Adamus, Ralf | 132 |
| Afrashteh, Behnaz | **3** |
| Ahlgrimm-Siess, Verena | 118 |
| Aigner, Ludwig | 3, 11, 72, 117, 121 |
| Alt, Eva | 75 |
| Altendorfer, Barbara | 11, 72, 121 |
| Aminzadeh-Gohari, Sepideh | 95, 125 |
| Ardelt, Maximilian | 1 |
| Arevalo-Martin, Angel | 72 |
| Aschauer-Wallner, Stephanie | 103 |
| Asslaber, Daniela | 121 |
| Astolfi, Laura | 9 |
| Auer-Hackenberg, Lorenz | 99 |
| Auffarth, Alexander | 38 |
| Augat, Peter | 4, 89, 106 |
| Austen, William G. | 22 |
| Avraham, Karen B. | 85 |
| **B** | |
| Bail, Hermann J. | 49 |
| Baillès, Eva | 90 |
| Barth, André A. | 18, 20 |
| Bauer, Andree | 116 |
| Bauer, Johann W. | 41, 61, 98, 118 |
| Baumbach, Jan | 61 |
| Baumeister, Dirk | **4** |
| Baumgärtel, Matthias | 120 |
| Baumgartner, Christian | 128 |
| Baumgartner, Christian F. | 129 |
| Beck, Sabrina | **5** |
| Bekric, Dino | **6, 7,** 31, 51, 86 |
| Benedetti, Ariane | 11, 46, 121 |
| Benedetti, Bruno | **8**, 105, 121 |
| Berger, Stefanie | 43 |
| Bernardinelli, Emanuele | **9**, 33 |
| Berns, Maresa | **10** |
| Bertsch, Thomas | 71, 77, 113, 116 |
| Bessa de Sousa, Diana M. | **11** |
| Beyreis, Marlena | 6, 7, 30, 31, 86 |
| Bieler, Lara | **12,** 105 |
| Billner, Moritz | 10, 18, 20 |
| Binder, Heide-Marie | 13, 25, 98, 130 |
| Bischof, Johannes | 61, 98 |
| Bittner, Severin | 110 |
| Blanch, Jordi | 90 |
| Blechschmidt, Cristiane | 35 |
| Blöchl, Constantin | 130 |
| Bolovis, Dimitrios I. | **14** |
| Bosque Varela, Pilar | **15,** 80 |
| Bott, Alexander | 115 |
| Brachtl, Gabriele | 13, 65, 130 |
| Brandauer, Anna | 43 |
| Braun, Alexandra | **16,** 40 |
| Braun, Bernd | 62 |
| Braun, Tobias | **17,** 63 |
| Breidung, David | **18** |
| Breier, Annette | 45, 122 |
| Brucker, Cosima | 14, 32, 132 |
| Brückl, Wolfgang | 133 |
| Brugger, Karin | 37 |
| Brunauer, Andreas | 96 |
| Brunner, Susanne M. | **19,** 101 |
| Buben, Philipp | **20** |
| Buchegger, Stephanie | **21** |
| Butkiene, Dominyka | 56 |
| Butler, Katrin | 120 |
| **C** | |
| Capelôa, Tânia | 125 |
| Casari, Maria E. | **22** |
| Catalano, Luca | **95,** 125 |
| Chartier, Christian | 22 |
| Chaudhari, Akshay | 128, 129 |
| Chaves, Gustavo | 77 |
| Chaves-Barboza, Gustavo | 39 |
| Christiane, Waller | 90 |
| Coletta, Anna F. | 23, 24 |
| Condello, Ignazio | **23, 24** |
| Conti, Chiara | 90 |
| Cosco, Valeria | 23 |
| Couillard-Després, Sébastien | 8, 12, 46, **105** |
| Criée, Carl-Peter | 108 |
| Critelli, Alessandra | 24 |
| Cronemberger Andrade, André | **25,** 48, 65, 130 |
| **D** | |
| Däbritz, Jan | 5 |
| Dallmann, Guido | 125 |
| Dankl, Daniel | 56 |
| Danklmaier, Lisa | 26 |
| DeFrance, Bryon | 119 |
| Degner, Noam L. | **27** |
| Deininger, Christian | **28,** 29 |
| Deluca, Amelie | 28, **29** |

Dennis, Clancy 108
Dinges, Christian 50
Distler, Florian 97
Dobias, Heidemarie 6, 7, **30, 31,** 86, 118
Dobrivojevic Radmilovic, Marina 105
Dormann, Christiane **32**
Dossena, Silvia 9, **33,** 85, 102
Duda, Georg 52
Dunne, Pádraic 90

E
Ebbert, Ronald **126**
Ebert, Lena 94
Ebner, Lisa 58
Ebner-Peking, Patricia 25, **34,** 48, 65, 130
Eckner, Dennis 53
Eckrich, Caroline 57
Eckstein, Felix 128, 129
Egle, Alexander 121
Eibl, Thomas **35**
el Helou, Salhab 70
Ellinghaus, Agnes 52
Elminger, Juri 52
Emberger, Michael 125
Eminger, Essi 130
Emmrich, Katrin 120
Erber, Sara 86
Erling, Rahel **36**
Evdokimov, Dimitar 16

F
Fadgyas Stanculete, Mihaela 90
Farré, Josep M. 90
Feichtinger, René G. 2, **37,** 125
Feil, Monika 104
Fejzic, Dzeneta 55
Felder, Thomas K. 125
Ficker, Joachim H. 77, 120, 133
Fischlein, Theodor 17, 23, 24, 47, 53, 63, 71, 82, 114, 116
Fittkau, Martin 47
Fittkau, Matthias 71, 114, 116
Flamm, Maria 21
Flesner, Ilka 126
Flunkert, Stefanie 117
Font, Elena 90
Förch, Stefan 106
Forner Puntonet, Mireia 90
Forster, Jennifer 121
Föttinger, Fabian 50
Frank, Johanna 16
Frank, Nino 56
Freywald, Nicole 43
Fricke, Leonard **38**
Fritsche, Milan 62
Fritzsche, Kurt 90
Fröhlich, Thomas 11
Frommeyer, Gerrit 56
Fuchs, Julia 118
Fuchs, Sarah 75
Fürst, David 129
Fusch, Christoph 5, 64, 70, 79, 119, 126
Fusch, Gerhard 5, 70

G
Gabriele, Gabriele 8
Gaisberger, Martin 6, 60, 118
Garcia-Ovejero, Daniel 72
Gayán, Elena 90
Gehwolf, Renate 110, 131
Geissler, Sven 52
Geltinger, Martin **39**
Gerber, Luis **40**
Gerner, Peter 21
Geroldinger, Martin **41**
Geßlein, Markus 49, 113
Geyer, Tatjana 108
Gfrerer, Lisa 22
Gharibeh, Sarah 50
Giese, Andreas 62
Gimona, Mario 105
Gisbert, Frank EM. 132
Glarcher, Manela 58
Gleichauf, Johanna **42**
Glöckl, Rainer 54, 73, 108
Gnass, Irmela **43,** 58
Gögele, Clemens **44, 45,** 112, 122
Golchert, Thomas 127
Gosch, Markus 57, 123
Gottardi, Roman 66
Grabner, Christian **46**
Grad, Sibylle 111
Granitz, Christina 50
Gräßel, Elmar 104
Grassner, Lukas 72
Grillhösl, Andreas 72
Großmann, Irena 82
Grothe, Valerian 37
Grünbart, Martin 87
Guagnano, Maria T. 90
Gueths Gomes, Fausto 25, **48,** 130
Günzler, Valentin **47,** 114
Guttmann-Gruber, Christina **61**

H
Haag, Nina P. **49**
Haarmeyer, Golo-Sung 77
Hahn, Judith 45, 122
Hähnel, Stefan 76
Hartl, Arnulf 69

Haslinger, Michael **50,** 96
Hauptmann, Laurenz 55
Heil, Hannah 19
Heimel, Patrick 105
Hell, Tobias 87
Helm, Katharina 51
Hennemann, Lukas 42
Hercher, David 105
Herrmann, Sven 42
Heuser, Thomas 13, 130
Hillemacher, Thomas 75
Hinterbuchner, Lynne 55
Hitzl, Wolfgang 14, 66, 108
Hochmann, Sarah 34, 48, **52,** 65
Hofbauer, Peter 37
Höfer, Kilian 55
Hofer-Dückelmann, Christina 21
Hoffmann, Bernd 45
Hoi, Hannes 87
Höller, Yvonne 103
Holtmannspötter, Markus 35
Holzinger, Stefanie 59
Hölzl, Bertram 118
Hoog, Anna 34, 121
Höppchen, Isabel 43
Hoppe, Uta C. 50, 55, 56, 96
Horna, Stine **53**
Hornfeck, Markus 44
Huber, Christian 48
Huber, Christian G. 130
Huber-Cantonati, Petra 1
Hüllen, Andreas 37
Hummer, Blake 2
Hutter-Paier, Birgit 117

J

Jäger, Tarkan 86
Jakab, Martin 6, **51,** 60
Jakubecova, Dominika 12, 105
Jarosch, Inga **54,** 73, 108
Jessl, Jürgen 53
Jirak, Peter 50, **55, 56,** 96
Jiven-Jetzelsberger, Fatima 82
Jurca, Maria T. **57**
Jurga-Freytag, Malgorzata 127

K

Kaiser, Annette 127
Kaiser, Karin **58**
Kalisnik, Jurij 63
Kališnik, Jurij M. 47, 71, 114, 116
Kaser-Eichberger, Alexandra 26, **59**
Kastl, Claus-Trutz 135
Kaufmann, Anna 61
Keller, Esra 3
Kemnitz, Jana 128
Kenn, Klaus 54, 73, 108
Kern, Jan M. 61
Kerry, Ghassan 76
Kiesslich, Tobias 1, 6, 7, 30, 31, 86
Kirnbauer, Michael 50, 96
Kittl, Michael 51, **60**
Klausner, Fritz 81
Klieser, Eckhard 86
Klinglmayer, Eva 91
Knab, Katja 79
Kniewallner, Kathrin M. 11
Kocet, Laura 47, 114
Koch, Thorsten 132
Kocher, Thomas 98
Köchl, Christina 61
Koczulla, Andreas R. 73, 108
Koczulla, Rembert 54
Kofler, Barbara 19, 95, 101, 125
Kohl, Benjamin 112
Kokozidou, Maria 17, **63,** 112
Kolaric, Julijana 79
Kölblinger, Peter 125
Koller, Andreas 37, 101
Koller, Ulrich 98
Kölpin, Alexander 42
König, Sarah 90
Konnoev, Samuel 116
Konrad, Jens 45
Konrat, Robert 33
Konukoglu, Ender 128, 129
Kopf, Daniel 62
Körber, Michael **62**
Kosmann, Pauline 64
Kottcke, Manfred 62
Kotzot, Dieter 37
Krauss, Hannes 42
Kreutzer, Christina 8, 12, 46, 105
Krisch, Linda 34, 48, **65**
Krombholz-Reindl, Philipp 50, 63, **66,** 96
Kuchukhidze, Giorgi 15, 80, 81
Kühl, Hannes 44
Kutschar, Patrick 43

L

Laimer, Martin 41
Landauer, Franz **67, 68**
Laner-Plamberger, Sandra **69**
Lang, Roland 19, 61, 125
Langegger, Doris 58
Lanzara, Roberta 90
Larbig, Robert 56
Ledwon, Miroslaw 53
Lee, Henry C. 64
Lehmann, Robert 104

Lehner, Christine 107
Leidinger, Sophia 54
Leier, Nicolas **70**
Leiler, Špela **71**
Leister, Iris **72**
Leitl, Daniela 54, **73**, 108
Leitner, Julia 19
Lell, Michael 57
Lenhart, Armin 44
Licht, Christiane **74, 75**
Lichtenauer, Michael 50, 55, 56, 96
Liebert, Adrian **76**
Liemberger, Bernadette 98
Linke, Annette 132
Linsenbühler, Simone 132
Lobmann, Sebastian **77**
Lobo, Antonio 90
Lösel, Ralf **78**, 122
Luciani, Francesco 62
Lücke, Lennart **79**
Lusuardi, Lukas 3

M
Mach, Orpheus 72
Machegger, Lukas 15, **80, 81**
Macrí, Lucrezia 23
Maeding, Nicole **13**, 91
Maier, Doris 72
Mamdooh, Hazem 71, **82**
Manava, Panagiota 57, 115
Manstein, Felix 25
March, Oliver P. 98
Marino, Angela 102
Marti, Alejandro 18, 20
Maruszczak, Katharina **83, 84**
Maschek, Susanne 128
Mastroroberto, Pasquale 23, 24
Matulevicius, Arnoldas **85**
Maurer, Alexander 88
Mayr, Christian 1, 6, 7, 30, 31, 51, **86**
Mayr, Edgar 106
Mayr, Johannes A. 2, 37
McCoy, Mark 15, 80, 81
Meisner-Kober, Nicole 48, 91
Meyer, Michael 45, 122
Meyersburg, Damian 118
Minnich, Bernd 96
Mittermair, Christof **87**
Mittermeir, Michaela 52
Mladek, Julia 17, 63
Möllenhoff, Christian **88**
Möllenhoff, Clemens 88
Morabito, Rossana 102
Motloch, Lukas J. 50, 55, 56, 96
Mrazek, Cornelia 69
Mrowetz, Heike 11
Mühling, Mischa **89**
Muigg, Katharina 34, **91**
Müller, Ernst 29
Müller, Markus 40
Müller, Markus M. **90**
Müller, Silvana 44
Mur, Linda **92, 93**
Musset, Boris 39, 77

N
Nausch, Lydia **94**
Neddens, Jörg 117
Nejatisafa, Ali-Akbar 90
Nell, Christoph 73
Nestler, Nadja 58
Neumayer, Bettina 86
Neuner, Matthias 50, 96
Neureiter, Daniel 1, 6, 7, 31, 86
Neureiter, Elen 31
Niebler, Christine 42
Nietzold, Steffen 120
Nitschke, Janina 42
Noseworthy, Michael 119
Novak, Michael 95

O
Obach, Amadeu 90
Obermayer, Astrid 13, 130
Oellerer, Andreas 15, 80, 81
Offiah, Gozie 90
Ölinger, Isabel 99
Öller, Michaela 65, 69, 91
Ou, Kristy 52

P
Paar, Vera 50, 55, **96**
Pachmayr, Johanna 1, 21, 99
Pahernik, Sascha 97
Paiement, Nadine 117
Pan, Zhen-Qiang 33
Pancis, Irina 1
Parise, Doglas 61
Parise, Marisol 61
Parramon, Gemma 90
Peri, Josep M. 90
Petersmann, Anna-Lena **97**
Petkovic, Igor **98**
Pfaff, Johannes 15, 80, 81
Pichler, Martin 6
Pinon-Hofbauer, Josefina 61
Pintar-Hitzl, Monika **99**
Pistulli, Rudin 56
Pjevac, Petra 61
Plank, Christian 111

Platzl, Christian 26, 59
Polánsky-Biskup, Julia 52
Pollari, Francesco 53, 82
Poupardin, Rodolphe 8, 11, 25, 34, 52, **100,** 121, 130, 131
Pradel, Andreas 44
Preishuber-Pflügl, Julia 51, 60
Pusch, Michael 102

Q
Quin, MK 64

R
Ramspacher, Andrea 19, **101**
Raninger, Anna M. 13, 130
Rapp, Erdmann 37
Rasp, Gerd 9
Redtenbacher, Anna-Sophia 125
Regl, Christof 48
Reich, Fabian 133
Reichelt, Julia 61, 98
Reichert, Bert 10, 18, 20
Reinecker, Holger 56
Reisinger, Maximilian 8
Remigante, Alessia **102**
Renner, Philipp 42
Renz, Nora **103**
Resch, Herbert 103
Retzer, Lukas **104**
Richter, Keginja 75
Richter, Kneginja 74, 104
Rieser, Caroline 19
Riminucci, Mara 52
Rip, Jaap 111
Ritter, Markus 1, 6, 7, 30, 31, 51, 60, 86, 118
Rochow, Niels 5, **64,** 70, 79, 119
Rohde, Eva 69, 105
Rohleder, Nicolas 40
Roider, Karin 3
Romanelli, Pasquale 46, 105
Rosa, Ilenia 90
Rösch, Sebastian 9
Roth, Dominik 113
Rousaud, Araceli 90
Rübling, Achim 44
Ruff, Marleen 40
Russe, Elisabeth 34
Rüther, Johannes 49
Ruttmann, Axel 75

S
Sackarnd, Jan 56
Salaheddine, Ali 52
Salewski, Birgit 5
Salgado Albarran, Marisol 61
Sandriesser, Sabrina 89, **106**
Santarpino, Giuseppe 23, 24
Sarikas, Antonio 9, 33, 85, 102
Schachinger, Judit **107,** 128
Schäfer, Stefan 79
Schäfer-Eckart, Kerstin 44, 122
Schallmoser, Katharina 13, 25, 34, 48, 65, 69, 91, 130
Schänzer, Anne 2
Scharler, Cornelia 34
Schernthaner, Christiana 55, 66
Schmelzer, Sebastian 94
Schmidbauer, Josef 62
Schmidhuber, Sabine 34
Schmidt-Bleek, Katharina 52
Schneeberger, Achim 34
Schneeberger, Tessa 54, 73, **108**
Schneider, Sophia **109**
Schrey, Michael 35
Schrödl, Falk **26,** 59, 96
Schröpfer, Michaela 45, 122
Schulze-Tanzil, Gundula 17, 44, 45, 63, 112, 113, 122
Schürger, Gabriele 88
Schuster, Daniela 51, 134
Schuster, Philipp 51
Schuster, Sara K. 90
Schwarz, Silke 113
Schwemberger, Bettina 28, 29, **110, 111,** 131
Schwenker, Kerstin 103
Seelmaier, Clemens 56
Seiler, Hans 120
Seitelberger, Rainald 50, 63, 66, 96
Shi, Jingjian **112**
Shomanova, Zornitsa 56
Sievers, Reiner 20
Silawal, Sandeep **113**
Sindermann, Jürgen 56
Sirch, Joachim 47, 71, 114, 116
Skokic, Sinisa 105
Sluet, Patrick 47, **114**
Smolcic, Tomislav 105
Söhn, Claudius **115**
Sommer, Claudia 16
Sonntag, Simon 120
Sonveaux, Pierre 125
Speziale, Giuseppe 23, 24
Spittler, Andreas 130
Stachelscheid, Harald 34
Stein, Barbara 40, 90
Steinbacher, Jürgen 15, 80, 81
Steindl, Johannes 66
Steiner, Hans-Herbert 35, 76
Steinmann, Jörg 77

Stemmler, Mark 109
Stenzel, Nikola 73
Stickl, Franziska J. **116**
Strempfl, Katharina **117**
Strobl, Annemarie 43
Strobl, Victoria 60, **118**
Strohmer, Bernhard 56
Strunk, Dirk 13, 25, 34, 48, 52, 61, 65, 69, 98, 100, 130
Sturm, Lisa 111
Surmann, David **119**
Swann, Victoria 12
Swol, Justyna **120**
Szakacs-Fusch, Adel 79, 126

T
Tallmann, Richard 120
Tatarski, Rafaella 118
Tausch, Andreas 40
Temml, Veronika 134
Tempfer, Herbert 28, 29, 107
Teuschl, Andreas 28
Textor, Martin 52
Thapa, Maheshwor 125
Thiel, Christian 37
Thurner, Marco 46
Tockner, Birgit 61
Topf, Albert 55
Torres, Xavier 90
Traweger, Andreas 28, 29, 107, 110, 111, 131
Trieb, Klemens 67, 68
Triebel, Jakob 113
Trinka, Eugen 15, 80, 81, 103
Tuchscherr de Hauschopp, Lorena 61

U
Üçeyler, Nurcan 16
Unger, Michael S. 11, 117, **121**

V
Vári, Balász 13, 34, 130
Vazeille, Thibaut 125
Vogelmeier, Claus F. 73
Vogt, Ferdinand 53, 82
Vogt, Julia **122**
Voit-Hoehne, Heinz-Leonhard 76
Volk, Hans-Dieter 130
Volp, Alexandra **123**
von Lutz, Lea S. **124**
Vötsch, Andreas 66

W
Wagner, Andrea 28, 29, 110
Wagner, Roland 61
Wald, Martin 99
Waller, Christiane 40, 109
Wally, Verena 19
Walter, Carola 43
Weber, Axel 2
Weber, Daniela 95
Weber, Daniela D. **125**
Weber, Miriam 78
Weigel, Carla 88
Weiger, Thomas M. 44
Weilgony, Nicolas 126
Weiss, Helmut 87
Weißenbacher, Nadja 28
Welker, Jan 57
Wenk, Jonathan 62
Werner, Christian 112
Wernly, Bernhard 55
Wiederhold, Jian 54
Wildner, Dane **127**
Willauschus, Maximilian 49, 113
Wiltzsch, Sven 44
Winkelmann, Paul 86
Winkler, Andreas 66
Winkler, Martin 4
Winklmayr, Martina 7, 60
Winterholler, Fabian 32
Wirth, Wolfgang **128,** 129
Wisser, Anna **129**
Wittig, Jörn 38
Wittig-Draenert, Alice 38
Wolf, Martin 13, 25, 34, 48, 100, **130**
Wolfmeier, Heidi 26, 59
Wortmann, Saskia B. 2, 37
Wunner, Christina 109
Würflein, Dieter 133
Wutte, Christof 72
Wutzke, Klaus 5

Y
Yiu So, Hon 64, 70

Z
Zabelt, Franziska **131**
Zaunmair, Pia 105
Zauter, Sigrid 104
Zeder-Göß, Christine **132**
Zeitler, Gloria **133**
Zell, Lukas **134**
Zerbe, Horst 117
Žibert, Janez 47, 71, 114
Zimmermann, Georg 15, 41, 80, 103
Zimmermann, Jasper 79
Zinterhof, Peter **135**
Zweigerdt, Robert 25